Recent Developments in the Antiferromagnetic Quantum Critical Metal: Pairing Instability, Emergent Momentum-Spacetime Geometry and Kondo Effect

Recent Developments in the Antiferromagnetic Quantum Critical Metal: Pairing Instability, Emergent Momentum-Spacetime Geometry and Kondo Effect

by

Francisco Borges M.Sc.

A Thesis
Submitted to the School of Graduate Studies
in Partial Fulfillment of the Requirements
for the degree Doctor of Philosophy

McMaster University

Doctor of Philosophy, Department of Physics and Astronomy, McMaster University (2025), Hamilton, Ontario.

Title: Recent Developments in the Antiferromagnetic Quantum Critical Metal: Pairing Instability, Emergent Momentum-Spacetime Geometry and Kondo Effect
Author: Francisco Borges, M.Sc. (University of Waterloo and Perimeter Institute for Theoretical Physics)
Supervisor: Dr. Sung-Sik Lee
Number of Pages: xviii, 188

Abstract

This thesis is concerned with recent progress made for the antiferromagnetic quantum critical metal in two space dimensions.

Firstly, we develop a field-theoretic functional renormalization group formalism for the low-energy effective field theories for non-Fermi liquids by using renormalizable field theories for metals. The formalism is applied to the antiferromagnetic quantum critical metal in two space dimensions. In the space of coupling functions, we identify the interacting fixed point with a vanishing nesting angle. For theories with non-zero nesting angles, the coupling functions acquire universal momentum dependent profiles controlled by the bare nesting angle before flowing towards a superconducting state in the low-energy limit. The superconducting instability is inevitable because "lukewarm" electrons that are coherent enough to be susceptible to pairing are subject to a universal attractive interaction mediated by the critical spin fluctuations. Despite the superconducting instability being unavoidable, theories with repulsive or weakly attractive four-fermion interaction at a UV scale must flow through a "bottleneck" where there is a slow RG flow due to the proximity to non-Hermitian fixed points. This bottleneck of the RG flow controls the scaling behaviour of the normal state and the "quasi-universal" pathway to superconductivity.

Secondly, we show that momentum-dependent quantum corrections dynamically give rise to a curved momentum-spacetimes for quasiparticles. In the antiferromagnetic quantum critical metal, the curved momentum-spacetime geometry arises from a momentum-dependent red shift. With increasing nesting angle, the red shift near the hot spots becomes stronger while the hot region on the Fermi surface with the strong red shift shrinks. This creates the possibility of realizing a momentum-space black hole horizon where electrons are perpetually slowed down as they approach the hot spots. However, the singularity in the momentum-dependent red shift is cut off at finite temperatures above the superconducting transition temperature.

Finally, we study a magnetic impurity immersed in the antiferromagnetic quantum critical metal. Critical spin fluctuations represented by bosonic fields compete with the conduction electrons to couple with the impurity spin. In the low-energy limit, the electron-impurity (Kondo) coupling dominates over the boson-impurity coupling. However, the Kondo screening is suppressed by the boson with an increasing severity when the hot spots connected by the antiferromagnetic ordering wavevector are better nested. The origin of this suppression of Kondo screening lies in the ultraviolet/infrared (UV/IR) mixing: bosons that carry large momenta up to the UV cutoff actively suppress the Kondo screening at low energies.

Contents

List of Figures

List of Tables

Acknowledgement

I want to start by thanking my supervisor, Sung-Sik Lee, for his continuous support, guidance, patience, his immense experience, and for his exceptional disposition to the role of teacher. Sung-Sik has shaped me to be a more effective researcher, and his approach to devise clever analogies to communicate difficult subjects has definitely rubbed off on me. Throughout my Ph.D. journey, Sung-Sik has influenced me to strive not only to achieve quality research and results, but also thoroughness, honesty, and a fearless approach towards science.

I am also very grateful to my collaborators and members of our group Anton Borissov, Shubham Kukreja, Afshin Besharat, Peter Lunts, Ashutosh Singh and Andrés Schlief. It was truly an amazing experience to collaborate with you, and to have all the amazing and insightful conversations about physics and many other diverse and interesting topics.

I want to thank the members of my committee, Cliff Burgess and Sergey Sibiryakov for their feedback and advice during my Ph.D. I want to extend that very same gratitude to all the faculty members who have taught and mentor me inside and outside the classrooms of McMaster University. I had the privilege to attend lectures and engage in physics discussion with An-Chang Shi, Erik Sørensen and Bruce Gaulin despite the challenges of the COVID-19 pandemic. Finally I want to thank the staff at the Department of Physics and Astronomy at McMaster University for their support, patience and great human quality. In particular, I would like to thank Rosemary McNeice, Jennifer Ayres and Aileen Pineda.

I spent most of my time at the Perimeter Institute for Theoretical Physics. It is a place defined by the curiosity, resilience, academic excellence and undeniable humane qualities of its members. I would like to thank Freddy Cachazo for his initial advice and support when I first came to PI. I want to give thanks to the postdocs who have given me advice through the mentorship program at PI Céline Zwikel and Barbara Šoda. I would also like to give special thanks to Barbara for all the conversations about physics, health, stand-up comedy, MBTI, AI, philosophy, for taking improv classes with me[1] and all things that might not be practical for everyday life but are nonetheless interesting. I would also like to thank Suvendu Giri for sharing his incredible physical intuition during his stay at Perimeter, his advice on how to look dapper and crazy new ideas for a new science-fiction book franchise. I want to thank all the rest of the Ph.D. students and postdocs I met at PI and McMaster, past and present. The Ph.D. community at PI is very special to me, it is a melting pot of a ideas and approaches the form the perfect nurture for anyone with a curious mind. It has been an immense pleasure to learn from them, as they are learning themselves. I would like to start with my former flatmates Fabián Bautista, Bruno Gimenéz and Alexandre Homrich, with whom I shared a lot of adventures in Waterloo and beyond. I would also like to thank my officemates for the majority of my Ph.D. studies, Amir-Reza Negari and Bruno Torres for providing a top-quality working environment at office 354. Finally, I would like to thank Aiden Suter, Amalia Madden, Kasia Budzik, Ramiro Cayuso, Sara Bogojević, Jury Radkovski, Jordan Krywonos, Σωτήρης Μυγδαλάς[2], Guillaume Dideron, Dalila Pîrvu, Hassan Khalvati, Conner Dailey, Alice Chen, Adrián López, and many others, for the numerous activities and conversations including physics, mathematics, Coulomb branches, Higgs branches, QFT, TQFT, QEC, QED, QCD, AdS/CFT, CMB, QMC, MRAM, ML, AI, ANI, AGI, LLMs, and many other acronyms, space and time travel, movies, evolution, birding, photography, investing and banking, biking, baking, barbecuing, geopolitics, economy, war, peace, crime, punishment, running, the five D's of dodgeball[3], language, etymology, horses, and many, many other enriching topics and things to do.

For the non academic side of PI, I would like to start by thanking Debbie Guenther, for her steadfast attitude and industriousness in the administrative side of PI until her retirement. I would like to thank Angela Hovestad and Sunny Tsang for the hard work on the administrative side of things regarding my Ph.D. residence at PI.

I would also like to thank my long-time friends: Jeinny Pérez, María Dias, and Gustavo Kufatty,

[1] Yes, and...

[2] Sotiris Mygdalas, spelled in Greek by his request.

[3] Dodge, Duck, Dip, Dive, and Dodge.

for their moral support and for keeping in touch all this years despite this permanently busy state of world around us. I want to thank the Perdomo-Blanco family: Benjamin, Laura and their son Antonio (Tato), for being tremendous neighbours during the entirety of my Ph.D., for being amazing friends and my small piece of Latin America right here in Waterloo. Last, but not least, I want to give my special thanks to the kitchen and server staff of The Black Hole Bistro. In particular, I want to thank past and present members, including Daniel Lynch, Olivia Taylor, Angela Malaythong, Angelina Malaythong, Megan Lindner, Chandy Thach, Amy Luce, Aislinn Moores and Belén Ponciano.

To conclude, I want to thank the most important people on my life. To my mother, Ysabel Zapata, I am infinitely grateful. I admire her strength, perseverance, and constant support, which have continuously inspired me to continue moving forward. To my father, Miguel Borges, who has always reminded me there is light at the end of the tunnel, and that talent means nothing without discipline. To my sister, Mariana, thank you from afar, for keeping an eye on our parents during my absence. I have nothing but everlasting love for all of you. Thank you for helping me believing in myself.

Declaration of Authorship and Academic Achievement

This thesis is based on two published works and another that under review for journal publication.

- Chapter 2

  F. Borges, A. Borissov, A. Singh, A. Schlief, and S.-S. Lee, *Field-theoretic functional renormalization group formalism for non-Fermi liquids and its application to the antiferromagnetic quantum critical metal in two dimensions*, Annals of Physics **450** (2023).

  DOI: https://doi.org/10.1016/j.aop.2023.169221

- Chapter 3

  F. Borges and S.-S. Lee, *Emergence of curved momentum-spacetime and its effect on cyclotron motion in the antiferromagnetic quantum critical metal*, Physical Review B **108** (2023).

  DOI: https://doi.org/10.1103/PhysRevB.108.245112

- Chapter 4

  F. Borges, P. Lunts and S.-S. Lee, *Ultraviolet/infrared mixing-driven suppression of Kondo screening in the antiferromagnetic quantum critical metal*, arXiv.2505.01561, (2025). Under review for publication in Phys. Rev. B.

  DOI: https://doi.org/10.48550/arXiv.2505.01561

In Chapter 2, Francisco Borges is primarily responsible for Sections 2.5.2, 2.6.3 and 2.7. All Authors where involved in Sections 2.3 and 2.4. Anton Borissov is responsible for the results in Sections 2.5.1 and 2.6.1. Ashutosh Singh was responsible for the results in Section 2.6.2, plots in Section 2.6.3, and other aspects of the publication. Andrés Schlief was responsible for the calculations at an early stage of the project. Francisco Borges performed most of the calculations in Appendix B and D. Anton Borissov is responsible for the calculations of Appendices A and C, and was partially involved in the calculation in Appendix B.3. Ashutosh Singh was partially involved in the calculations of Appendix B.1.1 and Appendix B.2.1. Sung-Sik Lee provided guidance and direction, wrote the majority of the draft, and all authors were responsible for editing the final manuscript.

In Chapter 3, Francisco Borges performed all calculations in Appendices E, F and G. Francisco Borges was also responsible for writing the draft of the manuscript. Sung-Sik Lee provided guidance throughout the development and completion of the project and edited the final version of the manuscript.

In Chapter 4, Francisco Borges was responsible for the calculations in Appendices H, I and J. Additionally, Borges was responsible for writing the draft of the manuscript. Peter Lunts contributed through discussion and suggestions throughout the completion of the work and was responsible for some initial calculations in an early version the project. Sung-Sik Lee provided guidance throughout the completion of the project. All authors were involved in the discussion and shaping the final version of the manuscript.

Chapter 1

Introduction

One core question that defines the field of condensed matter physics is: *What are the macroscopic behaviours that can emerge in quantum matter?* Answering this question involves extracting the *universal long-distance* physics in distinct *phases of matter*. In particular, quantum critical points host novel states of matter described by strongly interacting theories with no well-defined quasiparticle description. Understanding the nature of critical states that arise at a continuous phase transition also provides a unified understanding of the phases that are separated by the critical point.

An important class of continuous phase transitions is the one that involves spontaneous symmetry breaking [102, 103]. From the context of symmetry breaking, the *Ginzburg-Landau theory* that describes the long-distance physics in terms of the dynamical order parameter is one of the milestones of statistical physics, and its principles are the first foundational tool upon which this thesis is built [172, 115, 65]. The second tool we employ in this thesis is the *renormalization group*. Introduced by Kadanoff [91] and Wilson [224, 225], it allows a systematic extraction of the effects of fast fluctuations of the order parameter for slow modes by organizing physical degrees of freedom in terms of their energy scale. Low-energy effective theories obtained from coarse graining generally include all terms allowed by locality and symmetry, and we only need universal properties like spacetime dimension and the symmetries of the order parameter as ingredients when constructing effective field theories. From *scale-invariant fixed points* of the renormalization group flow, one can extract the universal low-energy physics.

Many phase transitions found in nature occur in dimensions that are below the upper critical dimension, making the low-energy effective theory strongly coupled at low energies, and thus, non-perturbative [233, 11, 207]. The effective field theory for metals is further complicated by the presence of the *Fermi surface*, where infinitely many gapless modes reside. While the low energy physics of the conventional metals is well described by *Landau's Fermi Liquid Theory* [101, 100, 163], non-Fermi liquids that arise at quantum critical points remain poorly understood. This thesis is concerned with the *non-Fermi liquid* metal realized at the antiferromagnetic quantum critical point in two space dimensions [78, 77, 153]. Specifically, we study the pathway of the non-Fermi liquid to superconductivity, the cyclotron motion of electrons, and the fate of a magnetic impurity immersed in the unconventional metal. We dedicate the rest of this chapter to a review of several key concepts used in the thesis.

1.1 Fermi Liquid Theory

The focus of this thesis is metals. Naively, studying the ground state of a metal would involve solving a many-body Schödinger equation with the Coulomb potential in the thermodynamic limit. Thankfully, we do not need to solve the full Schödinger equation for the purpose of understanding the low-energy physics. For that purpose, *Landau's Fermi Liquid Theory* [101, 100] is the low-energy theory of conventional metals that support quasiparticles. Landau's Fermi liquid theory is one of the two cornerstones

of traditional many-body theory[1]. We dedicate this section to review the basic intuition and key properties of the Fermi liquid theory.

1.1.1 Landau's Fermi Liquid Theory

Let us begin with the non-interacting Fermi gas. In a ion lattice, conduction electrons have their wavefunctions spread over the interstitial positions, organizing themselves in a similar periodic structure according to Bloch's theorem [19]. A single-particle quantum state in each band is specified by crystal momentum $\vec{k}$ and spin σ (generally along the z-axis). Because fermions obey Pauli's exclusion principle, the many-body energy eigenstates of the system as a whole can be specified through the occupation number of particles $n_{\vec{k},\sigma} = 0, 1$ in each of the single-particle states. In particular, the ground state of the system is one in which all single-particle states with momenta less than the *Fermi momentum*, k_F, are occupied ($n_{\vec{k},\sigma} = 1$) and all other single-particle states are empty ($n_{\vec{k},\sigma} = 0$). Excited stated can only be created by adding particles with momentum larger than k_F, or by removing particles with momentum less than k_F. We call these excited states *particles* and *holes*, respectively. At zero temperature, the occupation number has a sharp discontinuity at the Fermi surface,

$$n_{\text{g.s.}}(\vec{k}) = \Theta\left(k_F - \left|\vec{k}\right|\right), \tag{1.1}$$

where $\Theta(x)$ is the unit step function. At finite temperature T, states with energy $O(T)$ below the Fermi surface can become excited to states of energy $O(T)$ above the Fermi surface due to thermal fluctuations, and the occupation number above is replaced by the Fermi-Dirac distribution,

$$n_{\text{F-D}}(\vec{k}) = \frac{1}{e^{\frac{\varepsilon(\vec{k})-\mu}{T}} + 1}, \tag{1.2}$$

where the Boltzmann constant k_B is set to be 1, $\varepsilon(\vec{k})$ is the energy of the electron and μ is the chemical potential which at zero temperature is equal to the *Fermi energy* $E_F = \varepsilon(\vec{k}_F)$.

Now let us consider an interacting Fermi system. Landau's Fermi Liquid Theory (FLT) posits that there is a one-to-one correspondence between the eigenstates of the free Fermi gas and those of the interacting system at low energies. To be more precise, if one takes an eigenstate of Fermi gas and adiabatically turns on the interaction between particles, one obtains a state of the interacting system. This allows us to label the low-energy many-body eigenstates of the interacting system by using the occupation/particle distribution $n(\vec{k})$ of the corresponding state of the Fermi gas. Consequently, the elementary excitations of the Fermi liquid are in one-to-one correspondence with those of the Fermi gas, but with a renormalized spectrum due to the interaction; they are called *quasiparticles* and quasiholes. The distribution $n(\vec{k})$ of the Fermi gas is then promoted to the *quasiparticle distribution function*, or *quasiparticle occupation number* in interacting Fermi liquids.

The above conclusion can only be true if the relaxation time of the quasiparticle excitations is larger than the period of oscillation associated with its energy. Naively, one might expect the electron-electron scattering rate to be quite high, due to the Coulomb interaction[2]. However, Pauli's exclusion principle greatly suppresses the scattering rate for particles near the Fermi surface. Let us illustrate this point with a simple example [19], depicted in Fig. 1.1. Suppose we have electron 1 above the Fermi surface at energy $\varepsilon_1 \gtrsim E_F$. Suppose it interacts with an electron 2 with energy $\varepsilon_2 \lesssim E_F$. The exclusion principle requires these two electrons to scatter to final states 3 and 4 above the Fermi surface, i.e., $\varepsilon_3, \varepsilon_4 \gtrsim E_F$. Additionally, energy conservation requires that

$$\varepsilon_1 + \varepsilon_2 = \varepsilon_3 + \varepsilon_4. \tag{1.3}$$

[1] The other one being symmetry breaking theory.

[2] In fact, the Coulomb potential is as large as the Fermi energy E_F in ordinary metals, and definitely larger than the energy-level spacing near E_F

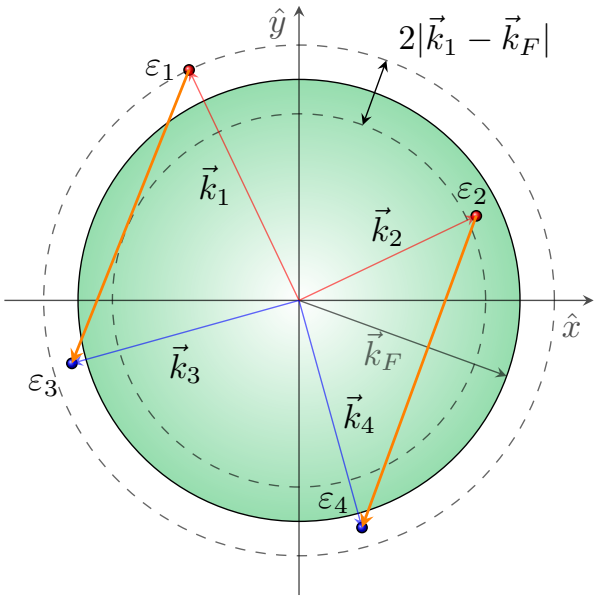

Figure 1.1: Scattering of particles around a one-dimensional Fermi surface. Here, the Fermi sea is represented by the green disk and the solid black circle demarcating the boundary is the Fermi surface. For the initial states with energies $\varepsilon_1, \varepsilon_2$ to get scattered to the final state with energies $\varepsilon_3, \varepsilon_4$, all the electron momenta must lie within the shell $2\left|\vec{k}_1 - \vec{k_F}\right|$. This is equivalent to the energy of the particles being within the shell $2|\varepsilon_1 - E_F|$ around E_F.

At zero temperature, electrons 2, 3 and 4 should have energies within a shell of thickness $2|\varepsilon_1 - E_F|$ around the Fermi energy. With one energy conservation for three undetermined energies, the total scattering rate scales as

$$\frac{1}{\tau} \sim (\varepsilon_1 - E_F)^2. \tag{1.4}$$

As the energy is reduced to that of the Fermi energy, the scattering rate is reduced quadratically. Therefore, low-lying excitations become more stable as the energy approaches the Fermi energy.

Let us turn our focus on the physical properties of the Fermi liquid. At low temperature T, it is only electrons within T away from the Fermi energy that contribute the most to the low-energy metallic properties. Let us consider a distribution of quasiparticles written as a 2×2 density matrix $n_{\sigma\bar{\sigma}}(\vec{k})$ in spin space. The total energy E is a functional of the variation $\delta n_{\sigma\bar{\sigma}}(\vec{k}) = n_{\sigma\bar{\sigma}}(\vec{k}) - 2\delta_{\sigma\bar{\sigma}} n_{\mathrm{F-D}}(\vec{k})$ [101]:

$$\begin{aligned} E[\delta n] =& E_{\text{g.s.}} + \sum_{\sigma\bar{\sigma}=\uparrow\downarrow} \int \frac{\mathrm{d}^3 k}{(2\pi)^3} \varepsilon^{(0)}_{\bar{\sigma}\sigma}(\vec{k}) \delta n_{\sigma\bar{\sigma}}(\vec{k}) \\ &+ \frac{1}{2} \sum_{\sigma\bar{\sigma};\sigma'\bar{\sigma}'=\uparrow\downarrow} \int \frac{\mathrm{d}^3 k \mathrm{d}^3 k'}{(2\pi)^6} f_{\sigma\bar{\sigma};\sigma'\bar{\sigma}'}(\vec{k};\vec{k}') \delta n_{\bar{\sigma}\sigma}(\vec{k}) \delta n_{\bar{\sigma}'\sigma'}(\vec{k}') + O(\delta n)^3. \end{aligned} \tag{1.5}$$

The first term, $E_{\text{g.s.}}$, is the energy of the ground state. In the second term, $\varepsilon^{(0)}_{\sigma\bar{\sigma}}(\vec{k})$ is the quasiparticle energy relative to E_F in the neighbourhood of the Fermi surface,

$$\varepsilon^{(0)}_{\sigma\bar{\sigma}}(\vec{k}) = \epsilon^{(0)}(\vec{k}) \delta_{\sigma\bar{\sigma}} + \vec{h}(\vec{k}) \cdot \vec{\tau}_{\sigma\bar{\sigma}}. \tag{1.6}$$

$\epsilon^{(0)}(\vec{k}) \approx \frac{1}{m^*}\left(\vec{k} - \vec{k}_F\right) \cdot \vec{k}_F$ with m^* being the quasiparticle effective mass, which is different from the bare electronic mass m. $\vec{h}(\vec{k})$ is proportional to an external magnetic field. Finally, $\vec{\tau} = (\tau^x, \tau^y, \tau^z)$ denotes the vector of Pauli matrices. In the second term of Eq. (1.5), the interaction energy $f_{\sigma\bar{\sigma};\sigma'\bar{\sigma}'}(\vec{k};\vec{k}')$

is referred to as *Landau's interaction function*, and it captures the forward scattering of quasiparticles. In the absence of spin-orbit coupling, we can write

$$f_{\sigma\bar{\sigma};\sigma'\bar{\sigma}'}(\vec{k};\vec{k}') = f^S(\vec{k};\vec{k}')\delta_{\sigma\bar{\sigma}}\delta_{\sigma'\bar{\sigma}'} + f^A(\vec{k};\vec{k}')\vec{\tau}_{\sigma\bar{\sigma}}\cdot\vec{\tau}_{\sigma'\bar{\sigma}'}, \tag{1.7}$$

where the f^S and f^A represent the density-density and spin-spin interactions, respectively. At low energies, we are concerned only with interactions of quasiparticles that are close to the Fermi surface, and we write

$$f^S(\vec{k};\vec{k}') = \sum_{l=0}^{\infty} f_l^S P_l(\cos\theta), \quad f^A(\vec{k};\vec{k}') = \sum_{l=0}^{\infty} f_l^A P_l(\cos\theta), \tag{1.8}$$

where $P_l(z)$ are the Legendre polynomials and θ is the angle between $\vec{k}$ and $\vec{k}'$. The coefficients are determined by

$$f_l^S = \frac{2l+1}{2}\int_{-1}^{1} \mathrm{d}(\cos\theta) P_l(\cos\theta) f^S(\vec{k};\vec{k}'), \quad f_l^A = \frac{2l+1}{2}\int_{-1}^{1} \mathrm{d}(\cos\theta) P_l(\cos\theta) f^A(\vec{k};\vec{k}'). \tag{1.9}$$

The coefficients f_l^S and f_l^A define the *Landau parameters* [100]:

$$F_l^S = N(0) f_l^S, \qquad F_l^A = N(0) f_l^A, \tag{1.10}$$

where $N(0)$ is the density of quasiparticle states at the Fermi surface. The Landau parameters provide a useful dimensionless measures of the strengths of quasiparticle interactions on the Fermi surface in each angular momentum channel. In systems with Galilean invariance, the effective mass is related to the bare electronic mass m through the relation

$$\frac{m^*}{m} = 1 + \frac{F_1^S}{3}. \tag{1.11}$$

We can express thermodynamic potentials in terms of the parameter in Eqs. (1.5) and (1.10) at the Fermi surface[24]. The specific heat at constant volume is

$$c_V = \frac{1}{3} m^* k_F T, \tag{1.12}$$

which is essentially that of a Fermi gas of mass m^*. Similarly, the compressibility κ, and the spin susceptibility χ, become

$$\kappa = \frac{1}{n^2}\frac{N(0)}{1+F_0^S}, \qquad \chi = \frac{\gamma^2}{4}\frac{N(0)}{1+F_0^A}, \tag{1.13}$$

respectively. Here, n is the total particle density and γ is the gyromagnetic ratio. The factors $1+F_0^S$ and $1+F_0^A$ both encapsulate the effects of renormalization due to the quasiparticle interaction [101, 100]. In order to retain thermodynamic stability in the presence of the interaction, the Landau parameters must satisfy[163]:

$$F_l^S > -(2l+1), \qquad F_l^A > -(2l+1) \tag{1.14}$$

for all l. When this condition is violated, the energy can be lowered by condensing quasiparticle-quasihole excitations near the Fermi surface, which leads to a phase separation or a symmetry breaking.

1.1.2 Fermi Liquid Theory in the Language of Effective Field Theory

Despite being a phenomenological framework, Landau's Fermi liquid theory saw great success in describing the low-energy physics of a large class of metals. A solid theoretical foundation for the theory was eventually found in the language of effective field theory (EFT) when the problem of many fermions at finite density was studied from the point of view of the Renormalization group (RG) [124, 194, 40, 39, 38]. In the language of EFT and the RG, Landau's FLT is a class of *low-energy fixed points* of a

finite density of fermions subject to a short-range interaction. Below we will unpack the meaning of the above statement.

The starting point is the *microscopic action* written in the $d+1$ dimensional Euclidean space as

$$S = \sum_{\sigma=\uparrow,\downarrow} \int \frac{\mathrm{d}k_0 \mathrm{d}^d k}{(2\pi)^{d+1}} \psi^\dagger_\sigma(k_0,\vec{k}) \left(ik_0 + \varepsilon(\vec{k}) - E_F \right) \psi_\sigma(k_0,\vec{k}) + \prod_{i=1}^{4} \left[\sum_{\sigma_i=\uparrow,\downarrow} \int \frac{\mathrm{d}k_{i,0}\mathrm{d}^d k_i}{(2\pi)^{d+1}} \right] \delta_{1+2,3+4} \lambda^{\left(\begin{smallmatrix}\sigma_1 & \sigma_2\\ \sigma_4 & \sigma_3\end{smallmatrix}\right)}_{\left(\begin{smallmatrix}\vec{k}_1 & \vec{k}_2\\ \vec{k}_4 & \vec{k}_3\end{smallmatrix}\right)} \psi^\dagger_{\sigma_1}(k_{1,0},\vec{k}_1)\psi^\dagger_{\sigma_2}(k_{2,0},\vec{k}_2)\psi_{\sigma_3}(k_{3,0},\vec{k}_3)\psi_{\sigma_4}(k_{4,0},\vec{k}_4). \tag{1.15}$$

Here, k_0 is the Matsubara frequency for fermions, $\vec{k}$ is the spatial $d-$dimensional momentum and $\psi_\sigma(k_0,\vec{k})$ is the Grassmann field variable representing the electrons, which depends on $(k_0,\vec{k})$ and spin $\sigma =\uparrow,\downarrow$. The fermion dispersion energy is denoted as $\varepsilon(\vec{k})$ and the Fermi energy is defined by $E_F = \varepsilon(\vec{k}_F)$. The local four-fermion interaction satisfies the energy and momentum conservation enforced through the $d+1$-dimensional delta function $\delta_{1+2,3+4} = (2\pi)\delta(k_{1,0}+k_{2,0}-k_{3,0}-k_{4,0})(2\pi)^d\delta(\vec{k}_1+\vec{k}_2-\vec{k}_3-\vec{k}_4)$. $\lambda^{\left(\begin{smallmatrix}\sigma_1 & \sigma_2\\ \sigma_4 & \sigma_3\end{smallmatrix}\right)}_{\left(\begin{smallmatrix}\vec{k}_1 & \vec{k}_2\\ \vec{k}_4 & \vec{k}_3\end{smallmatrix}\right)}$ are the *coupling functions* representing an inter-fermion interaction. The matrix notation $\left(\begin{smallmatrix}1 & 2\\ 4 & 3\end{smallmatrix}\right)$ in λ explicitly organizes the labelled parameter of the electron-electron interaction as they would appear in the external legs of a four-fermion vertex, with the initial state on the bottom row and the final state on the top row. Locality requires that λ is an analytic function of momenta. In the presence of the SU(2) spin rotation symmetry, λ can be written as

$$\lambda^{\left(\begin{smallmatrix}\sigma_1 & \sigma_2\\ \sigma_4 & \sigma_3\end{smallmatrix}\right)}_{\left(\begin{smallmatrix}\vec{k}_1 & \vec{k}_2\\ \vec{k}_4 & \vec{k}_3\end{smallmatrix}\right)} = \lambda^{D}_{\left(\begin{smallmatrix}\vec{k}_1 & \vec{k}_2\\ \vec{k}_4 & \vec{k}_3\end{smallmatrix}\right)} \delta_{\sigma_1\sigma_4}\delta_{\sigma_2\sigma_3} + \lambda^{E}_{\left(\begin{smallmatrix}\vec{k}_1 & \vec{k}_2\\ \vec{k}_4 & \vec{k}_3\end{smallmatrix}\right)} \vec{\tau}_{\sigma_1\sigma_4}\cdot\vec{\tau}_{\sigma_2\sigma_3}, \tag{1.16}$$

where D (E) stands for "direct" ("exchange") and $\lambda^{D,E}$ are analytic functions of momenta (See Eq. (1.7)).

Equation (1.15) generally contains non-universal data for high-energy modes far away from the Fermi surface, and the the Landau parameters can be understood as the fixed point profile of λ in the forward scattering channel. Let us briefly describe the intuition of the RG that connects the microscopic interaction and the low-energy observables such as the Landau parameters. When we compute physical observables from the action Eq. (1.15), the result can be formally expressed as a series of the coupling λ, where the coefficients are written as integrals over loop momenta. In general, physical observables depend on the ultraviolet cutoff Λ. However, we can choose a set of Λ-dependent couplings so that the physical observables become cutoff-independent at momenta much smaller than Λ. If we can make this choice at any given order of the perturbation series, the theory is *renormalizable*. Under the change of cutoff by a small factor $s<1$, accompanied by a suitable change of the couplings, low-energy physical observables remain invariant. By lowering the cutoff as $\Lambda \to \Lambda s$ with $s<1$, we effectively decimate high-energy modes that contain microscopic details of the system. This defines an RG transformation of the scale-dependent couplings, and the objective is to perform it iteratively to extract the low energy properties. The result is a series of dynamical equations for the couplings whose *fixed points* contain only universal low-energy information of the system [11]. In our particular case, we know that the low-energy modes reside near the Fermi surface. Therefore, the EFT action for the FL can be defined by considering the UV cutoff Λ defining a shell of thickness $2\Lambda \ll k_F$ around

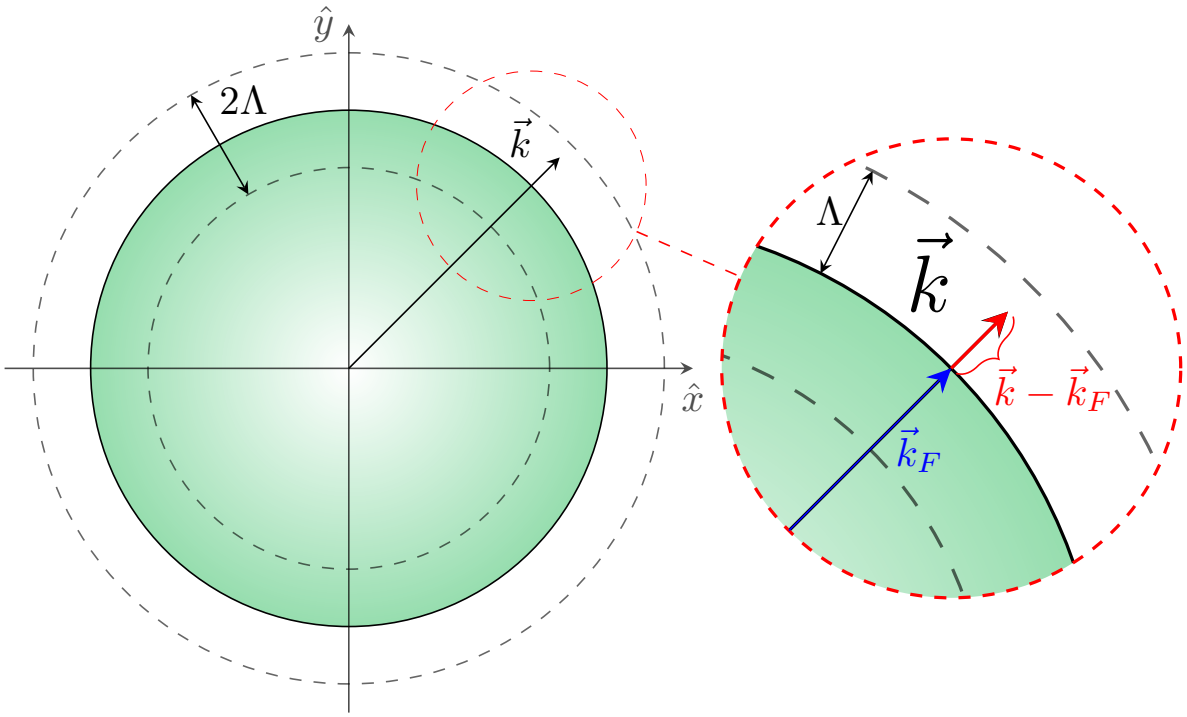

Figure 1.2: One dimensional Fermi surface (solid black circle) in a two dimensional momentum space. The dashed circles represent the boundaries of the shell of thickness $2\Lambda \ll k_F$ enclosing the low energy degrees of freedom.

the Fermi surface [160, 194]:

$$S = \sum_{\sigma=\uparrow,\downarrow} \int_\Lambda \frac{\mathrm{d}k_0 \mathrm{d}^d k}{(2\pi)^{d+1}} \psi^\dagger_\sigma(k_0, \vec{k}) \left[ik_0 + \vec{v}_F(\hat{k}) \cdot \left(\vec{k} - \vec{k}_F(\hat{k}) \right) \right] \psi_\sigma(k_0, \vec{k})$$
$$+ \prod_{i=1}^{4} \left[\sum_{\sigma_i=\uparrow,\downarrow} \int_\Lambda \frac{\mathrm{d}k_{i,0} \mathrm{d}^d k_i}{(2\pi)^{d+1}} \right] \delta_{1+2,3+4} \lambda^{\begin{pmatrix} \sigma_1 & \sigma_2 \\ \sigma_4 & \sigma_3 \end{pmatrix}}_{\begin{pmatrix} \hat{k}_1 & \hat{k}_2 \\ \hat{k}_4 & \hat{k}_3 \end{pmatrix}} \psi^\dagger_{\sigma_1}(k_{1,0}, \vec{k}_1) \psi^\dagger_{\sigma_2}(k_{2,0}, \vec{k}_2) \psi_{\sigma_3}(k_{3,0}, \vec{k}_3) \psi_{\sigma_4}(k_{4,0}, \vec{k}_4), \tag{1.17}$$

where the Fermi velocity $\vec{v}_F(\hat{k}) = \vec{\nabla}_{\vec{k}} \varepsilon(\vec{k})\Big|_{k=k_F}$ and Fermi momentum $\vec{k}_F(\hat{k})$ depend only on their angular position on the Fermi surface, encoded by the unit vector "orientation" $\hat{k}$. This is depicted in Fig. 1.2. We have linearized the dispersion energy in the direction perpendicular to the Fermi surface as allowed by proximity to the Fermi surface. Likewise, we expand the four-fermion coupling in powers of small $\vec{k} - \vec{k}_F$, keeping only the dependences on the direction of momenta as $\lambda^{\begin{pmatrix} \sigma_1 & \sigma_2 \\ \sigma_4 & \sigma_3 \end{pmatrix}}_{\begin{pmatrix} \vec{k}_1 & \vec{k}_2 \\ \vec{k}_4 & \vec{k}_3 \end{pmatrix}} \approx \lambda^{\begin{pmatrix} \sigma_1 & \sigma_2 \\ \sigma_4 & \sigma_3 \end{pmatrix}}_{\begin{pmatrix} \hat{k}_1 & \hat{k}_2 \\ \hat{k}_4 & \hat{k}_3 \end{pmatrix}}$. $\int_\Lambda$ denotes the integration done over momenta satisfying $\left| \vec{v}_F(\hat{k}) \cdot \left(\vec{k} - \vec{k}_F(\hat{k}) \right) \right| \ll \Lambda \ll k_F$.

Now that we have determined the EFT action (1.17), we need to address the challenge that the nature of the Fermi surface adds to the RG. Because the Fermi surface is extended in the momentum space, interactions at low energy are not necessarily limited to processes with small momentum transfers, unlike for example, in relativistic field theory. To see this explicitly, let us consider the simple case of a spherically symmetric Fermi surface. In this case we can use generalized spherical coordinates in momentum space to rewrite the action; $\vec{k} = (k, \vec{\Omega}_{d-1})$, where k is the magnitude of $\vec{k}$ labelling the coordinate *normal* to the Fermi surface, and $\vec{\Omega}_{d-1}$ are the coordinates on the $(d-1)-$sphere S_{d-1}

representing the directions *along* the Fermi surface. The action becomes [160, 194]

$$\begin{aligned} S = &\sum_{\sigma=\uparrow,\downarrow} \int_{S_{d-1}} \frac{\mathrm{d}\Omega_{d-1}}{(2\pi)^{d-1}} \int_{-\infty}^{\infty} \frac{\mathrm{d}k_0}{2\pi} \int_{-\Lambda}^{\Lambda} \frac{\mathrm{d}k}{2\pi} \psi^{\dagger}_{\sigma}(k_0,\vec{k})\left[ik_0 + v_F k\right]\psi_{\sigma}(k_0,\vec{k}) \\ &+ \prod_{i=1}^{4}\left[\sum_{\sigma_i=\uparrow,\downarrow}\int_{S_{d-1}} \frac{\mathrm{d}\Omega_{i,d-1}}{(2\pi)^{d-1}} \int_{-\infty}^{\infty} \frac{\mathrm{d}k_{i,0}}{2\pi} \int_{-\Lambda}^{\Lambda} \frac{\mathrm{d}k_i}{2\pi}\right] \tilde{\delta}_{1+2,3+4}\tilde{\lambda}^{\left(\begin{smallmatrix}\sigma_1 & \sigma_2\\ \sigma_4 & \sigma_3\end{smallmatrix}\right)}_{\left(\begin{smallmatrix}\vec{\Omega}_{1,d-1} & \vec{\Omega}_{2,d-1}\\ \vec{\Omega}_{4,d-1} & \vec{\Omega}_{3,d-1}\end{smallmatrix}\right)} \\ &\times \psi^{\dagger}_{\sigma_1}(k_{1,0},\vec{k}_1)\psi^{\dagger}_{\sigma_2}(k_{2,0},\vec{k}_2)\psi_{\sigma_3}(k_{3,0},\vec{k}_3)\psi_{\sigma_4}(k_{4,0},\vec{k}_4), \end{aligned} \tag{1.18}$$

where we have shifted $\vec{k} \to \vec{k} + \vec{k}_F(\hat{k})$. The integration measures in Eq. (1.18) has now become $\mathrm{d}^d k \approx k_F^{d-1}\mathrm{d}k\mathrm{d}\Omega_{d-1}$ with $\mathrm{d}\Omega_{d-1}$ being the solid angle element in S_{d-1}, and we have taken the extra step to set $k + k_F \approx k_F$ on the measure due to the integration support being very close to the Fermi surface. Additionally, we have defined $\psi_{\sigma}(k_0,\vec{k}) = k_F^{\frac{d-1}{2}}\psi_{\sigma}(k_0, k+k_F, \vec{\Omega}_{d-1})$, and the delta distribution is now given by $\tilde{\delta}_{1+2,3+4} = (2\pi)\delta(k_{1,0}+k_{2,0}-k_{3,0}-k_{4,0})(2\pi)^d\delta(\hat{k}_1(\vec{\Omega}_{1,d-1})+\hat{k}_2(\vec{\Omega}_{2,d-1})-\hat{k}_3(\vec{\Omega}_{3,d-1})-\hat{k}_4(\vec{\Omega}_{4,d-1}))$. Finally, $\tilde{\lambda} = k_F^{d-1}\lambda$ is the four-fermion coupling function. From the action we can see that for electrons arbitrarily close to the Fermi surface the interaction strength only depends on the orientation of the initial and final states. In principle, the momentum transfer $\left|\vec{k}_1 - \vec{k}_4\right|$ can be as large as $2k_F$. This follows from the fact that all electrons on the Fermi surface have the same energy E_F, so the energy cost to scatter from one point to another on the Fermi surface is essentially zero. In this sense, the angles $\Omega_{i,d-1}$ are *dimensionless continuous flavours* that label gapless modes on the metal. In contrast, the normal coordinate k is dimensionful in the RG sense (it scales with energy)[3].

In the Wilsonian RG, the action (1.18) depends on both the cutoff and Fermi momentum implicitly. The hierarchy $\Lambda \ll k_F$ of the theory defines the low energy phase space of the system. Consider the RG transformation $\Lambda \to \Lambda s$ ($s < 1$). This transformation amounts to taking Λ/k_F to zero, making this ratio a dimensionless small parameter of the theory. The scale transformation amounts to continuously shaving thin shells off the 2Λ shell. In the $\Lambda/k_F \to 0$ limit, the only interactions with available phase space are on the k_F-shell. The momentum conservation enforced by

$$\hat{k}_1(\vec{\Omega}_{1,d-1}) + \hat{k}_2(\vec{\Omega}_{2,d-1}) = \hat{k}_3(\vec{\Omega}_{3,d-1}) + \hat{k}_4(\vec{\Omega}_{4,d-1}). \tag{1.19}$$

only leaves the *forward scattering* and the *Bardeen-Cooper-Schrieffer* (BCS) [22, 23] channels [160, 194, 40, 39, 38]. The forward scattering channel, is characterized by $\hat{k}_1 = \hat{k}_3$, $\hat{k}_2 = \hat{k}_4$, or $\hat{k}_1 = \hat{k}_4$, $\hat{k}_2 = \hat{k}_3$ while the BCS channel is characterized by $\hat{k}_1 = -\hat{k}_2$, $\hat{k}_3 = -\hat{k}_4$. In both channels, there are only two independent momenta in the zero-energy limit. In the presence of spherical symmetry, the interaction only depends on the relative angle between initial and final particles.

With the scaling dimension of frequency and momentum set to be $[k_0] = [k] = 1$, the scaling dimension of the fermion field becomes $[\psi] = -3/2$. This scaling dimension allows us to determine the dimension of the four-fermion coupling in Eq. (1.18) to be $\left[\tilde{\lambda}^{\{\sigma_i\}}_{\{\vec{\Omega}_{i,d-1}\}}\right] = 0$, where $\{\sigma_i\}$ and $\{\vec{\Omega}_{i,d-1}\}$ are a shorthand for the matrix notation. Therefore, $\tilde{\lambda}^{\{\sigma_i\}}_{\{\vec{\Omega}_{i,d-1}\}}$ is marginal for both forward scattering and BCS interactions at the tree level. This remains true for the forward scattering even in the presence of loop corrections. For the BCS coupling, it becomes marginally irrelevant if the bare interaction is a repulsive, and marginally relevant for attractive interaction [160, 194, 40, 39, 38]. The attractive pairing interaction grows logarithmically in Fermi liquids, signifying a superconducting instability at low temperatures [22, 23].

[3] In fact, after expanding the four-fermion coupling λ to the leading order, the mapping from action (1.17) to (1.18) just makes explicit that the Fermi liquid problem in EFT is a $(1+1)$-dimensional problem, where the only relevant direction (that is, the direction that involves a relevant energy cost in scattering), is the direction normal to the Fermi surface. This problem is simplified from the $(d+1)$-dimensional problem in Eq. (1.15).

The four-fermion interaction renormalizes the single-particle Green's function as

$$G^R(\omega,\vec{k}) = \frac{1}{-\omega - i0^+ + \vec{v}_F(\hat{k})\cdot(\vec{k}-\vec{k}_F(\hat{k})) + \Sigma^R(\omega,\vec{k})}. \tag{1.20}$$

Here, we use the real frequency. $\Sigma^R(\omega,\vec{k})$ is the self-energy. The spectral function $A(\omega,\vec{k}) = -2\mathrm{Im}G^R(\omega,\vec{k})$, can be written as [33]

$$A(\omega,\vec{k}) = \frac{2\mathrm{Im}\Sigma^R(\omega,\vec{k})}{\left[-\omega + \vec{v}_F(\hat{k})\cdot(\vec{k}-\vec{k}_F(\hat{k})) + \mathrm{Re}\Sigma^R(\omega,\vec{k})\right]^2 + \left[\mathrm{Im}\Sigma^R(\omega,\vec{k})\right]^2}. \tag{1.21}$$

If $\mathrm{Im}\Sigma^R(\omega,\vec{k})$ is sufficiently small at low frequencies, the spectral function has a well-defined peak in ω-space at the (renormalized) excitation energy $\omega_{\vec{k}}$:

$$\omega_{\vec{k}} = \vec{v}_F(\hat{k})\cdot(\vec{k}-\vec{k}_F(\hat{k})) + \mathrm{Re}\Sigma^R(\omega_{\vec{k}},\vec{k}). \tag{1.22}$$

Expanding around the peak $\omega = \omega_{\vec{k}}$, the spectral function acquires the form

$$A(\omega,\vec{k}) = \frac{2}{\tau_{\vec{k}}}\frac{Z_{\vec{k}}}{\left(\omega-\omega_{\vec{k}}\right)^2 + \frac{1}{\tau_{\vec{k}}^2}}, \tag{1.23}$$

where $Z_{\vec{k}} = \left[1 - \frac{\partial\Sigma^R(\omega,\vec{k})}{\partial\omega}\right]^{-1}_{\omega=\omega_{\vec{k}}}$ is the *quasiparticle weight* which can be interpreted as the overlap between the bare electron and quasiparticle states. The set of points $\vec{k'}$ that satisfy $\omega_{\vec{k'}} = 0$ define the renormalized Fermi surface. The renormalized Fermi surface is, in general, deformed with respect to the bare Fermi surface, but it encloses the same volume of Fermi sea as the non interacting theory; this in known as the *Luttinger theorem* [124]. $Z_{\vec{k}_F} \lesssim 1$ represents the magnitude of the step in the distribution function $n(\vec{k})$ at $\vec{k} = \vec{k}_F$ [128][4]. Finally, The width of the quasiparticle peak in $A(\omega,\vec{k})$ is controlled by the imaginary part of the self-energy through $\tau_{\vec{k}}^{-1} = Z_{\vec{k}}\mathrm{Im}\Sigma^R(\omega_{\vec{k}},\vec{k})$, the decay rate of the single particle excitations. In Fermi liquids, the decay rate goes as $\tau_{\vec{k}}^{-1} \approx \omega_{\vec{k}}^2$. These features of the spectral function such as the quasiparticle weight $Z_{\vec{k}}$, quasiparticle lifetime $\tau_{\vec{k}}$, and the excitation spectrum $\omega_{\vec{k}}$ are physical observables that can be probed through the angle-resolved photoemission spectroscopy (ARPES).

Landau's Fermi liquid theory has been very successful in describing conventional metals and their instabilities. However, not all metals belong to Fermi liquids. In metals that that undergo continuous quantum phase transitions, strong critical fluctuations of order parameters destroy the coherence of quasiparticles. Metals without coherent quasiparticles are generally referred to as *non-Fermi Liquids* (NFL). Below, we introduce one such NFL state, known as the *Antiferromagnetic Quantum Critical Metal* (AFQCM), which is be the main focus of this thesis.

1.2 The Antiferromagnetic Quantum Critical Metal

In Fermi liquids, the low-energy physics is specified by the topology and geometric shape of the Fermi surface, the Berry phase around the Fermi surface [74], the angle-dependent effective mass and the forward scattering amplitude. As we have seen above, the effectiveness and simplicity of the low-energy effective theory of Fermi liquids is due to the existence of well-defined quasiparticles. In non-Fermi liquids, however, the quasiparticle picture is not valid [202, 185], and extracting dynamical information out of effective field theories is significantly harder [84, 79, 108, 167, 109, 144, 10, 93, 150, 161, 2, 3, 1, 121, 190, 110, 148, 140, 141, 76, 4, 90, 59, 48, 203, 205, 154, 206, 169, 83, 155, 210, 54, 180, 204, 120, 230, 118, 41, 211, 26, 119][5]. The simplest example of NFL is the one-dimensional system of interacting

[4] Here, $n(\vec{k}) = \int \frac{\mathrm{d}\omega}{2\pi} A(\omega,\vec{k}) n_{\mathrm{F-D}}(\omega)$, with $n_{\mathrm{F-D}}(\omega)$ given by Eq. (1.2)(with $\varepsilon - \mu \equiv \omega$). Thus, $Z_{\vec{k}}$ is a measure of the quasiparticle distribution's overlap with the Fermi gas particle distribution [128].

[5] For recent progress in non-Fermi liquid theories with random couplings, see Refs [174, 95, 131, 228, 57].

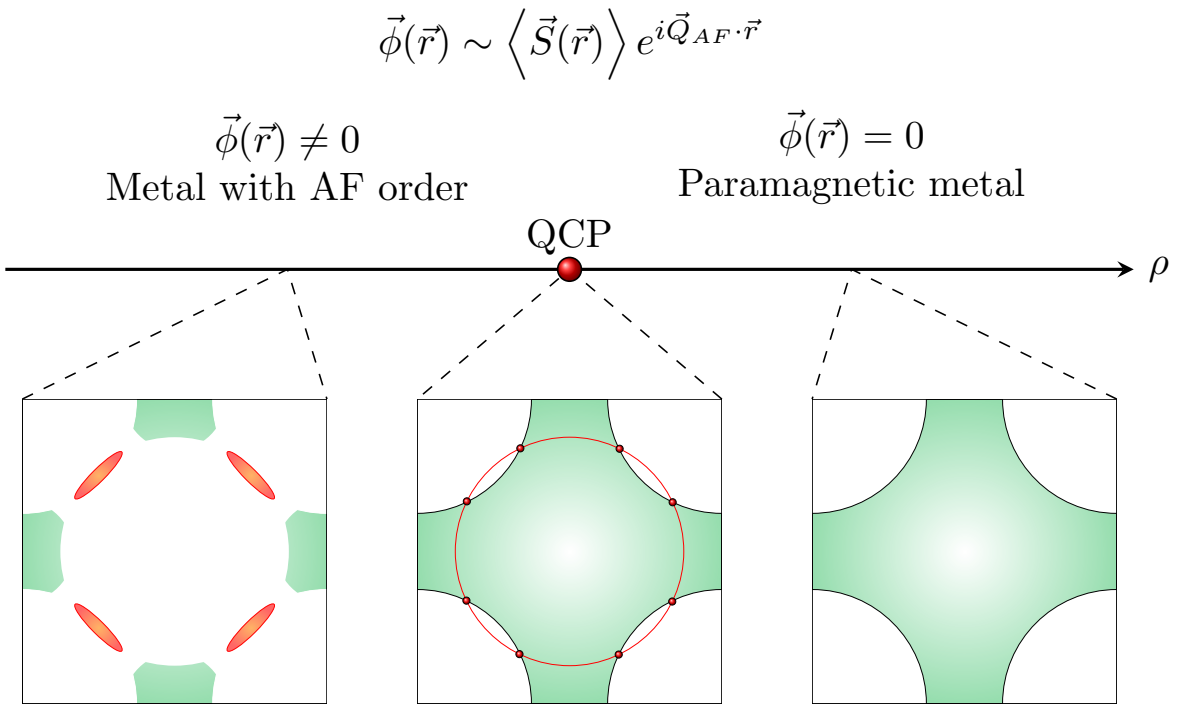

Figure 1.3: A schematic diagram for the antiferromagnetic quantum ($T = 0$) phase transition of a two-dimensional metal. The tuning parameter ρ drives the transition from a paramagnetic (Fermi liquid) phase ($\phi = 0$) to an antiferromagnecially ordered phase ($\phi \neq 0$). ρ can represent electron/hole doping in cuprates. At the quantum critical point (QCP), the Fermi surface hosts a number of hot spots, where electrons remain strongly coupled to the critical spin fluctuations Φ at all energy scales. The red circle in critical Fermi surface represents the Fermi surface when the Brillouin zone is shifted by $\vec{Q}_{AF}$. In the antiferromagnetic phase, the metal undergoes a "Fermi surface reconstruction": gaps open at the hot spots leading to electron (green) and hole (red) pockets [172].

fermions known as the *Tomonaga-Luttinger liquid* [208, 125, 137, 75, 213]. In one space dimension, the strong quantum fluctuations leads to a charge-spin separation, and the single-particle spectral function has no well-defined quasiparticle peaks. In higher dimensions, NFL can be realized in the vicinity of quantum critical points of continuous quantum phase transitions. Examples include high T_c superconductors [36, 71, 18, 227, 147, 184, 78, 77, 78], iron pnictides [77], and heavy fermion compounds [153]. Among the additional data that are needed for non-Fermi liquids in higher dimensions are the singularity of the critical Fermi surface characterized by anomalous dimensions of fermions, dynamical critical exponents, and scaling properties of other critical modes that are present in the system[190]. Since the momentum coordinates parallel to the Fermi surface play the role of a continuous flavour, critical exponents (such as the scaling dimension of fermions) can depend on the momentum along the Fermi surface.

The focus of this thesis is the *antiferromagnetic quantum critical metal* (AFQCM), which is potentially relevant for the cuprates, iron pnictides and heavy fermion compounds mentioned above. This theory has been intensively studied both theoretically and numerically [2, 3, 1, 76, 4, 107, 34, 35, 155, 154, 210, 130, 211, 141, 206, 204, 112, 25, 117, 179, 62, 116, 219]. The AFQCM arises at the critical point of a antiferromagnetic quantum phase transition, driven by a spatially-modulated spin density wave (SDW) order parameter $\vec{\phi}(\vec{r}) \sim \langle \vec{S}(\vec{r}) \rangle e^{i\vec{Q}_{AF}\cdot\vec{r}}$ ($\vec{S}(\vec{r})$ is the spin density), where the spatial $\vec{r}$-modulation is given by the ordering vector $\vec{Q}_{AF}$. Here, we focus on $\vec{Q}_{AF}$ that is *commensurate* with

$2\vec{Q}_F$ equivalent to a reciprocal lattice vector, i.e., $2\vec{Q}_F \equiv 0$. A schematic description can be found in Fig. 1.3. The minimal description includes the antiferromagnetic critical spin fluctuations, represented by a boson field $\Phi_{\sigma\sigma'}$, and electrons residing near the Fermi surface. On the Fermi surface, the *hot spots* play a special role. Here, the hot spots refer to points on the Fermi surface connected by the antiferromagnetic wave vector $\vec{Q}_{AF}$ and remain strongly coupled with spin fluctuations at low energies, as depicted in Fig. 1.4a. The hot spots have a degree of nesting measured by the *nesting angle* v, as depicted in Fig. 1.4b. The bare kinetic energy of the critical spin fluctuation is written as

$$S_{0,\mathrm{SDW}} = \int \frac{\mathrm{d}q_0 \mathrm{d}^2 q}{(2\pi)^3} \left[q_0^2 + c_0^2 |\vec{q}|^2\right] \mathrm{Tr}\left[\Phi(q_0, \vec{Q}_{AF} + \vec{q})\Phi(-q_0, -\vec{Q}_{AF} - \vec{q})\right], \tag{1.24}$$

where $\Phi_{\sigma\sigma'}(q_0, \vec{Q}_{AF} + \vec{q}) \equiv \vec{\phi}(q_0, \vec{Q}_{AF} + \vec{q}) \cdot \vec{\tau}_{\sigma\sigma'} = \sum_{a=1}^{3} \phi^a(q_0, \vec{Q}_{AF} + \vec{q})\tau^a_{\sigma\sigma'}$ is written in the adjoint representation of $SU(2)$, $\vec{q}$ is measured relative to $\vec{Q}_{AF}$, c_0 is the bare speed of the collective mode, and the trace is in the spin indices σ, σ'. The interaction between the boson and electrons near the hot spots can be written as

$$\begin{aligned} S_{\mathrm{Yuk}} = \sum_{N=1}^{8} \sum_{\sigma\sigma'=\uparrow,\downarrow} \int_{\Lambda} \frac{\mathrm{d}k_0 \mathrm{d}^2 k \mathrm{d}k_0' \mathrm{d}^2 k'}{(2\pi)^6} g_{\vec{k}_F(\hat{k}_{\overline{N}})+\vec{k}, \vec{k}_F(\hat{k}_N)+\vec{k}'} \\ \times \psi^\dagger_\sigma(k_0, \vec{k}_F(\hat{k}_{\overline{N}}) + \vec{k})\Phi_{\sigma\sigma'}(k_0 - k_0', \vec{Q}_{AF}(N \to \overline{N}) + \vec{k} - \vec{k}')\psi_{\sigma'}(k_0', \vec{k}_F(\hat{k}_N) + \vec{k}') \end{aligned} \tag{1.25}$$

where $N = 1, 2, \ldots, 8$ labels the hot spots, $\overline{N}$ is the hot spot connected to N by an ordering vector $\vec{Q}_{AF}$, $\vec{k}_F(\hat{k}_N)$ is the Fermi momentum oriented at hot spot N, $\vec{k}$ is the momentum measured from the hot spot, $\vec{Q}_{AF}(N \to \overline{N})$ is $\vec{Q}_{AF}$ pointing towards $\overline{N}$ from N. $g_{\vec{k}_F(\hat{k}_{\overline{N}})+\vec{k}, \vec{k}_F(\hat{k}_N)+\vec{k}'}$ is the Yukawa exchange interaction between electrons near N and $\overline{N}$. When $v = 0$, patches connected by $\vec{Q}_{AF}$ are *nested*. If the phase transition is continuous, the energy of the spin fluctuations with wavevector $\vec{Q}_{AF} + \vec{q}$ vanishes with vanishing $\vec{q}$. Electrons can be scattered from hot spot to hot spot connected by $\vec{Q}_{AF}$ by emitting or absorbing a zero-energy boson Φ.

1.2.1 Theoretical Descriptions of Non-Fermi Liquids

One approach to non-Fermi liquids that has proven to be useful is the patch theory[6]. For the AFQCM, the patch theory is commonly known as *hot-spot theory*. The goal of a patch theory is to "divide and conquer" the full theory by considering only a minimal set of small patches of Fermi surface at a time. The patch description is valid if large-momentum scatterings that connect different parts of Fermi surface are negligible (for example, a scattering between a particle near hot spot 1 and hot spot 5 in Fig. 1.4a). However, the patch theory is not enough when large-angle scatterings are important. To capture the low-energy physics of the whole Fermi surface, the patch theory has to be extended to a theory that includes all gapless modes around the Fermi surface. Such theories are characterized by couplings that are functions of momentum along the Fermi surface. The universal low-energy data should be encoded in fixed points that arise in the space of coupling functions. Ultimately, one would like to identify the space of fixed points and extract the universal data associated with each fixed point. The natural theoretical framework for this is the functional renormalization group (FRG) method [162, 222] [146, 168, 170, 81, 85, 64, 63, 31, 143, 159, 232, 217, 73, 181, 88, 139, 107, 55, 218, 89, 129, 53, 54, 87, 130, 209]. The functional renormalization group flow describes how the momentum dependent vertex function evolves as a function of an energy scale. However, the exact renormalization group equation for the full vertex function is usually too difficult to solve for interacting theories. As a result, some forms of truncation, which are often uncontrolled, are employed to make the flow equation manageable. Fortunately, one does not need to know the full momentum-dependent vertex function to characterize the universal low-energy physics. Because gapless modes are residing on Fermi surface with a dimension lower than the space dimension, one should be able to throw away a great deal of

[6] See [112] for a recent review.

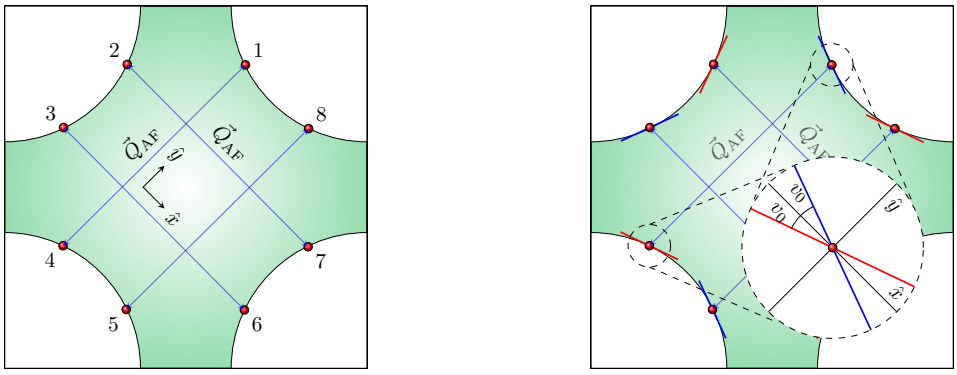

(a) (b)

Figure 1.4: Figure taken from [30]. (a) A C_4-symmetric Fermi surface in two dimensions. The red dots on the Fermi surface represent the hot spots connected by the antiferromagnetic wave vector, $\vec{Q}_{AF}$. The coordinate $\hat{x}$ ($\hat{y}$) is chosen to be perpendicular (parallel) to $\vec{Q}_{AF}$ that ends at hot spot 1. (b) Near hot spot 1, the Fermi surface is denoted as $k_y = -v_{k_x} k_x$, where v_k is generally a function of a component of momentum along the Fermi surface. In the hot spot theory, v_k is expanded around $k = 0$ and only the leading order term is kept. In the small v limit, the patches of Fermi surface connected by $\vec{Q}_{AF}$ become locally nested.

non-universal information associated with modes away from the Fermi surface. For relativistic field theories, there exists a systematic way of achieving this: renormalizable field theory. Born out of the locality principle and the gradient expansion, a renormalizable field theory is the minimal theory that captures the low-energy physics shared by all theories within one universality class. They are simple enough that one can in principle study them with pen and paper, yet powerful enough to produce among the most accurate predictions in the physical sciences [60]. Then, it is natural to combine the functional renormalization group formalism with the notion of renormalizable field theory to capture the universal low-energy physics of metals. The objective of this thesis is to describe the recent progress by the author and collaborators in achieving this goal, and the important consequences it entails for the non-Fermi liquid that arises at the antiferromagnetic quantum critical point in two space dimensions. Specifically, the focus will be upon three subjects: the formulation of the theory of the full Fermi surface and the description of the superconducting instability, the consequences of the momentum-dependent renormalization for the cyclotron motion of electron, and the fate of a magnetic impurity immersed in the non-Fermi liquid. We know give a brief synopsis to each one of these topics.

1.2.2 The Superconducting Instability in the AFQCM

Since most non-Fermi liquids exhibit superconductivity at low temperatures, there is a natural interest in understanding intrinsic superconducting fluctuations of non-Fermi liquids. However, the patch theory that only includes the electrons near the hot spots is not sufficient for this task because superconducting fluctuations generally involve large-angle scatterings between Cooper pairs across the entire Fermi surface. Furthermore, the hot-spot theory of AFQCM is not capable of describing the momentum-dependent universal properties of electrons on the Fermi surface and potentially important interplay between *hot* (incoherent, at the hot spots) and *cold* (coherent, far away from the hot spots) electrons for superconductivity [220]. The patch theory does not include the four-fermion coupling either because it is deemed irrelevant in the scaling that leaves the patch theory invariant. However, the four-fermion coupling should play an important role for superconductivity, which is another indication that the patch theory is incomplete. In Chapter 2, we consider the full low-energy effective theory that include all gapless modes around the Fermi surface and the four-fermion coupling. We then describe

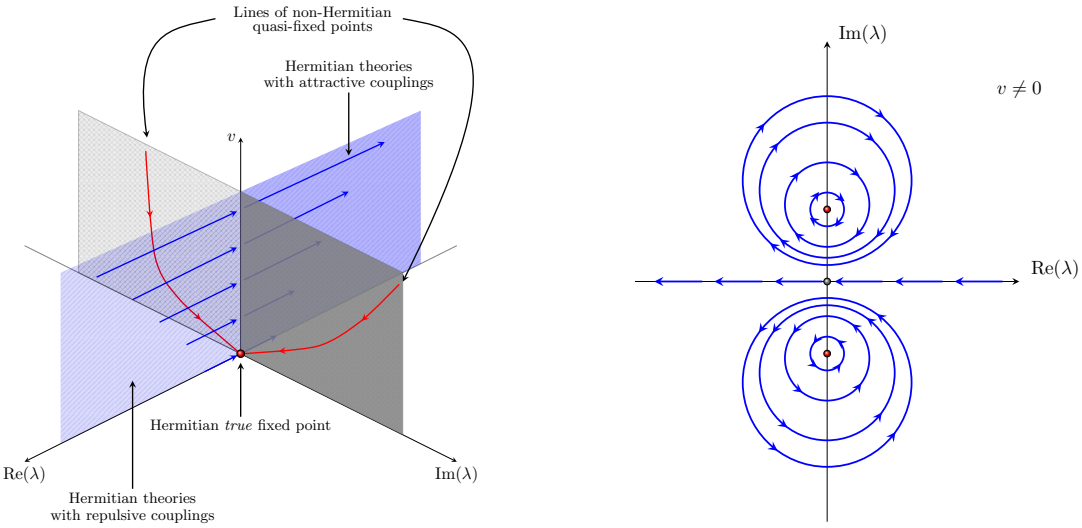

(a) (b)

Figure 1.5: Figure taken from [30]. (a) The schematic functional renormalization (RG) group flow depicted in the space of the complexified four-fermion coupling function (λ) and the nesting angle (v). For each nesting angle v, there exist a pair of non-Hermitian (complex) fixed points for the RG flow projected to the space of coupling functions with fixed v. These are called quasi-fixed points and the pairs of non-Hermitian quasi-fixed points are related to each other through the Hermitian conjugation. As v decreases, the non-Hermitian quasi-fixed points merge to the true Hermitian fixed point located at $v = 0$. While v flows towards zero under the full RG flow, a Hermitian theory with a non-zero nesting angle necessarily flows to the superconducting state before the nesting angle changes significantly. (b) A schematic functional RG flow projected to the space of complex four-fermion coupling function at a non-zero v. The proximity of the non-Hermitian quasi-fixed points to the space of Hermitian theories creates a bottleneck region with constricted RG flow for physical theories with small nesting angles.

how the critical spin fluctuations play a central role by providing pairing glue that forms Cooper pairs while making electrons incoherent near the hot spots (a pair -breaking effect). Finally, we describe the *non-Hermitian quasi-fixed point* arising from the competitions between spin fluctuations and the four-fermion coupling, which controls the universal pathway towards superconductivity (see Fig. 1.5).

Of particular importance of this thesis is the concept of *ultraviolet/infrared* (UV/IR) mixing in metals [133, 132, 231]. In the BCS pairing channel, the four-fermion couplings with large differences in momentum along the Fermi surface can mix with each other as Cooper pairs can be scattered around the Fermi surface even at low energies. This is because the momentum along the Fermi surface is not necessarily bounded by any external energy scale, and quantum corrections are generally expressed as integrals of coupling functions along the Fermi surface. If the coupling functions do not decay fast enough at large momenta, the contribution from large momenta along the Fermi surface can be important. In particular, the critical boson with large momenta contributes to the mixing between Cooper pairs with different relative momenta even in the low-energy limit. The fact that operators defined on different parts of the Fermi surface can mix with each other is not surprising in that they all describe gapless degrees of freedom. What is peculiar though is the fact that the mixing between low-energy operators with large differences in momentum along the Fermi surface can be influenced by the critical boson with large momenta. Due to this UV/IR mixing, the four-point vertex function itself can not be extracted from the low-energy effective field theory. Although the predictability of the low-energy effective theory seems at risk, there are still observables protected from the UV/IR

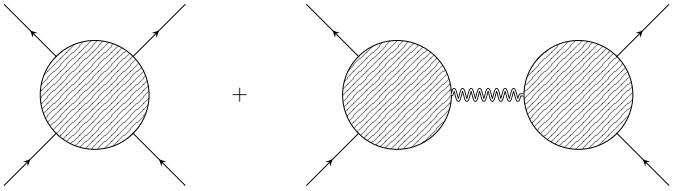

Figure 1.6: Figure taken from [30]. The net two-body electron-electron interaction composed of the one-particle irreducible (1PI) four-point function and two 1PI three-point functions connected with the dressed boson propagator. Here, the directed solid lines represent electrons and the double wiggly line represents the boson spin fluctuations.

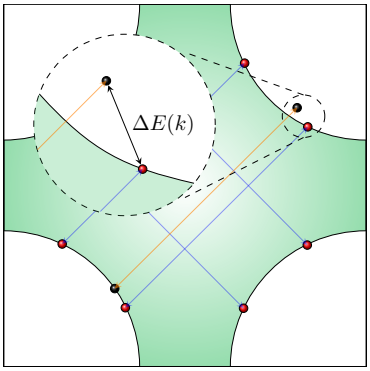

Figure 1.7: Figure taken from [30]. By absorbing/emitting a boson with zero energy, an electron on the Fermi surface (black dot) is scattered into a state away from the Fermi surface if the initial momentum is away from the hot spots. Alternatively, the electron must absorb/emit a boson with non-zero energy to scatter onto the Fermi surface. The minimum energy that virtual particles have to carry within a loop gives rise to a crossover energy scale below which electrons decouple from spin fluctuations at each point on the Fermi surface. Electrons closer to the hot spots remain coupled with spin fluctuations down to lower energy scales, which gives rise to a momentum dependent life time of electrons that gradually vanishes as one approaches hot spots.

mixing. The 'protected' low-energy observable that describes the fermionic four-point function is the net two-body electron-electron interaction given by the sum of the one-particle irreducible (1PI) four-point vertex function and the tree graph formed by connecting two 1PI three-point function with the boson propagator (see Fig. 1.6). The net interaction determines physical correlation functions at low energies, and it can be determined within the low-energy effective field theory without reference to high-energy physics. The RG flow of the net two-body interaction is insensitive to the ultra-violet (UV) physics.

1.2.3 Cyclotron Motion of Quasiparticles

The semi-classical equation of motion of quasiparticles in solids is remarkably symmetric under the interchange of position and momentum. The momentum-dependent quasiparticle energy is the counter part of the position-dependent potential in real space. Moreover, the Berry curvature associated with the Bloch wavefunctions plays the role of the magnetic field in momentum space[229]. It is then natural to ask if the symmetry can be further extended to spacetime geometry[44, 98, 106, 20, 49]. A real-space curvature can be created through buckling of lattices or topological defects in solids[12, 221, 157, 134, 214, 43, 223, 178, 145]. Recent studies on the semi-classical equations of motion of quasiparticles have suggested the emergence of a curved momentum space in lattice models. In particular, it has been

pointed out that the non-linear response of quasiparticles to the external electromagnetic field can be captured geometrically[198, 82]. In those examples, the metric[135] is ultimately traced back to the single-particle wavefunction fixed by the underlying lattice. In Chapter 3, we consider an intrinsic physical mechanism by which momentum space and time is integrated into a curved *momentum-spacetime* through the electron-electron interactions. While electrons at the hot spots are incoherent in AFQCM, the Fermi surface far away from the hot spots still supports coherent quasiparticles. Therefore, the dynamics of quasiparticles away from the hot spots can be understood semi-classically. However, the quasiparticle dynamics acquires a strong momentum dependence due to the momentum-dependent quantum corrections. We point out that curved momentum-spacetimes naturally arise from anisotropic (momentum-dependent) quantum corrections in the AFQCM and even a momentum-space black hole horizon can emerge if quantum corrections are sufficiently singular near the hot spots (see Fig. 1.7).

1.2.4 The Kondo Effect

Collective phenomena that arises from the interplay between local magnetic moments and itinerant electrons continue to attract considerable attention in condensed matter physics [14, 97, 151, 51, 80, 201, 113, 195, 152, 192, 193, 52, 196, 37, 61, 187, 158, 156]. The *Kondo impurity model* was originally introduced to describe the behaviour of such impurities of transition metal ions in simple metals. In the classic Kondo model, a magnetic impurity put in a Fermi liquid is screened by the conduction (or *itinerant*) electrons in the metal. The result is a non-magnetic state (singlet) where the impurity's magnetic moment is screened by the conduction electron's spin. This quantum phenomenon is known as the *Kondo effect* [97] and it is responsible for the observed minimum of resistance of some single-element metals with magnetic impurities [72]. It also represents one of the better known examples of asymptotic freedom in physics, akin to what causes the confinement of quarks [17]. The Kondo impurity model is the building block of the Kondo lattice models for heavy fermions systems [201, 195, 193, 61, 187, 156] and Kondo insulators [138, 52].

Before we discuss the problem of a magnetic impurity in the AFQCM, we first review the Kondo effect in Fermi liquids. Well studied examples of magnetic impurities that exhibit Curie-Weiss contributions to the susceptibility [80] are from the $3d$ transition series or $4f$ rare earth series in the periodic table, like Fe in Cu [200, 175], and Ce in $LaAl_2$ and LaB_6 [58, 176]. The minimal model that describes an impurity put in Fermi liquids is the *Anderson impurity model* [14]

$$\begin{aligned} H_A = &\sum_{\sigma=\uparrow,\downarrow} \int \frac{\mathrm{d}^d k}{(2\pi)^d} E(\vec{k}) \psi^\dagger_{\vec{k},\sigma} \psi_{\vec{k},\sigma} + \sum_{\sigma=\uparrow,\downarrow} \varepsilon_d \; d^\dagger_\sigma d_\sigma \\ &+ \sum_{\sigma=\uparrow,\downarrow} \int \frac{\mathrm{d}^d k}{(2\pi)^d} \left[V_{\vec{k}} d^\dagger_\sigma \psi_{\vec{k},\sigma} + V^*_{\vec{k}} \psi^\dagger_{\vec{k},\sigma} d_\sigma \right] + U_d \; d^\dagger_\uparrow d_\uparrow d^\dagger_\downarrow d_\downarrow . \end{aligned} \tag{1.26}$$

A schematic description of the model can be found in Fig. 1.8a. Here, $\psi_{\vec{k},\sigma}$ is the fermion operator at momentum $\vec{k}$ with spin σ, d_σ is the fermion operator at the site of the impurity, which is assumed to be at the origin ($\vec{x} = 0$), $E(\vec{k})$ is the electron energy, and ε_d is the energy of the d level of the impurity ion. The term that mixes $\psi_{\vec{k},\sigma}$ and d_σ with tunnelling matrix element $V_{\vec{k}}$ is the *hybridization* that describes the hopping between conduction band and the atomic d-level of the impurity. Finally, U_d is the Coulomb interaction between the electrons in the impurity ion d-states.

The analysis for large U_d proceeds most naturally by performing a canonical transformation to an effective Hamiltonian acting on the low energy subspace (*à la* Hubbard). To figure out what this subspace should be, let us examine the spectrum of the d level, assuming that $|\varepsilon_d|, U_d \gg \left|V_{\vec{k}}\right|$. There

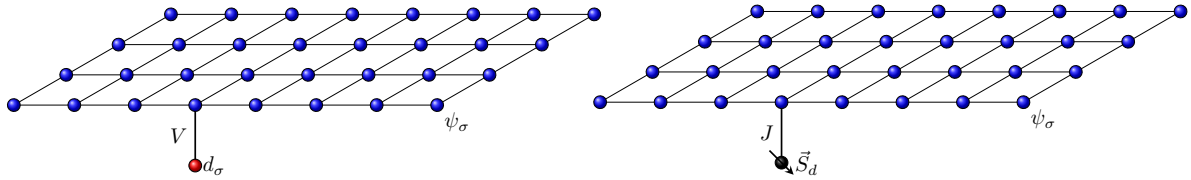

(a) (b)

Figure 1.8: Models of magnetic impurities. Here, the electrons ψ_σ are represented as the blue lattice. (a) Set-up for the non-interacting ($U_d = 0$) Anderson model (1.26). Also referred to as a resonant-level model, the conduction electrons ψ_σ hybridize with the d-level electrons of the impurity d_σ with an amplitude V. (b) Kondo impurity model: conduction electrons ψ_σ couple to a spin $\vec{S}_d$ with a exchange interaction strength J.

are four possible states on the d level:

$$\begin{aligned} |0\rangle, \text{ with energy } E &= 0, \\ d_\alpha^\dagger|0\rangle, \text{ with energy } E &= \varepsilon_d, \\ d_\uparrow^\dagger d_\downarrow^\dagger|0\rangle, \text{ with energy } E &= 2\varepsilon_d + U_d. \end{aligned} \tag{1.27}$$

The first state corresponds to the state with zero occupation at the impurity level, the second corresponds to singly occupied states with energy ε_d where $\alpha = \uparrow, \downarrow$, and the third state corresponds to the doubly occupied state. The impurity sites becomes magnetic when $\varepsilon_d \ll 0, 2\varepsilon_d + U_d$, where the d level is doubly-degenerate, making the d level behave effectively as a $S = 1/2$ spin. In the presence of a Fermi surface, the d level interacts with conduction electrons as a $S = 1/2$ local magnetic moment (*local moment regime*). This can be made explicit by the Schrieffer-Wolff transformation on the Hamiltonian (1.26) [32] resulting in the *Kondo Hamiltonian*[7] [186, 80, 97]

$$H_K = \sum_{\sigma=\uparrow,\downarrow} \int \frac{\mathrm{d}^d k}{(2\pi)^d} E(\vec{k}) \psi_{\vec{k},\sigma}^\dagger \psi_{\vec{k},\sigma} + \sum_{\sigma,\sigma'=\uparrow,\downarrow} \int \frac{\mathrm{d}^d k \mathrm{d}^d k'}{(2\pi)^{2d}} J_{\vec{k},\vec{k}'} \vec{S}_d \cdot \psi_{\vec{k},\sigma}^\dagger \frac{\vec{\tau}_{\sigma\sigma'}}{2} \psi_{\vec{k}',\sigma'}. \tag{1.28}$$

Here, $\vec{S}_d$ is an $S = 1/2$ spin operator acting on the two states $d_\alpha^\dagger|0\rangle$ on the d site. A schematic description of the model can be seen in Fig. 1.8b. The *Kondo exchange interaction* $J_{\vec{k},\vec{k}'}$ is given by

$$J_{\vec{k},\vec{k}'} = V_{\vec{k}}^* V_{\vec{k}'} \left(\frac{1}{U_d + \varepsilon_d - E(\vec{k}')} + \frac{1}{E(\vec{k}) - \varepsilon_d} \right), \tag{1.29}$$

and is antiferromagnetic (positive) in the local moment regime for electrons near the Fermi energy ($E(\vec{k}), E(\vec{k}') \sim 0$).

Generating a perturbative expansion for the Hamiltonian (1.28) in powers of $J_{\vec{k},\vec{k}'}$ is not straightforward because the d spins are now no longer free fermions, and there is no Wick's theorem for the correlations of the spin operators. However, it is still possible to treat the problem diagrammatically

[7] There is also and additional potential scattering term

$$\sum_{\sigma=\uparrow,\downarrow} \int \frac{\mathrm{d}^d k \mathrm{d}^d k'}{(2\pi)^{2d}} W_{\vec{k},\vec{k}'} \psi_{\vec{k},\sigma}^\dagger \psi_{\vec{k}',\sigma},$$

where

$$W_{\vec{k},\vec{k}'} = \frac{V_{\vec{k}}^* V_{\vec{k}'}}{2} \left(\frac{1}{E(\vec{k}) - \varepsilon_d} - \frac{1}{U_d + \varepsilon_d - E(\vec{k}')} \right).$$

We assume this term to be unimportant for now, so we drop it [80].

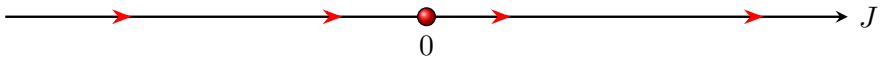

Figure 1.9: Renormalization group flow of the Kondo coupling in Eq. (1.33). When the UV coupling is ferromagnetic, i.e., $J(0) < 0$, the flow runs to the fixed point $J(\ell \to \infty) = 0$. For antiferromagnetic coupling, $J(0) > 0$, the flow goes towards strong coupling $J(\ell \to \infty) \to \infty$.

with the Abrikosov's method [5]. Specifically, by performing a Schwinger fermion decomposition of the spin operator, subject to the condition that at each impurity site there is only one pseudo-fermion,

$$\vec{S}_d = \sum_{\sigma,\sigma'=\uparrow,\downarrow} f^\dagger_\sigma \frac{\vec{\tau}_{\sigma\sigma'}}{2} f_{\sigma'}, \qquad \sum_{\sigma=\uparrow,\downarrow} f^\dagger_\sigma f_\sigma = 1. \tag{1.30}$$

The unit fermion constraint above can be imposed by introducing an imaginary chemical potential $-\zeta$ on the fermions f. Here, the Grassmann variable f now represents a *pseudo-fermion* in the Popov-Fedotov representation, where $\zeta = i\frac{\pi}{2\beta}$ ($\beta^{-1} = T$) enforces the unit fermion constraint $\sum_{\sigma=\uparrow,\downarrow} f^\dagger_\sigma f_\sigma = 1$ by cancelling out the contributions of the unphysical states $\sum_{\sigma=\uparrow,\downarrow} f^\dagger_\sigma f_\sigma = 0, 2$ in the partition function. This ensures that the only pseudo-fermion operators in the Hamiltonian are projection operators in the unit fermion subspace [164]. In practice, we are interested in the zero temperature limit ($\beta^{-1} \to 0$) on the diagrammatic expansion, and this constraint can be implemented by ignoring diagrams with external f-lines that flow both forwards and backwards in time. In Hamiltonian form, this generalizes Eq. (1.28) to [164, 173]

$$\begin{aligned} H_K = &\sum_{\sigma=\uparrow,\downarrow} \int \frac{\mathrm{d}^d k}{(2\pi)^d} E(\vec{k}) \psi^\dagger_{\vec{k},\sigma} \psi_{\vec{k},\sigma} + \sum_{\alpha=\uparrow,\downarrow} i\frac{\pi}{2\beta} f^\dagger_\alpha f_\alpha \\ &+ \sum_{\sigma,\sigma',\alpha,\beta=\uparrow,\downarrow} \int \frac{\mathrm{d}^d k \mathrm{d}^d k'}{(2\pi)^{2d}} J_{\vec{k},\vec{k}'} f^\dagger_\alpha \frac{\vec{\tau}_{\alpha\beta}}{2} f_\beta \cdot \psi^\dagger_{\vec{k},\sigma} \frac{\vec{\tau}_{\sigma\sigma'}}{2} \psi_{\vec{k}',\sigma'}. \end{aligned} \tag{1.31}$$

The key physics of the Kondo model becomes apparent upon considering the renormalization of the Kondo coupling to second order in J. In its simplest form, we assume a constant density of states for itinerant electrons with bandwidth $2D$. Additionally, let us assume constant J (by setting $V_{\vec{k}} \approx V, E(\vec{k}) \approx 0$) to simplify the analysis. Then, we integrate out the highest energy conduction electrons with $D - \delta D < \left|E(\vec{k})\right| < D$. The renormalization of the exchange coupling results in

$$J \to J + \rho(E_F)\frac{\delta D}{D} J^2, \tag{1.32}$$

where $\rho(E_F)$ is the density of states of the conduction electrons at E_F. Writing $\delta D = D\delta\ell$, where ℓ is the logarithmic length scale, we obtain the "poor person" renormalization group flow equation, [13]

$$\frac{\mathrm{d}J(\ell)}{\mathrm{d}\ell} = \rho(E_F) J^2(\ell) + O(J^3). \tag{1.33}$$

The RG flow governed by Eq. (1.33) is shown in Fig. 1.9. A ferromagnetic coupling $J(0) < 0$ flows towards $J(\ell \to \infty) = 0$: in this case the impurity spin decouples from the conduction itinerant electrons, and J can be treated perturbatively. For the antiferromagnetic coupling with $J(0) > 0$, $J(\ell)$ increases logarithmically. Specifically, the integration of Eq. (1.33) yields the result:

$$J(\ell) = \frac{1}{\frac{1}{J(0)} - \rho(E_F)\ell}. \tag{1.34}$$

This gives rise to a logarithmic contribution to the resistivity,

$$R_{\text{imp}} = R_0 \left[1 + 2J\rho(E_F) \log \left(\frac{D}{T} \right) \right], \tag{1.35}$$

where R_0 is the resistivity due to potential scattering at the impurity site. If we start from small positive $J(0)$, we see from this equation that the renormalized exchange reaches order 1 at scale $\ell^* = \frac{1}{\rho(E_F)J(0)}$; this defines the Kondo temperature:

$$T_K \sim D \exp \left(-\frac{1}{\rho(E_F)J(0)} \right). \tag{1.36}$$

In principle, this expression is only valid perturbatively. However, using numerical RG, Wilson showed that the $J(\ell \to \infty) \to \infty$ flow predicted by Eq. (1.34) is ultimately correct (qualitatively) and that the low energy physics of the Kondo Hamiltonian (1.28) is adiabatically connected to the non-interacting Anderson model ($U_d = 0$) in Eq. (1.26) [226]. Qualitatively, when $J(\ell)$ flows to large coupling, the way to minimize the ground state energy of Eq. (1.28) is for the spin $\vec{S}_d$ to lock into a *spin singlet* with an itinerant electron at the impurity site, forming a non-magnetic impurity described by an effective Hamiltonian,

$$H_R = \sum_{\sigma=\uparrow,\downarrow} \int \frac{\mathrm{d}^d k}{(2\pi)^d} E(\vec{k}) \psi^\dagger_{\vec{k},\sigma} \psi_{\vec{k},\sigma} + \sum_{\sigma=\uparrow,\downarrow} \int \frac{\mathrm{d}^d k \mathrm{d}^d k'}{(2\pi)^{2d}} W_{\vec{k},\vec{k}'} \psi^\dagger_{\vec{k},\sigma} \psi_{\vec{k}',\sigma}. \tag{1.37}$$

In the large $W_{\vec{k},\vec{k}'}$ limit, other electrons are prevented from occupying the impurity site. In other words, the impurity becomes a "rigid" scattering target at the impurity site with potential $W_{\vec{k},\vec{k}'}$. Due to the lack of dynamical degrees of freedom at the impurity site, this is an effective Fermi liquid description of the scattering states for $T \ll T_K$, similar to that of the non-interacting Anderson model.

We can use this interpretation to deduce the temperature dependent impurity spin susceptibility:

$$\chi_{\text{imp}} = \frac{1}{4T} \Phi(T/T_K), \tag{1.38}$$

where $\Phi(t)$ is a universal function for $J \ll D$. At temperatures $T \gg T_K$, the perturbation of the Kondo coupling is reliable; $\Phi \to 1$ and we obtain the Curie-Weiss susceptibility

$$\chi_{\text{imp}} = \frac{1}{4T}, \qquad T_K \ll T \ll U_d. \tag{1.39}$$

For $T \ll T_K$ we have $\Phi \sim T/T_K$, and the susceptibility becomes constant:

$$\chi_{\text{imp}} \sim \frac{1}{T_K}, \qquad T \ll T_K. \tag{1.40}$$

In AFQCM, critical spin fluctuations compete with itinerant electrons to couple with the impurity through the spin-spin interaction. The interaction between spin fluctuations and the impurity spin has the form

$$S_{\text{impurity}-\text{boson}} = g_f \sum_{\sigma\sigma'=\uparrow,\downarrow} \int_\Lambda \frac{\mathrm{d}p_0}{2\pi} \frac{\mathrm{d}q_0 \mathrm{d}^2 q}{(2\pi)^3} f^\dagger_\sigma(p_0 + q_0) \frac{\Phi_{\sigma\sigma'}(q_0, \vec{Q}_{AF} + \vec{q})}{2} f_{\sigma'}(p_0). \tag{1.41}$$

Here, the Grassmann variable $f(p_0)$ now represents a pseudo-fermion field depending on frequency. Through g_f, the spin fluctuations dress the impurity spin, which generates an anomalous dimension of J. As a result, the Kondo screening is weakened by the boson with an increasing T. We will discuss how the critical spin fluctuations suppress the Kondo screening in Chapter 4.

1.3 Structure of the Thesis

In Chapter 2, which is based on the work of Ref. [30], we present the field-theoretical functional RG formalism applied to the AFQCM in 2+1 dimensions. In this scheme, we go beyond the patch theory by including all gapless degrees of freedom along the Fermi surface and promoting couplings to coupling functions of momentum along the Fermi surface. In the space of coupling functions, we identify an interacting fixed point at a point with vanishing nesting angle. In theories deformed with non-zero nesting angles, coupling functions acquire momentum-dependent profiles controlled by the bare nesting angles at low energies before flowing to superconducting states in the low-energy limit. The superconducting instability is unavoidable because lukewarm electrons that are coherent enough to be susceptible to pairing end up being subject to a renormalized attractive interaction with its minimum strength set by the nesting angle irrespective of the bare four-fermion coupling. Despite the inevitable superconducting instability, theories with small bare nesting angles and bare four-fermion couplings that are repulsive or weakly attractive must pass through the region with slow RG flow due to the proximity to the non-Fermi liquid fixed point. This "bottleneck" region controls the quasi-universal scaling behaviour of the normal state above the superconducting transition temperature.

In Chapter 3, based on Ref. [28], we show that the momentum-dependent quantum corrections can give rise to curved momentum-spacetimes in metals. In the AFQCM, a curved momentum-spacetime is demonstrated to arise as the critical spin fluctuations generate a red shift that dilates frequency of the electron unevenly on the Fermi surface. As the shape of the Fermi surface controls the momentum-dependent red shift, the momentum-spacetime geometry that emerges at low energies depends on the bare nesting angle of the Fermi surface. Larger bare nesting angles reduce the region where the critical spin fluctuations slow down an electron. At the same time, the increasing nesting angle weakens the screening of the interactions, making the red shift stronger near the hot spots. These two effects compete to create a non-monotonic dependence of the electron's cyclotron frequency on the nesting angle. The red shift that becomes more singular at the hot spots with increasing nesting angle creates a possibility of realizing a momentum-space black hole horizon beyond a critical nesting angle: the electron motion becomes "perpetually" slowed down as it approaches a hot spot in the same way that the motion of a free falling object freezes near the event horizon of a black hole with respect to an asymptotic observer. However, the analogous horizon is not fully realized because the metric singularity at the hot spots is cut off by thermal effects present above the non-zero superconducting transition temperature.

Finally, in Chapter 4, which is based on Ref. [29], we study a magnetic impurity immersed in AFQCM. Critical spin fluctuations represented by bosonic fields compete with itinerant electrons to couple with the impurity through the spin-spin interaction. At long distances, the antiferromagnetic electron-impurity (Kondo) coupling dominates over the boson-impurity coupling. However, the Kondo screening is weakened by the boson with an increasing severity as the hot spots connected by the magnetic ordering wave-vector are better nested. The dramatic hampering of the Kondo screening by the critical boson results from UV/IR mixing, where spin fluctuations of all length scales actively suppress Kondo screening by itinerant electrons even at low energies.

We end this thesis with a few concluding remarks and an outlook on future research directions.

1.4 Notation

Throughout the the rest of this thesis the following notation will be encountered:

1. scales
    - Λ : UV energy cutoff
    - k_F : Fermi momentum / size of Fermi surface
    - μ : floating energy scale at which renormalization conditions are imposed

2. momentum
   - $\vec{k} = (k_x, k_y)$: two-dimensional momentum measured with respect to the hot spot in each patch
   - $\mathbf{k} = (k_0, \vec{k})$: three-momentum vector made of Matsubara frequency and two-dimensional momentum
   - $\vec{Q}_{AF}$: the antiferromagnetic ordering vector
   - k_N : the component of $\vec{k}$ that is perpendicular to $\vec{Q}_{AF}$
   - k : abbreviation for k_N used when the associated hot spot index is obvious
   - $k_\perp$: the component of $\vec{k}$ that is parallel to $\vec{Q}_{AF}$
   - $K = ke^\ell$: rescaled momentum associated with the logarithmic length scale ℓ
3. coupling functions
   - $V_{F,k}$: the momentum dependent Fermi velocity parallel to the antiferromagnetic ordering vector
   - v_k : the momentum dependent local nesting angle
   - c : the speed of the overdamped collective spin fluctuation
   - $w_k \equiv v_k/c$ ($w \equiv v_0/c$)
   - $g_{k,p}$: the momentum dependent fermion-boson coupling function
   - $\lambda^{\binom{N_1\ N_2}{N_4\ N_3};\binom{\sigma_1\ \sigma_2}{\sigma_4\ \sigma_3}}_{\binom{k_1\ k_2}{k_4\ k_3}}$: the momentum dependent four-fermion coupling function
   - $J^{(N,N')}_{k_N,k'_{N'}}$: Kondo coupling function that describes the scattering of electrons through interaction with the impurity
   - g_f : the boson-impurity coupling
   - u_a ($a = 1, 2$) : quartic boson couplings

Chapter 2

Field-theoretic functional renormalization group formalism for non-Fermi liquids and its application to the antiferromagnetic quantum critical metal in two dimensions

2.1 Introduction

A recent study has uncovered a strongly interacting fixed point for the antiferromagnetic quantum critical metal in two dimensions, where exact critical exponents are extracted [182]. The fixed point is characterized by the anomalous dimension of the spin fluctuations 1, the dynamical critical exponent $z = 1$ and an emergent nesting of Fermi surface near the hot spots. Due to a slow flow of the nesting angle under the RG flow, at finite length scales one expects to see scaling behaviours controlled by transient exponents that depend on the nesting angle[123]. A recent quantum Monte Carlo study[122] that employs a sign problem-free lattice regularization[25, 62, 26, 179] shows scaling behaviours that are in qualitative agreement with the predictions. However, the previous approach based on the patch theory is insufficient for studying superconducting instabilities because Cooper pairs can be scattered across the entire Fermi surface beyond a local patch. In order to take into account large-angle scatterings of Cooper pairs, one has to study the full low-energy effective field theory that include all gapless modes around the Fermi surface. In this chapter, we develop a field-theoretic functional renormalization group formalism for the full low-energy effective field theories of non-Fermi liquids beyond the patch theory. We apply this formalism to the non-Fermi liquid state that arises at the antiferromagnetic quantum critical metal.

The first half of this chapter (Secs. 2.2-2.4) is dedicated to the development of the formalism, and forms the theoretical backbone of the entire thesis. The second half of this chapter (Secs. 2.5-2.7) is dedicated to the functional RG flow of the coupling functions. In particular, Sections 2.5.1 and 2.6.1 include the RG flows of the nesting angle, Fermi velocity and Yukawa coupling functions. These results will be important for Chapters 3 and 4. Sections 2.6.2, 2.6.3 and 2.7 discuss the RG flow of the four-fermion coupling and the superconducting instability.

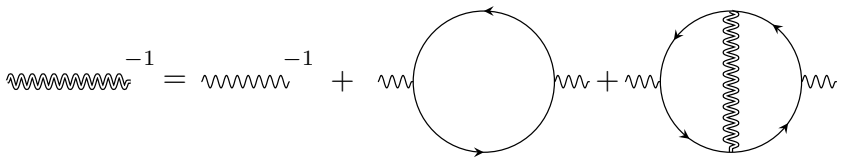

Figure 2.1: The truncated Schwinger-Dyson equation that becomes exact in the small v limit with $v \ll c(v) \ll 1$. The wiggly and solid lines denote the bare boson and fermion propagators, respectively. The double wiggly line represents the dressed boson propagator.

2.2 Review of the hot spot theory

The hot spot theory that describes the gapless spin fluctuations and the electrons near the hot spots is written as[182]

$$\begin{aligned} S = &\sum_{N=1}^{8}\sum_{\sigma=1}^{N_c}\sum_{j=1}^{N_f}\int \mathrm{d}\mathbf{k}\ \psi^{\dagger}_{N,\sigma,j}(\mathbf{k})\left[ik_0 + e_N(\vec{k};v)\right]\psi_{N,\sigma,j}(\mathbf{k}) \\ &+ \frac{1}{4}\int \mathrm{d}\mathbf{q}\ \left(q_0^2 + c_0^2|\vec{q}|^2\right)\mathrm{Tr}\left[\Phi(\mathbf{q})\Phi(-\mathbf{q})\right] \\ &+ \frac{g}{\sqrt{N_f}}\sum_{N=1}^{8}\sum_{\sigma\sigma'=1}^{N_c}\sum_{j=1}^{N_f}\int \mathrm{d}\mathbf{k}\ \int \mathrm{d}\mathbf{q}\ \psi^{\dagger}_{N,\sigma',j}(\mathbf{k}+\mathbf{q})\Phi_{\sigma'\sigma}(\mathbf{q})\psi_{\bar{N},\sigma,j}(\mathbf{k}). \end{aligned} \tag{2.1}$$

Here $\mathbf{k} = (k_0, \vec{k})$ denotes the three momentum that includes the Matsubara frequency k_0 and the two-dimensional momentum $\vec{k}$, and $\mathrm{d}\mathbf{k} \equiv \frac{\mathrm{d}k_0 \mathrm{d}k_x \mathrm{d}k_y}{(2\pi)^3}$. We consider a C_4-symmetric Fermi surface that supports eight hot spots labeled by $N = 1, 2, \ldots, 8$ as shown in Fig. 1.4a. $\psi_{N,\sigma,j}(\mathbf{k})$ represents the electron field near hot spot N with spin $\sigma = 1, 2, \ldots, N_c$ and flavour $j = 1, 2, \ldots, N_f$, where $\vec{k}$ is measured relative to hot spot N. The electron is in the fundamental representation of spin $SU(N_c)$ and flavour $SU(N_f)$ groups. The case that is most relevant to experiments is $N_c = 2$ and $N_f = 1$, but we keep N_c and N_f general. All results discussed in this chapter hold for any $N_c \geq 2$ and $N_f \geq 1$. The electron dispersion expanded to the linear order in momentum away from each hot spot is

$$\begin{aligned} e_1(\vec{k};v) = -e_5(\vec{k};v) =& vk_x + k_y, \\ e_2(\vec{k};v) = -e_6(\vec{k};v) =& -k_x - vk_y, \\ e_3(\vec{k};v) = -e_7(\vec{k};v) =& -k_x + vk_y, \\ e_4(\vec{k};v) = -e_8(\vec{k};v) =& vk_x - k_y. \end{aligned} \tag{2.2}$$

The coordinate is chosen so that $\vec{Q}_{\mathrm{AFM}}$ is parallel to $\hat{y}$ at hot spot 1. The component of the Fermi velocity along $\vec{Q}_{\mathrm{AFM}}$ is set to be 1 through a choice of momentum scale, and v denotes the dimensionless ratio between the component of the Fermi velocity perpendicular to $\vec{Q}_{\mathrm{AFM}}$ and the component parallel to $\vec{Q}_{\mathrm{AFM}}$. The patches of Fermi surface connected by $\vec{Q}_{\mathrm{AFM}}$ have relative slope $2v$, and v is referred to as *nesting angle* (see Fig. 1.4b). The collective antiferromagnetic spin fluctuations are represented by a bosonic field in the adjoint representation of $SU(N_c)$, $\Phi(\mathbf{q}) = \sum_{a=1}^{N_c^2-1}\phi^a(\mathbf{q})\tau^a$, where τ^a's denote the $N_c \times N_c$ generators of SU(N_c) with $\mathrm{Tr}[\tau^a\tau^b] = 2\delta_{ab}$ and $\phi^a(\mathbf{q}) = \phi^a(-\mathbf{q})^*$. Momentum $\vec{q}$ of the boson is measured relative to $\vec{Q}_{\mathrm{AFM}}$. c_0 is the bare speed of the boson. Finally, g denotes the Yukawa coupling between the boson and electrons near the hot spots. The cubic vertex describes the processes where an electron near hot spot $\bar{N}$ is scattered to hot spot N by absorbing or emitting a boson, where $\bar{1} = 4, \bar{2} = 7, \bar{3} = 6$, $\bar{4} = 1$, $\bar{5} = 8$, $\bar{6} = 3$, $\bar{7} = 2$ and $\bar{8} = 5$.

Under the Gaussian scaling in which the kinetic terms are kept invariant, the fields have dimension $[\Psi] = -2$, $[\Phi] = -5/2$ and the Yukawa coupling has dimension $[g] = 1/2$. The four-fermion coupling, which is not included in the hot-spot theory, has dimension -1. The usual perturbative expansion in which physical observables are expressed in powers of dimensionless coupling $g/E^{1/2}$ at energy scale E is bound to fail at low energies. Even if g is small compared to the UV cutoff, non-perturbative effects become important at low energies. Fortunately, the theory is solvable in the limit that the nesting angle v is small. If v is non-zero but small at a UV scale, it dynamically flows toward zero in the low energy limit, and the solution obtained in the small v limit becomes asymptotically exact in the low energy limit. This makes it possible to extract the exact critical exponents at the infrared fixed point with vanishing v[182, 123, 183][1]. At the fixed-point, both g and v vanish with $g^2/v \sim O(1)$, where the anomalous dimension of the boson is controlled by g^2/v. This interacting two-dimensional fixed point is distinct both from the Gaussian fixed point with $g^2/v = 0$ and the one-dimensional Fermi surface with the perfect nesting, $g^2/v = \infty$[42].

To the leading order in v, the dynamics of the boson is generated by the infinite set of diagrams included in Fig. 2.1. At low energies, the solution to the self-consistent Schwinger-Dyson equation is given by[182, 183]

$$D(\mathbf{q})^{-1} = \frac{2g^2}{\pi v}\Big[|q_0| + c(v)(|q_x| + |q_y|)\Big], \tag{2.3}$$

where

$$c(v) = \sqrt{\frac{v}{8N_cN_f}\log\left(\frac{1}{v}\right)} \tag{2.4}$$

is the speed of the over-damped collective mode[2]. Interestingly, Eq. (2.4) is only a function of v and independent of the bare speed of the boson (c_0). This is because the renormalization generated from gapless particle-hole excitations is more singular than the local kinetic term at low momenta and energies. The bare kinetic term, which is irrelevant, can be dropped from Eq. (2.1) at low energies. Without the boson kinetic term, one can rescale the boson field as $\Phi \to \sqrt{\frac{\pi v}{2g^2}}\Phi$ so that the dressed boson propagator has the canonical normalization, which gives rise to anomalous dimension 1 for the boson. After this rescaling, the Yukawa coupling becomes $\sqrt{\frac{\pi v}{2}}$. Physically, this implies that the Yukawa coupling and the nesting angle become dynamically related to each other at low energies.

While the boson is strongly dressed by particle-hole fluctuations, its feedback to electrons is weak in the small v limit. The magnitude of a general L-loop quantum correction with E external legs and L_f fermion loops computed with the renormalized boson propagator is bounded by

$$\mathcal{G}(L, L_f, E) \leq v^{\frac{E-2}{2}} w^{L-L_f} \tag{2.5}$$

up to logarithms of v, where $w = v/c$[182]. According to Eq. (2.5), only Fig. 2.2a can potentially give the leading order contribution to the fermion self-energy that renormalizes v. However, Eq. (2.5) is only an upper-bound, and the actual correction to v generated by Fig. 2.2a is further suppressed in c. This is because Fig. 2.2a depends on external momentum $\vec{k}$ only through the combination, $c\vec{k}$ as the external momentum can be directed to flow only through the boson propagator. As a consequence, Fig. 2.2a becomes of the same order as Fig. 2.2b which saturates the inequality in Eq. (2.5), and we have

[1] It is in principle possible that there exist other fixed points with large nesting angle. However, alternative perturbative analysis based on a dimensional regularization which is under control for any value of nesting angle near three dimensions[206, 123] indicates that there is no other fixed point besides the $z = 1$ fixed point that continuously evolves to the non-perturbative fixed point found in two dimensions[183].

[2] When $q_0 \neq 0$, $|q_x|+|q_y|$ in Eq. (2.3) should be replaced with a function $f(q_0, \vec{q})$ that approaches $f(q_0, \vec{q}) \approx |q_x|+|q_y|$ for $|\vec{q}| \gg |q_0|$. For a small $c(v)$, $c(v)(|q_x| + |q_y|)$ is important only for $|\vec{q}| \gg |q_0|$. Therefore, Eq. (2.3) holds for all $\vec{q}$ and q_0 to the leading order in $c(v)$ in the small v limit.

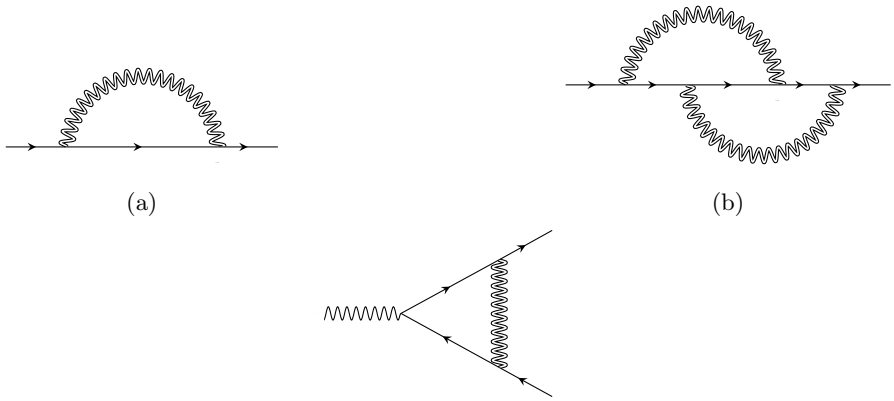

(a) (b) (c)

Figure 2.2: The leading order fermion self-energy and the vertex correction in the small v limit.

to include both Fig. 2.2a and Fig. 2.2b as the leading order correction to v. The quantum corrections in Fig. 2.2 renormalize the nesting angle at the hot spots, and give rise to the beta function,

$$\frac{dv}{d\ell} = -\frac{2(N_c^2-1)}{\pi^2 N_c N_f} v^2 \log\left(\frac{1}{v}\right), \tag{2.6}$$

where ℓ is the logarithmic length scale. The solution of the beta function is written as

$$\mathrm{Ei}\left[\log\left(\frac{1}{v(\ell)}\right)\right] = \mathrm{Ei}\left[\log\left(\frac{1}{v(0)}\right)\right] + \frac{2(N_c^2-1)}{\pi^2 N_c N_f}\ell, \tag{2.7}$$

where ℓ is the logarithmic length scale, $v(0)$ is the value of v measured at a UV scale set by $\ell = 0$ and $\mathrm{Ei}(x)$ is the exponential integral function which goes as $\mathrm{Ei}(x) = e^x(1/x + \mathcal{O}(1/x^2))$ for $x \gg 1$. For $v(0) \ll 1$, the solution becomes

$$v(\ell) = \frac{\pi^2 N_c N_f}{2(N_c^2-1)} \frac{1}{(\ell+\ell_0)\log(\ell+\ell_0)}, \tag{2.8}$$

where

$$\ell_0 = \frac{\pi^2 N_c N_f}{2(N_c^2-1)} \frac{1}{v(0)\log(1/v(0))} \tag{2.9}$$

is the crossover scale associated with the bare nesting angle, $v(0)$. For $\ell \ll \ell_0$, the flow of v can be ignored, while v flows to zero logarithmically for $\ell \gg \ell_0$.

For $\ell_0 \gg 1$, there is a large window of scales, $1 < \ell \ll \ell_0$ in which the flow of v can be ignored. Within this window of length scales, physical observables obey approximate scaling relations that are controlled by a set of *transient critical exponents*,

$$z = 1 + \frac{(N_c^2-1)}{2\pi N_c N_f} w, \tag{2.10}$$

$$[\Psi] = -2 - \frac{(N_c^2-1)}{4\pi N_c N_f} w, \tag{2.11}$$

$$[\Phi] = -2 + \frac{1}{2\pi N_c N_f} w \log\left(\frac{1}{w}\right). \tag{2.12}$$

Here $w = v(\ell)/c(\ell)$ (note that c depends on ℓ through v). z is the dynamical critical exponent. $[\Psi]$ and $[\Phi]$ denote the scaling dimension of the fermion and boson fields in the momentum space. If v was independent of ℓ, these exponents would control the power-law scaling of correlation functions in the low energy limit, and the one-parameter family of theories labeled by v would form a line of fixed points. In reality, v is not an exactly marginal parameter, and it flows to zero logarithmically for $\ell \gg \ell_0$. Still, these transient exponents control the scaling behaviours over a finite window of length scales $1 < \ell \ll \ell_0$ in which the flow of v can be ignored. We call the one-parameter family of theories labeled by v *quasi-fixed points* as they only act as approximate fixed points in the intermediate energy scale. If the RG flow was not cut off by an instability driven by the four-fermion coupling, the theory would flow to the true fixed point with $v = 0$[182, 123, 183] at length scales bigger than ℓ_0. At the true fixed point, the critical exponents become $z = 1$ and $[\Psi] = [\Phi] = -2$.[3] The crossover created by the flow of v manifests itself in physical observables. For example, the spectral function of electrons at the hot spots ($\mathcal{A}(\omega)$) and the dynamical spin susceptibility at the antiferromagnetic ordering vector ($\chi''(\omega)$) take different scaling forms at high and low energies as

$$\mathcal{A}(\omega) \sim \begin{cases} \omega^{-\left(1-\frac{(N_c^2-1)}{2\pi N_c N_f} w(0)\right)} & \text{for} \quad \omega_0 \ll \omega \ll \Lambda, \\ \left[\omega\ e^{2\sqrt{N_c^2-1}\frac{\left(\log\frac{1}{\omega}\right)^{1/2}}{\log\log\frac{1}{\omega}}} \left(\log\frac{1}{\omega}\right)^{1/2} \log\log\frac{1}{\omega}\right]^{-1} & \text{for} \quad \omega \ll \omega_0 \end{cases}, \tag{2.13}$$

$$\chi''(\omega) \sim \begin{cases} \omega^{-\left(1-\frac{1}{\pi N_c N_f} w(0) \log\frac{1}{w(0)}\right)} & \text{for} \quad \omega_0 \ll \omega \ll \Lambda, \\ \left[\omega\ e^{\frac{2}{\sqrt{N_c^2-1}}\sqrt{\log\frac{1}{\omega}}}\right]^{-1} & \text{for} \quad \omega \ll \omega_0 \end{cases}.$$

Here, Λ is the UV cutoff scale and $\omega_0 = \Lambda e^{-z(0)\ell_0}$ is the crossover energy scale, where $z(0) = 1 + \frac{(N_c^2-1)}{2\pi N_c N_f} w(0)$ is the transient dynamical critical exponent defined at high energy. At energies higher than ω_0, the flow of v can be ignored, and the spectral function decays in a power-law controlled by the transient exponent that depends on $v(0)$. At low energies, the spectral function is controlled by the true fixed point with logarithmic corrections generated from the flow of v[182, 183].

Despite the success of the hot-spot theory in explaining scaling properties of the critical spin fluctuations and electrons at the hot spots, there are two important open issues. First, the four-fermion coupling has not been included in the hot-spot theory. While the four-fermion couplings have scaling dimension -1 at the fixed point with $v = 0$, it can not be ignored if it gives rise to IR singularities, which, for example, are responsible for superconducting instabilities. In priori, both hot and cold electrons can play important roles in superconducting instabilities because Cooper pairs from hot spots can be scattered to anywhere on the Fermi surface (and vice versa). To capture such superconducting fluctuations, it is crucial to include all gapless degrees of freedom on the equal footing. If superconducting instabilities are indeed present, as is seen ubiquitously in many quantum critical metals, the flow of v is cut off before the theory flows to the true fixed point located at $v = 0$. Second, the hot spot theory does not capture the universal low-energy properties that vary along the Fermi surface. The antiferromagnetic quantum critical metal hosts both Fermi liquid away from the hot spots and non-Fermi liquid at the hot spots within one physical system. Eq. (2.13) describes the spectral properties of the electrons right at the hot spots. The spectral function has no quasiparticle peak at the hot spots because the gapless spin fluctuations remain coupled with electrons down to zero energy. On the other hand, electrons away from the hot spots decouple from the low-energy spin fluctuations at sufficiently low energies, and they should be described by the Fermi liquid theory in the low-energy limit. As the hot spots are approached, the energy scale below which the electrons decouple from spin fluctuations is lowered, and the quasiparticle gradually loses coherence. For the same reason, all

[3] It turns out that these exact critical exponents can be extracted from the *interaction-driven scaling* in which the Yukawa coupling and the fermion kinetic term are kept marginal[205, 182].

other electronic properties such as the nesting angle, Fermi velocities, the quasiparticle weight and Landau parameters are expected to acquire singular momentum profiles near the hot spots. In order to understand such momentum dependent critical properties of the system, we have to go beyond the patch theory and include all gapless modes within our effective field theory.

2.3 The theory of the full Fermi surface

The full theory that includes all gapless modes and the four-fermion coupling is written as

$$\begin{aligned} S = & \sum_{N=1}^{8}\sum_{\sigma=1}^{N_c}\sum_{j=1}^{N_f}\int \mathrm{d}\mathbf{k}\ \psi^{\dagger}_{N,\sigma,j}(\mathbf{k})\left\{ik_0 + V^{(N)}_{F,k_N} e_N[\vec{k}, v^{(N)}_{k_N}]\right\}\psi_{N,\sigma,j}(\mathbf{k}) \\ & + \frac{1}{\sqrt{N}_f}\sum_{N=1}^{8}\sum_{\sigma\sigma'=1}^{N_c}\sum_{j=1}^{N_f}\int \mathrm{d}\mathbf{k}\mathrm{d}\mathbf{q}\ g^{(N)}_{k_N+q_N,k_N}\psi^{\dagger}_{N,\sigma',j}(\mathbf{k}+\mathbf{q})\Phi_{\sigma'\sigma}(\mathbf{q})\psi_{\bar{N},\sigma,j}(\mathbf{k}) \\ & + \frac{1}{4\mu}\sum_{\{N_i=1\}}^{8}\sum_{\{\sigma_i=1\}}^{N_c}\sum_{\{j_i=1\}}^{N_f}\int\prod_{i=1}^{4}\mathrm{d}\mathbf{k}_i\ \ \delta_{1+2,3+4}\lambda^{\binom{N_1\ N_2}{N_4\ N_3};\binom{\sigma_1\ \sigma_2}{\sigma_4\ \sigma_3}}_{\binom{k_{1;N_1}\ k_{2;N_2}}{k_{4,N_4}\ k_{3;N_3}}} \\ & \times \psi^{\dagger}_{N_1,\sigma_1,j_1}(\mathbf{k}_1)\psi^{\dagger}_{N_2,\sigma_2,j_2}(\mathbf{k}_2)\psi_{N_3,\sigma_3,j_2}(\mathbf{k}_3)\psi_{N_4,\sigma_4,j_1}(\mathbf{k}_4) \\ & + \frac{1}{4\mu}\int\prod_{i=1}^{4}\mathrm{d}\mathbf{k}_i\ \ \delta_{1+2+3+4,0}\Big\{u_1\mathrm{Tr}\left[\Phi(\mathbf{k}_1)\Phi(\mathbf{k}_2)\right]\mathrm{Tr}\left[\Phi(\mathbf{k}_3)\Phi(\mathbf{k}_4)\right] \\ & + u_2\mathrm{Tr}\left[\Phi(\mathbf{k}_1)\Phi(\mathbf{k}_2)\Phi(\mathbf{k}_3)\Phi(\mathbf{k}_4)\right]\Big\}. \end{aligned} \tag{2.14}$$

Here, the Fermi surface is still divided into eight disjoint patches each of which includes one hot spot as in the hot spot theory. However, unlike in the hot spot theory, the union of those patches cover the entire Fermi surface and the size of each patch is order of the Fermi momentum. Therefore, the coupling constants are promoted to general *coupling functions* that depend on momentum along the Fermi surface. μ is the floating energy scale at which physical observables are related to the coupling functions. Couplings that carry non-zero dimensions under the interaction driven scaling are expressed in the unit of μ. $\delta_{1+2,3+4} \equiv (2\pi)^3\delta(\mathbf{k}_1+\mathbf{k}_2-\mathbf{k}_3-\mathbf{k}_4)$ and $\delta_{1+2+3+4,0} \equiv (2\pi)^3\delta(\mathbf{k}_1+\mathbf{k}_2+\mathbf{k}_3+\mathbf{k}_4)$. k_N denotes the component of momentum that labels the Fermi surface near hot spot N (see Fig. 1.4a for the choice of coordinate system),

$$k_N = \begin{cases} k_x & \text{for } N = 1,4,5,8 \\ k_y & \text{for } N = 2,3,6,7 \end{cases}. \tag{2.15}$$

Although the $\hat{x}$ and $\hat{y}$ directions are not perfectly parallel to the Fermi surface in general, there is one-to-one correspondence between k_N and a point on the Fermi surface near hot spot N. We call k_N momentum 'along' the Fermi surface near hot spot N. $V^{(N)}_{F,k_N}$ is the momentum dependent Fermi velocity in the direction that is parallel to $\vec{Q}_{AF}$ near hot spot N. $e_N[\vec{k}, v^{(N)}_{k_N}]$, which determines the shape of the Fermi surface near each hot spot, is written as

$$\begin{aligned} e_1[\vec{k}; v^{(1)}_{k_x}] &= v^{(1)}_{k_x}k_x + k_y, & e_2[\vec{k}; v^{(2)}_{k_y}] &= -v^{(2)}_{k_y}k_y - k_x, \\ e_3[\vec{k}; v^{(3)}_{k_y}] &= v^{(3)}_{k_y}k_y - k_x, & e_4[\vec{k}; v^{(4)}_{k_x}] &= v^{(4)}_{k_x}k_x - k_y, \\ e_5[\vec{k}; v^{(5)}_{k_x}] &= -v^{(5)}_{k_x}k_x - k_y, & e_6[\vec{k}; v^{(6)}_{k_y}] &= v^{(6)}_{k_y}k_y + k_x, \\ e_7[\vec{k}; v^{(7)}_{k_y}] &= -v^{(7)}_{k_y}k_y + k_x, & e_8[\vec{k}; v^{(8)}_{k_x}] &= -v^{(8)}_{k_x}k_x + k_y, \end{aligned} \tag{2.16}$$

where the nesting angle in Eq. (2.2) is promoted to functions. The set of points that satisfy $e_N[\vec{k}, v^{(N)}_{k_N}] = 0$ forms the Fermi surface of a general shape. u_1 and u_2 represent quartic couplings

	allowed channels
Group 1	$\left[\begin{smallmatrix}1&1\\1&1\end{smallmatrix}\right]_p$, $\left[\begin{smallmatrix}1&4\\1&4\end{smallmatrix}\right]_p$, $\left[\begin{smallmatrix}4&4\\1&1\end{smallmatrix}\right]$
Group 2	$\left[\begin{smallmatrix}1&5\\1&5\end{smallmatrix}\right]_p$, $\left[\begin{smallmatrix}1&8\\1&8\end{smallmatrix}\right]_p$, $\left[\begin{smallmatrix}4&8\\1&5\end{smallmatrix}\right]$, $\left[\begin{smallmatrix}1&8\\4&5\end{smallmatrix}\right]$
Group 3	$\left[\begin{smallmatrix}1&2\\1&2\end{smallmatrix}\right]_p$, $\left[\begin{smallmatrix}1&3\\1&3\end{smallmatrix}\right]_p$, $\left[\begin{smallmatrix}1&6\\1&6\end{smallmatrix}\right]_p$, $\left[\begin{smallmatrix}1&2\\4&7\end{smallmatrix}\right]$, $\left[\begin{smallmatrix}1&3\\4&6\end{smallmatrix}\right]$, $\left[\begin{smallmatrix}1&6\\3&4\end{smallmatrix}\right]$, $\left[\begin{smallmatrix}1&7\\4&2\end{smallmatrix}\right]$
Group 4	$\left[\begin{smallmatrix}1&5\\2&6\end{smallmatrix}\right]$, $\left[\begin{smallmatrix}1&5\\3&7\end{smallmatrix}\right]$, $\left[\begin{smallmatrix}1&8\\2&3\end{smallmatrix}\right]$

Table 2.1: The primary and secondary channels for the four-fermion coupling, where the primary channels are the ones generated from the spin fluctuations at the leading order and the secondary channels are the ones generated from the primary channels through the linear mixing. The ones with subscript p denote primary channels.

between the collective modes. For $N_c = 2$, the terms with u_1 and u_2 are not independent, and one can set $u_2 = 0$ without loss of generality. The momentum-dependent Yukawa coupling is denoted as $g^{(N)}_{k',k}$. Unlike u_i, which are coupling constants, $g^{(N)}_{k',k}$ is a function that depends on two momenta along the Fermi surface. Similarly, $\lambda^{\left(\begin{smallmatrix}N_1&N_2\\N_4&N_3\end{smallmatrix}\right);\left(\begin{smallmatrix}\sigma_1&\sigma_2\\\sigma_4&\sigma_3\end{smallmatrix}\right)}_{\left(\begin{smallmatrix}k_1&k_2\\k_4&k_3\end{smallmatrix}\right)}$ ($\lambda^{\{N_i\};\{\sigma_i\}}_{\{k_i\}}$ in short) denotes the short-range four-fermion interactions labeled by momenta of electrons on the Fermi surface.

Due to the C_4 symmetry, $v^{(N)}_k$, $V^{(N)}_{F,k}$ and $g^{(N)}_{k',k}$ can be represented in terms of just three coupling functions v_k, $V_{F,k}$ and $g_{k',k}$ as

$$\left(v^{(N)}_k,\ V^{(N)}_{F,k},\ g^{(N)}_{k',k}\right) = \begin{cases} (v_k,\ V_{F,k},\ g_{k',k}), & N = 1,3,4,6 \\ (v_{-k},\ V_{F,-k},\ g_{-k',-k}), & N = 2,5,7,8 \end{cases}. \tag{2.17}$$

Similarly, four-fermion coupling functions that are mapped to each other under the C_4 symmetry are related. We set the coefficient of the ik_0 term in the fermion kinetic term to 1 by choosing the scaling of the fermion fields. The relative scale between frequency and momentum is chosen to set the Fermi velocity along $\vec{Q}_{AFM}$ to be 1 at the hot spots, and the normalization of the bosonic field is chosen so that the Yukawa coupling at the hot spots is tied to v_0,

$$V_{\mathrm{F},0} = 1, \quad g_{0,0} = \sqrt{\frac{\pi v_0}{2}}. \tag{2.18}$$

The allowed four-fermion couplings are constrained by the crystal momentum conservation because the hot spots are located at different points in the momentum space.[4] Even if the four-fermion coupling is zero at a UV scale, the Yukawa coupling generates four-fermion couplings. To the leading order in the Yukawa coupling, the diagrams in Fig. 2.7 generate the four-fermion couplings in channels $\left(\begin{smallmatrix}N&M\\N&M\end{smallmatrix}\right)$ for $1 \le N, M \le 8$. Due to the C_4 symmetry, we can focus on those channels with $N = 1$ without loss of generality. We call those couplings that are generated from the Yukawa coupling at the leading order *primary couplings*. Once the primary couplings are generated, secondary couplings are further generated through the linear mixing shown in Fig. 2.8. Because a set of coupling functions that forms a closed set of beta functionals has common primary couplings, it is convenient to group the four-fermion couplings according to their primary couplings. Group 1 includes the primary couplings

[4]For example, the coupling function $\lambda^{\left(\begin{smallmatrix}1&5\\4&8\end{smallmatrix}\right);\left(\begin{smallmatrix}\sigma_1&\sigma_2\\\sigma_4&\sigma_3\end{smallmatrix}\right)}_{\left(\begin{smallmatrix}k_1&k_2\\k_4&k_3\end{smallmatrix}\right)}$ with $k_i \approx 0$ is allowed because a pair of electrons on hot spots 1 and 5 carry the same total momentum as the pair made of electrons on hot spots 4 and 8. On the other hand, the coupling function $\lambda^{\left(\begin{smallmatrix}1&1\\2&5\end{smallmatrix}\right);\left(\begin{smallmatrix}\sigma_1&\sigma_2\\\sigma_4&\sigma_3\end{smallmatrix}\right)}_{\left(\begin{smallmatrix}k_1&k_2\\k_4&k_3\end{smallmatrix}\right)}$ with $k_i \approx 0$ is not allowed because of momentum mismatch.

generated by the Yukawa coupling in $(N, M) = (1, 1), (1, 4)$, and the secondary couplings that are further generated from mixing. The couplings in group 2 represent the primary ones generated in channels $(N, M) = (1, 5), (1, 8)$ and the associated secondary couplings. Group 3 includes the primary couplings for $(N, M) = (1, 2), (1, 3), (1, 6)$, and their secondary couplings. Those in group 4 have no primary couplings. The couplings in group 4 can be present only when there exists a bare short-range four-fermion couplings at a UV scale. These couplings are listed in Table 2.1. To avoid clutter in the table, we show only one channel among the ones that are related to each other through the C_4 symmetry, permutation of two incoming particles (or two outgoing particles), and Hermitian conjugate. Namely, each entry with the square brackets in Table 2.1 represents a group of channels obtained by the C_4 transformations, the Hermitian conjugate and the permutations between two incoming/outgoing particles,

$$\left[\begin{smallmatrix} N_1 & N_2 \\ N_4 & N_3 \end{smallmatrix}\right] = \left\{ \begin{array}{ll} \mathbf{R}_{N_1 N_1'} \cdots \mathbf{R}_{N_4 N_4'} \left(\begin{smallmatrix} N_1' & N_2' \\ N_4' & N_3' \end{smallmatrix}\right), & \mathbf{R}_{N_1 N_1'} \cdots \mathbf{R}_{N_4 N_4'} \left(\begin{smallmatrix} N_4' & N_3' \\ N_1' & N_2' \end{smallmatrix}\right), \\ \mathbf{R}_{N_1 N_1'} \cdots \mathbf{R}_{N_4 N_4'} \left(\begin{smallmatrix} N_2' & N_1' \\ N_4' & N_3' \end{smallmatrix}\right), & \mathbf{R}_{N_1 N_1'} \cdots \mathbf{R}_{N_4 N_4'} \left(\begin{smallmatrix} N_3' & N_4' \\ N_1' & N_2' \end{smallmatrix}\right) \end{array} \middle| \; \mathbf{R}_{N_i' N_i} \in C_4 \right\}, \tag{2.19}$$

where the repeated hot spot indices are summed over and $\mathbf{R}$ is the 8-dimensional representation of the C_4 group that acts as permutations on hot spot indices. For example, for the $\pi/2$ rotation we have $\mathbf{R}^{\pi/2}_{NN'} = \delta_{N,[N'+2]_8}$, where $[x]_8 = x \bmod 8$. $\left(\begin{smallmatrix} 1 & 7 \\ 1 & 7 \end{smallmatrix}\right)$ is related to $\left(\begin{smallmatrix} 1 & 3 \\ 1 & 3 \end{smallmatrix}\right)$ through the $\pi/2$ rotation, and it is not separately shown in group 3. In the table, channels with subscript p denotes the ones that include primary couplings.

The theory has the $U(1)$ charge, the $SU(N_f)$ flavour and the $SU(N_c)$ spin rotational symmetry. Due to the spin rotational symmetry, the four-fermion coupling function can be decomposed into two channels as $\lambda^{\left(\begin{smallmatrix} N_1 & N_2 \\ N_4 & N_3 \end{smallmatrix}\right);\left(\begin{smallmatrix} \sigma_1 & \sigma_2 \\ \sigma_4 & \sigma_3 \end{smallmatrix}\right)}_{\left(\begin{smallmatrix} k_1 & k_2 \\ k_4 & k_3 \end{smallmatrix}\right)} = \lambda^{\left(\begin{smallmatrix} N_1 & N_2 \\ N_4 & N_3 \end{smallmatrix}\right)}_{D,\left(\begin{smallmatrix} k_1 & k_2 \\ k_4 & k_3 \end{smallmatrix}\right)} \delta_{\sigma_1\sigma_4}\delta_{\sigma_2\sigma_3} + \lambda^{\left(\begin{smallmatrix} N_1 & N_2 \\ N_4 & N_3 \end{smallmatrix}\right)}_{E,\left(\begin{smallmatrix} k_1 & k_2 \\ k_4 & k_3 \end{smallmatrix}\right)} \delta_{\sigma_1\sigma_3}\delta_{\sigma_2\sigma_4}$. The action in Eq. (2.14) is also invariant under the particle-hole (PH) transformation,

$$\psi_{N,\sigma,j}(k) \longrightarrow \psi^\dagger_{N,\sigma,j}(-k), \quad \Phi(q) \longrightarrow -\Phi(q)^{\mathrm{T}} \tag{2.20}$$

if the coupling functions satisfy

$$v_{-k} = v_k, \qquad V_{\mathrm{F},-k} = V_{\mathrm{F},k}, \qquad g_{-k',-k} = g_{k,k'}, \qquad \lambda^{\left(\begin{smallmatrix} N_1 & N_2 \\ N_4 & N_3 \end{smallmatrix}\right);\left(\begin{smallmatrix} \sigma_1 & \sigma_2 \\ \sigma_4 & \sigma_3 \end{smallmatrix}\right)}_{\left(\begin{smallmatrix} k_1 & k_2 \\ k_4 & k_3 \end{smallmatrix}\right)} = \lambda^{\left(\begin{smallmatrix} N_4 & N_3 \\ N_1 & N_2 \end{smallmatrix}\right);\left(\begin{smallmatrix} \sigma_4 & \sigma_3 \\ \sigma_1 & \sigma_2 \end{smallmatrix}\right)}_{\left(\begin{smallmatrix} -k_4 & -k_3 \\ -k_1 & -k_2 \end{smallmatrix}\right)}. \tag{2.21}$$

For Fermi surfaces with general shapes, the PH symmetry is absent. In this thesis, we are going to focus on the general cases without the PH symmetry.

The theory has two cutoff scales. The first is k_F that represents the size of each patch. The second is the energy cutoff Λ. It sets the momentum cutoff of boson and the momentum of electrons in the direction perpendicular to the Fermi surface. Naturally, k_F is the largest momentum scale.

Under the interaction-driven scaling in which frequency and momentum are rescaled by a factor $\mathsf{b} > 1$, the fields are transformed as

$$\psi(\mathbf{k}) = \mathsf{b}^2 \psi'(\mathbf{k}'), \quad \Phi(\mathbf{k}) = \mathsf{b}^2 \Phi'(\mathbf{k}') \tag{2.22}$$

with $\mathbf{k} = \mathsf{b}^{-1}\mathbf{k}'$. Under this transformation, the coupling functions are transformed as

$$\begin{gathered} v'_k = v_{\mathsf{b}^{-1}k}, \qquad V'_{\mathrm{F},k} = V_{\mathrm{F},\mathsf{b}^{-1}k}, \qquad g'_{k+q,k} = g_{\mathsf{b}^{-1}(k+q),\mathsf{b}^{-1}k}, \\ \lambda'^{\{N_i\};\{\sigma_i\}}_{\{k_i\}} = \mathsf{b}^{-1} \lambda^{\{N_i\};\{\sigma_i\}}_{\{\mathsf{b}^{-1}k_i\}}, \qquad u'_n = \mathsf{b}^{-1} u_n. \end{gathered} \tag{2.23}$$

Here k, q and k_i represent the momentum along the Fermi surface. According to Eq. (2.23), both fermionic and bosonic quartic interactions are irrelevant by power counting. Unlike the pure ϕ^4 theory in $2 + 1$ dimension, the bosonic quartic coupling is irrelevant because the boson acquires a large anomalous dimension due to the strong coupling with the fermions near the hot spots. Indeed, loop

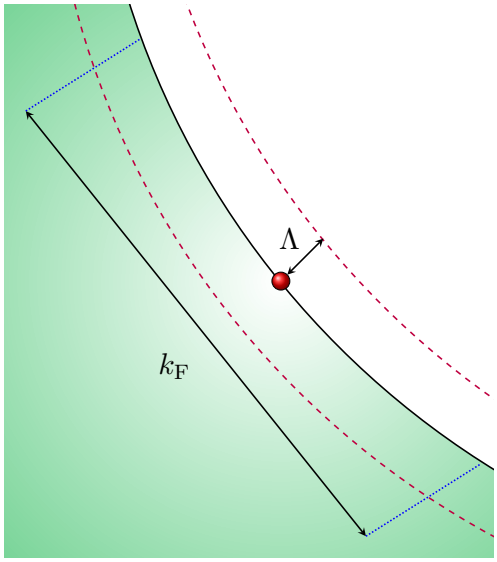

Figure 2.3: Energy and momentum cutoffs. Λ is the energy cutoff, and k_F denotes the size of the patch near each hot spot. The full Fermi surface consists of the union of the eight disjoint patches and the size of each patch is comparable to the Fermi momentum.

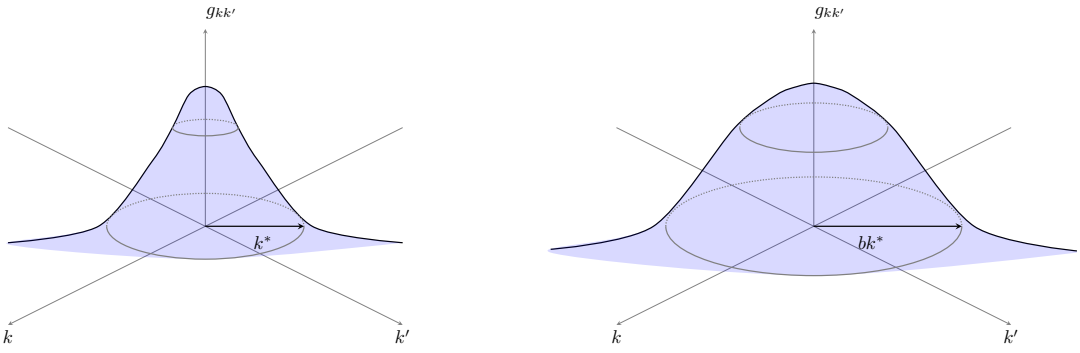

Figure 2.4: Under the tree-level scaling, the momentum along the Fermi surface is rescaled, which causes the momentum profiles of the coupling functions to be stretched out under the renormalization group flow.

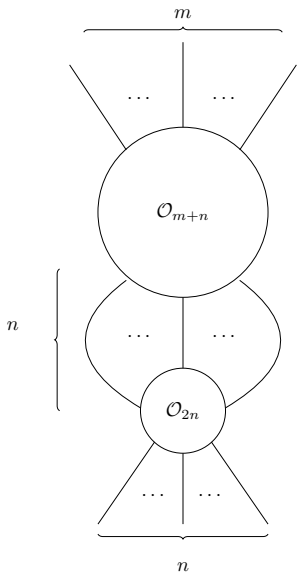

Figure 2.5: A loop correction in which an $m+n$-fermion operator is dressed with $2n$-fermion operator that results in an anomalous dimension of the $m+n$-fermion operator.

corrections that involve u_n are IR finite. Therefore, we can drop the bosonic quartic coupling in the low-energy limit.

On the contrary, one can not drop the four-fermion coupling because it can give rise to IR singularities through loop corrections. The disagreement between what is expected from the power-counting and the actual degree of IR divergence is caused by the scale associated with the size of Fermi surface. To see this, let us consider a process in which a $2n$-fermion operator fuses with another operator, generating an anomalous dimension for the latter. To the leading order in the perturbative expansion, this is represented by an $(n-1)$-loop process (see Fig. 2.5). The scaling dimension of λ_{2n} is $3-2n$, and no IR divergence is expected for $n \geq 2$ from the power-counting. However, the actual degree of IR divergence can be enhanced by the extended phase space for gapless fermions. If fermions in the loop can stay on the Fermi surface within a manifold with dimension α_{2n} in the space of internal momenta, the effective coupling that contributes to the quantum correction becomes $\lambda_{2n} k_F^{\alpha_{2n}}$ because the loop momenta within the manifold give the volume of the phase space, $k_F^{\alpha_{2n}}$. For one-dimensional Fermi surfaces, $\alpha_{2n} \leq (n-1)$. The upper bound is saturated if every momentum along the Fermi surface contributes a factor of k_F, which happens when the Fermi surface is straight. For Fermi surfaces with generic shapes, α_{2n} becomes smaller than $(n-1)$ as the perfect nesting is destroyed by curvature of Fermi surface. However, $n=2$ is special in that the upper bound is saturated in the pairing channel as far as the time-reversal symmetry is present. Since a pair of fermions with zero center of mass momentum can be placed anywhere on the Fermi surface in the one-dimensional Fermi surface, $\alpha_4 = 1$. This implies that the effective scaling dimension of the four-fermion coupling becomes zero, and the four-fermion coupling should be included within the low-energy effective theory. Indeed, the BCS scattering processes that involve the four-fermion coupling give rise to logarithmic divergences in the low-energy limit. On the other hand, λ_{2n}'s with $n > 2$ are too irrelevant to create IR singularities even with the help of the enhancement from Fermi surface. Therefore, we only keep the four-fermion coupling among the couplings that are irrelevant by power-counting.

Given that the action in Eq. (2.14) is local, all coupling functions can be expanded in the Taylor

series of momentum along the Fermi surface as

$$\begin{aligned} v_k &= \sum_{n=0}^{\infty} \frac{v^{[n]}}{n!} k^n, \qquad V_{\mathrm{F},k} = \sum_{n=0}^{\infty} \frac{V_F^{[n]}}{n!} k^n, \\ g_{k+q,k} &= \sum_{m,n=0}^{\infty} \frac{g^{[m,n]}}{m!n!} k^m q^n, \qquad \lambda_{\{k_i\}}^{\{N_i\};\{\sigma_i\}} = \sum_{\{l_i\}=0}^{\infty} \frac{\lambda^{[l_1,..,l_4];\{N_i\};\{\sigma_i\}}}{l_1!l_2!l_3!l_4!} k_1^{l_1} k_2^{l_2} k_3^{l_3} k_4^{l_4}. \end{aligned} \tag{2.24}$$

The interaction driven scaling fixes the scaling dimensions of the coefficients in Eq. (2.24) to $[v^{[n]}] = [V_F^{[n]}] = -n$, $[g^{[m,n]}] = -(m+n)$ and $\left[\lambda^{[l_1,..,l_4];\{N_i\};\{\sigma_i\}}\right] = -(1+l_1+l_2+l_3+l_4)$. Formally, allowing the general momentum dependence in the coupling functions amounts to introducing an infinite tower of coupling constants. Although the high-order coupling constants are highly 'irrelevant' in terms of their scaling dimensions, they are necessary to characterize the whole Fermi surface. This rather unusual role of irrelevant couplings is due to the fact that the momentum along the Fermi surface not only acts as a scale but also as a label for the gapless electronic degrees of freedom. In particular, the momentum dependence in coupling functions is important in understanding superconductivity that arises through an interplay between hot and cold electrons.

In Eq. (2.24), $g_{k+q,k}$ denotes the strength of the interaction in which an electron is scattered from momentum k to $k+q$ near the Fermi surface by absorbing or emitting boson with momentum q in magnitude. In relativistic quantum field theories, scatterings that involve high-energy particles are not important at low energies. For this reason, one may just keep the leading order term in the expansion in q. In the presence of Fermi surface, however, the processes in which electrons are scattered by high-energy bosons within the Fermi surface can give rise to IR singularities. The same mechanism is responsible for the logarithmic singularity associated with the BCS instability caused by short-range interactions mediated by a massive boson in Fermi liquids. For this reason, we include the Yukawa coupling with general k and q within the theory. The fact that the coupling associated with high-energy bosons should be included within the theory raises important questions on what constitute low-energy observables and what information the low-energy effective theory should include to be predictive. Later, we will see that the predictions of the theory do not depend on UV physics if we choose the right observables. For now, we proceed with the general Yukawa coupling function as an intermediate step toward identifying the universal observables that do not depend on UV physics.

2.4 The field-theoretic functional renormalization group formalism

In this section we discuss the fundamentals of the field theoretic functional RG scheme that is used throughout the thesis. For other functional RG approaches, see Refs. [162, 222, 146, 168, 170, 81, 85, 64, 63, 31, 143, 181, 88, 139, 107, 55, 159, 218, 89, 129, 53, 54, 87, 130, 171, 209].

2.4.1 Renormalizability

Explaining or predicting experiments is usually done in the following steps. One first identifies relevant degrees of freedom and symmetry to constructs a model that generally includes a set of free parameters. After physical observables are computed from the model, the parameters of the model are fixed from existing experimental data. Once the parameters are fixed, one can make predictions for new observables. Since there is freedom in choosing which observables are used to fix the parameters and which ones are used as predictions, what a theory captures is the relation among physical observables. A theory has stronger predictive power if more observables are fixed by fewer other observables.

In field theories, one aims to find relations among low-energy observables measured at energy scales much smaller than microscopic energy scales. While individual low-energy observables can sensitively depend on microscopic details, field theories can capture their relations that are independent of the

microscopic details. To achieve this goal, it is most convenient to use renormalizable field theories. A renormalizable theory contains a minimal set of couplings in terms of which all other low-energy observables of the theory can be expressed with errors that vanish in powers of μ/Λ, where μ is the energy scale at which observables are probed and Λ is a UV cutoff. Although microscopic systems in general include more parameters, one can use renormalizable theories to extract universal relations among low-energy observables. Two theories which differ by irrelevant couplings give rise to the same relations among low-energy observables within the power-law accuracy.

In the presence of Fermi surface, a low-energy theory includes momentum-dependent coupling functions. Once expanded around a point (say a hot spot) on the Fermi surface, the momentum-dependent coupling functions in Eq. (2.14) can be viewed as an infinite set of coupling constants. Under a transformation that rescales the momentum relative to the hot spots, the couplings associated with positive powers of momentum along the Fermi surface are formally irrelevant. However, this does not imply that those higher order terms in momentum are unimportant for all low-energy observables. Even if the higher order terms in Eq. (2.24) may not be needed for understanding the low-energy behaviours of electrons at the hot spots, they are still important for electrons on the Fermi surface far away from the hot spots. The higher order terms can be important even for electrons at the hot spots if large momentum-scatterings are not suppressed at low energies. Therefore, it is necessary to keep the full momentum-dependent coupling functions in order to characterize the low-energy physics of the entire system. Because the Fermi surface supports an infinite number of gapless modes, the amount of universal low-energy data is in general infinite[5].

The goal of low-energy effective theories for Fermi surface is to identify the minimal set of functions' worth of low-energy data, in terms of which all low-energy observables can be determined. To achieve this, we use Eq. (2.14) to compute a set of physical observables as functionals of the coupling functions. Local counter terms are added to the action so that those physical observables become what we set them to be as functions of momentum along the Fermi surface at an energy scale. Once the bare theory that includes the counter terms is fixed, it gives rise to the functional Callan-Symanzik equation that describes how the momentum dependent physical observables run as functions of energy. From the flow equations, we identify the set of low-energy observables in terms of which all other low-energy observables can be expressed without resorting to unknown high-energy physics. In particular, the RG flow of the coupling functions identified as low-energy observables should be captured solely in terms of those coupling functions themselves. Given that we don't know in priori what constitute universal low-energy observables, we first include all coupling functions $\{v_k, V_{\mathrm{F},k}, g_{k+q,k}, \lambda^{\{N_i\};\{\sigma_i\}}_{\{k_i\}}\}$ that can be potentially needed in characterizing all low-energy observables. From this, we isolate the minimal subset whose RG flow can be extracted solely from those couplings in the minimal subset without resorting to any unknown UV physics. The two-point function of fermion on the Fermi surface, which is related to the momentum dependent nesting angle and Fermi velocity, are low-energy observables. While the forward cubic vertex function related to $g_{k,k}$ is in the minimal set of low-energy observables, $g_{k+q,k}$ with a non-zero q is not because the off-diagonal Yukawa coupling function with large momentum transfer encodes the dynamics of the high-energy boson. Remarkably, the one-particle irreducible (1PI) four-fermion vertex function strictly defined on the Fermi surface does not belong to the minimal set of low-energy observables either. This is because the flow of $\lambda^{\{N_i\};\{\sigma_i\}}_{\{k_i\}}$ for general k_i's can not be determined within the low-energy effective field theory : quartic fermion operators defined on different points on the Fermi surface can mix with each other at low energies by exchanging high-energy bosons. Nonetheless, the RG flow of the net two-body interaction that combines the 1PI four-fermion vertex function and the tree-diagram associated with two 1PI three-point vertex functions connected by the renormalized boson propagator can be understood within the low-energy effective theory (see Fig. 1.6). This will be shown explicitly in Sec. 2.6.3.

In the present theory, there are two cutoff scales, k_F and Λ. Naively one might expect that

[5]The low-energy data, while being infinite, is still much smaller than the full information a microscopic theory can carry. This is because the low-energy effective theory only keeps track of the momentum dependence of the coupling functions along the Fermi surface.

the relations between observables at one scale, μ_1, and observables at another scale, μ_2, should be independent of all of those short distance scales for $\mu_1, \mu_2 \ll \Lambda, k_F$. This amounts to requiring that divergences in any of those large momentum scales can be removed by adding local counter terms. However, it is in general impossible to remove k_F dependences in all low-energy observables[6]. This is because k_F is a part of the low-energy data that reflects the 'number' of gapless modes in the system. As a result, the beta functionals for the four-fermion couplings may explicitly depend on k_F, and k_F needs to be included in characterizing low-energy physics. On the other hand, Λ represents the energy cutoffs, and it can be removed from low-energy observables by adding local counter terms. In field theories of Fermi surface, the validity of the low-energy effective field theory boils down to the question of whether one can remove Λ but not necessarily k_F in the relations among low-energy observables.

2.4.2 Extended minimal subtraction scheme

To understand the low-energy physics of the theory, the quantum effective action is computed order by order in v from the classical action in Eq. (2.14). Since the Yukawa coupling is marginal under the interaction-driven scaling, quantum corrections to the leading-order solution of the non-perturbative Schwinger-Dyson equation are logarithmically divergent in general. While the four-fermion coupling is irrelevant under the interaction driven scaling, it also gives rise to IR singularities as will be shown later. To capture how those singular corrections modify physical observables in the low-energy limit, we express the vertex functions in terms of the coupling functions, and keep track of the RG flow of the coupling functions as the energy scale is lowered. Since gapless electrons can be anywhere on the extended Fermi surface, the low-energy vertex functions and the couplings are functions of momentum along the Fermi surface and the energy scale.

The relation between the vertex functions and the coupling functions is set by a set of renormalization conditions, which is enforced by adding counter terms to Eq. (2.14). The renormalization conditions are written as

$$Re\Gamma_1^{(2,0)}(\mathbf{k})\Big|_{\mathbf{k}=(\mu,k_x,-v_{k_x}k_x)} = 0, \tag{2.25}$$

$$\frac{\partial}{\partial k_y} Re\Gamma_1^{(2,0)}(\mathbf{k})\Big|_{\mathbf{k}=(\mu,k_x,-v_{k_x}k_x)} = V_{\mathrm{F},k_x} + \mathscr{F}_{1,k_x}, \tag{2.26}$$

$$-i\frac{\partial}{\partial k_0} Im\Gamma_1^{(2,0)}(\mathbf{k})\Big|_{\mathbf{k}=(\mu,k_x,-v_{k_x}k_x)} = 1 + \mathscr{F}_{2,k_x}, \tag{2.27}$$

$$\Gamma_1^{(2,1)}(\mathbf{k}',\mathbf{k})\Big|_{\substack{\mathbf{k}'=(2\mu,k'_x,-v_{k'_x}k'_x)\\ \mathbf{k}=(\mu,k_x,v_{k_x}k_x)}} = \frac{g_{k'_x,k_x}}{\sqrt{N_f}} + \mathscr{F}_{3,(k'_x,k_x)}, \tag{2.28}$$

$$\Gamma^{(4,0);\{N_i\};\{\sigma_i\}}(\{\mathbf{k}_i\})\Big|_{\mathbf{k}_i=\mathbf{k}_i^*} = \frac{1}{4\mu}\left[\lambda^{\binom{N_1\ N_2}{N_4\ N_3};\binom{\sigma_1\ \sigma_2}{\sigma_4\ \sigma_3}}_{\binom{k_1\ k_2}{k_4\ k_3}} + \mathscr{F}^{\binom{N_1\ N_2}{N_4\ N_3};\binom{\sigma_1\ \sigma_2}{\sigma_4\ \sigma_3}}_{4,\binom{k_1\ k_2}{k_4\ k_3}}\right]. \tag{2.29}$$

Here, $\Gamma_N^{(2,0)}(\mathbf{k})$ is the two-point function of electrons near hot spot N. $\Gamma_N^{(2,1)}(\mathbf{k}',\mathbf{k})$ is the electron-boson vertex function that describes scattering of an electron from three-momentum $\mathbf{k}$ near hot spot $\bar{N}$ to $\mathbf{k}'$ near hot spot N. $\Gamma^{(4,0);\{N_i\};\{\sigma_i\}}(\{\mathbf{k}_i\})$ is the electron four-point function, where the i-th external electron is near hot spot N_i, spin σ_i and three-momentum $\mathbf{k}_i$. Eq. (2.25) is the defining equation for v_k that specifies the renormalized Fermi surface. Near hot spot 1, the renormalized Fermi surface at scale μ is given by the set of $(k_x, -v_{k_x}k_x)$ at which the real part of the two-point function vanishes. Eq. (2.26) defines the momentum dependent Fermi velocity, $V_{F,k}$. $\mathscr{F}_{1,k_x}$ corresponds to a

[6]For example, thermodynamic quantities such as the specific heat are proportional to k_F in the low temperature limit. k_F also determines the phase space of a pair of electrons with zero total momentum and energy, and controls the mixing between quartic fermion operators in the pairing channel.

scheme dependent function that is regular in the small μ limit. We choose the relative scale between frequency and spatial momentum to set

$$V_{F,0} = 1 \tag{2.30}$$

at the hot spots. To impose Eq. (2.30) at all μ, the relative scale between frequency and momentum should be chosen in an energy dependent way, which gives rise to a dynamical critical exponent different from 1 in general. The Fermi velocity away from the hot spots is in general different from that of the hot spots. Eq. (2.27) determines the momentum dependent scaling of the fermion field : it fixes the frequency dependent kinetic term of the fermion to be of the canonical form at all energy scales up to a regular correction, $\mathscr{F}_{2,k_x}$. Finally, Eq. (2.28) and Eq. (2.29) define the momentum dependent Yukawa coupling function and the four-fermion coupling functions, respectively. The renormalization condition for the four-point function is imposed at

$$\mathbf{k}_1^* = (3\mu, \vec{k}_1^*), \quad \mathbf{k}_2^* = (-\mu, \vec{k}_2^*), \quad \mathbf{k}_3^* = (\mu, \vec{k}_3^*), \quad \mathbf{k}_4^* = (\mu, \vec{k}_4^*), \tag{2.31}$$

where $\vec{k}_i^*$'s are the spatial momenta that are near the Fermi surface[7] and satisfy the momentum conservation. For generic shapes of Fermi surface, which is the main focus of this chapter, we can focus on the forward scattering and the pairing channels. Here, the external frequencies are chosen so that the energy that flows through the vertex function is 2μ in magnitude in all s, t, u channels.

Ideally, one would want to choose the counter terms so that they completely cancel the quantum corrections. In this total subtraction scheme, $\mathscr{F}_i = 0$, and the coupling functions at scale μ coincides with the vertex functions measured at that energy. However, the total subtraction scheme is rather impractical because it requires computing the full quantum corrections including finite parts. In this thesis, we use a minimal subtraction scheme, where counter terms remove only divergent contributions to the quantum effective action in the small μ/Λ limit. While the vertex functions do not exactly match the coupling functions in the minimal subtraction scheme, one can in principle infer one from the other as they are related to each other through relations that are regular in the small μ limit. For the purpose of extracting scaling behaviours, it suffices to know the existence of such finite functions but not their explicit forms. As far as IR singularities in all physical observables are encoded in the coupling functions, any instability of the system can be inferred from the RG flow of the coupling functions.

The minimal subtraction scheme is straightforward to implement for dimensionless couplings. Counter terms are added to remove singular corrections to the two and three-point functions as in Eqs. (2.25)-(2.28). In the minimal subtraction scheme, $\mathscr{F}_{1,2,3}$ are generally non-zero, but they stay finite in the small μ limit. This guarantees that the dimensionless physical observables are related to $v_k, V_{F,k}, g_{k',k}$ through non-singular relations.

Implementing the minimal subtraction scheme for the four-fermion couplings is more subtle. The four-fermion coupling is irrelevant, and $\Gamma^{(4,0)}$ has engineering scaling dimension -1. A renormalization condition should be imposed on dimensionless quantities constructed out of $\Gamma^{(4,0)}$ and a scale. $\mu\Gamma^{(4,0)}$ is one such dimensionless quantity. Naively, one may only require that $\mu\Gamma^{(4,0)}$ coincides with the dimensionless coupling function λ up to any non-singular correction. If this was the case, $\mathscr{F}_4$ in Eq. (2.29) could be an arbitrary finite function of momenta. However, this subtraction scheme is 'too minimal' in that λ does not capture all IR singularities of physical observables. This is because dimensionless observables constructed out of integrations of $\Gamma^{(4,0)}$ over momenta can exhibit singularities even if $\mu\Gamma^{(4,0)}$ is finite in the small μ limit. For example, the strength of the pairing interaction at energy scale μ is measured by eigenvalue E_μ defined through

$$\sum_{N_4} \sum_{\sigma_4,\sigma_3} \int dp \; \Gamma^{(4,0)}_{\begin{pmatrix} \mathbf{q+k} & \mathbf{-k} \\ \mathbf{p} & \mathbf{q-p} \end{pmatrix}}{}^{\begin{pmatrix} N_1 & [N_1+4]_8 \\ N_4 & [N_4+4]_8 \end{pmatrix};\begin{pmatrix} \sigma_1 & \sigma_2 \\ \sigma_4 & \sigma_3 \end{pmatrix}} f_p^{N_4;(\sigma_4,\sigma_3)} = E_\mu f_k^{N_1;(\sigma_1,\sigma_2)}. \tag{2.32}$$

[7] To be precise, the energy associated with each momentum should be at most order of μ.

Here $\mathbf{q} = (2\mu, 0, 0)$ is the three momentum of a Cooper pair. The frequencies of $\mathbf{k}$ and $\mathbf{p}$ are set to be μ. p and k label the components of $\vec{p}$ and $\vec{k}$ along the Fermi surface. The other components of the spatial momentum are chosen so that $\vec{p}$ and $\vec{k}$ are on the Fermi surface. $f_k^{N_1;(\sigma_1,\sigma_2)}$ is an eigen-wavefunction of the Cooper pair. Even if $\mathscr{F}^{\binom{N_1\ N_2}{N_4\ N_3};\binom{\sigma_1\ \sigma_2}{\sigma_4\ \sigma_3}}_{4,\binom{k_1\ k_2}{k_4\ k_3}}$ is finite at every k_i, its contribution to the eigenvalue may diverge in the small μ limit if it has an extended support in the momentum space. For example, $\mathscr{F}^{\binom{N_1\ [N_1+4]_8}{N_4\ [N_4+4]_8};\binom{\sigma_1\ \sigma_2}{\sigma_4\ \sigma_3}}_{4,\binom{k\ -k}{p\ -p}} \sim \frac{\mu}{\sqrt{(k-p)^2+\mu^2}}$ gives rise to a divergent correction to the eigenvalue E_μ although its element is finite in the small μ limit. Without subtracting such divergent contribution, the coupling function does not capture the IR singularity associated with the divergent pairing interaction. To remove any singular discrepancy between the eigenvalues of the vertex function and the coupling function, we need to impose a more stringent condition on the finite part : we require that not only $\mathscr{F}^{\binom{N_1\ N_2}{N_4\ N_3};\binom{\sigma_1\ \sigma_2}{\sigma_4\ \sigma_3}}_{4,\binom{k_1\ k_2}{k_4\ k_3}}$ is finite at all momenta but also

$$\lim_{\mu\to 0}\int_C \frac{dk}{\mu}\left|\mathscr{F}^{\binom{N_1\ N_2}{N_4\ N_3};\binom{\sigma_1\ \sigma_2}{\sigma_4\ \sigma_3}}_{4,\binom{k_1\ k_2}{k_4\ k_3}}\right| = \text{finite} \tag{2.33}$$

for any one-dimensional manifold C in the space of k_i's. With this condition, the eigenvalue of $\mathscr{F}^{\binom{N_1\ N_2}{N_4\ N_3};\binom{\sigma_1\ \sigma_2}{\sigma_4\ \sigma_3}}_{4,\binom{k_1\ k_2}{k_4\ k_3}}$ is non-divergent in the small μ limit[8]. In this extended minimal subtraction scheme, IR singularities of the four-point function are fully captured by λ.

2.4.3 Scale invariance and the lack of thereof

The local counter term action for Eq. (2.14) is written as

$$\begin{aligned}
&S_{\text{C.T}} = \\
&\sum_{N=1}^{8}\sum_{\sigma=1}^{N_c}\sum_{j=1}^{N_f}\int \mathrm{d}\mathbf{k}\ \psi^\dagger_{N,\sigma,j}(\mathbf{k})\left\{iA_1^{(N)}(k_N)k_0 + A_3^{(N)}(k_N)V^{(N)}_{\mathrm{F},k_N}e_N\left[\vec{k};\frac{A_2^{(N)}(k_N)}{A_3^{(N)}(k_N)}v^{(N)}_{k_N}\right]\right\}\psi_{N,\sigma,j}(\mathbf{k}) \\
&+\frac{1}{\sqrt{N_f}}\sum_{N=1}^{8}\sum_{\sigma\sigma'=1}^{N_c}\sum_{j=1}^{N_f}\int \mathrm{d}\mathbf{k}'\int \mathrm{d}\mathbf{k}\ A_4^{(N)}(k'_N,k_{\bar{N}})g^{(N)}_{k'_N,k_{\bar{N}}}\psi^\dagger_{N,\sigma',j}(\mathbf{k}')\Phi_{\sigma'\sigma}(\mathbf{k}'-\mathbf{k})\psi_{\bar{N},\sigma,j}(\mathbf{k}) \\
&+\frac{1}{4\mu}\sum_{\{N_i=1\}}^{8}\sum_{\{\sigma_i=1\}}^{N_c}\sum_{\{j_i=1\}}^{N_f}\left[\prod_{i=1}^{4}\int \mathrm{d}\mathbf{k}_i\right]\left\{A^{\{N_i\};\{\sigma_i\}}(\{k_{i;N_i}\})\lambda^{\{N_i\};\{\sigma_i\}}_{\{k_{i;N_i}\}}\delta_{1+2,3+4}\right. \\
&\left.\times\psi^\dagger_{N_1,\sigma_1,j_1}(\mathbf{k}_1)\psi^\dagger_{N_2,\sigma_2,j_2}(\mathbf{k}_2)\psi_{N_3,\sigma_3,j_2}(\mathbf{k}_3)\psi_{N_4,\sigma_4,j_1}(\mathbf{k}_4)\right\} \\
&+M_{CT}\sum_{N=1}^{8}\sum_{\sigma=1}^{N_c}\sum_{j=1}^{N_f}\int \mathrm{d}\mathbf{k}\ \psi^\dagger_{N,\sigma,j}(\mathbf{k})\psi_{N,\sigma,j}(\mathbf{k}) + \frac{m_{CT}}{4}\int \mathrm{d}\mathbf{k}\ \mathrm{Tr}\left[\Phi(\mathbf{k})\Phi(-\mathbf{k})\right].
\end{aligned} \tag{2.34}$$

Here, $A_i^{(N)}(k_N)$ with $i = 1, 2, 3$, $A_4^{(N)}(k', k)$ and $A^{\{N_i\};\{\sigma_i\}}(\{k_i\})$ are momentum-dependent local counter terms which are functionals of the coupling functions. They are determined from the quantum

[8] To see this, we consider matrix, $\mathcal{M}_{ij} = \frac{\Delta k}{\mu}\mathscr{F}^{\binom{N_i\ [N_i+4]_8}{N_j\ [N_j+4]_8};\binom{\sigma_i\ \sigma'_i}{\sigma_j\ \sigma'_j}}_{4,\binom{k_i\ -k_i}{k_j\ -k_j}}$, where the matrix indices i, j label hot spot index, spin and discretized momentum of a Cooper pair, and Δk denotes the mesh size of the discrete momentum. Eq. (2.33) implies that sum of the absolute values of elements in any row of $\mathcal{M}$ is finite in the small μ limit. Gershgorin's circle theorem implies that all eigenvalues are finite as well.

corrections so that the renormalization conditions in Eqs. (2.25) - (2.29) are satisfied. Due to the C_4 symmetry, $A_i^{(N)}(k)$ with $i = 1, 2, 3$ and $A_4^{(N)}(k', k)$ can be represented in terms of four counter term functions $A_i(k)$ with $i = 1, 2, 3$ and $A_4(k', k)$ as

$$\left(A_i^{(N)}(k),\ A_4^{(N)}(k', k)\right) = \begin{cases} \left(A_i(k),\ A_4(k', k)\right), & N = 1, 3, 4, 6 \\ \left(A_i(-k),\ A_4(-k', -k)\right), & N = 2, 5, 7, 8 \end{cases} . \tag{2.35}$$

M_{CT} is the counter term that is needed to make sure that the hot spots are located at $\mathbf{k} = 0$ in the fully renormalized Fermi surface. m_{CT} is the mass counter term for the boson, which is needed to keep the system at the quantum critical point.

Adding Eqs. (2.34) and (2.14) yields the renormalized action

$$\begin{aligned} S_{\text{Ren}} = & \sum_{N=1}^{8} \sum_{\sigma=1}^{N_c} \sum_{j=1}^{N_f} \int \mathrm{d}\mathbf{k}^{\mathsf{B}}\ \psi^{\mathsf{B}\dagger}_{N,\sigma,j}(\mathbf{k}^{\mathsf{B}}) \left\{ ik_0^{\mathsf{B}} + V^{\mathsf{B}(N)}_{\mathrm{F},k_N^{\mathsf{B}}} e_N \left[\vec{k}^{\mathsf{B}}; v^{\mathsf{B}(N)}_{k_N^{\mathsf{B}}} \right] \right\} \psi^{\mathsf{B}}_{N,\sigma,j}(\mathbf{k}^{\mathsf{B}}) \\ & + \frac{1}{\sqrt{N_f}} \sum_{N=1}^{8} \sum_{\sigma\sigma'=1}^{N_c} \sum_{j=1}^{N_f} \int \mathrm{d}\mathbf{k}'^{\mathsf{B}} \int \mathrm{d}\mathbf{k}^{\mathsf{B}}\ g^{\mathsf{B}(N)}_{k'^{\mathsf{B}}_N, k^{\mathsf{B}}_{\bar{N}}} \psi^{\mathsf{B}\dagger}_{N,\sigma',j}(\mathbf{k}'^{\mathsf{B}}) \Phi^{\mathsf{B}}_{\sigma'\sigma}(\mathbf{k}'^{\mathsf{B}} - \mathbf{k}^{\mathsf{B}}) \psi^{\mathsf{B}}_{\bar{N},\sigma,j}(\mathbf{k}^{\mathsf{B}}) \\ & + \frac{1}{4} \sum_{\{N_i=1\}}^{8} \sum_{\{\sigma_i=1\}}^{N_c} \sum_{\{j_i=1\}}^{N_f} \left[\prod_{i=1}^{4} \int \mathrm{d}\mathbf{k}_i^{\mathsf{B}} \right] \left\{ \lambda^{B\{N_i\};\{\sigma_i\}}_{\{k^{\mathsf{B}}_{i;N_i}\}} \delta_{1^B+2^B,3^B+4^B} \right. \\ & \left. \psi^{\mathsf{B}\dagger}_{N_1,\sigma_1,j_1}(\mathbf{k}_1^{\mathsf{B}}) \psi^{\mathsf{B}\dagger}_{N_2,\sigma_2,j_2}(\mathbf{k}_2^{\mathsf{B}}) \psi^{\mathsf{B}}_{N_3,\sigma_3,j_2}(\mathbf{k}_3^{\mathsf{B}}) \psi^{\mathsf{B}}_{N_4,\sigma_4,j_1}(\mathbf{k}_4^{\mathsf{B}}) \right\} \\ & + M^B \sum_{N=1}^{8} \sum_{\sigma=1}^{N_c} \sum_{j=1}^{N_f} \int \mathrm{d}\mathbf{k}^{\mathsf{B}}\ \psi^{\mathsf{B}\dagger}_{N,\sigma,j}(\mathbf{k}^B) \psi^{\mathsf{B}}_{N,\sigma,j}(\mathbf{k}^{\mathsf{B}}) + \frac{m^{\mathsf{B}}}{4} \int \mathrm{d}\mathbf{k}^{\mathsf{B}}\ \mathrm{Tr}\left[\Phi^{\mathsf{B}}(\mathbf{k}^{\mathsf{B}}) \Phi^{\mathsf{B}}(-\mathbf{k}^{\mathsf{B}}) \right], \end{aligned} \tag{2.36}$$

where $\delta_{1^B+2^B,3^B+4^B} \equiv (2\pi)^3 \delta(\mathbf{k}_1^{\mathsf{B}} + \mathbf{k}_2^{\mathsf{B}} - \mathbf{k}_3^{\mathsf{B}} - \mathbf{k}_4^{\mathsf{B}})$, and

$$\begin{aligned} & k_0^{\mathsf{B}} = Z_\tau k_0, \quad \vec{k}^{\mathsf{B}} = \vec{k}, \quad k_F^B = \mu \tilde{k}_F, \quad \Lambda^B = \mu \tilde{\Lambda}, \\ & \psi^{\mathsf{B}}_{N,\sigma,j}(\mathbf{k}^{\mathsf{B}}) = \sqrt{Z^{(\psi,N)}(k_N)} \psi_{N,\sigma,j}(\mathbf{k}), \quad \Phi^{\mathsf{B}}_{\sigma'\sigma}(\mathbf{q}^{\mathsf{B}}) = \sqrt{Z^{(\Phi)}} \Phi_{\sigma'\sigma}(\mathbf{q}), \\ & v^{\mathsf{B}(N)}_{k^{\mathsf{B}}} = \frac{Z_2^{(N)}(k)}{Z_3^{(N)}(k)} v_k^{(N)}, \quad V^{\mathsf{B}(N)}_{\mathrm{F},k^{\mathsf{B}}} = Z_\tau \frac{Z_3^{(N)}(k)}{Z_1^{(N)}(k)} V^{(N)}_{\mathrm{F},k}, \\ & g^{\mathsf{B}(N)}_{k'^{\mathsf{B}},k^{\mathsf{B}}} = \frac{Z_1(0)}{Z_4(0,0)} \sqrt{\frac{Z_2(0)}{Z_3(0)}} \frac{Z_4^{(N)}(k', k)}{\sqrt{Z_1^{(N)}(k') Z_1^{(\bar{N})}(k)}} g^{(N)}_{k',k}, \\ & \lambda^{B\{N_i\};\{\sigma_i\}}_{\{k_i^{\mathsf{B}}\}} = \mu^{-1} Z_\tau^{-3} \left[\prod_{i=1}^{4} Z^{(\psi,N_i)}(k_i) \right]^{-\frac{1}{2}} Z^{\{N_i\};\{\sigma_i\}}(\{k_i\}) \lambda^{\{N_i\};\{\sigma_i\}}_{\{k_i\}} \end{aligned} \tag{2.37}$$

with

$$Z^{(\psi,N)}(k) = \frac{Z_1^{(N)}(k)}{Z_\tau^2}, \quad Z^{(\Phi)} = \frac{Z_4^2(0,0) Z_3(0)}{Z_1^2(0) Z_2(0)}, \quad Z_\tau = \frac{Z_1(0)}{Z_3(0)}. \tag{2.38}$$

$Z_i^{(N)}(k) \equiv 1 + A_i^{(N)}(k)$ with $i = 1, 2, 3$, $Z_4^{(N)}(k', k) \equiv 1 + A_4^{(N)}(k', k)$ and $Z^{\{N_i\};\{\sigma_i\}}(\{k_i\}) \equiv 1 + A^{\{N_i\};\{\sigma_i\}}(\{k_i\})$ are the momentum-dependent multiplicative renormalization factors. $Z_i(0) = Z_i^{(N)}(0)$ for any N due to the C_4 symmetry. The field renormalization of the electron depends on momentum because gapless electronic modes are labeled by the momentum along the Fermi surface. On the contrary, the bosonic field is rescaled in a momentum-independent way because the boson has zero

energy only at one point in the momentum space. The frequency is also rescaled with the momentum-independent scaling factor, Z_τ. If we keep only the momentum independent pieces in the Taylor series of the coupling functions, these expressions reduce to those for the hot spot theory[182]. $\tilde{k}_F$ and $\tilde{\Lambda}$ represent the dimensionless size of Fermi surface and the UV energy cutoff measured in the unit of μ, respectively.

We denote the renormalized vertex function for $2m$ fermions at hot spots $\{N_i\}$ and n bosons as

$$\Gamma^{(2m,n);\{N_j\}}\left(\mathbf{k}_i;\left[v,g,V_{\rm F},\lambda^{\{M_i\};\{\sigma_i\}}\right];\tilde{k}_F,\tilde{\Lambda};\mu\right). \tag{2.39}$$

The vertex function depends on all external three-momenta, $\{\mathbf{k}_i\}$. It is also a functional of the coupling functions, $v_k, V_{{\rm F},k}, g_{k',k}, \lambda^{\{M_i\};\{\sigma_i\}}_{\{k_i\}}$. In general, the vertex function at a set of external momenta can depend on coupling functions at different momenta. The vertex function can also depend on $\tilde{\Lambda}$ and $\tilde{k}_F$. Although $\tilde{\Lambda}$ does not play any important role at low energies, for now both $\tilde{\Lambda}$ and $\tilde{k}_F$ are kept in Eq. (2.39) to contrast their different roles. It also depends on scale μ at which the coupling functions are defined in terms of the vertex functions. Using the facts that the bare vertex function is independent of μ and the vertex function has the scaling dimension $(3-2m-n)$ at the tree-level, we obtain the RG equation,

$$\begin{aligned}
&\Bigg\{(2m+n-1)z-2+n\eta^{(\Phi)}+\sum_{j=1}^{2m}\eta^{(\psi,N_j)}_{k_{N_j}}+\sum_{j=1}^{2m+n-1}\left[zk_{j;0}\frac{\partial}{\partial k_{j;0}}+\vec{k}_j\cdot\frac{\partial}{\partial\vec{k}_j}\right]\\
&-\beta_{\tilde{k}_F}\frac{\partial}{\partial\tilde{k}_F}-\beta_{\tilde{\Lambda}}\frac{\partial}{\partial\tilde{\Lambda}}-\int{\rm d}p\left(\left[p\frac{\partial v_p}{\partial p}+\beta^{(v)}_p\right]\frac{\delta}{\delta v_p}+\left[p\frac{\partial V_{{\rm F},p}}{\partial p}+\beta^{(V_{\rm F})}_p\right]\frac{\delta}{\delta V_{{\rm F},p}}\right)\\
&-\int{\rm d}p_1{\rm d}p_2\left(p_1\frac{\partial g_{p_1,p_2}}{\partial p_1}+p_2\frac{\partial g_{p_1,p_2}}{\partial p_2}+\beta^{(g)}_{p_1,p_2}\right)\frac{\delta}{\delta g_{p_1,p_2}}\\
&-\sum_{\{M_i\}}\sum_{\{\sigma_i\}}\sum_{\{j_i\}}\int{\rm d}p_1{\rm d}p_2{\rm d}p_3\left(\sum_{\{p_i\}}p_i\frac{\partial\lambda^{\{M_i\};\{\sigma_i\}}_{\{p_i\}}}{\partial p_i}+\beta^{(\lambda);\{M_i\};\{\sigma_i\}}_{\{p_i\}}\right)\frac{\delta}{\delta\lambda^{\{M_i\};\{\sigma_i\}}_{\{p_i\}}}\Bigg\}\\
&\times\Gamma^{(2m,n);\{N_j\}}(\{\mathbf{k}_i\};[V_{\rm F},v,g,\lambda];\tilde{k}_F,\tilde{\Lambda};\mu)=0.
\end{aligned} \tag{2.40}$$

$\delta/\delta\mathsf{A}$ denotes the functional derivative with respect to A with A denoting the momentum-dependent coupling functions. The dynamical critical exponent, the anomalous scaling dimensions, the beta functionals of the coupling functions, and the 'beta functions' for $\tilde{k}_F$ and $\tilde{\Lambda}$ are defined by

$$\begin{aligned}
z=&1+\frac{{\rm d}\log Z_\tau}{{\rm d}\log\mu}, & \beta^{(\tilde{k}_F)}=&\frac{{\rm d}\tilde{k}_F}{{\rm d}\log\mu}, & \beta^{(\tilde{\Lambda})}=&\frac{{\rm d}\tilde{\Lambda}}{{\rm d}\log\mu},\\
\eta^{(\psi,N)}_k=&\frac{1}{2}\frac{{\rm d}\log Z^{(\psi,N)}(k)}{{\rm d}\log\mu}, & \eta^{(\Phi)}=&\frac{1}{2}\frac{{\rm d}\log Z^{(\Phi)}}{{\rm d}\log\mu}, & \beta^{(v)}_k=&\frac{{\rm d}v_k}{{\rm d}\log\mu},\\
\beta^{(V_{\rm F})}_k=&\frac{{\rm d}V_{{\rm F},k}}{{\rm d}\log\mu}, & \beta^{(g)}_{k_1,k_2}=&\frac{{\rm d}g_{k_1,k_2}}{{\rm d}\log\mu}, & \beta^{(\lambda);\{N_i\};\{\sigma_i\}}_{\{k_i\}}=&\frac{{\rm d}\lambda^{\{N_i\};\{\sigma_i\}}_{\{k_i\}}}{{\rm d}\log\mu},
\end{aligned} \tag{2.41}$$

where the bare parameters are fixed in the derivatives. It is noted that due to the C_4 symmetry, we only need to keep track of one coupling function for each of the nesting angle, Fermi velocity and the Yukawa coupling as is shown in Eq. (2.17). Furthermore, the fermion anomalous dimensions at different hot spots can be written in terms of one function as

$$\eta^{(\psi,N)}_k=\begin{cases}\eta^{(\psi)}_k, & N=1,3,4,6\\ \eta^{(\psi)}_{-k}, & N=2,5,7,8\end{cases}. \tag{2.42}$$

From Eq. (2.37), one can express the beta functionals in terms of the counter terms as

$$\beta_k^{(v)} = v_k \left(\frac{\mathrm{d}\log Z_3(k)}{\mathrm{d}\log\mu} - \frac{\mathrm{d}\log Z_2(k)}{\mathrm{d}\log\mu} \right), \tag{2.43}$$

$$\beta_k^{(V_F)} = V_{F,k} \left(\frac{\mathrm{d}\log Z_1(k)}{\mathrm{d}\log\mu} - \frac{\mathrm{d}\log Z_3(k)}{\mathrm{d}\log\mu} - \frac{\mathrm{d}\log Z_1(0)}{\mathrm{d}\log\mu} + \frac{\mathrm{d}\log Z_3(0)}{\mathrm{d}\log\mu} \right), \tag{2.44}$$

$$\begin{aligned}\beta_{k',k}^{(g)} =& g_{k',k} \left(\left[\frac{\mathrm{d}\log Z_4(0,0)}{\mathrm{d}\log\mu} - \frac{\mathrm{d}\log Z_1(0)}{\mathrm{d}\log\mu} - \frac{1}{2}\frac{\mathrm{d}\log Z_2(0)}{\mathrm{d}\log\mu} + \frac{1}{2}\frac{\mathrm{d}\log Z_3(0)}{\mathrm{d}\log\mu} \right] \right. \\ & \left. - \frac{\mathrm{d}\log Z_4(k',k)}{\mathrm{d}\log\mu} + \frac{1}{2}\frac{\mathrm{d}\log Z_1(k')}{\mathrm{d}\log\mu} + \frac{1}{2}\frac{\mathrm{d}\log Z_1(k)}{\mathrm{d}\log\mu} \right),\end{aligned} \tag{2.45}$$

$$\begin{aligned}&\beta_{\{k_i\}}^{(\lambda);\{N_i\};\{\sigma_i\}} = \\ &\lambda_{\{k_i\}}^{\{N_i\};\{\sigma_i\}} \left(1 - \frac{\mathrm{d}\log Z_1(0)}{\mathrm{d}\log\mu} + \frac{\mathrm{d}\log Z_3(0)}{\mathrm{d}\log\mu} + \frac{1}{2}\sum_j \frac{\mathrm{d}\log Z_1(k_j)}{\mathrm{d}\log\mu} - \frac{\mathrm{d}\log Z^{\{N_i\};\{\sigma_i\}}(\{k_i\})}{\mathrm{d}\log\mu} \right),\end{aligned} \tag{2.46}$$

$$\beta^{(\tilde{k}_F)} = -\tilde{k}_F, \qquad \beta^{(\tilde{\Lambda})} = -\tilde{\Lambda}, \tag{2.47}$$

and the dynamical critical exponent and the anomalous dimensions as

$$z = 1 + \frac{\mathrm{d}\log Z_1(0)}{\mathrm{d}\log\mu} - \frac{\mathrm{d}\log Z_3(0)}{\mathrm{d}\log\mu}, \tag{2.48}$$

$$\eta_k^{(\psi)} = \frac{1}{2}\frac{\mathrm{d}\log Z_1(k)}{\mathrm{d}\log\mu} - \frac{\mathrm{d}\log Z_1(0)}{\mathrm{d}\log\mu} + \frac{\mathrm{d}\log Z_3(0)}{\mathrm{d}\log\mu}, \tag{2.49}$$

$$\eta^{(\Phi)} = \frac{\mathrm{d}\log Z_4(0,0)}{\mathrm{d}\log\mu} - \frac{\mathrm{d}\log Z_1(0)}{\mathrm{d}\log\mu} + \frac{1}{2}\frac{\mathrm{d}\log Z_3(0)}{\mathrm{d}\log\mu} - \frac{1}{2}\frac{\mathrm{d}\log Z_2(0)}{\mathrm{d}\log\mu}. \tag{2.50}$$

The beta functionals and the anomalous dimensions are obtained by replacing $\frac{\mathrm{d}Z_i(k)}{\mathrm{d}\log\mu}$ with

$$\begin{aligned}\frac{\mathrm{d}Z_i(k)}{\mathrm{d}\log\mu} =& \frac{\partial A_i(k)}{\partial\log\mu} + \int dp \frac{\delta A_i(k)}{\delta v_p}\beta_p^{(v)} + \int dp \frac{\delta A_i(k)}{\delta V_{F,p}}\beta_p^{(V_F)} + \int dp' dp \frac{\delta A_i(k)}{\delta g_{p',p}}\beta_{p',p}^{(g)} \\ & + \int dp_1 dp_2 dp_3 \, \frac{1}{\mu}\frac{\delta A_i(k)}{\delta\bar{\lambda}_{\{p_i\}}^{\{N_i\};\{\sigma_i\}}}\bigg|_{\bar{\lambda}=\lambda\mu^{-1}} \left(-\lambda_{\{p_i\}}^{\{N_i\};\{\sigma_i\}} + \beta_{\{k_i\}}^{(\lambda);\{N_i\};\{\sigma_i\}} \right)\end{aligned} \tag{2.51}$$

in Eqs. (2.43) - (2.50), and solve the resulting integro-differential equations for the beta functionals and the anomalous dimensions.

The beta functionals in Eqs. (2.43)-(2.47) describe the flow of the momentum-dependent coupling functions with increasing energy scale μ at fixed external momenta. In Eq. (2.40), the beta functionals appear along with the momentum dilation. This is due to the fact that the scale transformation rescales momentum in all directions. The momentum along the Fermi surface needs to be scaled together with the momentum perpendicular to the Fermi surface because change of momentum along the Fermi surface in non-forward scatterings is proportional to the momentum of the boson that carries a non-zero dimension. The momentum along the Fermi surface plays a dual role[205]. On the one hand, it labels gapless modes on the Fermi surface, and the momentum-dependent coupling functions encode how low-energy vertex functions vary along the Fermi surface. On the other hand, the momentum acts as a scale and is rescaled under the scale transformation. z represents the dynamical critical exponent that determines how the frequency is scaled relative to spatial momentum to keep Eq. (2.30).

Eq. (2.40) relates the vertex function of a theory at one set of frequencies and momenta with the vertex function of another theory with generally different couplings at rescaled frequencies and

momenta as

$$\begin{aligned}
&\varGamma^{(2m,n);\{N_j\}}(\{\mathbf{k}_i\};[\hat{v},\hat{g},\hat{V}_{\rm F}];\tilde{k}_F,\tilde{\Lambda}) \\
&= \exp\left\{\int_0^\ell \mathrm{d}\ell' \left[(2m+n-1)z(\ell') - 2 + n\eta^{(\Phi)}(\ell') + \sum_{j=1}^{2m}\hat{\eta}^{(\psi,N_j)}_{k_{N_j}(\ell')}(\ell')\right]\right\} \\
&\times \varGamma^{(2m,n);\{N_j\}}\left(\{k_{i,0}(\ell),\vec{k}_i(\ell)\};\left[\hat{v}(\ell),\hat{g}(\ell),\hat{V}_{\rm F}(\ell),\hat{\lambda}^{\{N_i\};\{\sigma_i\}}(\ell)\right];\tilde{k}_F(\ell),\tilde{\Lambda}(\ell)\right).
\end{aligned} \tag{2.52}$$

Here,

$$k_0(\ell) \equiv e^{\int_0^\ell z(\ell')\mathrm{d}\ell'} k_0, \qquad \vec{k}(\ell) \equiv e^\ell \vec{k}. \tag{2.53}$$

ℓ is the logarithmic length scale. The scale-dependent coupling functions obey

$$\frac{\partial\hat{v}_K(\ell)}{\partial\ell} = -\beta^{(v)}_K(\ell) - K\frac{\partial\hat{v}_K(\ell)}{\partial K}, \tag{2.54}$$

$$\frac{\partial\hat{V}_{{\rm F},K}(\ell)}{\partial\ell} = -\beta^{(V_{\rm F})}_K(\ell) - K\frac{\partial\hat{V}_{{\rm F},K}(\ell)}{\partial K}, \tag{2.55}$$

$$\frac{\partial\hat{g}_{K',K}(\ell)}{\partial\ell} = -\beta^{(g)}_{K',K}(\ell) - K'\frac{\partial\hat{g}_{K',K}(\ell)}{\partial K'} - K\frac{\partial\hat{g}_{K',K}(\ell)}{\partial K}, \tag{2.56}$$

$$\frac{\partial\hat{\lambda}^{\{N_i\};\{\sigma_i\}}_{\{K_i\}}(\ell)}{\partial\ell} = -\beta^{(\lambda);\{N_i\};\{\sigma_i\}}_{\{K_i\}}(\ell) - \sum_{j=1}^{4} K_j\frac{\partial\hat{\lambda}^{\{N_i\};\{\sigma_i\}}_{\{K_i\}}(\ell)}{\partial K_j}, \tag{2.57}$$

$$\frac{\partial\tilde{k}_F(\ell)}{\partial\ell} = \tilde{k}_F(\ell), \qquad \frac{\partial\tilde{\Lambda}(\ell)}{\partial\ell} = \tilde{\Lambda}(\ell) \tag{2.58}$$

with the initial conditions, $\hat{v}_K(0) = \hat{v}_K$, $\hat{V}_{{\rm F},K}(0) = \hat{V}_{{\rm F},K}$, $\hat{g}_{K',K}(0) = \hat{g}_{K',K}$, $\hat{\lambda}^{\{N_i\};\{\sigma_i\}}_{\{K_i\}}(0) = \hat{\lambda}^{\{N_i\};\{\sigma_i\}}_{\{K_i\}}$, $\tilde{k}_F(0) = \tilde{k}_F$ and $\tilde{\Lambda}(0) = \tilde{\Lambda}$. $\hat{\eta}^{(\psi,N)}_{ke^\ell}(\ell)$ denotes the anomalous dimension of the fermion measured at momentum ke^ℓ and energy scale Λ in the theory with coupling functions, $\{\hat{v}(\ell),\ \hat{g}(\ell),\ \hat{V}_{\rm F}(\ell),\ \hat{\lambda}^{\{N_i\};\{\sigma_i\}}(\ell)\}$. Eq. (2.52) relates a physical observable measured at $\{k_{i,0},\vec{k}_i\}$ in the theory with Fermi surface size $\mu\tilde{k}_F$, UV cutoff $\mu\tilde{\Lambda}$ and couplings $\{\hat{v},\ \hat{g},\ \hat{V}_{\rm F},\ \lambda^{\{N_i\};\{\sigma_i\}}\}$ to the observable measured at $\{e^{\int_0^\ell z(\ell')\mathrm{d}\ell'} k_{i,0}, e^\ell\vec{k}_i\}$ in the theory with Fermi surface size $e^\ell\mu\tilde{k}_F$, UV cutoff $e^\ell\mu\tilde{\Lambda}$ and couplings $\{\hat{v}(\ell),\ \hat{g}(\ell),\ \hat{V}_{\rm F}(\ell),\ \hat{\lambda}^{\{N_i\};\{\sigma_i\}}(\ell)\}$. It is noted that the RG equation relates observables in two theories not just with different UV cutoffs but with different sizes of Fermi surface, that is, with different numbers of IR degrees of freedom. Fixed points are characterized by coupling functions $\{\hat{v}^*,\ \hat{g}^*\ \hat{V}^*_{\rm F},\ \hat{\lambda}^{\{N_i\};\{\sigma_i\}*}\}$ at which the beta functionals in Eqs. (2.54)-(2.57) vanish, and $\tilde{\Lambda}^* = \infty$, $\tilde{k}^*_F = \infty$. If the physical observables can be expressed as regular functions of the renormalized couplings in the large Λ limit, we can set $\Lambda^* = \infty$ at the fixed point as is usually done in the continuum limit. On the other hand, k_F is an IR parameter of the theory that encapsulates the number of gapless modes in the system. Since there is no guarantee that all low-energy physical observables are well defined in the large k_F limit, we can not simply ignore the dependence on k_F as we do for Λ. This has an obvious consequence: *theories with Fermi surfaces do not have the usual sense of scale invariance that relates observables defined at different scales within one theory even in the continuum limit.* Consequently, Eq. (2.52) does not fully determine how physical observables actually scale with energy and momentum in a theory with a fixed k_F. Only for those vertex functions that are regular in the large k_F limit, $\left[(2m+n-1)z^* - 2 + n\eta^{(\Phi)^*} + \sum_{j=1}^{2m}\hat{\eta}^{(\psi)*}_{k_{N_j}}\right]$ in Eq. (2.52) determines the actual dependence on energy and momentum. For those observables that are singular in the large k_F limit, the scaling behaviour is modified from what is expected from the predicted scaling dimensions[9]. There is even no

[9]For example, the response functions to spatially uniform thermal/electromagnetic perturbations are sensitive to k_F.

guarantee that general low-energy observables depend on energy and momentum in power laws at a fixed point[133, 132]. Without knowing how general observables depend on k_F in priori, one has to keep k_F as a running coupling within the theory.

It is noted that the four-fermion couplings has dimension -1 at the tree-level. This causes the four-fermion couplings to decrease in amplitude under the RG flow. On the other hand, the momentum along the Fermi surface is rescaled, and the size of the Fermi surface measured in the unit of the running energy scale increases. This effectively promotes the four-fermion couplings to marginal couplings in the channels in which quantum corrections become proportional to the phase space. For example, this enhancement of the effective scaling dimension occurs in the pairing channel in which the phase space for low-energy Cooper pairs is extensive.

In keeping track of the momentum dependent coupling functions along the Fermi surface, it is sometimes convenient to define coupling functions at a fixed physical location on the Fermi surface as

$$\begin{aligned} &v_k(\ell) \equiv \hat{v}_{k(\ell)}(\ell), \quad V_{\mathrm{F},k}(\ell) \equiv \hat{V}_{\mathrm{F},k(\ell)}(\ell), \quad \eta_k^{(\psi)}(\ell) \equiv \hat{\eta}_{k(\ell)}^{(\psi)}(\ell), \\ &g_{k',k}(\ell) \equiv \hat{g}_{k'(\ell),k(\ell)}(\ell), \quad \lambda_{\{k_i\}}^{\{N_i\};\{\sigma_i\}}(\ell) \equiv \hat{\lambda}_{\{k_i(\ell)\}}^{\{N_i\};\{\sigma_i\}}(\ell). \end{aligned} \tag{2.59}$$

$v_k(\ell), V_{\mathrm{F},k}(\ell)$, $g_{k',k}(\ell)$ and $\lambda_{\{k_i\}}^{\{N_i\};\{\sigma_i\}}(\ell)$ satisfy the beta functionals that do not have the momentum dilatation,

$$\frac{\partial}{\partial \ell} v_k(\ell) = -\beta_k^{(v)}(\ell), \tag{2.60}$$

$$\frac{\partial}{\partial \ell} V_{\mathrm{F},k}(\ell) = -\beta_k^{(V_F)}(\ell), \tag{2.61}$$

$$\frac{\partial}{\partial \ell} g_{k',k}(\ell) = -\beta_{k',k}^{(g)}(\ell), \tag{2.62}$$

$$\frac{\partial}{\partial \ell} \lambda_{\{k_i\}}^{\{N_i\};\{\sigma_i\}}(\ell) = -\beta_{\{k_i\}}^{(\lambda);\{N_i\};\{\sigma_i\}}(\ell). \tag{2.63}$$

Eqs. (2.60) to (2.63) track the renormalization of the coupling functions with increasing logarithmic length scale ℓ at fixed momenta along the Fermi surface. It will be useful to go back and forth between Eqs. (2.54)-(2.57) and Eqs. (2.60)- (2.63)for different purposes. The ultimate fate of the system in the low-energy limit is determined by the RG flow of the full coupling functions, $\Big\{ v_k(\ell),\, V_{\mathrm{F},k}(\ell),\, g_{k',k}(\ell),\, \lambda_{\{k_i\}}^{\{N_i\};\{\sigma_i\}}(\ell) \Big\}$.

2.4.4 Quantum effective action

The full quantum effective action is written as

$$\begin{aligned} \mathbf{\Gamma} = &\sum_{N=1}^{8} \sum_{\sigma=1}^{N_c} \sum_{j=1}^{N_f} \int \mathrm{d}\mathbf{k}\ \psi_{N,\sigma,j}^{\dagger}(\mathbf{k}) \left\{ ik_0 + V_{\mathrm{F},k_N}^{(N)} e_N[\vec{k}; v_{k_N}^{(N)}] + \mathbf{\Sigma}_N(\mathbf{k}) \right\} \psi_{N,\sigma,j}(\mathbf{k}) \\ &+ \frac{1}{4} \int \mathrm{d}\mathbf{k}\ D^{-1}(\mathbf{k}) \mathrm{Tr}\left[\Phi(\mathbf{k})\Phi(-\mathbf{k})\right] \\ &+ \sum_{N=1}^{8} \sum_{\sigma\sigma'=1}^{N_c} \sum_{j=1}^{N_f} \int \mathrm{d}\mathbf{k}'\mathrm{d}\mathbf{k}\ \left\{ \frac{1}{\sqrt{N_f}} g_{k'_N,k_N}^{(N)} + \delta\mathbf{\Gamma}_N^{(2,1)}(\mathbf{k}',\mathbf{k}) \right\} \psi_{N,\sigma',j}^{\dagger}(\mathbf{k}') \Phi_{\sigma'\sigma}(\mathbf{k}'-\mathbf{k}) \psi_{\bar{N},\sigma,j}(\mathbf{k}) \\ &+ \sum_{\{N_i=1\}}^{8} \sum_{\{\sigma_i=1\}}^{N_c} \sum_{\{j_i=1\}}^{N_f} \int \prod_{i=1}^{4} \mathrm{d}\mathbf{k}_i \delta_{1+2,3+4} \left\{ \frac{1}{4\mu} \lambda^{\binom{N_1\ N_2}{N_4\ N_3};\binom{\sigma_1\ \sigma_2}{\sigma_4\ \sigma_3}}_{\binom{k_{1;N_1}\ k_{2;N_2}}{k_{4,N_4}\ k_{3;N_3}}} \right. \\ &\left. + \delta\mathbf{\Gamma}^{\binom{N_1\ N_2}{N_4\ N_3};\binom{\sigma_1\ \sigma_2}{\sigma_4\ \sigma_3}}(\{\mathbf{k}_{i;N_i}\}) \right\} \psi_{N_1,\sigma_1,j_1}^{\dagger}(\mathbf{k}_1) \psi_{N_2,\sigma_2,j_2}^{\dagger}(\mathbf{k}_2) \psi_{N_3,\sigma_3,j_2}(\mathbf{k}_3) \psi_{N_4,\sigma_4,j_1}(\mathbf{k}_4) + ..., \end{aligned} \tag{2.64}$$

where ... represents higher order terms in the fields. Here $D^{-1}(\mathbf{k})$ is the boson self-energy. Since the bare kinetic term of the boson is irrelevant, the self-energy determines the entire boson propagator at low energies. $\mathbf{\Sigma}_N(\mathbf{k})$ is the fermion self-energy. $\delta\mathbf{\Gamma}_N^{(2,1)}(\mathbf{k}', \mathbf{k})$ is the quantum correction to the Yukawa vertex. Finally, $\delta\mathbf{\Gamma}^{\binom{N_1\ N_2}{N_4\ N_3};\binom{\sigma_1\ \sigma_2}{\sigma_4\ \sigma_3}}(\{\mathbf{k}_{i;N_i}\})$ represents the quantum correction to the four-fermion coupling function.

In the present theory, the computation of the quantum effective action is organized in terms of the small parameter $v \sim g^2$. At the zeroth order in v, only $D^{-1}(\mathbf{k})$ is important among all quantum corrections. The infinite set of diagrams that contribute to the boson self-energy to the leading order in v can be summed through the Schwinger-Dyson equation in Fig. 2.1[182]. Other quantum corrections are at most order of $\frac{g^2}{c}\log(1/v) \sim \sqrt{v\log(1/v)}$ in the small v limit, and can be computed perturbatively as functionals of the coupling functions. The four-fermion couplings that is generated from the Yukawa coupling through Fig. 2.7 is order of g^4/c, where the phase space enhancement factor of $1/c$ arises because the largest speed of particles in the loop is c in one momentum direction. The interaction energy of two particles, given by the eigenvalues of the quartic vertex as in Eq. (2.32), goes as g^4/c^2, where there is an additional factor of $1/c$ because the typical momentum transfer of particle goes as μ/c at energy scale μ[10]. Since $g^4/c^2 \sim v/\log(1/v)$ in the small v limit, the electron-electron interaction is dominated by the interaction mediated by the gapless spin fluctuations whose strength is order of $g^2/c \sim \sqrt{v/\log(1/v)}$. We will see that there exists a large window of energy scale in which the four-fermion coupling remains smaller than g^2/c before it becomes dominant due to superconducting instabilities at low energies. Within this window, the feedback of the four-fermion coupling to the self-energies and the cubic vertex can be ignored. Our goal is to extract the universal normal state properties and the evolution of superconducting fluctuations that emerge within this range of energy scale.

Two faces of the four-fermion coupling

Under the interaction driven scaling, the Yukawa coupling is marginal, and quantum corrections that include the Yukawa coupling are logarithmically divergent, as expected. On the contrary, the four-fermion coupling has dimension -1. Naively, one would not expect infrared divergences associated with the four-fermion coupling. However, the actual degrees of IR divergence vary in different diagrams. In most diagrams that include the four-fermion coupling, there is indeed no IR divergence as expected from power-counting. Some diagrams, however, exhibit logarithmic IR divergences, defying the expectation based on the scaling dimension.

This disagreement arises because the momentum along the Fermi surface plays different roles in different scattering processes. In diagrams that involve patches of Fermi surface that are not nested, a loop momentum that is parallel to the Fermi surface in one patch is not parallel to the Fermi surface in another patch. Consequently, all components of momentum need to be small in order for virtual fermions to stay close to the Fermi surface. In this case, all components of momenta act as scale in the loop, and the power counting correctly captures the absence of IR divergence. On the contrary, in diagrams that include only those patches that are nested, the component of momentum parallel to the patches act as a continuous flavour. For example, the four-fermion interaction in the pairing channel involves opposite sides of Fermi surface which are perfectly nested in the particle-particle channel. Because all virtual particles can stay close to the Fermi surface irrespective of the momentum along the Fermi surface, actual IR divergences are controlled by the one-dimensional scaling under which the four-fermion coupling is marginal. In other words, the integration of the momentum along the nested patches gives rise to a volume of the low-energy phase space, and the scale associated with the volume of the phase space effectively promotes the four-fermion couplings to marginal couplings, resulting in logarithmic IR divergences.

[10]For example, the eigenvalue of the four-fermion coupling function in the BCS channel involves an integral over relative momentum of a Cooper pair, and it is enhanced by $1/c$ due to the slow decay of the coupling function at large momentum in the small c limit. This will be shown through explicit calculations in Appendix B.

Quantum corrections

We start with the propagator of the collective mode. To the leading order in v, the dressed boson propagator $D(\mathbf{q})$ satisfies the Schwinger-Dyson equation with the momentum dependent coupling functions,

$$\begin{aligned} D^{-1}(\mathbf{k}) =& m_{CT} + 2\sum_{N=1}^{8}\int d\mathbf{q}\; g^{(N)}_{q,q+k} g^{(\bar{N})}_{q+k,q} G_N(\mathbf{q}) G_{\bar{N}}(\mathbf{q}+\mathbf{k}) \\ &- \frac{4}{N_c N_f}\sum_{N=1}^{8}\int \mathrm{d}\mathbf{q}\mathrm{d}\mathbf{p}\; g^{(\bar{N})}_{p,p+k} g^{(N)}_{p+k,p+q+k} g^{(\bar{N})}_{p+q+k,p+q} g^{(N)}_{p+q,p} \\ &\times G_N(\mathbf{p}+\mathbf{q}) G_{\bar{N}}(\mathbf{p}) G_N(\mathbf{p}+\mathbf{k}) G_{\bar{N}}(\mathbf{p}+\mathbf{q}+\mathbf{k}) D(\mathbf{q}), \end{aligned} \tag{2.65}$$

where m_{CT} is the mass counter term that tunes the renormalized mass of the boson to zero. $G_N(\mathbf{k})$ is the bare fermionic Green's function for hot spot N,

$$G_N(\mathbf{k}) = \frac{1}{ik_0 + V^{(N)}_{F,k} e_N[\vec{k}; v^{(N)}_k]}. \tag{2.66}$$

It is noted that $G_N(\mathbf{k})$ depends on momentum not only through the explicit momentum dependence in the dispersion but also through $V^{(N)}_{F,k}$ and $v^{(N)}_k$ that depend on the momentum along the Fermi surface. Here and henceforth, we drop the patch index N in k_N for the momentum along the Fermi surface when there is no danger of confusion. For $\lambda \ll g^2/c$, the contribution of the short-ranged four-fermion coupling to the boson self-energy is sub-leading in the small v limit. Since the bare kinetic term of the boson is irrelevant under the interaction driven scaling, we don't need to add any counter term for the boson except for the mass counter term. In other diagrams, we use the non-perturbatively dressed boson propagator.

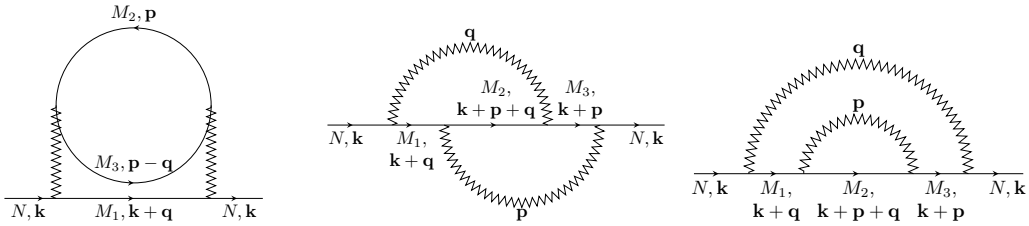

Figure 2.6: Contributions of the four-fermion coupling, represented by the zigzag lines, to the fermion self-energy.

To the leading order in v, the fermion self-energy is written as the sum of two terms as $\mathbf{\Sigma}_N(\mathbf{k}) = \mathbf{\Sigma}^{1\mathrm{L}}_N(\mathbf{k}) + \mathbf{\Sigma}^{2\mathrm{L}}_N(\mathbf{k})$ where

$$\mathbf{\Sigma}^{1\mathrm{L}}_N(\mathbf{k}) = -\frac{2(N_c^2-1)}{N_c N_f}\int \mathrm{d}\mathbf{q}\; g^{(N)}_{k,k+q} g^{(\bar{N})}_{k+q,k} G_{\bar{N}}(\mathbf{k}+\mathbf{q}) D(\mathbf{q}), \tag{2.67}$$

$$\begin{aligned} \mathbf{\Sigma}^{2\mathrm{L}}_N(\mathbf{k}) =& \frac{4(N_c^2-1)}{N_c^2 N_f^2}\int \mathrm{d}\mathbf{q}\int \mathrm{d}\mathbf{p}\; g^{(N)}_{k,k+q} g^{(\bar{N})}_{k+q,k+p+q} g^{(N)}_{k+p+q,k+p} g^{(\bar{N})}_{k+p,k} \\ &\times D(\mathbf{p}) D(\mathbf{q}) G_{\bar{N}}(\mathbf{k}+\mathbf{p}) G_N(\mathbf{k}+\mathbf{q}+\mathbf{p}) G_{\bar{N}}(\mathbf{k}+\mathbf{q}). \end{aligned} \tag{2.68}$$

Eq. (2.67) and Eq. (2.68) represent the one-loop and two-loop fermion self-energies generated from the Yukawa couplings as is shown in Fig. 2.2a and Fig. 2.2b respectively. To the leading order in v,

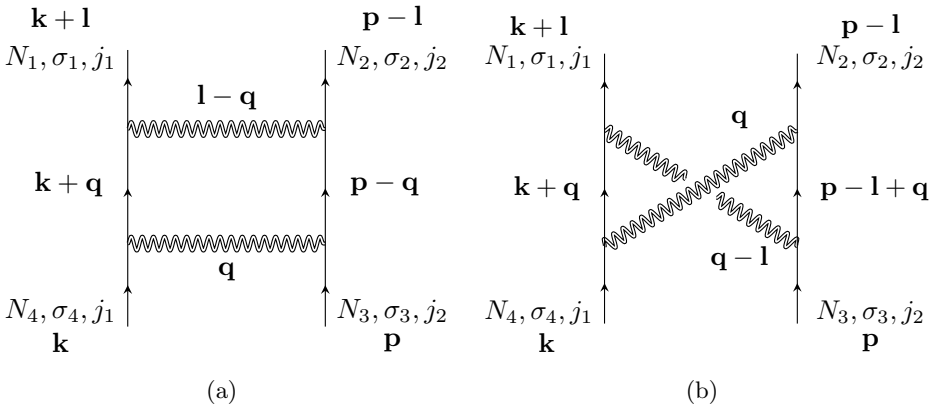

Figure 2.7: Quantum corrections to the four-fermion couplings that are independent of λ.

these are the only diagrams that are important[11]. The one-loop vertex correction shown in Fig. 2.2c is given by

$$\delta\mathbf{\Gamma}_1^{(2,1)}(\mathbf{k}',\mathbf{k}) = -\frac{2}{N_c N_f^{\frac{3}{2}}}\int \mathrm{d}\mathbf{q}\; g^{(N)}_{k',k'+q} g^{(\bar{N})}_{k'+q,k+q} g^{(N)}_{k+q,k}\; D(\mathbf{q}) G_{\bar{N}}(\mathbf{k}'+\mathbf{q}) G_N(\mathbf{k}+\mathbf{q}). \tag{2.70}$$

The contribution of the short-range four-fermion couplings to $\delta\mathbf{\Gamma}^{(2,1)}(\mathbf{k}',\mathbf{k})$ is sub-leading compared to Eq. (2.70).

The one-loop vertex correction to the four-fermion coupling is written as $\delta\mathbf{\Gamma}^{\{N_i\};\{\sigma_i\}} = \sum_{a=0}^{2}\mathbf{\Gamma}_{(a)}^{\{N_i\};\{\sigma_i\}}$, where $\mathbf{\Gamma}_{(a)}^{\{N_i\};\{\sigma_i\}}$ denotes the vertex correction that is of the a-th power of λ. The four-fermion vertex that is independent of λ is further divided into two parts as $\mathbf{\Gamma}_{(0)}^{\{N_i\};\{\sigma_i\}} = \mathbf{\Gamma}_{(0)PP}^{\{N_i\};\{\sigma_i\}} + \mathbf{\Gamma}_{(0)PH}^{\{N_i\};\{\sigma_i\}}$, where

$$\begin{aligned}\mathbf{\Gamma}_{(0)PP}^{\left(\begin{smallmatrix}N_1 & N_2\\ N_4 & N_3\end{smallmatrix}\right);\left(\begin{smallmatrix}\sigma_1 & \sigma_2\\ \sigma_4 & \sigma_3\end{smallmatrix}\right)}\left(\begin{smallmatrix}\mathbf{k+l} & \mathbf{p-l}\\ \mathbf{k} & \mathbf{p}\end{smallmatrix}\right) &= -\frac{1}{2N_f^2}\int \mathrm{d}\mathbf{q}\; g^{(N_1)}_{k+l,k+q} g^{(\bar{N}_4)}_{k+q,k} g^{(N_2)}_{p-l,p-q} g^{(\bar{N}_3)}_{p-q,p}\\ &\times D(\mathbf{q}) D(\mathbf{l}-\mathbf{q}) G_{\bar{N}_1}(\mathbf{k}+\mathbf{q}) G_{\bar{N}_2}(\mathbf{p}-\mathbf{q}) \delta_{N_1N_4}\delta_{N_2N_3} \mathsf{T}^{\sigma_1\sigma_2}_{\alpha\beta}\mathsf{T}^{\alpha\beta}_{\sigma_4\sigma_3}\end{aligned} \tag{2.71}$$

is the four-fermion vertex generated from the Yukawa coupling in the particle-particle channel (Fig. 2.7a), and

$$\begin{aligned}\mathbf{\Gamma}_{(0)PH}^{\left(\begin{smallmatrix}N_1 & N_2\\ N_4 & N_3\end{smallmatrix}\right);\left(\begin{smallmatrix}\sigma_1 & \sigma_2\\ \sigma_4 & \sigma_3\end{smallmatrix}\right)}\left(\begin{smallmatrix}\mathbf{k+l} & \mathbf{p-l}\\ \mathbf{k} & \mathbf{p}\end{smallmatrix}\right) &= -\frac{1}{2N_f^2}\int \mathrm{d}\mathbf{q}\; g^{(N_1)}_{k+l,k+q} g^{(\bar{N}_4)}_{k+q,k} g^{(N_2)}_{p-l,p-l+q} g^{(\bar{N}_3)}_{p-l+q,p}\times\\ &D(\mathbf{q}) D(\mathbf{l}-\mathbf{q}) G_{\bar{N}_1}(\mathbf{k}+\mathbf{q}) G_{\bar{N}_2}(\mathbf{p}-\mathbf{l}+\mathbf{q}) \delta_{N_1N_4}\delta_{N_2N_3} \mathsf{T}^{\beta\sigma_2}_{\sigma_4\alpha}\mathsf{T}^{\sigma_1\alpha}_{\beta\sigma_3}\end{aligned} \tag{2.72}$$

[11] The contribution of the four-fermion coupling to the fermion-self energy from Fig. 2.6 can be written as

$$\begin{aligned}\mathbf{\Sigma}_N^{\prime 2\mathrm{L}}(\mathbf{k}) =& \frac{1}{4\mu^2}\int \mathrm{d}\mathbf{q}\int \mathrm{d}\mathbf{p}\;\Bigg[N_f \lambda^{\left(\begin{smallmatrix}M_1 & M_3\\ N & M_2\end{smallmatrix}\right);\left(\begin{smallmatrix}\alpha_1 & \alpha_3\\ \sigma & \alpha_2\end{smallmatrix}\right)}_{\left(\begin{smallmatrix}k+q & p-q\\ k & p\end{smallmatrix}\right)} \lambda^{\left(\begin{smallmatrix}N & M_2\\ M_1 & M_3\end{smallmatrix}\right);\left(\begin{smallmatrix}\sigma & \alpha_2\\ \alpha_1 & \alpha_3\end{smallmatrix}\right)}_{\left(\begin{smallmatrix}k & p\\ k+q & p-q\end{smallmatrix}\right)} G_{M_1}(\mathbf{k}+\mathbf{q}) G_{M_2}(\mathbf{p}) G_{M_3}(\mathbf{p}+\mathbf{q})\\ &- \lambda^{\left(\begin{smallmatrix}M_1 & M_3\\ N & M_2\end{smallmatrix}\right);\left(\begin{smallmatrix}\alpha_1 & \alpha_3\\ \sigma & \alpha_2\end{smallmatrix}\right)}_{\left(\begin{smallmatrix}k+q & k+p\\ k & k+q+p\end{smallmatrix}\right)} \lambda^{\left(\begin{smallmatrix}M_2 & N\\ M_1 & M_3\end{smallmatrix}\right);\left(\begin{smallmatrix}\alpha_2 & \sigma\\ \alpha_1 & \alpha_3\end{smallmatrix}\right)}_{\left(\begin{smallmatrix}k+q+p & k\\ k+q & k+p\end{smallmatrix}\right)} G_{M_1}(\mathbf{k}+\mathbf{q}) G_{M_2}(\mathbf{k}+\mathbf{q}+\mathbf{p}) G_{M_3}(\mathbf{k}+\mathbf{p})\\ &- \lambda^{\left(\begin{smallmatrix}M_1 & N\\ N & M_3\end{smallmatrix}\right);\left(\begin{smallmatrix}\alpha_1 & \sigma\\ \sigma & \alpha_3\end{smallmatrix}\right)}_{\left(\begin{smallmatrix}k+q & k\\ k & k+q\end{smallmatrix}\right)} \lambda^{\left(\begin{smallmatrix}M_2 & M_3\\ M_1 & M_2\end{smallmatrix}\right);\left(\begin{smallmatrix}\alpha_2 & \alpha_3\\ \alpha_1 & \alpha_2\end{smallmatrix}\right)}_{\left(\begin{smallmatrix}k+q+p & k+q\\ k+q & k+p+q\end{smallmatrix}\right)} G_{M_1}(\mathbf{k}+\mathbf{q}) G_{M_2}(\mathbf{k}+\mathbf{q}+\mathbf{p}) G_{M_3}(\mathbf{k}+\mathbf{q})\Bigg].\end{aligned} \tag{2.69}$$

For $\lambda \ll g^2/c$, this is sub-leading compared to $\mathbf{\Sigma}_N^{1\mathrm{L}}(\mathbf{k})$ and $\mathbf{\Sigma}_N^{2\mathrm{L}}(\mathbf{k})$.

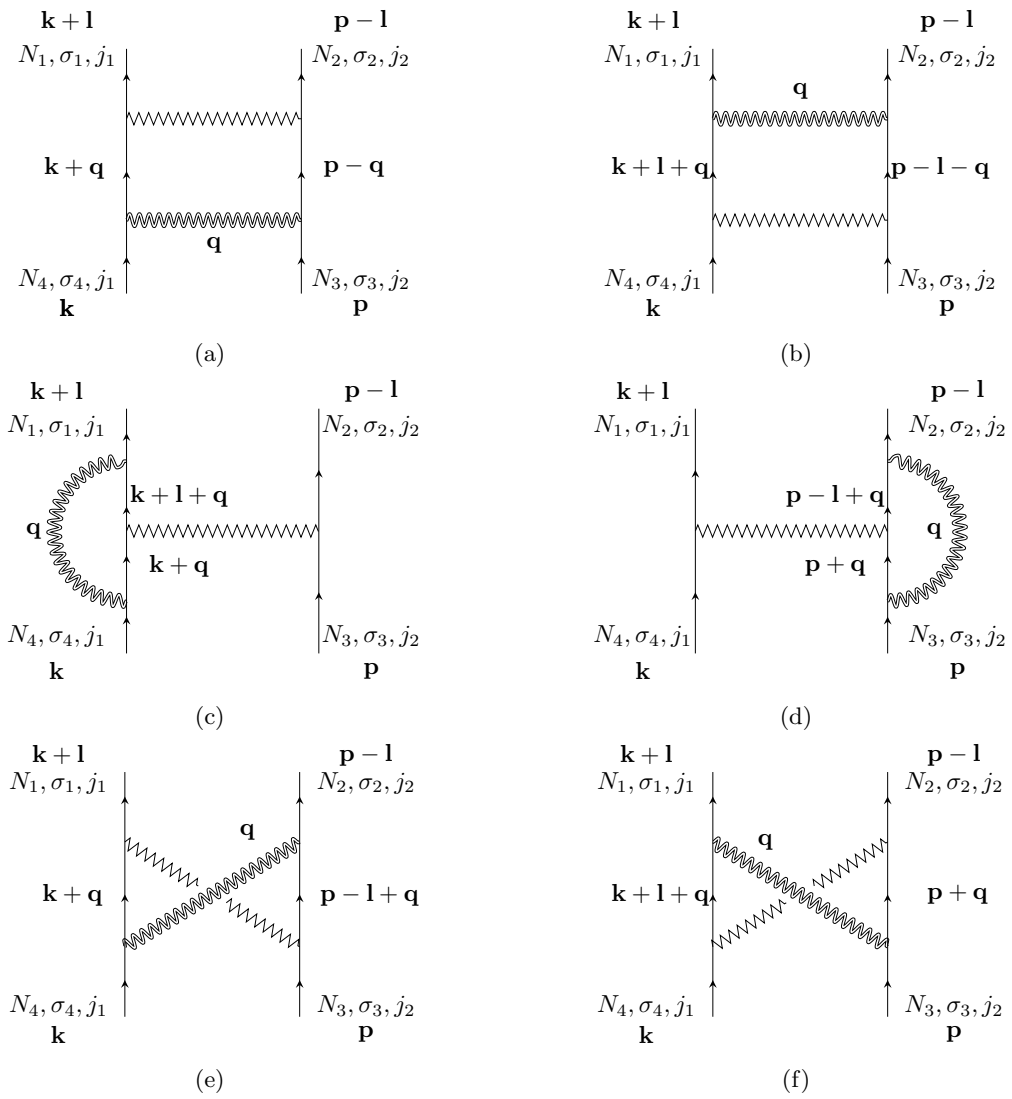

Figure 2.8: Quantum corrections to the four-fermion couplings linear in λ.

is the four-fermion vertex generated from the Yukawa coupling in the particle-hole channel (Fig. 2.7b). $\mathsf{T}^{\sigma_1\sigma_2}_{\sigma_4\sigma_3}$ is the spin structure factor for the interaction mediated by the critical spin fluctuations between incoming electrons with spin σ_4, σ_3 and outgoing electrons with spin σ_1, σ_2,

$$\mathsf{T}^{\sigma_1\sigma_2}_{\sigma_4\sigma_3} = \sum_{a=1}^{N_c^2-1} \tau^a_{\sigma_1\sigma_4}\tau^a_{\sigma_2\sigma_3} = 2\left(\delta_{\sigma_1\sigma_3}\delta_{\sigma_2\sigma_4} - \frac{1}{N_c}\delta_{\sigma_1\sigma_4}\delta_{\sigma_2\sigma_3}\right). \tag{2.73}$$

The four-fermion vertex that is linear in λ can be also divided into the one in which the vertex correction is in the particle-particle (PP) channel and the one in which the vertex correction is in the particle-hole (PH) channel, $\mathbf{\Gamma}_{(1)}^{\binom{N_1\ N_2}{N_4\ N_3};\binom{\sigma_1\ \sigma_2}{\sigma_4\ \sigma_3}} = \mathbf{\Gamma}_{(1)PP}^{\binom{N_1\ N_2}{N_4\ N_3};\binom{\sigma_1\ \sigma_2}{\sigma_4\ \sigma_3}} + \mathbf{\Gamma}_{(1)PH}^{\binom{N_1\ N_2}{N_4\ N_3};\binom{\sigma_1\ \sigma_2}{\sigma_4\ \sigma_3}}$. The vertex

correction in the PP channel (Figs. 2.8a and 2.8b) is

$$\begin{aligned}
&\mathbf{\Gamma}^{\binom{N_1\ N_2}{N_4\ N_3};\binom{\sigma_1\ \sigma_2}{\sigma_4\ \sigma_3}}_{(1)PP}\left(\begin{smallmatrix}\mathbf{k+l} & \mathbf{p-l}\\ \mathbf{k} & \mathbf{p}\end{smallmatrix}\right)\\
&= \frac{1}{4\mu N_f}\int d\mathbf{q}\; g^{(\overline{N}_4)}_{k+q,k} g^{(\overline{N}_3)}_{p-q,p} D(\mathbf{q}) G_{\overline{N}_4}(\mathbf{k}+\mathbf{q}) G_{\overline{N}_3}(\mathbf{p}-\mathbf{q}) \lambda^{\binom{N_1\ N_2}{\overline{N}_4\ \overline{N}_3};\binom{\sigma_1\ \sigma_2}{\alpha\ \ \beta}}_{\binom{k+l\ \ p-l}{k+q\ p-q}} \mathsf{T}^{\alpha\beta}_{\sigma_4\sigma_3}\\
&+ \frac{1}{4\mu N_f}\int d\mathbf{q}\; g^{(N_1)}_{k+l,k+l+q} g^{(N_2)}_{p-l,p-l-q} D(\mathbf{q}) G_{\overline{N}_1}(\mathbf{k}+\mathbf{l}+\mathbf{q}) G_{\overline{N}_2}(\mathbf{p}-\mathbf{l}-\mathbf{q}) \mathsf{T}^{\sigma_1\sigma_2}_{\alpha\beta} \lambda^{\binom{\overline{N}_1\ \overline{N}_2}{N_4\ \ N_3};\binom{\alpha\ \ \beta}{\sigma_4\ \sigma_3}}_{\binom{k+l+q\ \ p-l-q}{k\ \ \ \ p}},
\end{aligned} \tag{2.74}$$

and the vertex correction in the PH channel (Figs. 2.8c - 2.8f) is

$$\begin{aligned}
&\mathbf{\Gamma}^{\binom{N_1\ N_2}{N_4\ N_3};\binom{\sigma_1\ \sigma_2}{\sigma_4\ \sigma_3}}_{(1)PH}\left(\begin{smallmatrix}\mathbf{k+l} & \mathbf{p-l}\\ \mathbf{k} & \mathbf{p}\end{smallmatrix}\right)\\
&= \frac{1}{4\mu N_f}\int \mathrm{d}\mathbf{q}\; g^{(\overline{N}_4)}_{k+q,k} g^{(N_1)}_{k+l,k+l+q} D(\mathbf{q}) G_{\overline{N}_1}(\mathbf{k}+\mathbf{l}+\mathbf{q}) G_{\overline{N}_4}(\mathbf{k}+\mathbf{q}) \mathsf{T}^{\alpha\sigma_1}_{\sigma_4\beta} \lambda^{\binom{\overline{N}_1\ N_2}{\overline{N}_4\ N_3};\binom{\beta\ \sigma_2}{\alpha\ \sigma_3}}_{\binom{k+l+q\ \ p-l}{k+q\ \ \ p}}\\
&+ \frac{1}{4\mu N_f}\int \mathrm{d}\mathbf{q}\; g^{(\overline{N}_3)}_{p+q,p} g^{(N_2)}_{p-l,p-l+q} D(\mathbf{q}) G_{\overline{N}_3}(\mathbf{p}+\mathbf{q}) G_{\overline{N}_2}(\mathbf{p}-\mathbf{l}+\mathbf{q}) \mathsf{T}^{\alpha\sigma_2}_{\sigma_3\beta} \lambda^{\binom{N_1\ \overline{N}_2}{N_4\ \overline{N}_3};\binom{\sigma_1\ \beta}{\sigma_4\ \alpha}}_{\binom{k+l\ \ p-l+q}{k\ \ \ p+q}}\\
&+ \frac{1}{4\mu N_f}\int \mathrm{d}\mathbf{q}\; g^{(\overline{N}_4)}_{k+q,k} g^{(N_2)}_{p-l,p-l+q} D(\mathbf{q}) G_{\overline{N}_4}(\mathbf{k}+\mathbf{q}) G_{\overline{N}_2}(\mathbf{p}-\mathbf{l}+\mathbf{q}) \mathsf{T}^{\alpha\sigma_2}_{\sigma_4\beta} \lambda^{\binom{N_1\ \overline{N}_2}{\overline{N}_4\ N_3};\binom{\sigma_1\ \beta}{\sigma_3\ \alpha}}_{\binom{k+l\ \ p-l+q}{k+q\ \ \ p}}\\
&+ \frac{1}{4\mu N_f}\int \mathrm{d}\mathbf{q}\; g^{(\overline{N}_3)}_{p+q,p} g^{(N_1)}_{k+l,k+l+q} D(\mathbf{q}) G_{\overline{N}_1}(\mathbf{k}+\mathbf{l}+\mathbf{q}) G_{\overline{N}_3}(\mathbf{p}+\mathbf{q}) \mathsf{T}^{\alpha\sigma_1}_{\sigma_3\beta} \lambda^{\binom{\overline{N}_1\ N_2}{N_4\ \overline{N}_3};\binom{\beta\ \ \sigma_2}{\sigma_4\ \alpha}}_{\binom{k+l+q\ \ p-l}{k\ \ \ \ p+q}}.
\end{aligned} \tag{2.75}$$

The four-fermion vertex that is quadratic in λ is given by $\mathbf{\Gamma}^{\binom{N_1\ N_2}{N_4\ N_3};\binom{\sigma_1\ \sigma_2}{\sigma_4\ \sigma_3}}_{(2)} = \mathbf{\Gamma}^{\binom{N_1\ N_2}{N_4\ N_3};\binom{\sigma_1\ \sigma_2}{\sigma_4\ \sigma_3}}_{(2)PP} + \mathbf{\Gamma}^{\binom{N_1\ N_2}{N_4\ N_3};\binom{\sigma_1\ \sigma_2}{\sigma_4\ \sigma_3}}_{(2)PH}$, where the vertex correction in the PP channel (Fig. 2.9a) is

$$\mathbf{\Gamma}^{\binom{N_1\ N_2}{N_4\ N_3};\binom{\sigma_1\ \sigma_2}{\sigma_4\ \sigma_3}}_{(2)PP}\left(\begin{smallmatrix}\mathbf{k+l} & \mathbf{p-l}\\ \mathbf{k} & \mathbf{p}\end{smallmatrix}\right) = -\frac{1}{8\mu^2}\int d\mathbf{q}\; G_{M_1}(\mathbf{k}+\mathbf{q}) G_{M_2}(\mathbf{p}-\mathbf{q}) \lambda^{\binom{N_1\ N_2}{M_1\ M_2};\binom{\sigma_1\ \sigma_2}{\beta\ \ \alpha}}_{\binom{k+l\ \ p-l}{k+q\ p-q}} \lambda^{\binom{M_1\ M_2}{N_4\ N_3};\binom{\beta\ \ \alpha}{\sigma_4\ \sigma_3}}_{\binom{k+q\ p-q}{k\ \ \ p}} \tag{2.76}$$

and the vertex correction in the PH channel (Fig. 2.9b) is

$$\begin{aligned}
&\mathbf{\Gamma}^{\binom{N_1\ N_2}{N_4\ N_3};\binom{\sigma_1\ \sigma_2}{\sigma_4\ \sigma_3}}_{(2)PH}\left(\begin{smallmatrix}\mathbf{k+l} & \mathbf{p-l}\\ \mathbf{k} & \mathbf{p}\end{smallmatrix}\right)\\
&= -\frac{1}{8\mu^2}\int d\mathbf{q}\; \Bigg[G_{M_1}(\mathbf{q}-\mathbf{l}) G_{M_2}(\mathbf{q}) \Bigg(-N_f \lambda^{\binom{N_1\ M_1}{N_4\ M_2};\binom{\sigma_1\ \alpha}{\sigma_4\ \beta}}_{\binom{k+l\ q-l}{k\ \ \ q}} \lambda^{\binom{M_2\ N_2}{M_1\ N_3};\binom{\beta\ \sigma_2}{\alpha\ \sigma_3}}_{\binom{q\ \ p-l}{q-l\ p}}\\
&+ \lambda^{\binom{N_1\ M_1}{N_4\ M_2};\binom{\sigma_1\ \alpha}{\sigma_4\ \beta}}_{\binom{k+l\ q-l}{k\ \ \ q}} \lambda^{\binom{M_2\ N_2}{N_3\ M_1};\binom{\beta\ \sigma_2}{\sigma_3\ \alpha}}_{\binom{q\ p-l}{p\ q-l}} + \lambda^{\binom{N_1\ M_1}{M_2\ N_4};\binom{\sigma_1\ \alpha}{\beta\ \ \sigma_4}}_{\binom{k+l\ q-l}{q\ \ \ k}} \lambda^{\binom{M_2\ N_2}{M_1\ N_3};\binom{\beta\ \sigma_2}{\alpha\ \sigma_3}}_{\binom{q\ \ p-l}{q-l\ p}} \Bigg)\\
&+ G_{M_1}(\mathbf{q}-\mathbf{l}+\mathbf{p}-\mathbf{k}) G_{M_2}(\mathbf{q}) \lambda^{\binom{N_1\ M_1}{M_2\ N_3};\binom{\sigma_1\ \alpha}{\beta\ \ \sigma_3}}_{\binom{k+l\ q-l+p-k}{q\ \ \ \ \ p}} \lambda^{\binom{M_2\ N_2}{N_4\ M_1};\binom{\beta\ \sigma_2}{\sigma_4\ \alpha}}_{\binom{q\ \ \ p-l}{k\ q-l+p-k}} \Bigg].
\end{aligned} \tag{2.77}$$

2.4.5 Space of IR singularity

The renormalization of the coupling functions is determined from quantum corrections that depend on momenta along the Fermi surface. In each diagram, the momentum dependence of the quantum

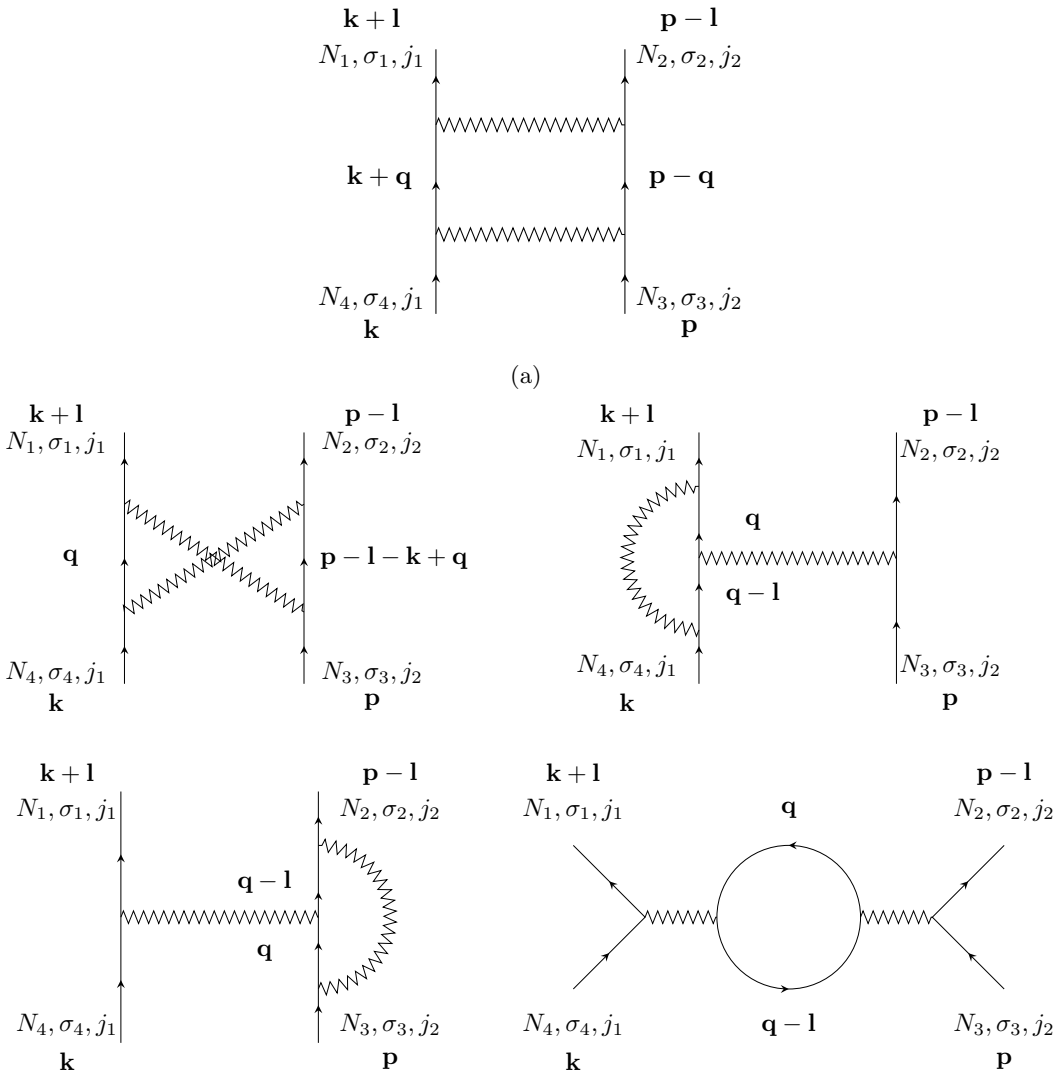

Figure 2.9: Quantum corrections to the four-fermion couplings quadratic in λ.

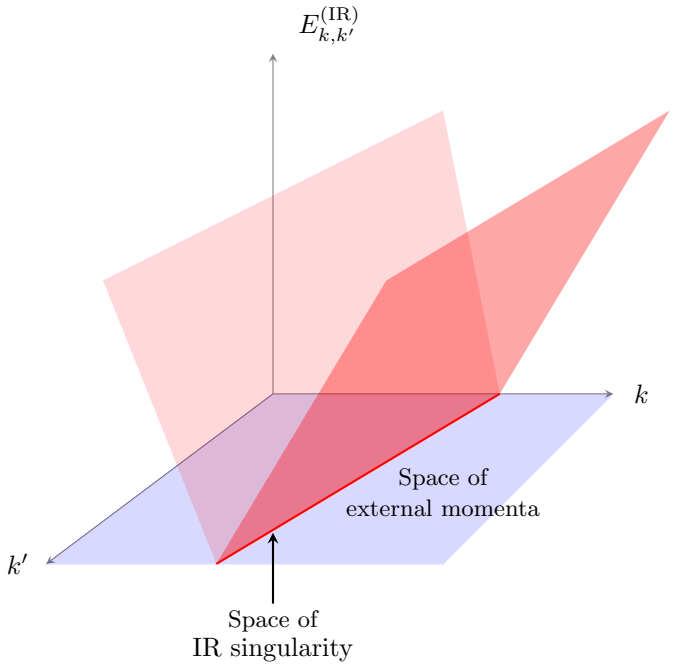

Figure 2.10: Schematic diagram of a momentum dependent crossover scale defined in the space of external momenta of a diagram. The set of external momenta at which the crossover scale vanishes forms the space of IR singularity for the diagram. Away from the space of IR singularity, the crossover scale becomes non-zero, causing a crossover from the high-energy region in which the quantum correction is significant to the low-energy region in which the quantum correction turns off.

correction is controlled by two crucial pieces of information. The first is *the space of IR singularity*, the set of external momenta at which a diagram is singular in the zero energy limit. The second is *the momentum dependent crossover scale* that cuts off the IR singularity when external momenta are away from the space of IR singularity.

Suppose there is a diagram that contributes to the vertex function, where all external electrons are on the Fermi surface. In the space of external momenta allowed by the momentum conservation, there exists a subset of external momenta in which the diagram exhibits an IR singularity in the limit that all external frequencies become zero. This subset is referred to as the space of IR singularity for the diagram, and its dimension is denoted as d_s. If external momenta lie within the space of IR singularity, the quantum correction exhibits IR divergence with a strength determined from the kinematics of virtual particles created within the loop[12]. If external momenta are outside of the space of IR singularity, a non-zero energy scale cuts off the IR divergence. The crossover energy scale is determined from the minimum energy that internal particles have to carry for given external momenta. At energies above the crossover energy scale, the quantum correction renormalizes the coupling functions even if the external momenta are outside the space of IR singularity. At energies below the crossover scale, the quantum correction becomes essentially independent of the energy scale,

[12]In an L-loop diagram, the space of internal three-momenta is $3L$-dimensional. If there exists a sub-manifold of co-dimension y in which x internal particles can have zero energy simultaneously, the diagram exhibits an IR singularity with degree $y-x$. If $y = x$ ($x > y$), a logarithmic (power-law) IR divergence can arise. If $x < y$, there is no IR singularity.

and the coupling functions stop receiving renormalization from the diagram. This is illustrated in Fig. 2.10. In this subsection, we discuss the space of IR singularity for each quantum correction in more detail.

Fermion self-energy

An electron has zero energy anywhere on the one-dimensional Fermi surface. The space of IR singularity for a fermion self-energy diagram is a subset of the one-dimensional Fermi surface in which the diagram is singular in the low-energy limit. To the leading order in v, only the diagrams in Figs. 2.2a and 2.2b are important. To be concrete, we consider the self-energy of electron at hot spot 1. With the frequency of the external electron set to be zero, we would like to figure out the set of k_x at which $\frac{\partial \mathbf{\Sigma}_1(\mathbf{k})}{\partial k_\rho}\Big|_{\mathbf{k}=(0,k_x,-v_{k_x}k_x)}$ is IR divergent. Let us first consider the one-loop self-energy in Eq. (2.67). If the external electron is at the hot spot 1, the electron can be scattered right onto the hot spot 4 by emitting a boson with zero energy. Because all internal particles can have zero energy at a loop momentum, a logarithmic singularity arises. If the external electron is away from the hot spots, there is no choice of loop momentum at which both electron and boson have zero energy in the loop, which removes the logarithmic singularity. The same conclusion holds for the two-loop self-energy diagrams. Therefore, the space of IR singularity for the fermion self-energy is the set of hot spots with dimension $d_s = 0$. Away from the hot spots, the IR singularity is cut off by a momentum dependent scale that is proportional to k_x[13]. This means that electrons away from the hot spots are eventually decoupled from spin fluctuations at sufficiently low energies.

Electron-boson vertex correction

Next, let us consider the cubic vertex where an electron at momentum $(k_x, -v_{k_x}k_x)$ in hot spot 1 is scattered to $(k'_x, v_{k'_x}k'_x)$ in hot spot 4 (Fig. 2.2c). In Eq. (2.70), the energies of the boson and two internal electrons in the loop are given by $c\,(|q_x| + |q_y|)$, $V_{F,k_x+q_x}\,(v_{k_x+q_x}(k_x+q_x) - q_y + v_{k_x}k_x)$, and $V_{F,k'_x+q_x}\left(v_{k'_x+q_x}(k'_x+q_x) + q_y + v_{k'_x}k'_x\right)$, respectively. As is the case for the self-energy, all internal particles can have zero energy at $\vec{q} = 0$ if $k_x = k'_x = 0$. This gives rise to the logarithmic IR singularity. [14] For non-zero k_x, k'_x, it is impossible to put all internal particles at zero energy, and the logarithmic singularity disappears. The expressions for the IR energy cutoff scales are derived in Sec. 2.5 and Appendix A. Since the vertex correction is singular at zero energy only when both the incoming and outgoing electrons are at the hot spots, we have $d_s = 0$. Away from the hot spots, the quantum corrections 'turn off' below the crossover energy scale.

Four-fermion vertex correction

At the one-loop order, there are three types of quantum corrections that contribute to the beta functional of the four-fermion couplings. The first is the quantum correction generated from the Yukawa coupling as is shown in Fig. 2.7. These give rise to contributions that are independent of λ in the beta functional, and act as the sources for the four-fermion coupling. The second, shown in Fig. 2.8, is the one that describes mixing among four-fermion couplings in different channels. Finally, diagrams in Fig. 2.9 describe the BCS-like scatterings. Here, we examine the spaces of IR singularity in these quantum corrections.

The primary couplings Through Eqs. (2.71) and (2.72), the primary four-fermion couplings are generated in channel $\left(\begin{smallmatrix} N & M \\ N & M \end{smallmatrix}\right)$ for any N and M. Without loss of generality, we can focus on the case with $N = 1$ because all other channels are related to the one with $N = 1$ through the C_4 symmetry. Let us start with the primary couplings with $(N, M) = (1, 1)$ and $(1, 5)$ in Table 2.1. In these channels,

[13] We will derive the crossover scale in Sec. 2.5 and Appendix A.

[14] This is because the product of the three propagators have IR singularity with dimension -3 at $\mathbf{q} = 0$, which is a subspace of co-dimension 3 in the space of internal energy-momentum.

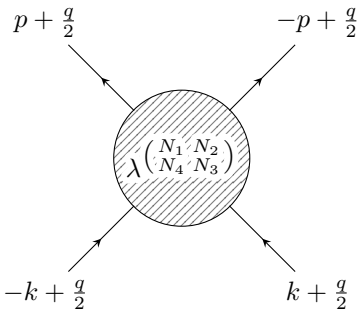

Figure 2.11: The momentum dependent four-fermion coupling function. q denotes the center of momentum in the particle-particle (PP) channel. $p-k$ and $p+k$ denote the center of mass momenta in two particle-hole (PH) channels. The gapless spin fluctuations generate singular four-fermion couplings in the PP plane with $q=0$ and the PH plane with $p-k=0$.

the Fermi velocities of the two internal fermions of Fig. 2.7 are parallel or anti-parallel to each other at the hot spots. As a result, there exist channels in which a pair of fermions within the loop can be far away from the hot spots while staying arbitrarily close to the Fermi surface. Contributions from states far away from the hot spots are only suppressed by the energy cost of the boson. Since the speed of the boson is c, the phase space of the low-energy states becomes proportional to $1/c$. Consequently, the quantum correction is enhanced from g^4 to g^4/c. For $(N,M)=(1,4)$ and $(1,8)$, the patches of Fermi surface are not perfectly nested, and the virtual electronic excitations in the loop can not stay on the Fermi surface at large momentum. Nonetheless, the main energy penalty for creating virtual excitations far away from the hot spots still comes from the boson because the nesting angle v is smaller than c in the small v limit as is shown in Eq. (2.4). Since the phase space of low-energy states is still controlled by the speed of the boson, the diagrams are still enhanced by $1/c$. For the primary couplings in group 3 in Table 2.1, the Fermi velocities of the two internal fermions are almost perpendicular to each other. In this case, the Fermi velocity, which is order of 1, controls the phase space of virtual electronic excitations, and the quantum corrections are simply order of g^4. Therefore, we can ignore the couplings in group 3 to the leading order in v. The couplings in group 4 are not generated from spin fluctuations.

When all external fermions are at the hot spots in Fig. 2.7, there exists a choice of the loop momentum at which all four internal particles (two fermions and two bosons) have zero energy. Because four internal particles have zero three-momentum at the origin (the manifold of co-dimension three) in the space of loop energy-momentum, it exhibits an IR singularity with degree -1. However, this power-law IR divergence is cut off as soon as any of the external momenta becomes non-zero. If an external electron is away from the hot spots, the electron has to absorb or emit a boson with non-zero momentum to scatter onto the Fermi surface inside the loop. Alternatively absorbing or emitting a boson with zero momentum (relative to $\vec{Q}_{AF}$), a virtual electron has to be away from the Fermi surface. Since the power-law divergence is removed for any external momentum away from the hot spots, the space of IR singularity with degree -1 is only zero-dimensional ($d_s=0$). Under the extended minimal subtraction scheme, no counter term is needed for the IR divergence with degree -1 localized within a zero-dimensional manifold of external momenta because Eq. (2.33) remains finite in the small μ limit. Although the IR singularity with degree -1 is localized within the zero-dimensional manifold of external momenta, IR singularities with degree 0 (logarithmic divergence) can arise in an extended space. These are the quantum corrections for which counter terms are needed. Below, we identify the channels in groups 1 and 2 for which logarithmic IR singularities arise in spaces with $d_s \geq 1$.

In the $\left(\begin{smallmatrix}1 & 4\\ 1 & 4\end{smallmatrix}\right)$ channel, there is no space of IR singularity with $d_s>0$. A logarithmic IR divergence can arise only if there exists a choice of internal momentum at which both electrons and at least one

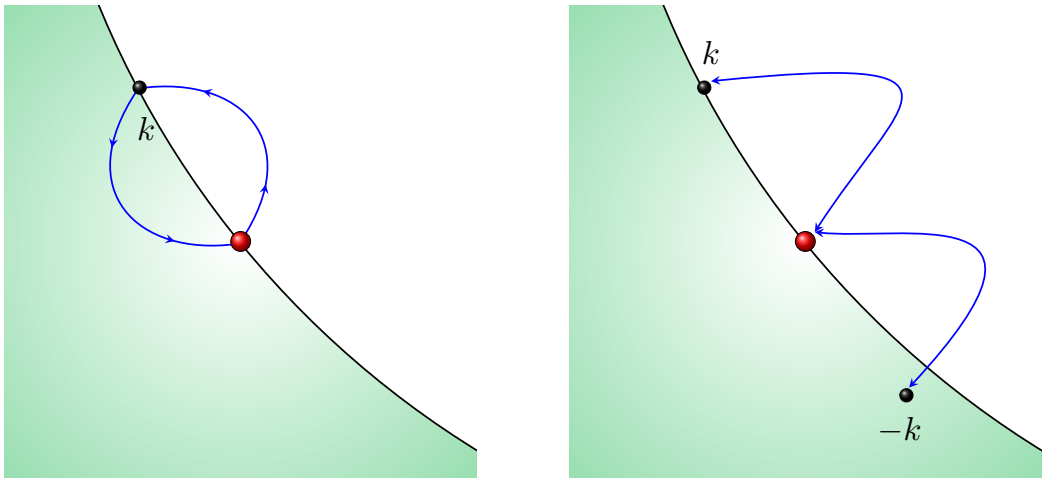

(a) (b)

Figure 2.12: (a) The forward scattering between an electron at a hot spot and an electron away from the hot spot. Irrespective of the shape of the Fermi surface, the forward scattering receives singular quantum corrections. (b) The Fulde–Ferrell–Larkin–Ovchinnikov (FFLO) scattering where a pair of electrons are scattered in and out of a hot spot. The FFLO scattering remains singular at low energies only if the Fermi surface has the particle-hole symmetry, for example, if the Fermi surface is straight. In general, two electrons from a hot spot can not scatter onto the Fermi surface due to the curvature of Fermi surface.

boson in the loop have zero energy in Fig. 2.7[15]. This forces a pair of external momenta in hot spots 1 and 4 to be zero. The fact that the patches at hot spots 1 and 4 are not nested with each other[16], combined with the constraint that external electrons are on the Fermi surface, further forces the other two external momenta to be zero as well. This shows that there is no extended space of IR singularity in the $\left(\begin{smallmatrix}1&4\\1&4\end{smallmatrix}\right)$ channel. The exact same argument applies to the $\left(\begin{smallmatrix}1&8\\1&8\end{smallmatrix}\right)$ channel.

In contrast, the quartic coupling in the $\left(\begin{smallmatrix}1&1\\1&1\end{smallmatrix}\right)$ channel supports an extended space of IR singularity. Fig. 2.7b is logarithmically divergent in the $\left(\begin{smallmatrix}1&1\\1&1\end{smallmatrix}\right)$ channel as far as a pair of external electron and hole are at the hot spots even if the other pair are away from the hot spots. Because there exists a choice of loop momentum at which two fermions and one boson in the loop have zero energy when one external electron-hole pair are at the hot spot, it gives rise to the logarithmic singularity. The space of IR singularity is one-dimensional ($d_s = 1$) because the other external momenta are arbitrary. The four-fermion couplings in the one-dimensional space of IR singularity is parameterized as

$$\left\{\lambda^{\left(\begin{smallmatrix}1&1\\1&1\end{smallmatrix}\right)}_{\left(\begin{smallmatrix}0&k\\k&0\end{smallmatrix}\right)}, \lambda^{\left(\begin{smallmatrix}1&1\\1&1\end{smallmatrix}\right)}_{\left(\begin{smallmatrix}k&0\\0&k\end{smallmatrix}\right)}\right\}. \tag{2.78}$$

This coupling describes the forward scattering between an electron at the hot spot and an electron at a general momentum on the Fermi surface (Fig. 2.12a).

The space of IR singularity is even bigger for the $\left(\begin{smallmatrix}1&5\\1&5\end{smallmatrix}\right)$ channel in group 2. As far as the center of mass momentum of the electron pair is zero in Fig. 2.7a, the quantum correction is logarithmically divergent irrespective of the relative momentum of the incoming *and* outgoing pairs. When the total momentum of the electron pair is zero, two internal electrons in the loop can stay close to the Fermi surface irrespective of the relative momentum along the Fermi surface. Since the two internal fermions can have zero energy within the manifold of internal energy-momentum with co-dimension 2, it gives

[15]The case in which two bosons and only one electron have zero energy does not give rise to an IR singularity because the electron propagator is odd under $\mathbf{k} \to -\mathbf{k}$.

[16]It is important to consider a small but non-zero v.

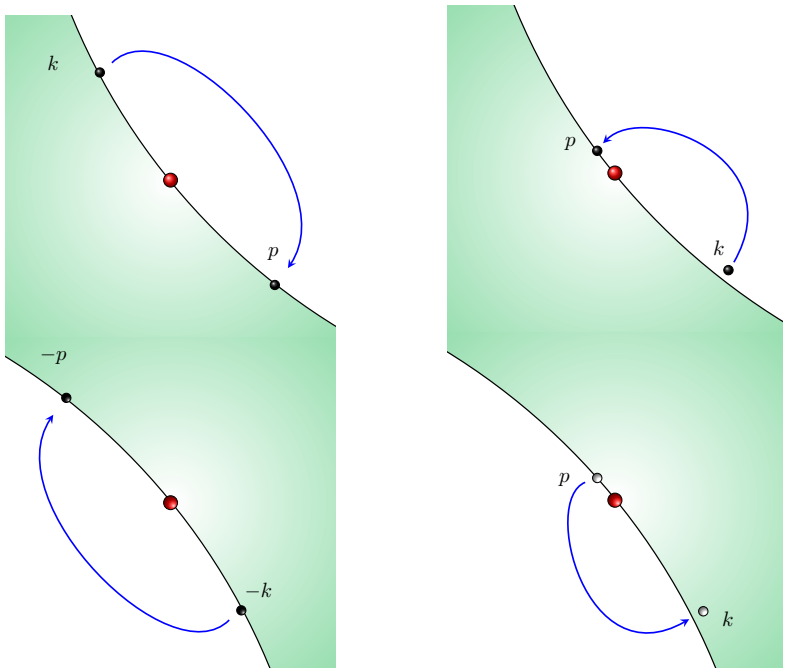

(a) (b)

Figure 2.13: (a) The Bardeen-Cooper-Schrieffer (BCS) scattering between a pair of electrons with zero center of mass momentum. Irrespective of the shape of the Fermi surface, the BCS scattering receives singular quantum corrections. (b) The $2k_F$ particle-hole scattering associated with a pair of particle and hole on the anti-podal patches of Fermi surface. The $2k_F$ particle-hole scattering remains singular at low energies only if the Fermi surface has the particle-hole symmetry. In general, a non-zero curvature of Fermi surface prevents particle-hole pairs with fixed momentum from staying on the Fermi surface.

rise to the logarithmic IR singularity. It is noted that this IR singularity is generated purely from gapless fermions, and whether the boson is gapless or not does not matter. Since the relative momentum of incoming and outgoing fermion pairs can be arbitrary, $d_s = 2$. The four-fermion couplings in the two-dimensional space of IR singularity is parameterized as

$$\left\{ \lambda^{\left(\begin{smallmatrix} 1 & 5 \\ 1 & 5 \end{smallmatrix}\right)}_{\left(\begin{smallmatrix} p & -p \\ k & -k \end{smallmatrix}\right)} \right\}. \tag{2.79}$$

This coupling describes the BCS pairing interaction for pairs of electrons with zero total momentum (Fig. 2.13a).

In summary, Fig. 2.7 generates primary four-fermion couplings within extended spaces of external momenta with $d_s > 0$ in groups 1 and 2 to the leading order in v. In the following, we consider the couplings that are further generated from the primary couplings through operator mixing.

The secondary couplings Once the Yukawa coupling generates the primary four-fermion couplings in the $\left(\begin{smallmatrix} 1 & 1 \\ 1 & 1 \end{smallmatrix}\right)$ and $\left(\begin{smallmatrix} 1 & 5 \\ 1 & 5 \end{smallmatrix}\right)$ channels, the vertex corrections in Fig. 2.8 generate secondary couplings by scattering a pair of electrons in the PP and PH channels, respectively. For example, a pair of indices in $\lambda^{\left(\begin{smallmatrix} N_1 & N_2 \\ N_4 & N_3 \end{smallmatrix}\right)}_{\left(\begin{smallmatrix} k_1 & k_2 \\ k_4 & k_3 \end{smallmatrix}\right)}$ can change from (N_a, N_b) to $(\overline{N}_a, \overline{N}_b)$ through the one-loop mixing as is shown in Fig. 2.14. The resulting operators can generate yet another set of operators through mixing. This in

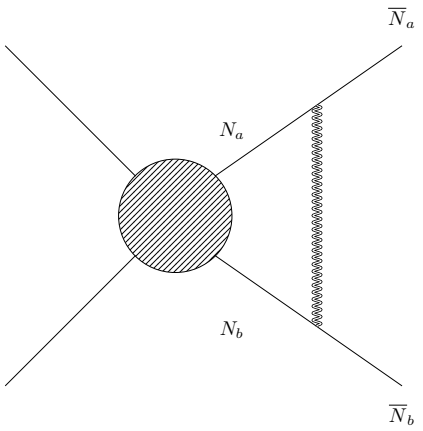

Figure 2.14: The quantum correction that linearly mixes four-fermion couplings with different hot spot indices to the lowest order in v. A pair of fermions can change their hot spot indices from (N_a, N_b) to $(\overline{N}_a, \overline{N}_b)$ by exchanging a boson.

	d_s	Primary couplings	Secondary couplings
Group 1	1	$\lambda^{\binom{1\ 1}{1\ 1}}_{\binom{0\ k}{k\ 0}}$, $\lambda^{\binom{1\ 1}{1\ 1}}_{\binom{k\ 0}{0\ k}}$	$\lambda^{\binom{4\ 1}{1\ 4}}_{\binom{0\ k}{k\ 0}}$, $\lambda^{\binom{1\ 4}{4\ 1}}_{\binom{k\ 0}{0\ k}}$
Group 2	2	$\lambda^{\binom{1\ 5}{1\ 5}}_{\binom{p\ -p}{k\ -k}}$, $\lambda^{\binom{4\ 8}{4\ 8}}_{\binom{p\ -p}{k\ -k}}$	$\lambda^{\binom{4\ 5}{1\ 8}}_{\binom{p\ -p}{k\ -k}}$, $\lambda^{\binom{1\ 8}{4\ 5}}_{\binom{p\ -p}{k\ -k}}$

Table 2.2: The primary four-fermion couplings generated from the Yukawa coupling and the secondary couplings further generated through the linear mixings in the spaces of IR singularity with dimensions $d_s \geq 1$.

general creates a network of operators described by a mixing matrix in the space of hot spot indices, spin indices and momentum. However, we only need to focus on those channels in which operator mixings are present within the space of IR singularity with $d_s > 0$. We don't need to add counter terms for the mixings that are present in zero-dimensional space of IR singularity. The secondary couplings that are generated within the extended spaces of IR singularity are summarized in Table 2.2.

In the $\left(\begin{smallmatrix}1&1\\1&1\end{smallmatrix}\right)$ channel, the quantum correction is IR singular only when the external legs that are associated with the vertex correction carry zero momenta. Each of $\lambda^{\left(\begin{smallmatrix}1&1\\1&1\end{smallmatrix}\right)}_{\left(\begin{smallmatrix}0&k\\k&0\end{smallmatrix}\right)}$ and $\lambda^{\left(\begin{smallmatrix}1&1\\1&1\end{smallmatrix}\right)}_{\left(\begin{smallmatrix}k&0\\0&k\end{smallmatrix}\right)}$ mixes with $\lambda^{\left(\begin{smallmatrix}4&1\\1&4\end{smallmatrix}\right)}_{\left(\begin{smallmatrix}0&k\\k&0\end{smallmatrix}\right)}$ and $\lambda^{\left(\begin{smallmatrix}1&4\\4&1\end{smallmatrix}\right)}_{\left(\begin{smallmatrix}k&0\\0&k\end{smallmatrix}\right)}$, respectively. The linear mixing is generated from Figs. 2.8e and 2.8f. In the $\left(\begin{smallmatrix}1&5\\1&5\end{smallmatrix}\right)$ channel, the vertex correction is IR singular within a two-dimensional manifold in which a particle-particle pair in hot spots 1 and 5 carry net zero momenta. As a result, $\lambda^{\left(\begin{smallmatrix}1&5\\1&5\end{smallmatrix}\right)}_{\left(\begin{smallmatrix}p&-p\\k&-k\end{smallmatrix}\right)}$ mixes with $\lambda^{\left(\begin{smallmatrix}4&8\\1&5\end{smallmatrix}\right)}_{\left(\begin{smallmatrix}p'&-p'\\k&-k\end{smallmatrix}\right)}$, $\lambda^{\left(\begin{smallmatrix}1&5\\4&8\end{smallmatrix}\right)}_{\left(\begin{smallmatrix}p&-p\\k'&-k'\end{smallmatrix}\right)}$ through Figs. 2.8a and 2.8b.

At the quadratic order in λ, the standard BCS diagram give rise to the logarithmic divergence for the coupling in group 2 within the two-dimensional manifold of external momenta in which the center of mass momentum of Cooper pair is zero.

Additional channels that become singular in the presence of the particle-hole symmetry In the presence of the PH symmetry, $v_k = v_{-k}$. In this case, the phase space of low-energy scatterings is further enlarged due to an enhanced nesting, and additional couplings receive singular quantum corrections in extended spaces of IR singularity. Although we focus on the generic case in which the PH symmetry is absent, here we list those additional couplings for completeness.

With $v_k = v_{-k}$, a pair of electrons with momenta k and $-k$ can simultaneously stay on the Fermi surface near one hot spot. As a result, Fig. 2.7a is also logarithmically divergent in the $\left(\begin{smallmatrix}1&1\\1&1\end{smallmatrix}\right)$ channel. The coupling function that receives IR singular quantum corrections is parameterized as

$$\left\{\lambda^{\left(\begin{smallmatrix}1&1\\1&1\end{smallmatrix}\right)}_{\left(\begin{smallmatrix}0&0\\k&-k\end{smallmatrix}\right)}, \lambda^{\left(\begin{smallmatrix}1&1\\1&1\end{smallmatrix}\right)}_{\left(\begin{smallmatrix}k&-k\\0&0\end{smallmatrix}\right)}\right\}. \tag{2.80}$$

This coupling describes the processes where a pair of electrons with total momentum $2k_F$ scatter in and out of the hot spots in the Fulde–Ferrell–Larkin–Ovchinnikov (FFLO) pairing channel (Fig. 2.12b). In group 2, Fig. 2.7b is also IR singularity for

$$\left\{\lambda^{\left(\begin{smallmatrix}1&5\\1&5\end{smallmatrix}\right)}_{\left(\begin{smallmatrix}p&k\\k&p\end{smallmatrix}\right)}\right\}. \tag{2.81}$$

These couplings are defined in the two-dimensional space with zero center of mass momentum in the PH channel. Eq. (2.81) describes scatterings of particle-hole pairs with momentum $2k_F$ (Fig. 2.13b). In the presence of the PH symmetry, this plane of the IR singularity intersects with Eq. (2.79) at a line with zero center of mass momentum both in the PP and PH channels.

Once those additional primary couplings are generated, additional secondary couplings are generated. In group 1, $\lambda^{\left(\begin{smallmatrix}1&1\\1&1\end{smallmatrix}\right)}_{\left(\begin{smallmatrix}0&0\\k&-k\end{smallmatrix}\right)}$, $\lambda^{\left(\begin{smallmatrix}1&1\\1&1\end{smallmatrix}\right)}_{\left(\begin{smallmatrix}k&-k\\0&0\end{smallmatrix}\right)}$, mixes with $\lambda^{\left(\begin{smallmatrix}4&4\\1&1\end{smallmatrix}\right)}_{\left(\begin{smallmatrix}0&0\\k&-k\end{smallmatrix}\right)}$, $\lambda^{\left(\begin{smallmatrix}1&1\\4&4\end{smallmatrix}\right)}_{\left(\begin{smallmatrix}k&-k\\0&0\end{smallmatrix}\right)}$ through Figs. 2.8a and 2.8b. In group 2, $\lambda^{\left(\begin{smallmatrix}1&5\\1&5\end{smallmatrix}\right)}_{\left(\begin{smallmatrix}k&p\\p&k\end{smallmatrix}\right)}$ mixes with $\lambda^{\left(\begin{smallmatrix}4&5\\1&8\end{smallmatrix}\right)}_{\left(\begin{smallmatrix}k'&p\\p&k'\end{smallmatrix}\right)}$ and $\lambda^{\left(\begin{smallmatrix}1&8\\4&5\end{smallmatrix}\right)}_{\left(\begin{smallmatrix}k&p'\\p'&k\end{smallmatrix}\right)}$ through Figs. 2.8e and 2.8f.

2.4.6 Adiabaticity

Now we turn our attention to the computation of the quantum effective action expressed as integrations of loop momenta in Sec. 2.4.4. The salient feature of theories with continuously many gapless

degrees of freedom is that quantum corrections are functionals of coupling functions. Even if the coupling functions are independent of momentum at one scale, they in general acquire non-trivial momentum dependences at low energies unless protected by symmetry. This makes it necessary to compute quantum corrections in the presence of general momentum dependent coupling functions. A simplification arises for quantum corrections generated from small angle scatterings in which loop momentum is bounded by the external energy. Thanks to the locality in real space, the rate at which coupling functions vary in momentum is controlled by the energy scale at which the coupling functions are defined. If the momentum carried by virtual particles in a loop is limited by a momentum that is proportional to external frequencies, quantum corrections can be computed approximately by treating the coupling functions as constants as far as the coupling functions do not vary significantly over that momentum scale. This motivates us to introduce the notion of *adiabaticity* in the momentum space. We say that coupling functions are adiabatic in a diagram if no coupling functions change appreciably within the range of loop momenta from which IR divergent contributions arise. Below, we make this precise and examine how adiabaticity is invoked to efficiently compute quantum corrections for non-nested diagrams.

We start with the Schwinger-Dyson equation for the boson propagator in Eq. (2.65). At energy scale μ, we need to know the boson propagator up to momentum μ/c, where c is the speed of the boson. After the mass renormalization is subtracted, Eq. (2.65) is finite in the limit that k_F and Λ are large. With all momentum cutoffs set to be infinite, the external momentum is the only scale in the integration, and it plays the role of a soft UV energy cutoff for the loop integration. When the external momentum is μ/c, the upper bound for the soft UV energy cutoff is $V_{F,0}\mu/c$. This is because the singular renormalization of the collective mode arises from electrons near the hot spots, and $V_{F,0}$ is the largest component of velocity near the hot spots. This energy cutoff is translated into the upper bound for the momentum cutoff,

$$\Pi_\mu = \frac{1}{V_{F,0}v_0}\frac{V_{F,0}\mu}{c} = \frac{\mu}{cv_0}, \tag{2.82}$$

where we use the fact that $V_{F,0}v_0$ is the smallest component of velocity[17]. We say the coupling functions satisfy adiabaticity at energy scale μ if the relative variation of $v_k, V_{F,k}$ and $g_{k',k}$ is small within the range of momentum Π_μ, that is,

$$\epsilon_\mu \equiv \max_{|k_i'-k_i|<\Pi_\mu}\left\{\left|\frac{V_{F,k_1'}-V_{F,k_1}}{V_{F,k_1}}\right|, \left|\frac{v_{k_1'}-v_{k_1}}{v_{k_1}}\right|, \left|\frac{g_{k_1',k_2'}-g_{k_1,k_2}}{g_{k_1,k_2}}\right|\right\} \ll 1, \tag{2.83}$$

where all couplings are defined at energy μ. Here, we don't expect the four-fermion coupling function satisfies adiabaticity at general momenta because the four-fermion coupling function, being irrelevant, has stronger momentum dependence than the marginal coupling functions. In Sec. 2.6, we will show that if $\epsilon_\Lambda \ll 1$[18], $\epsilon_\mu \ll 1$ at all $\mu \le \Lambda$. For now, we assume that the adiabaticity is satisfied at all energy scales and show how it simplifies the computation of quantum corrections. With Eq. (2.83), one can ignore the variation of the coupling functions within the loop, and Eq. (2.65) can be approximated as

$$\begin{aligned} D^{-1}(\mathbf{k}) = {} & m_{CT} + 2g_{0,0}^2\sum_{N=1}^{8}\int \mathrm{d}\mathbf{q}\; G_N(\mathbf{q}|0)G_{\overline{N}}(\mathbf{q}+\mathbf{k}|0) \\ & - \frac{4}{N_cN_f}g_{0,0}^4\sum_{N=1}^{8}\int \mathrm{d}\mathbf{q}\mathrm{d}\mathbf{p}\; G_N(\mathbf{p}+\mathbf{q}|0)G_{\overline{N}}(\mathbf{p}|0)G_N(\mathbf{p}+\mathbf{k}|0)G_{\overline{N}}(\mathbf{p}+\mathbf{q}+\mathbf{k}|0)D(\mathbf{q}), \end{aligned} \tag{2.84}$$

where the coupling functions are evaluated at the hot spots, and

$$G_N(\mathbf{k}|k') = \frac{1}{ik_0 + V_{F,k'}^{(N)}e_N[\vec{k}; v_{k'}^{(N)}]} \tag{2.85}$$

[17] For example, with energy $V_{F,0}\mu/c$, electron-hole pairs can be created near hot spots 1 and 4 up to momentum $k_x \sim \frac{\mu}{v_0 c}$ away from the hot spots.

[18] This is a reasonable starting point in that bare coupling functions are smooth functions of momentum

is the fermion propagator at $\mathbf{k}$ in which the coupling functions inside the propagator are evaluated at k'. As in Eq. (2.4), the self-consistent equation in Eq. (2.84) gives

$$c(v_0) = \sqrt{\frac{v_0}{8N_cN_f} \log\left(\frac{1}{v_0}\right)}, \tag{2.86}$$

where v_0 denotes the nesting angle at the hot spots. Provided that Eq. (2.83) is satisfied at energy scale μ, Eq. (2.3) is the valid expression up to momentum μ/c with the boson velocity given by Eq. (2.86).

Now, let us consider other vertex functions. Unlike the boson propagator, other diagrams that contribute to the counter terms in Eq. (2.34) are in general UV divergent logarithmically in Λ, k_F or both. This implies that internal momenta in those diagrams can be much bigger than μ, and we can not use adiabaticity to compute the quantum corrections. However, what we need is the derivative of the counter terms with respect to $\log \mu$ not the counter terms themselves. The derivatives capture the contributions generated from the fast modes within an infinitesimal window of energy scales, and determine the beta functionals. Because Λ is the UV energy cutoff, the derivative of the counter terms are finite in the large Λ limit. However, they are not necessarily finite in the large k_F limit as there are gapless fermionic modes with large momenta.

Therefore, we are led to consider two types of UV divergent quantum corrections separately. The quantum corrections of the first type are those whose derivative with respect to $\log \mu$ are finite in the large k_F limit. Quantum corrections that are generated by small-angle scatterings belong to this type. For example, in diagrams that involve only the Yukawa couplings, spin fluctuations scatter electrons between patches that are not nested with each other for $v \neq 0$. Consequently, internal fermions can not be scattered far away from external momenta modulo $\vec{Q}_{AF}$. In the derivative of quantum corrections, all components of internal momenta become dynamically bounded by the external energy, and its contribution to the beta functional is finite even in the large k_F limit. Their contributions to the beta functional can be computed by treating the coupling functions inside loops as constants as far as the adiabaticity condition is satisfied. The quantum corrections of the second type are the ones whose derivative with respect to $\log \mu$ are not finite in the large k_F limit while being finite in the large Λ limit. The second type of quantum corrections arise from large-angle scatterings in the channels in which fermions can stay close to the Fermi surface over an extended phase space that is not bounded by energy. For example, Cooper pairs with zero net momentum can be created far away from the hot spots without electronic energy penalty, and the phase space for virtual low-energy excitations is not limited by the external energy. In those cases, even the derivative of the counter terms remain sensitive to the size of the Fermi surface, and we can not ignore the momentum profiles of the coupling functions within loops. For the second type, the beta functionals should be expressed as integrations over the momenta along the Fermi surface. We will come back to the second type of quantum corrections when we explicitly compute quantum corrections that include the four-fermion couplings in the nested channels in Sec. 2.5.2. In the rest of the section, we discuss how adiabaticity is invoked to simplify the computation of quantum corrections of the first type.

Let us start with the contributions of $A^{(i)}(k)$ with $i = 1, 2, 3$ to the beta functionals. Let $\mathbf{\Sigma}_1(\mathbf{k})$ be the exact fermion-self energy in Eq. (2.67) at hot spot 1. While $\frac{\partial \mathbf{\Sigma}_1(\mathbf{k})}{\partial k_\rho}$ is UV divergent logarithmically, $\frac{\partial}{\partial \log \mu} \frac{\partial \mathbf{\Sigma}_1(\mathbf{k})}{\partial k_\rho}\Big|_{\mathbf{k}=(\mu, k_x, -v_{k_x} k_x)}$ is UV finite. Since external fermions are on the Fermi surface with frequencies that are $O(\mu)$, the soft UV cutoff for the loop momentum is μ for the UV finite integral. Since there is no loop that is purely made of fermions in this case, one necessarily creates bosonic virtual particle in the loop whose energy increases as $c|q_x| + c|q_y|$, where $\vec{q}$ is the loop momentum. This makes the momentum cutoff for the internal loop to be μ/c. Therefore, the adiabaticity is satisfied if the variation of the coupling functions can be ignored over μ/c. If Eq. (2.83) is satisfied, this condition is automatically satisfied. Because the integrand is peaked at $q = 0$, we can replace $g_{k+q,k} g_{k,k+q}$, v_{k+q} and $V_{F,k+q}$ with those evaluated at $q = 0$ in Eq. (2.67) to the leading order in ϵ_μ. The derivative of

the counter term for the fermion kinetic term can be written as

$$\frac{\partial}{\partial \log \mu} \frac{\partial \mathbf{\Sigma}_1(\mathbf{k})}{\partial k_\rho}\bigg|_{\mathbf{k}=(\mu,k_x,-v_{k_x}k_x)} = \frac{\partial}{\partial \log \mu} \frac{\partial \Sigma_1(\mathbf{k})}{\partial k_\rho}\bigg|_{\mathbf{k}=(\mu,k_x,-v_{k_x}k_x)} + \dots, \tag{2.87}$$

where $\Sigma_1(\mathbf{k})$ is the self-energy computed in the adiabatic limit,

$$\Sigma_1(\mathbf{k}) = -g_{k,k}^2 \frac{2(N_c^2-1)}{N_c N_f} \int \mathrm{d}\mathbf{q}\; G_4(\mathbf{k}+\mathbf{q}|k) D(\mathbf{q}), \tag{2.88}$$

and ... represents corrections that are further suppressed by ϵ_μ. In Sec. 2.6, it will be shown that $\epsilon_\mu \sim \sqrt{v}$. Therefore, the terms that are ignored in the adiabatic approximation are sub-leading in the small v limit. In Eq. (2.87), the momentum dependent coupling functions are evaluated at the external momentum, k_x because the integrand is peaked at $\mathbf{q} = 0$ with the soft UV cutoff that is order of μ/c. It is noted that external fermions can be far away from the hot spots, and momentum dependent coupling functions can not be replaced with those evaluated at the hot spots in general. However, one can still invoke adiabaticity locally in the momentum space at any point on the Fermi surface. Even if a coupling function at k is significantly different from its value at the hot spots, the coupling functions are still adiabatic if their variation is slow locally at that momentum. Since the derivative of the coupling functions is largest near the hot spots as will be shown in Sec. 2.6, the adiabatic condition is most stringent near the hot spots. Namely, Eq. (2.83) is satisfied for general k_i's on the Fermi surface, if it is satisfied near the hot spots.

Similarly, the contribution of the vertex correction in Fig. 2.2c to the beta functional of the Yukawa coupling is given by

$$\begin{aligned}&\frac{\partial A^{(4)}(k_x', k_x)}{\partial \log \mu} \\ &= \frac{2}{N_c N_f^{\frac{3}{2}}} \frac{\partial}{\partial \log \mu} \int \mathrm{d}\mathbf{q}\; g_{k',k'+q} g_{k'+q,k+q} g_{k+q,k} D(\mathbf{q}) G_4(\mathbf{k}'+\mathbf{q}) G_1(\mathbf{k}+\mathbf{q}) \Big|_{\substack{\mathbf{k}'=(2\mu,k_x',-v_{k_x'}k_x') \\ \mathbf{k}=(\mu,k_x,v_{k_x}k_x)}}.\end{aligned} \tag{2.89}$$

The degree of divergence of $A^{(4)}$ is 0, and its derivative with respect to μ is UV finite. Consequently, the singular part of Eq. (2.89) can be computed as

$$\begin{aligned}&\frac{\partial A^{(4)}(k_x', k_x)}{\partial \log \mu} \\ &= \frac{2}{N_c N_f^{\frac{3}{2}}} g_{k',k'} g_{k',k} g_{k,k} \frac{\partial}{\partial \log \mu} \int \mathrm{d}\mathbf{q}\; D(\mathbf{q}) G_4(\mathbf{k}'+\mathbf{q}|k') G_1(\mathbf{k}+\mathbf{q}|k) \Big|_{\substack{\mathbf{k}'=(2\mu,k_x',-v_{k_x'}k_x') \\ \mathbf{k}=(\mu,k_x,v_{k_x}k_x)}} + \dots\end{aligned} \tag{2.90}$$

to the leading order in v.

2.5 Beta functionals

In this section, we compute the beta functionals for the nesting angle, Fermi velocity, electron-boson coupling and four-fermion coupling functions.

2.5.1 Nesting angle, Fermi velocity and electron-boson coupling

To the leading order in v, the counter terms to the fermion kinetic term and the cubic coupling are given by (see Appendix A for derivation)

$$\begin{aligned}
A^{(1)}(k) &= -h_k^{(1)} \log\left(\frac{\Lambda}{\mathscr{H}_1(\mu, 2v_k ck)}\right) + A_{reg}^{(1)}(k), \\
A^{(2)}(k) &= \frac{2}{\pi} h_k^{(1)} \frac{c}{V_{F,k}} \log\left(\frac{V_{F,k}}{c}\right) \log\left(\frac{\Lambda}{\mathscr{H}_1(\mu, 2v_k ck)}\right) + 3h_k^{(2)} \log\left(\frac{\Lambda}{\mathscr{H}_1(\mu, 4V_{F,k} v_k k)}\right) + A_{reg}^{(2)}(k), \\
A^{(3)}(k) &= -\frac{2}{\pi} h_k^{(1)} \frac{c}{V_{F,k}} \log\left(\frac{V_{F,k}}{c}\right) \log\left(\frac{\Lambda}{\mathscr{H}_1(\mu, 2v_k ck)}\right) - h_k^{(2)} \log\left(\frac{\Lambda}{\mathscr{H}_1(\mu, 4V_{F,k} v_k k)}\right) + A_{reg}^{(3)}(k), \\
A^{(4)}(k', k) &= -h_{k',k}^{(1)} \log\left(\frac{\Lambda}{\mathscr{H}_3(\mu, 2v_k ck, 2v_{k'} ck', \mathscr{R}_{k',k})}\right) + A_{reg}^{(4)}(k', k),
\end{aligned} \tag{2.91}$$

where

$$h_k^{(1)} = \frac{N_c^2 - 1}{\pi^2 N_c N_f} \frac{g_k^2}{c V_{F,k}}, \tag{2.92}$$

$$h_{k',k}^{(1)} = \frac{2 g_k g_{k'}}{\pi^2 c N_c N_f (V_{F,k} + V_{F,k'})} \log\left(\frac{c(V_{F,k}^{-1} + V_{F,k'}^{-1})}{v_k + v_{k'}}\right), \tag{2.93}$$

$$h_k^{(2)} = \frac{N_c^2 - 1}{2\pi^4 N_c^2 N_f^2} \frac{g_k^4}{c^2 V_{F,k}^2} \log^2\left(\frac{V_{F,k} v_k}{c}\right) \tag{2.94}$$

with $g_k \equiv g_{k,k}$ and $\mathscr{R}_{k',k} = 4(v_{k'} k' + v_k k)/(V_{F,k'}^{-1} + V_{F,k}^{-1})$. $\mathscr{H}_i(x_1, k_2, .., x_{i+1})$'s represent smooth crossover functions that satisfy

$$\mathscr{H}_i(x_1, x_2, .., x_{i+1}) \approx |x_j| \quad \text{if } |x_j| \gg |x_1|, .., |x_{j-1}|, |x_{j+1}|, .., |x_{i+1}| \ . \tag{2.95}$$

The form of the crossover functions depend on the subtraction scheme. The specific form of $\mathscr{H}_i$ is not important for us as far as the counter term removes all IR divergences in physical observables. Choosing different $\mathscr{H}_i$ amounts to modifying the finite parts, $\mathscr{F}_i$ in Eqs. (2.26)-(2.29) and imposing a different set of renormalization conditions. Each counter term is proportional to

$$\log\left[\frac{\Lambda}{\mathscr{H}_i(\mu, \Delta_1, .., \Delta_i)}\right], \tag{2.96}$$

where μ is the energy scale at which the RG condition is imposed, and Δ_i represents crossover energy scales that depend on external momenta. Physically, these energy scales correspond to the energies that virtual particles have to carry within loops for given external momenta. If μ is much larger than all Δ_i's, Eq. (2.96) becomes $\log\left(\frac{\Lambda}{\mu}\right)$, and the quantum correction gives rise to the logarithmic flow of the coupling functions as the energy is lowered. If μ becomes much smaller than any of Δ_i, the quantum correction becomes independent of μ, and no longer contributes to the flow of coupling functions. Roughly speaking, the contribution to the beta function turns off below the energy scale which is given by the largest of Δ_i's. Since quantum corrections turn off at different energy scales at different points on the Fermi surface, the renormalized coupling functions acquire momentum dependence at low energies even if one starts with momentum independent coupling functions at the UV cutoff scale. $A_{reg.}^{(i)}$ represent terms that are regular in the limit that $\log \frac{\Lambda}{\mathscr{H}_i}$ is large. In our minimal subtraction scheme, we can set $A_{reg.}^{(i)} = 0$ for $i = 1, 4$. One still needs to include $A_{reg.}^{(2)}$ and $A_{reg.}^{(2)}$ to enforce the RG condition in Eq. (2.25) because the finite parts of the fermion self-energy affect the shape of the renormalized Fermi surface. However, the contribution of the regular counter terms to the flow of the coupling function diminishes in the small μ limit.

$A^{(i)}(k)$ for $i = 1, 2, 3$ are the counter terms for the kinetic term of the electron at momentum k away from the hot spot 1 along the Fermi surface. $A^{(4)}(k', k)$ is the counter term for the cubic vertex that describes the scattering of electron from momentum k near hot spot 4 to momentum k' near hot spot 1. In general, the quantum corrections are functionals of the coupling functions. However, $h_k^{(1)}$ and $h_k^{(2)}$ depend only on the coupling functions at momentum k. Similarly, $A^{(4)}(k', k)$ depends only on the coupling functions that are defined at k and k' due to adiabaticity. Through explicit calculations, we will show that the coupling functions that satisfy the adiabaticity at a UV scale continue to satisfy the adiabaticity below the UV scale.

The counter terms that include $h_k^{(1)}$ are the contributions of the one-loop fermion self-energy in Fig. 2.2a. Besides the factor of g_k^2, there are factors of $1/V_{F,k}$ and $1/c$ inside $h_k^{(1)}$ because the phase space of the loop momentum is controlled by the Fermi velocity in one direction and the boson velocity in another direction. For $A^{(2)}(k)$ and $A^{(3)}(k)$, there is an additional factor of $c/V_{F,k}$ because the quantum correction that renormalizes the Fermi velocity is controlled by the boson velocity[19]. Inside $\mathscr{H}_1$, $2v_k ck$ denotes the crossover energy scale determined from the kinematics of the virtual particles in the loop. For the external fermion at momentum $(k_x, -v_{k_x} k_x)$ on the Fermi surface near hot spot 1, the energies of the intermediate boson and electron in the loop can be written as $c\,(|q_x| + |q_y|)$ and $V_{F,k_x+q_x}\,(v_{k_x+q_x}(k_x + q_x) - q_y + v_{k_x} k_x)$, respectively, where $\vec{q}$ is the momentum carried by the internal boson. For $\vec{k} = 0$, the electron can be scattered right onto the hot spot 4 by emitting or absorbing a boson with zero energy. In this case, all virtual particles have zero energy at $\vec{q} = 0$, and an infrared divergence arises in the low-energy limit. If the external electron is away from the hot spot ($k \neq 0$), it is impossible for the electron to be scattered onto the Fermi surface with a zero-energy boson. If it is to be scattered onto the Fermi surface in hot spot 4, it must create a boson with energy that is order of $2cv_{k_x} k_x$. On the other hand, if the virtual boson carries zero energy, the internal electron should be created away from the Fermi surface with energy that is order of $V_{F,k_x} v_{k_x} k_x$ as is illustrated in Fig. 1.7. Since the boson is slower than fermion ($c \ll V_F$) in the small v limit, it is energetically 'cheaper' to create a bosonic excitation while keeping virtual fermions on the Fermi surface. The crossover scale is given by the minimum energy that virtual particles have to carry among all possible choices of internal momentum, and the crossover scale for the one-loop self-energy becomes

$$E_k^{(1L)} = 2v_k c|k|. \tag{2.97}$$

Below the crossover energy scale, the energy cost for creating virtual excitations becomes bigger than μ, and the one-loop quantum correction is dynamically turned off.

The counter terms that are proportional to $h_k^{(2)}$ are from the two-loop fermion self-energy shown in Fig. 2.2b. In the two-loop diagram, the crossover energy scale is different from that of the one-loop diagram. The energies of the two internal bosons and three internal fermions created in the loops can be written as $E_1 = c\,(|q_x| + |q_y|)$, $E_2 = c\,(|p_x| + |p_y|)$, $E_3 = V_{F,k_x+q_x}\,(v_{k_x+q_x}(k_x + q_x) - q_y + v_{k_x} k_x)$, $E_4 = V_{F,k_x+p_x}\,(v_{k_x+p_x}(k_x + p_x) - p_y + v_{k_x} k_x)$, $E_5 = V_{F,k_x+q_x+p_x}\,(v_{k_x+p_x+q_x}(k_x + p_x + q_x) - v_{k_x} k_x + p_y + q_y)$, as functions of internal momenta $\vec{q}$ and $\vec{p}$. For $k \neq 0$, it is kinematically impossible to put all virtual particles at zero energy. If all internal fermions are to be on the Fermi surface, at least one boson has to carry energy that is order of ck_x. Alternatively, zero-energy bosons with $\vec{q} = \vec{p} = 0$ put internal fermions away from the Fermi surface with energy that is order of $V_F vk$. Since $c \gg V_F v$ in the small v limit, it is energetically favourable to create fermions away from the Fermi surface while keeping bosons at zero energy. The crossover energy scale, obtained by minimizing $\max\{|E_1|, |E_2|, |E_3|, |E_4|, |E_5|\}$ over difference choices of $\vec{q}$ and $\vec{p}$, becomes

$$E_k^{(2L)} = 4V_{F,k} v_k |k|. \tag{2.98}$$

Since $E_k^{(2L)} > E_k^{(1L)}$ for $k \neq 0$, electrons away from the hot spots disengage with the two-loop quantum correction at higher energy scales than the one-loop correction.

[19] The one-loop self-energy diagram depends on the external momentum only through the combination of $c\vec{k}$.

The counter term that is proportional to $h^{(1)}_{k',k}$ is from the vertex correction in Fig. 2.2c. When the electron at momentum k near hot spot 1 is scattered to momentum k' near hot spot 4, the virtual particles are created with energies, $E_1 = c\,(|q_x| + |q_y|)$, $E_2 = V_{F,k_x+q_x}\,(v_{k_x+q_x}(k_x+q_x) - q_y + v_{k_x}k_x)$ and $E_3 = V_{F,k'_x+q_x}\left(v_{k'_x+q_x}(k'_x+q_x) + q_y + v_{k'_x}k'_x\right)$, where $\vec{q}$ is the momentum of the internal boson. The crossover energy scale is given by minimizing $\max\{|E_1|, |E_2|, |E_3|\}$ over $\vec{q}$. To have a rough estimation of the crossover scale, one can first set the energy of one of the internal fermions (say E_2) to zero by choosing $q_y = v_{k_x+q_x}(k_x+q_x) + v_{k_x}k_x$. With difference choices of q_x, one can tilt the balance between E_1 and E_3. Since $c \gg v$, it is energetically favourable to minimize the energy of boson at the expense of the energy of fermion : with $q_x = 0$, we have $E_1 = 2cv_{k_x}k_x$ and $E_3 = 2V_{F,k'_x}\left(v_{k'_x}k'_x + v_{k_x}k_x\right)$. The bigger between these two determines the crossover scale. An explicit calculation (Appendix A A.2) shows that the crossover scale is symmetric between k and k', and can be written as $\max\{E^{(1L)}_k, E^{(1L)}_{k'}, E^{(1L)}_{k',k}\}$, where

$$E^{(1L)}_{k',k} = \frac{4v_k k + 4v_{k'}k'}{V^{-1}_{F,k} + V^{-1}_{F,k'}}. \tag{2.99}$$

From Eqs. (2.43) - (2.45), one obtains the beta functionals for $v_k, V_{F,k}$ and $g_{k',k}$, and the anomalous dimension of fermion $\eta^{(\psi)}_k$. To the leading order in v, solving the beta functionals from the quantum corrections can be greatly simplified as one can use

$$\frac{\mathrm{d}Z_i(k)}{\mathrm{d}\log\mu} = \frac{\partial A_i(k)}{\partial\log\mu} \tag{2.100}$$

in Eqs. (2.43) - (2.47) and Eqs. (2.48)-(2.50). The rest of the terms in Eq. (2.51) are of higher order in v. At low energies, one can drop the contributions from the finite counter terms. The resulting beta functionals and the anomalous dimension are given by

$$\beta^{(v)}_k = v_k\left[\frac{4}{\pi}h^{(1)}_k\frac{c}{V_{F,k}}\log\left(\frac{V_{F,k}}{c}\right)\theta_1(\mu, E^{(1L)}_k) + 4h^{(2)}_k\theta_1(\mu, E^{(2L)}_k)\right], \tag{2.101}$$

$$\begin{aligned}\beta^{(V_F)}_k =& V_{F,k}\left[-\frac{2}{\pi}h^{(1)}_k\frac{c}{V_{F,k}}\log\left(\frac{V_{F,k}}{c}\right)\theta_1(\mu, E^{(1L)}_k) + h^{(1)}_k\theta_1(\mu, E^{(1L)}_k) + \frac{2}{\pi}h^{(1)}_0 c\log\left(\frac{1}{c}\right) - h^{(1)}_0\right.\\ &\left. + h^{(2)}_0 - h^{(2)}_k\theta_1(\mu, E^{(2L)}_k)\right],\end{aligned} \tag{2.102}$$

$$\begin{aligned}\beta^{(g)}_{k',k} =& g_{k',k}\left[h^{(1)}_{0,0} - h^{(1)}_{k',k}\theta_3(\mu, E^{(1L)}_k, E^{(1L)}_{k'}, E^{(1L)}_{k',k}) - h^{(1)}_0\right.\\ &\left. + \frac{h^{(1)}_k\theta_1(\mu, E^{(1L)}_k) + h^{(1)}_{k'}\theta_1(\mu, E^{(1L)}_{k'})}{2} + 2h^{(2)}_0 + \frac{2}{\pi}h^{(1)}_0 c\log\frac{1}{c}\right],\end{aligned} \tag{2.103}$$

$$\eta^{(\psi)}_k = \frac{h^{(1)}_k}{2}\theta_1(\mu, E^{(1L)}_k) - (z-1), \tag{2.104}$$

where $h^{(1)}_k$, $h^{(1)}_{k',k}$ and $h^{(2)}_k$ are defined in Eqs. (2.92)-(2.94), and

$$\theta_i(\mu, \Delta_1, .., \Delta_i) = \frac{\partial\log\mathscr{H}_i(\mu, \Delta_1, .., \Delta_i)}{\partial\log\mu} \tag{2.105}$$

is the derivative of the crossover function with respect to the energy scale. It controls whether each term in the beta functional is turned on or off depending on whether μ is greater or less than the momentum dependent the crossover energy scales.

2.5.2 Four-fermion coupling

In this section, we compute the beta functional for the four-fermion coupling. To the lowest order in v, Eq. (2.46) can be written as

$$\beta^{(\lambda);\{N_i\};\{\sigma_i\}}_{\{k_i\}} = \left(1 + 3(z-1) + \sum_{j=1}^{4} \eta^{(\psi,N_j)}_{k_j}\right) \lambda^{\{N_i\};\{\sigma_i\}}_{\{k_i\}} - 4\mu \frac{\partial \tilde{\mathbf{\Gamma}}^{\{N_i\};\{\sigma_i\}}_{CT}(\{k_i\})}{\partial \log \mu}, \tag{2.106}$$

where $\tilde{\mathbf{\Gamma}}^{\{N_i\};\{\sigma_i\}}_{CT}(\{k_{i,N_i}\})$ represents the local counter terms that are needed to remove the singular parts of the vertex correction. On the right hand side of Eq. (2.106), the first term represents the fact that the four-fermion couplings have scaling dimension -1 at the tree-level. The next two terms are the contributions from the anomalous dimension of frequency $(z-1)$ and the momentum-dependent anomalous dimension of the fermion field $(\eta^{(\psi,N)}_k)$, respectively. These are common in all channels. What is channel dependent is the last term that represents the vertex corrections. To the leading order, there are three distinct vertex corrections. The first is the one in which four-fermion couplings are generated from the spin fluctuations. This gives rise to a term in the beta function that is independent of the four-fermion couplings. The diagrams that source the four-fermion coupling at the lowest order in v are shown in Fig. 2.7. The second type of the vertex correction describes the processes in which spin fluctuations mix quartic fermion operators in different channels and momenta. The leading order diagrams that describe the linear mixing are shown in Fig. 2.8. It generates a term that is linear in the four-fermion couplings but off-diagonal in the space of channel and momentum. Finally, quantum corrections that are quadratic in the four-fermion couplings are shown in Fig. 2.9. This is the process that drives the pairing instability (or particle-hole instability if there is a nesting) in the presence of attractive interactions in Fermi liquids.

For general Fermi surface without the PH symmetry, we only need to consider the forward scattering channel in group 1 and the BCS channel in group 2. For the derivation of the counter terms that lead to the beta functional through Eq. (2.106), see Appendix B. In Appendix D, we discuss the additional channels that need to be considered in the presence of the PH symmetry.

Group 1 : small-angle scatterings

Before we show the result of explicit calculation, let us first describe the physics that determines the beta functionals. In group 1, the critical spin fluctuations generate the source term in the $\left(\begin{smallmatrix}1&1\\1&1\end{smallmatrix}\right)$ channel. In the small v limit, only the ladder diagrams shown in Fig. 2.7 give the leading order contribution. It is noted that tree-diagrams do not contribute to the 1PI vertex function. In the ladder diagrams, a pair of electron and hole near hot spot 1 are scattered to intermediate states near hot spot 4 before they are scattered back to the region near hot spot 1 by exchanging critical bosons. In the absence of the PH symmetry, there is no IR singularity for the diagram in the PP channel due to a lack of nesting. The coupling in the forward scattering channel that is potentially IR singular can be written as $\lambda^{\left(\begin{smallmatrix}1&1\\1&1\end{smallmatrix}\right)}_{\left(\begin{smallmatrix}p&k\\k&p\end{smallmatrix}\right)}$. On the dimensional ground, one expects to encounter a logarithmic divergence for general k and p because both fermions in the loop of Fig. 2.7 can stay on the Fermi surface irrespective of the relative momentum along the Fermi surface [20]. However, the actual IR singularity arises only for

$$\lambda^{\left(\begin{smallmatrix}1&1\\1&1\end{smallmatrix}\right)}_{\left(\begin{smallmatrix}0&k\\k&0\end{smallmatrix}\right)}, \quad \lambda^{\left(\begin{smallmatrix}1&1\\1&1\end{smallmatrix}\right)}_{\left(\begin{smallmatrix}k&0\\0&k\end{smallmatrix}\right)}, \tag{2.107}$$

where at least one electron-hole pair are at the hot spot. This is because the Pauli exclusion principle suppresses the low-energy phase space for particle-hole pairs created on one side of the Fermi surface.

[20] Even if both k and p are non-zero, a boson that carries a non-zero momentum can scatter external fermions to virtual states on the Fermi surface. One naively expects a logarithmic divergence as two fermions can have zero three-momentum in the space of internal three-momentum with co-dimension 2.

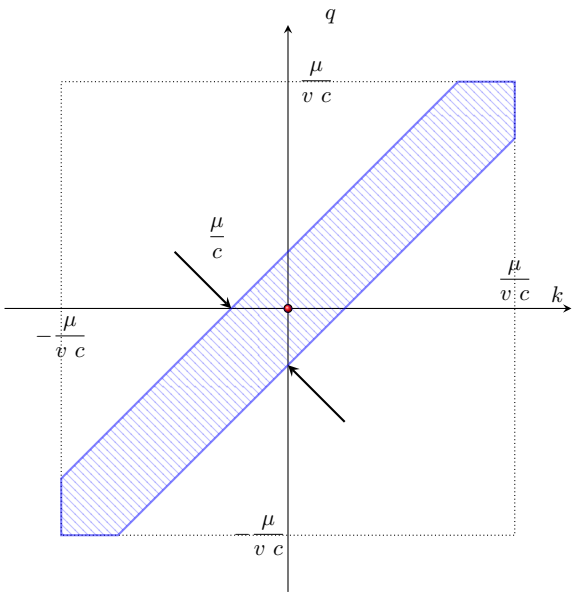

Figure 2.15: When an electron with momentum k near hot spot 1 on the Fermi surface is scattered to momentum p near hot spot 4 on the Fermi surface by exchanging a boson with energy μ, the interaction is largest in the shaded region in which both k and p are less than $\mu/(vc)$ and their difference is less then μ/c in magnitude. Outside the shaded region, the interaction decays in a power-law.

For example, the phase space that is available for an electron-hole pair with total momentum $\vec{q}$ vanishes in the zero $\vec{q}$ limit. As a result, the diagram exhibits a logarithmic singularity only with the help of the critical boson. When a pair of external electron-hole pair are at the hot spot 1, they can be scattered right onto the hot spot 4 through the boson with zero energy. Since two fermions and one boson can simultaneously have zero three-momentum, a logarithmic divergence arises. Once the spin fluctuations generate the source term in the $\left(\begin{smallmatrix}1&1\\1&1\end{smallmatrix}\right)$ channel, it spreads to other channels through linear mixing (Fig. 2.8). The same reasoning that determines the IR singularity of the source term shows that the mixing terms exhibit IR singularity only for external momenta shown in Eq. (2.107). In the $\left(\begin{smallmatrix}1&1\\1&1\end{smallmatrix}\right)$ channel, the diagrams in Fig. 2.9 do not have IR singularity because the critical boson is not involved in those processes.

The fact that the coupling function receives singular vertex correction only for Eq. (2.107) can be checked from the full expression of the beta functional for $\lambda^{\left(\begin{smallmatrix}1&1\\1&1\end{smallmatrix}\right)}_{\left(\begin{smallmatrix}p&k\\k&p\end{smallmatrix}\right)}$ at general k and p

$$\begin{aligned}\beta^{(\lambda);\left(\begin{smallmatrix}1&1\\1&1\end{smallmatrix}\right);\left(\begin{smallmatrix}\sigma_1&\sigma_2\\\sigma_4&\sigma_3\end{smallmatrix}\right)}_{\left(\begin{smallmatrix}p&k\\k&p\end{smallmatrix}\right)} &= \left(1+3(z-1)+2\eta^{(\psi)}_p+2\eta^{(\psi)}_k\right)\lambda^{\left(\begin{smallmatrix}1&1\\1&1\end{smallmatrix}\right);\left(\begin{smallmatrix}\sigma_1&\sigma_2\\\sigma_4&\sigma_3\end{smallmatrix}\right)}_{\left(\begin{smallmatrix}p&k\\k&p\end{smallmatrix}\right)}\\ &- \int \mathrm{d}\rho(q)\left\{\frac{\mathsf{D}_\mu(k;q)^2}{2\pi N_f g^2_{q,k}}\lambda^{\left(\begin{smallmatrix}1&4\\4&1\end{smallmatrix}\right);\left(\begin{smallmatrix}\sigma_1&\alpha\\\beta&\sigma_3\end{smallmatrix}\right)}_{\left(\begin{smallmatrix}p&q\\q&p\end{smallmatrix}\right)}\mathsf{T}^{\beta\sigma_2}_{\sigma_4\alpha}+\frac{\mathsf{D}_\mu(p;q)^2}{2\pi N_f g^2_{p,q}}\mathsf{T}^{\sigma_1\alpha}_{\beta\sigma_3}\lambda^{\left(\begin{smallmatrix}4&1\\1&4\end{smallmatrix}\right);\left(\begin{smallmatrix}\beta&\sigma_2\\\sigma_4&\alpha\end{smallmatrix}\right)}_{\left(\begin{smallmatrix}q&k\\k&q\end{smallmatrix}\right)}\right.\\ &\left.- \frac{\mathsf{D}_\mu(p;q)\mathsf{D}_\mu(q;k)}{\pi N_f^2}\mathsf{T}^{\beta\sigma_2}_{\sigma_4\alpha}\mathsf{T}^{\sigma_1\alpha}_{\beta\sigma_3}\left(\frac{\mathsf{D}_\mu(q;k)}{g^2_{q,k}}+\frac{\mathsf{D}_\mu(p;q)}{g^2_{p,q}}\right)\right\}.\end{aligned} \tag{2.108}$$

Here all repeated spin indices are understood to be summed over. $\mathsf{T}^{\sigma_1\sigma_2}_{\sigma_4\sigma_3}$ is defined in Eq. (2.73). $\int \mathrm{d}\rho(q) = \int \frac{\mathrm{d}q}{2\pi\mu V_{F,q}}$ represents integration along the Fermi surface with the measure normalized by

energy scale μ and the Fermi velocity.

$$\mathsf{D}_\mu(q;k) = g_{q,k}^2 \frac{\mu}{\mu + c\left(|q-k|_\mu + |v_q q + v_k k|_\mu\right)} \tag{2.109}$$

with $|k|_\mu = \sqrt{k^2+\mu^2}$ represents the contribution of the gapless spin fluctuations that renormalizes the short-range four-fermion coupling at energy scale μ. This arises from local counter terms that remove IR singularities of the loop correction in the small μ limit. For $|q-k| \gg \mu$, $\mathsf{D}_\mu(q;k)$ coincides with the interaction mediated by the collective mode with spatial momentum $(q-k, v_q q + v_k k)$ at energy μ, where $(q-k, v_q q + v_k k)$ denotes the momentum that is needed to scatter an electron from $(k, -v_k k)$ near hot spot 1 to $(q, v_q q)$ near hot spot 4 on the Fermi surface. In the limit that q and k are small, $\mathsf{D}_\mu(q;k)$ smoothly saturates to a constant and represents a local interaction in the real space. The main support of $\mathsf{D}_\mu(q;k)$ in the space of q and k is given by $S_D = \{(q,k) || q-k| < \mu/c, |q| < \mu/(vc), |k| < \mu/(vc)\}$ as is illustrated in Fig. 2.15. $\eta_k^{(\psi)}$ is the momentum dependent anomalous dimension of fermion defined in Eq. (2.104). To the leading order in v, $\eta_k^{(\psi)}$ is given by

$$\eta_k^{(\psi)} = \frac{N_c^2-1}{2\pi^2 N_c N_f} \frac{g_k^2}{c V_{F,k}} \frac{\mu}{\mu + 2c v_k |k|_\mu} - (z-1). \tag{2.110}$$

The first line in Eq. (2.108) is the contribution of the tree-level scaling dimension and the anomalous dimensions of frequency and the fermion fields. The second line represents the mixings between $\lambda^{\left(\begin{smallmatrix}1&1\\1&1\end{smallmatrix}\right);\left(\begin{smallmatrix}\sigma_1&\sigma_2\\\sigma_4&\sigma_3\end{smallmatrix}\right)}_{\left(\begin{smallmatrix}p&k\\k&p\end{smallmatrix}\right)}$ and $\left\{\lambda^{\left(\begin{smallmatrix}1&4\\1&1\end{smallmatrix}\right);\left(\begin{smallmatrix}\sigma_1&\alpha\\\beta&\sigma_3\end{smallmatrix}\right)}_{\left(\begin{smallmatrix}p&q\\q&p\end{smallmatrix}\right)}, \lambda^{\left(\begin{smallmatrix}4&1\\1&4\end{smallmatrix}\right);\left(\begin{smallmatrix}\beta&\sigma_2\\\sigma_4&\alpha\end{smallmatrix}\right)}_{\left(\begin{smallmatrix}q&k\\k&q\end{smallmatrix}\right)}\right\}$. Since the momentum along the Fermi surface acts as a continuous flavour, the mixing with coupling functions at different momenta is represented as the integration over q. The last line is the contribution of the ladder diagrams that source the four-fermion coupling. It is essentially the convolution of two boson propagators that are needed to scatter an electron from momentum k to the intermediate momentum q and finally to momentum p. The additional factor $\left(\frac{\mathsf{D}_\mu(q;k)}{g_{k,q}^2} + \frac{\mathsf{D}_\mu(q;p)}{g_{p,q}^2}\right)$ arises from the derivative of $\mathsf{D}_\mu(q;k)$ with respect to $\log\mu$ to the leading order in v limit[21]. It is noted that the full vertex correction is written as integrations over the momentum along the Fermi surface in Eq. (2.108).

If both p and k are away from the hot spots, the vertex corrections vanish in the small μ limit. On the other hand, the phase space in which both k and p are near the hot spot is negligible. Therefore, we focus on the forward scattering between an electron near the hot spot and an electron away from the hot spot. For $k \approx 0$ and $|p| \gg \mu/(vc)$, $\lambda_{\left(\begin{smallmatrix}p&q\\q&p\end{smallmatrix}\right)}$ and $\mathsf{D}_\mu(q;p)$ as functions of q vary much more slowly compared to $\mathsf{D}_\mu(k;q)^2$ which is sharply peaked at $q=k$[22]. Then, we can use $\int dq\ \mathsf{D}_\mu(k;q)^2 f(q;p) \approx f(k;p)\int dq\ \mathsf{D}_\mu(k;q)^2$ for $f(q;p) = \lambda_{\left(\begin{smallmatrix}p&q\\q&p\end{smallmatrix}\right)}$ or $\mathsf{D}_\mu(q;p)$ to simplify the beta functional as[23]

$$\begin{aligned}
\beta^{(\lambda);\left(\begin{smallmatrix}1&1\\1&1\end{smallmatrix}\right);\left(\begin{smallmatrix}\sigma_1&\sigma_2\\\sigma_4&\sigma_3\end{smallmatrix}\right)}_{\left(\begin{smallmatrix}p&k\\k&p\end{smallmatrix}\right)} &= \left(1 + 3(z-1) + 2\eta_p^{(\psi)} + 2\eta_k^{(\psi)}\right) \lambda^{\left(\begin{smallmatrix}1&1\\1&1\end{smallmatrix}\right);\left(\begin{smallmatrix}\sigma_1&\sigma_2\\\sigma_4&\sigma_3\end{smallmatrix}\right)}_{\left(\begin{smallmatrix}p&k\\k&p\end{smallmatrix}\right)} \\
&- \frac{g_{k,k}^2}{2\pi^2 c N_f V_{F,k}} \frac{\mu}{\mu + 2v_k c|k|_\mu} \lambda^{\left(\begin{smallmatrix}1&4\\1&1\end{smallmatrix}\right);\left(\begin{smallmatrix}\sigma_1&\alpha\\\beta&\sigma_3\end{smallmatrix}\right)}_{\left(\begin{smallmatrix}p&k\\k&p\end{smallmatrix}\right)} \mathsf{T}^{\beta\sigma_2}_{\sigma_4\alpha} - \frac{g_{p,p}^2}{2\pi^2 c N_f V_{F,p}} \frac{\mu}{\mu + 2v_p c|p|_\mu} \mathsf{T}^{\sigma_1\alpha}_{\beta\sigma_3} \lambda^{\left(\begin{smallmatrix}4&1\\1&4\end{smallmatrix}\right);\left(\begin{smallmatrix}\beta&\sigma_2\\\sigma_4&\alpha\end{smallmatrix}\right)}_{\left(\begin{smallmatrix}p&k\\k&p\end{smallmatrix}\right)} \\
&+ \mathsf{T}^{\beta\sigma_2}_{\sigma_4\alpha} \mathsf{T}^{\sigma_1\alpha}_{\beta\sigma_3} \frac{\mathsf{D}_\mu(p;k)}{\pi^2 c N_f^2} \left[\frac{\mu g_{k,k}^2}{V_{F,k}(\mu + 2v_k c|k|_\mu)} + \frac{\mu g_{p,p}^2}{V_{F,p}(\mu + 2v_p c|p|_\mu)}\right]
\end{aligned} \tag{2.111}$$

[21] Because the beta functional is given by the derivative of the quantum correction with respect to $\log\mu$, and the gapless fermions alone do not exhibit IR singularity in the small μ limit, the derivative only acts on the boson propagator.

[22] The profile of λ will be confirmed from the solution of the beta functional in Sec. 2.6.

[23] We can also use $\int dq\ \mathsf{D}_\mu(p;q)^2 f(q;k) \approx f(p;k)\int dq\ \mathsf{D}_\mu(p;q)^2$ because both sides vanish in the small μ limit for $k \approx 0$ and $|p| \gg \mu/(vc)$.

in the small μ limit. Here, $\frac{g_{k,k}^2}{2\pi^2 c N_f V_{F,k}} \frac{\mu}{\mu+2vc|k|_\mu}$ corresponds to the momentum dependent mixing matrix element. For $k=0$ and $p\neq 0$ ($k\neq 0$ and $p=0$), $\lambda^{\binom{1\ 1}{1\ 1};\binom{\sigma_1\ \sigma_2}{\sigma_4\ \sigma_3}}_{\binom{p\ k}{k\ p}}$ mixes only with $\lambda^{\binom{1\ 4}{4\ 1};\binom{\sigma_1\ \alpha}{\beta\ \sigma_3}}_{\binom{p\ k}{k\ p}}$ $\left(\lambda^{\binom{4\ 1}{1\ 4};\binom{\beta\ \sigma_2}{\sigma_4\ \alpha}}_{\binom{p\ k}{k\ p}}\right)$ in the small μ limit. This implies that the forward scattering amplitude is mainly renormalized through the electrons at the hot spots as is indicated in Table. 2.2.

Since the beta functional for $\lambda^{\binom{1\ 1}{1\ 1}}$ depend on $\lambda^{\binom{1\ 4}{4\ 1}}$, $\lambda^{\binom{4\ 1}{1\ 4}}$, and their beta functionals depend on $\lambda^{\binom{4\ 4}{4\ 4}}$, we need to compute the beta functionals for those couplings to have a closed set of beta functionals. The beta functionals for the other couplings are obtained to be

$$\beta^{(\lambda);\binom{1\ 4}{4\ 1};\binom{\sigma_1\ \sigma_2}{\sigma_4\ \sigma_3}}_{\binom{p\ k}{k\ p}} = \left(1+3(z-1)+2\eta_p^{(\psi)}+2\eta_k^{(\psi)}\right)\lambda^{\binom{1\ 4}{4\ 1};\binom{\sigma_1\ \sigma_2}{\sigma_4\ \sigma_3}}_{\binom{p\ k}{k\ p}}$$
$$-\frac{g_{k,k}^2}{2\pi^2 c N_f V_{F,k}}\frac{\mu}{\mu+2v_k c|k|_\mu}\lambda^{\binom{1\ 1}{1\ 1};\binom{\sigma_1\ \alpha}{\beta\ \sigma_3}}_{\binom{p\ k}{k\ p}}\mathsf{T}^{\beta\sigma_2}_{\sigma_4\alpha}-\frac{g_{p,p}^2}{2\pi^2 c N_f V_{F,p}}\frac{\mu}{\mu+2v_p c|p|_\mu}\mathsf{T}^{\sigma_1\alpha}_{\beta\sigma_3}\lambda^{\binom{4\ 4}{4\ 4};\binom{\beta\ \sigma_2}{\sigma_4\ \alpha}}_{\binom{p\ k}{k\ p}}, \tag{2.112}$$

$$\beta^{(\lambda);\binom{4\ 1}{1\ 4};\binom{\sigma_1\ \sigma_2}{\sigma_4\ \sigma_3}}_{\binom{p\ k}{k\ p}} = \left(1+3(z-1)+2\eta_p^{(\psi)}+2\eta_k^{(\psi)}\right)\lambda^{\binom{4\ 1}{1\ 4};\binom{\sigma_1\ \sigma_2}{\sigma_4\ \sigma_3}}_{\binom{p\ k}{k\ p}}$$
$$-\frac{g_{k,k}^2}{2\pi^2 c N_f V_{F,k}}\frac{\mu}{\mu+2v_k c|k|_\mu}\lambda^{\binom{4\ 4}{4\ 4};\binom{\sigma_1\ \alpha}{\beta\ \sigma_3}}_{\binom{p\ k}{k\ p}}\mathsf{T}^{\beta\sigma_2}_{\sigma_4\alpha}-\frac{g_{p,p}^2}{2\pi^2 c N_f V_{F,p}}\frac{\mu}{\mu+2v_p c|p|_\mu}\mathsf{T}^{\sigma_1\alpha}_{\beta\sigma_3}\lambda^{\binom{1\ 1}{1\ 1};\binom{\beta\ \sigma_2}{\sigma_4\ \alpha}}_{\binom{p\ k}{k\ p}}, \tag{2.113}$$

$$\beta^{(\lambda);\binom{4\ 4}{4\ 4};\binom{\sigma_1\ \sigma_2}{\sigma_4\ \sigma_3}}_{\binom{p\ k}{k\ p}} = \left(1+3(z-1)+2\eta_p^{(\psi)}+2\eta_k^{(\psi)}\right)\lambda^{\binom{4\ 4}{4\ 4};\binom{\sigma_1\ \sigma_2}{\sigma_4\ \sigma_3}}_{\binom{p\ k}{k\ p}}$$
$$-\frac{g_{k,k}^2}{2\pi^2 c N_f V_{F,k}}\frac{\mu}{\mu+2v_k c|k|_\mu}\lambda^{\binom{4\ 1}{1\ 4};\binom{\sigma_1\ \alpha}{\beta\ \sigma_3}}_{\binom{p\ k}{k\ p}}\mathsf{T}^{\beta\sigma_2}_{\sigma_4\alpha}-\frac{g_{p,p}^2}{2\pi^2 c N_f V_{F,p}}\frac{\mu}{\mu+2v_p c|p|_\mu}\mathsf{T}^{\sigma_1\alpha}_{\beta\sigma_3}\lambda^{\binom{1\ 4}{4\ 1};\binom{\beta\ \sigma_2}{\sigma_4\ \alpha}}_{\binom{p\ k}{k\ p}}$$
$$+\mathsf{T}^{\beta\sigma_2}_{\sigma_4\alpha}\mathsf{T}^{\sigma_1\alpha}_{\beta\sigma_3}\frac{\mathsf{D}_\mu(p;k)}{\pi^2 c N_f^2}\left[\frac{\mu g_{k,k}^2}{V_{F,k}(\mu+2v_k c|k|_\mu)}+\frac{\mu g_{p,p}^2}{V_{F,p}(\mu+2v_p c|p|_\mu)}\right]. \tag{2.114}$$

The beta functional for $\lambda^{\binom{4\ 4}{4\ 4};\binom{\sigma_1\ \sigma_2}{\sigma_4\ \sigma_3}}_{\binom{p\ k}{k\ p}}$ takes the same form as that of $\lambda^{\binom{1\ 1}{1\ 1};\binom{\sigma_1\ \sigma_2}{\sigma_4\ \sigma_3}}_{\binom{p\ k}{k\ p}}$ because those two are related to each other through the C_4 symmetry. On the other hand, there is no source term for $\lambda^{\binom{1\ 4}{4\ 1};\binom{\sigma_1\ \sigma_2}{\sigma_4\ \sigma_3}}_{\binom{p\ k}{k\ p}}$ and $\lambda^{\binom{4\ 1}{1\ 4};\binom{\sigma_1\ \sigma_2}{\sigma_4\ \sigma_3}}_{\binom{p\ k}{k\ p}}$ to the leading order in v as is shown in Eqs. (2.111) and (2.114).

Group 2 : BCS pairing

In group 2, the ladder diagrams in Fig. 2.7 generate $\lambda^{\binom{1\ 5}{1\ 5}}$. It then mixes with $\lambda^{\binom{4\ 8}{1\ 5}}$, $\lambda^{\binom{1\ 5}{4\ 8}}$ through diagrams in Fig. 2.8. In terms of how couplings are mixed in the space of hot spots, the structure of the beta functionals is similar to the $\binom{1\ 1}{1\ 1}$ channel except that the mixing occurs in the particle-particle channel for general k and p in group 2. There are more important differences in how operators with different momenta mix in this channel compared to the $\binom{1\ 1}{1\ 1}$ channel. The difference arises from the fact that the couplings in the $\binom{1\ 5}{1\ 5}$ channel describe scatterings of fermions on the opposite sides of the Fermi surface, and the phase space of a pair of fermions in antipodal patches is not suppressed by the Pauli exclusion principle. Namely, a Cooper pair with zero center of mass momentum can be placed anywhere above but arbitrarily close to the Fermi surface. As a result, IR divergences arise within a two-dimensional space of external momenta irrespective of the relative momenta of electrons within incoming and outgoing Cooper pairs.

The beta functional for $\lambda^{\binom{1\ 5}{1\ 5};\binom{\sigma_1\ \sigma_2}{\sigma_4\ \sigma_3}}_{\binom{p\ -p}{k\ -k}}$ at generic k and p is given by

$$\begin{aligned}\beta^{(\lambda);\binom{1\ 5}{1\ 5};\binom{\sigma_1\ \sigma_2}{\sigma_4\ \sigma_3}}_{\binom{p\ -p}{k\ -k}} &= \left(1+3(z-1)+2\eta_p^{(\psi)}+2\eta_k^{(\psi)}\right)\lambda^{\binom{1\ 5}{1\ 5};\binom{\sigma_1\ \sigma_2}{\sigma_4\ \sigma_3}}_{\binom{p\ -p}{k\ -k}} \\ &+\int \mathrm{d}\rho(q)\left\{-\frac{\mathsf{D}_\mu(p;q)}{2\pi N_f}\mathsf{T}^{\sigma_1\sigma_2}_{\alpha\beta}\lambda^{\binom{4\ 8}{1\ 5};\binom{\alpha\ \beta}{\sigma_4\ \sigma_3}}_{\binom{q\ -q}{k\ -k}}-\frac{\mathsf{D}_\mu(q;k)}{2\pi N_f}\lambda^{\binom{1\ 5}{4\ 8};\binom{\sigma_1\ \sigma_2}{\alpha\ \beta}}_{\binom{p\ -p}{q\ -q}}\mathsf{T}^{\alpha\beta}_{\sigma_4\sigma_3}\right. \\ &+\frac{1}{\pi N_f^2}\mathsf{T}^{\sigma_1\sigma_2}_{\alpha\beta}\mathsf{T}^{\alpha\beta}_{\sigma_4\sigma_3}\mathsf{D}_\mu(p;q)\mathsf{D}_\mu(q;k) \\ &\left.+\frac{1}{4\pi}\left(\lambda^{\binom{1\ 5}{1\ 5};\binom{\sigma_1\ \sigma_2}{\beta\ \alpha}}_{\binom{p\ -p}{q\ -q}}\lambda^{\binom{1\ 5}{1\ 5};\binom{\beta\ \alpha}{\sigma_4\ \sigma_3}}_{\binom{q\ -q}{k\ -k}}+\lambda^{\binom{1\ 5}{4\ 8};\binom{\sigma_1\ \sigma_2}{\beta\ \alpha}}_{\binom{p\ -p}{q\ -q}}\lambda^{\binom{4\ 8}{1\ 5};\binom{\beta\ \alpha}{\sigma_4\ \sigma_3}}_{\binom{q\ -q}{k\ -k}}\right)\right\}.\end{aligned} \tag{2.115}$$

$\lambda^{\binom{1\ 5}{1\ 5};\binom{\sigma_1\ \sigma_2}{\sigma_4\ \sigma_3}}_{\binom{p\ -p}{k\ -k}}$ describes the interaction in which a pair of electrons with zero center of mass momentum are scattered in antipodal hot patches. The first line in Eq. (2.115) is the contribution from the tree-level scaling dimension and the anomalous dimensions. The second line represents the linear mixing between $\lambda^{\binom{1\ 5}{1\ 5};\binom{\sigma_1\ \sigma_2}{\sigma_4\ \sigma_3}}_{\binom{p\ -p}{k\ -k}}$ and $\left\{\lambda^{\binom{4\ 8}{1\ 5};\binom{\alpha\ \beta}{\sigma_4\ \sigma_3}}_{\binom{q\ -q}{k\ -k}},\lambda^{\binom{1\ 5}{4\ 8};\binom{\sigma_1\ \sigma_2}{\alpha\ \beta}}_{\binom{p\ -p}{q\ -q}}\right\}$. Unlike in Eq. (2.108), the mixing between coupling functions at different momenta decays only in a single power of D_μ, and there is no additional suppression even when both p and k are way from the hot spots. This is because the vertex correction is IR divergent for any p and k. For example, the first term in the second line describes the process in which a pair of electrons at momenta k and $-k$ near hot spots 1 and 5 are scattered to momenta q and $-q$ near hot spots 4 and 8 through the short-range four-fermion interaction and then to momenta p and $-p$ near hot spots 1 and 5 by exchanging a boson. The next term can be understood similarly. In this process, the internal fermions can simultaneously stay outside but close to the Fermi surface for any q. This gives rise to a logarithmic IR singularity that is not tied to the criticality of the boson. In the beta functional that is given by the integration over q, the amplitude of mixing is simply controlled by the interaction mediated by the boson that carries the momentum needed to scatter the pair of electrons within the Fermi surface. Since the mixing amplitude scales as $\mathsf{D}_\mu(q,k)\sim g_{q,k}^2/|q-k|$ at large momenta, the contributions from large-angle scatterings are not strongly suppressed.

If the coupling functions are weakly dependent on momentum, the slow decay of the mixing matrix gives rise to a logarithmic divergence $\log\Lambda'/\mu$, where Λ' is a scale at which the large momentum is cut off[24]. The explicit dependence of the beta functional on a UV scale is a manifestation of the fact that the quantum correction itself exhibits a $\log^2$ divergence, where one logarithm is from the BCS scatterings of the gapless fermions and the other logarithm is from the criticality of the boson. In the functional RG formalism, the physical origins of these two logarithms are naturally resolved, and they manifest themselves in different ways : μ in the fermionic log acts as an IR energy cutoff that controls the 'distance' away from the Fermi surface and μ in the bosonic log acts as an IR cutoff that regulates how operators with different momentum along the Fermi surface mix. Interestingly, the mixing between operators with momenta q and k along the Fermi surface is controlled by $\mathsf{D}_\mu(q,k)$. The fact that the mixing between low-energy operators with large $q-k$ is determined from the dynamics of the high-energy boson implies that the four-fermion coupling function is not a low-energy observable that can be predicted within the low-energy effective field theory. While the 1PI quartic vertex function, represented by the four-fermion coupling function, can not be predicted within the low-energy effective field theory, the theory is still predictive for a different low-energy observable that captures the strength of two-body interaction. In Sec. 2.6, this will be discussed in full details. For now, let us set this issue aside and complete the rest of the beta functionals. Once the full beta functionals are completed, we will be in the better position to address the issue of UV/IR mixing more

[24]For example, the scale associated with the irrelevant kinetic term of the boson can act as a large momentum cutoff.

systematically. The term in the third line is the source that is generated from the spin fluctuations. Because there exists the fermionic logarithmic singularity associated with the virtual fermions that are on the antipodal patches of the Fermi surface, the contribution to the beta function is simply given by a convolution of two boson propagators without an additional suppression as in Eq. (D.7). Finally, the last line is the usual term that drives the BCS instability in the presence of attractive four-fermion couplings in Fermi liquids. Its contribution is expressed as a convolution of two four-fermion coupling functions.[25]

Together with the beta functional for $\lambda^{\binom{1\ 5}{1\ 5};\binom{\sigma_1\ \sigma_2}{\sigma_4\ \sigma_3}}_{\binom{p\ -p}{k\ -k}}$, the beta functionals for $\lambda^{\binom{4\ 8}{1\ 5};\binom{\sigma_1\ \sigma_2}{\sigma_4\ \sigma_3}}_{\binom{p\ -p}{k\ -k}}$, $\lambda^{\binom{1\ 5}{4\ 8};\binom{\sigma_1\ \sigma_2}{\sigma_4\ \sigma_3}}_{\binom{p\ -p}{k\ -k}}$, $\lambda^{\binom{4\ 8}{4\ 8};\binom{\sigma_1\ \sigma_2}{\sigma_4\ \sigma_3}}_{\binom{p\ -p}{k\ -k}}$ form a closed set of flow equations at generic momenta in the two-dimensional plane of IR singularity. The beta functionals for the remaining coupling functions are written as

$$\begin{aligned}
\beta^{(\lambda);\binom{4\ 8}{1\ 5};\binom{\sigma_1\ \sigma_2}{\sigma_4\ \sigma_3}}_{\binom{p\ -p}{k\ -k}} &= \left(1+3(z-1)+2\eta_p^{(\psi)}+2\eta_k^{(\psi)}\right)\lambda^{\binom{4\ 8}{1\ 5};\binom{\sigma_1\ \sigma_2}{\sigma_4\ \sigma_3}}_{\binom{p\ -p}{k\ -k}} \\
&+\int \mathrm{d}\rho(q)\left\{-\frac{1}{2\pi N_f}\left[\mathsf{D}_\mu(p;q)\mathsf{T}^{\sigma_1\sigma_2}_{\alpha\beta}\lambda^{\binom{1\ 5}{1\ 5};\binom{\alpha\ \beta}{\sigma_4\ \sigma_3}}_{\binom{q\ -q}{k\ -k}}+\mathsf{D}_\mu(q;k)\lambda^{\binom{4\ 8}{4\ 8};\binom{\sigma_1\ \sigma_2}{\alpha\ \beta}}_{\binom{p\ -p}{q\ -q}}\mathsf{T}^{\alpha\beta}_{\sigma_4\sigma_3}\right]\right. \\
&\left.+\frac{1}{4\pi}\left(\lambda^{\binom{4\ 8}{1\ 5};\binom{\sigma_1\ \sigma_2}{\beta\ \alpha}}_{\binom{p\ -p}{q\ -q}}\lambda^{\binom{1\ 5}{1\ 5};\binom{\beta\ \alpha}{\sigma_4\ \sigma_3}}_{\binom{q\ -q}{k\ -k}}+\lambda^{\binom{4\ 8}{4\ 8};\binom{\sigma_1\ \sigma_2}{\beta\ \alpha}}_{\binom{p\ -p}{q\ -q}}\lambda^{\binom{4\ 8}{1\ 5};\binom{\beta\ \alpha}{\sigma_4\ \sigma_3}}_{\binom{q\ -q}{k\ -k}}\right)\right\},
\end{aligned} \tag{2.116}$$

$$\begin{aligned}
\beta^{(\lambda);\binom{1\ 5}{4\ 8};\binom{\sigma_1\ \sigma_2}{\sigma_4\ \sigma_3}}_{\binom{p\ -p}{k\ -k}} &= \left(1+3(z-1)+2\eta_p^{(\psi)}+2\eta_k^{(\psi)}\right)\lambda^{\binom{1\ 5}{4\ 8};\binom{\sigma_1\ \sigma_2}{\sigma_4\ \sigma_3}}_{\binom{p\ -p}{k\ -k}} \\
&+\int \mathrm{d}\rho(q)\left\{-\frac{1}{2\pi N_f}\left[\mathsf{D}_\mu(p;q)\mathsf{T}^{\sigma_1\sigma_2}_{\alpha\beta}\lambda^{\binom{4\ 8}{4\ 8};\binom{\alpha\ \beta}{\sigma_4\ \sigma_3}}_{\binom{q\ -q}{k\ -k}}+\mathsf{D}_\mu(q;k)\lambda^{\binom{1\ 5}{1\ 5};\binom{\sigma_1\ \sigma_2}{\alpha\ \beta}}_{\binom{p\ -p}{q\ -q}}\mathsf{T}^{\alpha\beta}_{\sigma_4\sigma_3}\right]\right. \\
&\left.+\frac{1}{4\pi}\left(\lambda^{\binom{1\ 5}{1\ 5};\binom{\sigma_1\ \sigma_2}{\beta\ \alpha}}_{\binom{p\ -p}{q\ -q}}\lambda^{\binom{1\ 5}{4\ 8};\binom{\beta\ \alpha}{\sigma_4\ \sigma_3}}_{\binom{q\ -q}{k\ -k}}+\lambda^{\binom{1\ 5}{4\ 8};\binom{\sigma_1\ \sigma_2}{\beta\ \alpha}}_{\binom{p\ -p}{q\ -q}}\lambda^{\binom{4\ 8}{4\ 8};\binom{\beta\ \alpha}{\sigma_4\ \sigma_3}}_{\binom{q\ -q}{k\ -k}}\right)\right\},
\end{aligned} \tag{2.117}$$

$$\begin{aligned}
\beta^{(\lambda);\binom{4\ 8}{4\ 8};\binom{\sigma_1\ \sigma_2}{\sigma_4\ \sigma_3}}_{\binom{p\ -p}{k\ -k}} &= \left(1+3(z-1)+2\eta_p^{(\psi)}+2\eta_k^{(\psi)}\right)\lambda^{\binom{4\ 8}{4\ 8};\binom{\sigma_1\ \sigma_2}{\sigma_4\ \sigma_3}}_{\binom{p\ -p}{k\ -k}} \\
&+\int \mathrm{d}\rho(q)\left\{-\frac{\mathsf{D}_\mu(p;q)}{2\pi N_f}\mathsf{T}^{\sigma_1\sigma_2}_{\alpha\beta}\lambda^{\binom{1\ 5}{4\ 8};\binom{\alpha\ \beta}{\sigma_4\ \sigma_3}}_{\binom{q\ -q}{k\ -k}}-\frac{\mathsf{D}_\mu(q;k)}{2\pi N_f}\lambda^{\binom{4\ 8}{1\ 5};\binom{\sigma_1\ \sigma_2}{\alpha\ \beta}}_{\binom{p\ -p}{q\ -q}}\mathsf{T}^{\alpha\beta}_{\sigma_4\sigma_3}\right. \\
&+\frac{1}{\pi N_f^2}\mathsf{T}^{\sigma_1\sigma_2}_{\alpha\beta}\mathsf{T}^{\alpha\beta}_{\sigma_4\sigma_3}\mathsf{D}_\mu(p;q)\mathsf{D}_\mu(q;k) \\
&\left.+\frac{1}{4\pi}\left(\lambda^{\binom{4\ 8}{1\ 5};\binom{\sigma_1\ \sigma_2}{\beta\ \alpha}}_{\binom{p\ -p}{q\ -q}}\lambda^{\binom{1\ 5}{4\ 8};\binom{\beta\ \alpha}{\sigma_4\ \sigma_3}}_{\binom{q\ -q}{k\ -k}}+\lambda^{\binom{4\ 8}{4\ 8};\binom{\sigma_1\ \sigma_2}{\beta\ \alpha}}_{\binom{p\ -p}{q\ -q}}\lambda^{\binom{4\ 8}{4\ 8};\binom{\beta\ \alpha}{\sigma_4\ \sigma_3}}_{\binom{q\ -q}{k\ -k}}\right)\right\}.
\end{aligned} \tag{2.118}$$

Eq. (2.118) is related to Eq. (2.115) through the C_4 symmetry. Similarly, Eq. (2.117) is related to Eq. (2.116) through the symmetry. It is noted that there is no λ-independent source term for Eq. (2.116) and Eq. (2.117).

[25] Here, we focus on the four-fermion couplings that are generated from the critical spin fluctuations to the leading order in v. In the presence of a bare four-fermion coupling, more channels such as $\lambda^{\binom{1\ 5}{2\ 6}}\lambda^{\binom{2\ 6}{1\ 5}}$ and $\lambda^{\binom{1\ 5}{3\ 7}}\lambda^{\binom{3\ 7}{1\ 5}}$ should be included in the BCS term.

2.5.3 The true fixed point

The full beta functionals that describe the flow of the coupling functions under the lowering of the energy scale and the dilatation of momentum along the Fermi surface are Eqs. (2.54)-(2.57), where $\beta_k^{(v)}$, $\beta_k^{(V_F)}$, $\beta_{k'k}^{(g)}$ and $\beta_{\{k_i\}}^{(\lambda)}$ are given by Eqs. (2.101)- (2.104), Eqs. (2.111) -(2.114), Eqs. (2.115) -(2.118) [26]. In the space of the coupling functions, a fixed point arises at

$$v_k = 0, \quad V_{F,k} = 1, \quad g_{k'k} = 0, \quad \lambda^{\binom{N_1\ N_2}{N_4\ N_3};\binom{\sigma_1\ \sigma_2}{\sigma_4\ \sigma_3}}_{\binom{k+l\ p-l}{k\ \ p}} = 0, \tag{2.119}$$

with $\frac{g_{k'k}^2}{v_k} = \frac{\pi}{2}$. Since the coupling functions in Eq. (2.119) are independent of momentum, $\beta_k^{(v)}$, $\beta_k^{(V_F)}$, $\beta_{k'k}^{(g)}$ and $\beta_{\{k_i\}}^{(\lambda)}$ also vanish at the fixed point. In the space of coupling functions, Eq. (2.119) is a singular point, and the theory with $g_{k'k} = 0$ and $v_k = 0$ is well defined only after the ratio between the Yukawa coupling and the nesting angle is specified as the singular point is approached. Since the leading-order quantum corrections for the renormalized boson propagator are proportional to g^2/v, the ratio determines the anomalous dimension of the boson. For the non-interacting Gaussian theory, $\frac{g_{k'k}^2}{v_{k''}} = 0$. With $\frac{g_{k'k}^2}{v_{k''}} = \frac{\pi}{2}$, there are infinitely many diagrams that renormalize the boson propagator non-perturbatively. These are included in Schwinger-Dyson equation in Eq. (2.3), which gives rise to anomalous dimension 1 for the boson. On the other hand, the anomalous dimension of the fermion is proportional to g^2/c (Eq. (2.104)). At the interacting fixed point with $\frac{g_{k'k}^2}{v_{k''}} = \frac{\pi}{2}$, $g_{k'k}^2/c$ vanishes because v_k and c are related to each other through Eq. (2.4). Consequently, the fermion has no anomalous dimension, and the dynamical critical exponent is 1 at the fixed point.

It turns out that Eq. (2.119) is an unstable fixed point as a generic perturbation added to the fixed point drives the theory toward a superconducting state at low energies. We establish this by solving the full beta functionals of theories that are tuned away from the fixed point. To be concrete, we consider a UV theory with

$$\begin{aligned} v_k = v_0 \ll 1, \quad V_{\mathrm{F},k} = 1, \\ g_{k',k} = \sqrt{\frac{\pi}{2}} v_0, \quad \lambda_{\{k_i\}}^{\{N_i\};\{\sigma_i\}} = 0 \end{aligned} \tag{2.120}$$

at a UV energy scale Λ. Here, we consider a small but non-zero nesting angle. The UV theory has momentum independent nesting angle, Fermi velocity and Yukawa coupling with zero four-fermion coupling. Considering this particular UV theory is not a strong constraint for the following reasons. First, although the bare four-fermion coupling is zero at a UV scale in Eq. (2.120), non-zero four-fermion couplings are generated from the spin fluctuations at low energies. Conclusions drawn for the UV theory in Eq. (2.120) also apply to theories in which the bare four-fermion coupling is weaker than the four-fermion coupling generated from the spin fluctuations. Second, even if the bare coupling functions are chosen to be momentum-independent in Eq. (2.120), renormalized coupling functions acquire non-trivial momentum dependence at low energies. We will see that the universal momentum profiles of the coupling functions become singular near the hot spots in the low energy limit[27]. If a UV theory has momentum dependent bare coupling functions, which must be smooth as functions of momentum due to locality, the renormalized coupling functions acquire the same universal singularities near the hot spots on top of the smooth profile of coupling functions. Third, the value of the Yukawa coupling is merely a convention. It can be chosen to be any $O(1)$ number in the absence of the bare boson kinetic term that can be dropped at low energies in the vicinity of the interacting fixed point. Finally, the simple momentum independent coupling functions chosen in Eq. (2.120) happens to possess the PH symmetry. In this case, the four-fermion couplings also receive singular quantum corrections

[26] It is reminded that $\beta_k^{(v)}$, $\beta_k^{(V_F)}$, $\beta_{k'k}^{(g)}$ and $\beta_{\{k_i\}}^{(\lambda)}$ describe the flow of the coupling functions with increasing energy at *fixed* momenta without momentum dilatation.

[27] Below the superconducting transition temperature scale, the singularity is cut off.

in the $2k_F$ scattering channels in which the external momenta take values shown in Eq. (2.80) and Eq. (2.81). The full beta functionals that include the $2k_F$ scattering channels are derived in Appendix D. However, at low energies, one can ignore the contributions from those additional couplings to the flow of the couplings in the BCS pairing channel that drives the superconducting instability. This is because the volume of the phase space in which the $2k_F$ scattering channels overlap with the BCS pairing channels vanishes in the low energy limit. For details, see Appendix D.

As it is the case for the hot spot theory, we organize quantum corrections in terms of $v \sim g^2$ to understand the full functional RG flow in the vicinity of the fixed point. $g^2/c \sim \sqrt{v/\log(1/v)}$ controls the strength of the quantum corrections associated with the Yukawa coupling beyond the non-perturbative quantum corrections that is included through Eq. (2.3). The four-fermion coupling generated from the critical spin fluctuations is order of g^4/c. Since the four-fermion coupling generated from the loop corrections is smaller than the tree-level interaction mediated by the spin fluctuations, one can understand the RG flow of v, V_F and g without including the feedback of the four-fermion coupling until the four-fermion coupling become large due to superconducting instability in the low-energy limit. We will see that in the small v limit there is a large window of energy scale in which the feedback of the four-fermion coupling can be ignored. In the low-energy limit in which the four-fermion coupling becomes stronger than the interaction mediated by the spin fluctuations, the four-fermion coupling dominates the physics and the spin fluctuations become largely unimportant.

2.6 Quasi-fixed points

In this section, we study the RG flow of the UV theory that are tuned away from the fixed point as in Eq. (2.120). Because the feedback of the four-fermion coupling to the nesting angle, Fermi velocity and the Yukawa coupling is negligible over a large window of length scale, we can first focus on the flow equations of v, V_F and g. Then, we discuss the beta functional for the four-fermion coupling.

2.6.1 Fermi velocity and electron-boson coupling

From Eqs. (2.101)- (2.104), the beta functionals for $v_k, V_{F,k}$ and $g_{k',k}$ are written as

$$\begin{aligned}\frac{\partial v_k(\ell)}{\partial \ell} =& v_k(\ell)\Bigg[-\frac{4(N_c^2-1)}{\pi^3 N_c N_f}\frac{g_k(\ell)^2}{V_{F,k}(\ell)^2}\log\left(\frac{V_{F,k}(\ell)}{c(\ell)}\right)\Theta_1(\ell, L^{(1L)}(k;\ell)) \\ &- \frac{2(N_c^2-1)}{\pi^4 N_c^2 N_f^2}\frac{g_k(\ell)^4}{c(\ell)^2 V_{F,k}(\ell)^2}\log^2\left(\frac{V_{F,k}(\ell)v_k(\ell)}{c(\ell)}\right)\Theta_1(\ell, L^{(2L)}(k;\ell))\Bigg],\end{aligned} \tag{2.121}$$

$$\begin{aligned}\frac{\partial V_{F,k}(\ell)}{\partial \ell} =& V_{F,k}(\ell)\Bigg[\frac{2(N_c^2-1)}{\pi^3 N_c N_f}\frac{g_k(\ell)^2}{V_{F,k}(\ell)^2}\log\left(\frac{V_{F,k}(\ell)}{c(\ell)}\right)\Theta_1(\ell, L^{(1L)}(k;\ell)) \\ &- \frac{N_c^2-1}{\pi^2 N_c N_f}\frac{g_k(\ell)^2}{c(\ell)V_{F,k}(\ell)}\Theta_1(\ell, L^{(1L)}(k;\ell)) \\ &- \frac{3}{2}\frac{N_c^2-1}{\pi^2 N_c N_f}v_0(\ell)\log\left(\frac{1}{c(\ell)}\right) + \frac{N_c^2-1}{2\pi N_c N_F}w_0(\ell) \\ &+ \frac{(N_c^2-1)}{2\pi^4 N_c^2 N_f^2}\frac{g_k(\ell)^4}{c(\ell)^2 V_{F,k}(\ell)^2}\log^2\left(\frac{V_{F,k}(\ell)v_k(\ell)}{c(\ell)}\right)\Theta_1(\ell, L^{(2L)}(k;\ell))\Bigg],\end{aligned} \tag{2.122}$$

$$\begin{aligned}\frac{\partial g_{k',k}(\ell)}{\partial \ell} =& g_{k',k}(\ell)\Bigg[-\frac{1}{2\pi N_c N_f}w_0(\ell)\log\left(\frac{1}{w_0(\ell)}\right) + \frac{N_c^2-1}{2\pi N_c N_f}w_0(\ell) \\ &- \frac{(N_c^2-1)}{\pi^2 N_c N_f}v_0(\ell)\log\left(\frac{1}{v_0(\ell)}\right) - \frac{(N_c^2-1)g_k(\ell)^2\Theta_1(\ell, L^{(1L)}(k;\ell))}{2\pi^2 N_c N_f c(\ell)V_{F,k}(\ell)} \\ &- \frac{(N_c^2-1)g_{k'}(\ell)^2\Theta_1(\ell, L^{(1L)}(k';\ell))}{2\pi^2 N_c N_f c(\ell)V_{F,k'}(\ell)} \\ &+ \frac{2g_k(\ell)g_{k'}(\ell)}{\pi^2 c(\ell)N_c N_f(V_{F,k}(\ell)+V_{F,k'}(\ell))}\log\left(\frac{c(V_{F,k}(\ell)^{-1}+V_{F,k'}(\ell)^{-1})}{v_k(\ell)+v_{k'}(\ell)}\right) \\ &\times \Theta_2(\ell, L^{(1L)}(k;\ell), L^{(1L)}(k';\ell), L^{(1L)}(k',k;\ell))\Bigg].\end{aligned} \tag{2.123}$$

Here ℓ is the logarithmic length scale, $\ell = \log\Lambda/\mu$. $\Theta_i(\ell,\ell_1,..,\ell_i) = \theta_i(\Lambda e^{-\ell}, \Lambda e^{-\ell_1},.., \Lambda e^{-\ell_i})$ are crossover functions written in terms of the logarithmic length scale, where θ_i is defined in Eq. (2.105). At short (long) distance scales with $\ell \ll \min_i\{\ell_i\}$ ($\ell \gg \min_i\{\ell_i\}$), $\Theta_i(\ell_1,..,\ell_i,\ell) \approx 1$ ($\Theta_i(\ell_1,..,\ell_i,\ell) \approx 0$), and the corresponding term in the beta function is turned on (off). $L^{(2L)}(k';\ell)$, $L^{(1L)}(k';\ell)$ and $L^{(1L)}(k',k;\ell)$ are the logarithmic length scales that mark three crossovers,

$$L^{(2L)}(k;\ell) = \log\left(\frac{\Lambda}{E_k^{(2L)}}\right), \quad L^{(1L)}(k;\ell) = \log\left(\frac{\Lambda}{E_k^{(1L)}}\right), \quad L^{(1L)}(k',k;\ell) = \log\left(\frac{\Lambda}{E_{k',k}^{(1L)}}\right), \tag{2.124}$$

where $L^{(2L)}(k;\ell)$, $L^{(1L)}(k;\ell)$ and $L^{(1L)}(k',k;\ell)$ are implicit functions of ℓ through $v_k(\ell)$, $V_{F,k}(\ell)$ and $c(\ell)$ that enter in Eqs. (2.97)- (2.99). Crossovers occur when ℓ crosses one or more of these length scales defined by the self-consistent equations[28],

$$\begin{aligned}\ell_k^{(2L)} =& L^{(2L)}(k;\ell_k^{(2L)}), \\ \ell_k^{(1L)} =& L^{(1L)}(k;\ell_k^{(1L)}), \\ \ell_{k',k}^{(1L)} =& \min\Big\{L^{(1L)}(k;\ell_{k',k}^{(1L)}), L^{(1L)}(k';\ell_{k',k}^{(1L)}), L^{(1L)}(k',k;\ell_{k',k}^{(1L)})\Big\}.\end{aligned} \tag{2.125}$$

[28]It is noted that $E_k^{(1L)}$, $E_{k',k}^{(1L)}$ and $E_k^{(2L)}$ are functions of ℓ because the coupling functions in Eqs. (2.97)-(2.99) depend on ℓ.

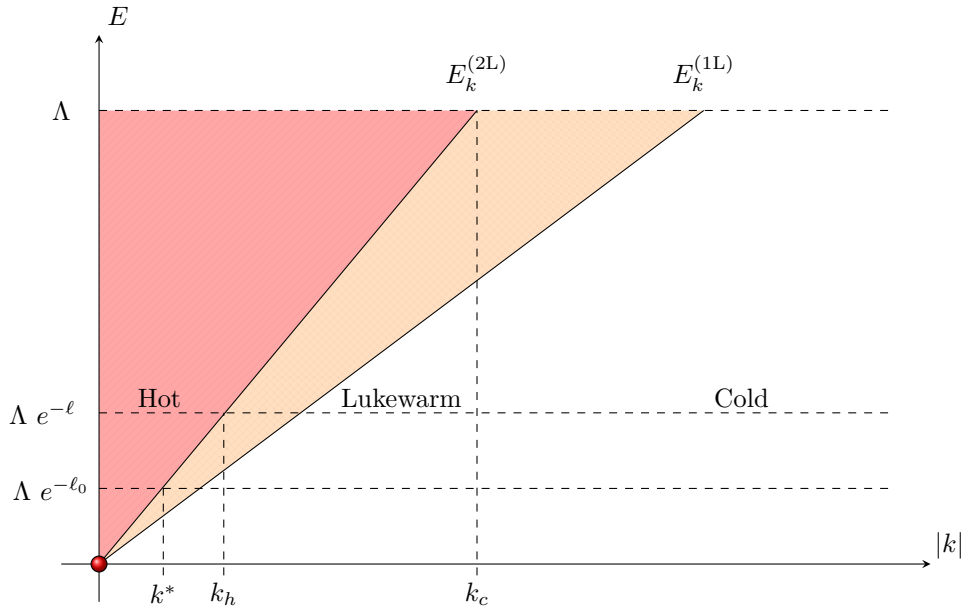

Figure 2.16: Crossover energy scales associated with the two-loop fermion self-energy ($E_k^{(2L)}$) and the one-loop fermion self-energy ($E_k^{(1L)}$), respectively. Since the flow of the couplings between $E_k^{(2L)}$ and $E_k^{(1L)}$ is negligible, one can consider only one crossover, say $E_k^{(2L)}$. At energy scale $\Lambda e^{-\ell}$, the momentum space is divided into three regions. In the hot region ($k < k_h$), electrons receive quantum correction from the UV scale all the way down to the current energy scale $\Lambda e^{-\ell}$. In the lukewarm region ($k_h < k < k_c$), electrons received some quantum correction at high energies but are decoupled from spin fluctuations at the current energy scale. In the cold region ($k > k_c$), electrons do not receive any quantum correction. Below the energy scale $\Lambda e^{-\ell_0}$, the flow of v cannot be ignored for $k < k^*$ (Ch. 3).

The solutions to Eq. (2.125) are given by (see Appendices C.1.2)

$$\begin{aligned}
\ell_k^{(2L)} &\approx \log\left(\frac{\Lambda}{4v_0(0)k}\right) + \log\left(1 + \frac{1}{\ell_0}\log\left(\frac{\Lambda}{4v_0(0)k}\right)\right), \\
\ell_k^{(1L)} &\approx \ell_k^{(2L)} + \log\frac{2}{c(\ell_k^{(2L)})}, \\
\ell_{k',k}^{(1L)} &\approx \min(\ell_{(k+k')/2}^{(2L)}, \ell_k^{(1L)}, \ell_{k'}^{(1L)}).
\end{aligned} \tag{2.126}$$

Here ℓ_0 is the length scale that parameterizes the bare nesting angle at $\ell = 0$ as defined in Eq. (2.9).

Since the RG flow equations for $v_k, V_{F,k}, g_k$ do not depend on the off-diagonal Yukawa coupling $g_{k',k}$, we first solve the beta functions for $v_k(\ell), V_{F,k}(\ell), g_k(\ell) \equiv g_{kk}(\ell)$. For $k' = k$, $\ell_{k',k}^{(1L)} = \ell_k^{(2L)}$. The beta functionals in Eq. (2.103) take different forms in each of the three windows of length scale : (i) $\ell < \ell_k^{(2L)}$, (ii) $\ell_k^{(2L)} < \ell < \ell_k^{(1L)}$, and (iii) $\ell_k^{(1L)} < \ell$. These regions are depicted in Fig. 2.16. In region i), electrons receive renormalization from all quantum corrections generated by spin fluctuations to the leading order in v. In region ii), the two-loop correction is turned off, but the one-loop quantum corrections are still present. In region iii), electrons are decoupled from spin fluctuations. To have the global solution, we solve the beta functions to obtain $J_k^{(i)}(\ell)$, $J_k^{(ii)}(\ell)$, $J_k^{(iii)}(\ell)$ for $J_k = v_k, V_{F,k}, g_k$ in each energy window, and the coupling functions are matched at the boundary to ensure continuity.

In the small v limit, $h_k^{(1)}$, $h_k^{(2)}$, $h_{k'k}^{(1)}$ scale as $w = v/c \sim \sqrt{v/\log(1/v)}$. As a result, the beta functionals for $J_k = v_k, V_{F,k}, g_k$ are bounded by $\frac{1}{J}\frac{\partial J}{\partial \ell} \sim w \ll 1$. Since $\ell_k^{(1L)} - \ell_k^{(2L)} \sim \log 1/c$, the net change of the couplings that occur in $\ell_k^{(2L)} < \ell < \ell_k^{(1L)}$ is only $\frac{|J(\ell_k^{(1L)}) - J(\ell_k^{(2L)})|}{J(\ell_k^{(2L)})} \sim w \log(1/c) \ll 1$ in the small v limit. Since the flow of couplings can be ignored in region (ii), we can use $J_k^{(iii)}$ in both regions (ii) and (iii). In this case, we only need to consider one crossover scale $E_k^{(2)}$ besides the UV cutoff scale Λ. At a given length scale ℓ, the Fermi surface can be divided into hot, lukewarm and cold regions separated by two momentum scales $k_h(\ell)$ and $k_c(\ell)$ defined by

$$\ell_{k_h(\ell)}^{(2L)} = \ell, \quad \ell_{k_c(\ell)}^{(2L)} = 0. \tag{2.127}$$

Below, we summarize the solution to the RG equation in each region. The derivation can be found in Appendix C.

- Hot region : In $0 \le |k| \le k_h(\ell)$, the momentum dependent IR cutoffs are smaller than the energy scale ($\Lambda e^{-\ell}$), and electrons remains strongly coupled with spin fluctuations. Accordingly, v_k, $V_{F,k}$ and g_k flow in the same way as in the hot spots : $v_k(\ell) = \frac{\pi^2 N_c N_f}{2(N_c^2-1)} \frac{1}{(\ell+\ell_0)\log(\ell+\ell_0)}$, $V_{F,k}(\ell) = 1$ and $g_k(\ell) = \sqrt{\frac{\pi v_0(\ell)}{2}}$ as in Eq. (2.18). Here $V_{F,k}(\ell)$ at the hot spot is chosen to be 1 as the reference speed with respect to which all other speeds are measured.

- Lukewarm region : In $k_h(\ell) \le |k| \le k_c(\ell)$, the momentum dependent IR cutoff is larger than the floating energy scale, $\mu = \Lambda e^{-\ell}$, but smaller than the UV cut off, Λ. Electrons in this range of momentum receive quantum corrections within a window of energy scale given by $\Lambda e^{-\ell_k^{(2L)}} < E < \Lambda$ before they decouple below $\Lambda e^{-\ell_k^{(2L)}}$. Once electrons are decoupled, the coupling with spin fluctuations decreases with increasing ℓ while $v_k(\ell)$ freezes out. Since spin fluctuations no longer slow electrons down, $V_{F,k}(\ell)$ increases relative to $V_{F,0}(\ell)$. The momentum profiles of the coupling functions are determined from the momentum dependent IR cutoff. Since electrons farther away from the hot spots decouple from spin fluctuations at higher energies, $g_k(\ell)$ decays while $v_k(\ell)$ and $V_{F,k}(\ell)$ increases with increasing momentum. It is noted that the division of the hot and lukewarm regions depends on the energy scale. As the energy is lowered, the hot region shrinks while the lukewarm region grows as more electrons on the Fermi surface are decoupled from spin fluctuations.

- Cold region : In $|k| \ge k_c(\ell)$, electrons are too far away from the hot spots to receive any significant renormalization from spin fluctuations at energies below Λ. In this region, $v_k(\ell)$ does not run, while $g_k(\ell)$ ($V_{F,k}(\ell)$) constantly decreases (increases) with increasing ℓ.

At a given scale ℓ, the momentum dependent coupling functions are obtained to be

$$v_k(\ell) = \begin{cases} v_0(\ell) & k < k_h(\ell) \\ v_0(\ell_k^{(2L)}) & k_h(\ell) < k < k_c(\ell) \\ v_0(0) & k_c(\ell) < k \end{cases} \tag{2.128}$$

$$g_k(\ell) = \begin{cases} \sqrt{\pi v_0(\ell)/2} & k < k_h(\ell) \\ \sqrt{\frac{\pi}{2} v_0(\ell_k^{(2L)})}\ \mathcal{E}_0(\ell; \ell_k^{(2L)}) & k_h(\ell) < k < k_c(\ell) \\ \sqrt{\pi v_0(0)/2}\ \mathcal{E}_0(\ell; 0) & k_c(\ell) < k \end{cases}, \tag{2.129}$$

$$V_{F,k}(\ell) = \begin{cases} 1 & k < k_h(\ell) \\ \mathcal{E}_1(\ell; \ell_k^{(2L)}) & k_h(\ell) < k < k_c(\ell) \\ \mathcal{E}_1(\ell; 0) & k_c(\ell) < k \end{cases}, \tag{2.130}$$

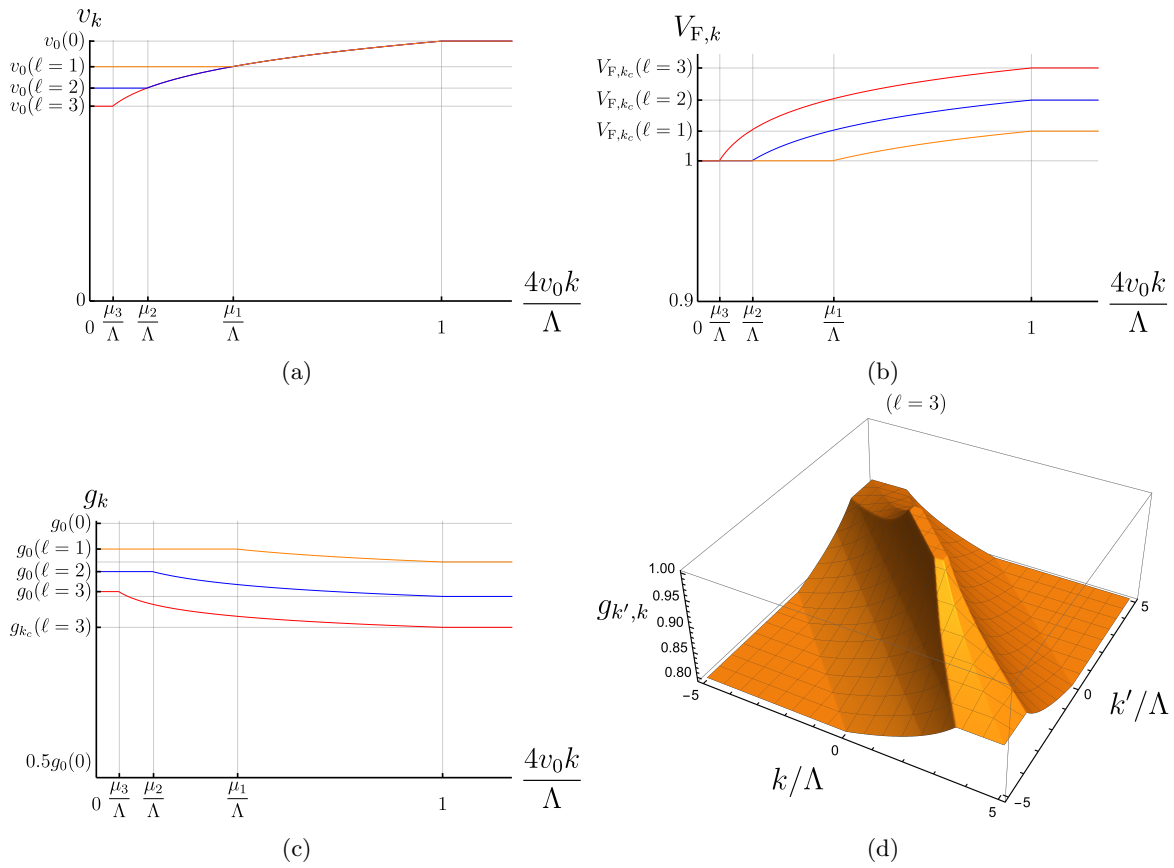

Figure 2.17: (a) $v_k(\ell)$, (b) $V_{F,k}(\ell)$, (c) $g_k(\ell) \equiv g_{kk}(\ell)$ and (d) $g_{k'k}(\ell)$ plotted as functions of momentum along the Fermi surface for the theory with a constant bare nesting angle, $v_0(0) = 0.1$. For plots in (a)-(c), the coupling functions are shown for $\ell = 1, 2, 3$, where $\mu_\ell = \Lambda e^{-\ell}$ denotes the energy scale associated with $\ell = 1, 2, 3$. In the hot region near $k = 0$, the coupling functions are essentially independent of momentum, taking the values of the coupling constants of the hot spot theory. The coupling functions are also constants in the cold region as electrons far away from the hot spots are not normalized. In the lukewarm region that interpolates the hot and cold regions, the coupling functions acquire non-trivial momentum dependence. As the energy is lowered, the size of the hot region near the hot spot decreases as more electrons become decoupled from spin fluctuations. At a fixed energy, v_k and $V_{F,k}$ decreases with decreasing k because spin fluctuations remain coupled with electrons down to lower energies ($V_{F,k}$ is measured in the unit of the hot spot velocity which is set to be 1). On the contrary, the Yukawa coupling increases with decreasing k. The kinks in the plots are the artifact of not keeping the precise crossover functions between the regions. For the off-diagonal Yukawa coupling in (d), $\ell = 3$ is chosen.

where

$$v_0(\ell) = \frac{\pi^2 N_c N_f}{2(N_c^2-1)} \frac{1}{(\ell+\ell_0)\log(\ell+\ell_0)}, \tag{2.131}$$

$$\mathcal{E}_0(X,Y) \equiv \exp\left(-\frac{\sqrt{X+\ell_0}-\sqrt{Y+\ell_0}}{\sqrt{N_c^2-1}}\right), \tag{2.132}$$

$$\mathcal{E}_1(X,Y) \equiv \exp\left(\sqrt{N_c^2-1}\left(\mathrm{Ei}(\log\sqrt{X+\ell_0}) - \mathrm{Ei}(\log\sqrt{Y+\ell_0})\right)\right). \tag{2.133}$$

For the general Yukawa coupling, the solution of the beta functional is given by

$$g_{k,k'}(\ell) = \begin{cases} \sqrt{\frac{\pi}{2} v_0(\ell)} & \ell \leq \ell^{(1L)}_{k',k} \\ \sqrt{\frac{\pi}{2} v_0(\ell^{(1L)}_{k',k})}\mathcal{E}_0(\ell, \ell^{(1L)}_{k',k}) & \ell \geq \ell^{(1L)}_{k',k}. \end{cases} \tag{2.134}$$

Eq. (2.134) can be understood in the following way. The RG flow of $g_{k',k}$ is controlled by the vertex correction and the self-energy corrections to the electrons at momenta k and k'. In the small v limit, the vertex correction is the dominant factor, and the momentum dependence of the renormalized Yukawa coupling is largely determined by the crossover scale at which the vertex correction turns off. At the hot spots, the vertex correction is present at all energy scales. The vertex correction tends to enhances the Yukawa coupling at low energies due to the anti-screening effect associated with the non-Abelian nature of the $SU(N_c)$ group[204]. Once this vertex correction is absorbed by the field renormalization of the boson, the Yukawa coupling between the boson and electrons near the hot spots is kept to be the order of $\sqrt{v_0}$ at all energy scales, while the boson is endowed with the large anomalous dimension. For electrons away from hot spots, the vertex correction turns off for $\ell > \ell^{(1L)}_{k',k}$. At low energies, the Yukawa coupling decays because the boson that remains strongly renormalized by electrons near the hot spots is too 'heavy' to stay coupled with electrons away from hot spots without the help of the anti-screening vertex correction : the large scaling dimension of the boson caused by hot electrons makes the boson to decouple from lukewarm electrons at low energies. The momentum dependent coupling functions are shown in Fig. 2.17.

It is noted that $v_0(\ell)$ flows to zero in the large ℓ limit. Therefore, only $v_0 = 0$ is a true fixed point. However, for $\ell_0 \gg 1$ there exists a large window of scale $0 < \ell \ll \ell_0$ within which $v_k(\ell)$ does not change appreciably as a function of k and ℓ. Within this window of length scale, $v_k(\ell)$ is well approximated by $v_0(0)$, and physical observables obey scaling relations controlled by exponents that depend on $v_0(0)$. Therefore, we can consider an one-parameter family of *quasi-fixed points* labeled by v_0. To characterize those quasi-fixed points, let us first extract the scaling behaviour of the coupling functions. Eqs. (2.130)-(2.134) describes how the coupling functions at a fixed physical momentum evolve as the energy scale is lowered. The coupling functions will exhibit scale invariance if the momentum along the Fermi surface is simultaneously scaled as the energy scale is lowered. To find a scale invariant fixed point, we consider the coupling functions defined in Eq. (2.59),

$$\hat{v}_K = v_k, \quad \hat{V}_{F,K} = V_{F,k}, \quad \hat{g}_{K,K'} = g_{k,k'}, \tag{2.135}$$

where $K = ke^{\ell}$, $K' = k'e^{\ell}$ are the rescaled momenta. For fixed K and K', the hatted coupling functions in Eq. (2.135) become independent of ℓ to the leading order in ℓ/ℓ_0,

$$\hat{v}_K = v_0(0), \tag{2.136}$$

$$\hat{V}_{F,K} = \begin{cases} 1 & |K| < K_h \\ \left(\frac{|K|}{K_h}\right)^{\alpha_1(0)} & K_h < |K| < K_c \\ \left(\frac{K_c}{K_h}\right)^{\alpha_1(0)} & K_c < |K| \end{cases}, \tag{2.137}$$

$$\hat{g}_K = \begin{cases} \sqrt{\frac{\pi}{2} v_0(0)} & |K| < K_h \\ \sqrt{\frac{\pi}{2} v_0(0)} \left(\frac{K_h}{|K|}\right)^{\alpha_0(0)} & K_h < |K| < K_c \\ \left(\frac{K_h}{K_c}\right)^{\alpha_0(0)} & K_c < |K| \end{cases}, \tag{2.138}$$

$$\hat{g}_{K,K'} = \begin{cases} \sqrt{\frac{\pi}{2} v_0(0)} & \max\{\frac{|K+K'|}{2}, \frac{c|K|}{2}, \frac{c|K'|}{2}\} < K_h \\ \sqrt{\frac{\pi}{2} v_0(0)} \left(\frac{K_h}{\max\{\frac{|K+K'|}{2}, \frac{c|K|}{2}, \frac{c|K'|}{2}\}}\right)^{\alpha_0(0)} & K_h < \max\{\frac{|K+K'|}{2}, \frac{c|K|}{2}, \frac{c|K'|}{2}\} < K_c \\ \sqrt{\frac{\pi}{2} v_0(0)} \left(\frac{K_h}{K_c}\right)^{\alpha_0(0)} & K_c < \max\{\frac{|K+K'|}{2}, \frac{c|K|}{2}, \frac{c|K'|}{2}\} \end{cases}, \tag{2.139}$$

where $K_h = e^{\ell} k_h(\ell) = \frac{\Lambda}{4v_0(0)}$ and $K_c = e^{\ell} k_c(\ell) = \frac{\Lambda e^{\ell}}{4v_0(0)}$ represent the rescaled crossover momenta from hot to lukewarm, and from lukewarm to cold region, respectively, and

$$\begin{aligned} \alpha_1(\ell) =& \frac{\sqrt{N_c^2-1}}{\sqrt{\ell_0+\ell}\log(\ell_0+\ell)}, \\ \alpha_0(\ell) =& \frac{1}{2\sqrt{N_c^2-1}\sqrt{\ell_0+\ell}} \end{aligned} \tag{2.140}$$

are the critical exponents that govern the universal power-law decays of the coupling functions in the momentum space. The exponents only depend on the nesting angle within the line of quasi-fixed points. It is noted that $\hat{V}_{F,K}$ and $\hat{g}_{K',K}$ depend on momentum more strongly than $\hat{v}_K$. As a result, the momentum dependence of the former two can not be ignored even if the latter is regarded as constant to the leading order in ℓ/ℓ_0. Across the lukewarm region, each of the coupling functions changes by $\frac{\hat{v}_{K_c}}{\hat{v}_{K_h}} \approx 1 + \frac{\ell}{\ell_0}$, $\frac{\hat{V}_{F,K_c}}{\hat{V}_{F,K_h}} \approx e^{\sqrt{N_c^2-1}\frac{\ell}{\sqrt{\ell_0 \log \ell_0}}}$, and $\frac{\hat{g}_{K_c}}{\hat{g}_{K_h}} \approx e^{-\frac{1}{2\sqrt{N_c^2-1}}\frac{\ell}{\sqrt{\ell_0}}}$. For $\ell/\ell_0 \ll 1$, $\frac{\hat{v}_{K_c}}{\hat{v}_{K_h}} \approx 1$. However, the variations of the Fermi velocity and the Yukawa coupling are not negligible if $\ell/\sqrt{\ell_0} \geq 1$.

Although the coupling functions acquire non-trivial momentum profiles at low energies, they do not vary much over momentum scales that are proportional to the energy scale μ. From the momentum profiles of the coupling functions in Eqs. (2.136)- (2.139), we can now check the validity of the adiabaticity in Eq. (2.83). The relative variation of the couplings within the range of $\Pi_\mu = \frac{\mu}{vc}$ is given by

$$\epsilon_\mu \sim \alpha_0 \log \frac{1}{vc} \tag{2.141}$$

in the small v limit. Up to a logarithmic correction, $\epsilon_\mu \sim \sqrt{v} \ll 1$ and Eq. (2.83) is satisfied at all energy scales.

$\hat{g}_{K',K}$ in Eq. (2.139) decays in a power law as a function of momenta in all directions in the space of K' and K. The power-law decay of the off-diagonal elements of $\hat{g}_{K',K}$ signifies the importance of the non-forward scatterings. Consequently, the number of electrons at each momentum is not conserved. There is still a sense in which a large symmetry emerges at low energies without the four-fermion coupling[56]. In the space of rescaled momentum, k_F runs to infinity in the low-energy limit. Because the range of the off-diagonal elements are fixed and the size of Fermi surface blows up under the RG flow, the number of electrons within a finite fraction of the total system becomes better conserved as the energy is lowered. This can be also understood by examining the coupling function in the space of physical momenta, $k = Ke^{-\ell}$, $k' = K'e^{-\ell}$. If the large ℓ limit is taken for fixed k and k', the Yukawa coupling function vanishes for k and k' away from the hot spots. The four-fermion coupling functions generated from the Yukawa coupling give rise to stronger large-angle scatterings that invalidate the patch description more severely. In the following two sections, we examine the RG flow of the four-fermion coupling function projected to the space of a fixed nesting angle.

2.6.2 Four-fermion coupling in group 1 : the singular Landau function

We now turn our attention to the four-fermion coupling functions. The couplings in group 1 describes the forward scattering whose beta functional is written as

$$\begin{aligned} \frac{\partial}{\partial \ell} \lambda^{\binom{N_1\ N_2}{N_4\ N_3};\binom{\sigma_1\ \sigma_2}{\sigma_4\ \sigma_3}}_{\binom{p\ k}{k\ p}} =& -\left(1 + 3(z-1) + 2\eta_k^{(\psi)} + 2\eta_p^{(\psi)}\right) \lambda^{\binom{N_1\ N_2}{N_4\ N_3};\binom{\sigma_1\ \sigma_2}{\sigma_4\ \sigma_3}}_{\binom{p\ k}{k\ p}} - \frac{S_{k,p}}{N_f^2} \mathsf{T}^{\beta\sigma_2}_{\sigma_4\alpha} \mathsf{T}^{\sigma_1\alpha}_{\beta\sigma_3} \delta^{N_1}_{N_4} \delta^{N_2}_{N_3} \\ &+ \frac{B_k}{2N_f} \lambda^{\binom{N_1\ \bar{N}_2}{\bar{N}_4\ N_3};\binom{\sigma_1\ \alpha}{\beta\ \sigma_3}}_{\binom{p\ k}{k\ p}} \mathsf{T}^{\beta\sigma_2}_{\sigma_4\alpha} + \frac{B_p}{2N_f} \mathsf{T}^{\sigma_1\beta}_{\alpha\sigma_3} \hat{\lambda}^{\binom{\bar{N}_1\ N_2}{N_4\ \bar{N}_3};\binom{\alpha\ \sigma_2}{\sigma_4\ \beta}}_{\binom{p\ k}{k\ p}}. \end{aligned} \tag{2.142}$$

Here $\binom{N_1\ N_2}{N_4\ N_3}$ is one of the elements in the set of

$$H^{PH}_{1111} = \left\{ \binom{1\ 1}{1\ 1}, \binom{1\ 4}{4\ 1}, \binom{4\ 1}{1\ 4}, \binom{4\ 4}{4\ 4} \right\}, \tag{2.143}$$

and

$$B_k = \frac{g_k^2}{\pi^2 c V_{F,k}} \frac{\mu}{\mu + 2v_k c|k|_\mu}, \qquad S_{k,p} = \mathsf{D}_\mu(k;p)(B_k + B_p) \tag{2.144}$$

represent the momentum dependent vertex correction and the source term generated from the spin fluctuations, respectively. Since the coupling measured in the unit of the Fermi velocity represents the physical strength of interaction[29], we define

$$\lambda^{V;\left(\begin{smallmatrix}N_1 & N_2\\ N_4 & N_3\end{smallmatrix}\right);\left(\begin{smallmatrix}\alpha & \beta\\ \gamma & \delta\end{smallmatrix}\right)}_{1PH\left(\begin{smallmatrix}p & k\\ k & p\end{smallmatrix}\right)} = \frac{1}{\sqrt{V_{F,p}V_{F,k}}} \lambda^{\left(\begin{smallmatrix}N_1 & N_2\\ N_4 & N_3\end{smallmatrix}\right);\left(\begin{smallmatrix}\alpha & \beta\\ \gamma & \delta\end{smallmatrix}\right)}_{1PH\left(\begin{smallmatrix}p & k\\ k & p\end{smallmatrix}\right)}, \tag{2.145}$$

where the coupling is divided by $\sqrt{V_{F,p}V_{F,k}}$ to keep λ^V symmetric. Its beta functional reads

$$\begin{aligned}\frac{\partial}{\partial \ell}\lambda^{V;\left(\begin{smallmatrix}N_1 & N_2\\ N_4 & N_3\end{smallmatrix}\right);\left(\begin{smallmatrix}\sigma_1 & \sigma_2\\ \sigma_4 & \sigma_3\end{smallmatrix}\right)}_{1PH\left(\begin{smallmatrix}p & k\\ k & p\end{smallmatrix}\right)} &= -\left(1+\eta_k+\eta_p\right)\lambda^{V;\left(\begin{smallmatrix}N_1 & N_2\\ N_4 & N_3\end{smallmatrix}\right);\left(\begin{smallmatrix}\sigma_1 & \sigma_2\\ \sigma_4 & \sigma_3\end{smallmatrix}\right)}_{1PH\left(\begin{smallmatrix}p & k\\ k & p\end{smallmatrix}\right)} - \frac{S^V_{k,p}}{N_f^2}\mathsf{T}^{\beta\sigma_2}_{\sigma_4\alpha}\mathsf{T}^{\sigma_1\alpha}_{\beta\sigma_3}\delta^{N_1}_{N_4}\delta^{N_2}_{N_3} \\ &+ \frac{B_k}{2N_f}\lambda^{V;\left(\begin{smallmatrix}N_1 & \bar{N}_2\\ \bar{N}_4 & N_3\end{smallmatrix}\right);\left(\begin{smallmatrix}\sigma_1 & \alpha\\ \beta & \sigma_3\end{smallmatrix}\right)}_{1PH\left(\begin{smallmatrix}p & k\\ k & p\end{smallmatrix}\right)}\mathsf{T}^{\beta\sigma_2}_{\sigma_4\alpha} + \frac{B_p}{2N_f}\mathsf{T}^{\sigma_1\beta}_{\alpha\sigma_3}\hat{\lambda}^{V;\left(\begin{smallmatrix}\bar{N}_1 & N_2\\ N_4 & \bar{N}_3\end{smallmatrix}\right);\left(\begin{smallmatrix}\alpha & \sigma_2\\ \sigma_4 & \beta\end{smallmatrix}\right)}_{1PH\left(\begin{smallmatrix}p & k\\ k & p\end{smallmatrix}\right)},\end{aligned} \tag{2.146}$$

where

$$\eta_k = \frac{(N_c^2-1)g_k^2}{2\pi^2 N_c N_f c V_{F,k}} \frac{\mu}{\mu + 2cv_k\,|k|_\mu}, \tag{2.147}$$

$$S^V_{k,p} = \frac{1}{\sqrt{V_{F,p}V_{F,k}}}\mathsf{D}_\mu(k;p)(B_k+B_p). \tag{2.148}$$

Just as the Fermi velocity and the Yukawa coupling functions acquire momentum profiles that are solely determined from the nesting angle at the quasi-fixed point, the forward scattering amplitude acquires a singular momentum profile near the hot spots. To extract the universal momentum profile of the forward scattering amplitude that is scale invariant at the quasi-fixed point, we consider the beta functional for the four-fermion coupling functions defined in the space of rescaled momentum, $\hat{\lambda}^{\left(\begin{smallmatrix}N_1 & N_2\\ N_3 & N_4\end{smallmatrix}\right);\left(\begin{smallmatrix}\sigma_1 & \sigma_2\\ \sigma_4 & \sigma_3\end{smallmatrix}\right)}_{1PH;\left(\begin{smallmatrix}K_1 & K_2\\ K_4 & K_3\end{smallmatrix}\right)} = \lambda^{V;\left(\begin{smallmatrix}N_1 & N_2\\ N_3 & N_4\end{smallmatrix}\right);\left(\begin{smallmatrix}\sigma_1 & \sigma_2\\ \sigma_4 & \sigma_3\end{smallmatrix}\right)}_{1PH;\left(\begin{smallmatrix}k_1 & k_2\\ k_4 & k_3\end{smallmatrix}\right)}$, where $K_i = e^\ell k_i$. The beta functionals for the four-fermion coupling functions defined in the space of rescaled momentum is written as

$$\begin{aligned}\left[\frac{\partial}{\partial\ell} + K\frac{\partial}{\partial K} + P\frac{\partial}{\partial P}\right]\hat{\lambda}^{\left(\begin{smallmatrix}N_1 & N_2\\ N_4 & N_3\end{smallmatrix}\right);\left(\begin{smallmatrix}\sigma_1 & \sigma_2\\ \sigma_4 & \sigma_3\end{smallmatrix}\right)}_{1PH;\left(\begin{smallmatrix}P & K\\ K & P\end{smallmatrix}\right)} &= -\left(1+\hat{\eta}_K+\hat{\eta}_P\right)\hat{\lambda}^{\left(\begin{smallmatrix}N_1 & N_2\\ N_4 & N_3\end{smallmatrix}\right);\left(\begin{smallmatrix}\sigma_1 & \sigma_2\\ \sigma_4 & \sigma_3\end{smallmatrix}\right)}_{1PH;\left(\begin{smallmatrix}P & K\\ K & P\end{smallmatrix}\right)} \\ + \frac{\hat{B}_K}{2N_f}\hat{\lambda}^{\left(\begin{smallmatrix}N_1 & \bar{N}_2\\ \bar{N}_4 & N_3\end{smallmatrix}\right);\left(\begin{smallmatrix}\sigma_1 & \alpha\\ \beta & \sigma_3\end{smallmatrix}\right)}_{1PH;\left(\begin{smallmatrix}P & K\\ K & P\end{smallmatrix}\right)}\mathsf{T}^{\beta\sigma_2}_{\sigma_4\alpha} + \frac{\hat{B}_P}{2N_f}\mathsf{T}^{\sigma_1\beta}_{\alpha\sigma_3}\hat{\lambda}^{\left(\begin{smallmatrix}\bar{N}_1 & N_2\\ N_4 & \bar{N}_3\end{smallmatrix}\right);\left(\begin{smallmatrix}\alpha & \sigma_2\\ \sigma_4 & \beta\end{smallmatrix}\right)}_{1PH;\left(\begin{smallmatrix}P & K\\ K & P\end{smallmatrix}\right)} - \frac{\hat{S}_{K,P}}{N_f^2}\mathsf{T}^{\beta\sigma_2}_{\sigma_4\alpha}\mathsf{T}^{\sigma_1\alpha}_{\beta\sigma_3}\delta^{N_1}_{N_4}\delta^{N_2}_{N_3},\end{aligned} \tag{2.149}$$

where $\hat{\eta}_K = \eta_{Ke^{-\ell}}$, $\hat{B}_K = B_{Ke^{-\ell}}$ and $\hat{S}_{K,P} = S^V_{Ke^{-\ell},Pe^{-\ell}}$. We combine the four coupling functions into a matrix as

$$\hat{\lambda}^{\left(\begin{smallmatrix}\sigma_1 & \sigma_2\\ \sigma_4 & \sigma_3\end{smallmatrix}\right)}_{1PH\left(\begin{smallmatrix}P & K\\ K & P\end{smallmatrix}\right)} = \begin{pmatrix}\hat{\lambda}^{\left(\begin{smallmatrix}1 & 1\\ 1 & 1\end{smallmatrix}\right);\left(\begin{smallmatrix}\sigma_1 & \sigma_2\\ \sigma_4 & \sigma_3\end{smallmatrix}\right)}_{\left(\begin{smallmatrix}P & K\\ K & P\end{smallmatrix}\right)} & \hat{\lambda}^{\left(\begin{smallmatrix}1 & 4\\ 4 & 1\end{smallmatrix}\right);\left(\begin{smallmatrix}\sigma_1 & \sigma_2\\ \sigma_4 & \sigma_3\end{smallmatrix}\right)}_{\left(\begin{smallmatrix}P & K\\ K & P\end{smallmatrix}\right)} \\ \hat{\lambda}^{\left(\begin{smallmatrix}4 & 1\\ 1 & 4\end{smallmatrix}\right);\left(\begin{smallmatrix}\sigma_1 & \sigma_2\\ \sigma_4 & \sigma_3\end{smallmatrix}\right)}_{\left(\begin{smallmatrix}P & K\\ K & P\end{smallmatrix}\right)} & \hat{\lambda}^{\left(\begin{smallmatrix}4 & 4\\ 4 & 4\end{smallmatrix}\right);\left(\begin{smallmatrix}\sigma_1 & \sigma_2\\ \sigma_4 & \sigma_3\end{smallmatrix}\right)}_{\left(\begin{smallmatrix}P & K\\ K & P\end{smallmatrix}\right)}\end{pmatrix} \tag{2.150}$$

[29] For example, the perturbation series in the four-fermion coupling is organized in terms of the ratio between the four-fermion coupling and the Fermi velocity.

to write the set of beta functionals as a matrix differential equation,

$$\left[\frac{\partial}{\partial\ell}+K\frac{\partial}{\partial K}+P\frac{\partial}{\partial P}\right]\hat{\lambda}^{\left(\begin{smallmatrix}\sigma_1 & \sigma_2\\ \sigma_4 & \sigma_3\end{smallmatrix}\right)}_{1PH\left(\begin{smallmatrix}P & K\\ K & P\end{smallmatrix}\right)}=-\left(1+\hat{\eta}_K+\hat{\eta}_P\right)\hat{\lambda}^{\left(\begin{smallmatrix}\sigma_1 & \sigma_2\\ \sigma_4 & \sigma_3\end{smallmatrix}\right)}_{1PH\left(\begin{smallmatrix}P & K\\ K & P\end{smallmatrix}\right)}$$
$$+\frac{\hat{B}_K}{2N_f}\hat{\lambda}^{\left(\begin{smallmatrix}\sigma_1 & \alpha\\ \beta & \sigma_3\end{smallmatrix}\right)}_{1PH\left(\begin{smallmatrix}P & K\\ K & P\end{smallmatrix}\right)}\mathsf{T}^{\beta\sigma_2}_{\sigma_4\alpha}\begin{pmatrix}0&1\\1&0\end{pmatrix}+\frac{\hat{B}_P}{2N_f}\mathsf{T}^{\sigma_1\beta}_{\alpha\sigma_3}\begin{pmatrix}0&1\\1&0\end{pmatrix}\hat{\lambda}^{\left(\begin{smallmatrix}\alpha & \sigma_2\\ \sigma_4 & \beta\end{smallmatrix}\right)}_{1PH\left(\begin{smallmatrix}P & K\\ K & P\end{smallmatrix}\right)}-\frac{\hat{S}_{K,P}}{N_f^2}\mathsf{T}^{\beta\sigma_2}_{\sigma_4\alpha}\mathsf{T}^{\sigma_1\alpha}_{\beta\sigma_3}\begin{pmatrix}1&0\\0&1\end{pmatrix}. \tag{2.151}$$

In the PH channel, the spin tensor of the interaction can be decomposed as

$$\mathsf{T}^{\alpha\beta}_{\gamma\delta}=Y^{(t)}_{PH}\mathsf{I}^{\alpha\beta}_{\gamma\delta}+Y^{(a)}_{PH}\chi^{\alpha\beta}_{\gamma\delta}. \tag{2.152}$$

Here

$$\mathsf{I}^{\sigma_1\sigma_2}_{\sigma_4\sigma_3}=\frac{1}{N_c}\delta_{\sigma_1\sigma_3}\delta_{\sigma_2\sigma_4},\qquad \chi^{\sigma_1\sigma_2}_{\sigma_4\sigma_3}=\left(\delta_{\sigma_1\sigma_4}\delta_{\sigma_2\sigma_3}-\frac{1}{N_c}\delta_{\sigma_1\sigma_3}\delta_{\sigma_2\sigma_4}\right) \tag{2.153}$$

project a spin state of a pair of particle and hole into the trivial representation and the adjoint representation of the $SU(N_c)$ group, respectively, and

$$Y^{(t)}_{PH}=2\left(N_c-\frac{1}{N_c}\right),\qquad Y^{(a)}_{PH}=-\frac{2}{N_c} \tag{2.154}$$

denotes the eigenvalue of $\mathsf{T}^{\alpha\beta}_{\gamma\delta}$ in each channel. Similarly, the matrix that controls the mixing in the space of hot spots can be decomposed as

$$\begin{pmatrix}0&1\\1&0\end{pmatrix}=1^s\mathscr{P}_s+1^d\mathscr{P}_d, \tag{2.155}$$

where

$$\mathscr{P}_s=\frac{1}{2}\begin{pmatrix}1&1\\1&1\end{pmatrix},\qquad \mathscr{P}_d=\frac{1}{2}\begin{pmatrix}1&-1\\-1&1\end{pmatrix} \tag{2.156}$$

project the four-fermion couplings into the s-wave and d-wave channels, respectively, and

$$1^s=1,\qquad 1^d=-1 \tag{2.157}$$

are the associated eigenvalues. Naturally, the coupling function is decomposed into four different channels as

$$\hat{\lambda}^{\left(\begin{smallmatrix}\sigma_1 & \sigma_2\\ \sigma_4 & \sigma_3\end{smallmatrix}\right)}_{1PH\{K_i\}}=\hat{\lambda}^{(t)(s)}_{1PH\{K_i\}}\mathsf{I}^{\sigma_1\sigma_2}_{\sigma_4\sigma_3}\mathscr{P}_s+\hat{\lambda}^{(t)(d)}_{1PH\{K_i\}}\mathsf{I}^{\sigma_1\sigma_2}_{\sigma_4\sigma_3}\mathscr{P}_d+\hat{\lambda}^{(a)(s)}_{1PH\{K_i\}}\chi^{\sigma_1\sigma_2}_{\sigma_4\sigma_3}\mathscr{P}_s+\hat{\lambda}^{(a)(d)}_{1PH\{K_i\}}\chi^{\sigma_1\sigma_2}_{\sigma_4\sigma_3}\mathscr{P}_d. \tag{2.158}$$

The beta functional for the coupling function in each channel becomes

$$\begin{aligned}&\left[\frac{\partial}{\partial\ell}+K\frac{\partial}{\partial K}+P\frac{\partial}{\partial P}\right]\hat{\lambda}^{\left(\begin{smallmatrix}t\\ a\end{smallmatrix}\right),\left(\begin{smallmatrix}s\\ d\end{smallmatrix}\right)}_{1PH\left(\begin{smallmatrix}P & K\\ K & P\end{smallmatrix}\right)}\\&=-\left(1+\hat{\eta}_K+\hat{\eta}_P-\frac{1^{\left(\begin{smallmatrix}s\\ d\end{smallmatrix}\right)}Y^{\left(\begin{smallmatrix}t\\ a\end{smallmatrix}\right)}_{PH}}{2N_f}\left[\hat{B}_K+\hat{B}_P\right]\right)\hat{\lambda}^{\left(\begin{smallmatrix}t\\ a\end{smallmatrix}\right),\left(\begin{smallmatrix}s\\ d\end{smallmatrix}\right)}_{1PH\left(\begin{smallmatrix}P & K\\ K & P\end{smallmatrix}\right)}-\left(Y^{\left(\begin{smallmatrix}t\\ a\end{smallmatrix}\right)}_{PH}\right)^2\frac{\hat{S}_{K,P}}{N_f^2}.\end{aligned} \tag{2.159}$$

Due to the momentum dilatation, the coupling functions at different momenta mix under the RG flow. However, only the overall magnitude of external momenta is rescaled, and the relative magnitudes do not change. To integrate the beta functional, it is convenient to introduce a polar coordinate for the space of external momenta,

$$(K,P)=X\hat{\Omega}, \tag{2.160}$$

where $X = \sqrt{K^2 + P^2}$ represents the overall magnitude, and $\hat{\Omega} = (\Omega_K, \Omega_P)$ represents the unit vector that specifies direction in the space of external momenta. At the fixed point, the coupling function satisfies

$$X\frac{\partial}{\partial X}\hat{\lambda}^{*\binom{t}{a},\binom{s}{d}}_{1PH,X,\hat{\Omega}} + \left(1 + \hat{\eta}_{X\Omega_K} + \hat{\eta}_{X\Omega_P} - \frac{1^{\binom{s}{d}} Y^{\binom{t}{a}}_{PH}}{2N_f}\left[\hat{B}_{X\Omega_K} + \hat{B}_{X\Omega_P}\right]\right)\hat{\lambda}^{*\binom{t}{a},\binom{s}{d}}_{1PH,X,\hat{\Omega}} + \frac{1}{N_f^2}\left(Y^{\binom{t}{a}}_{PH}\right)^2 \hat{S}_{X,\hat{\Omega}} = 0. \tag{2.161}$$

The fixed point solution is readily obtained to be

$$\hat{\lambda}^{*\binom{t}{a},\binom{s}{d}}_{1PH,X,\hat{\Omega}} = \psi^{\binom{s}{d}}(X)\left[\frac{\hat{\lambda}^{\binom{t}{a},\binom{s}{d}}_{1PH,\Lambda_0,\hat{\Omega}}}{\psi^{\binom{s}{d}}(\Lambda_0)} - \frac{1}{N_f^2}\, Y^{\binom{t}{a}}_{PH}{}^2 \int_{\Lambda_0}^{X}\frac{dX'}{X'}\frac{1}{\psi^{\binom{s}{d}}(X')}\hat{S}_{X',\hat{\Omega}}\right], \tag{2.162}$$

where

$$\psi^{\binom{s}{d}}(X) = \mathrm{Exp}\left[-\int_{\Lambda}^{X}\frac{dX'}{X'}\left(1 + \hat{\eta}_{X'\Omega_K} + \hat{\eta}_{X'\Omega_P} - \frac{1^{\binom{s}{d}} Y^{\binom{t}{a}}_{PH}}{2N_f}(\hat{B}_{X'\Omega_K} + \hat{B}_{X'\Omega_P})\right)\right] \tag{2.163}$$

and Λ_0 is a reference scale at which the boundary condition is imposed for $\hat{\lambda}^{*\binom{t}{a},\binom{s}{d}}_{1PH,X,\hat{\Omega}}$. Since $\psi^{\binom{s}{d}}(X)$ diverges in the small X limit, the solution that is regular at the hot spot is obtained by choosing $\Lambda_0 = 0$[30],

$$\hat{\lambda}^{*\binom{t}{a},\binom{s}{d}}_{1PH,X,\hat{\Omega}} = -\frac{1}{N_f^2}\, Y^{\binom{t}{a}}_{PH}{}^2\, \psi^{\binom{s}{d}}(X)\int_0^X \frac{dX'}{X'}\frac{1}{\psi^{\binom{s}{d}}(X')}\hat{S}_{X',\hat{\Omega}}. \tag{2.164}$$

In the small v limit, $\psi^{\binom{s}{d}}(X)$ is well approximated by Λ/X, and the anomalous dimension and the $\hat{B}$ terms are sub-leading. At the fixed point, the coupling function takes the scale invariant form given by

$$\hat{\lambda}^{*\binom{t}{a},\binom{s}{d}}_{1PH\binom{P\ K}{K\ P}} = -\frac{\hat{g}^2_{P,K}\, Y^{\binom{t}{a}}_{PH}{}^2}{\pi^2 c N_f^2\sqrt{\hat{V}_{F,K}\hat{V}_{F,P}}}\left[\frac{\hat{g}^2_{K,K}}{\hat{V}_{F,K}}\frac{\Lambda\log\left(\frac{c|\hat{v}_K K + \hat{v}_P P|_\Lambda + c|K-P|_\Lambda + \Lambda}{2\hat{v}_K c|K|_\Lambda + \Lambda}\right)}{c(|\hat{v}_K K + \hat{v}_P P|_\Lambda + |K-P|_\Lambda - 2\hat{v}_K|K|_\Lambda)} + \frac{\hat{g}^2_{P,P}}{\hat{V}_{F,P}}\frac{\Lambda\log\left(\frac{c|\hat{v}_K K + \hat{v}_P P|_\Lambda + c|K-P|_\Lambda + \Lambda}{2\hat{v}_P c|P|_\Lambda + \Lambda}\right)}{c(|\hat{v}_K K + \hat{v}_P P|_\Lambda + |K-P|_\Lambda - 2\hat{v}_P|P|_\Lambda)}\right] \tag{2.165}$$

to the leading order in v[31]. Just as other coupling functions discussed in the previous section, the forward scattering amplitude becomes independent of ℓ when the rescaled momenta K and P are fixed. This implies that the scale invariance emerges when the forward scattering amplitude is probed at momenta increasingly closer to the hot spots as the energy is lowered. If one of the electron is in the hot region and the other is at momentum p far away from the hot region, the forward scattering amplitude decays as $1/p$ with a logarithmic correction as

$$\frac{1}{4\mu}\lambda^{V;\binom{t}{a},\binom{s}{d}}_{1PH\binom{p\ 0}{0\ p}} = -\frac{g^2_{p,0}g_0^2\, Y^{\binom{t}{a}}_{PH}{}^2}{4\pi^2 c^2 N_f^2\sqrt{V_{F,p}}}\frac{1}{|p|}\log\left(\frac{c|p|}{\mu}\right), \tag{2.166}$$

where $p = Pe^{-\ell}$ represents the physical momentum. The momentum profile of the forward scattering amplitude is shown in Fig. 2.18.

[30] The coupling functions are regular at all momenta including the hot spots at any non-zero energy scale.

[31] In the small v limit, we ignored the momentum dependence of the coupling functions and use the approximation $\Lambda + c|K|_\Lambda \approx \Lambda + c|K|$ in $\hat{S}_{K,P}$.

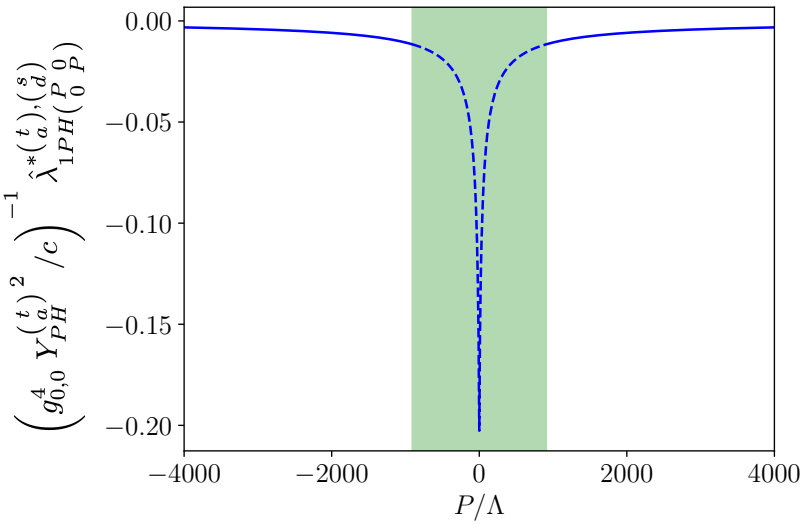

Figure 2.18: The forward scattering amplitude $\hat{\lambda}^{*\binom{t}{a},\binom{s}{d}}_{1PH\binom{P\ 0}{0\ P}}$ in Eq. (2.165) plotted in units of $\left(g_{0,0}^4\, Y_{PH}^{\binom{t}{a}\,2}/c\right)$ as a function of P/Λ at $K = 0$ for $\ell_0 = 50$ (equivalently, $1/(v_0 c) \approx 907$). The width of the shaded region is $2/(v_0 c)$.

2.6.3 Four-fermion coupling in group 2

UV/IR mixing

In group 2, $\lambda^{\binom{1\ 5}{1\ 5};\binom{\sigma_1\ \sigma_2}{\sigma_4\ \sigma_3}}_{\binom{p\ -p}{k\ -k}}$, $\lambda^{\binom{4\ 8}{4\ 8};\binom{\sigma_1\ \sigma_2}{\sigma_4\ \sigma_3}}_{\binom{p\ -p}{k\ -k}}$, $\lambda^{\binom{1\ 5}{4\ 8};\binom{\sigma_1\ \sigma_2}{\sigma_4\ \sigma_3}}_{\binom{p\ -p}{k\ -k}}$, $\lambda^{\binom{4\ 8}{1\ 5};\binom{\sigma_1\ \sigma_2}{\sigma_4\ \sigma_3}}_{\binom{p\ -p}{k\ -k}}$ form a closed set of beta functionals given by Eqs. (2.115)- (2.118). The beta functionals are expressed as integrations over q because of the significant mixing between operators that carry different momenta along the Fermi surface. To simplify the system of beta functionals, we combine the four coupling functions into one matrix,

$$\lambda^{\binom{\sigma_1\ \sigma_2}{\sigma_4\ \sigma_3}}_{2PP\binom{p\ -p}{k\ -k}} = \begin{pmatrix} \lambda^{\binom{1\ 5}{1\ 5};\binom{\sigma_1\ \sigma_2}{\sigma_4\ \sigma_3}}_{\binom{p\ -p}{k\ -k}} & \lambda^{\binom{1\ 5}{4\ 8};\binom{\sigma_1\ \sigma_2}{\sigma_4\ \sigma_3}}_{\binom{p\ -p}{k\ -k}} \\ \lambda^{\binom{4\ 8}{1\ 5};\binom{\sigma_1\ \sigma_2}{\sigma_4\ \sigma_3}}_{\binom{p\ -p}{k\ -k}} & \lambda^{\binom{4\ 8}{4\ 8};\binom{\sigma_1\ \sigma_2}{\sigma_4\ \sigma_3}}_{\binom{p\ -p}{k\ -k}} \end{pmatrix} \tag{2.167}$$

to rewrite Eqs. (2.115)- (2.118) as

$$\begin{aligned}\frac{\partial}{\partial\ell}\lambda^{\left(\begin{smallmatrix}\sigma_1 & \sigma_2\\ \sigma_4 & \sigma_3\end{smallmatrix}\right)}_{2PP\left(\begin{smallmatrix}p & -p\\ k & -k\end{smallmatrix}\right)} =& -\left(1+3(z-1)+2\eta_k^{(\psi)}+2\eta_p^{(\psi)}\right)\lambda^{\left(\begin{smallmatrix}\sigma_1 & \sigma_2\\ \sigma_4 & \sigma_3\end{smallmatrix}\right)}_{2PP\left(\begin{smallmatrix}p & -p\\ k & -k\end{smallmatrix}\right)}\\ &-\frac{1}{4\pi}\int\frac{\mathrm{d}q}{2\pi\mu V_{F,q}}\left[\lambda^{\left(\begin{smallmatrix}\sigma_1 & \sigma_2\\ \beta & \alpha\end{smallmatrix}\right)}_{2PP\left(\begin{smallmatrix}p & -p\\ q & -q\end{smallmatrix}\right)}-\frac{2\mathsf{T}^{\sigma_1\sigma_2}_{\beta\alpha}}{N_f}\mathsf{D}_\mu(p;q)\begin{pmatrix}0&1\\1&0\end{pmatrix}\right]\\ &\times\left[\lambda^{\left(\begin{smallmatrix}\beta & \alpha\\ \sigma_4 & \sigma_3\end{smallmatrix}\right)}_{2PP\left(\begin{smallmatrix}q & -q\\ k & -k\end{smallmatrix}\right)}-\frac{2\mathsf{T}^{\beta\alpha}_{\sigma_4\sigma_3}}{N_f}\mathsf{D}_\mu(q;k)\begin{pmatrix}0&1\\1&0\end{pmatrix}\right].\end{aligned}\tag{2.168}$$

As in Eq. (2.145), we symmetrically normalize the four-fermion coupling in the unit of the Fermi velocity by defining

$$\lambda^{V;\left(\begin{smallmatrix}\alpha & \beta\\ \gamma & \delta\end{smallmatrix}\right)}_{2PP\left(\begin{smallmatrix}p & -p\\ k & -k\end{smallmatrix}\right)}=\frac{1}{\sqrt{V_{F,p}V_{F,k}}}\lambda^{\left(\begin{smallmatrix}\alpha & \beta\\ \gamma & \delta\end{smallmatrix}\right)}_{2PP\left(\begin{smallmatrix}p & -p\\ k & -k\end{smallmatrix}\right)}.\tag{2.169}$$

Its beta functional is given by

$$\begin{aligned}\frac{\partial}{\partial\ell}\lambda^{V;\left(\begin{smallmatrix}\sigma_1 & \sigma_2\\ \sigma_4 & \sigma_3\end{smallmatrix}\right)}_{2PP\left(\begin{smallmatrix}p & -p\\ k & -k\end{smallmatrix}\right)} =& -\left(1+\eta_k+\eta_p\right)\lambda^{V;\left(\begin{smallmatrix}\sigma_1 & \sigma_2\\ \sigma_4 & \sigma_3\end{smallmatrix}\right)}_{2PP\left(\begin{smallmatrix}p & -p\\ k & -k\end{smallmatrix}\right)}\\ &-\frac{1}{4\pi}\int\frac{\mathrm{d}q}{2\pi\mu}\left[\lambda^{V;\left(\begin{smallmatrix}\sigma_1 & \sigma_2\\ \beta & \alpha\end{smallmatrix}\right)}_{2PP\left(\begin{smallmatrix}p & -p\\ q & -q\end{smallmatrix}\right)}-\frac{2\mathsf{T}^{\sigma_1\sigma_2}_{\beta\alpha}}{N_f}\frac{\mathsf{D}_\mu(p;q)}{\sqrt{V_{F,p}V_{F,q}}}\begin{pmatrix}0&1\\1&0\end{pmatrix}\right]\\ &\times\left[\lambda^{V;\left(\begin{smallmatrix}\beta & \alpha\\ \sigma_4 & \sigma_3\end{smallmatrix}\right)}_{2PP\left(\begin{smallmatrix}q & -q\\ k & -k\end{smallmatrix}\right)}-\frac{2\mathsf{T}^{\beta\alpha}_{\sigma_4\sigma_3}}{N_f}\frac{\mathsf{D}_\mu(q;k)}{\sqrt{V_{F,q}V_{F,k}}}\begin{pmatrix}0&1\\1&0\end{pmatrix}\right],\end{aligned}\tag{2.170}$$

where η_k is defined in Eq. (2.147).

In the space of spin wavefunctions for two electrons, the four-fermion coupling can be decomposed into the symmetric and anti-symmetric channels of $SU(N_c)$. For $N_c=2$, the symmetric and anti-symmetric representations correspond to the spin triplet and spin singlet representations, respectively. Combined with the wavefunction defined in the space of hot spot indices, the four-fermion coupling can be decomposed into spin-symmetric s-wave $(+,s)$, spin-symmetric d-wave $(+,d)$, spin-anti-symmetric s-wave $(-,s)$ and spin-anti-symmetric d-wave $(-,d)$ channels as

$$\lambda^{V;\left(\begin{smallmatrix}\sigma_1 & \sigma_2\\ \sigma_4 & \sigma_3\end{smallmatrix}\right)}_{2PP\{k_i\}}=\lambda^{V;(+)(s)}_{2PP\{k_i\}}\mathsf{S}^{\sigma_1\sigma_2}_{\sigma_4\sigma_3}\mathscr{P}_s+\lambda^{V;(+)(d)}_{2PP\{k_i\}}\mathsf{S}^{\sigma_1\sigma_2}_{\sigma_4\sigma_3}\mathscr{P}_d+\lambda^{V;(-)(s)}_{2PP\{k_i\}}\mathsf{A}^{\sigma_1\sigma_2}_{\sigma_4\sigma_3}\mathscr{P}_s+\lambda^{V;(-)(d)}_{2PP\{k_i\}}\mathsf{A}^{\sigma_1\sigma_2}_{\sigma_4\sigma_3}\mathscr{P}_d.\tag{2.171}$$

Here $\mathscr{P}_s$ and $\mathscr{P}_d$ are defined in Eq. (2.156).

$$\mathsf{S}^{\sigma_1\sigma_2}_{\sigma_4\sigma_3}=\frac{1}{2}\left(\delta_{\sigma_1\sigma_4}\delta_{\sigma_2\sigma_3}+\delta_{\sigma_1\sigma_3}\delta_{\sigma_2\sigma_4}\right),\qquad \mathsf{A}^{\sigma_1\sigma_2}_{\sigma_4\sigma_3}=\frac{1}{2}\left(\delta_{\sigma_1\sigma_4}\delta_{\sigma_2\sigma_3}-\delta_{\sigma_1\sigma_3}\delta_{\sigma_2\sigma_4}\right)\tag{2.172}$$

project a spin state of two particles into the $SU(N_c)$ symmetric and anti-symmetric representations. The spin dependence in the interaction mediated by the spin fluctuations can be resolved into

$$\mathsf{T}^{\alpha\beta}_{\gamma\delta}=Y^{(+)}_{PP}\mathsf{S}^{\alpha\beta}_{\gamma\delta}+Y^{(-)}_{PP}\mathsf{A}^{\alpha\beta}_{\gamma\delta}\tag{2.173}$$

with

$$Y^{(+)}_{PP}=2\left(1-\frac{1}{N_c}\right),\qquad Y^{(-)}_{PP}=-2\left(1+\frac{1}{N_c}\right).\tag{2.174}$$

The beta functional for the coupling function in each channel is written as

$$\begin{aligned}\frac{\partial}{\partial\ell}\lambda^{V;(\pm),\binom{s}{d}}_{2PP\binom{p\ -p}{k\ -k}} =& -(1+\eta_k+\eta_p)\,\lambda^{V;(\pm),\binom{s}{d}}_{2PP\binom{p\ -p}{k\ -k}} \\ &- \frac{1}{4\pi}\int\frac{\mathrm{d}q}{2\pi\mu}\left[\lambda^{V;(\pm),\binom{s}{d}}_{2PP\binom{p\ -p}{q\ -q}} - \frac{2}{N_f}Y^{(\pm)}_{PP}1^{\binom{s}{d}}\frac{\mathsf{D}_\mu(p;q)}{\sqrt{V_{F,p}V_{F,q}}}\right] \\ &\times\left[\lambda^{V;(\pm),\binom{s}{d}}_{2PP\binom{q\ -q}{k\ -k}} - \frac{2}{N_f}Y^{(\pm)}_{PP}1^{\binom{s}{d}}\frac{\mathsf{D}_\mu(q;k)}{\sqrt{V_{F,q}V_{F,k}}}\right],\end{aligned} \tag{2.175}$$

where $1^{\binom{s}{d}}$ is defined in Eq. (2.157).

What is interesting for the beta functionals in group 2 is the fact that the strength of mixing between two low-energy operators defined near the Fermi surface but with a large difference in momentum is controlled by high-energy bosons. Since $D_\mu(q;k)$ decays as $\frac{g^2_{qk}}{c|q-k|}$ at large $|q-k|$, the contribution from q far away from k can be important. The potential UV divergence associated with the q integration in Eq. (2.175) is cut off by either the momentum profile of the Yukawa coupling included in $D_\mu(q;k)$ at large $|q-k|$ in Eq. (2.109) or the irrelevant boson kinetic term[32]. The trouble is that whichever cuts off the UV divergence is related to the dynamics of boson at large energy/momentum, which is not a part of the universal low-energy data. This implies that the four-fermion coupling can not be determined without including the high-energy physics. *Namely, the one-particle irreducible (1PI) quartic vertex function is not an observable that can be determined solely in terms of other low-energy observables.* What is then the low-energy observable that measures the strength of the two-body interaction? To identify the right low-energy observable, we note that the four-point functions, which determine physical susceptibilities, are determined by the sum of the 1PI four-point function and the tree-diagram that involves the 1PI three-point functions and the boson propagator (see Fig. 1.6). Therefore, we consider the net two-body interaction that combines the contributions of the four-fermion coupling and the interaction mediated by the spin fluctuations,

$$\lambda^{'(\pm),\binom{s}{d}}_{2PP\binom{p\ -p}{k\ -k}} = \lambda^{V;(\pm),\binom{s}{d}}_{2PP\binom{p\ -p}{k\ -k}} - \frac{2}{N_f}Y^{(\pm)}_{PP}1^{\binom{s}{d}}\frac{\mathsf{D}_\mu(p;k)}{\sqrt{V_{F,p}V_{F,k}}}. \tag{2.176}$$

The net two-body interaction is what determines the pairing interaction as is shown in the complete square term in Eq. (2.175)[33]. The RG flow equation for the net two-body interaction reads

$$\begin{aligned}\frac{\partial}{\partial\ell}\lambda^{'(\pm),\binom{s}{d}}_{2PP\binom{p\ -p}{k\ -k}} =& -(1+\eta_k+\eta_p)\,\lambda^{'(\pm),\binom{s}{d}}_{2PP\binom{p\ -p}{k\ -k}} - \frac{1}{4\pi}\int\frac{\mathrm{d}q}{2\pi\mu}\lambda^{'(\pm),\binom{s}{d}}_{2PP\binom{p\ -p}{q\ -q}}\lambda^{'(\pm),\binom{s}{d}}_{2PP\binom{q\ -q}{k\ -k}} \\ &- \frac{2}{N_f}Y^{(\pm)}_{PP}1^{\binom{s}{d}}\mathsf{r}(p,k),\end{aligned} \tag{2.177}$$

where

$$\mathsf{r}(k,p) = \left(-\mu\frac{\partial}{\partial\mu}+1+\eta_k+\eta_p\right)\frac{\mathsf{D}_\mu(p;k)}{\sqrt{V_{F,p}V_{F,k}}} \tag{2.178}$$

corresponds to the contribution of the spin fluctuations that arises between energy μ and $\mu-d\mu$. The spin fluctuations generate attractive interactions in the spin anti-symmetric d-wave channel and the spin symmetric s-wave channel. Its magnitude is strongest near the hot spots. To the leading order in v, $\mathsf{r}(k,p) = \frac{g^2_{k,p}}{\sqrt{V_{F,k}V_{F,p}}}\frac{\mu^2}{(\mu+c|k-p|+c|v_k k+v_p p|)^2}$. Because $\mathsf{r}(k,p)$ is the low-energy contribution to the net two-body interaction, it decays as $1/|k-p|^2$ at large momentum, and its contribution becomes

[32] For instance, the scale associated with the crossover from high-energy 'Gaussian physics' to low-energy 'critical physics' can act as a cutoff momentum for q integration.

[33] The Wilsonian RG scheme is also naturally formulated in terms of the net two-body interaction[142].

negligible at momentum much larger than $\mu/(vc)$. Due to the fast decay of $\mathsf{r}(k,p)$ at large momenta, the flow of the net two-body interaction is no longer sensitive to UV scales. Once the net two-body interaction is known at a scale, within a power-law accuracy its value at a lower energy scale can be determined from Eq. (2.177) without having to resort to UV physics.

Absence of Hermitian quasi-fixed point at non-zero nesting angle

To find a fixed point of the beta functional, we have to examine the flow equation for the four-fermion coupling function defined in the space of rescaled momentum,

$$\tilde{\lambda}^{(\pm),\binom{s}{d}}_{2PP\binom{P\ -P}{K\ -K}} = \lambda'^{(\pm),\binom{s}{d}}_{2PP\binom{p\ -p}{k\ -k}}, \tag{2.179}$$

where $K = e^{\ell}k$, $P = e^{\ell}p$. The beta functionals for $\tilde{\lambda}$ becomes

$$\begin{aligned}\frac{\partial}{\partial\ell}\tilde{\lambda}^{(\pm),\binom{s}{d}}_{2PP\binom{P\ -P}{K\ -K}} =& -\left(1+K\frac{\partial}{\partial K}+P\frac{\partial}{\partial P}+\hat{\eta}_K+\hat{\eta}_P\right)\tilde{\lambda}^{(\pm),\binom{s}{d}}_{2PP\binom{P\ -P}{K\ -K}} \\ &-\frac{1}{4\pi}\int\frac{\mathrm{d}Q}{2\pi\Lambda}\tilde{\lambda}^{(\pm),\binom{s}{d}}_{2PP\binom{P\ -P}{Q\ -Q}}\tilde{\lambda}^{(\pm),\binom{s}{d}}_{2PP\binom{Q\ -Q}{K\ -K}}-\frac{2}{N_f}Y^{(\pm)}_{PP}1^{\binom{s}{d}}\hat{\mathsf{R}}(P,K),\end{aligned} \tag{2.180}$$

where

$$\begin{aligned}\hat{\mathsf{R}}(K,P) &= \frac{\hat{g}^2_{K,P}}{\sqrt{\hat{V}_{F,K}\hat{V}_{F,P}}}\frac{\Lambda^2}{\left(\Lambda+c\,|K-P|+c\,|\hat{v}_K K+\hat{v}_P P|\right)^2}, \\ \hat{\eta}_K &= \frac{(N_c^2-1)\hat{g}^2_K}{2\pi^2 c N_c N_f \hat{V}_{F,K}}\frac{\Lambda}{\Lambda+2c\hat{v}_K\,|K|}.\end{aligned} \tag{2.181}$$

Here, the attractive interaction $\hat{\mathsf{R}}(K,P)$ generated from the spin fluctuations tends to drive the system to a superconducting state. On the other hand, $\hat{\eta}_K$, that represents the momentum dependent anomalous dimension, tends to suppress growth of the four-fermion coupling by making electrons incoherent. The fate of the theory is determined by the competition between the attractive interaction that favours superconductivity and the pair-breaking effect caused by incoherence. If the pairing effect dominates, the theory flows to a superconducting state, and quasi-fixed points arise only outside the space of Hermitian theories. On the other hand, if the pair-breaking effect dominates, there can be Hermitian quasi-fixed points. Once the theory is attracted to the quasi-fixed point with a non-zero v, the theory would gradually flow to the true fixed point at $v=0$ under the full RG flow. In the latter case, a stable non-Fermi liquid state would be realized at zero temperature. This scenario is realized near three space dimensions where the co-dimension of the Fermi surface is close to 2[123, 183]. Our goal is to understand the fate of the system that results as an outcome of this competition in two space dimensions.

In principle, there can be multiple quasi-fixed points. Here we focus on the one-parameter families of quasi-fixed points that are continuously connected to the true fixed point at $v=0$. It is difficult to write down the momentum dependent coupling function explicitly at the quasi-fixed points. However, we can understand the asymptotic form of $\tilde{\lambda}$ at large momenta. To the leading order in v, the last term in Eq. (2.180) decays in a power-law as $\hat{\mathsf{R}}(K,P)\sim\frac{\Lambda^2}{(c|K-P|+c|\hat{v}_K K+\hat{v}_P P|)^2}$ at large $|K|$ and $|P|$. Since $\left(1+K\frac{\partial}{\partial K}+P\frac{\partial}{\partial P}\right)\hat{\mathsf{R}}(K,P)\approx-\hat{\mathsf{R}}(K,P)$, at large momenta the coupling function at the quasi fixed-point can be determined from balancing the first and the last terms of the beta functional as

$$\tilde{\lambda}^{*\binom{\sigma_1\ \sigma_2}{\sigma_4\ \sigma_3}}_{2PP\binom{P\ -P}{K\ -K}} \approx \frac{2}{N_f}\hat{\mathsf{R}}(K,P)\mathsf{T}^{\sigma_1\sigma_2}_{\sigma_4\sigma_3}(\mathscr{P}_s-\mathscr{P}_d). \tag{2.182}$$

Here $\tilde{\lambda}^2$ term and $\hat{\eta}\tilde{\lambda}$ term can be ignored in the small v limit. This is a special solution of the fixed point equation which can be augmented with a homogeneous solution of $(1+K\partial_K+P\partial_P)\tilde{\lambda}=0$. The

homogeneous solution also vanishes as $1/K$ or $1/P$ at large momenta. This shows that $\tilde{\lambda}^{(\pm),\binom{s}{d}}_{2PP\binom{P\ -P}{K\ -K}}$ has to vanish in the limit that either K or P, or both are large at the quasi-fixed points.

We now prove that the quasi-fixed points have to be non-Hermitian at $v \neq 0$. To show this, we rewrite Eq. (2.180) as a matrix equation,

$$\frac{\partial}{\partial \ell}\tilde{\lambda}^{(n)} = -\tilde{\lambda}^{(n)} - L\tilde{\lambda}^{(n)} - \tilde{\lambda}^{(n)}L^{\dagger} - H\tilde{\lambda}^{(n)} - \tilde{\lambda}^{(n)}H - \frac{1}{4\pi}\tilde{\lambda}^{(n)}\tilde{\lambda}^{(n)} + \alpha^{(n)}R. \tag{2.183}$$

Here, $\tilde{\lambda}^{(n)}_{QK} = \tilde{\lambda}^{(n)}_{2PP\binom{Q\ -Q}{K\ -K}}$ with $n = (+,s),(+,d),(-,s),(-,d)$ represent the four-fermion coupling functions written as matrices in the space of momentum. $L_{PK} = 2\pi\Lambda P\partial_P\delta(P-K)$, $H_{PK} = 2\pi\Lambda\hat{\eta}_P\delta(P-K)$, $R_{PK} = \hat{\mathsf{R}}(P,K)$ are also viewed as matrices, where the multiplication of matrices is defined as $(AB)_{PK} = \int \frac{\mathrm{d}Q}{2\pi\Lambda}A_{PQ}B_{QK}$. $\alpha^{(n)}$ denotes the parameter that determines the sign and the strength of interaction in each channel,

$$\begin{aligned}
\alpha^{(+,s)} &= -\frac{4}{N_f}\left(1-\frac{1}{N_c}\right), \quad \alpha^{(+,d)} = \frac{4}{N_f}\left(1-\frac{1}{N_c}\right), \\
\alpha^{(-,s)} &= \frac{4}{N_f}\left(1+\frac{1}{N_c}\right), \quad \alpha^{(-,d)} = -\frac{4}{N_f}\left(1+\frac{1}{N_c}\right).
\end{aligned} \tag{2.184}$$

The beta functionals can be written in the complete square form as

$$\frac{\partial}{\partial \ell}\tilde{\lambda}^{(n)} = -\frac{1}{4\pi}\left[\tilde{\lambda}^{(n)} + 4\pi\left(\frac{I}{2}+L+H\right)\right]\left[\tilde{\lambda}^{(n)} + 4\pi\left(\frac{I}{2}+L^{\dagger}+H\right)\right] + \mathcal{D}^{(n)}, \tag{2.185}$$

where $\mathcal{D}^{(n)}$ is the discriminant matrix given by

$$\mathcal{D}^{(n)} = \alpha^{(n)}R + 4\pi\left(\frac{I}{2}+L+H\right)\left(\frac{I}{2}+L^{\dagger}+H\right). \tag{2.186}$$

I is the identity matrix with $I_{PK} = 2\pi\Lambda\delta(P-K)$. At the fixed point, the four-fermion coupling function should satisfy

$$\left[\tilde{\lambda}^{(n)} + 4\pi\left(\frac{I}{2}+L+H\right)\right]\left[\tilde{\lambda}^{(n)} + 4\pi\left(\frac{I}{2}+L^{\dagger}+H\right)\right] - 4\pi\mathcal{D}^{(n)} = 0. \tag{2.187}$$

It is noted that $\mathcal{D}^{(n)}$ and H are Hermitian matrices, but L is not. Even if $\left[\tilde{\lambda}^{(n)} + 4\pi\left(\frac{I}{2}+L^{\dagger}+H\right)\right]$ is not Hermitian, the polar decomposition theorem guarantees that there exists a unitary matrix U that makes $U\left[\tilde{\lambda}^{(n)} + 4\pi\left(\frac{I}{2}+L^{\dagger}+H\right)\right]$ Hermitian. The solution to Eq. (2.187) is then written as

$$\tilde{\lambda}^{(n)} = -4\pi\left(\frac{I}{2}+L^{\dagger}+H\right) + (4\pi)^{1/2}U^{\dagger}\mathcal{E}^{(n)}, \tag{2.188}$$

where $\mathcal{E}^{(n)}$ represents a matrix that satisfies $[\mathcal{E}^{(n)}]^2 = \mathcal{D}^{(n)}$[34].

To show that $\tilde{\lambda}^{(n)}$ is non-Hermitian at the quasi-fixed point with $v \neq 0$, we consider a vector of the form,

$$f_K = \left(\frac{\Lambda}{|K|}\right)^{1/2} e^{\int_{\Lambda'}^{|K|}\frac{dK'}{K'}\hat{\epsilon}_{K'}} \tag{2.189}$$

[34]For an $N \times N$ Hermitian matrix $\mathcal{D}^{(n)}$, there are $2^{(N-N_0)}$ distinct solution for $[\mathcal{E}^{(n)}]^2 = \mathcal{D}^{(n)}$, where N_0 is the number of zero eigenvalues.

with a real function $\hat{\epsilon}_K$ and a scale Λ'. For f_K to be square integrable, $\hat{\epsilon}_K$ has to be positive (negative) in the limit that $|K|$ is small (large). The expectation value of the both sides of Eq. (2.187) for f_K is written as

$$\int \frac{dK}{2\pi\Lambda} \tilde{f}'^{*}_K \tilde{f}_K - 4\pi\alpha^{(n)} \int \frac{dKdP}{(2\pi\Lambda)^2} f^*_K R_{KP} f_P - (4\pi)^2 \int \frac{dK}{2\pi\Lambda} (\hat{\eta}_K - \hat{\epsilon}_K)^2 |f_K|^2 = 0, \tag{2.190}$$

where $\tilde{f}_K = \int \frac{dP}{2\pi\Lambda} \tilde{\lambda}^{(n)}_{KP}\ f_P + 4\pi(\hat{\eta}_K - \hat{\epsilon}_K) f_K$ and $\tilde{f}'_K = \int \frac{dP}{2\pi\Lambda} \tilde{\lambda}^{(n)\dagger}_{KP}\ f_P + 4\pi(\hat{\eta}_K - \hat{\epsilon}_K) f_K$. If $\tilde{\lambda}$ is Hermitian, $\tilde{f}'_K = \tilde{f}_K$, and the first term in Eq. (2.190) is non-negative. The second term is strictly positive for $n = (-, d)$ and $(+, s)$ because $\alpha^{(n)}$ is negative for these channels (see Eq. (2.184)), and R_{KP}, f_K, f_P are positive for all K and P. The third term is negative, but we can make it arbitrarily small by tuning $\hat{\epsilon}_K$ and Λ' as far as $\hat{\eta}_K$ goes to zero in the large K limit. Let us choose $\hat{\epsilon}_K$ to be

$$\hat{\epsilon}_K = \begin{cases} \hat{\eta}_K & \text{for} \quad |K| < \Lambda', \\ -\delta & \text{for} \quad |K| > \Lambda' \end{cases} \tag{2.191}$$

with $\delta > 0$. Since $\hat{\eta}_K$ approaches zero in the large K limit, for any non-zero δ, there exists a sufficiently large Λ' such that $|\hat{\eta}_K| \ll \delta$ for $|K| > \Lambda'$. In this case,

$$\int \frac{dK}{2\pi\Lambda} (\hat{\eta}_K - \hat{\epsilon}_K)^2 |f_K|^2 \approx 2\delta^2 \int_{\Lambda'}^{\infty} \frac{dK}{2\pi K} \left(\frac{\Lambda'}{K}\right)^{2\delta} = \frac{\delta}{2\pi}. \tag{2.192}$$

This can be made arbitrarily small by choosing δ that is nonzero but small enough. On the other hand, the second term in Eq. (2.190) remains strictly positive even in the limit in which δ is small and Λ' is large. This implies that there exist normalizable vectors for which the left hand side of Eq. (2.190) is positive definite if $\tilde{\lambda}$ was Hermitian. This proves that $\tilde{\lambda}$ can not be Hermitian, and *the quasi-fixed point must be non-Hermitian for* $v \neq 0$[69].

Because the beta functionals have real coefficients, non-Hermitian quasi-fixed points arise in pairs that are related to each other through the Hermitian conjugation. On the other hand, the true Hermitian fixed point in Eq. (2.119) is at $\tilde{\lambda} = 0$ in the $v \to 0$ limit. As v approaches zero, a pair of non-Hermitian quasi-fixed points should merge into the true Hermitian-fixed point due to continuity. This implies that at least one pair of non-Hermitian fixed points are close to the space of Hermitian theories for a small v. This is illustrated in Fig. 1.5.

Collision of projected quasi-fixed points

Given that the RG flow is defined in the infinite dimensional space of coupling functions, it is not easy to visualize it. However, one can have a glimpse of the RG flow by projecting it onto a finite dimensional subspace of coupling functions. For this, we view the space of coupling functions as a vector space and decompose the four-fermion coupling function as an infinite sum of orthonormal basis,

$$\tilde{\lambda}^{(n)}_{QK}(\ell) = \sum_{j=0}^{\infty} c_{n,j}(\ell) \tilde{\lambda}^{[j]}_{QK}. \tag{2.193}$$

Here $\tilde{\lambda}^{[j]}_{QK}$ represents the j-th basis of the coupling function that obeys the orthonormality condition, $\int \frac{dKdP}{(2\pi\Lambda)^2} \tilde{\lambda}^{[i]}_{KP} \tilde{\lambda}^{[j]}_{PK} = \delta_{ij}$. $c_{n,j}(\ell)$ denotes the strength of the coupling function projected to the j-th basis function in channel n. The space of coupling function is viewed as the infinite dimensional space of the coupling constants, $\{c_{n,j}(\ell)\}$, and the full beta functional can be written as a coupled differential equations for $c_{n,j}(\ell)$. Within the infinite dimensional space of coupling constants, let us consider a subspace spanned by one basis coupling,

$$\tilde{\lambda}^{[0]}_{KP}(\ell) = f_K f^*_P, \tag{2.194}$$

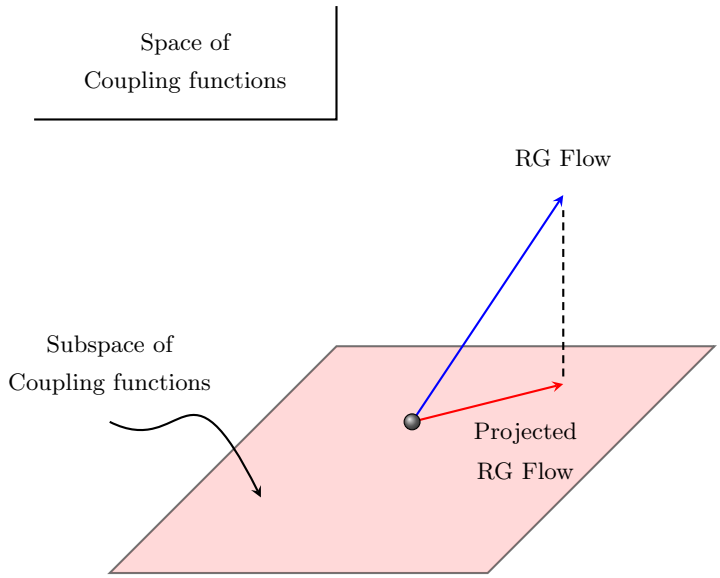

Figure 2.19: The full RG flow defined in the infinite dimensional space of coupling functions can be projected onto a finite dimensional subspace by restricting the flow vector to the tangent space of the subspace.

where f_K denotes a wavefunction defined in the space of relative momentum of a Cooper pair with zero center of mass momentum. The corresponding coupling, denoted as $c_{n,0}(\ell) = t(\ell)$, measures the strength of the interaction in that specific pairing channel. For Hermitian theories, $t(\ell)$ is real, but here we allow it to be complex to accommodate non-Hermitian quasi-fixed points. We choose the Cooper pair wavefunction to be of the form,

$$f_K = A\sqrt{\frac{\Lambda}{|K|}}\Theta(|K| - \varepsilon)\Theta(\Delta - |K|), \tag{2.195}$$

where $A = \left[\frac{1}{\pi}\log\left(\frac{\Delta}{\varepsilon}\right)\right]^{-\frac{1}{2}}$ is the normalization constant [35]. Here ε and Δ correspond to the small and large momentum cutoffs for the wavefunction, respectively. Since the norm of the wavefunction diverges both in the small ε and the large Δ limits, one has to consider finite Δ/ε. With decreasing ε, the wavefunction has more weight for electrons near the hot spots. In contrast, a larger Δ puts more weight on cold electrons away from the hot spots. The nature of the projected RG flow depends on the relative weight between hot and cold electrons.

Even if one starts with a theory within the subspace in Eq. (2.194), the theory in general flows out of the subspace because the beta functions for other coupling constants are not generally zero within the subspace. Here, we consider the RG flow that is projected onto the subspace (see Fig. 2.19). The projected beta function[111] is defined as

$$\frac{\partial t(\ell)}{\partial \ell} = \int \frac{\mathrm{d}K\mathrm{d}P}{(2\pi\Lambda)^2}\left[\frac{\partial \tilde{\lambda}^{(n)}_{KP}(\ell)}{\partial \ell}\right]_{c_{n,0}=t,\ c_{n,j\neq 0}=0} \tilde{\lambda}^{[0]}_{PK}. \tag{2.196}$$

[35] The rest of the basis coupling functions can be chosen to be orthogonal to Eq. (2.195).

From Eqs. (2.183) and (2.194), the projected beta function can be written as

$$\frac{\partial t(\ell)}{\partial \ell} = -\left\{ \int \frac{\mathrm{d}P\mathrm{d}K}{(2\pi\Lambda)^2} f_P^* \left(1 + K\frac{\partial}{\partial K} + P\frac{\partial}{\partial P} + \hat{\eta}_K + \hat{\eta}_P\right) \tilde{\lambda}_{PK}^{(n)} f_K \right. \\ \left. + \frac{1}{4\pi} \int \frac{\mathrm{d}P\mathrm{d}Q\mathrm{d}K}{(2\pi\Lambda)^3} f_P^* \tilde{\lambda}_{PQ}^{(n)} \tilde{\lambda}_{QK}^{(n)} f_K - \alpha^{(n)} \int \frac{\mathrm{d}P\mathrm{d}K}{(2\pi\Lambda)^2} f_P^* R(P,K) f_K \right\}, \tag{2.197}$$

where the momentum dilatation on the first line only act on $\tilde{\lambda}_{PK}^{(n)}$. The resulting projected beta function is written as a differential equation for t only,

$$\frac{\partial t(\ell)}{\partial \ell} = -\left[\frac{1}{4\pi} t(\ell)^2 + 2\langle f|\hat{\eta}|f\rangle t(\ell) - \alpha^{(n)} \langle f|R|f\rangle\right], \tag{2.198}$$

where $\langle f|T|f\rangle \equiv \int \frac{dPdK}{(2\pi\Lambda)^2} f_K^* T_{KP} f_P$. The fixed points of the projected beta function arise at

$$t_\star = -4\pi\langle f|\eta|f\rangle \pm 2\pi\sqrt{d_\star}, \tag{2.199}$$

where $d_\star \equiv 4\langle f|\eta|f\rangle^2 + \frac{\alpha^{(n)}}{\pi}\langle f|R|f\rangle$ is the discriminant. $\langle f|\eta|f\rangle$ is the contribution from the anomalous dimension of electrons, and $\langle f|R|f\rangle$ is from the interaction generated from the spin fluctuations. The anomalous dimension makes electrons incoherent and tends to suppress pairing instability. On the other hand, the attractive interaction promotes superconductivity in the channels with $\alpha^{(n)} < 0$. While $\langle f|\eta|f\rangle$ contributes to the discriminant with the higher power than $\langle f|R|f\rangle$, for a non-zero w, the discriminant can be dominated by either one of the two depending on the choice of ε and Δ. In channels in which the pair breaking effect (attractive interaction) dominates over the other, $d_\star > 0$ ($d_\star < 0$) and the quasi-fixed points are Hermitian (non-Hermitian).

Let us examine the discriminant in the limit that $\varepsilon/\Lambda \ll 1/c$ and $\Delta/\Lambda \gg 1/(vc)$. In this case, $\langle f|\eta|f\rangle$ and $\langle f|R|f\rangle$ can be computed analytically,

$$\langle f|\hat{\eta}|f\rangle = \frac{(N_c^2-1)}{4\pi N_c N_f} w \frac{\log\left(\frac{\Lambda}{2vc\varepsilon}\right)}{\log\left(\frac{\Delta}{\varepsilon}\right)}, \quad \langle f|R|f\rangle = \frac{1}{2} w \log\left(\frac{2}{v}\right) \frac{1}{\log\left(\frac{\Delta}{\varepsilon}\right)}. \tag{2.200}$$

Here, $K\partial_K f_K = -\frac{1}{2} f_K + A\sqrt{\varepsilon\Lambda}\,\mathrm{sgn}(K)\delta(|K|-\varepsilon) - A\sqrt{\Delta\Lambda}\,\mathrm{sgn}(K)\delta(\Delta - |K|)$ is used and $w \equiv v/c$ with $v = v_0$ and $c = c(v_0)$. In the spin anti-symmetric d-wave channel, the discriminant becomes

$$d_\star = \frac{1}{\log\left(\frac{\Delta}{\varepsilon}\right)} \left[\frac{(N_c^2-1)^2}{4\pi^2 N_c^2 N_f^2} w^2 \frac{\log^2\left(\frac{\Lambda}{2vc\varepsilon}\right)}{\log\left(\frac{\Delta}{\varepsilon}\right)} - \frac{2}{\pi N_f}\left(1 + \frac{1}{N_c}\right) w \log\left(\frac{2}{v}\right)\right]. \tag{2.201}$$

The relative magnitude between the two terms in Eq. (2.201) is controlled by $\frac{\log^2\left(\frac{\Lambda}{2vc\varepsilon}\right)}{\log\left(\frac{\Delta}{\varepsilon}\right)}$. If we take the small ε/Λ limit for a fixed Δ/Λ, the wavefunction has a large weight for incoherent electrons close to the hot spots. While the attractive interaction is also strong near the hot spots, the interaction is not singular enough to overcome the pair breaking effect. In those channels with small ε/Λ, the discriminant is positive and the projected RG flow supports two fixed points on the real axis of the coupling. One is a stable fixed point and the other is an unstable fixed point. Near the stable fixed point, the pairing interaction does not grow due to the pair breaking effect. Alternatively, if we take the large Δ/Λ limit for a fixed ε/Λ, the wavefunction has a large weight for cold electrons. Since electrons away from the hot spots are largely coherent, they are more susceptible to pairing instability. While the attractive interaction is also weak away from the hot spots, the pairing effect prevails over the pair breaking effect in these channels because $\langle f|\eta|f\rangle^2$ goes to zero faster than $\langle f|R|f\rangle$ with increasing Δ/Λ. As a result, the discriminant is negative in the channels with large Δ/Λ[36], and the fixed points arise

[36] However, $d_\star$ eventually approaches zero in the $\Delta/\Lambda \to \infty$ limit because the attractive interaction becomes vanishingly small for electrons that are very far from the hot spots. Therefore, there exists an optimal choice of ε and Δ at which the discriminant is most negative.

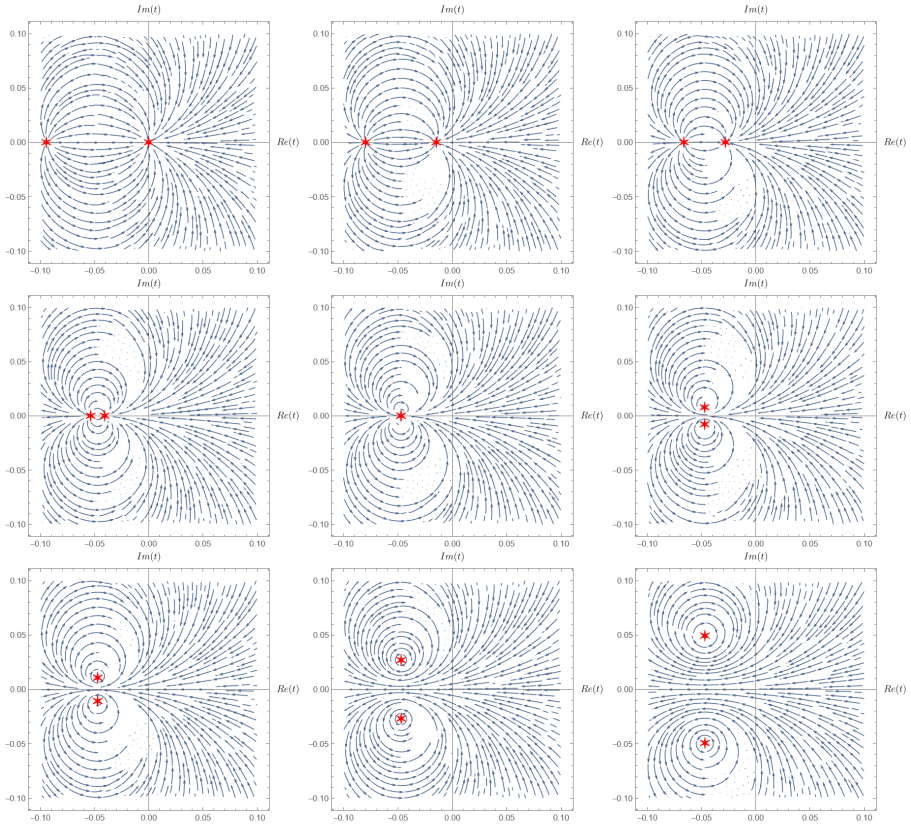

Figure 2.20: The RG flow projected onto the subspace of one complex four-fermion coupling in the spin anti-symmetric d-wave pairing channel with Cooper-pair wave function given in Eq. (2.195) for $v = 0.000476257$, $N_c = 2$ and $N_f = 1$. Here $\Delta/\Lambda = 1000/(vc) \approx 1.39 \times 10^8$ and ε/Λ is chosen to be $\exp(-10^a)$ with $a = 6$, 4, 3.8, 3.73, 3.721826341, 3.71, 3.7, 3.6 and 3.4 from the top left panel to the bottom right. The quasi-fixed points are marked as (red) stars. For small values of ε/Λ, the pair breaking effect for hot electrons dominates, resulting in the quasi-fixed points on the real axis. At the (approximate) critical value $\varepsilon/\Lambda = \exp(-10^{3.721826341})$, the stable and unstable quasi-fixed points collide. For larger values of ε/Λ, the pair forming effect dominates, and the quasi-fixed points move away from the real axis, resulting in a runaway flow for Hermitian theories on the real axis.

away from the real axis. This corresponds to a non-Hermitian fixed point for the projected RG flow. On the real axis, the couplings in those channels exhibit run-away flows toward the strong coupling regime with large attractive interactions, signifying a superconducting instability. These two different behaviours are separated by critical wavefunctions at which the discriminant vanishes and two fixed points collide on the real axis[92]. Here, the collision of fixed points arises within one theory as the plane onto which the RG flow is projected is rotated in the space of coupling functions. The evolution of the projected RG flow with different values of ε/Λ and Δ/Λ is shown in Fig. 2.20.

A small perturbation around the projected quasi-fixed point evolves under the linearized beta function given by

$$\frac{\partial \delta t(\ell)}{\partial \ell} = \mp\sqrt{d_\star}\ \delta t(\ell), \tag{2.202}$$

where $\delta t(\ell) = t(\ell) - t_\star$. The eigenvalues $\mp\sqrt{d_\star}$ are real at the Hermitian fixed points and purely imaginary at the non-Hermitian quasi-fixed points. The RG flow in the vicinity of the real quasi-fixed points exhibits the usual converging or diverging behaviour depending on whether the fixed point

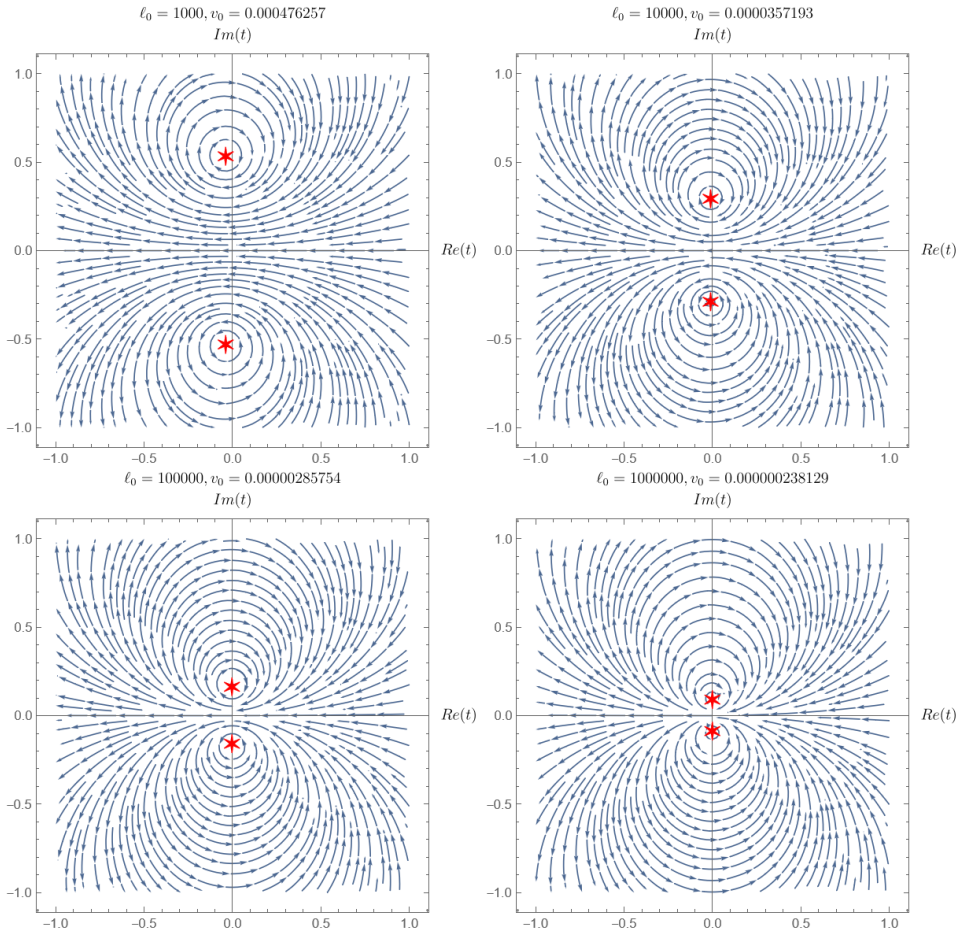

Figure 2.21: The RG flow projected onto the subspace of one complex four-fermion coupling in the spin anti-symmetric d-wave pairing channel with Cooper-pair wave function given in Eq. (2.195) for $N_c = 2$, $N_f = 1$, $\Delta/\Lambda = 10^8$ and $\varepsilon/\Lambda = 10^{-10}$ with $\ell_0 = 10^3, 10^4, 10^5, 10^6$ from top left to bottom right. With increasing ℓ_0 (decreasing $v_0(0)$), the pair of complex quasi-fixed points approach to the real axis, creating a bottleneck region in the real axis.

is stable or unstable, respectively. Near the non-Hermitian fixed points, the RG flow is rotational, exhibiting limit cycles[212, 67, 105, 66, 45].

The existence of channels in which the quasi-fixed points arise away from the real axis suggests that a Hermitian theory eventually flows toward a superconducting fixed point at low energies. When the nesting angle is small, we expect a weaker superconducting instability as the pairing interaction generated from the spin fluctuations is weak. Indeed, the non-Hermitian quasi-fixed points get closer to the space of Hermitian theories as v decreases. In Fig. 2.21, we plot the projected RG flow around the non-Hermitian quasi fixed point in the spin anti-symmetric d-wave channel for different values of v. With decreasing v, the quasi-fixed points approach the real axis, creating a bottleneck in the RG flow of Hermitian theories. The bottleneck creates a large window of length scale in which the theory exhibits an approximate scale invariance before the system eventually becomes superconducting in the low energy limit.

Our next task is to understand how Hermitian theories undergo superconducting instabilities at low energies. We can not use Eq. (2.198) to describe the actual superconducting instability because the full RG flow does not stay within the one-dimensional subspace spanned by Eq. (2.194). The RG flow

that is projected to a fixed channel does not capture how the Cooper pair wavefunction evolves under the RG flow. In particular, the dilatation term in the beta functional continuously push electrons from the hot region to the cold region under the RG flow, which broadens the width of the pair wavefunction relative to the width of the hot spot region[37]. Therefore, we go back to the full beta functional to address superconducting instability.

2.7 Superconducting instability

In this section, we study superconducting instability by solving the beta functional for the four-fermion coupling function in the pairing channel with a fixed nesting angle. This is justified because the theory undergoes a superconducting instability before the nesting angle changes appreciably in the small v limit, as will be shown later. Since we already know that there is no Hermitian fixed point with $v \neq 0$, for the purpose of understanding superconductivity, it is simpler to use the beta functional for the coupling function defined in the space of physical momentum. The way superconductivity emerges at low energies can be understood from the solution of the beta functional for the four-fermion coupling function. Since $\lambda^{V;(\pm),\binom{s}{d}}_{2PP\binom{p\ -p}{k\ -k}}$ is sensitive to the boson propagator at large momenta, only the net two-body interaction function defined in Eq. (2.176) can be determined within the low-energy effective field theory. Nonetheless, we can still understand superconducting instabilities by solving Eq. (2.175) for $\lambda^{V;(\pm),\binom{s}{d}}_{2PP\binom{p\ -p}{k\ -k}}$, assuming that the boson propagator takes the form of Eq. (2.109) at all momenta. Although $\mathsf{D}_\mu(q;k)$ in Eq. (2.109) and $\lambda^{V;(\pm),\binom{s}{d}}_{2PP\binom{p\ -p}{k\ -k}}$ obtained from Eq. (2.175) are not individually reliable at large momenta, the combination in Eq. (2.176) is insensitive to the unknown UV physics. In particular, if the net two-body interaction diverges due to a superconducting instability, so does $\lambda^{V;(\pm),\binom{s}{d}}_{2PP\binom{p\ -p}{k\ -k}}$ because Eq. (2.109) is regular. Therefore, we directly solve the beta functional in Eq. (2.175). The manner superconductivity arises crucially depends on whether the bare coupling function has any channel with attractive interaction which is stronger than the interaction mediated by the spin fluctuations or not [96]. Therefore, discussion on superconductivity is divided into two parts.

2.7.1 Attractive bare interaction

If the bare interaction is attractive in any channel with its strength greater than $w = v/c$, Eq. (2.175) is dominated by the BCS term that is quadratic in the four-fermion coupling. In this case, Eq. (2.175) is well approximated by

$$\frac{\partial}{\partial \ell}\lambda^{V;(\pm),\binom{s}{d}}_{2PP\binom{p\ -p}{k\ -k}} = -\lambda^{V;(\pm),\binom{s}{d}}_{2PP\binom{p\ -p}{k\ -k}} - \frac{1}{4\pi}\int \frac{\mathrm{d}q}{2\pi\mu}\lambda^{V;(\pm),\binom{s}{d}}_{2PP\binom{p\ -p}{q\ -q}}\lambda^{V;(\pm),\binom{s}{d}}_{2PP\binom{q\ -q}{k\ -k}}. \tag{2.203}$$

The first term on the right hand side reflects the fact that the four-fermion coupling is irrelevant by power-counting under the scaling in which all components of momentum are scaled. The flip side of the scaling is the scale dependent measure $\frac{\mathrm{d}q}{2\pi\mu}$ in the second term. It describes the BCS process in which Cooper pairs are scattered to intermediate states on the Fermi surface. The volume of the phase space for virtual Cooper pairs measured in the unit of the running energy scale $\mu = \Lambda e^{-\ell}$ increases with decreasing energy. The enhancement from the phase space volume compensates the suppression from the power-counting, effectively promoting the four-fermion coupling to a marginal coupling as expected. This can be easily seen by absorbing a factor of e^ℓ into the coupling to write the beta

[37] This reflects the fact that more and more electrons are decoupled from spin fluctuations as the low-energy limit is taken.

functional as

$$\frac{\partial}{\partial \ell}\left(e^{\ell}\lambda^{V;(\pm),\binom{s}{d}}_{2PP\binom{p\ -p}{k\ -k}}\right)=-\frac{1}{4\pi}\int\frac{\mathrm{d}q}{2\pi\Lambda}\left(e^{\ell}\lambda^{V;(\pm),\binom{s}{d}}_{2PP\binom{p\ -p}{q\ -q}}\right)\left(e^{\ell}\lambda^{V;(\pm),\binom{s}{d}}_{2PP\binom{q\ -q}{k\ -k}}\right). \tag{2.204}$$

Its solution is given by

$$\lambda^{V;(\pm),\binom{s}{d}}(\ell)=e^{-\ell}\lambda^{V;(\pm),\binom{s}{d}}(0)\left[1+\frac{\ell}{4\pi}\lambda^{V;(\pm),\binom{s}{d}}(0)\right]^{-1}. \tag{2.205}$$

Here $\lambda^{V;(\pm),\binom{s}{d}}$ is viewed as a matrix defined in the space of momentum. In this expression, the matrix multiplications are defined with the measure $(AB)_{p,k}=\int\frac{\mathrm{d}q}{2\pi\Lambda}A_{pq}B_{qk}$. If $\lambda^V(0)$ has any channel with negative eigenvalue, the four-fermion coupling blows up around scale $\ell_c\sim\frac{4\pi}{|E|}$, where $E<0$ is the most negative eigenvalue of the bare coupling[165]. For $|E|>w$, $\ell_c<1/w\ll\ell_0$, and the flow of v is negligible between $\ell=0$ and ℓ_c. When the bare interaction is attractive and stronger than w, the superconducting transition temperature and the pairing wavefunction are sensitive to the bare four-fermion coupling. In this case, gapless spin fluctuations have little effect on superconductivity, and the manner in which superconductivity emerges is not universal.

2.7.2 Repulsive bare interaction

Theories in which the bare coupling is not strongly attractive in any channel are more interesting in that the emergence of superconductivity is governed by the universal physics associated with the nearby non-Fermi liquid fixed point. This is because those theories necessarily flow through the bottleneck region where the RG flow is constricted. To see this, we view λ^V_{2PP} in Eq. (2.169) as a matrix and decompose it as $\lambda^V_{2PP}=\sum_i\lambda_i|i\rangle\langle i|$. Here, the channel indices $((\pm),(\begin{smallmatrix}s\\d\end{smallmatrix}))$ are dropped to avoid clutter in notation. $|i\rangle$'s ($\langle i|$'s) represent normalized column (row) eigenvectors that diagonalize the four fermion coupling function, and λ_i's represent the eigenvalues. Eigenvalues and eigenvectors obey the flow equations given by

$$\begin{aligned}\frac{\partial}{\partial\ell}\lambda_i=&-\lambda_i-2\langle i|\eta|i\rangle_\mu\lambda_i-\frac{1}{4\pi}\langle i|(\lambda')^2|i\rangle_\mu,\\ \frac{\partial|i\rangle}{\partial\ell}=&-\sum_{j\neq i}\frac{(\lambda_i+\lambda_j)\left(\langle j|\eta|i\rangle_\mu-\frac{\alpha^{(n)}}{4\pi}\langle j|\mathsf{D}^V|i\rangle_\mu\right)+\frac{(\alpha^{(n)})^2}{4\pi}\langle j|\left(\mathsf{D}^V\right)^2|i\rangle_\mu}{\lambda_i-\lambda_j}|j\rangle.\end{aligned} \tag{2.206}$$

Here, $\langle i|C|j\rangle_\mu\equiv\int\frac{\mathrm{d}k\mathrm{d}p}{(2\pi\mu)^2}f^*_{i,k}C_{kp}f_{j,p}$ with $f_{i,k}$ representing the i-th eigenvector written in the momentum space. η is a diagonal matrix with $\eta_{p,k}=2\pi\mu\delta(p-k)\eta_p$. $\lambda'^{(\pm),\binom{s}{d}}_{\binom{p\ -p}{q\ -q}}$ is defined in Eq. (2.176) and $D^V_{p,k}\equiv\frac{\mathsf{D}_\mu(p;k)}{\sqrt{V_{F,p}V_{F,k}}}$. Since η and $(\lambda')^2$ are non-negative matrices, $\frac{d\lambda_i}{d\ell}\leq0$ for $\lambda_i\geq0$. This means that theories with repulsive couplings flow toward $\lambda_i=0$ at low energies. In the small v limit, theories with bare repulsive couplings flow to the fixed point at $\lambda_i=0$. For $v\neq0$, $\lambda_i=0$ is no longer a fixed point. Since $\frac{\partial\lambda_i}{\partial\ell}<0$ for $\lambda_i\geq0$, all theories with $v\neq0$ develop at least one channel with attractive interactions at sufficiently low energies[38]. Although $\lambda=0$ is not a fixed point, it still acts as an approximate focal point in the space of theories because at $\lambda=0$ the beta functional is proportional to D^2_μ whose eigenvalues are order of w^2. In the small v limit, the slow RG speed near $\lambda=0$ creates a bottleneck region in which a theory spends a long RG 'time'. Consequently, bare theories with $O(1)$ repulsive interactions are naturally attracted to the region with $|\lambda_i|\leq w$ at scale $\ell^*\sim w^{-1}$ before they become negative. For $v\neq0$, there is no perfect focusing of the RG flow. Nonetheless, theories spend longer RG time in the bottleneck region as v decreases. This makes the theory within the bottleneck an

[38] This is expected from the absence of Hermitian quasi-fixed points with $v\neq0$.

approximate attractor of UV theories[234, 216]. Once theories are attracted to the bottleneck region, the superconducting transition temperature is determined by the RG time that is needed for theories to pass through it. In this section, we examine how superconductivity emerges in a theory that is within the bottleneck region with $\lambda \approx 0$ at a scale ℓ^*.

To remove the explicit scale dependence in the measure of the momentum integration of the beta functional, we consider

$$\bar{\lambda}^{V;(\pm),\binom{s}{d}}_{2PP\binom{p\ -p}{k\ -k}} = e^{\ell}\lambda^{V;(\pm),\binom{s}{d}}_{2PP\binom{p\ -p}{k\ -k}}. \tag{2.207}$$

Its beta functional reads

$$\begin{aligned}\frac{\partial}{\partial\ell}\bar{\lambda}^{V;(\pm),\binom{s}{d}}_{2PP\binom{p\ -p}{k\ -k}} =& -(\eta_k+\eta_p)\,\bar{\lambda}^{V;(\pm),\binom{s}{d}}_{2PP\binom{p\ -p}{k\ -k}} \\ &- \frac{1}{4\pi}\int\frac{\mathrm{d}q}{2\pi\Lambda}\left[\bar{\lambda}^{V;(\pm),\binom{s}{d}}_{2PP\binom{p\ -p}{q\ -q}} - \frac{2}{N_f}Y^{(\pm)}_{PP}1^{\binom{s}{d}}\frac{e^{\ell}\mathsf{D}_{\Lambda e^{-\ell}}(p;q)}{\sqrt{V_{F,p}V_{F,q}}}\right] \\ &\times\left[\bar{\lambda}^{V;(\pm),\binom{s}{d}}_{2PP\binom{q\ -q}{k\ -k}} - \frac{2}{N_f}Y^{(\pm)}_{PP}1^{\binom{s}{d}}\frac{e^{\ell}\mathsf{D}_{\Lambda e^{-\ell}}(q;k)}{\sqrt{V_{F,q}V_{F,k}}}\right].\end{aligned} \tag{2.208}$$

Here, $\mathsf{D}_\mu(q;k)$ is defined in Eq. (2.109). A theory that is at the bottleneck point at scale ℓ^* corresponds to the 'initial' condition

$$\bar{\lambda}^{V;(\pm),\binom{s}{d}}_{2PP\binom{p\ -p}{k\ -k}}(\ell^*) = 0. \tag{2.209}$$

In the following, we focus on the d-wave and spin anti-symmetric sector in which the attractive interaction is strongest[177, 165]. At energy scales that are not too smaller than $\Lambda^* = \Lambda e^{-\ell^*}$, we can ignore $\bar{\lambda}^V_{2PP}$ on the right hand side of Eq. (2.208). As the energy scale is lowered, the spin fluctuations generate attractive interaction which, in turn, accelerates the flow of $\bar{\lambda}^V_{2PP}$[39]. At sufficiently low energies, the magnitude of $\bar{\lambda}^V_{2PP}$ surpasses that of $-\frac{2}{N_f}Y^{(\pm)}_{PP}1^{\binom{s}{d}}\frac{e^{\ell}\mathsf{D}_{\Lambda e^{-\ell}}(p;q)}{\sqrt{V_{F,p}V_{F,q}}}$ in Eq. (2.208). As the four-fermion coupling becomes stronger than the attractive interaction generated by spin fluctuations at low energies, the further growth of the four-fermion coupling is dominated by the BCS process. We denote this crossover scale as ℓ_1. Since the beta function is dominated by different terms below and above the crossover scales, we write the approximate solution of the beta functional as

$$\bar{\lambda}^V_{2PP} = \begin{cases} \bar{\lambda}_I & \text{for } \ell < \ell_1 \\ \bar{\lambda}_{II} & \text{for } \ell > \ell_1 \end{cases}. \tag{2.210}$$

For $\ell < \ell_1$, the RG flow is approximated by

$$\frac{\partial}{\partial\ell}\bar{\lambda}^{(-),(\,d\,)}_{I,\binom{p\ -p}{k\ -k}} \approx -\frac{1}{4\pi}\left(\frac{2Y^{(-)}_{PP}}{N_f}\right)^2\int\frac{\mathrm{d}q}{2\pi\Lambda}\frac{e^{\ell}\mathsf{D}_{\Lambda e^{-\ell}}(p;q)}{\sqrt{V_{F,p}V_{F,q}}}\frac{e^{\ell}\mathsf{D}_{\Lambda e^{-\ell}}(q;k)}{\sqrt{V_{F,q}V_{F,k}}}. \tag{2.211}$$

It describes the process in which the four-fermion coupling is generated from gapless spin fluctuations. The contribution of the anomalous dimension can be also ignored because λ^V_{2PP} is small. The solution of Eq. (2.211) is written as

$$\begin{aligned}\bar{\lambda}^{(-),(\,d\,)}_{I,\binom{p\ -p}{k\ -k}}(\ell) =& -\frac{1}{4\pi}\left(\frac{2Y^{(-)}_{PP}}{N_f}\right)^2\int_{\ell^*}^{\ell}d\ell'\frac{1}{\sqrt{V_{F,p}V_{F,k}}} \\ &\times\int\frac{dq}{2\pi V_{F,q}}\frac{g^2_{p,q}g^2_{q,k}\Lambda}{\left[\mu'+c\,|p-q|_{\mu'}+c\,|v_pp+v_qq|_{\mu'}\right]\left[\mu'+c\,|q-k|_{\mu'}+c\,|v_qq+v_kk|_{\mu'}\right]},\end{aligned} \tag{2.212}$$

[39] This follows from the fact that the largest eigenvalue of D_μ is positive and $Y^{(-)}_{PP}1^{(\,d\,)} = 2\left(1+\frac{1}{N_c}\right) > 0$.

where $\mu' = \Lambda e^{-\ell'}$, and all coupling functions on the right hand side of the equation are evaluated at scale ℓ'. Let us denote the most negative eigenvalue and the associated eigenvector of $\bar{\lambda}_I(\ell)$ as $E_0(\ell)$ and $F_k(\ell)$, respectively. The crossover scale ℓ_1 is determined from the condition that $E_0(\ell)$ becomes comparable to the spin fluctuation-induced interaction projected onto $F_k(\ell)$,

$$E_0(\ell_1) \sim \frac{2}{N_f} Y_{PP}^{(-)} \left\langle \frac{e^{\ell_1} \mathsf{D}_{\Lambda e^{-\ell_1}}(p;k)}{\sqrt{V_{F,p} V_{F,k}}} \right\rangle_F , \tag{2.213}$$

where $\left\langle \frac{e^{\ell_1} \mathsf{D}_{\Lambda e^{-\ell_1}}(p;k)}{\sqrt{V_{F,p} V_{F,k}}} \right\rangle_F = \int \frac{dpdk}{(2\pi\Lambda)^2} \frac{e^{\ell_1} \mathsf{D}_{\Lambda e^{-\ell_1}}(p;k)}{\sqrt{V_{F,p} V_{F,k}}} F_p^*(\ell_1) F_k(\ell_1)$. To the leading order in v, the four-fermion coupling function generated by the Yukawa coupling in Eq. (2.212) decays as $1/|p-k|$ at large momenta up to a logarithmic correction. The slow decay of the large-angle scatterings give rise to inter-patch couplings that invalidates the patch description.

Since it is difficult to analytically compute the eigenvector of $\bar{\lambda}_{I,\binom{p\ -p}{k\ -k}}^{(-),(d)}(\ell)$, we first estimate the crossover scale using a simple Ansatz. At energy scale Λ^*, electrons within the range of momentum $|k| < \Lambda^*/(vc)$ are strongly coupled with spin fluctuations. Therefore, we consider a Cooper pair wavefunction whose width is order of $\Lambda^*/(vc)$ in the momentum space,

$$f_k = \left(\frac{2\pi vc}{\Lambda^*}\right)^{1/2} \Theta\left(\frac{1}{2} - \frac{vc\,|k|}{\Lambda^*}\right). \tag{2.214}$$

The expectation value of $\frac{e^{\ell} \mathsf{D}_{\mu}}{\sqrt{V_F}\sqrt{V_F}}$ for this Ansatz is written as

$$\left\langle \frac{e^{\ell} \mathsf{D}_{\mu}}{\sqrt{V_F}\sqrt{V_F}} \right\rangle = \int \frac{\mathrm{d}k\mathrm{d}p}{(2\pi\Lambda)^2} \frac{g_{kp}(\ell)^2}{\sqrt{V_{F,k}(\ell) V_{F,p}(\ell)}} \frac{\Lambda}{\Lambda e^{-\ell} + c\,|k-p| + cv\,|k+p|} f_k^*(\ell) f_p(\ell), \tag{2.215}$$

where

$$g_{k,p}(\ell) = g_{k,p}(0) \left(\frac{\mu}{\max\{\mu, 2v\,|k+p|\,, 2vc\,|k|\,, 2vc\,|p|\}}\right)^{\alpha_0(\ell_0)}, \quad V_{F,k}(\ell) = \left(\frac{\mu}{\max\{\mu, 4v|k|\}}\right)^{\alpha_1(\ell_0)/2} \tag{2.216}$$

with $\mu = \Lambda e^{-\ell}$ and α_0, α_1 defined in Eq. (2.140). To simplify the computation of Eq. (2.215), we first use a few assumptions, and later justify them from the solution. First, we assume that the Yukawa coupling function does not change significantly as a function of ℓ for $\ell^* < \ell < \ell_1$:

$$\frac{g_{k,p}(\ell_1)}{g_{k,p}(\ell^*)} \sim 1, \tag{2.217}$$

where ℓ^* is the scale at which the theory is in the bottleneck region and ℓ_1 is the crossover scale. If Eq. (2.217) is satisfied, the scale dependence of $V_{F,k}(\ell)$ can be also ignored in $\ell^* < \ell < \ell_1$ because $\alpha_1 \ll \alpha_0$ in the small v limit. Second, we assume that the coupling functions are almost constant within the support of f_k :

$$V_{F,k}(\ell) \approx 1, \quad g_{k,p}(\ell) \approx g_0(\ell) \tag{2.218}$$

for $|k| < \Lambda^*/(vc)$ and $\ell^* < \ell < \ell_1$. Finally, we assume that the crossover occurs at an energy that is much smaller than Λ^*,

$$\ell_1 \gg \ell^*. \tag{2.219}$$

These assumptions allow us to approximate (2.215) as

$$\left\langle \frac{e^{\ell} \mathsf{D}_{\mu}}{\sqrt{V_F}\sqrt{V_F}} \right\rangle \approx g_0(\ell^*)^2 \int \frac{\mathrm{d}k\mathrm{d}p}{(2\pi\Lambda)^2} \frac{\Lambda}{c\,|k-p| + cv\,|k+p|} f_k^*(\ell) f_p(\ell) \tag{2.220}$$

for $\ell^* < \ell < \ell_1$. The direct integrations over the momenta gives

$$\left\langle \frac{e^{\ell}\mathsf{D}_{\mu}}{\sqrt{V_F}\sqrt{V_F}} \right\rangle \approx \frac{g_0(\ell^*)^2}{\pi c} \log\left(\frac{1}{v}\right) = \frac{w_0(\ell^*)}{2} \log\left(\frac{1}{v}\right). \tag{2.221}$$

Eq. (2.221) is largely independent of ℓ[40]. On the other hand, $E_0(\ell)$ grows linearly in ℓ as

$$E_0(\ell) \sim -\frac{1}{4\pi N_f^2} \left(Y_{PP}^{(-)}\right)^2 (\ell - \ell^*) \left\langle \frac{e^{\ell}\mathsf{D}_{\mu}}{\sqrt{V_F}\sqrt{V_F}} \right\rangle_f^2 \sim -\frac{1}{4\pi N_f^2} \left(Y_{PP}^{(-)}\right)^2 (\ell - \ell^*) w^2 \log^2\left(\frac{1}{v}\right). \tag{2.222}$$

Inserting Eqs. (2.221)-(2.222) to Eq. (2.213), we obtain the crossover scale to be

$$\ell_1 \sim \ell^* + \frac{2\pi N_f}{\left(1 + \frac{1}{N_c}\right)} \frac{1}{w \log(1/v)}, \tag{2.223}$$

and the strength of the four-fermion coupling at the crossover scale is

$$E_0(\ell_1) \sim -\frac{2}{N_f} \left(1 + \frac{1}{N_c}\right) w \log\left(\frac{1}{v}\right). \tag{2.224}$$

The consistency of the assumptions used in Eqs. (2.217) -(2.219) can be checked[41].

We confirm this estimation of the crossover scale by numerically diagonalizing Eq. (2.212). Fig. 2.22a shows the numerical results for the most negative eigenvalue of $\bar{\lambda}^{(-),(d)}_{I,\left(\begin{smallmatrix} p & -p \\ k & -k \end{smallmatrix}\right)}(\ell)$ and the expectation value of $\frac{e^{\ell_1}\mathsf{D}_{\Lambda e^{-\ell_1}}(p;k)}{\sqrt{V_{F,p}V_{F,k}}}$ evaluated for the corresponding eigenvector. While the magnitude of the former increases more or less linearly in $\ell - \ell^*$, the expectation value of the latter is largely constant, as expected. This results in the crossover at a scale ℓ_1. At the crossover scale, the eigenvector shown in Fig. 2.22b is peaked at the hot spot but its support is extended to $\Lambda^*/(vc)$. As is expected, the crossover scale increases with decreasing v (or increasing ℓ_0) as is shown in Fig. 2.22c.

For $\ell > \ell_1$, the magnitude of $\bar{\lambda}^V$ exceeds the contribution of $\frac{2}{N_f} Y_{PP}^{(\pm)} 1^{\left(\begin{smallmatrix} s \\ d \end{smallmatrix}\right)} \frac{e^{\ell}\mathsf{D}_{\Lambda e^{-\ell}}(q;k)}{\sqrt{V_{F,q}V_{F,k}}}$ in Eq. (2.208) at least in the channel with the most negative eigenvalue. The growth of the eigenvalue in that channel is then mostly driven by $\bar{\lambda}^V$ itself. This marks the start of the second stage. In the small v limit, $E_0(\ell_1) \gg \int \frac{dk}{2\pi\Lambda} \eta_k |f_k(\ell_1)|^2$, and we can further ignore the contribution of the anomalous dimension in Eq. (2.208) to write the beta functional as

$$\frac{\partial}{\partial \ell} \bar{\lambda}^{(-),(d)}_{II,\left(\begin{smallmatrix} p & -p \\ k & -k \end{smallmatrix}\right)}(\ell) \approx -\frac{1}{4\pi} \int \frac{\mathrm{d}q}{2\pi\Lambda} \bar{\lambda}^{(-),(d)}_{II,\left(\begin{smallmatrix} p & -p \\ q & -q \end{smallmatrix}\right)} \bar{\lambda}^{(-),(d)}_{II,\left(\begin{smallmatrix} q & -q \\ k & -k \end{smallmatrix}\right)} \tag{2.225}$$

with the matching condition, $\bar{\lambda}^{(-),(d)}_{II,\left(\begin{smallmatrix} p & -p \\ k & -k \end{smallmatrix}\right)}(\ell_1) = \bar{\lambda}^{(-),(d)}_{I,\left(\begin{smallmatrix} p & -p \\ k & -k \end{smallmatrix}\right)}(\ell_1)$. The solution to Eq. (2.225) is given by $\bar{\lambda}^{(-),(d)}_{II}(\ell) = \frac{\bar{\lambda}^{(-),(d)}_{I}(\ell_1)}{1 + \frac{1}{4\pi}(\ell - \ell_1)\bar{\lambda}^{(-),(d)}_{I}(\ell_1)}$, and the renormalized four-fermion coupling blows up around the scale, $\ell_c \sim \ell_1 + \frac{4\pi}{|E_0(\ell_1)|} = \ell^* + \frac{4\pi N_f}{\left(1 + \frac{1}{N_c}\right) w \log\left(\frac{1}{v}\right)}$. The superconducting transition temperature is given by

$$T_c \sim \Lambda^* e^{-\frac{4\pi N_f}{\left(1 + \frac{1}{N_c}\right) w \log\left(\frac{1}{v}\right)}}. \tag{2.226}$$

[40] While $\frac{e^{\ell}\mathsf{D}_{\Lambda e^{-\ell}}(p;k)}{\sqrt{V_{F,p}V_{F,k}}}$ at the hot spot ($p = k = 0$) increases without a bound with increasing ℓ, its eigenvalues remain bounded at all ℓ. In particular, $\int_{-k_F}^{k_F} \frac{\mathrm{d}p}{2\pi\Lambda} \int_{-k_F}^{k_F} \frac{\mathrm{d}k}{2\pi\Lambda} f_p^* \frac{\Lambda}{c|k-p| + cv_0|k+p|} f_k$ is finite for all square integrable functions f_k.

[41] Eq. (2.219) directly follows from Eq. (2.223). With α_0 and c expressed in terms of v as $\alpha_0(v) = \frac{\sqrt{v \log(1/v)}}{\sqrt{2}\pi\sqrt{N_c N_f}}$, $c(v) = \sqrt{\frac{v}{8N_c N_f} \log\left(\frac{1}{v}\right)}$, Eq. (2.217) becomes $\frac{g_{k,p}(\ell_1)}{g_{k,p}(\ell^*)} \sim e^{-\alpha_0(\ell_0)(\ell_1 - \ell^*)} \sim e^{-\frac{1}{2(N_c+1)}} \sim 1$. For $N_c = 2, N_f = 1$, $g(\ell_1)/g(\ell^*) \approx 0.846482$. Eq. (2.218) for the diagonal Yukawa coupling can be checked from $\frac{g_{\frac{\Lambda^*}{vc}}(\ell_1)}{g_0(\ell_1)} \sim \left(\frac{\Lambda e^{-\ell_1}}{\Lambda^*}\right)^{\alpha_0} = e^{-\alpha_0(\ell_1 - \ell^*)} \sim 1$. Similarly, Eq. (2.218) for the off-diagonal Yukawa coupling and $V_{F,k}$ follow.

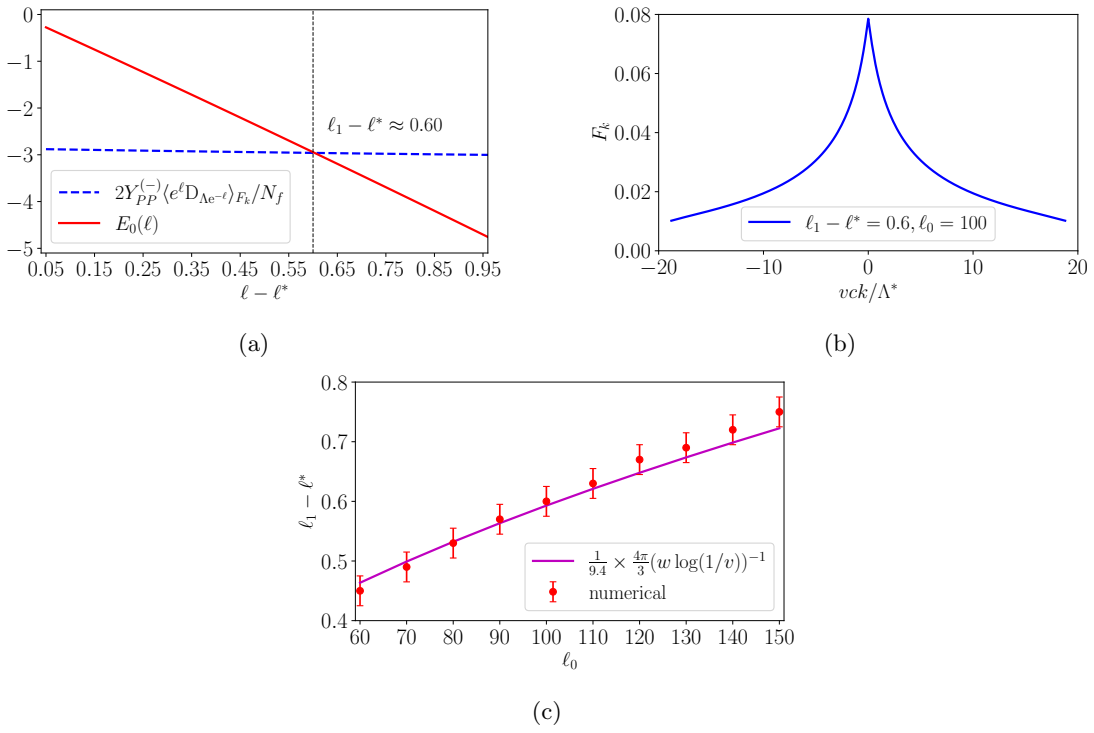

Figure 2.22: Numerical results for the crossover scale and the Cooper pair wavefunction. (a) The solid and dashed lines denote the most negative eigenvalue of Eq. (2.212) ($E_0(\ell)$) and the expectation value of $\mathsf{D}_\mu(k,p)$ in Eq. (2.215) for the associated eigenvector, respectively, plotted as functions of $\ell - \ell^*$ for $\ell_0 = 100$, $N_c = 2$ and $N_f = 1$. The eigenvalue and the expectation value cross at scale $\ell \approx \ell^* + 0.6$. (b) The normalized eigenvector associated with the most negative eigenvalue of Eq. (2.212) at the crossover scale. (c) The ℓ_0 dependence of the crossover scale. The solid line represents the analytic estimation for the crossover scale obtained in Eq. (2.223) with a multiplicative factor determined from a fit of the numerical crossover scales denoted as dots. The uncertainty in the numerical data is due to the grid size of $\ell - \ell^*$, which is taken to be 0.05.

In the second stage of the RG flow, the eigenvector with the most negative eigenvalue is more or less frozen, and the eigenvectors of $\bar{\lambda}^{(-),(d)}_{I,\binom{p\ -p}{k\ -k}}(\ell_1)$ (Fig. 2.22b) determines the channel that becomes superconducting. It is noted that the pairing wavefunction is extended far beyond the hot spot region defined at scale ℓ_c. This shows the importance of large-angle scatterings beyond the hot spot region. Therefore, the hot spot theory can not capture the superconducting instability properly. Since $\ell_c - \ell^* \sim 1/(w \log(1/v)) \ll 1/v$ in the small v limit, the nesting angle does not change much between the scale where the theory is in the bottleneck and the scale at which the superconductivity sets in. This justifies our analysis in which the flow of the nesting angle is ignored.

For the superconductivity, the physics of non-Fermi liquid and the Fermi liquid play important roles in different length scales. When the theory is within the bottleneck region say at energy scale Λ^*, the gapless spin fluctuations generate an attractive interaction for electrons within the range of momentum $|k| < \frac{\Lambda^*}{vc}$ from the hot spots. The spin fluctuations also make those same electrons incoherent, causing a 'pair-breaking' effect. At lower energy scale, the momentum region where the spin fluctuations generate attractive interaction becomes increasingly localized near the hot spots as more and more electrons are decoupled from spin fluctuations. At the same time, the pair breaking effect caused by the spin fluctuations subsides except for the small region near the hot spots. At low energies, what remains away from the hot spots is the heavy but largely coherent electrons that are

subject to the attractive four-fermion interaction that has been accumulated at high energies. The spin fluctuations continue to add more attractive interaction near the hot spots. But, once the accumulated four-fermion coupling becomes comparable to the interaction mediated by the spin fluctuations, the further growth of the four-fermion coupling is mainly driven by those more abundant cold electrons through the BCS scatterings[42]. The RG time that is needed to reach the crossover scale $(\ell_1 - \ell^*)$ is comparable to the RG time that is further needed for the BCS process to finally drive the instability from the crossover $(\ell_c - \ell_1)$. Interestingly, the residual attractive interaction that is left for the coherent electrons at low energies is only dependent on the bare nesting angle and so is the superconducting transition temperature.

2.8 Summary

In this chapter, a field-theoretic functional renormalization group formalism is developed for full low-energy effective field theories of non-Fermi liquids that include all gapless modes around the Fermi surface. The formalism, which is beyond the traditional patch description, captures the universal low-energy physics of the entire Fermi surface in the minimal way through renormalizable field theories. Due to the Fermi momentum that does not generally decouple from the low-energy physics, the usual notions of renormalizable field theories and scale invariance need to be generalized. We use this functional renormalization group formalism to understand the non-Fermi liquid state realized at the 2+1 dimensional antiferromagnetic quantum critical point and the pathway from the non-Fermi liquid to superconductivity.

The low-energy effective field theory of the antiferromagnetic quantum critical metal is characterized by couplings that are functions of momentum along the Fermi surface. The full functional renormalization group flow, which is controlled in the limit that the bare nesting angle is small allows us to identify the non-Fermi liquid fixed point in the space of coupling functions and extract universal low-energy physics controlled by the fixed point. At low energies, the renormalized coupling functions acquire universal profiles as functions of momentum along the Fermi surface. Those coupling functions, in turn, fix physical observables that depend on momentum along the Fermi surface such as the shape of the renormalized Fermi surface, the Fermi velocity, the quasiparticle weight, the single-electron decay rate and the superconducting instability. When the bare four-fermion coupling is weak, the superconducting instability is controlled by the universal attractive interaction generated by the gapless spin fluctuations. Below the superconducting transition temperature, which is exponentially suppressed in the limit that the nesting angle is small, the non-Fermi liquid state becomes unstable against the spin-singlet d-wave pairing instability. The pairing wavefunction includes significant weight of electrons away from the hot spot region defined at the scale of the superconducting transition temperature. Therefore, the hot spot theory cannot capture the superconducting instability that involves large-angle scatterings.

[42] This is in contrast to the cases in which the Fermi surface is coupled with a critical bosonic mode centered at zero momentum. In those cases, the entire Fermi surface remains strongly renormalized down to the zero energy, and the pairing must arise out of hot fermions.

Chapter 3

Emergence of Curved Momentum-Spacetime and its Effect on Cyclotron Motion in the Antiferromagnetic Quantum Critical metal

3.1 Introduction

The semi-classical equations of motion of electrons in a metal present a position-momentum duality similar to that of the electric-magnetic duality of Maxwell's equations [86]. In this analogy, the momentum-dependent quasiparticle energy and the Berry curvature associated with the Bloch wavefunctions play the roles of the position-dependent potential in real space and magnetic field in momentum space, respectively [229]. Can this symmetry be further expended to spacetime geometry [44, 98, 106, 20, 49]? Examples of both real space curvature and momentum space curvature in lattices have been explored in the past [12, 221, 157, 134, 214, 43, 223, 178, 145, 198, 82]. However, in both types of examples, the origin of the momentum space curvature can be traced to the underlying lattice [135]. In this work, we point out that curved momentum-spacetimes can also arise from anisotropic quantum corrections and even a momentum-space black hole horizon can emerge if quantum corrections are strongly singular in momentum space.

In Chapter 2, we saw that strongly momentum-dependent quantum corrections arise in metals close to quantum critical points associated with order parameters carrying non-zero momenta. At spin or charge density-wave critical points, electrons residing on hot manifolds, sub-manifolds of Fermi surface that can be connected by the ordering wave vectors, are more strongly scattered by critical fluctuations than electrons away from the hot manifolds. This leads to a momentum-dependent renormalization of electron. In particular, the Fermi velocity can acquire a strong dependence on momentum along the Fermi surface as electrons become significantly heavier near the hot manifold. Interestingly, a strongly momentum-dependent Fermi velocity arises as a consequence of momentum-dependent red shift even without a direct renormalization of the band dispersion energy. Namely, the Fermi velocity can acquire momentum-dependence through a momentum-dependent dilatation of frequency. This momentum-dependent red shift is indeed the primary mechanism by which the Fermi velocity acquires a strong momentum dependence in the antiferromagnetic quantum critical metal in two space dimensions (Sec. 2.6.1).

Here is the outline of the chapter. In Sec. 3.2, we cast the theory of the fully renormalized

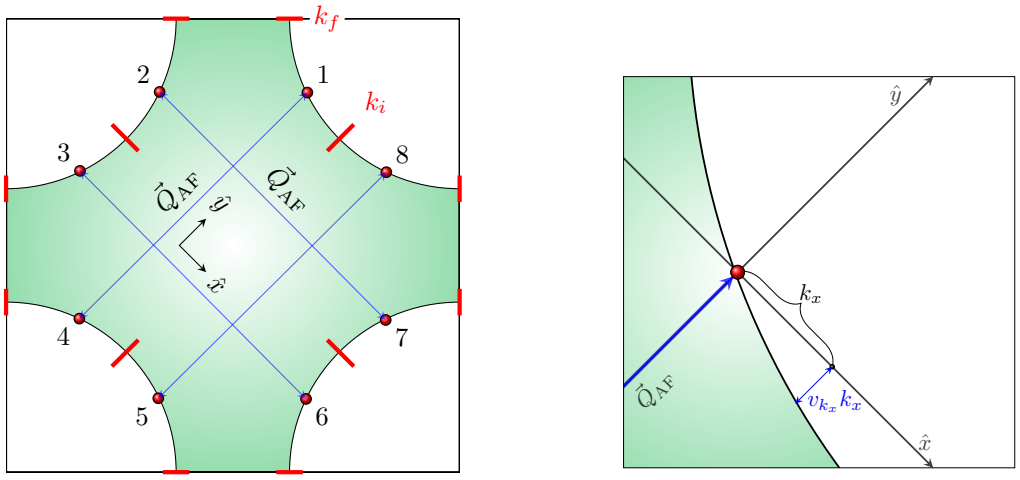

(a) (b)

Figure 3.1: For simplicity, we have omitted the superscript B in all the quantities in this figure. (a) The full Fermi surface divided into eight segments (separated by the red bars.) Segment 1 is bounded by k_i and k_f, and other segments are related to it through the C_4 and reflection symmetries. Each segment contains one hot spot denoted as red dots on the Fermi surface. The hot spots are connected by the antiferromagnetic ordering wave vector, $\vec{Q}_{AF}$. $\hat{x}$ ($\hat{y}$) is chosen to be perpendicular (parallel) to $\vec{Q}_{AF}$ at hot spot 1. (b) The Fermi surface in segment 1 is at $v_{k_x}k_x + k_y = 0$. Here, $v_{k_x}k_x$ represents the displacement of the Fermi surface from what the perfectly nested Fermi surface would have been.

quasiparticles away from the hot spots into a theory of spinors propagating in a curved momentum-spacetime. In Sec. 3.3, we compute the cyclotron period of electron and the attribute its non-trivial dependence on the bare nesting angle of the Fermi surface to a curved momentum-spacetime geometry generated by the critical spin fluctuations. We conclude with a summary in Sec. 3.4.

3.2 Emergence of a curved momentum-spacetime

Before we start, let us list up the necessary ingredients to carry out the calculations of this chapter. First, focusing on the renormalized shape of the Fermi surface and the Fermi velocity that control the dynamics of low-energy quasiparticles, we consider the renormalized low-energy effective field theory from Eq. (2.36) that includes all gapless modes on the Fermi surface,

$$\begin{aligned} S = &\sum_{N=1}^{8}\sum_{\sigma=1}^{N_c}\sum_{j=1}^{N_f}\int \mathrm{d}\mathbf{k}^{\mathsf{B}}\ \psi^{\mathsf{B}\dagger}_{N,\sigma,j}(\mathbf{k}^{\mathsf{B}})\left\{ik_0^{\mathsf{B}} + V^{\mathsf{B};(N)}_{F,k_N^{\mathsf{B}}} e_N[\vec{k}^{\mathsf{B}}; v^{\mathsf{B};(N)}_{k_N^{\mathsf{B}}}]\right\}\psi^{\mathsf{B}}_{N,\sigma,j}(\mathbf{k}^{\mathsf{B}}) \\ &+ \frac{1}{\sqrt{N_f}}\sum_{N=1}^{8}\sum_{\sigma\sigma'=1}^{N_c}\sum_{j=1}^{N_f}\int \mathrm{d}\mathbf{k}^{\mathsf{B}}\mathrm{d}\mathbf{q}^{\mathsf{B}}\ g^{\mathsf{B};(N)}_{k_N^{\mathsf{B}}+q_N^{\mathsf{B}},k_N^{\mathsf{B}}}\psi^{\mathsf{B}\dagger}_{N,\sigma',j}(\mathbf{k}^{\mathsf{B}}+\mathbf{q}^{\mathsf{B}})\Phi^{\mathsf{B}}_{\sigma'\sigma}(\mathbf{q}^{\mathsf{B}})\psi^{\mathsf{B}}_{N,\sigma,j}(\mathbf{k}^{\mathsf{B}}) \\ &+ \frac{1}{4}\sum_{\{N_i=1\}}^{8}\sum_{\{\sigma_i=1\}}^{N_c}\sum_{\{j_i=1\}}^{N_f}\int\prod_{i=1}^{4}\mathrm{d}\mathbf{k}_i^{\mathsf{B}}\ \delta^{\mathsf{B}}_{1+2,3+4}\lambda^{\mathsf{B};\left(\begin{smallmatrix}N_1 & N_2\\ N_4 & N_3\end{smallmatrix}\right);\left(\begin{smallmatrix}\sigma_1 & \sigma_2\\ \sigma_4 & \sigma_3\end{smallmatrix}\right)}_{\left(\begin{smallmatrix}k^{\mathsf{B}}_{1;N_1} & k^{\mathsf{B}}_{2;N_2}\\ k^{\mathsf{B}}_{4;N_4} & k^{\mathsf{B}}_{3;N_3}\end{smallmatrix}\right)} \\ &\times \psi^{\mathsf{B}\dagger}_{N_1,\sigma_1,j_1}(\mathbf{k}_1^{\mathsf{B}})\psi^{\mathsf{B}\dagger}_{N_2,\sigma_2,j_2}(\mathbf{k}_2^{\mathsf{B}})\psi^{\mathsf{B}}_{N_3,\sigma_3,j_2}(\mathbf{k}_3^{\mathsf{B}})\psi^{\mathsf{B}}_{N_4,\sigma_4,j_1}(\mathbf{k}_4^{\mathsf{B}}). \end{aligned} \tag{3.1}$$

Here, we consider a Fermi surface with the C_4 and reflection symmetries that supports eight hot spots labelled by $N = 1, 2, \ldots, 8$ as is shown in Fig. 3.1a. The Fermi surface is divided into eight disjoint

segments whose union covers the entire Fermi surface. All quantities with superscript B are bare ones in terms of which the microscopic theory is written (see Eq. (2.37)). The full Fermi velocity vector in term of $V^{\mathsf{B};(N)}_{F,k^{\mathsf{B}}_N}$ and $v^{\mathsf{B};(N)}_{k^{\mathsf{B}}_N}$ is given by

$$\vec{v}^{\mathsf{B}}_F(k^{\mathsf{B}}_x) = V^{\mathsf{B};(1)}_{F,k^{\mathsf{B}}_x}\left(\frac{\partial v^{\mathsf{B};(1)}_{k^{\mathsf{B}}_x}}{\partial k^{\mathsf{B}}_x}k^{\mathsf{B}}_x + v^{\mathsf{B};(1)}_{k^{\mathsf{B}}_x}\right)\hat{x} + V^{\mathsf{B};(1)}_{F,k^{\mathsf{B}}_x}\hat{y}, \tag{3.2}$$

where $N = 1$ (See Fig. 3.1b).

Our second ingredient is the crossover scale is given by (see Eq. (2.126)) $E^{(2L)}_k \equiv \Lambda e^{-\ell^{(2L)}_k}$ where

$$\ell^{(2L)}_k = \log\left(\frac{\Lambda}{4V_{F,k}v_k\,|k|}\right) \tag{3.3}$$

denotes the logarithmic length scale associated with the crossover. Let us recall that this crossover occurs because electrons away from hot spots can not interact with with critical spin fluctuations with zero energy while staying on the Fermi surface due to a lack of the perfect nesting for $v_k \neq 0$. Here, we emphasize that v_k is small but non-zero in the non-perturbative solution. This momentum-dependent crossover creates two *momentum scales*, $k_c(\ell)$ and $k_h(\ell)$ determined from $\ell^{(2L)}_{k_c} = 0$ and $\ell^{(2L)}_{k_h} = \ell$, respectively. They divide the momentum space into three regions at a finite length scale ℓ. To the leading order in v_k, these momentum scales can be approximated as $k_c \approx \frac{\Lambda}{4v_0(0)}$ and $k_h \approx \frac{\Lambda e^{-\ell}}{4v_0(0)}$. In the 'cold' region with $k > k_c$, electrons are too far away from the hot spot to receive significant quantum correction at energies below Λ. In the 'lukewarm' region with $k_h(\ell) < k < k_c$, electrons receive non-trivial quantum corrections between Λ and $E^{(2L)}_k$. But, the electrons in the lukewarm region are largely decoupled from spin fluctuations at energy scale ℓ. In the 'hot' region with $k < k_h(\ell)$, electrons remain strongly coupled with critical spin fluctuations at scale ℓ. This gives rise to the following momentum profiles for the renormalized nesting angle v_k and Fermi velocity $V_{F,k}$ at scale ℓ (Eqs. (2.128) and (2.130)),

$$v_k = \begin{cases} \frac{\ell_0\log(\ell_0)}{(\ell+\ell_0)\log(\ell+\ell_0)}v_0(0) & 0 \le k < k_h \\ \frac{\ell_0\log(\ell_0)}{(\ell^{(2L)}_k+\ell_0)\log(\ell^{(2L)}_k+\ell_0)}v_0(0) & k_h \le k < k_c \\ v_0(0) & k_c \le k \end{cases}, \tag{3.4}$$

$$V_{F,k} = \begin{cases} 1 & 0 \le k < k_h \\ \exp\left(\sqrt{N_c^2-1}\left(\mathrm{Ei}(\log\sqrt{\ell+\ell_0}) - \mathrm{Ei}(\log\sqrt{\ell^{(2L)}_k+\ell_0})\right)\right) & k_h \le k < k_c \\ \exp\left(\sqrt{N_c^2-1}\left(\mathrm{Ei}(\log\sqrt{\ell+\ell_0}) - \mathrm{Ei}(\log\sqrt{\ell_0})\right)\right) & k_c \le k \end{cases}. \tag{3.5}$$

Here, $\mathrm{Ei}(x)$ is the exponential integral function and

$$\ell_0 = \frac{\pi^2 N_c N_f}{2(N_c^2-1)}\frac{1}{v_0(0)\log(1/v_0(0))} \tag{3.6}$$

represents the logarithmic length scale below which the flow of the nesting angle is negligible. The nesting angle is unchanged for $k \ge k_c$ because the Fermi surface is not renormalized far away from the hot spots.

As ℓ increases, the size of hot region shrinks as more electrons become decoupled from spin fluctuations. In the strict zero temperature limit, the theory develops superconducting instabilities due to the run-away flow of the four-fermion coupling function (Sec. 2.6.3). However, the normal state remains stable down to an energy scale that is exponentially small in $1/\sqrt{v_0(0)}$ in the limit that $v_0(0)$ is small and the bare four-fermion coupling is weak. Here, we study the dynamics of electrons at energies low enough that electrons are decoupled from the critical spin fluctuations almost everywhere on the Fermi

surface except for the immediate vicinity of the hot spots but high enough that the superconducting instability is absent. As a first step, we consider the dynamics of quasiparticles at zero temperature, ignoring the superconducting instability. Later, we consider the thermal effect that arises above the superconducting transition temperature.

At zero energy ($\ell = \infty$) the Fermi velocity away from the hot spots becomes infinite. This represents the fact that electrons at the hot spots becomes infinitely slower than the rest of electrons. While the choice of the renormalized frequency is convenient for describing the scaling behaviour of electrons at the hot spots and the critical spin fluctuations[182], it is not useful for describing the dynamics of electrons away from the hot spots. What really happens is that electrons in the the hot region are slowed down by spin fluctuations while electrons in the cold region are not. For electrons away from hot spots, it is more convenient to use the bare clock with respect to which the velocity of the cold electrons is fixed to be 1. We can go back to the bare unit of frequency by undoing the rescaling the frequency as

$$k_0 = \left(\frac{V_{F,k_c}^{(N)}}{V_{F,0}^{(N)}}\right)\omega, \qquad \psi_{N,\sigma,j}(\mathbf{k}) = \left(\frac{V_{F,k_c}^{(N)}}{V_{F,0}^{(N)}}\right)^{-1} \tilde{\psi}_{N,\sigma,j}(\omega, \vec{k}), \tag{3.7}$$

where we use $\omega \equiv k_0^{\mathsf{B}}$ for simplicity of notation, and the normalization of the field is chosen to keep the canonical form of the quantum effective action,

$$\Gamma_{\text{kin}} = \sum_{N=1}^{8}\sum_{\sigma=1}^{N_c}\sum_{j=1}^{N_f}\int \frac{\mathrm{d}\omega \mathrm{d}^2\vec{k}}{(2\pi)^3}\tilde{\psi}_{N,\sigma,j}^{\dagger}(\omega,\vec{k})\left\{i\omega + \mathcal{V}_{F,k_N}^{(N)} e_N\left[\vec{k}; v_{k_N}^{(N)}\right]\right\}\tilde{\psi}_{N,\sigma,j}(\omega,\vec{k}). \tag{3.8}$$

For the rest of the chapter, we will use the bare frequency. Here, $\mathcal{V}_{F,k_N}^{(N)} = \left(\frac{V_{F,0}^{(N)}}{V_{F,k_c}^{(N)}}\right) V_{F,k_N}^{(N)}$ denotes the Fermi velocity measured in the bare time.

In the low-energy limit, k_h approaches zero and the hot region shrinks to points. This implies that quasiparticles are well defined everywhere on the Fermi surface except at the hot spots. The dynamics of the fully renormalized quasiparticles is described by the quadratic action[1] in Eq. (3.8) with nesting angle v_k and Fermi velocity (along $\vec{Q}_{AF}$) $\mathcal{V}_{F,k}$ given by

$$\begin{aligned} v_k &= \begin{cases} \frac{\pi^2 N_c N_f}{2(N_c^2-1)} \frac{1}{(\ell_k^{(2L)}+\ell_0)\log(\ell_k^{(2L)}+\ell_0)} & 0 \le k < k^* \\ v_0(0) & k^* \le k \end{cases}, \\ &\text{and} \\ \mathcal{V}_{F,k} &= \begin{cases} e^{\sqrt{N_c^2-1}\left(-\mathrm{Ei}(\log\sqrt{\ell_k^{(2L)}+\ell_0})+\mathrm{Ei}(\log\sqrt{\ell_0})\right)} & 0 \le k < k^* \\ \left(\frac{k}{k_c}\right)^{\alpha_1} & k^* < k < k_c \\ 1 & k_c \le k \end{cases}, \end{aligned} \tag{3.9}$$

respectively, where $k^* = \frac{\Lambda e^{-\ell_0}}{4v_0(0)}$ is the momentum scale below which the flow of the nesting angle is appreciable and is determined from $\ell_0 = \ell_{k^*}^{(2L)}$ (see Fig. 2.16). It is noted that the renormalized nesting angle in Eq. (3.4) can be well approximated to be $v_0(0)$ for $k > k^*$ in the limit that $v_0(0)$ is small (equivalently $\ell_0 \gg 1$).

$$\alpha_1 = \frac{\sqrt{N_c - 1}}{\sqrt{\ell_0}\log\ell_0} \tag{3.10}$$

is the critical exponent of the Fermi velocity. As expected in Eq. (3.9), $\mathcal{V}_{F,k} = 1$ for $k > k_c$ and vanishes at the hot spots. There are two noteworthy features in Eq. (3.9). First, in $k^* < k < k_c$,

[1] Besides the quadratic action, there also exists the four-fermion coupling that has been generated by the critical spin fluctuations. However, their effects on the quasiparticle motion is sub-leading compared to the quantum corrections that have been already incorporated into v_k and $V_{F,k}$ in the limit that the nesting angle is small.

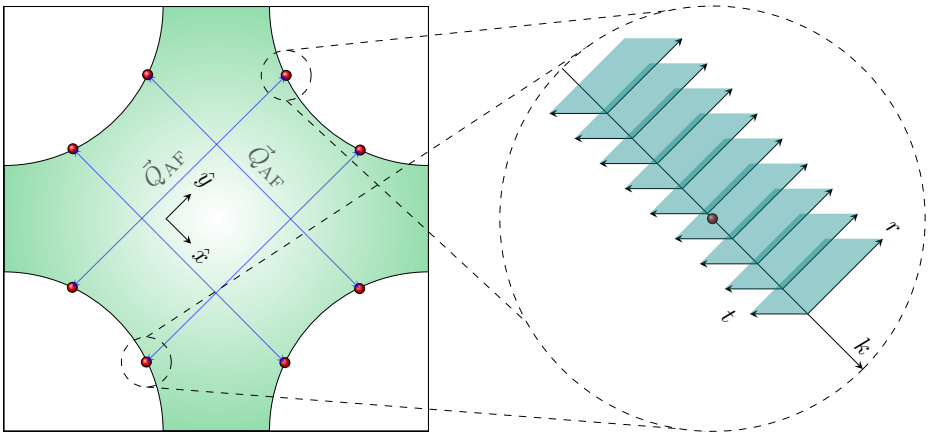

Figure 3.2: The spinor composed of the electrons in segments 1 and 5 is defined in the hybrid spacetime (t, r, k), where t is time, r is space conjugate to k_y and $k = k_x$. At fixed k, electrons at hot spots 1 and 5 have the same dynamics due to the time-reversal symmetry, and can be naturally described by the two-component spinor Ψ in Eq. (3.11).

$\mathcal{V}_{F,k}$ scales with k algebraically while v_k is almost constant. This is because the quantum correction that renormalizes $\mathcal{V}_{F,k}$ is stronger than what renormalizes v_k (Sec. 2.5.1). As a result, v_k is almost momentum-independent except in the vicinity of the hot spot within $k < k^*$, as expressed in Eq. (3.9) for v_k. Second, with virtually k-independent v_k in $k > k^*$, both x and y components of Fermi velocity are renormalized in the same fashion although there is no symmetry that protects the direction of the Fermi velocity. This peculiarity arises because the dominant renormalization of Fermi velocity is from the quantum correction to the frequency-dependent (ik_0) term of the action in Eq. (3.1). In other words, the momentum dependence of $\mathcal{V}_{F,k}$ arises because the strength of the quantum correction that dilates frequency depends on momentum along the Fermi surface. In the scheme that uses one global clock for the entire system, we are forced to transfer the momentum dependence of the quantum correction to the field renormalization and Fermi velocity. While this is a perfectly legitimate picture, what the theory is really suggesting is to view the momentum-dependent Fermi velocity as a consequence of non-uniform temporal metric on the Fermi surface. Here, we adopt this perspective in which electrons have momentum-independent Fermi velocity in $k^* < k < k_c$ once the velocity is measured with a proper time defined with respect to a momentum-dependent metric.

We formulate this geometric description by casting Eq. (3.8) into a theory of quasiparticles propagating in a curved spacetime that incorporates the momentum-dependent metric. For a brief review of the fermionic action defined in curved spacetime, see Appendix E. For our particular case, we view the Fermi surface as a collection of $1+1$-dimensional Dirac fermions stacked along the direction of Fermi surface, and combine a pair of chiral fermions at anti-podal points of the Fermi surface into a two-component Dirac spinor[48]. Let us focus on segments 1 and 5 in this representation. Electrons in these anti-podal hot spots can be naturally paired since they have the same dynamics (See Fig. 3.1.) The two-component spinor is given by the Fourier transform

$$\Psi_{\sigma,j}(t, r, k_x) \equiv \int \frac{\mathrm{d}\omega \mathrm{d}k_y}{(2\pi)^2} e^{i(\omega t + k_y r)} \begin{bmatrix} \psi_{1,\sigma,j}(\omega, k_x, k_y) \\ \psi^*_{5,\sigma,j}(-\omega, -k_x, -k_y) \end{bmatrix}. \tag{3.11}$$

Here, the hot spot index is dropped as we focus on $N = 1$ and 5 (it is straightforward to write down the theory for other segments.) The theory is written in the hybrid spacetime of (t, r, k)[205], where t is time, r is the conjugate variable of k_y, and $k = k_x$ labels points on the Fermi surface in segments

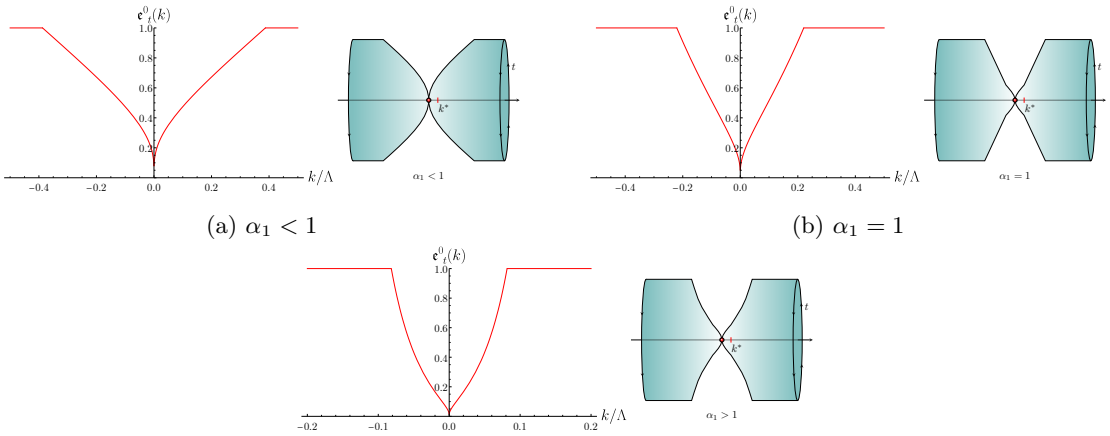

(a) $\alpha_1 < 1$ (b) $\alpha_1 = 1$

(c) $\alpha_1 > 1$

Figure 3.3: The vielbein $\mathfrak{e}^0{}_t(k)$ that depends on momentum along the Fermi surface determines the rate at which the proper time lapses at momentum k per unit proper time of cold electrons far away from the hot spots. The vielbein that vanishes at the hot spots represents the fact that the motion of electrons at the hot spots become infinitely slowed down compared to cold electrons. (Left) The momentum-dependent vielbein $\mathfrak{e}^0{}_t$ for (a) $\alpha_1 \approx 0.663$, (b) $\alpha_1 \approx 1$ and (c) $\alpha_1 \approx 2.169$. The choice in (b) corresponds to the critical nesting angle at which the cyclotron period exhibits a logarithmic dependence on momentum (see Eq. (3.19)). (Right) The $t-k$ slice of the hybrid spacetime for fixed r. For the purpose of illustrating the momentum-dependence of the vielbein, the temporal coordinate has been compactified so that the size of the circumference at each k represents the proper time lapsed at that momentum for every unit proper time of cold electrons. The circumference pinches off at the hot spots due to the infinitely large red shift at those points.

1 and 5 (See Fig. 3.2.) From Eq. (3.11), it is straightforward to write the action in Eq. (3.8) for segments 1 and 5 in the hybrid space of t, r, k_x. The resulting action in terms of the spinors is

$$\Gamma^{(1,5)}_{\text{kin}} = \sum_{\sigma=1}^{N_c}\sum_{j=1}^{N_f}\int\frac{\mathrm{d}k}{2\pi}\int \mathrm{d}t\mathrm{d}r|\mathfrak{e}|\ \bar{\Psi}_{\sigma,j}(t,r,k)\left\{\gamma^0\mathfrak{e}_0{}^t D_t + \gamma^1\mathfrak{e}_1{}^r D_r\right\}\Psi_{\sigma,j}(t,r,k), \tag{3.12}$$

where $\bar{\Psi} = \Psi^\dagger\gamma^0$, where $\gamma^0 = \sigma_y$, $\gamma^1 = \sigma_x$, $\gamma^2 = \sigma_z$ denote 2×2 gamma matrices that furnish the two-dimensional spinor representation. $\mathfrak{e}_a{}^\mu$ is the inverse of the vielbein $\mathfrak{e}^a{}_\mu$ with $a = 0, 1, 2$ and $\mu = t, r, k$. The vielbein determines the metric in the $2+1$-dimensional spacetime through $g_{\mu\nu} = \sum_{a=0}^{2}\mathfrak{e}^a{}_\mu\mathfrak{e}^a{}_\nu$. In general, the vielbein is a function of t, r, k, but in our case it depends only on k : $\mathfrak{e}^0{}_t(k) = \mathcal{V}_{F,k}$, $\mathfrak{e}^1{}_r(k) = \mathfrak{e}^2{}_k(k) = 1$ with all other elements being zero. $|\mathfrak{e}|$ is the determinant of $\mathfrak{e}^a{}_\mu$. $D_\mu = \partial_\mu + \frac{i}{2}\omega_{\mu,ab}\Sigma^{ab} + iA_\mu$ denotes the covariant derivative, where $\omega_{\mu,ab}$ is the spin connection with $\Sigma^{ab} = \frac{i}{4}[\gamma^a, \gamma^b]$ and A_μ is the U(1) gauge field. Eq. (3.12) becomes equivalent to Eq. (3.8) for the trivial spin connection $\omega_{\mu,ab} = 0$ and the gauge field given by $A_t = 0$, $A_r = v_k k$, $A_k = 0$. The gauge field A_r gives a k_x-dependent shift of momentum in the r direction so that quasiparticles have zero energy at $k_y = -v_{k_x}k_x$.

Eq. (3.12) describes quasiparticles moving in a curved hybrid spacetime with a non-trivial torsion. It expresses the fact that the Fermi velocity along the direction of $\vec{Q}_{AF}$ is 1 everywhere on the Fermi surface if the momentum-dependent proper time interval $\mathrm{d}\tau = \mathfrak{e}^0{}_t(k)\mathrm{d}t$ is used in measuring velocity at momentum k. The 'apparent' variation of Fermi velocity along the Fermi surface arises only when one chooses to probe the dynamics of quasiparticles in one fixed clock. For an external lab observer whose clock ticks once for every unit proper time defined in $k > k_c$, quasiparticles appear to slow down near hot spots due to the momentum-dependent red-shift in the same way that a free falling object

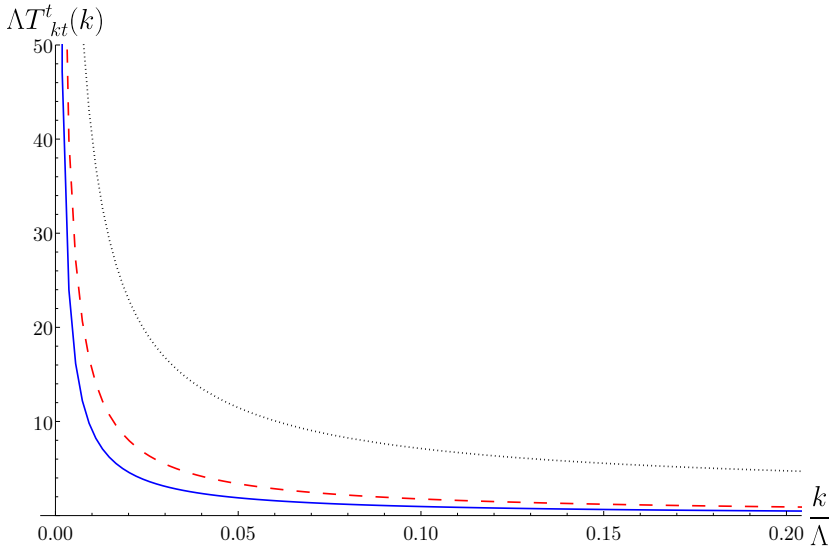

Figure 3.4: The non-zero component of torsion shown as a function of momentum along the Fermi surface near the hot spots. The torsion, as a gauge-invariant geometric quantity, represents how much the momentum-spacetime in which quasiparticles propagate has been distorted from the flat one that arises in the absence of momentum-dependent quantum corrections. The plot is obtained from $\frac{1}{\mathfrak{e}^0{}_t}\frac{\mathrm{d}\mathfrak{e}^0{}_t}{\mathrm{d}k}$ by substituting Eq. (3.9) into $\mathfrak{e}^0{}_t$, and with the help of Eqs. (3.3), (3.6), and (3.10). The solid blue, dashed red and dotted black curves correspond to $v_0(0) \approx 0.04$, $v_0(0) \approx 0.13$ and $v_0(0) \approx 1.13$, respectively. This shows that the spacetime is more strongly distorted near the hot spots and for larger bare nesting angles.

appears to undergo a slower time evolution near the surface of a massive object with respect to the far observer due to the gravitational red shift.

The t-k slice of the momentum-spacetime is illustrated in Fig. 3.3 for the case in which the temporal direction is compact. In $k \gg k_c$, the proper length of the temporal direction remains equal to the periodicity of t since $\mathfrak{e}^0{}_t = 1$. In $k^* < k < k_c$, the proper length scales with k algebraically with exponent α_1 ($\mathfrak{e}^0{}_t \sim k^{\alpha_1}$). Hence, the proper time lapses slower as the hot spot is approached. In $k < k^*$, the power-law decay is replaced with a slower decay due to a flow of the nesting angle as is shown in Eq.(3.9).

With the vielbein and spin connection fully fixed by the renormalized coupling functions, Cartan's structure equation determines the torsion of the spacetime to be $T^t = \frac{1}{\mathfrak{e}^0{}_t}\frac{\mathrm{d}\mathfrak{e}^0{}_t}{\mathrm{d}k}\mathrm{d}k \wedge \mathrm{d}t$, $T^r = T^k = 0$. The torsion measures the failure of closure when each of two vector is parallel transported along the other vector. The non-zero component of the torsion indicates a non-trivial structure of the hybrid spacetime. For the present hybrid spacetime, the torsion diverges in the $k \to 0$ limit as is shown in Fig. 3.4. In principle, the torsion can be measured from the rate at which the red shift varies along the Fermi surface. However, it is not clear how the momentum-dependent torsion can be directly measured from an experimental probe that is local in momentum space. Here, we consider a physical observable that probes the global aspect of the distorted momentum-spacetime, which is sensitive to the torsion yet much easier to measure experimentally.

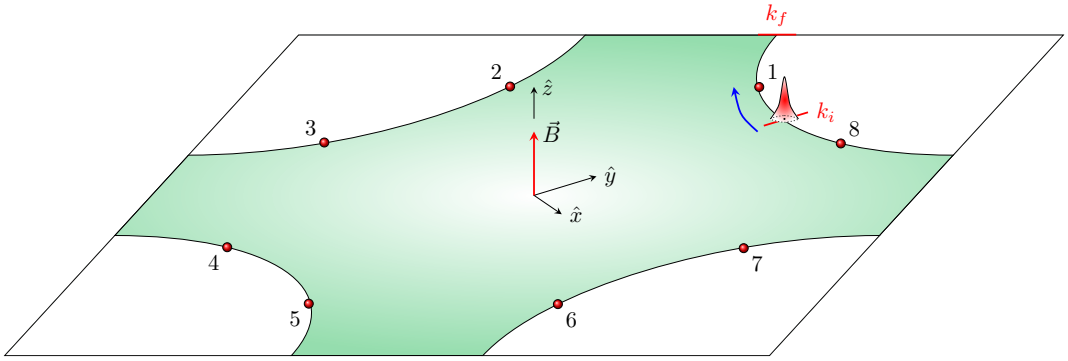

Figure 3.5: Initial setup of the quasiparticle wavepacket. The initial wavepacket of a quasiparticle is placed at the boundary between segments 1 and 8 (k_i). In the presence of magnetic field applied in the z direction, the wavepacket moves along the Fermi surface towards hot spot 1. As it approaches hot spot 1, it slows down due to the momentum-dependent red shift.

3.3 Cyclotron motion of quasiparticles in the curved momentum-spacetime

In this section, we examine how the curved momentum-spacetime affects the dynamics of quasiparticles by computing the cyclotron period of electron in the presence of magnetic field[199, 191]. Due to the C_4 symmetry and the reflection symmetry around the boundary between segments, the cyclotron period at bare nesting angle v_0[2] is eight times the time it takes for a quasiparticle to traverse segment 1 : $T(v_0) = 8\left[T(k_i, 0; v_0) + T(0, k_f; v_0)\right]$, where $T(k_i, 0; v_0)$ denotes the time that it takes for a quasiparticle to traverse from the boundary between segments 1 and 8 to hot spot 1, and $T(0, k_f; v_0)$, from hot spot 1 to the Brillouin zone boundary between segments 1 and 6 (see Fig. 3.1). The setup is depicted in Fig. 3.5. For simplicity, we assume $T(0, k_f; v_0) = T(k_i, 0; v_0)$ and focus on the computation of $T(k_i, 0; v_0)$ here[3].

In the zero temperature limit, well-defined quasiparticles exist away from the hot spots and we can use the semi-classical description of their dynamics. Strictly speaking, electrons right at the hot spots are not described by quasiparticle even at zero temperature. However, the hot spots are a set of measure zero on the Fermi surface and do not affect the cyclotron period. For a quasiparticle localized at momentum $\vec{k}$, its time evolution is entirely determined by the kinetic action at that momentum. According to Eq. (3.12), the quasiparticle has Fermi velocity given by

$$\vec{v}_F(k) = \left(k\frac{\partial v_k}{\partial k} + v_k\right)\hat{x} + \hat{y} \tag{3.13}$$

when the Fermi velocity is measured with respect to the proper time τ defined at that momentum through $\mathrm{d}\tau = \mathfrak{e}^0{}_t \mathrm{d}t$, where t represents the time associated with the bare frequency ω. Since the equation of quasiparticle at momentum k is entirely determined from the Fermi velocity and the proper time defined at that momentum, the equation of motion for the the wavepacket of a quasiparticle is given by the standard equation of motion[19],

$$\frac{\mathrm{d}\vec{r}}{\mathrm{d}\tau} = \vec{v}_F(k), \qquad \frac{\mathrm{d}\vec{k}}{\mathrm{d}\tau} = -e\ \vec{v}_F(k) \times \vec{B}, \tag{3.14}$$

[2]In this section, we use v_0 and $v_0(0)$ interchangeably for the momentum-independent bare nesting angle.

[3]In general, $T(0, k_f; v_0) \neq T(k_i, 0; v_0)$ because there is no reflection symmetry around the hot spots. However, the computation of $T(0, k_f; v_0)$ is exactly parallel to that of $T(k_i, 0; v_0)$. This is because the singular part of the quantum corrections are symmetric around the hot spots[30].

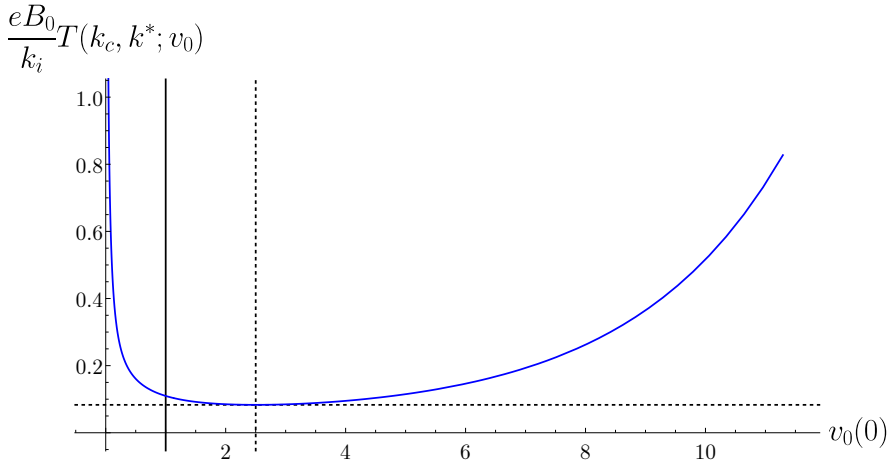

Figure 3.6: The time that it takes for a quasiparticle to traverse from k_c to k^* plotted in the unit of $k_i/(eB_0)$ as a function of the bare nesting angle from $v_0 \approx 0.04$ to $v_0 \approx 11$ for the choice $k_i/\Lambda = 6$. The solid vertical line denotes the nesting angle ($v_0 \approx 1.13$) at which $\alpha_1 = 1$. The dashed lines mark the minimum of $T(k_c, k_i; v_0)$. The non-monotonic behaviour of $T(k_c, k_i; v_0)$ arises from the interplay between two effects : with increasing nesting angle, the size of the lukewarm region shrinks but the intensity of the red shift induced by quantum corrections is increased.

when written in terms of the local proper time coordinate τ, where $\vec{B} = B_0\hat{z}$ is the magnetic field applied along the $\hat{z}$ direction. B_0 is assumed to be weak so that it does not affect the renormalized coupling functions. To measure the cyclotron period in the lab frame, however, we need to recast the equations of motion in the bare time t,

$$\frac{1}{\mathfrak{e}^0{}_t}\frac{\mathrm{d}\vec{r}}{\mathrm{d}t} = \left(k\frac{\partial v_k}{\partial k} + v_k\right)\hat{x} + \hat{y}, \qquad \frac{1}{\mathfrak{e}^0{}_t}\frac{\mathrm{d}\vec{k}}{\mathrm{d}t} = -eB_0\left[\hat{x} - \left(k\frac{\partial v_k}{\partial k} + v_k\right)\hat{y}\right], \tag{3.15}$$

where the effects of the curved spacetime are captured by the vielbein $\mathfrak{e}^0{}_t$. We consider quasiparticles on the Fermi surface, which allows us to focus on the equation of motion for the momentum along the Fermi surface.

Now let us proceed with the solutions. For $k_c < k_i$ ($k_i > \frac{\Lambda}{4v_0}$), there exists a region of Fermi surface near the zone boundary where the renormalization from spin fluctuations is negligible at energies below UV cutoff Λ. In this case, $T(k_i, 0; v_0)$ can be written as the sum of three intervals, $T(k_i, 0; v_0) = T(k_i, k_c; v_0) + T(k_c, k^*; v_0) + T(k^*, 0; v_0)$. $T(k_i, k_c; v_0)$ denotes the time that the quasiparticle spends in the region where the quantum correction from spin fluctuations is negligible and the hybrid spacetime is almost flat. $T(k_c, k^*; v_0)$ arises from the region with algebraically decaying $\mathfrak{e}^0{}_t(k)$. Finally, $T(k^*, 0; v_0)$ denotes the time that the quasiparticle spends in the very vicinity of the hot spot where the flow of the nesting angle modifies the spacetime geometry from the algebraic form. In the following, we compute each time interval one by one.

In the cold region with $k_c < k < k_i$, $\mathfrak{e}^0{}_t \approx 1$ (see the third line for $\mathcal{V}_{F,k}$ in Eq. (3.9)). From $\frac{\mathrm{d}\vec{r}}{\mathrm{d}t} = v_0(0)\hat{x} + \hat{y}$, $\frac{\mathrm{d}\vec{k}}{\mathrm{d}t} = -eB_0\,(\hat{x} - v_0(0)\hat{y})$, one readily obtains

$$T(k_i, k_c; v_0) = \frac{k_i - k_c}{eB_0}. \tag{3.16}$$

In $k^* < k < k_c$, the nesting angle can be still regarded as momentum-independent while the vielbein decays as $\mathfrak{e}^0{}_t = (k/k_c)^{\alpha_1}$, following the second line in Eq. (3.9), where the exponent α_1 is determined

from the bare nesting angle through Eqs. (3.6) and (3.10). The equations of motion become

$$\frac{\mathrm{d}\vec{r}}{\mathrm{d}t} = \left(\frac{k(t)}{k_c}\right)^{\alpha_1} (v_0(0)\hat{x} + \hat{y}), \qquad \frac{\mathrm{d}\vec{k}}{\mathrm{d}t} = -eB_0 \left(\frac{k(t)}{k_c}\right)^{\alpha_1} (\hat{x} - v_0(0)\hat{y}), \tag{3.17}$$

where $k(t)$ denotes the x-component of $\vec{k}(t)$. Integrating $\frac{\mathrm{d}k(t)}{\mathrm{d}t} = -eB_0 \left(\frac{k(t)}{k_c}\right)^{\alpha_1}$ from k_c to k^*, we obtain

$$T(k_c, k^*; v_0) = \frac{k_c^{\alpha_1}}{eB_0} \int_{k^*}^{k_c} \frac{\mathrm{d}k'}{k'^{\alpha_1}} = \frac{k_c}{(1-\alpha_1)eB_0} \left[1 - \left(\frac{k^*}{k_c}\right)^{1-\alpha_1}\right]. \tag{3.18}$$

$T(k_c, k^*; v_0)$ is plotted as a function of $v_0(0)$ in Fig. 3.6. This plot is obtained by substituting the expressions in Eqs. (3.10) and (3.6) in Eq. (3.18). For small nesting angle, $T(k_c, k^*; v_0)$ rapidly decreases with increasing $v_0(0)$. This is because the range of lukewarm region decreases with increasing nesting angle for a fixed Λ (see Eqs. (2.97), (2.98) and Fig. 2.16). Furthermore, at larger nesting angles, even those electrons in the lukewarm region decouple from spin fluctuations at higher energy scales. Remarkably, $T(k_c, k^*; v_0)$ bounces back as $v_0(0)$ increases further. This non-monotonic behaviour is due to a competing effect that an increasing nesting angle has. At larger nesting angles, a reduction in the density of states of low-energy particle-hole excitations weakens the screening of interaction[182]. This makes the quantum-correction-induced red shift stronger for electrons close to the hot spots.

As the nesting angle increases, the portion of Fermi surface affected by spin fluctuations shrinks while electrons close to the hot spots are more significantly renormalized. The disparity in the strength of quantum correction in different parts of Fermi surface causes a more strongly curved spacetime at a large nesting angle. This is also reflected in the torsion that increases with increasing nesting angle as is shown in Fig. 3.4. The metric that becomes more singular at the hot spots with increasing nesting angle creates a possibility of realizing an analogous black hole horizon in momentum space. As α_1 approaches 1, the prefactor $\frac{k_c}{(1-\alpha_1)eB_0}$ in Eq. (3.18) diverges and $T(k_c, k^*; v_0)$ becomes

$$\lim_{\alpha_1 \to 1} T(k_c, k^*; v_0) = \frac{k_c}{eB_0} \log\left(\frac{k_c}{k^*}\right). \tag{3.19}$$

The leading small-angle expansion predicts that α_1 becomes 1 at $v_0 \approx 1.13$ for $N_c = 2$ and $N_f = 1$. Even though the small v_0 expansion is not valid for theories with $v_0 \sim 1$, here we proceed with the assumption that the qualitative feature of the theory remains unchanged even at nesting angles that are not so small[122]. In this case, there may well be a critical nesting angle at which α_1 becomes 1 even if the actual critical value of v_0 differs from what is predicted from the small-v_0 expansion. The way the time interval depends on k^* in Eq. (3.19) is reminiscent of the logarithmic divergence in the time needed for a free-falling object to reach the horizon of the Schwarzschild black hole as measured by an asymptotic observer. This behaviour is analogous; nevertheless, it is not a coincidence. It is a consequence of the fact that at $\alpha_1 = 1$ the metric of a t and k slice of the hybrid spacetime in $k > k^*$ is conformally equivalent to that of the Schwazschild black hole outside the horizon. For a review of the Schwarzchild metric and the time needed for a free-falling object to reach the horizon, see Appendix F. If k^* was zero, the cyclotron period would diverge and a quasiparticle would not be able to go through the hot spot for $\alpha_1 \geq 1$. In our case, the divergence is cut off by k^* because the momentum-spacetime geometry is modified from that of the Schwarschild horizon for $k < k^*$ due to the flow of the nesting angle [4].

For $0 < k < k^*$, the electrons stay coupled with spin fluctuations at energy scales that are low enough that one has to consider the flow of the nesting angle. This modifies the temporal vielbein from the algebraic form to a 'super-logarithmic' form[5] in the first line of Eq. (3.9), $\mathfrak{e}^0{}_t \approx$

[4] For this reason, the geometry that emerges in the $\alpha_1 = 1$ limit is more a fuzzball[136] or a firewall[9] than a horizon with no 'drama'. The fact that the horizon is a special place is also seen from the fact that the torsion diverges at the hot spots (see Fig. 3.4). Another difference from the Schwarzschild horizon is that there is no interior of the black hole in our analogous horizon.

[5] For this, we use $\mathrm{Ei}(X) \approx \frac{e^X}{X}$ for $X \gg 1$.

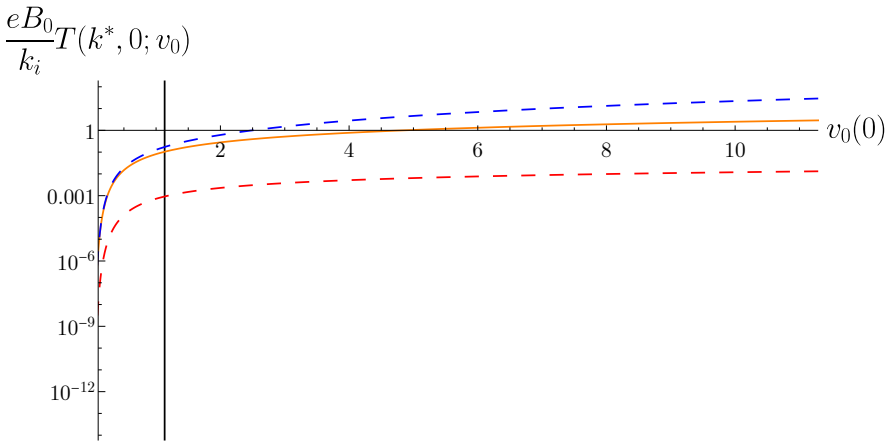

Figure 3.7: The solid curve represents $T(k^*,0;v_0)$ plotted as a function of $v_0(0)$. Two dashed lines that sandwich the solid curve are upper and lower bounds whose expressions can be obtained analytically (see text), which shows that $T(k^*,0;v_0)$ is finite at all values of $v_0(0)$. The vertical line marks the nesting angle at which $\alpha_1 = 1$.

$\frac{1}{\nu(\ell_0)}\exp\left(-\sqrt{N_c^2-1}\frac{\sqrt{\ell_k^{(2L)}+\ell_0}}{\log\sqrt{\ell_k^{(2L)}+\ell_0}}\right)$, where $\nu(\ell_0)=\exp\left(-\sqrt{N_c^2-1}\,\mathrm{Ei}\left(\log\sqrt{\ell_0}\right)\right)$. Because the nesting angle decreases in the vicinity of the hot spot, the quantum correction becomes weaker. As k approaches 0, $\mathfrak{e}^0{}_t$ decreases to zero only as $e^{-\sqrt{\log 1/k}}$, which is slower than any power-law. This results in the time interval that remains finite even for $\alpha_1 \geq 1$, $T(k^*,0;v_0)=\frac{\nu(\ell_0)}{eB_0}\int_0^{k^*}\exp\left(\sqrt{N_c^2-1}\frac{\sqrt{\ell_{k'}^{(2L)}+\ell_0}}{\log\sqrt{\ell_{k'}^{(2L)}+\ell_0}}\right)\mathrm{d}k'$.

Substitution $s=\sqrt{\ell_{k'}^{(2L)}+\ell_0}$ yields

$$T(k^*,0;v_0)=\frac{\Lambda}{2v_0(0)}\frac{\nu(\ell_0)e^{\ell_0}}{eB_0}\int_{\sqrt{2\ell_0}}^{\infty}s\exp\left(-s^2+\sqrt{N_c^2-1}\frac{s}{\log s}\right)\mathrm{d}s. \tag{3.20}$$

It is hard to evaluate Eq. (3.20) exactly. But, we can bound it as $T^{(\mathrm{l})}(k^*,0;v_0) < T(k^*,0;v_0) < T^{(\mathrm{u})}(k^*,0;v_0)$, where the lower bound is obtained by dropping $s/\log s$ in the exponent on the integrand of Eq. (3.20),

$$T^{(\mathrm{l})}(k^*,0;v_0)=\frac{\nu(\ell_0)}{eB_0}k^*, \tag{3.21}$$

and the upper bound is obtained by using $\log s \approx \log\sqrt{2\ell_0}$,

$$T^{(\mathrm{u})}(k^*,0;v_0)=\frac{\nu(\ell_0)}{eB_0}k^*\left[e^{\sqrt{N_c^2-1}\frac{\sqrt{2\ell_0}}{\log\sqrt{2\ell_0}}}+\sqrt{\frac{\pi(N_c^2-1)}{4}}e^{\frac{N_c^2-1}{4\log^2\sqrt{2\ell_0}}+2\ell_0}\frac{1+\mathrm{erf}\left(\frac{\sqrt{N_c^2-1}}{2\log\sqrt{2\ell_0}}-\sqrt{2\ell_0}\right)}{\log\sqrt{2\ell_0}}\right]. \tag{3.22}$$

Here, $\mathrm{erf}(z)=\frac{2}{\sqrt{\pi}}\int_0^z e^{-t^2}\mathrm{d}t$ is the error function. Fig. 3.7 shows $T(k^*,0;v_0)$, $T^{(\mathrm{u})}(k^*,0;v_0)$ and $T^{(\mathrm{l})}(k^*,0;v_0)$ as functions of $v_0(0)$. The upper and lower bounds are direct plots of Eqs. (3.21) and (3.22). The solid line is obtained by numerically evaluating Eq. (3.20). This shows that $T(k^*,0,v_0)$ is finite even for v_0 with $\alpha_1 \geq 1$. $T(k^*,0,v_0)$ decreases with decreasing nesting angle. Especially, the sharp drop of $T(k^*,0,v_0)$ in the small v_0 limit is due to the decrease of $k^*=\frac{\Lambda e^{-\ell_0}}{4v_0(0)}$ with decreasing v_0 (see Eq. (3.6)). The cyclotron period given by the sum of time lapse in each segment,

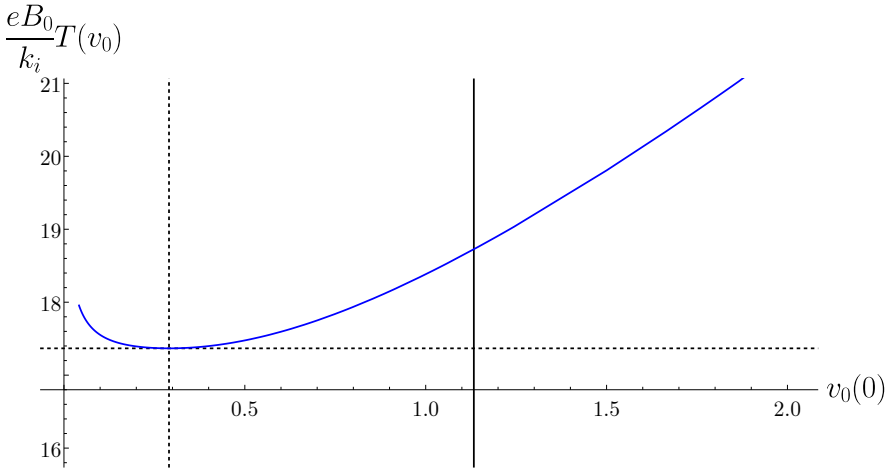

Figure 3.8: The cyclotron period $T(v_0)$ plotted as a function of the bare nesting angle for $k_i/\Lambda = 6$. This plot is obtained by adding the times computed for Figs. 3.6 and 3.7. The solid vertical line denotes the nesting angle with $\alpha_1 = 1$, and the dashed lines mark the minimum of $T(v_0)$.

$T(v_0) = 16\left[T(k_i, k_c; v_0) + T(k_c, k^*; v_0) + T(k^*, 0; v_0)\right]$. $T(v_0)$ is plotted in Fig. 3.8. The non-monotonic behaviour of $T(v_0)$ as a function of v_0 is attributed to the non-monotonicity of $T(k_c, k^*; v_0)$ created by the increasing disparity in the strength of red shift across the Fermi surface with increasing v_0.

So far, we have consider the zero-temperature limit in which the entire Fermi surface supports coherent quasiparticles except at the hot spots. Since electrons are decoupled from spin fluctuations away from the hot spots and all quantum effects that renormalize electrons have been fully incorporated into the renormalized couplings, the semi-classical description is valid at zero temperature. The hot spots, which is a set of measure zero, does not affect the cyclotron period of electrons. At non-zero temperatures, the hot spots become hot regions with a non-zero width proportional to temperature (Sec. 2.6.1), and the contribution from the incoherent electrons can not be completely ignored. Nonetheless, at low temperatures, their contribution remains sub-leading for the cyclotron period compared to the contribution away from the segments of Fermi surface outside the hot regions. In particular, our conclusion on the non-monotonic behaviour of the cyclotron period as a function of the bare nesting angle, which originates from outside the hot region, remains robust as far as the size of hot regions remain much smaller than the remaining segments of Fermi surface. However, for completeness, we consider the effect of finite temperatures below based on the scaling analysis. We defer the more detailed study of the finite temperature correction from incoherent electrons to a future work.

In reality, the superconducting instability is inevitable in theories with non-zero bare nesting angle (Secs. 2.6.3, 2.7), and we have to consider a non-zero temperature to be in the normal state. In order to understand the transport in the hot region, one can not use the quasiparticle picture. At temperature $\mathcal{T}$ (we have changed the notation of the temperature here in order to avoid confusion with the period T) that is higher than the energy scale below which the nesting angle flows ($\mathcal{T} > \Lambda e^{-\ell_0}$)[6], the expression for the cyclotron period should be revised to $T(v_0) = 16\left[T(k_i, k_c; v_0) + T(k_c, k^{\#}; v_0) + T(k^{\#}, 0; v_0)\right]$. Here $T(k_i, k_c; v_0)$ in Eq. (3.16) is unchanged because we are still too far away from the hot spot ($k > k_c$.) $T(k_c, k^{\#}; v_0)$ is still given by Eq. (3.18) except that $k^{\#} \sim \mathcal{T}/v$ now represents the momentum cut-off scale associated with temperature $\mathcal{T}$ ($\mathcal{T}/4v_0 > \Lambda e^{-\ell_0}/4v_0 = k^*$.) Finally, $T(k^{\#}, 0; v_0)$ represents the time that it takes for an incoherent electron pass through the hot region. In the small v_0 limit, the quasiparticle is only marginally destroyed and $T(k^{\#}, 0; v_0)$ can be estimated to be $T(k^{\#}, 0; v_0) \sim$

[6] In the small v_0 limit, the superconducting temperature is given by $T_c \sim \Lambda e^{-\frac{a}{\sqrt{v_0 \log 1/v_0}}}$ which is is higher than the energy scale below which the nesting angle flows significantly, $\Lambda e^{-\frac{b}{v_0 \log(1/v_0)}}$, where a and b are constants independent of v_0 (Eq. (2.226)).

$\frac{k^{\#}}{eB_0(k^{\#}/k_c)^{\alpha_1}}$. Here, the Fermi velocity has the form $(k^{\#}/k_c)^{\alpha_1}$ because the dynamics of the hot region at temperature $\mathcal{T}$ now replaces the zero-temperarture dynamics that previously contained the nesting angle profile ($k^{\#} > k^*$.)

In the zero-temperature superconducting state, one has to include the effect of the pair condensate to describe the dynamics of the Bogoliubov quasiparticles. Suppose that the ground state has the d-wave pairing[177] with a momentum-dependent pairing wavefunction Δ_k. For the physical case with $N_c = 2$ and $N_f = 1$, we need to add the following action for quasiparticles in segments 1 and 5,

$$S'^{1,5} = \sum_{\sigma,\sigma'=\uparrow,\downarrow} \int \frac{\mathrm{d}\omega \mathrm{d}^2 k}{(2\pi)^3} \left\{ \psi^*_{1,\sigma}(\omega,\vec{k}) \Delta_k^{\sigma\sigma'} \psi^*_{5,\sigma'}(-\omega,-\vec{k}) + \psi_{5,\sigma}(-\omega,-\vec{k})\ \Delta_k^{\dagger\ \sigma\sigma'}\ \psi_{1,\sigma'}(\omega,\vec{k}) \right\}, \quad (3.23)$$

where $\Delta_k^{\sigma\sigma'} = \Delta_k \epsilon^{\sigma\sigma'}$ with $\epsilon = \begin{pmatrix} 0 & 1 \\ -1 & 0 \end{pmatrix}$. The derivation of this equation can be found in Appendix G. Eqs. (3.8) and (3.23) can be combined into an action of a spinor field that represents Bogoliubov quasiparticles in the superconducting state,

$$S^{1,5}_{\mathrm{kin}} + S'^{1,5} = \int \frac{\mathrm{d}\omega \mathrm{d}^2 k}{(2\pi)^3} \bar{\Psi}(\omega,\vec{k}) \left\{ i\omega\Gamma^0 + i\mathcal{V}_{F,k}(v_k k_x + k_y)\Gamma^1 - i\Delta_k \Gamma^2 \right\} \Psi(\omega,\vec{k}), \quad (3.24)$$

where $S^{1,5}_{\mathrm{kin}}$ are the terms of the kinematic action corresponding to electrons in hot spots 1 and 5, and $\Psi^T(\omega,\vec{k}) = \left(\psi_{1,\uparrow}(\omega,\vec{k}), \psi_{1,\downarrow}(\omega,\vec{k}), \psi^*_{5,\downarrow}(-\omega,-\vec{k}), -\psi^*_{5,\uparrow}(-\omega,-\vec{k})\right)$ is a 4-component spinor. $\bar{\Psi}(\omega,\vec{k}) = \Psi^\dagger(\omega,\vec{k})\Gamma^0$ with $\Gamma^0 = \sigma_y \otimes \mathbb{1}_2$, $\Gamma^1 = \sigma_x \otimes \mathbb{1}_2$, $\Gamma^2 = \sigma_z \otimes \mathbb{1}_2$ being 4×4 gamma matrices, where the first Pauli matrices act on the Nambu spinor basis and the second Pauli matrices act on the spin space. Using the same transform as in Eq. (3.11) for the Dirac spinor Ψ in the hybrid momentum-spacetime (t, r, k), Eq. (3.24) can be written as

$$S^{1,5}_{\mathrm{kin}} + S'^{1,5} = \int \frac{\mathrm{d}k}{2\pi} \int \mathrm{d}t\mathrm{d}r\, |\mathfrak{e}|\, \bar{\Psi}(t,r,k) \left\{ \Gamma^0 \mathfrak{e}_0{}^t D_t + \Gamma^1 \mathfrak{e}_1{}^r D_r \right\} \Psi(t,r,k). \quad (3.25)$$

Here, the vielbein and the U(1) gauge field are unchanged, but the pairing term gives rise to a complex spin connection, $\omega_{t,02} = 4i\Delta_k$. It will be of interest to find geometric interpretation of physical observables in the superconducting state.

3.4 Summary

In this chapter, we show that the momentum-dependent quantum correction that dilates frequency of electron anisotropically on the Fermi surface gives rise to a curved momentum-spacetime for low-energy quasiparticles in the 2+1 dimensional antiferromagnetic quantum critical metal. The non-trivial dependence of the emergent geometry on the shape of the Fermi surface causes a non-monotonic dependence of the cyclotron frequency on the bare nesting angle of the Fermi surface. With increasing nesting angle, the stronger disparity in the strength of quantum correction in different parts of Fermi surface makes the momentum-dependent red shift more singular at the hot spots. This creates a possibility of realizing an analogous black hole horizon at the hot spots where the motion of the quasiparticle tend to freeze beyond a critical bare nesting angle of the Fermi surface. However, an analogous horizon is not fully realized because the metric in the vicinity of the hot spots is modified by thermal effects above the superconducting transition temperature. Our prediction can be in principle tested through a measurement of the cyclotron frequency as a function of the nesting angle near the hot spots.

Chapter 4

Ultraviolet-Infrared Mixing-Driven Suppression of Kondo Screening in the Antiferromagnetic Quantum Critical Metal

4.1 Introduction

The interaction between local magnetic moments and conduction electrons continue to attract considerable attention in condensed matter physics [14, 97, 151, 51, 80, 201, 113, 195, 152, 192, 193, 52, 196, 37, 61, 187, 158, 156]. In the classic Kondo problem, a magnetic impurity put in Fermi liquid metals is screened into a spin singlet due to the quantum effect that is akin to what causes the confinement of quarks [97, 17]. Recent discoveries of correlated compounds that can be tuned across quantum phase transitions have opened opportunities for exploring new cooperative magnetism facilitated by critical fluctuations [104, 126, 127, 8, 149, 46]. However, the current theoretical understanding remains limited because quantum critical metals are usually described by strongly interacting theories [112].

In this chapter, we study a single magnetic impurity immersed in the two-dimensional AFQCM [3, 141] based on the non-perturbative understanding of the strongly coupled theory in Chapter 2 [182]. This problem has been studied in Ref. [127], but we find that strong coupling effects make a qualitative difference for the behaviour of the impurity. In AFQCM, itinerant electrons and critical spin fluctuations compete to get entangled with the impurity spin. One may naively expect that critical fluctuations, described by bosonic fields, is no match for itinerant electrons with an extensive Fermi surface. However, critical spin fluctuations turn out to be almost on the par with the Fermi surface in the competition. Through the strong electron-boson coupling, the boson 'recruits' low-energy particle-hole excitations with a wide range of momenta to enhance its density of states and suppress Kondo screening at low energies. While Kondo coupling still becomes strong at long distances, it only happens at a much larger distance scale compared to Fermi liquids when the Fermi surface connected by the antiferromagnetic wavevector is close to nesting.

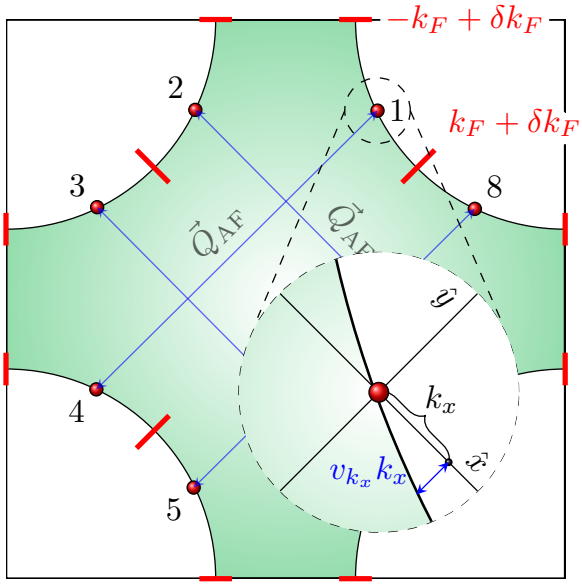

Figure 4.1: In AFQCM, the hot spots (red dots) connected by the antiferromagnetic wave-vector $\vec{Q}_{AF}$ are strongly coupled with the boson that represents critical spin fluctuations. v_0, which represents the nesting angle between the pairs of hot spots connected by $\vec{Q}_{AF}$, determines the low-energy dynamics of the clean AFQCM.

4.2 Kondo Interaction in the AFQCM

We start with the low-energy theory for the clean AFQCM in two space dimensions in Eq. (2.14), restricted to $N_c = 2, N_f = 1$,

$$\begin{aligned} S_0 = & \sum_{N=1}^{8} \sum_{\sigma=\uparrow,\downarrow} \int \mathrm{d}\mathbf{k}\ \psi^{\dagger}_{N,\sigma}(\mathbf{k}) \left\{ ik_0 + V^{(N)}_{F,k_N} e_N \left[\vec{k}; v^{(N)}_{k_N} \right] \right\} \psi_{N,\sigma}(\mathbf{k}) \\ & + \sum_{N=1}^{8} \int \mathrm{d}\mathbf{k}\mathrm{d}\mathbf{q}\ g^{(N)}_{k_N+q_N,k_{\bar{N}}} \psi^{\dagger}_{N,\sigma'}(\mathbf{k}+\mathbf{q}) \vec{\tau}_{\sigma'\sigma} \psi_{\overline{N},\sigma}(\mathbf{k}) \cdot \vec{\phi}(\mathbf{q}) \\ & + \frac{1}{4\mu} \sum_{\{N_i\}} \sum_{\{\sigma_i\}} \int \prod_{i=1}^{3} \mathrm{d}\mathbf{k}_i\ \ \lambda^{\{N_i\};\{\sigma_i\}}_{\{k_{i;N_i}\}}\ \psi^{\dagger}_{N_1,\sigma_1}(\mathbf{k}_1) \psi^{\dagger}_{N_2,\sigma_2}(\mathbf{k}_2) \psi_{N_3,\sigma_3}(\mathbf{k}_3) \psi_{N_4,\sigma_4}(\mathbf{k}_1+\mathbf{k}_2-\mathbf{k}_3). \end{aligned} \tag{4.1}$$

For $N_c = 2, N_f = 1$, $O(3)$ symmetric critical spin fluctuations are described by a three-component bosonic field $\vec{\phi}(\mathbf{q})$. In each segment, the momentum component k_N perpendicular to $\vec{Q}_{AF}$ is used to label points on the Fermi surface within $-(k_F - \delta k_F) \le k_N < k_F + \delta k_F$, where $2k_F$ is the linear size of a segment, as depicted in Fig. 4.1. We choose the scale of frequency so that $V_{\mathrm{F},0} = 1$, just as in Chapter 2.

Now, we add a magnetic impurity to this critical metal. We represent the impurity spin as $\vec{S}_{\mathrm{imp}} = \sum_{\alpha,\beta} f^{\dagger}_{\alpha} \frac{\vec{\tau}_{\alpha,\beta}}{2} f_{\beta}$, where f_α is a pseudo-fermion field with spin α. The dynamics of the impurity is

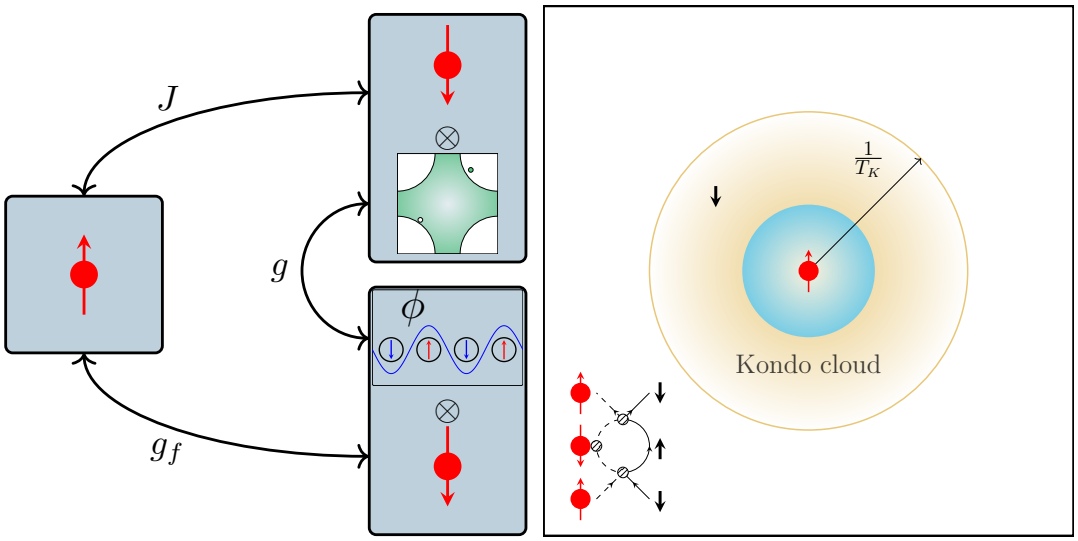

(a) (b)

Figure 4.2: (a) The electron-impurity coupling (J) and boson-impurity coupling (g_f) cause the impurity spin to flip by creating a particle-hole excitation and a boson, respectively, while the latter two are strongly mixed through the electron-boson coupling (g). (b) The Kondo temperature vanishes in the small v_0 limit due to the dressing of the impurity by the critical spin fluctuations subject to strong UV/IR mixing.

described by

$$\begin{aligned} S_1 = & \sum_{\alpha=\uparrow,\downarrow} \int \frac{\mathrm{d}p_0}{2\pi} \left(ip_0 + i\frac{\pi}{2\beta} \right) f_\alpha^\dagger(p_0) f_\alpha(p_0) \\ & + \sum_{\alpha\beta=\uparrow,\downarrow} \sum_{\sigma\sigma'=\uparrow,\downarrow} \int \mathrm{d}\mathbf{q} \left(\int \frac{\mathrm{d}p_0}{2\pi} f_\alpha^\dagger(p_0) \frac{\vec{\tau}_{\alpha\beta}}{2} f_\beta(p_0+q_0) \right) \\ & \cdot \left(\sum_{N,N'=1}^{8} \int \mathrm{d}\mathbf{k} \frac{J^{(N,N')}_{(k+q)_N, k_{N'}}}{\mu} \psi^\dagger_{N,\sigma}(\mathbf{k}+\mathbf{q}) \frac{\vec{\tau}_{\sigma\sigma'}}{2} \psi_{N',\sigma'}(\mathbf{k}) + g_f \vec{\phi}(-\mathbf{q}) \right). \end{aligned} \tag{4.2}$$

The imaginary chemical potential projects out states with $f_\alpha^\dagger f_\alpha = 0, 2$, where $\beta = 1/T$ becomes infinity at zero temperature [164]. $J^{(N,N')}_{k_N, k'_{N'}}$ is the Kondo coupling function that describes the scattering of electrons from $(N', k'_{N'})$ to (N, k_N) through interaction with the impurity. g_f represents the boson-impurity coupling (see Fig. 4.2a). At the impurity-free fixed point, the fields have scaling dimensions $[\Psi(\mathbf{k})] = [\vec{\phi}(\mathbf{k})] = -2$ with respect to the transformation that rescales both components of momentum with dimension $[\mathbf{k}] = 1$. Under this scale transformation, the dimensionless size of Fermi surface (k_F), measured in the unit of the floating energy scale (μ) that is sent to zero in the low-energy limit, grows, playing the role of a relevant parameter [30, 99]. g_f and J have dimensions 0 and -1, respectively. Accordingly, the power of μ has been factored out in each coupling. It is noted that g_f is marginal due to the large anomalous dimension of the boson generated at the strongly coupled clean fixed point. Without it, g_f would be strictly relevant [127].

4.3 Suppression of the Kondo screening in the AFQCM

While the Kondo coupling has the negative scaling dimension, we have to keep it within the low-energy theory, as it gives rise to a logarithmic divergence. Due to scatterings that involve large momentum transfer, quantum corrections are proportional to k_F, which alters the relevancy of a coupling from what is expected from its scaling dimension. Kondo coupling is particularly prone to this large-momentum/low-energy (in short, UV/IR) mixing [133, 231, 30, 99] because the phase space available for low-energy electrons becomes even greater without the momentum conservation[1]. To understand this, let us first consider the beta functional of the Kondo coupling in the absence of critical boson:

$$\frac{\mathrm{d}J^{(N,N')}_{k,k'}}{\mathrm{d}\ell} = -J^{(N,N')}_{k,k'} + \sum_{M=1}^{8} \frac{1}{2\pi} \int_{-k_F}^{k_F} \frac{\mathrm{d}q}{2\pi\mu V_{F,q}} J^{(N,M)}_{k,q} J^{(M,N')}_{q,k'}. \tag{4.3}$$

The interaction that scatters an electron from k' to k is renormalized by a virtual electron that can be placed anywhere on the Fermi surface (hence, q and M are integrated and summed over). As the volume of the phase space is controlled by the relevant parameter k_F, the expansion is actually controlled by a dimensionless parameter $\tilde{J} \sim \int \mathrm{d}q J \sim k_F J$, which is marginally relevant for $J > 0$ [97].

In the AFQCM, the beta function is modified by critical spin fluctuations, and is augmented with the beta function for the boson-impurity coupling. To the leading order in v, J and g_f, the beta functions become (see Appendices H and I for details)

$$\frac{\mathrm{d}J^{(N,N')}_{k,k'}}{\mathrm{d}\ell} = -\left(2 - z + \eta_f\right) J^{(N,N')}_{k,k'} + \sum_{M} \frac{1}{2\pi} \int \frac{\mathrm{d}q}{2\pi\mu V_{F,q}} J^{(N,M)}_{k,q} J^{(M,N')}_{q,k'}, \tag{4.4}$$

$$\frac{\partial g_f}{\partial \ell} = -\left(\eta_f + \eta^{(\Phi)}\right) g_f, \tag{4.5}$$

where $z = 1 + \frac{3}{4\pi}\frac{v_0}{c}$ is the dynamical critical exponent corrected from 1 by the non-zero nesting angle and $\eta_f = \frac{\tilde{g}_f}{\pi^3}\ell$ with $\tilde{g}_f \equiv \frac{g_f^2}{c^2}$. Both g_f and J have the common component of anomalous dimension η_f, which arises from the self-energy and vertex correction of pseudo-fermion. The flow of g_f is also affected by the finite v-correction to the anomalous dimension of the boson, $\eta^{(\Phi)} = \frac{1}{4\pi}\frac{v_0}{c}\log\frac{c}{v_0}$ [182]. Acting on top of the anomalous dimension 1 of the boson at the $v = 0$ fixed point, $\eta^{(\Phi)}$ makes the boson-impurity coupling slightly irrelevant at a small but non-zero nesting angle. The self-energy and vertex correction for itinerant electrons would generate additional contributions to the beta functional of J. However, those corrections have been dropped. They are not important at low energies because critical spin fluctuations renormalize itinerant electrons only within patches of size $\mu/(v_0 c)$ around the hot spots at energy scale μ [30]. This can be understood as follows. An electron on the Fermi surface at momentum k_N away from hot spot N must interact with a boson with minimum momentum $q \sim v_0 k_N$ (and energy $\sim c v_0 k_N$) to be scattered onto the Fermi surface in segment $\bar{N}$ due to an imperfect nesting for $v_0 \neq 0$. So, electrons with $k_N \gg \mu/(v_0 c)$ decouple from spin fluctuations at energies lower than μ. Since the size of the 'hot patches' shrinks linearly in μ, those quantum corrections do not affect $J^{(N,N')}_{k,k'}$ for most k, k'. Therefore, quantum corrections to those hot electrons are suppressed by μ/k_F for the s-wave Kondo coupling. On the contrary, the pseudo-fermion self-energy and the vertex correction for the impurity-boson coupling gives rise to the anomalous dimension η_f for $J^{(N,N')}_{k,k'}$ regardless of k and k'. Remarkably, $\eta_f = \tilde{g}_f \ell/\pi^3$ depends on $\ell = \log\Lambda/\mu$ explicitly. This unusual sensitivity on the UV cutoff is traced back to the propagator of the boson at the impurity site,

$$\begin{aligned} \bar{D}(q_0) &= \int \frac{\mathrm{d}q_x \mathrm{d}q_y}{(2\pi)^2} D(\mathbf{q}) \\ &= \frac{1}{\pi^2 c^2}\left\{2\Lambda \log\left(1 + \frac{\Lambda}{\Lambda + |q_0|}\right) + |q_0|\left[\log\left(1 + \frac{\Lambda}{\Lambda + |q_0|}\right) - \log\left(1 + \frac{\Lambda}{|q_0|}\right)\right]\right\}. \end{aligned} \tag{4.6}$$

[1] Another such coupling is the four-fermion coupling

The UV divergence in the term $-|q_0|\log\left(1+\frac{\Lambda}{|q_0|}\right) \sim -|q_0|\log\left(\frac{\Lambda}{|q_0|}\right)$, which is non-analytic in q_0, implies that short-wavelength bosons significantly contribute to the long-time correlation. Namely, short-wavelength spin textures whose wave-vectors deviate significantly from $\vec{Q}_{AF}$ still fluctuate slowly temporally. This is caused by the strong mixing of the boson with low-energy particle-hole excitations that carry large momenta. The low-energy spectral weight enhanced by large-momentum modes also gives rise to a logarithmically divergent specific heat coefficient from the boson[182]. This *UV/IR mixing* plays the crucial role in determining the fate of the Kondo coupling at low energies. Eqs. (4.4) and (4.5) are valid for $\ell > \ell_i \sim O(1)$ where this UV/IR-driven contribution is dominant over terms that are $O(\ell^0)$ in η_f.

To simplify the task of solving the beta functional, we focus on the 's-wave' channel of the form

$$J^{(N,N')}_{k,k'} = \frac{\pi^2}{4}\frac{\mu}{k_F}\sqrt{V^{(N)}_{F,k}V^{(N')}_{F,k'}}\,\tilde{J}^V, \tag{4.7}$$

where $J^{(N,N')}_{k,k'}$ is momentum-independent modulo the factor of Fermi velocity. Fermi velocity outside the hot patches increases as $\frac{\partial V_{F,k}}{\partial \ell} = (z-1)V_{F,k}$ relative to $V_{F,0}$, which is set to be 1, because only electrons within the hot patches are renormalized by spin fluctuations (Sec. 2.6.1). The s-wave Kondo coupling $\tilde{J}^V$, which includes the effect of growing phase space k_F/μ, satisfies a simple beta function,

$$\frac{\partial \tilde{J}^V(\ell)}{\partial \ell} = -\eta_f(\ell)\tilde{J}^V(\ell) + \left(\tilde{J}^V(\ell)\right)^2, \tag{4.8}$$

where $\eta_f = \frac{\tilde{g}_f}{\pi^3}\ell$. In this problem, there are three parameters that are marginal up to logarithmic corrections: the nesting angle at the hot spots (v_0), Kondo coupling ($\tilde{J}^V$), and the boson-impurity coupling (g_f). Let $v_{0,i} \sim 1/(\ell_0 \log \ell_0)$, $\tilde{J}^V_i$ and $g_{f,i}$ denote the nesting angle, Kondo coupling and boson-impurity coupling, respectively, defined at short-distance cutoff scale $\ell_i \sim O(1)$. Our main goal is to understand how the critical spin fluctuations affect the behaviour of Kondo coupling. In particular, we would like to extract how the Kondo scale, the scale at which $\tilde{J}^V(\ell)$ becomes large, depends on $v_{0,i}$ and $\tilde{g}_{f,i}$ in the small $\tilde{J}^V_i$ limit. Our calculation is controlled in the limit that $v_{0,i}$, $\tilde{J}^V$ and $\tilde{g}_f$ are small without a particular order among them.

We first solve Eq. (4.5). Since $\eta^{(\Phi)}_i$ and $\tilde{g}_{f,i}\ell$ set the rates at which g_f decays with increasing ℓ, we define the following characteristic scales: $1/\eta^{(\Phi)}_i \sim \sqrt{\ell_0}$ and $\ell_1 \sim 1/\sqrt{\tilde{g}_{f,i}}$. Naturally, the RG flow exhibits different behaviours, depending on the relative magnitude of $1/\ell_0$ and $\tilde{g}_{f,i}$.

If $\tilde{g}_{f,i} \ll 1/\ell_0$, the effect of the boson-impurity coupling is weak compared to the quantum correction that arises from a non-zero nesting angle. Since $\eta^{(\Phi)}$ plays the dominant role over $\tilde{g}_f$ in determining the flow of $\tilde{g}_f$, one can ignore $\tilde{g}_f$ in Eq. (4.5) to obtain

$$g_f(\ell) = e^{-\frac{\sqrt{\ell+\ell_0}-\sqrt{\ell_0+\ell_i}}{\sqrt{3}}}\, g_{f,i}. \tag{4.9}$$

In this case, the boson-impurity coupling decays to zero exponentially at large ℓ due to the relatively large correction to the anomalous dimension of the boson, and $\tilde{g}_f$ remains negligible for the flow of g_f at all scales. With small $\tilde{g}_f$, one essentially recovers the Kondo effect in Fermi liquids: $\ell_K \sim 1/\tilde{J}^V_i$ with a small correction.

A qualitatively new behaviour emerges for $\tilde{g}_{f,i} \gg 1/\ell_0$. In this case, the bare boson-impurity coupling is strong enough that $\eta^{(\Phi)}$ is negligible in Eq. (4.5) at short distance scales. The $\tilde{g}_f$-dominated flow gives

$$\tilde{g}_f(\ell) = \frac{3\pi^3\tilde{g}_{f,i}(\ell+\ell_0)}{3\pi^3(\ell_0+\ell_i) + \tilde{g}_{f,i}\left[2\ell^3 + 3\ell^2\ell_0 - \ell_i^2(3\ell_0+2\ell_i)\right]}. \tag{4.10}$$

This slowly decaying $\tilde{g}_f$ gives rise to a relatively large anomalous dimension, which suppresses the Kondo coupling significantly. To understand this quantitatively (see Appendix J for details), we note that $\tilde{g}_f\ell/\pi^3 \approx 1/\ell$ within length scale $\ell_1 \ll \ell \ll \ell_0$, and Eq. (4.8) becomes $\frac{\partial \tilde{J}^V}{\partial \ell} = -\tilde{J}^V/\ell + (\tilde{J}^V)^2$.

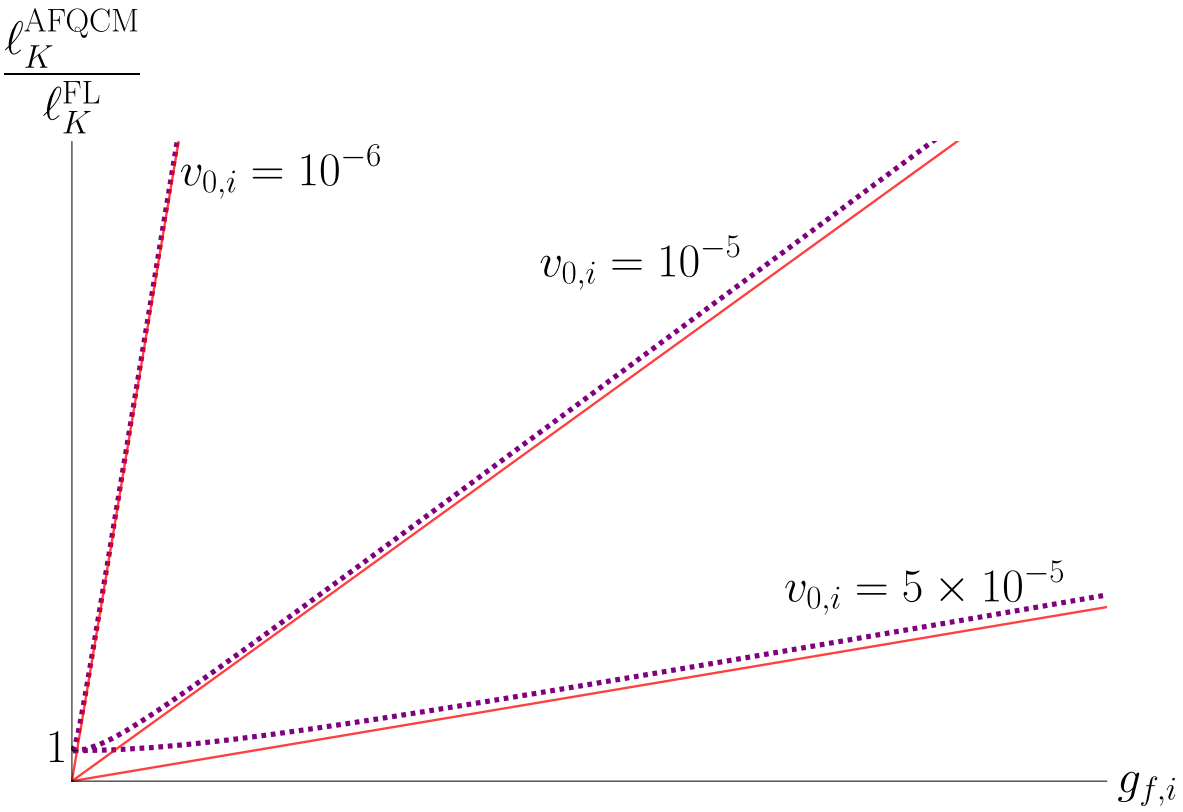

Figure 4.3: Logarithmic Kondo scale of the AFQCM relative to that of the Fermi liquid with the same electronic density of state and bare Kondo coupling plotted as a function of the bare boson-impurity coupling, $g_{f,i}$ for three different bare nesting angles $v_{0,i}$. The dashed lines represent the numerical solutions of Eqs. (4.5) and (4.8) obtained with $\tilde{J}_i^V = 10^{-8}$, and the solid lines are $\frac{\ell^{\mathrm{AFQCM}}}{\ell^{\mathrm{FL}}} = A\frac{g_{f,i}}{v_{0,i}\log(1/v_{0,i})}$ with $A = \frac{8e^{3/4}}{3\sqrt{\pi}}$.

Its solution is given by $\tilde{J}^V(\ell)^{-1} \approx \ell\left[\frac{1}{\tilde{J}^V(\ell_1)\ell_1} - \log\frac{\ell}{\ell_1}\right]$. According to this, Kondo coupling only grows as a logarithm of ℓ, and the Kondo scale becomes $\ell_K = \ell_1 e^{\frac{1}{\tilde{J}^V(\ell_1)\ell_1}}$. This implies that the Kondo temperature $T_K = \Lambda e^{-\ell_K}$ is suppressed by an exponential of an exponential of $1/\tilde{J}^V(\ell_1)$. In a sense, the critical boson demotes Kondo coupling from a marginally relevant coupling to a 'marginally marginally relevant' coupling. However, this rapid increase of ℓ_K with decreasing $\tilde{J}_i^V$ is cut off once ℓ_K becomes large enough that one can not drop $\eta^{(\Phi)}$ in Eq. (4.5) anymore. Because $\eta_f = \tilde{g}_f\ell/\pi^3 \sim 1/\ell$ decays faster than $\eta^{(\Phi)} \sim 1/(\ell+\ell_0)^{1/2}$, g_f exhibits a crossover from the $\tilde{g}_f$-dominated flow to the $\eta^{(\Phi)}$-dominated flow around $\ell_f \sim \sqrt{\ell_0}$. For $\ell > \ell_f$, the flow of g_f is dominated by $\eta^{(\Phi)}$ and decays exponentially. As the anomalous dimension for $\tilde{J}^V$ becomes exponentially small for $\ell > \ell_f$, the flow of Kondo coupling is reduced to that of the Fermi liquids. Consequently, the Kondo scale is given by $\ell_K \sim \ell_f + \frac{1}{\tilde{J}^V(\ell_f)}$, where $\tilde{J}^V(\ell_f) \sim \tilde{J}_i^V \frac{v_{0,i}\log 1/v_{0,i}}{g_{f,i}}$ is the Kondo coupling at scale ℓ_f. In the small $\tilde{J}_i^V$ limit, $\frac{1}{\tilde{J}^V(\ell_f)} \gg \ell_f$ and the Kondo scale becomes $\ell_K \sim \frac{1}{\tilde{J}_i^V}\frac{g_{f,i}}{v_{0,i}\log 1/v_{0,i}}$ to the leading order in $\tilde{J}_i^V$. At small $v_{0,i}$, ℓ_K is enhanced by the factor of $\frac{g_{f,i}}{v_{0,i}\log 1/v_{0,i}}$ compared to that of Fermi liquid ($\ell_K^{FL} \sim 1/\tilde{J}_i^V$) with the same density of state (see Fig. 4.2b). This is confirmed through solving the beta functions numerically as is shown in Fig. 4.3. Given that the superconducting instability arises at $\ell_{SC} \sim 1/\sqrt{v_{0,i}\log 1/v_{0,i}}$ [30], Kondo screening won't be observable in AFQCM at sufficiently small

nesting angles.

4.4 Summary

In summary, the Kondo screening is greatly suppressed in AFQCM through a UV/IR mixing when the hot spots on the Fermi surface are well nested. Our analysis fully takes into account the strong electron-boson coupling in the limit that the nesting angle is small. In the future, it is of great interest to understand the regime with the strong Kondo coupling non-perturbatively[226, 15, 16, 6, 7].

Chapter 5

Conclusion

In this thesis, we studied the functional renormalization group flow of the four-fermion coupling for understanding the superconducting instability, the emergence of singular momentum-spacetime geometry on the Fermi surface, and the anomalous suppression of the Kondo screening in the 2+1 dimensional antiferromagnetic quantum critical metal.

In Chapter 2, we present the field-theoretic functional renormalization group formalism for non-Fermi liquids. We apply it to the low-energy effective field theory for the non-Fermi liquid realized at the onset of an antiferromagnetic quantum phase transition in two space dimensions. We find that the notions of renormalizable field theory and scale invariance must be generalized by incorporating the existence of the Fermi momentum. This generalized formalism is a necessity in the theoretical treatment of metals that is born out the fact that the Fermi momentum is an intrinsic scale of the system. With the implementation of the functional renormalization group formalism, we identify the non-Fermi liquid fixed point in the space of coupling functions and extract the universal low-energy physics from the critical point. Crucially, we are able to uncover the dual role that critical spin fluctuations play for superconductivity: while spin fluctuations make electrons incoherent at the hot spots, they also provide the "glue" for Cooper pairing. Despite the inevitable superconducting instability, systems with small bare nesting angles must pass through a region of slow RG flow when the bare four-fermion interaction is repulsive or weakly attractive due to the proximity of the theory to the fixed point. This "bottleneck" region controls the scaling behaviours of the normal state and the quasi-universal pathway from the non-Fermi liquid to superconductivity.

In Chapter 3, we show that a curved momentum-spacetime arises at the antiferromagnetic quantum critical metal as the critical spin fluctuations generate red shift that dilates frequency of electron unevenly on the Fermi surface. The momentum-spacetime geometry that emerges at low energies depends on the bare nesting angle of the Fermi surface and is encoded in the Fermi velocity. With increasing nesting angle, the region in which electron motion is slowed down by critical spin fluctuations shrinks. On the other hand, the increasing nesting angle makes the red shift stronger near the hot spots due to the weakened screening of the interaction. These competing effects result in a non-monotonic dependence of the cyclotron frequency of electron on the nesting angle of the Fermi surface. This geometric approach can expose interesting alternative picture on the origin of cyclotron mass enhancement in strongly correlated materials where electrons become incoherent in hot manifolds of the Fermi surface [166, 47, 189, 188, 114, 68, 50, 197, 21, 70, 94].

In Chapter 4, we present the effects of an isolated magnetic impurity added to the antiferromagnetic quantum critical metal. Since critical spin fluctuations are present in the low energy theory, the impurity not only interacts with the itinerant electrons, but also with the collective mode through the spin-spin interactions. We use the beta functions of both interactions to describe how the itinerant electrons compete with the spin fluctuations to couple with the impurity. Naively, one would expect the bosonic spin fluctuation to be no match of the extensive Fermi surface that supports infinitely many gapless modes. However, critical spin fluctuations turn out to be almost on the par with the

Fermi surface in the competition. Through the strong electron-boson coupling, the boson 'recruits' low-energy particle-hole excitations with a wide range of momenta to enhance its density of states and suppress Kondo screening at low energies. While Kondo coupling still becomes strong at long distances, it only happens at a much larger distance scale compared to Fermi liquids when the Fermi surface connected by the antiferromagnetic wavevector is close to nesting.

We conclude with some outlook, future directions and open questions.

- Beyond the small nesting angle: We can not exclude the possibility of new strongly interacting fixed points in the region where the nesting angle is not small. It will be of great interest to understand the fate of the theories with general nesting angles in more detail. In particular, the results for the cyclotron period show the metric becomes more singular when the nesting angle becomes $O(1)$.

- Momentum-spacetime geometry near cold spots: In the Ising-nematic quantum critical metal in two dimensions, the Fermi surface has cold spots at which the Yukawa coupling vanishes. Therefore, the entire Fermi surface is 'hot' except for a discrete set of cold spots. It would be interesting to understand the dynamics of incoherent electrons in the Ising-nematic quantum critical metal in terms of the emergent momentum-space geometry. One expects to have an enhanced blue-shift of electrons near the cold spots where quantum corrections vanish.

- Stable non-Fermi liquids: In AFQCM, critical spin fluctuations create a strong pair-breaking effect on electrons at the hot spots by making them in coherent. Nonetheless, superconducting instabilities are unavoidable due to the lukewarm electrons that are subject to strong pairing interaction yet coherent enough to be susceptible to pairing instability. It will also be of great interest to examine a possibility in which the pair breaking effect due to incoherence prevents superconductivity even at zero temperature for hot Fermi surfaces. Recent progress in the study of effective field theories of hot Fermi surfaces has revealed metallic fixed points to be defined only modulo a rescaling of Fermi momentum [99]. In this study it was revealed that near the upper critical dimension, two exactly marginal coupling functions span the space of stable projective fixed points: one specifies the shape of the Fermi surface and the other sets the angle-dependent Fermi velocity.

- Non-perturbative Kondo coupling: The Kondo problem in this thesis was solved in the limit where the impurity-boson and the impurity-electron couplings are weak. In the future, it is of great interest to extend the study to the non-perturbative regime [226, 15, 16, 6, 7].

- Kondo lattice and heavy fermions: Another interesting direction of extending the result of Chapter 4 is to consider the Kondo lattice problem in the presence of critical spin fluctuations [51, 80, 201, 113, 195, 152, 192, 193, 52, 196, 37, 61, 187, 158, 156]. It is of great interest to tackle the quantum critical points associated with Fermi surface reconstruction through the field-theoretic functional renormalization group scheme.

Appendix A

Quantum corrections for the two and three-point functions

In this appendix, we compute the quantum corrections for the fermion two-point function and the Yukawa vertex. In this computation, we assume that all coupling functions satisfy the adiabaticity condition in Eq. (2.83). In this case, the singular parts of the quantum corrections for the two and three-point functions can be computed by replacing the coupling functions with the values at which the integrand is peaked. Later we will verify that the coupling functions that arise from the beta functionals obtained under the assumption of adiabaticity at a UV energy scale satisfy the adiabaticity at all energy scales.

A.1 Fermion self-energy

A.1.1 One-loop

The real and imaginary part of the one-loop self-energy in Eq. (2.67) reads

$$\mathrm{Im}\left[\Sigma_N^{\mathrm{1L}}(\mathbf{k})\right] = \frac{2g_k^{(N)}g_k^{(\bar{N})}(N_c^2-1)}{N_cN_f}\int \mathrm{d}\boldsymbol{q}\left[\frac{(k_0+q_0)}{(k_0+q_0)^2+(V_{F,k}^{(\bar{N})})^2 e_{\bar{N}}[\vec{k}+\vec{q};v_k^{(\bar{N})}]^2}\frac{1}{|q_0|+|cq_x|+|cq_y|}\right], \tag{A.1}$$

$$\mathrm{Re}\left[\Sigma_N^{\mathrm{1L}}(\mathbf{k})\right] = -\frac{2g_k^{(N)}g_k^{(\bar{N})}(N_c^2-1)}{N_cN_f}\int \mathrm{d}\boldsymbol{q}\left[\frac{V_{F,k}^{(\bar{N})}e_{\bar{N}}[\vec{k}+\vec{q};v_k^{(\bar{N})}]}{(k_0+q_0)^2+(V_{F,k}^{(\bar{N})})^2 e_{\bar{N}}[\vec{k}+\vec{q};v_k^{(\bar{N})}]^2}\frac{1}{|q_0|+|cq_x|+|cq_y|}\right]. \tag{A.2}$$

Without loss of generality, we can consider the quantum correction for $N=1$. The self-energy at other hot spots can be obtained from this through a C_4-transformation.

Imaginary part $\mathrm{Im}\left[\Sigma_N^{\mathrm{1L}}(\mathbf{k})\right]$

We first compute the imaginary part,

$$\mathrm{Im}\left[\Sigma_1^{\mathrm{1L}}(\mathbf{k})\right] = \frac{2g_k^2(N_c^2-1)}{N_cN_f}\int \mathrm{d}\mathbf{q}\left[\frac{(k_0+q_0)}{(k_0+q_0)^2+V_{F,k}^2(v_kq_x-q_y+e_4[\vec{k},v_k])^2}\frac{1}{|q_0|+|cq_x|+|cq_y|}\right], \tag{A.3}$$

where Eq. (2.17) is used to express coupling functions in terms of the generic coupling functions. We shift the internal momentum as $q_y \to q_y + v_kq_x + e_4[\vec{k},v_k]$ so that the internal fermion has zero energy

at $q_y = 0$. The integration over q_y is convergent even if we drop the cq_y term in the boson propagator in the small v limit. We further simply the expression by replacing $|cq_x| + |cv_k q_x + ce_4[\vec{k}, v_k]|$ with $c|q_x| + |ce_4[\vec{k}, v_k]|$ in the small v limit,

$$\mathrm{Im}\left[\Sigma_1^{1\mathrm{L}}(\mathbf{k})\right] = \frac{2g_k^2(N_c^2-1)}{N_c N_f}\int \mathrm{d}\mathbf{q}\left[\frac{(k_0+q_0)}{(k_0+q_0)^2 + V_{F,k}^2 q_y^2}\frac{1}{|q_0|+|cq_x|+|\bar{\Delta}(\vec{k};v_k)|}\right], \tag{A.4}$$

where $\bar{\Delta}(\vec{k};v_k) = ce_4[\vec{k},v_k]$. The integration over q_y leads to

$$\mathrm{Im}\left[\Sigma_1^{1\mathrm{L}}(\mathbf{k})\right] = \frac{g_k^2(N_c^2-1)}{V_{F,k}N_c N_f}\int_{\mathbb{R}}\frac{\mathrm{d}q_0}{2\pi}\int_{-\Lambda/c}^{\Lambda/c}\frac{\mathrm{d}q_x}{2\pi}\left[\frac{\mathrm{sgn}(k_0+q_0)}{|q_0|+|cq_x|+|\bar{\Delta}(\vec{k};v_k)|}\right]. \tag{A.5}$$

Here Λ is a UV energy cutoff, which is translated to the momentum cutoff for the boson, Λ/c. The subsequent integrations over q_0 and q_x yield

$$\mathrm{Im}\left[\Sigma_1^{1\mathrm{L}}(\mathbf{k})\right] = \frac{g_k^2(N_c^2-1)}{V_{F,k}N_c N_f}\frac{1}{\pi^2 c}k_0\log\left(\frac{\Lambda}{|\bar{\Delta}(\vec{k};v_k)|+|k_0|}\right) + reg., \tag{A.6}$$

where $reg.$ represents terms that are regular in the large Λ limit. To remove the singular part of $\frac{\partial \mathrm{Im}\left[\Sigma_1^{1\mathrm{L}}(\mathbf{k})\right]}{\partial k_0}\Big|_{\mathbf{k}=(\mu,k_x,-v_k k_x)}$ in the small μ limit, the counter-term is chosen to be

$$A^{(1);1\mathrm{L}}(k) = -\frac{N_c^2-1}{\pi^2 N_c N_f}\frac{g_k^2}{cV_{F,k}}\log\left(\frac{\Lambda}{\mu+2v_k c|k|}\right), \tag{A.7}$$

where we use $\bar{\Delta}(\vec{k};v_k) = 2v_k ck$ when the external fermion is on the Fermi surface.

Real part $\mathrm{Re}\left[\Sigma_N^{1\mathrm{L}}(\mathbf{k})\right]$

We rewrite the real part of the self-energy in Eq. (A.2) by shifting q_y to $q_y + e_4[\vec{k},v_k] + v_k q_x$,

$$\begin{aligned}&\mathrm{Re}\left[\Sigma_1^{1\mathrm{L}}(\mathbf{k})\right]\\ &= \frac{2g_k^2(N_c^2-1)}{N_c N_f}\int \mathrm{d}\mathbf{q}\left[\frac{V_{F,k}q_y}{(k_0+q_0)^2+V_{F,k}^2q_y^2}\right]\left[\frac{1}{|q_0|+|cq_x|+|cq_y+\bar{\Delta}(\vec{k};v_k)+cv_k q_x|}\right],\end{aligned} \tag{A.8}$$

where $\bar{\Delta}(\vec{k};v_k) = ce_4[\vec{k},v_k]$. As in the calculation of the imaginary part, we can neglect $cv_k q_x$ in the boson propagator since the leading q_x dependence comes from $|cq_x|$. However, cq_y can not be ignored as the integration vanishes without it. Therefore, we consider

$$\mathrm{Re}\left[\Sigma_1^{1\mathrm{L}}(\mathbf{k})\right] = \frac{2g_k^2(N_c^2-1)}{N_c N_f}\int \mathrm{d}\mathbf{q}\left[\frac{V_{F,k}q_y}{(k_0+q_0)^2+V_{F,k}^2q_y^2}\right]\left[\frac{1}{|q_0|+|cq_x|+|cq_y+\bar{\Delta}(\vec{k};v_k)|}\right]. \tag{A.9}$$

For the imaginary part of the self-energy, the full self-energy has been obtained at general frequency and momentum. For the real part, we focus on the asymptotic limits: (i) $|k_0| \gg |\bar{\Delta}(\vec{k};v_k)|$ and (ii) $|k_0| \ll |\bar{\Delta}(\vec{k};v_k)|$.

For $|k_0| \gg |\bar{\Delta}(\vec{k};v_k)|$, we rescale the internal momentum as $q_0 \to k_0 q_0$ and $\vec{q} \to k_0\vec{q}/c$ to rewrite Eq. (A.9) as

$$\mathrm{Re}\left[\Sigma_1^{1\mathrm{L}}(\mathbf{k})\right] = \frac{2g_k^2(N_c^2-1)k_0}{cV_{F,k}N_c N_f}\int \mathrm{d}\mathbf{q}\left[\frac{q_y}{\mathfrak{c}_k^2(1+q_0)^2+q_y^2}\right]\left[\frac{1}{|q_0|+|q_x|+|q_y+\mathfrak{h}(\mathbf{k};v_k)|}\right], \tag{A.10}$$

where $\mathfrak{h}(\mathbf{k};v_k)=\bar{\Delta}(\vec{k};v_k)/k_0$ and $\mathfrak{c}_k\equiv c/V_{F,k}$. One has to be careful in taking the small c and small $\mathfrak{h}(\mathbf{k};v_k)$ limits in this expression. On the one hand, the integration over q_y vanishes if $\mathfrak{h}(\mathbf{k};v_k)=0$. On the other hand, setting $\mathfrak{c}_k=0$ inside the integrand makes the integration logarithmically divergent. These imply that the quantum correction is proportional to $\mathfrak{h}(\mathbf{k},v_k)$ and diverges logarithmically in $\mathfrak{c}_k\ll 1$. After the integration over q_y is done for general $\mathfrak{c}_k$ and $\mathfrak{h}(\mathbf{k};v_k)$, the leading order contribution in $\mathfrak{h}(\mathbf{k};v_k)$ is given by

$$\begin{aligned}&\mathrm{Re}\left[\Sigma_1^{1\mathrm{L}}(\mathbf{k})\right]\\&=\frac{2g_k^2(N_c^2-1)\bar{\Delta}(\vec{k};v_k)}{\pi cV_{F,k}N_cN_f}\int_{\mathbb{R}}\frac{\mathrm{d}q_0}{(2\pi)}\int_{\mathbb{R}}\frac{\mathrm{d}q_x}{(2\pi)}\left(\frac{\mathfrak{c}_k^2(1+q_0)^2+(|q_0|+|q_x|)^2-\pi\mathfrak{c}_k|q_0+1|(|q_x|+|q_0|)}{[\mathfrak{c}_k^2(1+q_0)^2+(|q_0|+|q_x|)^2]^2}\right.\\&\left.+\frac{1}{2}\frac{\mathfrak{c}_k^2(1+q_0)^2-(|q_0|+|q_x|)^2}{[\mathfrak{c}_k^2(1+q_0)^2+(|q_0|+|q_x|)^2]^2}\log\left(\frac{(|q_0|+|q_x|)^2}{\mathfrak{c}_k^2(1+q_0)^2}\right)\right).\end{aligned}\tag{A.11}$$

The integration over q_x can be done exactly and is given by

$$\mathrm{Re}\left[\Sigma_1^{1\mathrm{L}}(\mathbf{k})\right]=\frac{2g_k^2(N_c^2-1)\bar{\Delta}(\vec{k};v_k)}{\pi cV_{F,k}N_cN_f}\int_{-\Lambda/|k_0|}^{\Lambda/|k_0|}\frac{\mathrm{d}q_0}{(2\pi)}\frac{|q_0|\log(\mathfrak{c}_k^2(1+q_0)^2/q_0^2)-\pi\mathfrak{c}_k|1+q_0|}{2\pi(q_0^2+\mathfrak{c}_k^2(1+q_0)^2)},\tag{A.12}$$

where the cutoff for the rescaled frequency becomes $\Lambda/|k_0|$. The frequency integration gives

$$\mathrm{Re}\left[\Sigma_1^{1\mathrm{L}}(\mathbf{k})\right]=-\frac{2g_k^2(N_c^2-1)\bar{\Delta}(\vec{k};v_k)}{\pi^3cV_{F,k}N_cN_f}\log\frac{V_{F,k}}{c}\log\frac{\Lambda}{|k_0|}+reg.,\tag{A.13}$$

where $reg.$ represents terms that are regular in the large Λ/k_0 limit. For $|\bar{\Delta}(\vec{k};v_k)|\gg|k_0|$, $\bar{\Delta}(\vec{k};v_k)$ cuts off the IR singularity, and the self-energy becomes

$$\mathrm{Re}\left[\Sigma_1^{1\mathrm{L}}(\mathbf{k})\right]=-\frac{2g_k^2(N_c^2-1)}{\pi^3cV_{F,k}N_cN_f}\log\left(\frac{V_{F,k}}{c}\right)\bar{\Delta}(\vec{k};v_k)\log\left(\frac{\Lambda}{|\bar{\Delta}(\vec{k};v_k)|}\right)+reg.,\tag{A.14}$$

where $reg.$ represents terms that are regular in the large $\Lambda/\bar{\Delta}$ limit. Using Eqs. (A.13) and (A.14), we can write the real part of the one-loop fermion self-energy as

$$\mathrm{Re}\left[\Sigma_1^{1\mathrm{L}}(\mathbf{k})\right]=-\frac{2g_k^2(N_c^2-1)}{\pi^3V_{F,k}N_cN_f}\log\left(\frac{V_{F,k}}{c}\right)e_4[\vec{k};v_k]\log\left(\frac{\Lambda}{\mathscr{H}_1(k_0,ce_4[\vec{k};v_k])}\right)+reg..\tag{A.15}$$

Here, $\mathscr{H}_1(x,y)$ is a crossover function that satisfies $\mathscr{H}_1(x,y)\sim\max(|x|,|y|)$ if $|x|\gg|y|$ or $|y|\gg|x|$. Counter terms that remove IR divergent parts of $\left.\frac{\partial\mathrm{Re}\left[\Sigma_1^{1\mathrm{L}}(\mathbf{k})\right]}{\partial k_x}\right|_{\mathbf{k}=(\mu,k_x,-v_kk_x)}$ and $\left.\frac{\partial\mathrm{Re}\left[\Sigma_1^{1\mathrm{L}}(\mathbf{k})\right]}{\partial k_y}\right|_{\mathbf{k}=(\mu,k_x,-v_kk_x)}$ in the small μ limit are given by

$$A^{(2);1\mathrm{L}}(k)=\frac{2g_k^2(N_c^2-1)}{\pi^3V_{F,k}^2N_cN_f}\log\left(\frac{V_{F,k}}{c}\right)\log\left(\frac{\Lambda}{\mathscr{H}_1(\mu,2v_kck)}\right)+A_{reg}^{(2);1\mathrm{L}}(k),\tag{A.16}$$

$$A^{(3);1\mathrm{L}}(k)=-\frac{2g_k^2(N_c^2-1)}{\pi^3V_{F,k}^2N_cN_f}\log\left(\frac{V_{F,k}}{c}\right)\log\left(\frac{\Lambda}{\mathscr{H}_1(\mu,2v_kck)}\right)+A_{reg}^{(3);1\mathrm{L}}(k),\tag{A.17}$$

where $A_{reg}^{(2);1\mathrm{L}}(k)$ and $A_{reg}^{(3);1\mathrm{L}}(k)$ represent terms that are regular in the large $\frac{\Lambda}{\mathscr{H}_2(\mu,2v_kck)}$ limit.

A.1.2 Two-loop

The two-loop fermion self-energy reads

$$\Sigma_N^{2\mathrm{L}}(\mathbf{k}) = \frac{4(g_k^{(N)})^2(g_k^{(\bar{N})})^2(N_c^2-1)}{N_c^2 N_f^2}\int \mathrm{d}\mathbf{q}\int \mathrm{d}\mathbf{p} D(\mathbf{p})D(\mathbf{q})G_{\bar{N}}(\mathbf{k}+\mathbf{p})G_N(\mathbf{k}+\mathbf{p}+\mathbf{q})G_{\bar{N}}(\mathbf{k}+\mathbf{q}). \quad (A.18)$$

With the shifts $q_y \to q_y + v_k q_x + e_4[\vec{k}; v_k]$ and $p_y \to p_y + v_k p_x + e_4[\vec{k}; v_k]$, Eq. (A.18) for $N = 1$ is written as

$$\begin{aligned}\Sigma_1^{2\mathrm{L}}(\mathbf{k}) = \frac{4g_k^4(N_c^2-1)}{N_c^2N_f^2}\int \mathrm{d}\mathbf{q}\int \mathrm{d}\mathbf{p}\Bigg\{ &\frac{1}{|q_0|+c|q_x|+|cq_y+v_kcq_x+\bar{\Delta}(\vec{k};v_k)|}\\ &\times\frac{1}{|p_0|+c|p_x|+|cp_y+v_kcp_x+\bar{\Delta}(\vec{k};v_k)|}\Bigg[\frac{1}{i(k_0+p_0)-V_{F,k}p_y}\frac{1}{i(k_0+q_0)-V_{F,k}q_y}\\ &\times\frac{1}{i(k_0+p_0+q_0)+(V_{F,k}p_y+V_{F,k}q_y+V_{F,k}\gamma(\vec{k};v_k)+2v_kV_{F,k}(p_x+q_x))}\Bigg]\Bigg\},\end{aligned} \quad (A.19)$$

where $\bar{\Delta}(\vec{k};v_k) = ce_4[\vec{k};v_k]$ and $\gamma(\vec{k};v_k) = 2e_4[\vec{k};v_k] + e_1[\vec{k};v_k]$. In the small v limit, the cq_y and cp_y terms can be dropped in the boson propagators as the integrations of q_y and p_y are convergent without them. Furthermore, we drop v_kcq_x and v_kcp_x as the IR singular term is unaffected by them to the leading order in v. With the rescaling of internal momentum as $(p_x, q_x) \to (p_x/c, q_x/c)$, the integration over p_y and q_y yields

$$\begin{aligned}&\Sigma_1^{2\mathrm{L}}(\mathbf{k})\\ &= -\frac{4g_k^4(N_c^2-1)}{c^2V_{F,k}^2N_c^2N_f^2}\int_{\mathbb{R}}\frac{\mathrm{d}q_0}{(2\pi)}\int_{\mathbb{R}}\frac{\mathrm{d}p_0}{(2\pi)}\int_{\mathbb{R}}\frac{\mathrm{d}q_x}{(2\pi)}\int_{\mathbb{R}}\frac{\mathrm{d}p_x}{(2\pi)}\Bigg\{\frac{[\Theta(p_0+2q_0+2k_0)-\Theta(-k_0-p_0)]}{|q_0|+|q_x|+|\bar{\Delta}(\vec{k};v_k)|}\\ &\times\frac{[\Theta(p_0+q_0+k_0)-\Theta(-k_0-q_0)]}{|p_0|+|p_x|+|\bar{\Delta}(\vec{k};v_k)|}\frac{[2\widetilde{w}_k(p_x+q_x)+\widetilde{\gamma}(\vec{k};v_k)]-i\,[2(p_0+q_0)+3k_0]}{(3k_0+2p_0+2q_0)^2+[2\widetilde{w}_k(p_x+q_x)+\widetilde{\gamma}(\vec{k};v_k)]^2}\Bigg\},\end{aligned} \quad (A.20)$$

where $w_k = v_k/c$, $\widetilde{w}_k = V_{F,k}w_k$, $\widetilde{\gamma}(\vec{k},v_k) = V_{F,k}\gamma(\vec{k};v_k)$ and $\Theta(x)$ denotes the Heaviside function. Since only the real part of the two-loop self-energy is of the same order as the one-loop self-energy[182], we only compute the real part of the self-energy.

The real part of the two-loop fermion self-energy reads

$$\begin{aligned}&\mathrm{Re}\left[\Sigma_1^{2\mathrm{L}}(\mathbf{k})\right]\\ &= -\frac{4g_k^4(N_c^2-1)}{c^2V_{F,k}^2N_c^2N_f^2}\int_{\mathbb{R}}\frac{\mathrm{d}q_0}{(2\pi)}\int_{\mathbb{R}}\frac{\mathrm{d}p_0}{(2\pi)}\int_{\mathbb{R}}\frac{\mathrm{d}q_x}{(2\pi)}\int_{\mathbb{R}}\frac{\mathrm{d}p_x}{(2\pi)}\Bigg\{\frac{[\Theta(p_0+2q_0+2k_0)-\Theta(-k_0-p_0)]}{|q_0|+|q_x|+|\bar{\Delta}(\vec{k};v_k)|}\\ &\times\frac{[\Theta(p_0+q_0+k_0)-\Theta(-k_0-q_0)]}{|p_0|+|p_x|+|\bar{\Delta}(\vec{k};v_k)|}\frac{[2\widetilde{w}_k(p_x+q_x)+\widetilde{\gamma}(\vec{k};v_k)]}{(3k_0+2p_0+2q_0)^2+[2\widetilde{w}_k(p_x+q_x)+\widetilde{\gamma}(\vec{k};v_k)]^2}\Bigg\}.\end{aligned} \quad (A.21)$$

Let us make a change of variables as $a=(p_x+q_x)/2$ and $b=(p_x-q_x)/2$. The integration over b gives

$$\begin{aligned}
&\mathrm{Re}\left[\Sigma_1^{2\mathrm{L}}(\mathbf{k})\right] \\
&=-\frac{4g_k^4(N_c^2-1)}{\pi c^2 V_{F,k}^2 N_c^2 N_f^2}\int_{\mathbb{R}}\frac{\mathrm{d}q_0}{(2\pi)}\int_{\mathbb{R}}\frac{\mathrm{d}p_0}{(2\pi)}\int_{\mathbb{R}}\frac{\mathrm{d}a}{(2\pi)}\left\{\frac{\Theta(k_0;p_0,q_0)[4\widetilde{w}_k a+\widetilde{\gamma}(\vec{k};v_k)]}{(3k_0+2p_0+2q_0)^2+[4\widetilde{w}_k a+\widetilde{\gamma}(\vec{k};v_k)]^2}\right. \\
&\times\left(\frac{\log\left(\frac{2|a|+|p_0|+|\bar{\Delta}(\vec{k};v_k)|}{|q_0|+|\bar{\Delta}(\vec{k};v_k)|}\right)}{2|a|+|p_0|-|q_0|}+\frac{\log\left(\frac{2|a|+|q_0|+|\bar{\Delta}(\vec{k};v_k)|}{|p_0|+|\bar{\Delta}(\vec{k};v_k)|}\right)}{2|a|+|q_0|-|p_0|}\right. \\
&\left.\left.+\frac{\log\left(\frac{(2|a|+|p_0|+|\bar{\Delta}(\vec{k};v_k)|)(2|a|+|q_0|+|\bar{\Delta}(\vec{k};v_k)|)}{(|p_0|+|\bar{\Delta}(\vec{k};v_k)|)(|q_0|+|\bar{\Delta}(\vec{k};v_k)|)}\right)}{2|a|+|p_0|+|q_0|+2|\bar{\Delta}(\vec{k};v_k)|}\right)\right\},
\end{aligned}\tag{A.22}$$

where $\Theta(k_0;p_0,q_0)=[\Theta(p_0+2q_0+2k_0)-\Theta(-k_0-p_0)]\,[\Theta(p_0+q_0+k_0)-\Theta(-k_0-q_0)]$. Besides k_0, $\widetilde{\gamma}(\vec{k};v_k)$ and $\bar{\Delta}(\vec{k};v_k)$ enter as additional energy scales associated with the external momentum $\vec{k}$. If the external fermion is close to the Fermi surface, $|\widetilde{\gamma}(\vec{k};v_k)|\sim 4V_{F,k}v_k|k_x|\gg|\bar{\Delta}(\vec{k};v_k)|\sim 2v_k c|k_x|$. Therefore, the crossover is determined by the competition between k_0 and $\widetilde{\gamma}(\vec{k};v_k)$. In the $|\widetilde{\gamma}(\vec{k};v_k)/k_0|\ll 1$ limit, the integration over a, q_0 and p_0 gives

$$\mathrm{Re}\left[\Sigma_1^{2\mathrm{L}}(\mathbf{k})\right]=-\frac{4g_k^4(N_c^2-1)\widetilde{\gamma}(\vec{k},v_k)}{\pi c^2 V_{F,k}^2 N_c^2 N_f^2}\frac{\log^2\widetilde{w}_k}{8\pi^3}\log\frac{\Lambda}{k_0}.\tag{A.23}$$

In the opposite limit with $|k_0/\widetilde{\gamma}(\vec{k},v_k)|\ll 1$, the IR divergence is cutoff by $\widetilde{\gamma}(\vec{k},v_k)$ instead of k_0,

$$\mathrm{Re}\left[\Sigma_1^{2\mathrm{L}}(\mathbf{k})\right]=-\frac{4g_k^4(N_c^2-1)\widetilde{\gamma}(\vec{k},v_k)}{\pi c^2 V_{F,k}^2 N_c^2 N_f^2}\frac{\log^2\widetilde{w}_k}{8\pi^3}\log\frac{\Lambda}{\widetilde{\gamma}(\vec{k},v_k)}.\tag{A.24}$$

Collecting the results of Eq. (A.23) and Eq. (A.24), we conclude that the logarithmically divergent contribution to the real part of the two-loop fermion self-energy is given by

$$\begin{aligned}
\mathrm{Re}\left[\Sigma_1^{2\mathrm{L}}(\mathbf{k})\right]=&-\frac{g_k^4(N_c^2-1)}{2\pi^4 c^2 V_{F,k}^2 N_c^2 N_f^2}V_{F,k}\left[e_1[\vec{k};v_k]+2e_4[\vec{k};v_k]\right] \\
&\times\log^2\left(\frac{V_{F,k}v_k}{c}\right)\log\left(\frac{\Lambda}{\mathscr{H}_1(k_0,V_{F,k}(2e_4[\vec{k},v_k]+e_1[\vec{k},v_k]))}\right).
\end{aligned}\tag{A.25}$$

The two-loop counterterms are given by

$$A^{(2);2L}(k)=\frac{3g_k^4(N_c^2-1)}{2\pi^4 c^2 V_{F,k}^2 N_c^2 N_f^2}\log^2\left(\frac{V_{F,k}v_k}{c}\right)\log\left(\frac{\Lambda}{\mathscr{H}_1(\mu,4V_{F,k}v_k k)}\right)+A_{reg}^{(2);2L}(k),\tag{A.26}$$

$$A^{(3);2L}(k)=-\frac{g_k^4(N_c^2-1)}{2\pi^4 c^2 V_{F,k}^2 N_c^2 N_f^2}\log^2\left(\frac{V_{F,k}v_k}{c}\right)\log\left(\frac{\Lambda}{\mathscr{H}_1(\mu,4V_{F,k}v_k k)}\right)+A_{reg}^{(3);2L}(k),\tag{A.27}$$

where $A_{reg}^{(2);2L}(k)$ and $A_{reg}^{(3);2L}(k)$ represent the terms that are regular in the large $\frac{\Lambda}{\mathscr{H}_2(\mu,4V_{F,k}v_k k)}$ limit.

A.2 Fermion-boson vertex correction

The one-loop vertex function is given by:

$$\Gamma_N^{(2,1),1\mathrm{L}}(\mathbf{k}',\mathbf{k})=-\frac{2}{N_c N_f^{\frac{3}{2}}}g_{k'}^{(N)}g_{k,k'}^{(\bar{N})}g_k^{(N)}\int\mathrm{d}\mathbf{q}D(\mathbf{q})G_{\bar{N}}(\mathbf{k}'+\mathbf{q})G_N(\mathbf{k}+\mathbf{q}).\tag{A.28}$$

Without loss of generality, we consider the contribution to interaction vertex for the $N = 1$ hot spot,

$$\begin{aligned}
&\Gamma_1^{(2,1),1\mathrm{L}}(\mathbf{k}',\mathbf{k}) \\
&= -\frac{2g_k g_{k'} g_{k',k}}{N_c N_f^{\frac{3}{2}}} \int \frac{\mathrm{d}q_0}{2\pi}\frac{\mathrm{d}q_x}{2\pi}\frac{\mathrm{d}q_y}{2\pi} \frac{1}{|q_0|+|cq_x|+|cq_y|} \frac{1}{i(k'_0+q_0)+V_{F,k'}(e_4[\vec{k}',v_{k'}]+v_{k'}q_x-q_y)} \\
&\times \frac{1}{i(k_0+q_0)+V_{F,k}(e_1[\vec{k},v_k]+v_k q_x+q_y)}.
\end{aligned} \tag{A.29}$$

Let us integrate over q_y using a contour integration. To do this, we use $|cq_y| = c\sqrt{q_y^2+0^+}$ with the branch cuts located at $|Im\ q_y| > 0^+$. Across the branch cut, the square root is discontinuous : $c\sqrt{q_y^2+0^+} = c\,\mathrm{sgn}(\mathrm{Re}(q_y))q_y$. To ensure a symmetric expression, we close the contours in both the upper and lower-half planes and taking the average of these two expressions. In each case, we will consider a semicircular contour with a dip along the imaginary axis that avoids the branch cuts. The contour integral of Eq. (A.29) results in

$$\begin{aligned}
&\Gamma_1^{(2,1),1\mathrm{L}}(\mathbf{k}',\mathbf{k}) = \\
&\frac{ig_k g_{k'} g_{k',k}}{N_c N_f^{\frac{3}{2}} c(V_{F,k}+V_{F,k'})} \int \frac{\mathrm{d}q_0}{2\pi}\frac{\mathrm{d}q_x}{2\pi} \frac{1}{i(\mathscr{M}+q_0)+\mathscr{R}_{k',k}/2+\mathscr{W}q_x} \left(\frac{\mathrm{sgn}(k'_0+q_0)}{|q_0|+|q_x|+c|e_4(\vec{k}',v_{k'})|} \right. \\
&\left. + \frac{\mathrm{sgn}(k_0+q_0)}{|q_0|+|q_x|+c|e_1(\vec{k},v_k)|} \right) \\
&- \frac{2g_k g_{k'} g_{k',k} c}{N_c N_f^{\frac{3}{2}}} \int \frac{\mathrm{d}q_0}{2\pi}\frac{\mathrm{d}q_x}{2\pi} \int_{-\infty}^{\infty} \frac{\mathrm{d}x}{2\pi} \frac{|x|}{c^2x^2+(|q_0|+|cq_x|)^2} \\
&\times \frac{1}{i(k'_0+q_0)+V_{F,k'}(e_4(k',v_{k'})+v_{k'}q_x-ix)} \frac{1}{i(k_0+q_0)+V_{F,k}(e_1(k,v_k)+v_k q_x+ix)},
\end{aligned} \tag{A.30}$$

where $\mathscr{M} = (V_{F,k'}^{-1}k'_0 + V_{F,k}^{-1}k_0)/(V_{F,k'}^{-1}+V_{F,k}^{-1})$, $\mathscr{R}_{k',k} = 2(e_4(\vec{k}',v_{k'})+e_1(\vec{k},v_k))/(V_{F,k'}^{-1}+V_{F,k}^{-1})$ and $\mathscr{W} = (v_k+v_{k'})/(cV_{F,k'}^{-1}+cV_{F,k}^{-1})$. The first term is the contribution from the residues of the poles of the fermion propagators. The second term comes from the branch cut. In the small v limit, the first contribution dominates. The remaining integrand over q_0 and q_x leads to

$$\begin{aligned}
\Gamma_1^{(2,1),1\mathrm{L}}(\mathbf{k}',\mathbf{k})\Big|_{\substack{\mathbf{k}'=(2\mu,k'_x,-v_{k'}k'_x)\\ \mathbf{k}=(\mu,k_x,v_k k_x)}} &= \frac{g_k g_{k'} g_{k',k}}{\pi^2 c(V_{F,k}+V_{F,k'})N_c N_f^{\frac{3}{2}}} \log\left(\frac{c(V_{F,k}^{-1}+V_{F,k'}^{-1})}{v_k+v_{k'}}\right) \\
&\times \left(\log\left(\frac{\Lambda}{\mathscr{H}_2\left[\mu, \frac{4v_{k'}k'+4v_k k}{V_{F,k'}^{-1}+V_{F,k}^{-1}}, 2cv_k k\right]} \right) + \log\left(\frac{\Lambda}{\mathscr{H}_2\left[\mu, \frac{4v_{k'}k'+4v_k k}{V_{F,k'}^{-1}+V_{F,k}^{-1}}, 2cv_{k'} k'\right]} \right) \right)
\end{aligned} \tag{A.31}$$

to the leading order in c. $\mathscr{H}_2(x,y,z)$ is a crossover function that satisfies $\mathscr{H}_2(x,y,z) \sim \max(|x|,|y|,|z|)$ if $|x| \gg |y|,|z|$, $|y| \gg |x|,|z|$ or $|z| \gg |x|,|y|$[1]. Because $c \ll 1$, $\left|\frac{4v_{k'}k'+4v_k k}{V_{F,k'}^{-1}+V_{F,k}^{-1}}\right| \gg 2cv_k|k|, 2cv_{k'}|k'|$ for most k and k'. $\left|\frac{4v_{k'}k'+4v_k k}{V_{F,k'}^{-1}+V_{F,k}^{-1}}\right|$ becomes smaller than $2cv_k|k|$ or $2cv_{k'}|k'|$ only in a small wedge near

[1]For the future convenience, $\mathscr{R}_{k',k}$ is chosen as the crossover scale although $\mathscr{R}_{k',k}/2$ is what appears in Eq. (A.30). This is a freedom associated with the choice of the crossover function that only affects the finite part of the counter term.

$v_{k'}k' + v_k k = 0$. Since $|v_{k'}k'| \approx |v_k k|$ within the wedge, we can combine the two crossover functions into one as

$$\begin{aligned}
&\log\left(\frac{\Lambda}{\mathscr{H}_2\left[\mu, \frac{4v_{k'}k'+4v_k k}{V_{F,k'}^{-1}+V_{F,k}^{-1}}, 2cv_k k\right]}\right) + \log\left(\frac{\Lambda}{\mathscr{H}_2\left[\mu, \frac{4v_{k'}k'+4v_k k}{V_{F,k'}^{-1}+V_{F,k}^{-1}}, 2cv_{k'}k'\right]}\right) \\
&= 2\log\left(\frac{\Lambda}{\mathscr{H}_3\left[\mu, \frac{4v_{k'}k'+4v_k k}{V_{F,k'}^{-1}+V_{F,k}^{-1}}, 2cv_k k, 2cv_{k'}k'\right]}\right),
\end{aligned} \tag{A.32}$$

where $\mathscr{H}_3(w,x,y,z)$ is a crossover function that satisfies $\mathscr{H}_3(w,x,y,z) \sim \max(|w|,|x|,|y|,|z|)$. Therefore, we write the counter term as

$$\begin{aligned}
A^{(4)}(k',k) = &-\frac{2g_k g_{k'}}{\pi^2 c(V_{F,k}+V_{F,k'})N_c N_f} \\
&\times \log\left(\frac{c(V_{F,k}^{-1}+V_{F,k'}^{-1})}{v_k + v_{k'}}\right)\log\left(\frac{\Lambda}{\mathscr{H}_3\left[\mu, \frac{4v_{k'}k'+4v_k k}{V_{F,k'}^{-1}+V_{F,k}^{-1}}, 2cv_k k, 2cv_{k'}k'\right]}\right).
\end{aligned} \tag{A.33}$$

Appendix B

Quantum corrections for the four-point function

In this appendix, we compute the quantum corrections for the four-fermion vertex. We denote the fermionic four-point vertex function evaluated at external momenta on the Fermi surface as

$$\mathbf{\Gamma}^{\left(\begin{smallmatrix}N_1 & N_2\\ N_4 & N_3\end{smallmatrix}\right);\left(\begin{smallmatrix}\sigma_1 & \sigma_2\\ \sigma_4 & \sigma_3\end{smallmatrix}\right)}_{\left(\begin{smallmatrix}k_1 & k_2\\ k_4 & k_3\end{smallmatrix}\right)} \equiv \mathbf{\Gamma}^{\left(\begin{smallmatrix}N_1 & N_2\\ N_4 & N_3\end{smallmatrix}\right);\left(\begin{smallmatrix}\sigma_1 & \sigma_2\\ \sigma_4 & \sigma_3\end{smallmatrix}\right)}\left(\begin{smallmatrix}\mathbf{k}_1 & \mathbf{k}_2\\ \mathbf{k}_4 & \mathbf{k}_3\end{smallmatrix}\right)\Big|_{\mathbf{k}_i=\mathbf{k}_i^*}. \tag{B.1}$$

Here the external frequencies are chosen as in Eq. (2.31). k_i labels the component of $\vec{k}_i$ that is parallel to the Fermi surface near hot spot N_i in the small v limit. The other component of the spatial momentum is chosen so that external electrons are on the Fermi surface.

B.1 Generation of the primary couplings from spin fluctuations

We first consider the quantum corrections through which the primary four-fermion coupling are generated.

B.1.1 Group 1

In group 1, the diagram in Fig. 2.7a exhibits an IR singularity only when all external fermions are at the hot spots. In our minimal subtraction scheme, we don't need to add a counter term for it. Therefore, we focus on the diagram in Fig. 2.7b. Its contribution to the quantum effective action is given by Eq. (2.72),

$$\mathbf{\Gamma}^{\left(\begin{smallmatrix}1 & 1\\ 1 & 1\end{smallmatrix}\right);\left(\begin{smallmatrix}\sigma_1 & \sigma_2\\ \sigma_4 & \sigma_3\end{smallmatrix}\right)}_{(0)PH}\left(\begin{smallmatrix}\mathbf{k+l} & \mathbf{p-l}\\ \mathbf{k} & \mathbf{p}\end{smallmatrix}\right) = -\frac{\mathsf{T}^{\beta\sigma_2}_{\sigma_4\alpha}\mathsf{T}^{\sigma_1\alpha}_{\beta\sigma_3}}{2N_f^2}\int \mathrm{d}\mathbf{q}\frac{g^{(1)}_{k+l,k+q}g^{(4)}_{k+q,k}g^{(1)}_{p-l,p-l+q}g^{(4)}_{p-l+q,p}}{(|q_0|+c|q_x|+c|q_y|)\,(|q_0-l_0|+c|q_x-l_x|+c|q_y-l_y|)}\times$$
$$\frac{1}{i(k_0+q_0)+V^{(4)}_{F,k+q}e_4[\vec{k}+\vec{q};v^{(4)}_{k+q}]}\,\frac{1}{i(p_0-l_0+q_0)+V^{(4)}_{F,p-l+q}e_4[\vec{p}-\vec{l}+\vec{q};v^{(4)}_{p-l+q}]}. \tag{B.2}$$

Since it is possible to put all external fermions on the Fermi surface for $\vec{k}+\vec{l}=\vec{p}$, we focus on the quantum correction in the vicinity of the plane with $\vec{k}+\vec{l}=\vec{p}$. Near the plane, we can replace $k+l$

with p inside coupling functions. Shifting $q_y \to q_y + v_{k+q}q_x + \Delta_{1,\{1,1\}}/c$, we obtain

$$\mathbf{\Gamma}^{\left(\begin{smallmatrix}1&1\\1&1\end{smallmatrix}\right);\left(\begin{smallmatrix}\sigma_1&\sigma_2\\\sigma_4&\sigma_3\end{smallmatrix}\right)}_{(0)PH}\left(\begin{smallmatrix}\mathbf{k+l}&\mathbf{p-l}\\\mathbf{k}&\mathbf{p}\end{smallmatrix}\right) = -\frac{\mathsf{T}^{\beta\sigma_2}_{\sigma_4\alpha}\mathsf{T}^{\sigma_1\alpha}_{\beta\sigma_3}}{2N_f^2}\int\frac{\mathrm{d}\mathbf{q}}{V^2_{F,k+q}}\frac{g^2_{k+l,k+q}g^2_{k+q,k}}{\left(|q_0|+c|q_x|+c|q_y+v_{k+q}q_x+\Delta_{1,\{1,1\}}/c|\right)}\times$$
$$\frac{1}{\left(|q_0-l_0|+c|q_x-l_x|+c|q_y-l_y+v_{k+q}q_x+\Delta_{1,\{1,1\}}/c|\right)}\times$$
$$\frac{1}{i(k_0+q_0)/V_{F,k+q}-q_y+\Delta_{2,\{1,1\}}}\,\frac{1}{i(p_0-l_0+q_0)/V_{F,k+q}-q_y-\Delta_{2,\{1,1\}}}\,, \tag{B.3}$$

where $\Delta_{1,\{1,1\}} \equiv \Delta_{1,\{1,1\}}(q;k,p-l;v) = c(e_4[\vec{k};v^{(4)}_{k+q}]+e_4[\vec{p}-\vec{l};v^{(4)}_{p-l+q}])/2$ and $\Delta_{2,\{1,1\}} \equiv \Delta_{2,\{1,1\}}(q;k,p-l;v) = (e_4[\vec{k};v^{(4)}_{k+q}]-e_4[\vec{p}-\vec{l};v^{(4)}_{p-l+q}])/2$. We can drop cq_y from the two boson propagators in the small v limit because the integration is convergent without it. Using the RG condition for the frequencies $(k_0=\mu,\ p_0=\mu,\ l_0=2\mu)$ and doing the q_y integration, we obtain

$$\mathbf{\Gamma}^{\left(\begin{smallmatrix}1&1\\1&1\end{smallmatrix}\right);\left(\begin{smallmatrix}\sigma_1&\sigma_2\\\sigma_4&\sigma_3\end{smallmatrix}\right)}_{(0)PH;\left(\begin{smallmatrix}k+l&p-l\\k&p\end{smallmatrix}\right)} = -\frac{\mathsf{T}^{\beta\sigma_2}_{\sigma_4\alpha}\mathsf{T}^{\sigma_1\alpha}_{\beta\sigma_3}}{2N_f^2}\int\frac{\mathrm{d}q_0\mathrm{d}q_x}{8\pi^2V_{F,k+q}}\frac{g^2_{k+l,k+q}g^2_{k+q,k}}{\left(|q_0|+c|q_x|+c|v_{k+q}q_x+\Delta_{1,\{1,1\}}/c|\right)}\times$$
$$\frac{1}{\left(|q_0-2\mu|+c|q_x-l_x|+c|-l_y+v_{k+q}q_x+\Delta_{1,\{1,1\}}/c|\right)}\,\frac{i(\mathrm{sgn}(q_0+\mu)-\mathrm{sgn}(q_0-\mu))}{2V_{k+q}\Delta_{2,\{1,1\}}+2i\mu}\,. \tag{B.4}$$

We now construct a local counter term for this quantum correction. There are two crucial conditions that counter terms must satisfy : 1) counter terms must remove the IR divergence of quantum corrections in the small μ limit, and 2) counter terms should be analytic in external momenta as they are parts of the local action. Eq. (B.4) can not be directly used for the counter term because it is a non-analytic function of external momentum. We can construct analytic counter terms by making the momentum dependence smooth around $k=0$ and $p=0$ with energy scale μ. This smearing can be implemented by replacing

$$|x|_\mu \equiv \sqrt{x^2+\mu^2} \tag{B.5}$$

for momentum x. [1]. The modification only introduces a finite correction. The counter term can be further simplified by replacing $|q_0|$ and $|q_0-2\mu|$ with μ inside the boson propagators in Eq. (B.4). The latter procedure only affects the finite part of the quantum correction because q_0-integration is bounded by $-\mu$ and μ. The resulting counter term at energy scale μ is written as

$$\tilde{\mathbf{\Gamma}}^{\left(\begin{smallmatrix}1&1\\1&1\end{smallmatrix}\right);\left(\begin{smallmatrix}\sigma_1&\sigma_2\\\sigma_4&\sigma_3\end{smallmatrix}\right)}_{CT;(0)PH;\left(\begin{smallmatrix}k+l&p-l\\k&p\end{smallmatrix}\right)} = \frac{\mathsf{T}^{\beta\sigma_2}_{\sigma_4\alpha}\mathsf{T}^{\sigma_1\alpha}_{\beta\sigma_3}}{2N_f^2}\int\frac{\mathrm{d}q_0\mathrm{d}q_x}{8\pi^2V_{F,k+q}}\frac{g^2_{k+l,k+q}g^2_{k+q,k}}{\left(\mu+c|q_x|_\mu+c|v_{k+q}q_x+\Delta_{1,\{1,1\}}/c|_\mu\right)}\times$$
$$\frac{1}{\left(\mu+c|q_x-l_x|_\mu+c|-l_y+v_{k+q}q_x+\Delta_{1,\{1,1\}}/c|_\mu\right)}\,\frac{i(\mathrm{sgn}(q_0+\mu)-\mathrm{sgn}(q_0-\mu))}{2V_{k+q}\Delta_{2,\{1,1\}}+2i\mu}\,. \tag{B.6}$$

As expected, the counter term removes the IR singularity of the quantum correction in the plane $\vec{p}=\vec{k}+\vec{l}$[2]. The $\log\mu$ derivative of the counter term that determines the beta functional is given by

[1] Such smearing naturally would arise in the exact boson propagator evaluated at a finite frequency μ.

[2] The sum of the quantum correction and the counter term in the region away from the hot-spot $(|k|,|p| \gg \frac{\mu}{vc})$ is given by

$$\mathbf{\Gamma}^{\left(\begin{smallmatrix}1&1\\1&1\end{smallmatrix}\right);\left(\begin{smallmatrix}\sigma_1&\sigma_2\\\sigma_4&\sigma_3\end{smallmatrix}\right)}_{(0)PH;\left(\begin{smallmatrix}p&k\\k&p\end{smallmatrix}\right)} + \tilde{\mathbf{\Gamma}}^{\left(\begin{smallmatrix}1&1\\1&1\end{smallmatrix}\right);\left(\begin{smallmatrix}\sigma_1&\sigma_2\\\sigma_4&\sigma_3\end{smallmatrix}\right)}_{CT;(0)PH;\left(\begin{smallmatrix}p&k\\k&p\end{smallmatrix}\right)} \sim \frac{\mathsf{T}^{\beta\sigma_2}_{\sigma_4\alpha}\mathsf{T}^{\sigma_1\alpha}_{\beta\sigma_3}}{2N_f^2}\frac{1}{8\pi^2}\frac{g^2_{p,k}g^2_{k,k}}{cV_{F,k}}\left[-\frac{2\mu\log\left(\frac{(c|k_x-p_x|+cv|k_x|)(c|k_x-p_x|+cv|p_x|)}{c^2v^2|k_x||p_x|}\right)}{c^2(|k_x-p_x|+v|k_x|+v|p_x|)^2}\right.$$
$$\left.-\frac{2\mu(|k_x|+|p_x|)}{c^2v|k_x||p_x|(|k_x-p_x|+v|k_x|+v|p_x|)}\right] \tag{B.7}$$

In order to arrive at the above expression, we use momentum independent nesting angle.

$$
\begin{aligned}
&4\mu\frac{\partial}{\partial\log\mu}\tilde{\mathbf{\Gamma}}^{\left(\begin{smallmatrix}1&1\\1&1\end{smallmatrix}\right);\left(\begin{smallmatrix}\sigma_1&\sigma_2\\\sigma_4&\sigma_3\end{smallmatrix}\right)}_{CT;(0)PH;\left(\begin{smallmatrix}k+l&p-l\\k&p\end{smallmatrix}\right)}\\
&=-\frac{\mathsf{T}^{\beta\sigma_2}_{\sigma_4\alpha}\mathsf{T}^{\sigma_1\alpha}_{\beta\sigma_3}}{\pi N_f^2}\int\frac{\mathrm{d}q_x}{2\pi\mu V_{F,k+q}}\,\frac{i\mu}{i\mu+V_{F,k+q}\Delta_{2,\{1,1\}}}\Bigg[-\frac{V_{F,k+q}\Delta_{2,\{1,1\}}}{(i\mu+V_{F,k+q}\Delta_{2,\{1,1\}})}\\
&\times\frac{g^2_{k+q,k}\;\mu}{\left(\mu+c|q_x|_\mu+c|v_{k+q}q_x+\Delta_{1,\{1,1\}}/c|_\mu\right)}\frac{g^2_{k+l,k+q}\;\mu}{\left(\mu+c|q_x-l_x|_\mu+c|-l_y+v_{k+q}q_x+\Delta_{1,\{1,1\}}/c|_\mu\right)}\\
&+\frac{g^2_{k+q,k}\;\mu}{\left(\mu+c|q_x|_\mu+c|v_{k+q}q_x+\Delta_{1,\{1,1\}}/c|_\mu\right)}\frac{g^2_{k+l,k+q}\;\mu^2}{\left(\mu+c|q_x-l_x|_\mu+c|-l_y+v_{k+q}q_x+\Delta_{1,\{1,1\}}/c|_\mu\right)^2}\\
&+\frac{g^2_{k+q,k}\;\mu^2}{\left(\mu+c|q_x|_\mu+c|v_{k+q}q_x+\Delta_{1,\{1,1\}}/c|_\mu\right)^2}\frac{g^2_{k+l,k+q}\;\mu}{\left(\mu+c|q_x-l_x|_\mu+c|-l_y+v_{k+q}q_x+\Delta_{1,\{1,1\}}/c|_\mu\right)}\Bigg].
\end{aligned}
\tag{B.8}
$$

In the plane with $\vec{p}=\vec{k}+\vec{l}$, we have $\Delta_{1,\{1,1\}}=ce_4[\vec{k};v^{(4)}_{k+q}]$ and $\Delta_{2,\{1,1\}}=0$. Denoting q_x, p_x and k_x as q, p and k, respectively, Eq. (B.8) is written as

$$
4\mu\frac{\partial}{\partial\log\mu}\tilde{\mathbf{\Gamma}}^{\left(\begin{smallmatrix}1&1\\1&1\end{smallmatrix}\right);\left(\begin{smallmatrix}\sigma_1&\sigma_2\\\sigma_4&\sigma_3\end{smallmatrix}\right)}_{CT;(0)PH;\left(\begin{smallmatrix}p&k\\k&p\end{smallmatrix}\right)}=-\frac{\mathsf{T}^{\beta\sigma_2}_{\sigma_4\alpha}\mathsf{T}^{\sigma_1\alpha}_{\beta\sigma_3}}{\pi N_f^2}\int d\rho(q)\left[\mathsf{D}_\mu(q;k)\frac{\mathsf{D}_\mu(p;q)^2}{g^2_{p,q}}+\mathsf{D}_\mu(p;q)\frac{\mathsf{D}_\mu(q;k)^2}{g^2_{q,k}}\right],
\tag{B.9}
$$

where q is shifted to $q-k$ and

$$
\mathsf{D}_\mu(p;k)=g^2_{k,p}\frac{\mu}{\mu+c\left(|p-k|_\mu+|v_pp+v_kk|_\mu\right)},\qquad d\rho(q)=\frac{\mathrm{d}q}{2\pi\mu V_{F,q}}
\tag{B.10}
$$

represent the interaction mediated by gapless spin fluctuations and the phase space integration measure, respectively.

B.1.2 Group 2

In group 2, the diagram in Fig. 2.7a gives rise to a singular quantum correction to the couplings given by Eq. (2.79) in which the total momentum of the electron pair is zero. Eq. (2.71) for the quantum correction reads

$$
\begin{aligned}
\mathbf{\Gamma}^{\left(\begin{smallmatrix}1&5\\1&5\end{smallmatrix}\right);\left(\begin{smallmatrix}\sigma_1&\sigma_2\\\sigma_4&\sigma_3\end{smallmatrix}\right)}_{(0)PP}\left(\begin{smallmatrix}\mathbf{k+l}&\mathbf{p-l}\\\mathbf{k}&\mathbf{p}\end{smallmatrix}\right)=&-\frac{\mathsf{T}^{\sigma_1\sigma_2}_{\alpha\beta}\mathsf{T}^{\alpha\beta}_{\sigma_4\sigma_3}}{2N_f^2}\int\mathrm{d}\mathbf{q}\;\frac{1}{i(k_0+q_0)+V^{(4)}_{F,k+q}e_4[\vec{k}+\vec{q};v^{(4)}_{k+q}]}\;\frac{1}{i(p_0-q_0)+V^{(8)}_{F,p-q}e_8[\vec{p}-\vec{q};v^{(8)}_{p-q}]}\times\\
&\frac{g^{(4)}_{k+q,k}g^{(8)}_{p-q,p}g^{(1)}_{k+l,k+q}g^{(5)}_{p-l,p-q}}{\left(|q_0|+c|q_x|+c|q_y|\right)\left(|q_0-l_0|+c|q_x-l_x|+c|q_y-l_y|\right)}.
\end{aligned}
\tag{B.11}
$$

In the vicinity of the plane with $\vec{p}+\vec{k}=\vec{0}$, we can replace p_x with $-k_x$ in the coupling functions. Shifting $q_y\to q_y+v_{k+q}q_x+\Delta_{1,\{1,5\}}/c$, we obtain

$$
\begin{aligned}
\mathbf{\Gamma}^{\left(\begin{smallmatrix}1&5\\1&5\end{smallmatrix}\right);\left(\begin{smallmatrix}\sigma_1&\sigma_2\\\sigma_4&\sigma_3\end{smallmatrix}\right)}_{(0)PP}\left(\begin{smallmatrix}\mathbf{k+l}&\mathbf{p-l}\\\mathbf{k}&\mathbf{p}\end{smallmatrix}\right)=&-\frac{\mathsf{T}^{\sigma_1\sigma_2}_{\alpha\beta}\mathsf{T}^{\alpha\beta}_{\sigma_4\sigma_3}}{2N_f^2}\int\frac{\mathrm{d}\mathbf{q}}{V^2_{F,k+q}}\frac{g^2_{k+l,k+q}g^2_{k+q,k}}{\left(|q_0|+c|q_x|+c|q_y+v_{k+q}q_x+\Delta_{1,\{1,5\}}/c|\right)}\times\\
&\frac{1}{\left(|q_0-l_0|+c|q_x-l_x|+c|q_y-l_y+v_{k+q}q_x+\Delta_{1,\{1,5\}}/c|\right)}\times\\
&\frac{1}{i(k_0+q_0)/V_{F,k+q}-q_y+\Delta_{2,\{1,5\}}}\;\frac{1}{i(p_0-q_0)/V_{F,k+q}-q_y-\Delta_{2,\{1,5\}}},
\end{aligned}
\tag{B.12}
$$

where $\Delta_{1,\{1,5\}} \equiv \Delta_{1,\{1,5\}}(q;k,p;v) = c(e_4[\vec{k};v^{(4)}_{k+q}] + e_8[\vec{p};v^{(8)}_{p-q}])/2$ and $\Delta_{2,\{1,5\}} \equiv \Delta_{2,\{1,5\}}(q;k,p;v) = (e_4[\vec{k};v^{(4)}_{k+q}] - e_8[\vec{p};v^{(8)}_{p-q}])/2$. To the leading order in v, one can perform the q_y integration with dropping cq_y in the boson propagator to obtain

$$\mathbf{\Gamma}^{\left(\begin{smallmatrix}1&5\\1&5\end{smallmatrix}\right);\left(\begin{smallmatrix}\sigma_1&\sigma_2\\\sigma_4&\sigma_3\end{smallmatrix}\right)}_{(0)PP;\left(\begin{smallmatrix}k+l&p-l\\k&p\end{smallmatrix}\right)} = -\frac{\mathsf{T}^{\sigma_1\sigma_2}_{\alpha\beta}\mathsf{T}^{\alpha\beta}_{\sigma_4\sigma_3}}{2N_f^2}\int\frac{\mathrm{d}q_0\mathrm{d}q_x}{8\pi^2 V_{F,k+q}}\,\frac{\mathrm{sgn}(q_0+\mu)+\mathrm{sgn}(q_0-\mu)}{2(q_0-iV_{F,k+q}\Delta_{2,\{1,5\}})}\times$$
$$\frac{g^2_{k+q,k}g^2_{k+l,k+q}}{\left(|q_0|+c|q_x|+c|v_{k+q}q_x+\Delta_{1,\{1,5\}}/c|\right)\left(|q_0-2\mu|+c|q_x-l_x|+c|-l_y+v_{k+q}q_x+\Delta_{1,\{1,5\}}/c|\right)}. \tag{B.13}$$

Since the support of q_0-integration is $(-\infty,-\mu)\bigcup(\mu,\infty)$, the IR divergent part of the quantum correction is not affected by dropping 2μ from $|q_0-2\mu|$ in the second boson propagator. We further smear the non-analyticity in external momenta to write the counter term as

$$\tilde{\mathbf{\Gamma}}^{\left(\begin{smallmatrix}1&5\\1&5\end{smallmatrix}\right);\left(\begin{smallmatrix}\sigma_1&\sigma_2\\\sigma_4&\sigma_3\end{smallmatrix}\right)}_{CT;(0)PP;\left(\begin{smallmatrix}k+l&p-l\\k&p\end{smallmatrix}\right)} = \frac{\mathsf{T}^{\sigma_1\sigma_2}_{\alpha\beta}\mathsf{T}^{\alpha\beta}_{\sigma_4\sigma_3}}{2N_f^2}\int\frac{\mathrm{d}q_0\mathrm{d}q_x}{8\pi^2 V_{F,k+q}}\,\frac{\mathrm{sgn}(q_0+\mu)+\mathrm{sgn}(q_0-\mu)}{2(q_0-iV_{F,k+q}\Delta_{2,\{1,5\}})}\times$$
$$\frac{g^2_{k+q,k}g^2_{k+l,k+q}}{\left(|q_0|+c|q_x|_\mu+c|v_{k+q}q_x+\Delta_{1,\{1,5\}}/c|_\mu\right)\left(|q_0|+c|q_x-l_x|_\mu+c|-l_y+v_{k+q}q_x+\Delta_{1,\{1,5\}}/c|_\mu\right)}. \tag{B.14}$$

The counter term removes the IR singularity of the quantum correction in the $\vec{p}=-\vec{k}$ plane[3]. Integrating q_0 and taking the $\log\mu$ derivative of the counter term, we obtain

$$4\mu\frac{\partial}{\partial\log\mu}\tilde{\mathbf{\Gamma}}^{\left(\begin{smallmatrix}1&5\\1&5\end{smallmatrix}\right);\left(\begin{smallmatrix}\sigma_1&\sigma_2\\\sigma_4&\sigma_3\end{smallmatrix}\right)}_{CT;(0)PP;\left(\begin{smallmatrix}k+l&p-l\\k&p\end{smallmatrix}\right)} = -\frac{\mathsf{T}^{\sigma_1\sigma_2}_{\alpha\beta}\mathsf{T}^{\alpha\beta}_{\sigma_4\sigma_3}}{\pi N_f^2}\int\frac{\mathrm{d}q_x}{2\pi\mu V_{F,k+q}}\,\frac{\mu^2}{(\mu^2+V^2_{F,k+q}\Delta^2_{2,\{1,5\}})}\times$$
$$\frac{g^2_{k+q,k}\,\mu}{\left(\mu+c|q_x|_\mu+c|v_{k+q}q_x+\Delta_{1,\{1,5\}}/c|_\mu\right)}\,\frac{g^2_{k+l,k+q}\,\mu}{\left(\mu+c|q_x-l_x|_\mu+c|-l_y+v_{k+q}q_x+\Delta_{1,\{1,5\}}/c|_\mu\right)}. \tag{B.16}$$

Away from the plane with $\vec{p}+\vec{k}\neq 0$, $\Delta_{2,\{1,5\}}\neq 0$ and the counter term vanishes in the low-energy limit. Non-vanishing contribution to the beta functional arises only for $\Delta_{2,\{1,5\}}\ll\mu$. Within the space of IR singularity, Eq. (B.16) becomes

$$4\mu\frac{\partial}{\partial\log\mu}\tilde{\mathbf{\Gamma}}^{\left(\begin{smallmatrix}1&5\\1&5\end{smallmatrix}\right);\left(\begin{smallmatrix}\sigma_1&\sigma_2\\\sigma_4&\sigma_3\end{smallmatrix}\right)}_{CT;(0)PP;\left(\begin{smallmatrix}k+l&-k-l\\k&-k\end{smallmatrix}\right)} = -\frac{\mathsf{T}^{\sigma_1\sigma_2}_{\alpha\beta}\mathsf{T}^{\alpha\beta}_{\sigma_4\sigma_3}}{\pi N_f^2}\int\mathrm{d}\rho(q)\;\mathsf{D}_\mu(q;k)\mathsf{D}_\mu(k+l;q), \tag{B.17}$$

where $\mathsf{D}_\mu(p;k)$ and $d\rho(q)$ are defined in Eq. (B.10).

B.2 Linear mixing

Once the primary couplings are generated from the spin fluctuations, the secondary couplings are further generated through the linear mixing. When external fermions are on the Fermi surface, Eqs. (2.74) and (2.75) that describe mixing of the four-fermion couplings can be written as the sum of

[3]The sum of the quantum correction and the counter term in the region away from the hot-spot $\left(|k|,|k+l|\gg\frac{\mu}{vc}\right)$ is given by

$$\mathbf{\Gamma}^{\left(\begin{smallmatrix}1&5\\1&5\end{smallmatrix}\right);\left(\begin{smallmatrix}\sigma_1&\sigma_2\\\sigma_4&\sigma_3\end{smallmatrix}\right)}_{(0)PP;\left(\begin{smallmatrix}k+l&-k-l\\k&-k\end{smallmatrix}\right)} + \tilde{\mathbf{\Gamma}}^{\left(\begin{smallmatrix}1&5\\1&5\end{smallmatrix}\right);\left(\begin{smallmatrix}\sigma_1&\sigma_2\\\sigma_4&\sigma_3\end{smallmatrix}\right)}_{CT;(0)PP;\left(\begin{smallmatrix}k+l&-k-l\\k&-k\end{smallmatrix}\right)} \sim \frac{\mathsf{T}^{\sigma_1\sigma_2}_{\alpha\beta}\mathsf{T}^{\alpha\beta}_{\sigma_4\sigma_3}}{2N_f^2}\,\frac{1}{8\pi^2}\,\frac{g^2_{k,k}g^2_{k+l,k}}{cV_{F,k}}\,\frac{4\mu}{cv|k_x+l_x|(cv|k_x|+c|l_x|)} \tag{B.15}$$

where we use momentum independent nesting angle for the estimation.

contributions from different parts of the Fermi surface as

$$\begin{aligned}\mathbf{\Gamma}^{\binom{N_1\ N_2}{N_4\ N_3};\binom{\sigma_1\ \sigma_2}{\sigma_4\ \sigma_3}}_{(1)PP;\binom{k+l\ p-l}{k\ \ p}} = \frac{1}{4\mu N_f}\int\frac{\mathrm{d}q}{2\pi}\Bigg[& g^{(\bar{N}_4)}_{k+q,k}g^{(\bar{N}_3)}_{p-q,p}\ \mathcal{K}^{(PP)}_{N_4,N_3}(q;\mu,\mu,k,p)\lambda^{\binom{N_1\ N_2}{\bar{N}_4\ \bar{N}_3};\binom{\sigma_1\ \sigma_2}{\alpha\ \ \beta}}_{\binom{k+l\ p-l}{k+q\ p-q}}\mathsf{T}^{\alpha\beta}_{\sigma_4\sigma_3} \\ & + g^{(N_1)}_{k+l,k+l+q}g^{(N_2)}_{p-l,p-l-q}\ \mathcal{K}^{(PP)}_{N_1,N_2}(q;3\mu,-\mu,k+l,p-l)\mathsf{T}^{\sigma_1\sigma_2}_{\alpha\beta}\lambda^{\binom{\bar{N}_1\ \bar{N}_2}{N_4\ N_3};\binom{\alpha\ \ \beta}{\sigma_4\ \sigma_3}}_{\binom{k+l+q\ p-l-q}{k\ \ p}}\Bigg]\end{aligned} \tag{B.18}$$

and

$$\begin{aligned}\mathbf{\Gamma}^{\binom{N_1\ N_2}{N_4\ N_3};\binom{\sigma_1\ \sigma_2}{\sigma_4\ \sigma_3}}_{(1)PH;\binom{k+l\ p-l}{k\ \ p}} = \frac{1}{4\mu N_f}\int\frac{\mathrm{d}q}{2\pi}\Bigg[& g^{(\bar{N}_4)}_{k+q,k}g^{(N_1)}_{k+l,k+l+q}\ \mathcal{K}^{(PH)}_{N_1,N_4}(q;3\mu,\mu,k+l,k)\mathsf{T}^{\alpha\sigma_1}_{\sigma_4\beta}\lambda^{\binom{\bar{N}_1\ N_2}{N_4\ \bar{N}_3};\binom{\beta\ \sigma_2}{\alpha\ \sigma_3}}_{\binom{k+l+q\ p-l}{k+q\ \ p}} \\ & + g^{(\bar{N}_3)}_{p+q,p}g^{(N_2)}_{p-l,p-l+q}\ \mathcal{K}^{(PH)}_{N_2,N_3}(q;-\mu,\mu,p-l,p)\mathsf{T}^{\alpha\sigma_2}_{\sigma_3\beta}\lambda^{\binom{N_1\ \bar{N}_2}{N_4\ \bar{N}_3};\binom{\sigma_1\ \beta}{\sigma_4\ \alpha}}_{\binom{k+l\ p-l+q}{k\ \ p+q}} \\ & + g^{(\bar{N}_4)}_{k+q,k}g^{(N_2)}_{p-l,p-l+q}\ \mathcal{K}^{(PH)}_{N_2,N_4}(q;-\mu,\mu,p-l,k)\mathsf{T}^{\alpha\sigma_2}_{\sigma_4\beta}\lambda^{\binom{N_1\ \bar{N}_2}{\bar{N}_4\ N_3};\binom{\sigma_1\ \beta}{\alpha\ \sigma_3}}_{\binom{k+l\ p-l+q}{k+q\ \ p}} \\ & + g^{(\bar{N}_3)}_{p+q,p}g^{(N_1)}_{k+l,k+l+q}\ \mathcal{K}^{(PH)}_{N_1,N_3}(q;3\mu,\mu,k+l,p)\mathsf{T}^{\alpha\sigma_1}_{\sigma_3\beta}\lambda^{\binom{\bar{N}_1\ N_2}{N_4\ \bar{N}_3};\binom{\beta\ \sigma_2}{\sigma_4\ \alpha}}_{\binom{k+l+q\ p-l}{k\ \ p+q}}\Bigg].\end{aligned} \tag{B.19}$$

Here,

$$\mathcal{K}^{(PP)}_{N_a,N_b}(q;k_{a,0},k_{b,0},k_a,k_b) = \int\frac{\mathrm{d}q_\perp\mathrm{d}q_0}{(2\pi)^2}D(\mathbf{q})G_{\bar{N}_a}(\mathbf{k_a}+\mathbf{q})G_{\bar{N}_b}(\mathbf{k_b}-\mathbf{q}) \tag{B.20}$$

is the kernel that determines the strength of mixing between a particle-particle pair with momenta (k_a, k_b) in hot spots (N_a, N_b) with a particle-particle pair with momenta $(k_a + q, k_b - q)$ in hot spots $(\bar{N}_a, \bar{N}_b)$. k_a and k_b are the external momenta along the Fermi surface. $k_{a,0}$ and $k_{b,0}$ are the external frequencies. q ($q_\perp$) denotes the internal momentum that becomes parallel (perpendicular) to the Fermi surface in the small v limit. Similarly,

$$\mathcal{K}^{(PH)}_{N_a,N_b}(q;k_{a,0},k_{b,0},k_a,k_b) = \int\frac{\mathrm{d}q_\perp\mathrm{d}q_0}{(2\pi)^2}D(\mathbf{q})G_{\bar{N}_a}(\mathbf{k_a}+\mathbf{q})G_{\bar{N}_b}(\mathbf{k_b}+\mathbf{q}) \tag{B.21}$$

determines the strength of mixing between a particle-hole pair with momenta (k_a, k_b) in hot spots (N_a, N_b) with a particle-hole pair with momenta $(k_a + q, k_b + q)$ in hot spots $(\bar{N}_a, \bar{N}_b)$.

B.2.1 Group 1

In group 1, the primary couplings generated from the spin fluctuations takes the form of Eq. (2.78). The vertex correction that generates the secondary couplings exhibits IR singularity within the extended space of IR singularity only in the PH channel. In particular, only the last two terms in Eq. (B.19) exhibit IR singularity for $\left\{\lambda^{\binom{1\ 1}{1\ 1}}_{\binom{0\ k}{k\ 0}}, \lambda^{\binom{1\ 1}{1\ 1}}_{\binom{k\ 0}{0\ k}}\right\}$ at general k. This is because the primary coupling has zero total momentum only in two of the four PH channels at general k. While we only need $\mathcal{K}^{(PH)}_{1,1}(q;k_{a,0},k_{b,0},k,p)$ at $p = k$ for the last two terms in Eq. (B.19), let us compute it for general k and p to see how the vertex correction dies out at low energies when k deviates from p. In this case, $q = q_x$ and $q_\perp = q_y$. The kernel associated with a particle-hole pair at momenta k and p reads (see

Figs. 2.8c-2.8f)

$$\mathcal{K}^{(PH)}_{1,1}(q;3\mu,\mu,k,p)=\int\frac{\mathrm{d}q_0\mathrm{d}q_\perp}{(2\pi)^2}\frac{1}{|q_0|+c(|q|+|q_\perp|)}\frac{1}{i(q_0+3\mu)+V^{(4)}_{F,k+q}(v^{(4)}_{k+q}q-q_\perp+e_4[\vec{k};v^{(4)}_{k+q}])}\\ \times\frac{1}{i(q_0+\mu)+V^{(4)}_{F,p+q}(v^{(4)}_{p+q}q-q_\perp+e_4[\vec{p};v^{(4)}_{p+q}])}. \tag{B.22}$$

From Eq. (2.17), we can write $V^{(4)}_{F,p}=V_{F,p}$ and $v^{(4)}_p=v_p$. Since we are interested in the kernel near the space of IR singularity with $p=k$, we set $V_{F,k+q}=V_{F,p+q}$ and $v_{k+q}=v_{p+q}$ in the integrand. We shift the internal momenta as $q_0\to q_0-2\mu$, $q_\perp\to q_\perp+v_{k+q}q+\frac{1}{2}\left(e_4[\vec{k};v^{(4)}_{k+q}]+e_4[\vec{p};v^{(4)}_{p+q}]\right)$ and drop $cq_\perp$ from the boson propagator. The $q_\perp$ integration gives

$$\mathcal{K}^{(PH)}_{1,1}(q;3\mu,\mu,k,p)=\int\frac{\mathrm{d}q_0}{2\pi}\frac{1}{4V_{F,k+q}}\frac{\mathrm{sgn}(q_0+\mu)-\mathrm{sgn}(q_0-\mu)}{|q_0-2\mu|+c\,|q|+\left|cv_{k+q}q+\Delta_{1,\{1,1\}}\right|}\frac{1}{\mu-iV_{F,k+q}\Delta_{2,\{1,1\}}}, \tag{B.23}$$

where

$$\Delta_{1,\{1,1\}}(q;k,p;v)=\frac{c}{2}\left(e_4[\vec{k};v^{(4)}_{k+q}]+e_4[\vec{p};v^{(4)}_{p+q}]\right),\quad \Delta_{2,\{1,1\}}(q;k,p;v)=\frac{1}{2}\left(e_4[\vec{k};v^{(4)}_{k+q}]-e_4[\vec{p};v^{(4)}_{p+q}]\right). \tag{B.24}$$

The integration over the frequency results in

$$\mathcal{K}^{(PH)}_{1,1}(q;3\mu,\mu,k,p)=\frac{\log\left(1+\frac{2\mu}{\mu+c|q|+\left|cv_{k+q}q+\Delta_{1,\{1,1\}}\right|}\right)}{4\pi V_{F,k+q}\left(\mu-iV_{F,k+q}\Delta_{2,\{1,1\}}\right)}. \tag{B.25}$$

The subsequent integration over momentum q along the Fermi surface would give rise to a logarithmic IR divergence at $k=p=0$. A simple local counter term that removes the IR divergent part of the quantum correction can be obtained by regulating the non-analyticity in the external momenta and replacing q_0 with μ inside the boson propagator in Eq. (B.23) as

$$\tilde{\mathcal{K}}^{(PH)}_{1,1}(q;k,p)=\frac{1}{2\pi V_{F,k+q}}\frac{\mu}{\mu-iV_{F,k+q}\Delta_{2,\{1,1\}}}\frac{1}{\mu+c\,|q|_\mu+c\left|v_{k+q}q+\frac{1}{c}\Delta_{1,\{1,1\}}\right|_\mu}, \tag{B.26}$$

where $|q|_\mu=\sqrt{q^2+\mu^2}$ smears the non-analyticity of the boson propagator. One can explicitly check that Eq. (B.26) removes all IR singularity of the quantum correction [4]. The contribution to the beta functional is given by the derivative of Eq. (B.26) with respect to $\log\mu$[5],

$$\frac{\partial\tilde{\mathcal{K}}^{(PH)}_{1,1}(q;k,p)}{\partial\log\mu}=-\frac{1}{2\pi V_{F,k+q}}\frac{\mu\left[\mu^2+i\Delta_{2,\{1,1\}}V_{F,k+q}\left(c\,|q|_\mu+c\left|v_{k+q}q+\frac{1}{c}\Delta_{1,\{1,1\}}\right|_\mu\right)\right]}{\left(\mu-i\Delta_{2,\{1,1\}}V_{F,k+q}\right)^2\left(\mu+c\,|q|_\mu+c\left|v_{k+q}q+\frac{1}{c}\Delta_{1,\{1,1\}}\right|_\mu\right)^2}. \tag{B.28}$$

Eq. (B.28) vanishes in the small μ limit unless q, $\Delta_{2,\{1,1\}}$ and $\Delta_{1,\{1,1\}}$ all vanish. This implies that (1) the vertex correction is non-zero only when the pair of external fermions scattered by the critical

[4] To the leading order in the small v limit, the difference between Eq. (B.25) and Eq. (B.26) is given by

$$\int\frac{\mathrm{d}q}{2\pi}\left(\mathcal{K}^{(PH)}_{1,1}(q;3\mu,\mu,k,p)-\tilde{\mathcal{K}}^{(PH)}_{1,1}(q;k,p)\right)=\frac{\mu-(3\mu+|\Delta_{1,\{1,1\}}|)\mathrm{arctanh}\left(\frac{\mu}{2\mu+|\Delta_{1,\{1,1\}}|}\right)}{2c\pi^2V_{F,k}\left(\mu-i\Delta_{2,\{1,1\}}V_{F,k}\right)}, \tag{B.27}$$

where the momentum dependence of the coupling functions are ignored, and cv_kq is dropped in the boson propagator.

[5] In principle, the $\log\mu$ derivative affects the $|q|_\mu$ terms, but these result in sub leading contributions, which we ignore.

boson through quantum fluctuations are at the hot spots and (2) the non-zero vertex correction arises from the boson with small momenta near $q = 0$. We can use Eqs. (B.27) and (B.28) for the counter terms that cancel singular parts of quantum corrections with different choices of frequencies that are order of μ in Eq. (B.19).

The vertex correction in the particle-hole channel in Fig. 2.8 is given by the last two terms of Eq. (B.19). From Eq. (B.26), we can directly write the counter term,

$$\tilde{\mathbf{\Gamma}}^{\binom{1\ 1}{1\ 1};\binom{\sigma_1\ \sigma_2}{\sigma_4\ \sigma_3}}_{CT;(1)PH;\binom{k+l\ \ k}{k\ \ k+l}} = -\frac{1}{8\pi N_f}\int d\rho(q)\left[\frac{\mathsf{D}_\mu(k;q)}{\mu}\mathsf{T}^{\alpha\sigma_2}_{\sigma_4\beta}\lambda^{\binom{1\ 4}{4\ 1};\binom{\sigma_1\ \ \beta}{\alpha\ \ \sigma_3}}_{\binom{k+l\ \ q}{q\ \ k+l}} + \frac{\mathsf{D}_\mu(k+l;q)}{\mu}\mathsf{T}^{\sigma_1\alpha}_{\beta\sigma_3}\lambda^{\binom{4\ 1}{1\ 4};\binom{\beta\ \ \sigma_2}{\sigma_4\ \ \alpha}}_{\binom{q\ \ k}{k\ \ q}}\right], \tag{B.29}$$

where we have shifted $q_x \to q_x - k_x$ and $q_x \to q_x - k_x - l_x$, respectively. The contribution to the beta functional is given by the $\log\mu$ derivative of the counter term[6],

$$4\mu\frac{\partial}{\partial\log\mu}\tilde{\mathbf{\Gamma}}^{\binom{1\ 1}{1\ 1};\binom{\sigma_1\ \sigma_2}{\sigma_4\ \sigma_3}}_{CT;(1)PH;\binom{k+l\ \ k}{k\ \ k+l}} = \frac{1}{2\pi N_f}\int d\rho(q)\left[\frac{\mathsf{D}_\mu(k;q)^2}{g^2_{q,k}}\mathsf{T}^{\alpha\sigma_2}_{\sigma_4\beta}\lambda^{\binom{1\ 4}{4\ 1};\binom{\sigma_1\ \ \beta}{\alpha\ \ \sigma_3}}_{\binom{k+l\ \ q}{q\ \ k+l}} + \frac{\mathsf{D}_\mu(k+l;q)^2}{g^2_{k+l,q}}\mathsf{T}^{\sigma_1\alpha}_{\beta\sigma_3}\lambda^{\binom{4\ 1}{1\ 4};\binom{\beta\ \ \sigma_2}{\sigma_4\ \ \alpha}}_{\binom{q\ \ k}{k\ \ q}}\right]. \tag{B.30}$$

B.2.2 Group 2

In group 2, the primary couplings generated from the spin fluctuations are given by Eq. (2.79). The vertex correction that is linear in the four-fermion coupling further generates the secondary couplings in the PP channel through Figs. 2.8a- 2.8b. The relevant expression for the quantum correction is in Eq. (B.18). The kernel that goes into the quantum correction in the PP channel is written as

$$\mathcal{K}^{(PP)}_{1,5}(q;3\mu,-\mu,k,p) = \int\frac{\mathrm{d}q_0\mathrm{d}q_\perp}{(2\pi)^2}\frac{1}{|q_0|+c(|q|+|q_\perp|)}\frac{1}{i(q_0+3\mu)+V^{(4)}_{F,k+q}(v^{(4)}_{k+q}q-q_\perp+e_4[\vec{k};v^{(4)}_{k+q}])}\times \frac{1}{i(-q_0-\mu)+V^{(8)}_{F,p-q}(v^{(8)}_{p-q}q-q_\perp+e_8[\vec{p};v^{(8)}_{p-q}])}. \tag{B.31}$$

Shifting q_0 by -2μ and $q_\perp$ by $v_{k+q}q + \Delta_{1\{1,5\}}(q;k,p;v)/c$, and dropping $cq_\perp$ in the boson propagator in the small c limit leads to

$$\mathcal{K}^{(PP)}_{1,5}(q;3\mu,-\mu,k,p) = \int\frac{\mathrm{d}q_0\mathrm{d}q_\perp}{(2\pi)^2}\frac{1}{|q_0-2\mu|+c\,|q|+\left|cv_{k+q}q+\Delta_{1,\{1,5\}}\right|}\frac{1}{i(q_0+\mu)+V_{F,k+q}(-q_\perp+\Delta_{2,\{1,5\}})}\times \frac{1}{i(-q_0+\mu)+V_{F,-p+q}((v_{-p+q}-v_{k+q})q-q_\perp-\Delta_{2,\{1,5\}})}, \tag{B.32}$$

where

$$\Delta_{1,\{1,5\}}(q;k,p;v) = \frac{c}{2}\left(e_4[\vec{k};v^{(4)}_{k+q}]+e_8[\vec{p};v^{(8)}_{p-q}]\right),\quad \Delta_{2,\{1,5\}}(q;k,p;v) = \frac{1}{2}\left(e_4[\vec{k};v^{(4)}_{k+q}]-e_8[\vec{p};v^{(8)}_{p-q}]\right). \tag{B.33}$$

Integrating $q_\perp$ gives

$$\mathcal{K}^{(PP)}_{1,5}(q;3\mu,-\mu,k,p) = \int\frac{\mathrm{d}q_0}{2\pi}\frac{1}{|q_0-2\mu|+c\,|q|+\left|cv_{k+q}q+\Delta_{1,\{1,5\}}\right|}\times \frac{\frac{1}{2}\left(\mathrm{sgn}(q_0+\mu)+\mathrm{sgn}(q_0-\mu)\right)}{(V_{F,k+q}+V_{F,-p+q})q_0-(V_{F,k+q}-V_{F,-p+q})\mu-iV_{F,k+q}V_{F,-p+q}((v_{k+q}-v_{-p+q})q+2\Delta_{2,\{1,5\}})}. \tag{B.34}$$

Near the space of IR singularity with $k = -p$, we can set $V_{F,k+q} = V_{F,-p+q}$ and $v_{k+q} = v_{-p+q}$ to simplify the above expression. To construct a simple local and analytic counter term that removes

[6] To the leading order, fixing λ_B is equivalent to fixing λ/μ under the $\log\mu$ derivative.

the IR divergence, we can drop 2μ in the boson propagator and regularize the non-analyticity in the external momenta as

$$\tilde{\mathcal{K}}^{(PP)}_{1,5}(q;k,p) = \int \frac{\mathrm{d}q_0}{2\pi} \frac{1}{|q_0| + c\,|q|_\mu + c\left|v_{k+q}q + \frac{1}{c}\Delta_{1,\{1,5\}}\right|_\mu} \frac{\frac{1}{2}\left(\mathrm{sgn}(q_0+\mu)+\mathrm{sgn}(q_0-\mu)\right)}{2V_{F,k+q}q_0 - 2iV^2_{F,k+q}\Delta_{2,\{1,5\}}}. \tag{B.35}$$

Since $\tilde{\mathcal{K}}^{(pp)}_{1,5}$ differs from $\mathcal{K}^{(pp)}_{1,5}$ only by non-singular terms[7], we can use Eq. (B.35) in the counter term. After q_0 integration, the kernel becomes

$$\tilde{\mathcal{K}}^{(PP)}_{1,5}(q;k,p) = \frac{\left\{\begin{array}{c} 2\Delta_{2;\{1,5\}}V_{F,k+q}\arctan\left(\dfrac{\Delta_{2;\{1,5\}}V_{F,k+q}}{\mu}\right) \\ -\left(c\left|v_{k+q}q_x + \Delta_{1,\{1,5\}}/c\right|_\mu + c\,|q_x|_\mu\right)\log\left(\dfrac{\mu^2+\left(\Delta_{2;\{1,5\}}V_{F,k+q}\right)^2}{\left(c\left|v_{k+q}q_x+\Delta_{1;\{1,5\}}/c\right|_\mu + c\,|q_x|_\mu+\mu\right)^2}\right)\end{array}\right\}}{4\pi V_{F,k+q}\left[\left(c\,|q|_\mu + c\left|v_{k+q}q+\Delta_{1,\{1,5\}}/c\right|_\mu\right)^2 + \left(\Delta_{2;\{1,5\}}V_{F,k+q}\right)^2\right]}. \tag{B.38}$$

The contribution to the beta functional is given by the derivative of the kernel with respect to $\log\mu$,

$$\frac{\partial\tilde{\mathcal{K}}^{(PP)}_{1,5}(q;k,p)}{\partial\log\mu} = -\frac{1}{2\pi V_{F,k+q}}\frac{\mu^2}{\left(\Delta_{2,\{1,5\}}V_{F,k+q}\right)^2+\mu^2}\frac{1}{\mu + c\,|q|_\mu + c\left|v_{k+q}q+\Delta_{1,\{1,5\}}/c\right|_\mu}. \tag{B.39}$$

In the small μ limit, Eq. (B.39) remains non-zero as far as $\Delta_{2,\{1,5\}} = 0$. This implies that (1) the vertex corrections in the pairing channel remains important at low energies irrespective of the relative momentum of Cooper pairs, and (2) the singular vertex correction arises from bosons with all momenta. In particular, even a high-energy boson creates a singular vertex correction by scatterings Cooper pairs along the Fermi surface with large momentum transfers.

Using Eq. (B.38), we can directly write the counter term for the quantum correction in Eq. (B.18). From (B.39), the contribution to the beta functional is obtained to be

$$4\mu\frac{\partial}{\partial\log\mu}\tilde{\mathbf{\Gamma}}^{\left(\begin{smallmatrix}1&5\\1&5\end{smallmatrix}\right);\left(\begin{smallmatrix}\sigma_1&\sigma_2\\\sigma_4&\sigma_3\end{smallmatrix}\right)}_{CT;(1)PP;\left(\begin{smallmatrix}k+l&-k-l\\k&-k\end{smallmatrix}\right)} = \frac{1}{2\pi N_f}\int d\rho(q)\left[\mathsf{D}_\mu(k+l;q)\mathsf{T}^{\sigma_1\sigma_2}_{\alpha\beta}\lambda^{\left(\begin{smallmatrix}4&8\\1&5\end{smallmatrix}\right),\left(\begin{smallmatrix}\alpha&\beta\\\sigma_4&\sigma_3\end{smallmatrix}\right)}_{\left(\begin{smallmatrix}q&-q\\k&-k\end{smallmatrix}\right)} + \mathsf{D}_\mu(q;k)\lambda^{\left(\begin{smallmatrix}1&5\\4&8\end{smallmatrix}\right),\left(\begin{smallmatrix}\sigma_1&\sigma_2\\\alpha&\beta\end{smallmatrix}\right)}_{\left(\begin{smallmatrix}k+l&-k-l\\q&-q\end{smallmatrix}\right)}\mathsf{T}^{\alpha\beta}_{\sigma_4\sigma_3}\right], \tag{B.40}$$

where we have shifted $q_x \to q_x - k_x - l_x$ and $q_x \to q_x - k_x$ in the respective terms.

[7] To the leading order in v, the difference is given by

$$\begin{aligned}&(\mathcal{K}^{(PP)}_{1,5}(q;3\mu,-\mu,k,p) - \tilde{\mathcal{K}}^{(PP)}_{1,5}(q;k,p)) \\ &= \int\frac{dq_0}{2\pi}\frac{\frac{1}{2}\left(|q_0|-|q_0-2\mu|\right)\left(\mathrm{sgn}(q_0+\mu)+\mathrm{sgn}(q_0-\mu)\right)}{\left\{\begin{array}{c}\left[(V_{F,k+q}+V_{F,-p+q})q_0 - 2iV_{F,k+q}V_{F,-p+q}\Delta_{2,\{1,5\}}\right] \\ \times(|q_0-2\mu|+c\,|q|+|cv_{k+q}q+\Delta_{1,\{1,5\}}|)(|q_0|+c\,|q|+|cv_{k+q}q+\Delta_{1,\{1,5\}}|)\end{array}\right\}}.\end{aligned} \tag{B.36}$$

Here Δ_2 only makes the magnitude of the integrand strictly larger, thus we can set $\Delta_2 = 0$. For coupling functions that are weakly momentum dependent, one can perform the q integration by dropping $cv_{k+q}q$ for $v \ll c \ll 1$ to obtain

$$\int\frac{\mathrm{d}q}{2\pi}(\mathcal{K}^{(PP)}_{1,5}(q;3\mu,-\mu,k,p) - \tilde{\mathcal{K}}^{(PP)}_{1,5}(q;k,p)) = \left\{\begin{array}{ll}\frac{1-\log 4}{\pi^2 c(V_{F,k}+V_{F,-p})}\frac{\mu}{|\Delta_{1,\{1,5\}}|} + O(\mu^2) & \text{for} \quad \Delta_1 \neq 0, \Delta_2 = 0 \\ \frac{\pi^2 - 3\left(2\log^2(2)+\mathrm{Li}_2(1/4)\right)}{12c\pi^2(V_{F,k}+V_{F,-p})} & \text{for} \quad \Delta_1 = 0, \Delta_2 = 0\end{array}\right. . \tag{B.37}$$

B.3 BCS processes

The vertex corrections quadratic in the four-fermion coupling (Eqs. (2.76) - (2.77) for Fig. 2.9) can be written as

$$\mathbf{\Gamma}^{\binom{N_1\ N_2}{N_4\ N_3};\binom{\sigma_1\ \sigma_2}{\sigma_4\ \sigma_3}}_{(2)PP;\binom{k+l\ p-l}{k\ \ p}} = -\frac{1}{8\mu^2}\int\frac{\mathrm{d}q}{2\pi}\mathcal{Q}^{(PP)}_{M_1M_2}(q;\mu,\mu,k,p)\lambda^{\binom{N_1\ N_2}{M_1\ M_2};\binom{\sigma_1\ \sigma_2}{\beta\ \ \alpha}}_{\binom{k+l\ p-l}{k+q\ p-q}}\lambda^{\binom{M_1\ M_2}{N_4\ N_3};\binom{\beta\ \ \alpha}{\sigma_4\ \sigma_3}}_{\binom{k+q\ p-q}{k\ \ p}}, \tag{B.41}$$

and

$$\begin{aligned}\mathbf{\Gamma}^{\binom{N_1\ N_2}{N_4\ N_3};\binom{\sigma_1\ \sigma_2}{\sigma_4\ \sigma_3}}_{(2)PH;\binom{k+l\ p-l}{k\ \ p}} =& -\frac{1}{8\mu^2}\int\frac{\mathrm{d}q}{2\pi}\Bigg[\mathcal{Q}^{(PH)}_{M_1M_2}(q;-2\mu,0,-l,0)\Bigg(-N_f\lambda^{\binom{N_1\ M_1}{N_4\ M_2};\binom{\sigma_1\ \alpha}{\sigma_4\ \beta}}_{\binom{k+l\ q-l}{k\ \ q}}\lambda^{\binom{M_2\ N_2}{M_1\ N_3};\binom{\beta\ \sigma_2}{\alpha\ \sigma_3}}_{\binom{q\ \ p-l}{q-l\ p}}\\ &+\lambda^{\binom{N_1\ M_1}{N_4\ M_2};\binom{\sigma_1\ \alpha}{\sigma_4\ \beta}}_{\binom{k+l\ q-l}{k\ \ q}}\lambda^{\binom{M_2\ N_2}{N_3\ M_1};\binom{\beta\ \sigma_2}{\sigma_3\ \alpha}}_{\binom{q\ p-l}{p\ q-l}}+\lambda^{\binom{N_1\ M_1}{M_2\ N_4};\binom{\sigma_1\ \alpha}{\beta\ \ \sigma_4}}_{\binom{k+l\ q-l}{q\ \ k}}\lambda^{\binom{M_2\ N_2}{M_1\ N_3};\binom{\beta\ \sigma_2}{\alpha\ \sigma_3}}_{\binom{q\ \ p-l}{q-l\ p}}\Bigg)\\ &+\mathcal{Q}^{(PH)}_{M_1M_2}(q;-2\mu,0,p-l-k,0)\lambda^{\binom{N_1\ M_1}{M_2\ N_3};\binom{\sigma_1\ \alpha}{\beta\ \ \sigma_3}}_{\binom{k+l\ q+p-l-k}{q\ \ \ p}}\lambda^{\binom{M_2\ N_2}{N_4\ M_1};\binom{\beta\ \sigma_2}{\sigma_4\ \alpha}}_{\binom{q\ \ p-l}{k\ q+p-l-k}}\Bigg],\end{aligned} \tag{B.42}$$

where

$$\mathcal{Q}^{(PP)}_{N_1N_2}(q;k_{a,0},k_{b,0},k_a,k_b) = \int\frac{\mathrm{d}q_0\mathrm{d}q_\perp}{(2\pi)^2}G_{N_1}(\mathbf{k_a}+\mathbf{q})G_{N_2}(\mathbf{k_b}-\mathbf{q}), \tag{B.43a}$$

$$\mathcal{Q}^{(PH)}_{N_1N_2}(q;k_{a,0},k_{b,0},k_a,k_b) = \int\frac{\mathrm{d}q_0\mathrm{d}q_\perp}{(2\pi)^2}G_{N_1}(\mathbf{k_a}+\mathbf{q})G_{N_2}(\mathbf{k_b}+\mathbf{q}) \tag{B.43b}$$

are the kernels that determine the strength of the operator mixing in which two four-fermion operators 'fuse' into one four-fermion operator as a function of momentum along the Fermi surface and frequencies. For a generic shape of Fermi surface, the only kernel that produces an IR singularity in an extended space of external momenta is in the PP channel,

$$\begin{aligned}&\mathcal{Q}^{(PP)}_{15}(q;\mu,\mu,k,p)\\ &=\int\frac{1}{\Big[i(\mu+q_0)+V^{(1)}_{F,k+q}e_1[\vec{k}+\vec{q};v^{(1)}_{k+q}]\Big]\Big[i(\mu-q_0)+V^{(5)}_{F,p-q}e_5[\vec{p}-\vec{q};v^{(5)}_{p-q}]\Big]}\frac{\mathrm{d}q_\perp}{2\pi}\frac{\mathrm{d}q_0}{2\pi}.\end{aligned} \tag{B.44}$$

This is singular when the center of mass momentum is zero. For $\vec{p}=-\vec{k}$, the kernel becomes

$$\mathcal{Q}^{(PP)}_{15}(q;\mu,\mu,k,-k) = \frac{1}{2\pi V_{F,k+q}}\log\frac{\Lambda}{\mu}. \tag{B.45}$$

It is noted that this is IR divergent irrespective of k as far as $p=-k$.

Using the expressions above, we write down the quantum corrections that are quadratic in λ explicitly. With the help of Eq. (B.45) we obtain the counter term,

$$\begin{aligned}\tilde{\mathbf{\Gamma}}^{\binom{1\ 5}{1\ 5};\binom{\sigma_1\ \sigma_2}{\sigma_4\ \sigma_3}}_{CT;(2)PP;\binom{k+l\ -k-l}{k\ \ \ -k}} =&\frac{1}{8\mu^2}\int\frac{\mathrm{d}q}{2\pi}\frac{1}{2\pi V_{F,q}}\log\left(\frac{\Lambda}{\mu}\right)\Bigg[\lambda^{\binom{1\ 5}{1\ 5};\binom{\sigma_1\ \sigma_2}{\beta\ \ \alpha}}_{\binom{k+l\ -k-l}{q\ \ \ -q}}\lambda^{\binom{1\ 5}{1\ 5};\binom{\beta\ \ \alpha}{\sigma_4\ \sigma_3}}_{\binom{q\ -q}{k\ -k}}\\ &+\lambda^{\binom{1\ 5}{4\ 8};\binom{\sigma_1\ \sigma_2}{\beta\ \ \alpha}}_{\binom{k+l\ -k-l}{q\ \ \ -q}}\lambda^{\binom{4\ 8}{1\ 5};\binom{\beta\ \ \alpha}{\sigma_4\ \sigma_3}}_{\binom{q\ -q}{k\ -k}}\Bigg],\end{aligned} \tag{B.46}$$

where the internal momentum is shifted by $-k$. The contribution to the beta functional becomes

$$\begin{aligned}4\mu\frac{\partial}{\partial\log\mu}\tilde{\mathbf{\Gamma}}^{\binom{1\ 5}{1\ 5};\binom{\sigma_1\ \sigma_2}{\sigma_4\ \sigma_3}}_{CT;(2)PP;\binom{k+l\ -k-l}{k\ \ \ -k}} =&-\frac{1}{4\pi}\int d\rho(q)\Bigg[\lambda^{\binom{1\ 5}{1\ 5};\binom{\sigma_1\ \sigma_2}{\beta\ \ \alpha}}_{\binom{k+l\ -k-l}{q\ \ \ -q}}\lambda^{\binom{1\ 5}{1\ 5};\binom{\beta\ \ \alpha}{\sigma_4\ \sigma_3}}_{\binom{q\ -q}{k\ -k}}\\ &+\lambda^{\binom{1\ 5}{4\ 8};\binom{\sigma_1\ \sigma_2}{\beta\ \ \alpha}}_{\binom{k+l\ -k-l}{q\ \ \ -q}}\lambda^{\binom{4\ 8}{1\ 5};\binom{\beta\ \ \alpha}{\sigma_4\ \sigma_3}}_{\binom{q\ -q}{k\ -k}}\Bigg].\end{aligned} \tag{B.47}$$

Appendix C

RG Flow of the nesting angle, Fermi velocity and Yukawa coupling functions

C.1 Diagonal Coupling functions

We can solve the beta functionals for the diagonal couplings, $\{v_k, V_{F,k}, g_k \equiv g_{k,k}\}$ because Eqs. (2.101)-(2.103) do not depend on the off-diagonal elements of $g_{k,k'}$ with $k' \neq k$. The momentum dependent flow of the diagonal coupling functions is controlled by three length scales $\ell_k^{(2L)}$, $\ell_k^{(1L)}$, $\ell_{k,k}^{(1L)}$. defined through Eq. (2.125). The length scales satisfy $\ell_k^{(2L)} = \ell_{k,k}^{(1L)} < \ell_k^{(1L)}$. Since these logarithmic length scales depend on the scale dependent coupling functions, they need to be solved along with the beta functionals. To be concrete, we consider a UV theory which has momentum dependent coupling functions at scale Λ as is shown in Eq. (2.120).

C.1.1 Short-distance Regime

At length scales shorter than all crossover scales ($\ell < \ell_k^{(2L)}$, $\ell_k^{(1L)}$, $\ell_{k,k}^{(1L)}$), the beta functionals become

$$\begin{aligned}\frac{\partial v_k(\ell)}{\partial \ell} = v_k(\ell)\Bigg[&-\frac{4(N_c^2-1)}{\pi^3 N_c N_f}\frac{g_k(\ell)^2}{V_{F,k}(\ell)^2}\log\left(\frac{V_{F,k}(\ell)}{c(\ell)}\right)\\ &-\frac{2(N_c^2-1)}{\pi^4 N_c^2 N_f^2}\frac{g_k(\ell)^4}{c(\ell)^2 V_{F,k}(\ell)^2}\log^2\left(\frac{V_{F,k}(\ell)v_k(\ell)}{c(\ell)}\right)\Bigg],\end{aligned} \tag{C.1}$$

$$\begin{aligned}\frac{\partial V_{F,k}(\ell)}{\partial \ell} = V_{F,k}(\ell)\Bigg[&\frac{2(N_c^2-1)}{\pi^3 N_c N_f}\frac{g_k(\ell)^2}{V_{F,k}(\ell)^2}\log\left(\frac{V_{F,k}(\ell)}{c(\ell)}\right)-\frac{N_c^2-1}{\pi^2 N_c N_f}\frac{g_k(\ell)^2}{c(\ell)V_{F,k}(\ell)}\\ &-\frac{3}{2}\frac{N_c^2-1}{\pi^2 N_c N_f}v_0(\ell)\log\left(\frac{1}{c(\ell)}\right)+\frac{N_c^2-1}{2\pi N_c N_F}w_0(\ell)\\ &+\frac{(N_c^2-1)}{2\pi^4 N_c^2 N_f^2}\frac{g_k(\ell)^4}{c(\ell)^2 V_{F,k}(\ell)^2}\log^2\left(\frac{V_{F,k}(\ell)v_k(\ell)}{c(\ell)}\right)\Bigg],\end{aligned} \tag{C.2}$$

$$\begin{aligned}\frac{\partial g_k(\ell)}{\partial \ell} = g_k(\ell)\Bigg[&-\frac{1}{2\pi N_c N_f}w_0(\ell)\log\left(\frac{1}{w_0(\ell)}\right)+\frac{N_c^2-1}{2\pi N_c N_f}w_0(\ell)-\frac{N_c^2-1}{\pi^2 N_c N_f}v_0(\ell)\log\left(\frac{1}{v_0(\ell)}\right)\\ &-\frac{(N_c^2-1)g_k(\ell)^2}{\pi^2 N_c N_f c(\ell)V_{F,k}(\ell)}+\frac{g_k(\ell)^2}{\pi^2 N_c N_f V_{F,k}(\ell)c(\ell)}\log\left(\frac{c(\ell)}{V_{F,k}(\ell)v_k(\ell)}\right)\Bigg].\end{aligned} \tag{C.3}$$

The solution to the beta functional reproduces the results of the hot spot theory[182],

$$v_k(\ell) = \frac{\pi^2 N_c N_f}{2(N_c^2-1)}\frac{1}{(\ell+\ell_0)\log(\ell+\ell_0)}, \tag{C.4}$$

$$V_{F,k}(\ell) = 1, \tag{C.5}$$

$$g_k(\ell) = \sqrt{\frac{\pi^3 N_c N_f}{4(N_c^2-1)}\frac{1}{(\ell+\ell_0)\log(\ell+\ell_0)}}. \tag{C.6}$$

The speed of the collective mode is given by Eq. (2.4),

$$c(\ell) = \frac{\pi}{4\sqrt{N_c^2-1}}\frac{1}{\sqrt{\ell+\ell_0}}. \tag{C.7}$$

Here ℓ_0 is the parameter that sets the nesting angle at the UV scale $\ell = 0$. In the limit that the nesting angle is small, $\ell_0 \gg 1$.

C.1.2 The crossover scales

As the length scale increases, the theory encounters the first crossover at $\ell_k^{(2L)}$. Eq. (2.125) that determines the crossover scale reads

$$\ell_k^{(2L)} = \log\left(\frac{\Lambda}{4v_0(\ell_k^{(2L)})k}\right). \tag{C.8}$$

For $\ell_0 \gg 1$, $\log 1/v_0(\ell) \approx \log(\ell+\ell_0)$, and Eq. (C.8) can be written as

$$\ell_k^{(2L)} = \log\left(\frac{\Lambda}{4v_0(0)k}\right) + \log\left(\frac{\ell_0+\ell_k^{(2L)}}{\ell_0}\right). \tag{C.9}$$

To the leading order in the small v limit, its solution is obtained to be

$$\ell_k^{(2L)} = \log\left(\frac{\Lambda}{4v_0(0)k}\right) + \log\left[\frac{\ell_0 + \log\left(\frac{\Lambda}{4v_0(0)k}\right)}{\ell_0}\right]. \tag{C.10}$$

As ℓ increases further, the theory encounters the second crossover length scale at

$$\ell_k^{(1L)} = \log\frac{\Lambda}{2v_k(\ell_k^{(1L)})c(\ell_k^{(1L)})k}. \tag{C.11}$$

It turns out that $\ell_k^{(1L)} - \ell_k^{(2L)}$ is not large enough to generate any significant flow of coupling functions within this window of length scales. To see this, let us first assume that the logarithmic change of the coupling functions is negligible between the two length scales,

$$|\delta_k^{(J)}| \equiv |\log J(\ell_k^{(1L)}) - \log J(\ell_k^{(2L)})| \ll 1 \tag{C.12}$$

for all couplings $J = \{g_k, v_k, V_{F,k}\}$. The self-consistent equation in Eq. (C.11) can be written as

$$\ell_k^{(1L)} - \ell_k^{(2L)} = -\log c(\ell_k^{(2L)}) - \delta_k^{(v_k)} - \delta_k^{(c)} + \log 2 \approx \log\frac{2}{c(\ell_k^{(2L)})} \tag{C.13}$$

for $c \ll 1$. Since all beta functionals goes to zero in powers of w as

$$\begin{gathered}\left|\frac{1}{v_k(\ell)}\frac{\partial v_k(\ell)}{\partial \ell}\right| \lesssim \mathcal{O}(\, v\log(1/c)\,), \qquad \left|\frac{1}{V_{F,k}(\ell)}\frac{\partial V_{F,k}(\ell)}{\partial \ell}\right| \lesssim \mathcal{O}(\, w\,), \\ \left|\frac{1}{g_{k,k}(\ell)}\frac{\partial g_{k,k'}(\ell)}{\partial \ell}\right| \lesssim \mathcal{O}(\, w\log(1/w)\,),\end{gathered} \tag{C.14}$$

the change of the coupling that occurs in $\ell_k^{(2L)} < \ell < \ell_k^{(1L)}$ is at most

$$\left|\frac{J(\ell_k^{(1L)}) - J(\ell_k^{(2L)})}{J(\ell_k^{(2L)})}\right| \sim O(\, w\log(1/w)\log(1/c)\,) \ll 1 \tag{C.15}$$

for all couplings. This justifies the assumption made in Eq. (C.12). Therefore, the change of couplings is negligible between $\ell_k^{(2L)}$ and $\ell_k^{(1L)}$, and we can set

$$J_k(\ell) = J(k; \ell_k^{(2L)}) \quad \text{for} \quad \ell_k^{(2L)} \le \ell \le \ell_k^{(1L)}. \tag{C.16}$$

C.1.3 Low Energy Regime

In the long distance limit with $\ell > \ell_k^{(1L)}$, the beta functionals become

$$\left.\frac{\partial v_k(\ell)}{\partial \ell}\right|_{\ell \ge \ell_k^{(1L)}} = 0 \tag{C.17}$$

$$\left.\frac{\partial V_{F,k}(\ell)}{\partial \ell}\right|_{\ell \ge \ell_k^{(1L)}} = V_{F,k}(\ell)\left[\frac{N_c^2 - 1}{2\pi N_c N_F} w_0(\ell)\right], \tag{C.18}$$

$$\left.\frac{\partial g_k(\ell)}{\partial \ell}\right|_{\ell \ge \ell_k^{(1L)}} = g_k(\ell)\left[-\frac{1}{2\pi N_c N_f} w_0(\ell)\log\left(FR1 w_0(\ell)\right)\right] \tag{C.19}$$

to the leading order in v. With the quantum corrections turned off, the flow of v_k freezes out. $V_{F,k}$ that represents the Fermi velocity measured in the unit of the Fermi velocity at the hot spots increases

with increasing length scale. This is because the dynamical critical exponent is chosen to keep $V_{F,0} = 1$ at the hot spot. Cold electrons which are decoupled from spin fluctuations at low energies appear to be moving increasingly faster when the speed is measured with the sluggish clock that is tuned to keep the speed of hot electrons to be 1. Since the deviation of the dynamical critical exponent from 1 is order of w, the flow of $V_{F,k}$ is controlled by w. On the contrary, the Yukawa coupling decays to zero away from the hot spots in the low energy limit. This is because the vertex correction, which tends to strengthen the coupling through the anti-screening effect, turns off at low energies. With the anti-screening effect gone, the large anomalous dimension of the boson, which is $1 + O(w \log 1/w)$, forces the Yukawa coupling to decrease rapidly. Since the Yukawa coupling is marginal when the anomalous dimension is 1, the flow of the Yukawa coupling is proportional to $w \log 1/w$. From $w_0(\ell) = v_0(\ell)/c(\ell)$, the solutions are readily obtained to be

$$\begin{aligned} v_k(\ell \geq \ell_k^{(1L)}) &= \frac{\pi^2 N_c N_f}{2(N_c^2-1)} \frac{1}{(\ell_k^{(1L)} + \ell_0)\log(\ell_k^{(1L)} + \ell_0)}, \\ V_{F,k}(\ell \geq \ell_k^{(1L)}) &= \mathcal{E}_1(\ell, \ell_k^{(1L)}), \\ g_k(\ell \geq \ell_k^{(1L)}) &= \sqrt{\frac{\pi}{2} v_0(\ell_k^{(1L)})}\mathcal{E}_0(\ell, \ell_k^{(1L)}), \end{aligned} \tag{C.20}$$

where

$$\mathcal{E}_0(X,Y) \equiv \exp\left(-\frac{\sqrt{X+\ell_0} - \sqrt{Y+\ell_0}}{\sqrt{N_c^2-1}}\right), \tag{C.21}$$

$$\mathcal{E}_1(X,Y) \equiv \exp\left(\sqrt{N_c^2-1}\left(\mathrm{Ei}(\log\sqrt{X+\ell_0}) - \mathrm{Ei}(\log\sqrt{Y+\ell_0})\right)\right). \tag{C.22}$$

Because $v_k(\ell_k^{(1L)}) \approx v_k(\ell_k^{(2L)})$, $\mathcal{E}_0(\ell_k^{(1L)}, \ell_k^{(2L)}) \approx 1$, $\mathcal{E}_1(\ell_k^{(1L)}, \ell_k^{(2L)}) \approx 1$, the scale dependent diagonal couplings can be written in terms of only one crossover as

$$\begin{aligned} v_k(\ell) &= \begin{cases} v_0(\ell) & \ell \leq \ell_k^{(2L)} \\ v_0(\ell_k^{(2L)}) & \ell \geq \ell_k^{(2L)} \end{cases} \\ V_{F,k}(\ell) &= \begin{cases} 1 & \ell \leq \ell_k^{(2L)} \\ \mathcal{E}_1(\ell, \ell_k^{(2L)}) & \ell \geq \ell_k^{(2L)} \end{cases} \\ g_k(\ell) &= \begin{cases} \sqrt{\pi v_0(\ell)/2} & \ell \leq \ell_k^{(2L)} \\ \sqrt{\frac{\pi}{2} v_0(\ell_k^{(2L)})}\mathcal{E}_0(\ell, \ell_k^{(2L)}) & \ell \geq \ell_k^{(2L)} \end{cases}. \end{aligned} \tag{C.23}$$

C.2 Off-diagonal Yukawa Coupling

The crossover scale for the off-diagonal Yukawa vertex correction is given by

$$\ell_{k,k'}^{(1L)} = \min\left(\ell_{k',k}^{(\mathrm{ver})}, \ell_k^{(1L)}, \ell_{k'}^{(1L)}\right), \tag{C.24}$$

where $\ell_{k',k}^{(\mathrm{ver})} = L^{(1L)}(k,k';\ell_{k',k}^{(\mathrm{ver})})$ is the crossover scale associated with the vertex correction. Inside Eq. (C.24), we can use the expression for $\ell_{k',k}^{(\mathrm{ver})}$ that is valid for $\ell_{k',k}^{(\mathrm{ver})} \leq \ell_k^{(1L)}, \ell_{k'}^{(1L)}$[1]. Therefore, we can set $V_{F,k} = V_{F,k'} = 1$ and $v_k(\ell_{k',k}^{(\mathrm{ver})}), v_{k'}(\ell_{k',k}^{(\mathrm{ver})}) = v_0(\ell_{k',k}^{(\mathrm{ver})})$ to estimate $\ell_{k',k}^{(\mathrm{ver})}$. In this case, $\ell_{k',k}^{(\mathrm{ver})}$ satisfies $\ell_{k',k}^{(\mathrm{ver})} = \log\left(\frac{\Lambda}{2v_0(\ell_{k',k}^{(\mathrm{ver})})|k+k'|}\right)$. Since this is of the same form as Eq. (C.8) for $\ell_k^{(2L)}$ except

[1] If $\ell_{k',k}^{(\mathrm{ver})}$ is greater than $\ell_k^{(1L)}$ or $\ell_{k'}^{(1L)}$, $\ell_{k',k}^{(\mathrm{ver})}$ drops out from Eq. (C.24) anyway.

that k is replaced with $|k+k'|/2$, $\ell^{(\mathrm{ver})}_{k',k} = \ell^{(2L)}_{(k+k')/2}$. From this, we can write the crossover scale for the off-diagonal Yukawa coupling as

$$\ell^{(1L)}_{k',k} = \min(\ell^{(2L)}_{(k+k')/2}, \ell^{(1L)}_{k}, \ell^{(1L)}_{k'}). \tag{C.25}$$

For $\ell \leq \ell^{(1L)}_{k',k}$, Eq. (2.103) takes the same form as the beta functional for the diagonal Yukawa coupling at high energy in Eq. (C.3), and the solution is given by

$$g_{k,k'}(\ell) = \sqrt{\frac{\pi}{2} v_0(\ell)}. \tag{C.26}$$

For $\ell > \ell^{(1L)}_{k',k}$, the off-diagonal Yukawa coupling decreases as

$$\frac{\partial g_{k',k}(\ell)}{\partial \ell} = g_{k',k}(\ell) \left[-\frac{1}{2\pi N_c N_f} w_0(\ell) \log\left(\frac{1}{w_0(\ell)}\right) \right]. \tag{C.27}$$

All other terms in the beta function are sub-leading. Integrating this differential equation, we obtain

$$g(k', k; \ell) = \sqrt{\frac{\pi}{2} v_0(\ell^{(1L)}_{k',k})} \mathcal{E}_0(\ell, \ell^{(1L)}_{k',k}) \tag{C.28}$$

for $\ell > \ell^{(1L)}_{k',k}$. Combining Eqs. (C.26) and (C.28) we arrive at

$$g_{k,k'}(\ell) = \begin{cases} \sqrt{\frac{\pi}{2} v_0(\ell)} & \ell \leq \ell^{(1L)}_{k',k} \\ \sqrt{\frac{\pi}{2} v_0(\ell^{(1L)}_{k',k})} \mathcal{E}_0(\ell, \ell^{(1L)}_{k',k}) & \ell \geq \ell^{(1L)}_{k',k}. \end{cases} \tag{C.29}$$

Appendix D

Additional beta functionals in the presence of the particle-hole symmetry

If the PH symmetry is present, there exists a perfect nesting for the $2k_F$ scatterings both in the PP and PH channels[1]. In this case, there are additional channels with extended spaces of IR singularity. In group 1, one needs to include the interaction that describes pairings between electrons with total momentum $2k_F$ as is shown in Eq. (2.80). In group 2, the $2k_F$ scatterings of particle-hole pairs in Eq. (2.81) should be included. Below, we derive the beta functionals for those additional coupling functions and discuss they affect the flow of the couplings considered in the main text. In the presence of the PH symmetry, the coupling functions obey Eq. (2.21). Therefore, we can simply write $v_k^{(N)} = v_k, V_{F,k}^{(N)} = V_{F,k}$ and $g_{k',k}^{(N)} = g_{k',k}$, where $v_k = v_{-k}$ and $V_{F,k} = V_{F,-k}$. This implies that the fermion propagator satisfies

$$G_N(\mathbf{q}) = -G_N(-\mathbf{q}). \tag{D.1}$$

From this, we can derive relations between the vertex corrections in the PP and PH channels. The vertex correction that is independent of the four-fermion coupling in Eqs. (2.71) and (2.72) is determined by the kernels,

$$\gamma^{(PP)}_{N_1,N_2}(q;k_0,p_0,l_0,k,p,l) = \int \frac{\mathrm{d}q_0\mathrm{d}q_\perp}{(2\pi)^2} D(\mathbf{q})D(\mathbf{l}-\mathbf{q})G_{\bar{N}_1}(\mathbf{k}+\mathbf{q})G_{\bar{N}_2}(\mathbf{p}-\mathbf{q}), \tag{D.2}$$

$$\gamma^{(PH)}_{N_1,N_2}(q;k_0,p_0,l_0,k,p,l) = \int \frac{\mathrm{d}q_0\mathrm{d}q_\perp}{(2\pi)^2} D(\mathbf{q})D(\mathbf{l}-\mathbf{q})G_{\bar{N}_1}(\mathbf{k}+\mathbf{q})G_{\bar{N}_2}(\mathbf{p}-\mathbf{l}+\mathbf{q}). \tag{D.3}$$

Due to Eq. (D.1), $\gamma^{(PP)}_{N_1,N_2}$ and $\gamma^{(PH)}_{N_1,N_2}$ obey

$$\gamma^{(PH)}_{N_1,N_2}(q;k_0,p_0,l_0,k,p,l) = -\gamma^{(PP)}_{N_1,N_2}(q;k_0,-p_0+l_0,l_0,k,-p+l,l). \tag{D.4}$$

Similarly, the kernels that determines the linear mixing in Eqs. (B.20) and (B.21) satisfy

$$\mathcal{K}^{(PH)}_{N_a,N_b}(q;k_{a,0},k_{b,0},k_a,k_b) = -\mathcal{K}^{(PP)}_{N_a,N_b}(q;k_{a,0},-k_{b,0},k_a,-k_b). \tag{D.5}$$

[1]The time-reversal and parity symmetries guarantee that $V^{(N_T)}_{\mathrm{F},-k} e_{N_T}[-\vec{k};v^{(N_T)}_{-k}] = V^{(N)}_{\mathrm{F},k} e_N[\vec{k};v^{(N)}_k]$ for $N_T = [N+4]_8$. This makes it possible to put two electrons with zero center of mass momentum on the Fermi surface in antipodal patches irrespective of their relative momentum. In the presence of the PH symmetry, we also have $V^{(N)}_{\mathrm{F},-k} e_N[-\vec{k};v^{(N)}_{-k}] = -V^{(N)}_{\mathrm{F},k} e_N[\vec{k};v^{(N)}_k]$. This further makes it possible for a pair of electrons or an electron-hole pair with total momentum $2\vec{k}_F$ to stay on the Fermi surface irrespective of their relative momentum.

Finally, the kernels for the quantum corrections quadratic in the four fermion coupling in Eqs. (B.43a) and (B.43b) are related to each other through

$$Q^{(PH)}_{M_a,M_b}(q;k_{a,0},k_{b,0},k_a,k_b) = -Q^{(PP)}_{M_a,M_b}(q;k_{a,0},-k_{b,0},k_a,-k_b). \tag{D.6}$$

From these relations, we can readily compute the beta functions for the $2k_F$ scatterings using Eq. (2.106).

D.1 Group 1

D.1.1 Beta functional for the $2k_F$ pairing

Let us first consider $\lambda^{\binom{1\ 1}{1\ 1}}_{\binom{p\ -p}{k\ -k}}$, where the total momentum of two electrons is $2k_F$ (0 when measured with respect to the momentum of two electrons located at hot spot 1) in the PP channel. The beta functional for the coupling is

$$\begin{aligned}
\beta^{(\lambda);\binom{1\ 1}{1\ 1};\binom{\sigma_1\ \sigma_2}{\sigma_4\ \sigma_3}}_{\binom{p\ -p}{k\ -k}} &= \left(1+3(z-1)+2\eta^{(\psi)}_p+2\eta^{(\psi)}_k\right)\lambda^{\binom{1\ 1}{1\ 1};\binom{\sigma_1\ \sigma_2}{\sigma_4\ \sigma_3}}_{\binom{p\ -p}{k\ -k}} \\
&+\int \mathrm{d}\rho(q)\left\{\frac{\mathsf{D}_\mu(q;k)^2}{2\pi N_f g^2_{k,q}}\lambda^{\binom{1\ 1}{4\ 4};\binom{\sigma_1\ \sigma_2}{\alpha\ \ \beta}}_{\binom{p\ -p}{q\ -q}}\mathsf{T}^{\alpha\beta}_{\sigma_4\sigma_3}+\frac{\mathsf{D}_\mu(p;q)^2}{2\pi N_f g^2_{p,q}}\mathsf{T}^{\sigma_1\sigma_2}_{\alpha\beta}\lambda^{\binom{4\ 4}{1\ 1};\binom{\alpha\ \ \beta}{\sigma_4\ \sigma_3}}_{\binom{q\ -q}{k\ -k}}\right. \\
&\left.-\frac{\mathsf{D}_\mu(p;q)\mathsf{D}_\mu(q;k)}{\pi N_f^2}\mathsf{T}^{\sigma_1\sigma_2}_{\alpha\beta}\mathsf{T}^{\alpha\beta}_{\sigma_4\sigma_3}\left(\frac{\mathsf{D}_\mu(q;k)}{g^2_{q,k}}+\frac{\mathsf{D}_\mu(p;q)}{g^2_{p,q}}\right)\right\}.
\end{aligned} \tag{D.7}$$

Performing the q integration in the adiabatic limit, we obtain

$$\begin{aligned}
\beta^{(\lambda);\binom{1\ 1}{1\ 1};\binom{\sigma_1\ \sigma_2}{\sigma_4\ \sigma_3}}_{\binom{p\ -p}{k\ -k}} &= \left(1+3(z-1)+2\eta^{(\psi)}_p+2\eta^{(\psi)}_k\right)\lambda^{\binom{1\ 1}{1\ 1};\binom{\sigma_1\ \sigma_2}{\sigma_4\ \sigma_3}}_{\binom{p\ -p}{k\ -k}} \\
&+\frac{g^2_{k,k}}{2\pi^2 cN_f V_{F,k}}\frac{\mu}{\mu+2vc|k|_\mu}\lambda^{\binom{1\ 1}{4\ 4};\binom{\sigma_1\ \sigma_2}{\alpha\ \ \beta}}_{\binom{p\ -p}{k\ -k}}\mathsf{T}^{\alpha\beta}_{\sigma_4\sigma_3}+\frac{g^2_{p,p}}{2\pi^2 cN_f V_{F,p}}\frac{\mu}{\mu+2vc|p|_\mu}\mathsf{T}^{\sigma_1\sigma_2}_{\alpha\beta}\lambda^{\binom{4\ 4}{1\ 1};\binom{\alpha\ \ \beta}{\sigma_4\ \sigma_3}}_{\binom{p\ -p}{k\ -k}} \\
&-\mathsf{T}^{\sigma_1\sigma_2}_{\alpha\beta}\mathsf{T}^{\alpha\beta}_{\sigma_4\sigma_3}\frac{\mathsf{D}_\mu(p;k)}{\pi^2 cN_f^2}\left[\frac{\mu g^2_{k,k}}{V_{F,k}(\mu+2v_k c|k|_\mu)}+\frac{\mu g^2_{p,p}}{V_{F,p}(\mu+2v_p c|p|_\mu)}\right].
\end{aligned} \tag{D.8}$$

Since the coupling $\lambda^{\binom{1\ 1}{1\ 1}}$ mixes with $\lambda^{\binom{4\ 4}{1\ 1}}$, $\lambda^{\binom{1\ 1}{4\ 4}}$, $\lambda^{\binom{4\ 4}{4\ 4}}$, we need to compute the beta functionals for those couplings as well to have a closed set of beta functionals. The beta functionals for the rest of the couplings are obtained to be

$$\begin{aligned}
\beta^{(\lambda);\binom{4\ 4}{1\ 1};\binom{\sigma_1\ \sigma_2}{\sigma_4\ \sigma_3}}_{\binom{p\ -p}{k\ -k}} &= \left(1+3(z-1)+2\eta^{(\psi)}_p+2\eta^{(\psi)}_k\right)\lambda^{\binom{4\ 4}{1\ 1};\binom{\sigma_1\ \sigma_2}{\sigma_4\ \sigma_3}}_{\binom{p\ -p}{k\ -k}} \\
&+\frac{g^2_{k,k}}{2\pi^2 cN_f V_{F,k}}\frac{\mu}{\mu+2v_k c|k|_\mu}\lambda^{\binom{4\ 4}{4\ 4};\binom{\sigma_1\ \sigma_2}{\alpha\ \ \beta}}_{\binom{p\ -p}{k\ -k}}\mathsf{T}^{\alpha\beta}_{\sigma_4\sigma_3}+\frac{g^2_{p,p}}{2\pi^2 cN_f V_{F,p}}\frac{\mu}{\mu+2v_p c|p|_\mu}\mathsf{T}^{\sigma_1\sigma_2}_{\alpha\beta}\lambda^{\binom{1\ 1}{1\ 1};\binom{\alpha\ \ \beta}{\sigma_4\ \sigma_3}}_{\binom{p\ -p}{k\ -k}},
\end{aligned} \tag{D.9}$$

$$\begin{aligned}
\beta^{(\lambda);\binom{1\ 1}{4\ 4};\binom{\sigma_1\ \sigma_2}{\sigma_4\ \sigma_3}}_{\binom{p\ -p}{k\ -k}} &= \left(1+3(z-1)+2\eta^{(\psi)}_p+2\eta^{(\psi)}_k\right)\lambda^{\binom{1\ 1}{4\ 4};\binom{\sigma_1\ \sigma_2}{\sigma_4\ \sigma_3}}_{\binom{p\ -p}{k\ -k}} \\
&+\frac{g^2_{k,k}}{2\pi^2 cN_f V_{F,k}}\frac{\mu}{\mu+2v_k c|k|_\mu}\lambda^{\binom{1\ 1}{1\ 1};\binom{\sigma_1\ \sigma_2}{\alpha\ \ \beta}}_{\binom{p\ -p}{k\ -k}}\mathsf{T}^{\alpha\beta}_{\sigma_4\sigma_3}+\frac{g^2_{p,p}}{2\pi^2 cN_f V_{F,p}}\frac{\mu}{\mu+2v_p c|p|_\mu}\mathsf{T}^{\sigma_1\sigma_2}_{\alpha\beta}\lambda^{\binom{4\ 4}{4\ 4};\binom{\alpha\ \ \beta}{\sigma_4\ \sigma_3}}_{\binom{p\ -p}{k\ -k}},
\end{aligned} \tag{D.10}$$

$$\beta^{(\lambda);\left(\begin{smallmatrix}4&4\\4&4\end{smallmatrix}\right);\left(\begin{smallmatrix}\sigma_1&\sigma_2\\\sigma_4&\sigma_3\end{smallmatrix}\right)}_{\left(\begin{smallmatrix}p&-p\\k&-k\end{smallmatrix}\right)} = \left(1+3(z-1)+2\eta_p^{(\psi)}+2\eta_k^{(\psi)}\right)\lambda^{\left(\begin{smallmatrix}4&4\\4&4\end{smallmatrix}\right);\left(\begin{smallmatrix}\sigma_1&\sigma_2\\\sigma_4&\sigma_3\end{smallmatrix}\right)}_{\left(\begin{smallmatrix}p&-p\\k&-k\end{smallmatrix}\right)}$$
$$+\frac{g_{k,k}^2}{2\pi^2 c N_f V_{F,k}}\frac{\mu}{\mu+2v_k c|k|_\mu}\lambda^{\left(\begin{smallmatrix}4&4\\1&1\end{smallmatrix}\right);\left(\begin{smallmatrix}\sigma_1&\sigma_2\\\alpha&\beta\end{smallmatrix}\right)}_{\left(\begin{smallmatrix}p&-p\\k&-k\end{smallmatrix}\right)}\mathsf{T}^{\alpha\beta}_{\sigma_4\sigma_3}+\frac{g_{p,p}^2}{2\pi^2 c N_f V_{F,p}}\frac{\mu}{\mu+2v_p c|p|_\mu}\mathsf{T}^{\sigma_1\sigma_2}_{\alpha\beta}\lambda^{\left(\begin{smallmatrix}1&1\\4&4\end{smallmatrix}\right);\left(\begin{smallmatrix}\alpha&\beta\\\sigma_4&\sigma_3\end{smallmatrix}\right)}_{\left(\begin{smallmatrix}p&-p\\k&-k\end{smallmatrix}\right)}$$
$$-\mathsf{T}^{\sigma_1\sigma_2}_{\alpha\beta}\mathsf{T}^{\alpha\beta}_{\sigma_4\sigma_3}\frac{\mathsf{D}_\mu(p;k)}{\pi^2 c N_f^2}\left[\frac{\mu g_{k,k}^2}{V_{F,k}(\mu+2v_k c|k|_\mu)}+\frac{\mu g_{p,p}^2}{V_{F,p}(\mu+2v_p c|p|_\mu)}\right]. \tag{D.11}$$

For $\lambda^{\left(\begin{smallmatrix}4&4\\1&1\end{smallmatrix}\right)}$ and $\lambda^{\left(\begin{smallmatrix}1&1\\4&4\end{smallmatrix}\right)}$, there is no source term to the leading order in v.

D.1.2 Solution of the beta functional for the $2k_F$ pairing

In the space of the rescaled momentum, the set of four beta functionals in Eqs. (D.8)- (D.11) can be written as

$$\left[\frac{\partial}{\partial\ell}+K\frac{\partial}{\partial K}+P\frac{\partial}{\partial P}\right]\hat{\lambda}^{\left(\begin{smallmatrix}N_1&N_2\\N_4&N_3\end{smallmatrix}\right);\left(\begin{smallmatrix}\sigma_1&\sigma_2\\\sigma_4&\sigma_3\end{smallmatrix}\right)}_{\left(\begin{smallmatrix}P&-P\\K&-K\end{smallmatrix}\right)} = -\left(1+\hat{\eta}_K+\hat{\eta}_P\right)\hat{\lambda}^{\left(\begin{smallmatrix}N_1&N_2\\N_4&N_3\end{smallmatrix}\right);\left(\begin{smallmatrix}\sigma_1&\sigma_2\\\sigma_4&\sigma_3\end{smallmatrix}\right)}_{\left(\begin{smallmatrix}P&-P\\K&-K\end{smallmatrix}\right)}$$
$$-\frac{\hat{B}_K}{2N_f}\hat{\lambda}^{\left(\begin{smallmatrix}N_1&N_2\\\bar{N}_4&\bar{N}_3\end{smallmatrix}\right);\left(\begin{smallmatrix}\sigma_1&\sigma_2\\\alpha&\beta\end{smallmatrix}\right)}_{\left(\begin{smallmatrix}P&-P\\K&-K\end{smallmatrix}\right)}\mathsf{T}^{\alpha\beta}_{\sigma_4\sigma_3}-\frac{\hat{B}_P}{2N_f}\mathsf{T}^{\sigma_1\sigma_2}_{\alpha\beta}\hat{\lambda}^{\left(\begin{smallmatrix}\bar{N}_1&\bar{N}_2\\N_4&N_3\end{smallmatrix}\right);\left(\begin{smallmatrix}\alpha&\beta\\\sigma_4&\sigma_3\end{smallmatrix}\right)}_{\left(\begin{smallmatrix}P&-P\\K&-K\end{smallmatrix}\right)}+\frac{\hat{S}_{K,P}}{N_f^2}\mathsf{T}^{\sigma_1\sigma_2}_{\alpha\beta}\mathsf{T}^{\alpha\beta}_{\sigma_4\sigma_3}\delta^{N_1}_{N_4}\delta^{N_2}_{N_3}, \tag{D.12}$$

where $\hat{\lambda}^{\left(\begin{smallmatrix}N_1&N_2\\N_4&N_3\end{smallmatrix}\right);\left(\begin{smallmatrix}\alpha&\beta\\\gamma&\delta\end{smallmatrix}\right)}_{\left(\begin{smallmatrix}P&-P\\K&-K\end{smallmatrix}\right)} = \frac{1}{\sqrt{V_{F,p}V_{F,k}}}\lambda^{\left(\begin{smallmatrix}N_1&N_2\\N_4&N_3\end{smallmatrix}\right);\left(\begin{smallmatrix}\alpha&\beta\\\gamma&\delta\end{smallmatrix}\right)}_{1PH\left(\begin{smallmatrix}p&-p\\k&-k\end{smallmatrix}\right)}$ with $K=ke^\ell$, $P=pe^\ell$ for $\left(\begin{smallmatrix}N_1&N_2\\N_4&N_3\end{smallmatrix}\right)$ in

$$H^{PP}_{1111} = \left\{\left(\begin{smallmatrix}1&1\\1&1\end{smallmatrix}\right),\left(\begin{smallmatrix}1&1\\4&4\end{smallmatrix}\right),\left(\begin{smallmatrix}4&4\\1&1\end{smallmatrix}\right),\left(\begin{smallmatrix}4&4\\4&4\end{smallmatrix}\right)\right\}. \tag{D.13}$$

$\hat{B}_K$ and $\hat{S}_{K,P}$ are defined in Eq. (2.144) and Eq. (2.148). We combine the four coupling functions into a matrix as

$$\hat{\lambda}^{\left(\begin{smallmatrix}\sigma_1&\sigma_2\\\sigma_4&\sigma_3\end{smallmatrix}\right)}_{1PP\left(\begin{smallmatrix}P&-P\\K&-K\end{smallmatrix}\right)} = \begin{pmatrix}\hat{\lambda}^{\left(\begin{smallmatrix}1&1\\1&1\end{smallmatrix}\right);\left(\begin{smallmatrix}\sigma_1&\sigma_2\\\sigma_4&\sigma_3\end{smallmatrix}\right)}_{\left(\begin{smallmatrix}P&-P\\K&-K\end{smallmatrix}\right)} & \hat{\lambda}^{\left(\begin{smallmatrix}1&1\\4&4\end{smallmatrix}\right);\left(\begin{smallmatrix}\sigma_1&\sigma_2\\\sigma_4&\sigma_3\end{smallmatrix}\right)}_{\left(\begin{smallmatrix}P&-P\\K&-K\end{smallmatrix}\right)}\\ \hat{\lambda}^{\left(\begin{smallmatrix}4&4\\1&1\end{smallmatrix}\right);\left(\begin{smallmatrix}\sigma_1&\sigma_2\\\sigma_4&\sigma_3\end{smallmatrix}\right)}_{\left(\begin{smallmatrix}P&-P\\K&-K\end{smallmatrix}\right)} & \hat{\lambda}^{\left(\begin{smallmatrix}4&4\\4&4\end{smallmatrix}\right);\left(\begin{smallmatrix}\sigma_1&\sigma_2\\\sigma_4&\sigma_3\end{smallmatrix}\right)}_{\left(\begin{smallmatrix}P&-P\\K&-K\end{smallmatrix}\right)}\end{pmatrix} \tag{D.14}$$

to write the set of beta functionals in a compact form as

$$\left[\frac{\partial}{\partial\ell}+K\frac{\partial}{\partial K}+P\frac{\partial}{\partial P}\right]\hat{\lambda}^{\left(\begin{smallmatrix}\sigma_1&\sigma_2\\\sigma_4&\sigma_3\end{smallmatrix}\right)}_{1PP\left(\begin{smallmatrix}P&-P\\K&-K\end{smallmatrix}\right)} = -\left(1+\hat{\eta}_K+\hat{\eta}_P\right)\hat{\lambda}^{\left(\begin{smallmatrix}\sigma_1&\sigma_2\\\sigma_4&\sigma_3\end{smallmatrix}\right)}_{1PP\left(\begin{smallmatrix}P&-P\\K&-K\end{smallmatrix}\right)}$$
$$-\frac{\hat{B}_K}{2N_f}\hat{\lambda}^{\left(\begin{smallmatrix}\sigma_1&\sigma_2\\\alpha&\beta\end{smallmatrix}\right)}_{1PP\left(\begin{smallmatrix}P&-P\\K&-K\end{smallmatrix}\right)}\mathsf{T}^{\alpha\beta}_{\sigma_4\sigma_3}\begin{pmatrix}0&1\\1&0\end{pmatrix}-\frac{\hat{B}_P}{2N_f}\mathsf{T}^{\sigma_1\sigma_2}_{\alpha\beta}\begin{pmatrix}0&1\\1&0\end{pmatrix}\hat{\lambda}^{\left(\begin{smallmatrix}\alpha&\beta\\\sigma_4&\sigma_3\end{smallmatrix}\right)}_{1PP\left(\begin{smallmatrix}P&-P\\K&-K\end{smallmatrix}\right)}+\frac{\hat{S}_{K,P}}{N_f^2}\mathsf{T}^{\sigma_1\sigma_2}_{\alpha\beta}\mathsf{T}^{\alpha\beta}_{\sigma_4\sigma_3}\begin{pmatrix}1&0\\0&1\end{pmatrix}. \tag{D.15}$$

The matrix coupling function can be decomposed into the spin-symmetric s-wave $(+,s)$, spin-symmetric d-wave $(+,d)$, spin-anti-symmetric s-wave $(-,s)$ and spin-anti-symmetric d-wave $(-,d)$ channels as

$$\hat{\lambda}^{\left(\begin{smallmatrix}\sigma_1&\sigma_2\\\sigma_4&\sigma_3\end{smallmatrix}\right)}_{1PP\left(\begin{smallmatrix}P&-P\\K&-K\end{smallmatrix}\right)} = \hat{\lambda}^{(+)(s)}_{1PP\left(\begin{smallmatrix}P&-P\\K&-K\end{smallmatrix}\right)}\mathsf{S}^{\sigma_1\sigma_2}_{\sigma_4\sigma_3}\mathscr{P}_s+\hat{\lambda}^{(+)(d)}_{1PP\left(\begin{smallmatrix}P&-P\\K&-K\end{smallmatrix}\right)}\mathsf{S}^{\sigma_1\sigma_2}_{\sigma_4\sigma_3}\mathscr{P}_d+\hat{\lambda}^{(-)(s)}_{1PP\left(\begin{smallmatrix}P&-P\\K&-K\end{smallmatrix}\right)}\mathsf{A}^{\sigma_1\sigma_2}_{\sigma_4\sigma_3}\mathscr{P}_s+\hat{\lambda}^{(-)(d)}_{1PP\left(\begin{smallmatrix}P&-P\\K&-K\end{smallmatrix}\right)}\mathsf{A}^{\sigma_1\sigma_2}_{\sigma_4\sigma_3}\mathscr{P}_d. \tag{D.16}$$

where S and A defined in Eq. (2.172) represent the operators that project spin wavefunctions to the symmetric and anti-symmetric channels, respectively. $\mathscr{P}_s$ and $\mathscr{P}_d$ defined in Eq. (2.156) are the operators that project hot spot wavefunctions to the s and d wave channels, respectively. In each

channel, the beta functional becomes

$$\begin{aligned}&\left[\frac{\partial}{\partial \ell}+K\frac{\partial}{\partial K}+P\frac{\partial}{\partial P}\right]\hat{\lambda}^{(\pm)\binom{s}{d}}_{1PP\binom{P\ -P}{K\ -K}}\\&=-\left(1+\hat{\eta}_K+\hat{\eta}_P+\frac{1^{\binom{s}{d}}Y^{(\pm)}_{PP}}{2N_f}\left[\hat{B}_K+\hat{B}_P\right]\right)\hat{\lambda}^{(\pm)\binom{s}{d}}_{1PP\binom{P\ -P}{K\ -K}}+{Y^{(\pm)}_{PP}}^2\frac{\hat{S}_{K,P}}{N_f^2}.\end{aligned}\tag{D.17}$$

At the quasi-fixed points, the coupling function is given by

$$\begin{aligned}\hat{\lambda}^{*(\pm)\binom{s}{d}}_{1PP\binom{P\ -P}{K\ -K}}\Big|_{w\ll 1}=&\frac{\hat{g}^2_{P,K}\ {Y^{(\pm)}_{PP}}^2}{\pi^2 c N_f^2\sqrt{\hat{V}_{F,K}\hat{V}_{F,P}}}\left[\frac{\hat{g}^2_{K,K}}{\hat{V}_{F,K}}\frac{\Lambda\log\left(\frac{c|\hat{v}_K K+\hat{v}_P P|_\Lambda+c|K-P|_\Lambda+\Lambda}{2\hat{v}_K c|K|_\Lambda+\Lambda}\right)}{c(|\hat{v}_K K+\hat{v}_P P|_\Lambda+|K-P|_\Lambda-2\hat{v}_K|K|_\Lambda)}\right.\\&\left.+\frac{\hat{g}^2_{P,P}}{\hat{V}_{F,P}}\frac{\Lambda\log\left(\frac{c|\hat{v}_K K+\hat{v}_P P|_\Lambda+c|K-P|_\Lambda+\Lambda}{2\hat{v}_P c|P|_\Lambda+\Lambda}\right)}{c(|\hat{v}_K K+\hat{v}_P P|_\Lambda+|K-P|_\Lambda-2\hat{v}_P|P|_\Lambda)}\right].\end{aligned}\tag{D.18}$$

D.2 Group 2

In group 2, the space of IR singularity consists of two intersecting manifolds in the presence of the PH symmetry. The first manifold is the PP-plane in which the center of mass momentum of two incoming particles is zero. The second manifold is the PH-plane in which a particle-hole pair with momentum $2k_F$ is formed across anti-podal patches. (when the momentum is measured with respect to each hot spot the particle-hole pair has zero center of mass momentum). This space can be divided into three disjoint manifolds. The first is the PP-plane that excludes the intersecting line with the PH-plane. The second is the PH-plane that excludes the intersecting line with the PP-plane. The third is the intersecting line. Written as a function of three general external momenta as $\lambda^{\binom{1\ 5}{1\ 5}}_{\binom{p+q/2\ -p+q/2}{k+q/2\ -k+q/2}}$, the space of IR singularity can be divided into four disjoint sub-spaces as (see Fig. D.1)

$$1)\ q=0,\ p+k\neq 0,\qquad 2)\ q\neq 0,\ p+k=0,\qquad 3)\ q=0,\ p+k=0.\tag{D.19}$$

The beta functional in the PP-plane is computed in Sec. 2.5.2. In this section, we present the beta functionals for the couplings in the PH-plane and the intersecting line.

D.2.1 Beta functional for the $2k_F$ PH interaction

Within the PH plane, the coupling function describes the processes in which a pair of electron and hole fluctuate between different antipodal patches (1, 5 and 4, 8 patches) and different relative momenta. The derivation of the beta functional is parallel to the ones for the PP channel. The beta functional for $\lambda^{\binom{1\ 5}{1\ 5};\binom{\sigma_1\ \sigma_2}{\sigma_4\ \sigma_3}}_{\binom{p\ k}{k\ p}}$ in the PH plane but away from the intersecting line is obtained to be

$$\begin{aligned}\beta^{(\lambda);\binom{1\ 5}{1\ 5};\binom{\sigma_1\ \sigma_2}{\sigma_4\ \sigma_3}}_{\binom{p\ k}{k\ p}}=&\left(1+3(z-1)+2\eta_p^{(\psi)}+2\eta_k^{(\psi)}\right)\lambda^{\binom{1\ 5}{1\ 5};\binom{\sigma_1\ \sigma_2}{\sigma_4\ \sigma_3}}_{\binom{p\ k}{k\ p}}\\&+\int \mathrm{d}\rho(q)\left\{\frac{\mathsf{D}_\mu(q;k)}{2\pi N_f}\lambda^{\binom{1\ 8}{4\ 5};\binom{\sigma_1\ \alpha}{\beta\ \sigma_3}}_{\binom{p\ q}{q\ p}}\mathsf{T}^{\beta\sigma_2}_{\sigma_4\alpha}+\frac{\mathsf{D}_\mu(p;q)}{2\pi N_f}\lambda^{\binom{4\ 5}{1\ 8};\binom{\alpha\ \sigma_2}{\sigma_4\ \beta}}_{\binom{q\ k}{k\ q}}\mathsf{T}^{\sigma_1\beta}_{\alpha\sigma_3}\right.\\&-\frac{1}{\pi N_f^2}\mathsf{T}^{\beta\sigma_2}_{\sigma_4\alpha}\mathsf{T}^{\sigma_1\alpha}_{\beta\sigma_3}\mathsf{D}_\mu(p;q)\mathsf{D}_\mu(q;k)\\&\left.-\frac{1}{4\pi}\left(\lambda^{\binom{1\ 5}{1\ 5};\binom{\sigma_1\ \alpha}{\beta\ \sigma_3}}_{\binom{p\ q}{q\ p}}\lambda^{\binom{1\ 5}{1\ 5};\binom{\beta\ \sigma_2}{\sigma_4\ \alpha}}_{\binom{q\ k}{k\ q}}+\lambda^{\binom{1\ 8}{4\ 5};\binom{\sigma_1\ \alpha}{\beta\ \sigma_3}}_{\binom{p\ q}{q\ p}}\lambda^{\binom{4\ 5}{1\ 8};\binom{\beta\ \sigma_2}{\sigma_4\ \alpha}}_{\binom{q\ k}{k\ q}}\right)\right\}.\end{aligned}\tag{D.20}$$

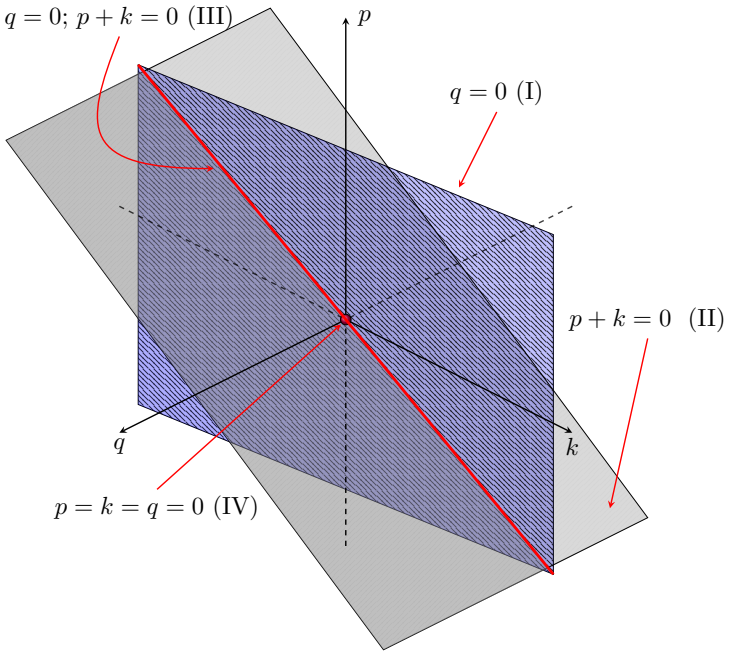

Figure D.1: The space of IR singularity for $\lambda^{\left(\begin{smallmatrix}1&5\\1&5\end{smallmatrix}\right)}_{\left(\begin{smallmatrix}p+q/2&-p+q/2\\k+q/2&-k+q/2\end{smallmatrix}\right)}$. Plane I (plane II) represents the set of external momenta at which the vertex correction is singular in the PP (PH) channel. On line III, where the two planes intersect, the vertex corrections from both channels contribute. As one deviates from the intersecting line but staying within plane I (II), the quantum corrections from plane II (I) dynamically turn off as the deviation of the momentum from the intersecting line is greater than μ/v. Since the volume of the intersecting 'line' vanishes in the small μ limit, one can ignore the contribution of the couplings in the intersecting line to the flow of the couplings within plane I or II far away from the intersecting line.

Here $\lambda^{\left(\begin{smallmatrix}1&5\\1&5\end{smallmatrix}\right);\left(\begin{smallmatrix}\sigma_1&\sigma_2\\\sigma_4&\sigma_3\end{smallmatrix}\right)}_{\left(\begin{smallmatrix}p&k\\k&p\end{smallmatrix}\right)}$ describes the interaction in which an electron with momentum k in hot spot 1 and a hole with $-k$ in hot spot 5 are scattered to electron with p in hot spot 1 and hole with $-p$ in hot spot 5. Since the momentum is measured with respect to the hot spots, the pair of electron and hole in this channel actually carry a non-zero momentum, $2\vec{k}_F$. The physical origin of each term in Eq. (D.20) can be understood in the same way as in Eq. (2.115). The beta functionals for the other couplings that form a closed set of flow equations in the PH-plane are given by

$$\begin{aligned}
\beta^{(\lambda);\left(\begin{smallmatrix}4&5\\1&8\end{smallmatrix}\right);\left(\begin{smallmatrix}\sigma_1&\sigma_2\\\sigma_4&\sigma_3\end{smallmatrix}\right)}_{\left(\begin{smallmatrix}p&k\\k&p\end{smallmatrix}\right)} &= \left(1+3(z-1)+2\eta_p^{(\psi)}+2\eta_k^{(\psi)}\right)\lambda^{\left(\begin{smallmatrix}4&5\\1&8\end{smallmatrix}\right);\left(\begin{smallmatrix}\sigma_1&\sigma_2\\\sigma_4&\sigma_3\end{smallmatrix}\right)}_{\left(\begin{smallmatrix}p&k\\k&p\end{smallmatrix}\right)} \\
&+\int \mathrm{d}\rho(q)\left\{\frac{1}{2\pi N_f}\mathsf{D}_\mu(q;k)\lambda^{\left(\begin{smallmatrix}4&8\\4&8\end{smallmatrix}\right);\left(\begin{smallmatrix}\sigma_1&\alpha\\\beta&\sigma_3\end{smallmatrix}\right)}_{\left(\begin{smallmatrix}p&q\\q&p\end{smallmatrix}\right)}\mathsf{T}^{\beta\sigma_2}_{\sigma_4\alpha}+\frac{1}{2\pi N_f}\mathsf{D}_\mu(p;q)\lambda^{\left(\begin{smallmatrix}1&5\\1&5\end{smallmatrix}\right);\left(\begin{smallmatrix}\alpha&\sigma_2\\\sigma_4&\beta\end{smallmatrix}\right)}_{\left(\begin{smallmatrix}q&k\\k&q\end{smallmatrix}\right)}\mathsf{T}^{\sigma_1\beta}_{\alpha\sigma_3}\right. \\
&\left.-\frac{1}{4\pi}\left(\lambda^{\left(\begin{smallmatrix}4&5\\1&8\end{smallmatrix}\right);\left(\begin{smallmatrix}\sigma_1&\alpha\\\beta&\sigma_3\end{smallmatrix}\right)}_{\left(\begin{smallmatrix}p&q\\q&p\end{smallmatrix}\right)}\lambda^{\left(\begin{smallmatrix}1&5\\1&5\end{smallmatrix}\right);\left(\begin{smallmatrix}\beta&\sigma_2\\\sigma_4&\alpha\end{smallmatrix}\right)}_{\left(\begin{smallmatrix}q&k\\k&q\end{smallmatrix}\right)}+\lambda^{\left(\begin{smallmatrix}4&8\\4&8\end{smallmatrix}\right);\left(\begin{smallmatrix}\sigma_1&\alpha\\\beta&\sigma_3\end{smallmatrix}\right)}_{\left(\begin{smallmatrix}p&q\\q&p\end{smallmatrix}\right)}\lambda^{\left(\begin{smallmatrix}4&5\\1&8\end{smallmatrix}\right);\left(\begin{smallmatrix}\beta&\sigma_2\\\sigma_4&\alpha\end{smallmatrix}\right)}_{\left(\begin{smallmatrix}q&k\\k&q\end{smallmatrix}\right)}\right)\right\},
\end{aligned} \tag{D.21}$$

$$\begin{aligned}
\beta^{(\lambda);\left(\begin{smallmatrix}1&8\\4&5\end{smallmatrix}\right);\left(\begin{smallmatrix}\sigma_1&\sigma_2\\\sigma_4&\sigma_3\end{smallmatrix}\right)}_{\left(\begin{smallmatrix}p&k\\k&p\end{smallmatrix}\right)} &= \left(1+3(z-1)+2\eta_p^{(\psi)}+2\eta_k^{(\psi)}\right)\lambda^{\left(\begin{smallmatrix}1&8\\4&5\end{smallmatrix}\right);\left(\begin{smallmatrix}\sigma_1&\sigma_2\\\sigma_4&\sigma_3\end{smallmatrix}\right)}_{\left(\begin{smallmatrix}p&k\\k&p\end{smallmatrix}\right)} \\
&+\int \mathrm{d}\rho(q)\left\{\frac{1}{2\pi N_f}\mathsf{D}_\mu(q;k)\lambda^{\left(\begin{smallmatrix}1&5\\1&5\end{smallmatrix}\right);\left(\begin{smallmatrix}\sigma_1&\alpha\\\beta&\sigma_3\end{smallmatrix}\right)}_{\left(\begin{smallmatrix}p&q\\q&p\end{smallmatrix}\right)}\mathsf{T}^{\beta\sigma_2}_{\sigma_4\alpha}+\frac{1}{2\pi N_f}\mathsf{D}_\mu(p;q)\lambda^{\left(\begin{smallmatrix}4&8\\4&8\end{smallmatrix}\right);\left(\begin{smallmatrix}\alpha&\sigma_2\\\sigma_4&\beta\end{smallmatrix}\right)}_{\left(\begin{smallmatrix}q&k\\k&q\end{smallmatrix}\right)}\mathsf{T}^{\sigma_1\beta}_{\alpha\sigma_3}\right. \\
&\left.-\frac{1}{4\pi}\left(\lambda^{\left(\begin{smallmatrix}1&5\\1&5\end{smallmatrix}\right);\left(\begin{smallmatrix}\sigma_1&\alpha\\\beta&\sigma_3\end{smallmatrix}\right)}_{\left(\begin{smallmatrix}p&q\\q&p\end{smallmatrix}\right)}\lambda^{\left(\begin{smallmatrix}1&8\\4&5\end{smallmatrix}\right);\left(\begin{smallmatrix}\beta&\sigma_2\\\sigma_4&\alpha\end{smallmatrix}\right)}_{\left(\begin{smallmatrix}q&k\\k&q\end{smallmatrix}\right)}+\lambda^{\left(\begin{smallmatrix}1&8\\4&5\end{smallmatrix}\right);\left(\begin{smallmatrix}\sigma_1&\alpha\\\beta&\sigma_3\end{smallmatrix}\right)}_{\left(\begin{smallmatrix}p&q\\q&p\end{smallmatrix}\right)}\lambda^{\left(\begin{smallmatrix}4&8\\4&8\end{smallmatrix}\right);\left(\begin{smallmatrix}\beta&\sigma_2\\\sigma_4&\alpha\end{smallmatrix}\right)}_{\left(\begin{smallmatrix}q&k\\k&q\end{smallmatrix}\right)}\right)\right\},
\end{aligned} \tag{D.22}$$

$$\begin{aligned}
\beta^{(\lambda);\left(\begin{smallmatrix}4&8\\4&8\end{smallmatrix}\right);\left(\begin{smallmatrix}\sigma_1&\sigma_2\\\sigma_4&\sigma_3\end{smallmatrix}\right)}_{\left(\begin{smallmatrix}p&k\\k&p\end{smallmatrix}\right)} &= \left(1+3(z-1)+2\eta_p^{(\psi)}+2\eta_k^{(\psi)}\right)\lambda^{\left(\begin{smallmatrix}4&8\\4&8\end{smallmatrix}\right);\left(\begin{smallmatrix}\sigma_1&\sigma_2\\\sigma_4&\sigma_3\end{smallmatrix}\right)}_{\left(\begin{smallmatrix}p&k\\k&p\end{smallmatrix}\right)} \\
&+\int \mathrm{d}\rho(q)\left\{\frac{\mathsf{D}_\mu(q;k)}{2\pi N_f}\lambda^{\left(\begin{smallmatrix}4&5\\1&8\end{smallmatrix}\right);\left(\begin{smallmatrix}\sigma_1&\alpha\\\beta&\sigma_3\end{smallmatrix}\right)}_{\left(\begin{smallmatrix}p&q\\q&p\end{smallmatrix}\right)}\mathsf{T}^{\beta\sigma_2}_{\sigma_4\alpha}+\frac{\mathsf{D}_\mu(p;q)}{2\pi N_f}\lambda^{\left(\begin{smallmatrix}1&8\\4&5\end{smallmatrix}\right);\left(\begin{smallmatrix}\alpha&\sigma_2\\\sigma_4&\beta\end{smallmatrix}\right)}_{\left(\begin{smallmatrix}q&k\\k&q\end{smallmatrix}\right)}\mathsf{T}^{\sigma_1\beta}_{\alpha\sigma_3}\right. \\
&-\frac{1}{\pi N_f^2}\mathsf{T}^{\beta\sigma_2}_{\sigma_4\alpha}\mathsf{T}^{\sigma_1\alpha}_{\beta\sigma_3}\mathsf{D}_\mu(p;q)\mathsf{D}_\mu(q;k) \\
&\left.-\frac{1}{4\pi}\left(\lambda^{\left(\begin{smallmatrix}4&5\\1&8\end{smallmatrix}\right);\left(\begin{smallmatrix}\sigma_1&\alpha\\\beta&\sigma_3\end{smallmatrix}\right)}_{\left(\begin{smallmatrix}p&q\\q&p\end{smallmatrix}\right)}\lambda^{\left(\begin{smallmatrix}1&8\\4&5\end{smallmatrix}\right);\left(\begin{smallmatrix}\beta&\sigma_2\\\sigma_4&\alpha\end{smallmatrix}\right)}_{\left(\begin{smallmatrix}q&k\\k&q\end{smallmatrix}\right)}+\lambda^{\left(\begin{smallmatrix}4&8\\4&8\end{smallmatrix}\right);\left(\begin{smallmatrix}\sigma_1&\alpha\\\beta&\sigma_3\end{smallmatrix}\right)}_{\left(\begin{smallmatrix}p&q\\q&p\end{smallmatrix}\right)}\lambda^{\left(\begin{smallmatrix}4&8\\4&8\end{smallmatrix}\right);\left(\begin{smallmatrix}\beta&\sigma_2\\\sigma_4&\alpha\end{smallmatrix}\right)}_{\left(\begin{smallmatrix}q&k\\k&q\end{smallmatrix}\right)}\right)\right\}.
\end{aligned} \tag{D.23}$$

D.2.2 Beta functional in the intersection between the PP and PH planes

Within the PP-plane with $k+p\neq 0$, an operator mixes with other operators only within the plane. Similarly, an operator at generic momenta within the PH-plane only mixes with other operators within the PH-plane. However, an operator at the intersection of the two planes can mix with operators in both planes. Within the one-dimensional manifold in which the PP and PH planes meet, the coupling function is parameterized by one variable as $\lambda^{\left(\begin{smallmatrix}1&5\\1&5\end{smallmatrix}\right);\left(\begin{smallmatrix}\sigma_1&\sigma_2\\\sigma_4&\sigma_3\end{smallmatrix}\right)}_{\left(\begin{smallmatrix}-k&k\\k&-k\end{smallmatrix}\right)}$. While the beta functional takes a more complicated form in the line, the underlying physics of each term is not different from the ones that determine the beta functionals in each of the PP and PH planes. The beta functional for the couplings at a generic momentum point ($k\neq 0$) on this line is

$$\begin{aligned}
\beta^{(\lambda);\left(\begin{smallmatrix}N_1&N_2\\N_4&N_3\end{smallmatrix}\right);\left(\begin{smallmatrix}\sigma_1&\sigma_2\\\sigma_4&\sigma_3\end{smallmatrix}\right)}_{\left(\begin{smallmatrix}-k&k\\k&-k\end{smallmatrix}\right)} &= \left(1+3(z-1)+\eta_{-k}^{(\psi,N_1)}+\eta_k^{(\psi,N_2)}+\eta_{-k}^{(\psi,N_3)}+\eta_k^{(\psi,N_4)}\right)\lambda^{\left(\begin{smallmatrix}N_1&N_2\\N_4&N_3\end{smallmatrix}\right);\left(\begin{smallmatrix}\sigma_1&\sigma_2\\\sigma_4&\sigma_3\end{smallmatrix}\right)}_{\left(\begin{smallmatrix}-k&k\\k&-k\end{smallmatrix}\right)} \\
&+\int \mathrm{d}\rho(q)\left\{-\frac{\mathsf{D}_\mu(-k;q)}{2\pi N_f}\left[\mathsf{T}^{\sigma_1\sigma_2}_{\alpha\beta}\lambda^{\left(\begin{smallmatrix}\bar N_1&\bar N_2\\N_4&N_3\end{smallmatrix}\right);\left(\begin{smallmatrix}\alpha&\beta\\\sigma_4&\sigma_3\end{smallmatrix}\right)}_{\left(\begin{smallmatrix}q&-q\\k&-k\end{smallmatrix}\right)}-\lambda^{\left(\begin{smallmatrix}\bar N_1&N_2\\N_4&\bar N_3\end{smallmatrix}\right);\left(\begin{smallmatrix}\alpha&\sigma_2\\\sigma_4&\beta\end{smallmatrix}\right)}_{\left(\begin{smallmatrix}q&k\\k&q\end{smallmatrix}\right)}\mathsf{T}^{\sigma_1\beta}_{\alpha\sigma_3}\right]\right. \\
&\left.-\frac{\mathsf{D}_\mu(q;k)}{2\pi N_f}\left[\lambda^{\left(\begin{smallmatrix}N_1&N_2\\\bar N_4&\bar N_3\end{smallmatrix}\right);\left(\begin{smallmatrix}\sigma_1&\sigma_2\\\alpha&\beta\end{smallmatrix}\right)}_{\left(\begin{smallmatrix}-k&k\\q&-q\end{smallmatrix}\right)}\mathsf{T}^{\alpha\beta}_{\sigma_4\sigma_3}-\lambda^{\left(\begin{smallmatrix}N_1&\bar N_2\\\bar N_4&N_3\end{smallmatrix}\right);\left(\begin{smallmatrix}\sigma_1&\alpha\\\beta&\sigma_3\end{smallmatrix}\right)}_{\left(\begin{smallmatrix}-k&q\\q&-k\end{smallmatrix}\right)}\mathsf{T}^{\beta\sigma_2}_{\sigma_4\alpha}\right]\right\} \\
&+\frac{1}{\pi N_f^2}\int \mathrm{d}\rho(q)\left[\mathsf{T}^{\sigma_1\sigma_2}_{\alpha\beta}\mathsf{T}^{\alpha\beta}_{\sigma_4\sigma_3}\mathsf{D}_\mu(-k;q)\mathsf{D}_\mu(q;k)-\mathsf{T}^{\sigma_1\beta}_{\alpha\sigma_3}\mathsf{T}^{\alpha\sigma_2}_{\sigma_4\beta}\mathsf{D}_\mu(-k;q)\mathsf{D}_\mu(q;k)\right]\delta^{N_1}_{N_4}\delta^{N_2}_{N_3} \\
&+\frac{1}{4\pi}\int \mathrm{d}\rho(q)\left[\left(\lambda^{\left(\begin{smallmatrix}N_1&N_2\\M&M'\end{smallmatrix}\right);\left(\begin{smallmatrix}\sigma_1&\sigma_2\\\beta&\alpha\end{smallmatrix}\right)}_{\left(\begin{smallmatrix}-k&k\\q&-q\end{smallmatrix}\right)}\lambda^{\left(\begin{smallmatrix}M&M'\\N_4&N_3\end{smallmatrix}\right);\left(\begin{smallmatrix}\beta&\alpha\\\sigma_4&\sigma_3\end{smallmatrix}\right)}_{\left(\begin{smallmatrix}q&-q\\k&-k\end{smallmatrix}\right)}-\lambda^{\left(\begin{smallmatrix}N_1&M\\M'&N_3\end{smallmatrix}\right);\left(\begin{smallmatrix}\sigma_1&\alpha\\\beta&\sigma_3\end{smallmatrix}\right)}_{\left(\begin{smallmatrix}-k&q\\q&-k\end{smallmatrix}\right)}\lambda^{\left(\begin{smallmatrix}M'&N_2\\N_4&M\end{smallmatrix}\right);\left(\begin{smallmatrix}\beta&\sigma_2\\\sigma_4&\alpha\end{smallmatrix}\right)}_{\left(\begin{smallmatrix}q&k\\k&q\end{smallmatrix}\right)}\right)\right].
\end{aligned} \tag{D.24}$$

Here $\left(\begin{smallmatrix}N_1&N_2\\N_4&N_3\end{smallmatrix}\right)$ represents any of the elements in the set of

$$h^{(1)}_{1515}=\left\{\left(\begin{smallmatrix}1&5\\1&5\end{smallmatrix}\right),\left(\begin{smallmatrix}1&5\\4&8\end{smallmatrix}\right),\left(\begin{smallmatrix}4&8\\1&5\end{smallmatrix}\right),\left(\begin{smallmatrix}4&8\\4&8\end{smallmatrix}\right),\left(\begin{smallmatrix}1&8\\4&5\end{smallmatrix}\right),\left(\begin{smallmatrix}4&5\\1&8\end{smallmatrix}\right)\right\}. \tag{D.25}$$

M and M' are summed over hot spot indices for which the four-fermion couplings are in $h^{(1)}_{1515}$. If $k=0$, the four-fermion operator mixes with an even larger set of operators. However, we don't

need to introduce counter terms for the operators right at the hot spots because the IR singularity is localized within the measure zero set in the low-energy limit.

How does Eq. (D.24) change to Eqs. (2.115)- (2.118) or Eqs. (D.20)- (D.23) as one moves away from the intersecting line staying either within the PP or PH plane? To answer this question, let us examine how the contribution of the PP diagram to $\lambda^{\binom{1\ 5}{1\ 5};\binom{\sigma_1\ \sigma_2}{\sigma_4\ \sigma_3}}_{\binom{p\ k}{k\ p}}$ decays as $p+k$ becomes non-zero away from the intersecting line. Away from the intersecting line but within the PH plane, the total momentum of the electron pair is non-zero, which makes it impossible to put both internal electrons on the Fermi surface within the loop: if a pair of electrons with momenta k and p on the Fermi surface near hot spots 1 and 5 are scattered to hot spots 4 and 8, the minimum energy that the virtual electron pair must carry is order of $v_p p + v_k k$. This cuts off the IR divergence in the PP diagram in the low energy limit. Therefore, the contribution of the PP diagram to $\lambda^{\binom{1\ 5}{1\ 5};\binom{\sigma_1\ \sigma_2}{\sigma_4\ \sigma_3}}_{\binom{p\ k}{k\ p}}$ becomes negligible for $\mu \ll |v_p p + v_k k|$. This is confirmed through an explicit calculation in Appendix B. Similarly, the contribution of the PH diagram to $\lambda^{\binom{1\ 5}{1\ 5};\binom{\sigma_1\ \sigma_2}{\sigma_4\ \sigma_3}}_{\binom{p\ -p}{k\ -k}}$ becomes negligible for $\mu \ll |v_p p + v_k k|$. This implies that Eq. (D.24) crossovers to Eqs. (2.115)- (2.118) or Eqs. (D.20)- (D.23) as the momentum deviates more than μ/v away from the intersecting line in each plane.

D.2.3 Decoupling between the PP and PH-planes

The full beta functionals that describe the coupling functions defined in this space are given by Eqs. (2.115)-(2.118), Eqs. (D.20)-(D.23) and Eq. (D.24). The couplings in the PP plane are coupled with the couplings in the PH plane through the intersection. However, a simplification arises at low energies. In the low-energy limit, the phase space of the intersection becomes vanishingly small compared to the phase space of the PP and PH planes. To see this in more detail, let us consider the beta functional of $\lambda^{\binom{1\ 5}{1\ 5};\binom{\sigma_1\ \sigma_2}{\sigma_4\ \sigma_3}}_{\binom{p\ -p}{k\ -k}}$ for p and k far away from the intersecting line, that is $|v_k k + v_p p| > \mu$. The q integration in Eq. (2.115) can be broken into the contribution that depends on the couplings in the intersecting line and the remaining contribution that does not depend on the couplings in the intersecting line as

$$\begin{aligned}\beta^{(\lambda);\binom{1\ 5}{1\ 5};\binom{\sigma_1\ \sigma_2}{\sigma_4\ \sigma_3}}_{\binom{p\ -p}{k\ -k}} &= \left(1+3(z-1)+2\eta_p^{(\psi)}+2\eta_k^{(\psi)}\right)\lambda^{\binom{1\ 5}{1\ 5};\binom{\sigma_1\ \sigma_2}{\sigma_4\ \sigma_3}}_{\binom{p\ -p}{k\ -k}} \\ &+ \int_{C_{k,p}} \mathrm{d}\rho(q)\ \ V^{(\lambda);\binom{1\ 5}{1\ 5};\binom{\sigma_1\ \sigma_2}{\sigma_4\ \sigma_3}}_{p,k,q} + \int_{C'_{k,p}} \mathrm{d}\rho(q)\ \ V^{(\lambda);\binom{1\ 5}{1\ 5};\binom{\sigma_1\ \sigma_2}{\sigma_4\ \sigma_3}}_{p,k,q},\end{aligned} \tag{D.26}$$

where

$$\begin{aligned}V^{(\lambda);\binom{1\ 5}{1\ 5};\binom{\sigma_1\ \sigma_2}{\sigma_4\ \sigma_3}}_{p,k,q} &= -\frac{\mathsf{D}_\mu(p;q)}{2\pi N_f}\mathsf{T}^{\sigma_1\sigma_2}_{\alpha\beta}\lambda^{\binom{4\ 8}{1\ 5};\binom{\alpha\ \ \beta}{\sigma_4\ \sigma_3}}_{\binom{q\ -q}{k\ -k}} - \frac{\mathsf{D}_\mu(q;k)}{2\pi N_f}\lambda^{\binom{1\ 5}{4\ 8};\binom{\sigma_1\ \sigma_2}{\alpha\ \ \beta}}_{\binom{p\ -p}{q\ -q}}\mathsf{T}^{\alpha\beta}_{\sigma_4\sigma_3} \\ &+ \frac{1}{\pi N_f^2}\mathsf{T}^{\sigma_1\sigma_2}_{\alpha\beta}\mathsf{T}^{\alpha\beta}_{\sigma_4\sigma_3}\mathsf{D}_\mu(p;q)\mathsf{D}_\mu(q;k) \\ &+ \frac{1}{4\pi}\left(\lambda^{\binom{1\ 5}{1\ 5};\binom{\sigma_1\ \sigma_2}{\beta\ \ \alpha}}_{\binom{p\ -p}{q\ -q}}\lambda^{\binom{1\ 5}{1\ 5};\binom{\beta\ \ \alpha}{\sigma_4\ \sigma_3}}_{\binom{q\ -q}{k\ -k}} + \lambda^{\binom{1\ 5}{4\ 8};\binom{\sigma_1\ \sigma_2}{\beta\ \ \alpha}}_{\binom{p\ -p}{q\ -q}}\lambda^{\binom{4\ 8}{1\ 5};\binom{\beta\ \ \alpha}{\sigma_4\ \sigma_3}}_{\binom{q\ -q}{k\ -k}}\right),\end{aligned} \tag{D.27}$$

and

$$\begin{aligned}C_{k,p} &= \left\{q \;\middle|\; |v_q q + v_k k| > \mu\ \&\ |v_q q + v_p p| > \mu\right\}, \\ C'_{k,p} &= (C_{k,p})^{\complement}.\end{aligned} \tag{D.28}$$

$C_{k,p}$ represents the set of q at which all coupling functions in $V^{(\lambda);\binom{1\ 5}{1\ 5};\binom{\sigma_1\ \sigma_2}{\sigma_4\ \sigma_3}}_{p,k,q}$ are away from the intersection and obey the beta functionals given by Eqs. (2.115)-(2.118). $C'_{k,p}$, being the complement

of $C_{k,p}$, represents the set of q at which at least one coupling function in $V^{(\lambda);\binom{1\ 5}{1\ 5};\binom{\sigma_1\ \sigma_2}{\sigma_4\ \sigma_3}}_{p,k,q}$ is in the intersection of the PP and PH planes and satisfy Eq. (D.24). In the small μ limit, the phase space of $C'_{k,p}$ vanishes linearly in μ. Consequently, the contribution of $C'_{k,p}$ to the beta functions of $\lambda^{\binom{1\ 5}{1\ 5};\binom{\sigma_1\ \sigma_2}{\sigma_4\ \sigma_3}}_{\binom{p\ -p}{k\ -k}}$ away from the intersection becomes negligible in the small μ limit. Similarly, the contributions of the intersection to the beta functional of the couplings in the PH plane away from the intersection are negligible in the low-energy limit. Therefore, one can ignore the intersection for the purpose of understanding the RG flow of the coupling functions in the PP and PH planes away from the intersecting line. As a result, the couplings in the PP plane and the couplings in the PH plane become effectively decoupled in the low-energy limit, and we can study Eqs. (2.115)-(2.118) and Eqs. (D.20)-(D.23), separately. The solution of the beta function in the PP-plane is discussed in Sec. 2.6.3. Here, we present the solution of the beta function for the couplings defined in the PH-plane.

D.2.4 Solution of the beta functional for the $2k_F$ PH interaction

The closed set of beta functionals for $\lambda^{\binom{1\ 5}{1\ 5};\binom{\sigma_1\ \sigma_2}{\sigma_4\ \sigma_3}}_{\binom{p\ k}{k\ p}}$, $\lambda^{\binom{1\ 8}{4\ 5};\binom{\sigma_1\ \sigma_2}{\sigma_4\ \sigma_3}}_{\binom{p\ k}{k\ p}}$, $\lambda^{\binom{4\ 5}{1\ 8};\binom{\sigma_1\ \sigma_2}{\sigma_4\ \sigma_3}}_{\binom{p\ k}{k\ p}}$, $\lambda^{\binom{4\ 8}{4\ 8};\binom{\sigma_1\ \sigma_2}{\sigma_4\ \sigma_3}}_{\binom{p\ k}{k\ p}}$ that describe four-fermion couplings in the PH channel with momentum $2\vec{k}_F$ are given by Eqs. (D.20)-(D.23). With

$$\lambda^{\binom{\sigma_1\ \sigma_2}{\sigma_4\ \sigma_3}}_{2PH\binom{p\ k}{k\ p}} = \begin{pmatrix} \lambda^{\binom{1\ 5}{1\ 5};\binom{\sigma_1\ \sigma_2}{\sigma_4\ \sigma_3}}_{\binom{p\ k}{k\ p}} & \lambda^{\binom{1\ 8}{4\ 5};\binom{\sigma_1\ \sigma_2}{\sigma_4\ \sigma_3}}_{\binom{p\ k}{k\ p}} \\ \lambda^{\binom{4\ 5}{1\ 8};\binom{\sigma_1\ \sigma_2}{\sigma_4\ \sigma_3}}_{\binom{p\ k}{k\ p}} & \lambda^{\binom{4\ 8}{4\ 8};\binom{\sigma_1\ \sigma_2}{\sigma_4\ \sigma_3}}_{\binom{p\ k}{k\ p}} \end{pmatrix}, \tag{D.29}$$

the set of beta functionals can be combined into

$$\begin{aligned} \frac{\partial}{\partial \ell}\lambda^{\binom{\sigma_1\ \sigma_2}{\sigma_4\ \sigma_3}}_{2PH\binom{p\ k}{k\ p}} =& -\left(1+3(z-1)+2\eta^{(\psi)}_k+2\eta^{(\psi)}_p\right)\lambda^{\binom{\sigma_1\ \sigma_2}{\sigma_4\ \sigma_3}}_{2PH\binom{p\ k}{k\ p}} \\ &+\frac{1}{4\pi}\int\frac{dq}{2\pi\mu V_{F,q}}\left[\lambda^{\binom{\sigma_1\ \alpha}{\beta\ \sigma_3}}_{2PH\binom{p\ q}{q\ p}}-\frac{2\mathsf{T}^{\sigma_1\alpha}_{\beta\sigma_3}}{N_f}\mathsf{D}_\mu(q;p)\begin{pmatrix}0&1\\1&0\end{pmatrix}\right] \\ &\times\left[\lambda^{\binom{\beta\ \sigma_2}{\sigma_4\ \alpha}}_{2PH\binom{q\ k}{k\ q}}-\frac{2\mathsf{T}^{\beta\sigma_2}_{\sigma_4\alpha}}{N_f}\mathsf{D}_\mu(q;k)\begin{pmatrix}0&1\\1&0\end{pmatrix}\right]. \end{aligned} \tag{D.30}$$

To make the analysis parallel with that of the PH channel, we define

$$\tilde{\lambda}^{\binom{\alpha\ \beta}{\gamma\ \delta}}_{2PH\binom{P\ K}{K\ P}} = \frac{1}{\sqrt{V_{F,p}V_{F,k}}}\left[-\lambda^{\binom{\alpha\ \beta}{\gamma\ \delta}}_{2PH\binom{p\ k}{k\ p}}+\frac{2\mathsf{T}^{\alpha\beta}_{\gamma\delta}}{N_f}\mathsf{D}_\mu(p;k)\begin{pmatrix}0&1\\1&0\end{pmatrix}\right] \tag{D.31}$$

with $P=pe^\ell$, $K=ke^\ell$ to rewrite the beta functional as

$$\begin{aligned} \frac{\partial}{\partial \ell}\tilde{\lambda}^{\binom{\sigma_1\ \sigma_2}{\sigma_4\ \sigma_3}}_{2PH\binom{P\ K}{K\ P}} =& -\left(1+K\frac{\partial}{\partial K}+P\frac{\partial}{\partial P}+\hat{\eta}_K+\hat{\eta}_P\right)\tilde{\lambda}^{\binom{\sigma_1\ \sigma_2}{\sigma_4\ \sigma_3}}_{2PH\binom{P\ K}{K\ P}} \\ &-\frac{1}{4\pi}\int\frac{\mathrm{d}Q}{2\pi\Lambda}\tilde{\lambda}^{\binom{\sigma_1\ \alpha}{\beta\ \sigma_3}}_{2PH\binom{P\ Q}{Q\ P}}\tilde{\lambda}^{\binom{\beta\ \sigma_2}{\sigma_4\ \alpha}}_{2PH\binom{Q\ K}{K\ Q}}+\frac{2\mathsf{T}^{\sigma_1\sigma_2}_{\sigma_4\sigma_3}}{N_f}\mathsf{R}(K,P)(\mathscr{P}_s-\mathscr{P}_d), \end{aligned} \tag{D.32}$$

where $\mathsf{R}(K,P)$ and $\hat{\eta}_K$, are defined in Eqs. (2.181). The coupling function is decomposed into four different channels as

$$\tilde{\lambda}^{\binom{\sigma_1\ \sigma_2}{\sigma_4\ \sigma_3}}_{2PH\{K_i\}} = \tilde{\lambda}^{(t)(s)}_{2PH\{K_i\}}\mathsf{I}^{\sigma_1\sigma_2}_{\sigma_4\sigma_3}\mathscr{P}_s+\tilde{\lambda}^{(t)(d)}_{2PH\{K_i\}}\mathsf{I}^{\sigma_1\sigma_2}_{\sigma_4\sigma_3}\mathscr{P}_d+\tilde{\lambda}^{(a)(s)}_{2PH\{K_i\}}\chi^{\sigma_1\sigma_2}_{\sigma_4\sigma_3}\mathscr{P}_s+\tilde{\lambda}^{(a)(d)}_{2PH\{K_i\}}\chi^{\sigma_1\sigma_2}_{\sigma_4\sigma_3}\mathscr{P}_d, \tag{D.33}$$

where $\mathsf{I}^{\sigma_1\sigma_2}_{\sigma_4\sigma_3}$ and $\chi^{\sigma_1\sigma_2}_{\sigma_4\sigma_3}$ are defined in Eq. (2.153). Each of the four channels are $SU(N_c)$-trivial s-wave, $SU(N_c)$-trivial d-wave, $SU(N_c)$-adjoint s-wave and $SU(N_c)$-adjoint d-wave channels. The beta functional in each channel becomes

$$\begin{aligned}\frac{\mathrm{d}}{\mathrm{d}\ell}\tilde{\lambda}^{\binom{t}{a},\binom{s}{d}}_{2PH\binom{P\ K}{K\ P}} &= -\left(1+K\frac{\partial}{\partial K}+P\frac{\partial}{\partial P}+\hat{\eta}_K+\hat{\eta}_P\right)\tilde{\lambda}^{\binom{t}{a},\binom{s}{d}}_{2PH\binom{P\ K}{K\ P}} \\ &\quad -\frac{1}{4\pi}\int\frac{\mathrm{d}Q}{2\pi\Lambda}\tilde{\lambda}^{\binom{t}{a},\binom{s}{d}}_{2PH\binom{P\ Q}{Q\ P}}\tilde{\lambda}^{\binom{t}{a},\binom{s}{d}}_{2PH\binom{Q\ K}{K\ Q}}+\frac{2}{N_f}Y^{\binom{t}{a}}_{PH}1^{\binom{s}{d}}\mathsf{R}(P,K),\end{aligned} \tag{D.34}$$

where $1^{\binom{s}{d}}$ is defined in Eq. (2.157).

Eq. (D.34) has the same form as Eq. (2.180). The only difference is the change in the spin wavefunction and the associated eigenvalue determined from the representations of two fermions in the PP and PH channels. The spin symmetric and anti-symmetric representations in the PP channel with eigenvalues $Y^{(\pm)}_{PP}$ in the last term of Eq. (2.180) are replaced with the trivial and adjoint representations in the PH channel with eigenvalues $Y^{\binom{t}{a}}_{PH}$ in Eq. (2.154) [2]. All discussions on $\tilde{\lambda}_{2PP}$ straightforwardly generalize to $\tilde{\lambda}_{2PH}$. In the PH channel, the spin fluctuations gives rise to an attractive interaction in the $SU(N_c)$-adjoint s-wave channel and the $SU(N_c)$-trivial d-wave channel with the $SU(N_c)$-trivial d-wave channel being the stronger. The other two channels, $SU(N_c)$-adjoint d-wave and $SU(N_c)$-trivial s-wave, are repulsive. Therefore, $\tilde{\lambda}^{(t)(d)}_{2PH}$ and $\tilde{\lambda}^{(a)(s)}_{2PH}$ become non-Hermitian (complex) at quasi-fixed point.

[2] For $N_c = 2$, even that difference goes away because the fundamental and anti-fundamental representations are identical for $SU(2)$.

Appendix E

Spinors in curved spacetime

In this appendix, we review the background material for the theory of spinor in curved spacetimes. For concreteness, we consider four-dimensional spacetimes, but the discussion can be generalized to any dimension (for more details, see Ref. [27] for example). Suppose manifold M is endowed with metric $g_{\mu\nu}$. One can define a set of orthonormal basis that spans the space of one-forms through which the metric two-form can be written as

$$g_{\mu\nu}\mathrm{d}x^\mu \otimes \mathrm{d}x^\nu = \eta_{ab}\hat{\theta}^a \otimes \hat{\theta}^b, \tag{E.1}$$

where $\hat{\theta}^a = \mathfrak{e}^a{}_\mu \mathrm{d}x^\mu$ is the orthonormal basis, $\mathfrak{e}^a{}_\mu$ is the vielbein and $\eta_{ab} = \mathrm{diag}(-1,+1,+1,+1)$[1]. One can also introduce a set of vectors that is dual to $\{\hat{\theta}^a\}$ through the relation $\langle \hat{\theta}^a, \hat{e}_b\rangle = \delta^a{}_b$, where $\hat{e}_a = \mathfrak{e}_a{}^\mu \partial_\mu$. The bases $\{\hat{e}_a\}$ and $\{\hat{\theta}^a\}$ are called the *non-coordinate bases*. There is clearly the freedom to rotate the orthonormal basis through the local Lorentz transformations. A relativistic fermion forms a spinor representation under this local Lorentz transformation. From the requirement that the action should be invariant under the local Lorentz transformation, the action for a Dirac spinor with mass m coupled to a gauge field $\mathcal{A}_\mu(x)$ is written as

$$\Gamma_\psi = \int_M \sqrt{|g|}\mathrm{d}^4x\ \bar{\psi}(x)\gamma^c \mathfrak{e}_c{}^\mu \left(\partial_\mu + \mathcal{A}_\mu(x) + \frac{i}{2}\omega_{\mu,ab}\Sigma^{ab} + m\right)\psi(x). \tag{E.2}$$

Here, $\sqrt{|g|} = |\mathfrak{e}|$ with $\mathfrak{e} = \det \mathfrak{e}^a{}_\mu$. $\bar{\psi} = \psi^\dagger\gamma^0$, where the gamma matrices γ^a satisfy the Clifford algebra $\{\gamma^a, \gamma^b\} = 2\eta^{ab}$ that furnishes the spinor representation of local Lorentz transformation. $\Sigma^{ab} = \frac{i}{4}\left[\gamma^a, \gamma^b\right]$ is the generator of the local Lorentz transformations. The matrix-valued one form with elements $\omega_{\mu,ab} = (\omega_{ab})_\mu$ is the spin connection that acts as the gauge connection for the local Lorentz transformation. The connection one-form and the vielbein completely determines the torsion and curvature of the spacetime through the *Cartan structure equations*,

$$\mathrm{d}\hat{\theta}^a + \omega^a{}_b \wedge \hat{\theta}^b = T^a, \tag{E.3a}$$

$$\mathrm{d}\omega^a{}_b + \omega^a{}_c \wedge \omega^c{}_b = R^a{}_b, \tag{E.3b}$$

where d is the exterior derivative, $\wedge$ is the wedge product, T^a is the torsion two-form and $R^a{}_b$ is the curvature two-form. T^a and $R^a{}_b$ are gauge covariant measures that characterize the geometry of the manifold M. The torsion measures the screw or twist on a frame when parallel transported along two directions in the manifold M. The curvature is a measure of the holonomy (gauge flux) acquired by a vector transported parallely around a loop.

[1] For Euclidean signature, the Minkowskian metric η_{ab} is replaced with $\delta_{ab} = \mathrm{diag}(+1,+1,+1,+1)$. In the following two paragraphs, we use the Einstein convention for the Greek and Latin indices.

Appendix F

Schwarzschild Geodesics

In this appendix, we briefly review the Schwarzschild spacetime that describes a black hole and the motion of a free falling object (for a more complete review, see [215] for example). The Schwarzschild metric is an exact solution to Einstein field equations, which describes the spacetime outside a static, neutral and spherically symmetric compact object. In the spherical coordinate, the line element for the Schwarzschild metric can be written as

$$ds^2 = \left(1 - \frac{r_s}{r}\right) c^2 \mathrm{d}t^2 - \frac{\mathrm{d}r^2}{1 - \frac{r_s}{r}} - r^2 \mathrm{d}\theta^2 - r^2 \sin^2\theta \mathrm{d}\phi^2, \tag{F.1}$$

where M is the mass and c is the sped of light. t is the time coordinate that describes the proper time of an asymptotic observer who is at $r = \infty$, where r is the radial coordinate.

$$r_s = \frac{2GM}{c^2} \tag{F.2}$$

is the Schwarzschild radius, where G is the gravitational constant. When the radius of the compact object is smaller than r_s, it describes a black hole with an event horizon at $r = r_s$ inside of which the future light cone always points toward $r = 0$, and thus no escape. As the free falling object approaches the horizon from the outside, the lapse of its proper time is infinitely slowed down as compared to that of the proper time of an asymptotic observer. This gives rise to a critical slowdown of the motion of the free falling object as observed by the asymptotic observer. For an object that falls radially to the black hole at a fixed angle (say $\theta = \pi/2$ and $\phi = 0$), the geodesic equation of motion gives

$$t \sim \frac{r_s}{c} \log\left(\frac{\left|\sqrt{\frac{r}{r_s}} + 1\right|}{\sqrt{\frac{r}{r_s}} - 1}\right) \tag{F.3}$$

near the horizon. As r approaches r_s, t diverges logarithmically. This implies that the asymptotic observer will never see the passing of the free falling object across the horizon.

Appendix G

The pairing term for Bogoliubov quasiparticles

In this appendix we derive Eq. (3.23). We begin by writing the pairing interaction between electrons in segments 1 and 5 (See Fig. 3.1),

$$S_{4\mathrm{f}}^{\left(\begin{smallmatrix}1&5\\1&5\end{smallmatrix}\right)} = \frac{1}{4\mu}\sum_{\{\sigma_i\}}\int \frac{\mathrm{d}\omega_p \mathrm{d}\omega_k \mathrm{d}\omega_q\ \mathrm{d}^2p\ \mathrm{d}^2k\ \mathrm{d}^2q}{(2\pi)^9}\psi^*_{1,\sigma_1}\left(\omega_p+\frac{\omega_q}{2},\vec{p}+\frac{\vec{q}}{2}\right)\psi^*_{5,\sigma_2}\left(-\omega_p+\frac{\omega_q}{2},-\vec{p}+\frac{\vec{q}}{2}\right)$$
$$\times\lambda^{\left(\begin{smallmatrix}1&5\\1&5\end{smallmatrix}\right);\left(\begin{smallmatrix}\sigma_1&\sigma_2\\\sigma_4&\sigma_3\end{smallmatrix}\right)}_{\left(\begin{smallmatrix}p+\frac{q}{2}&-p+\frac{q}{2}\\k+\frac{q}{2}&-k+\frac{q}{2}\end{smallmatrix}\right)}\psi_{5,\sigma_3}\left(-\omega_k+\frac{\omega_q}{2},-\vec{k}+\frac{\vec{q}}{2}\right)\psi_{1,\sigma_4}\left(\omega_k+\frac{\omega_q}{2},\vec{k}+\frac{\vec{q}}{2}\right). \tag{G.1}$$

Here, λ is the four fermion coupling function generated from the critical spin fluctuations. The specific momentum-dependence of the coupling function is not important for us. The functional renormalization group analysis shows that the strongest attractive interaction is generated in the spin-singlet and d-wave channel, and the significant pairing interaction is generated not only for the electrons at the hot spots but also for electrons that are far away from the hot spots [30]. We are using the frequency defined in Eq. (3.7). Performing a Hubbard-Stratonovich transformation on the quartic interaction yields

$$e^{-S_{4\mathrm{f}}^{\left(\begin{smallmatrix}1&5\\1&5\end{smallmatrix}\right)}} = \int \mathcal{D}\Delta\mathcal{D}\Delta^* \exp\left\{-\sum_{\{\sigma_i\}}\int\left(\prod_{l=p,q,k,q'}\frac{\mathrm{d}\omega_l\ \mathrm{d}^2l}{(2\pi)^3}\right)\left[\tilde{\Delta}^{\dagger\,\sigma_1\sigma_2}_{(\omega_p,\vec{p};\omega_q,\vec{q})}\left[-\bar{\lambda}\right]^{\sigma_1\sigma_2;\sigma_3\sigma_4}_{(\omega_p,\vec{p},\omega_q,\vec{q};\omega_k,\vec{k},\omega_{q'},\vec{q'})}\tilde{\Delta}^{\sigma_3\sigma_4}_{(\omega_k,\vec{k};\omega_{q'},\vec{q'})}\right.\right.$$
$$-\psi^*_{1,\sigma_1}\left(\omega_p+\frac{\omega_q}{2},\vec{p}+\frac{\vec{q}}{2}\right)\psi^*_{5,\sigma_2}\left(-\omega_p+\frac{\omega_q}{2},-\vec{p}+\frac{\vec{q}}{2}\right)\left[-\bar{\lambda}\right]^{\sigma_1\sigma_2;\sigma_3\sigma_4}_{(\omega_p,\vec{p},\omega_q,\vec{q};\omega_k,\vec{k},\omega_{q'},\vec{q'})}\tilde{\Delta}^{\sigma_3\sigma_4}_{(\omega_k,\vec{k};\omega_{q'},\vec{q'})}$$
$$\left.\left.-\tilde{\Delta}^{\dagger\,\sigma_1\sigma_2}_{(\omega_p,\vec{p};\omega_q,\vec{q})}\left[-\bar{\lambda}\right]^{\sigma_1\sigma_2;\sigma_3\sigma_4}_{(\omega_p,\vec{p},\omega_q,\vec{q};\omega_k,\vec{k},\omega_{q'},\vec{q'})}\psi_{5,\sigma_3}\left(-\omega_k+\frac{\omega_{q'}}{2},-\vec{k}+\frac{\vec{q'}}{2}\right)\psi_{1,\sigma_4}\left(\omega_k+\frac{\omega_{q'}}{2},\vec{k}+\frac{\vec{q'}}{2}\right)\right]\right\}, \tag{G.2}$$

where we use the matrix notation $\left[\bar{\lambda}\right]^{\sigma_1\sigma_2;\sigma_3\sigma_4}_{(\omega_p,\vec{p},\omega_q,\vec{q};\omega_k,\vec{k},\omega_{q'},\vec{q'})} = \frac{(2\pi)^3\delta(\omega_p-\omega_{q'})\delta^{(2)}(\vec{q}-\vec{q'})}{4\mu}\lambda^{\left(\begin{smallmatrix}1&5\\1&5\end{smallmatrix}\right);\left(\begin{smallmatrix}\sigma_1&\sigma_2\\\sigma_4&\sigma_3\end{smallmatrix}\right)}_{\left(\begin{smallmatrix}p+\frac{q}{2}&-p+\frac{q}{2}\\k+\frac{q'}{2}&-k+\frac{q'}{2}\end{smallmatrix}\right)}$ [1]. Writing the static component of the order parameter with zero center of mass momentum as

[1] The matrix elements of $\bar{\lambda}$ can be written as $\bar{\lambda}_{mn}$, where $m \equiv (\sigma_1\sigma_2;\omega_p,\vec{p},\omega_q,\vec{q})$ and $n \equiv (\sigma_3\sigma_4;\omega_k,\vec{k},\omega'_q,\vec{q'})$.

$\tilde{\Delta}^{\sigma_1\sigma_2}_{(\omega_p,\vec{p};\omega_q,\vec{q})} = (2\pi)^3\delta(\omega_q)\delta^{(2)}(\vec{q})\tilde{\Delta}^{\sigma_1\sigma_2}_{(\omega_p,\vec{p})}$ and making a further transformation through

$$\Delta^{\sigma_1\sigma_2}_{(\omega_p,\vec{p})} = \sum_{\sigma_3\sigma_4}\int \frac{\mathrm{d}\omega_k \mathrm{d}^2k}{(2\pi)^3}\frac{\lambda^{\binom{1\ 5}{1\ 5};\binom{\sigma_1\ \sigma_2}{\sigma_4\ \sigma_3}}_{\binom{p\ -p}{k\ -k}}}{4\mu}\tilde{\Delta}^{\sigma_3\sigma_4}_{(\omega_k,\vec{k})}, \tag{G.3}$$

we obtain the pairing term for the Bogoliubov quasiparticles,

$$e^{-S^{\binom{1\ 5}{1\ 5}}_{4\mathrm{f}}} = \int \mathcal{D}\Delta\mathcal{D}\Delta^* \exp\Bigg\{ -\sum_{\{\sigma_i\}}\int \frac{\mathrm{d}\omega_p\ \mathrm{d}^2p\mathrm{d}\omega_k\ \mathrm{d}^2k}{(2\pi)^6}\ \Delta^{\dagger\,\sigma_1\sigma_2}_{(\omega_p,\vec{p})}\,[\mathfrak{G}^{-1}]^{\binom{\sigma_1\ \sigma_2}{\sigma_4\ \sigma_3}}_{\binom{p\ -p}{k\ -k}}\Delta^{\sigma_3\sigma_4}_{(\omega_k,\vec{k})}$$
$$-\sum_{\sigma_1,\sigma_2}\int\frac{\mathrm{d}\omega_p\ \mathrm{d}^2p}{(2\pi)^3}\left[\psi^*_{1,\sigma_1}(\omega_p,\vec{p})\,\Delta^{\sigma_1\sigma_2}_{(\omega_p,\vec{p})}\psi^*_{5,\sigma_2}(-\omega_p,-\vec{p})+\psi_{5,\sigma_1}(-\omega_p,-\vec{p})\,\Delta^{\dagger\,\sigma_1\sigma_2}_{(\omega_p,\vec{p})}\,\psi_{1,\sigma_2}(\omega_p,\vec{p})\right]\Bigg\}, \tag{G.4}$$

where $[\mathfrak{G}^{-1}]^{\binom{\sigma_1\ \sigma_2}{\sigma_4\ \sigma_3}}_{\binom{p\ -p}{k\ -k}} = 4\mu(2\pi)^3\delta(0)\delta^{(2)}(\vec{0})\left[-\lambda^{-1}\right]^{\binom{1\ 5}{1\ 5};\binom{\sigma_1\ \sigma_2}{\sigma_4\ \sigma_3}}_{\binom{p\ -p}{k\ -k}}$. Once the momentum-dependent pairing amplitude is determined from the saddle-point equation, it together with the vielbein sets the background spacetime on which the Bogoliubov quasiparticles propagate.

Appendix H

Field-theoretic functional RG scheme for the Kondo problem

In this appendix, we describe the functional renormalization group (RG) scheme, closely following Ref. [30]. Let $\Gamma^{(2m,2n,l)}$ be the vertex function for $2m$ itinerant electrons, $2n$ pseudo fermions and l bosons. The normalization of the pseudo-fermion field, and the Kondo coupling function and the impurity-boson coupling are defined through the vertex function so that (see Fig. H.1)

$$-i\frac{\partial}{\partial p_0}\Gamma^{(0,2,0)}(p_0)\Big|_{p_0=\mu} = 1+\mathscr{F}_0, \tag{H.1}$$

$$\Gamma^{(0,2,1)}(p_0,q_0)\Big|_{p_0=q_0/2=\mu} = \frac{1}{2}\left(g_f+\mathscr{F}_1\right), \tag{H.2}$$

$$\Gamma^{(2,2,0);(N,N')}(\mathbf{k},\mathbf{k}',p_0)\Big|_{\substack{p_0/2=k'_0=-k_0=\mu \\ e_N[\vec{k};v_k^{(N)}]=e_{N'}[\vec{k}';v_{k'}^{(N')}]=0}} = \frac{1}{4\mu}\left[J^{(N,N')}_{k_N,k'_{N'}}+\mathscr{F}^{(N,N')}_{3;k_N,k'_{N'}}\right]. \tag{H.3}$$

Here, $\mathscr{F}_0,\mathscr{F}_1$ are scheme-dependent terms that are regular in the $\mu\to 0$ limit. For the Kondo coupling, which is a function of momentum along the Fermi surface, not only $\mathscr{F}^{(N,N')}_{3;k_N,k'_{N'}}$ is required to be regular in μ at each external momentum but also its integral done along the Fermi surface with the measure $\frac{dk}{\mu}$ should be regular [30]. This stricter condition is necessary to capture an IR divergence that may arise for a momentum-integrated dimensionless coupling such as the one in the s-wave Kondo coupling $\sim\int\frac{dk_N}{\mu}J_{k_N,k'_{N'}}$ while $J_{k_N,k'_{N'}}$ at each momentum is regular.

To impose these RG conditions, a local counter term action is added to as Eq. (4.2),

$$\begin{aligned}
S_1^{\text{C.T.}} &= \int\frac{\mathrm{d}p_0}{2\pi}A_{f,1}ip_0f^\dagger_\alpha(p_0)f_\alpha(p_0)\\
&+\frac{1}{\mu}\sum_{N,N'}\int\mathrm{d}\mathbf{k}\mathrm{d}\mathbf{q}\frac{\mathrm{d}p_0}{2\pi}A^{(N,N')}_{f,2}(k_N,q_{N'})J^{(N,N')}_{k_N,q_{N'}}\psi^\dagger_{N,\sigma}(\mathbf{k})\frac{\vec{\tau}_{\sigma,\sigma'}}{2}\psi_{N',\sigma'}(\mathbf{q})f^\dagger_\alpha(p_0+q_0)\frac{\vec{\tau}_{\alpha,\beta}}{2}f_\beta(p_0+k_0)\\
&+g_f\sum_{\alpha,\beta=\uparrow,\downarrow}\int\mathrm{d}\mathbf{q}\frac{\mathrm{d}p_0}{2\pi}A_{f,3}f^\dagger_\alpha(p_0+q_0)\frac{\Phi_{\alpha,\beta}(\mathbf{q})}{2}f_\beta(p_0),
\end{aligned} \tag{H.4}$$

where $\Phi_{\alpha,\beta}\equiv\vec{\phi}\cdot\vec{\tau}_{\alpha,\beta}$. For the RG conditions of the coupling functions that appear in Eq. (4.1) and their counter terms, we refer the reader to Ref. [30]. Adding Eq. (H.4) to Eq. (4.2), we obtain the

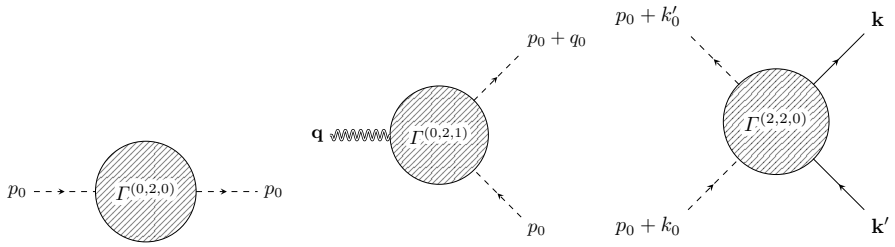

Figure H.1: (a) The inverse propagator of the pseudo-fermion. (b) The boson-impurity vertex. (c) The electron-impurity vertex. Here, the double wiggly lines, the dashed lines, and the solid lines represent the boson propagators, the pseudo-fermion propagators and the electron propagators, respectively.

renormalized action for the impurity,

$$\begin{aligned} S^{\mathrm{Ren}} &= \int \frac{\mathrm{d}p_0^{\mathsf{B}}}{2\pi} i p_0^{\mathsf{B}} f_\alpha^{\mathsf{B}\dagger}(p_0^{\mathsf{B}}) f_\alpha^{\mathsf{B}}(p_0^{\mathsf{B}}) \\ &+ \sum_{N,N'} \int \mathrm{d}\mathbf{k}^{\mathsf{B}} \mathrm{d}\mathbf{q}^{\mathsf{B}} \frac{\mathrm{d}p_0^{\mathsf{B}}}{2\pi} J^{\mathsf{B}(N,N')}_{k_N^{\mathsf{B}}, q_N^{\mathsf{B}}} \psi^{\mathsf{B}\dagger}_{N,\sigma}(\mathbf{k}^{\mathsf{B}}) \frac{\vec{\tau}_{\sigma,\sigma'}}{2} \psi^{\mathsf{B}}_{N',\sigma'}(\mathbf{q}^{\mathsf{B}}) \cdot f_\alpha^{\mathsf{B}\dagger}(p_0^{\mathsf{B}} + q_0^{\mathsf{B}}) \frac{\vec{\tau}_{\alpha,\beta}}{2} f_\beta^{\mathsf{B}}(p_0^{\mathsf{B}} + k_0^{\mathsf{B}}) \\ &+ \sum_{\alpha,\beta=\uparrow,\downarrow} \int \mathrm{d}\mathbf{q}^{\mathsf{B}} \frac{\mathrm{d}p_0^{\mathsf{B}}}{2\pi} g_f^{\mathsf{B}} f_\alpha^{\mathsf{B}\dagger}(p_0^{\mathsf{B}} + q_0^{\mathsf{B}}) \frac{\Phi^{\mathsf{B}}_{\alpha,\beta}(\mathbf{q}^{\mathsf{B}})}{2} f_\beta^{\mathsf{B}}(p_0^{\mathsf{B}}). \end{aligned} \tag{H.5}$$

Here,

$$\begin{gathered} k_0^{\mathsf{B}} = Z_\tau k_0, \quad \vec{k}^{\mathsf{B}} = \vec{k}, \\ \psi^{\mathsf{B}}_{N,\sigma}(\mathbf{k}^{\mathsf{B}}) = \sqrt{Z^{(\psi,N)}(k_N)} \psi_{N,\sigma}(\mathbf{k}), \quad \Phi^{\mathsf{B}}_{\sigma\sigma'}(\mathbf{q}^{\mathsf{B}}) = \sqrt{Z^{(\Phi)}} \Phi_{\sigma\sigma'}(\mathbf{q}), \quad f_\alpha^{\mathsf{B}}(p_0^{\mathsf{B}}) = \sqrt{Z^{(f)}} f_\alpha(p_0), \\ J^{\mathsf{B}(N,N')}_{k_N^{\mathsf{B}}, q_{N'}^{\mathsf{B}}} = \frac{Z^{(N,N')}_{f,2}(k_N, q_{N'})}{Z_\tau^3 Z^{(f)} \sqrt{Z^{(\psi,N)}(k_N) Z^{(\psi,N')}(q_{N'})}} \mu^{-1} J^{(N,N')}_{k_N, q_{N'}}, \quad g_f^{\mathsf{B}} = \frac{Z_{f,3}}{Z_\tau^2 Z^{(f)} \sqrt{Z^{(\Phi)}}} g_f \end{gathered} \tag{H.6}$$

are bare frequency, fields and couplings expressed in terms of the renormalized ones. Z_τ is the dynamical critical exponent. $\sqrt{Z^{(\psi,N)}(k_N)}$ and $\sqrt{Z^{(\Phi)}}$ are renormalization of the fermion and boson fields, respectively[30]. $Z^{(f)} = \frac{Z_{f,1}}{Z_\tau^2}$ is the field renormalization of the pseudo-fermion. The renormalization factors are given by $Z_{f,1} = 1 + A_{f,1}$, $Z^{(N,N')}_{f,2}(k_N, q_{N'}) = 1 + A^{(N,N')}_{f,2}(k_N, q_{N'})$ and $Z_{f,3} = 1 + A_{f,3}$. The beta functions capture how the renormalized couplings, which represent the vertex functions at energy scale μ, runs as μ is lowered for fixed bare couplings,

$$\beta^{(g_f)} = g_f \left(2(z-1) + 2\eta^{(f)} + \eta^{(\Phi)} - \frac{\mathrm{d}\log Z_{f,3}}{\mathrm{d}\log\mu} \right), \tag{H.7}$$

$$\beta^{(J);(N,N')}_{k,k'} = J^{(N,N')}_{k,k'} \left(1 + 3(z-1) + 2\eta^{(f)} + \eta^{(\psi,N)}_k + \eta^{(\psi,N')}_{k'} - \frac{\mathrm{d}\log Z^{(N,N')}_{f,2}(k,k')}{\mathrm{d}\log\mu} \right), \tag{H.8}$$

where

$$z = 1 + \frac{\mathrm{d}\log Z_\tau}{\mathrm{d}\log\mu}, \quad \eta^{(\psi,N)}_k = \frac{1}{2} \frac{\mathrm{d}\log Z^{(\psi,N)}(k)}{\mathrm{d}\log\mu}, \qquad \eta^{(\Phi)} = \frac{1}{2} \frac{\mathrm{d}\log Z^{(\Phi)}}{\mathrm{d}\log\mu}, \quad \eta^{(f)} = \frac{1}{2} \frac{\mathrm{d}\log Z^{(f)}}{\mathrm{d}\log\mu}. \tag{H.9}$$

In the small v_k limit, the dynamical critical exponent and the anomalous dimensions are given by [182, 30]

$$z = 1 + \frac{3}{4\pi^2} w, \qquad \eta^{(\Phi)} = \frac{1}{4\pi} w \log \frac{1}{w}, \qquad \eta_{k_N}^{(\psi,N)} = \frac{3(g_{k_N,k_N}^{(N)})^2}{4\pi^2 c V_{F,k_N}^{(\overline{N})}} \frac{\mu}{\mu + 2c v_{k_N}^{(N)} |k_N|} - (z-1), \tag{H.10}$$

where $w \equiv v_0/c(v_0)$ with $c(v_0) = \sqrt{\frac{v_0}{16} \log\left(\frac{1}{v_0}\right)}$.

Appendix I

Quantum corrections for the Kondo problem

In this appendix, we present the one-loop quantum corrections that renormalize the pseudo-fermion self-energy, the boson-impurity coupling and the electron-impurity (Kondo) coupling. The diagrams that are relevant to the boson-impurity coupling and the Kondo coupling are shown in Fig. I.1. For the quantum corrections for the impurity-free theory, we refer the readers to Refs. [182, 30].

I.1 Pseudo-fermion self-energy

The one-loop self-energy in Fig. I.1a gives

$$\mathbf{\Sigma}^{(f);1\mathrm{L}}(p_0) = -\frac{3g_f^2}{4}\int \mathrm{d}\mathbf{q} D(\mathbf{q}) G_f(p_0+q_0) = -\frac{3g_f^2}{4}\int \frac{\mathrm{d}q_0}{2\pi}\bar{D}(q_0)G_f(p_0+q_0), \tag{I.1}$$

where

$$\begin{aligned}\bar{D}(q_0) =& \int \frac{\mathrm{d}q_x \mathrm{d}q_y}{(2\pi)^2} D(\mathbf{q}) \\ =& \frac{1}{\pi^2 c^2}\left\{2c\Lambda_b \log\left(1+\frac{c\Lambda_b}{c\Lambda_b+|q_0|}\right) + |q_0|\left[\log\left(1+\frac{c\Lambda_b}{c\Lambda_b+|q_0|}\right) - \log\left(1+\frac{c\Lambda_b}{|q_0|}\right)\right]\right\}\end{aligned} \tag{I.2}$$

is the local boson propagator at the impurity site. Here, Λ_b is the momentum cutoff below which the self-energy of the boson generated from the particle-hole excitation $\Pi(\mathbf{q}) = [|q_0| + c(|q_x| + |q_y|)]^{-1}$ becomes dominant over the bare boson propagator dropped in this calculation. The logarithmic UV divergence $\log \Lambda_b/q_0$ in the coefficient of $|q_0|$ arises because the bosons with large momenta up to Λ_b have a significant spectral weight at low energies[182]. While the precise value of Λ_b is not important, it is crucial that Λ_b is a fixed UV momentum cutoff. From now on, we set $\Lambda_b = \Lambda/c$, where Λ is an energy cutoff. The frequency integration q_0 results in

$$\mathbf{\Sigma}^{(f);1\mathrm{L}}(p_0) \approx ip_0 \frac{3g_f^2 \log^2\left(\frac{\Lambda}{|p_0|}\right)}{8\pi^3 c^2} - ip_0 \frac{3g_f^2 \log(2)\log\left(\frac{\Lambda}{|p_0|}\right)}{4\pi^3 c^2} + ip_0 \frac{3g_f^2 \log\left(\frac{\Lambda}{|p_0|}\right)}{4\pi^3 c^2} \tag{I.3}$$

to the leading order in small p_0. With the renormalization conditions (H.1), the counter term in the small μ limit is chosen to be

$$A_{f,1}^{1\mathrm{L}} = \frac{3g_f^2 \log(2)\log\left(\frac{\Lambda}{\mu}\right)}{4\pi^3 c^2} - \frac{3g_f^2 \log^2\left(\frac{\Lambda}{\mu}\right)}{8\pi^3 c^2}. \tag{I.4}$$

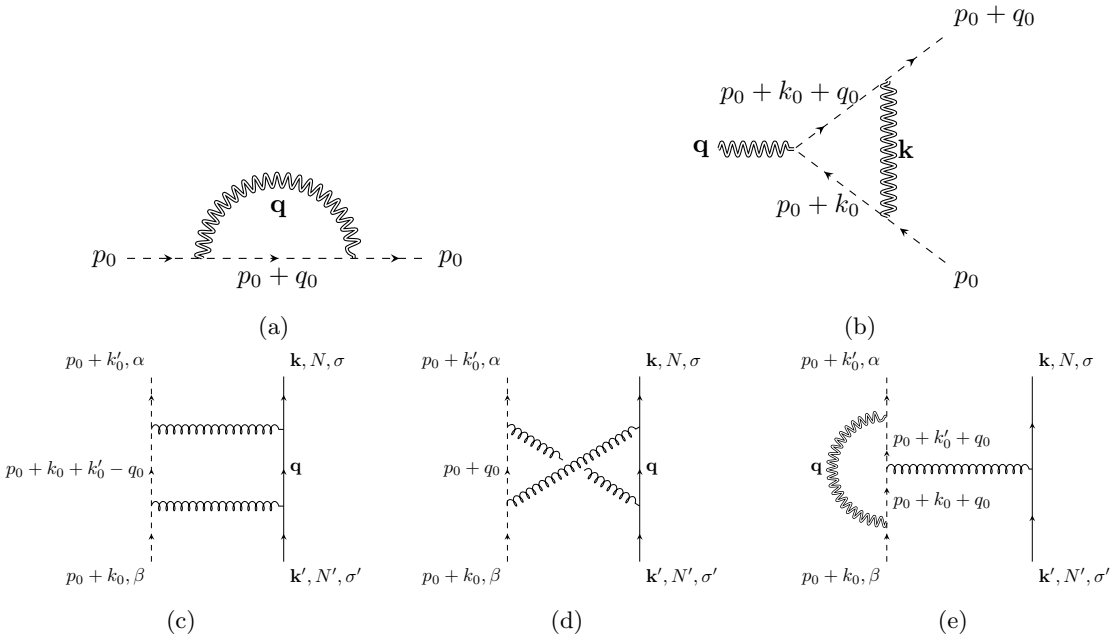

Figure I.1: The one-loop diagrams that renormalize the pseudo-fermion, the boson-impurity coupling and the Kondo coupling. (a) The pseudo-fermion self energy. (b) The boson-impurity vertex correction. (c-e) The vertex correction for the Kondo coupling. The boson propagator is non-perturbatively dressed by particle-hole excitations. Here, the double wiggly lines, the dashed lines, and the solid lines represent the boson propagators, the pseudo-fermion propagators and the electron propagators, respectively (See Fig. H.1). The coiled line represents the Kondo interaction.

I.2 Boson-impurity vertex correction

The one-loop boson-impurity vertex correction in Fig. I.1b reads

$$\mathbf{\Gamma}^{1\mathrm{L}}(p_0, q_0) = -\frac{g_f^3}{8}\int \mathrm{d}\mathbf{k} D(\mathbf{k}) G_f(p_0{+}k_0) G_f(p_0{+}q_0{+}k_0) = -\frac{g_f^3}{8}\int \frac{\mathrm{d}k_0}{2\pi}\bar{D}(k_0) G_f(p_0{+}k_0) G_f(p_0{+}q_0{+}k_0). \tag{I.5}$$

Integrating k_0 results in the quantum correction at external frequency μ,

$$\mathbf{\Gamma}^{1\mathrm{L}}(p_0, q_0)\big|_{p_0=q_0/2=\mu} = -\frac{g_f^3 \log^2\left(\frac{c\Lambda_b}{\mu}\right)}{16\pi^3 c^2} + \frac{g_f^3(\log(108)-2)\log\left(\frac{c\Lambda_b}{\mu}\right)}{16\pi^3 c^2} \tag{I.6}$$

upto terms that are regular in μ. The corresponding counter term is

$$A_{f,3}^{1\mathrm{L}} = \frac{g_f^2 \log^2\left(\frac{c\Lambda_b}{\mu}\right)}{8\pi^3 c^2} - \frac{g_f^2(\log(108)-2)\log\left(\frac{c\Lambda_b}{\mu}\right)}{8\pi^3 c^2}. \tag{I.7}$$

I.3 Kondo coupling vertex corrections

The diagrams in Figs. I.1c and I.1d, originally computed by Kondo, give

$$\mathbf{\Gamma}^{(N,N');\left(\begin{smallmatrix}\alpha & \sigma\\ \beta & \sigma'\end{smallmatrix}\right);(1L)}_{FL(PP);(k_N,k'_{N'},p_0)} = (3\delta_{\sigma\sigma'}\delta_{\alpha\beta} - 2\vec{\tau}_{\sigma\sigma'}\cdot\vec{\tau}_{\alpha\beta})\,\mathbf{\Gamma}^{(N,N');(1L)}_{FL(PP);(k_N,k'_{N'},p_0)}, \tag{I.8}$$

$$\mathbf{\Gamma}^{(N,N');\left(\begin{smallmatrix}\alpha & \sigma\\ \beta & \sigma'\end{smallmatrix}\right);(1L)}_{FL(PH);(k_N,k'_{N'},p_0)} = (3\delta_{\sigma\sigma'}\delta_{\alpha\beta} + 2\vec{\tau}_{\sigma\sigma'}\cdot\vec{\tau}_{\alpha\beta})\,\mathbf{\Gamma}^{(N,N');(1L)}_{FL(PH);(k_N,k'_{N'},p_0)}, \tag{I.9}$$

where

$$\mathbf{\Gamma}^{(N,N');(1L)}_{FL(PP);(k_N,k'_{N'},p_0)} = -\sum_M \int \mathrm{d}\mathbf{q} \frac{J^{(N,M)}_{k_N,q_M} J^{(M,N')}_{q_M,k'_{N'}}}{16\mu^2} G_M(\mathbf{q}) G_f(p_0+k_0+k'_0-q_0), \tag{I.10}$$

$$\mathbf{\Gamma}^{(N,N');(1L)}_{FL(PH);(k_N,k'_{N'},p_0)} = -\sum_M \int \mathrm{d}\mathbf{q} \frac{J^{(N,M)}_{k_N,q_M} J^{(M,N')}_{q_M,k'_{N'}}}{16\mu^2} G_M(\mathbf{q}) G_f(p_0+q_0). \tag{I.11}$$

At the external frequencies, $k'_0 = -k_0 = p_0/2 = \mu$ set by the RG condition, (I.10) gives rise to

$$\mathbf{\Gamma}^{(N,N');(1L)}_{FL(PP);(k_N,k'_{N'})} = -\sum_M \int \frac{\mathrm{d}q_M}{2\pi} \frac{J^{(N,M)}_{k_N,q_M} J^{(M,N')}_{q_M,k'_{N'}}}{32\pi\mu^2 V^{(M)}_{F,q_M}} \log\left(\frac{\Lambda}{\mu}\right). \tag{I.12}$$

The q_M integral is left undone because we do not know the explicit form of the Kondo coupling a priori. The corresponding counter term becomes $\mathbf{\Gamma}^{(N,N');(1L)}_{CT;FL(PP);(k_N,k'_{N'})} = \sum_M \int \frac{\mathrm{d}q_M}{2\pi} \frac{J^{(N,M)}_{k_N,q_M} J^{(M,N')}_{q_M,k'_{N'}}}{32\pi\mu^2 V^{(M)}_{F,q_M}} \log\left(\frac{\Lambda}{\mu}\right)$. The evaluation of Eq. (I.11) is similar and the resulting counter term is given by $\mathbf{\Gamma}^{(N,N');(1L)}_{CT;FL(PH);(k_N,k'_{N'})} = -\mathbf{\Gamma}^{(N,N');(1L)}_{CT;FL(PP);(k_N,k'_{N'})}$. In the net counter term, the density-density interaction cancels, leading to

$$\mathbf{\Gamma}^{(N,N');\left(\begin{smallmatrix}\alpha & \sigma\\ \beta & \sigma'\end{smallmatrix}\right);(1L)}_{CT;FL;(k_N,k_{N'})} = -\vec{\tau}_{\sigma\sigma'}\cdot\vec{\tau}_{\alpha\beta} \sum_M \int \frac{\mathrm{d}q_M}{2\pi} \frac{J^{(N,M)}_{k_N,q_M} J^{(M,N')}_{q_M,k'_{N'}}}{8\pi\mu^2 V^{(M)}_{F,q_M}} \log\left(\frac{\Lambda}{\mu}\right). \tag{I.13}$$

It contributes to the IR beta functional as

$$4\mu \frac{\partial \mathbf{\Gamma}^{(N,N');\left(\begin{smallmatrix}\alpha & \sigma\\ \beta & \sigma'\end{smallmatrix}\right);(1L)}_{CT;FL;(k_N,k_{N'})}}{\partial \log\mu}\bigg|_{J_B} = \vec{\tau}_{\sigma\sigma'}\cdot\vec{\tau}_{\alpha\beta} \sum_M \int \frac{\mathrm{d}q_M}{2\pi\mu V^{(M)}_{F,q_M}} \frac{J^{(N,M)}_{k_N,q_M} J^{(M,N')}_{q_M,k'_{N'}}}{2\pi}, \tag{I.14}$$

where the derivative with respect to $\log\mu$ is done with fixed bare Kondo coupling, which is $J^{B(N,M)}_{k_N,q_M} = J^{(N,M)}_{k_N,q_M}/\mu$ to the leading order.

In AFQCM, Fig. I.1e gives rise to an additional vertex correction to Kondo coupling. Since the critical boson renormalizes the Kondo coupling in the exact same way as it renormalizes the boson-impurity vertex through (I.5), the multiplicative renormalization factor is identical to that of Eq. (I.7),

$$\mathbf{\Gamma}^{(N,N');(1L)}_{CT;NFL} = \frac{J^{(N,N')}_{k_N,k'_{N'}}}{4\mu}\left[\frac{g_f^2 \log^2\left(\frac{\Lambda}{\mu}\right)}{8\pi^3 c^2} - \frac{g_f^2\left(\log(108)-2\right)\log\left(\frac{\Lambda}{\mu}\right)}{8\pi^3 c^2}\right]. \tag{I.15}$$

For the beta function, the term that is proportional to $\log^2\Lambda/\mu$ dominates and gives

$$4\mu \frac{\partial \mathbf{\Gamma}^{(N,N');\left(\begin{smallmatrix}\alpha & \sigma\\ \beta & \sigma'\end{smallmatrix}\right);(1L)}_{CT;NFL}}{\partial \log\mu} = -\vec{\tau}_{\sigma\sigma'}\cdot\vec{\tau}_{\alpha\beta} \frac{g_f^2 J^{(N,N')}_{k_N,k'_{N'}}}{4\pi^3 c^2} \log\left(\frac{\Lambda}{\mu}\right). \tag{I.16}$$

Appendix J

The solution of the beta functions for g_f and J

In this appendix, we compute Kondo scale ℓ_K as a function of the bare parameters $\tilde{J}_i^V$, $g_{f,i}$ and ℓ_0 defined at the short-distance cutoff scale ℓ_i by solving Eqs. (4.4) and (4.5). In the small $\tilde{J}_i^V$ limit, the flow of $\tilde{J}^V$ can be understood in two steps. At short distance scales smaller than a crossover scale denoted by $\ell_{\rm cross}$, $\tilde{J}^V$ undergoes a suppression due to the anomalous dimension generated from the boson-impurity coupling. Its flow is described by $\frac{\partial \tilde{J}^V(\ell)}{\partial \ell} = -\eta_f(\ell)\tilde{J}^V(\ell)$. Then, $\tilde{J}^V$ at the crossover scale becomes $\tilde{J}^V(\ell_{\rm cross}) \sim \tilde{J}_i^V e^{-\gamma}$ with $\gamma = \int_{\ell_i}^{\ell_{\rm cross}} d\ell' \eta_f(\ell')$. For $\ell \gg \ell_{\rm cross}$, the flow of $\tilde{J}^V$ can be approximated by $\frac{\partial \tilde{J}^V(\ell)}{\partial \ell} = \left(\tilde{J}^V(\ell)\right)^2$ as is in Fermi liquids, and $\tilde{J}^V$ becomes strong at Kondo scale $\ell_K \sim \ell_{\rm cross} + e^{\gamma}/\tilde{J}_i^V$. This is illustrated in Fig. J.1. Since $\ell_{\rm cross}$ is largely independent of $\tilde{J}_i^V$ in the small $\tilde{J}_i^V$ limit, ℓ_K is mainly determined by the renormalized Kondo coupling at $\ell_{\rm cross}$.

In order to compute this suppression factor of the Kondo coupling ($e^{-\gamma}$) at $\ell_{\rm cross}$, we first need to know how η_f evolves as a function of ℓ by solving the beta function of g_f. The flow of g_f exhibits different behaviours depending on the relative magnitude between $1/\ell_0$ and $\tilde{g}_f = g_f^2/c^2$ at ℓ_i. Three different cases are illustrated in Fig. J.2. Below, we discuss each case one by one.

J.1 $\tilde{g}_{f,i} \ll 1/\ell_0$

In this case, the boson-impurity coupling is weak, and its flow is mainly controlled by the anomalous dimension of the boson $\eta^{(\Phi)}$. In particular, $\tilde{g}_f$ can be dropped in Eq. (4.5) in the beta function of g_f, $\frac{\partial g_f(\ell)}{\partial \ell} = -\frac{1}{4\pi} w \log\left(\frac{1}{w}\right) g_f(\ell)$, where $w = v/c$. The finite w-correction to the anomalous dimension of the boson makes the boson-impurity coupling irrelevant and flow to zero at large distance scales. From $w(\ell)$ determined from Eq. (2.8), one obtains $g_f(\ell) = e^{-\frac{\sqrt{\ell+\ell_0}-\sqrt{\ell_0+\ell_i}}{\sqrt{3}}} g_{f,i}$, and the effective boson-impurity coupling $\tilde{g}_f = g_f^2/c^2$ becomes

$$\tilde{g}_f(\ell) = \frac{\ell_0+\ell}{\ell_0+\ell_i} e^{-\frac{2\left(\sqrt{\ell+\ell_0}-\sqrt{\ell_i+\ell_0}\right)}{\sqrt{3}}} \tilde{g}_{f,i}, \tag{J.1}$$

where subscript i denote the coupling defined at initial length scale $\ell_i \sim O(1)$. As ℓ increases $\eta_f = (\tilde{g}_f \ell/\pi^3)$ reaches its maximum $\tilde{g}_{f,i}\sqrt{\ell_0}$ around scale $\sqrt{\ell_0}$ before it decays exponentially. Since $\eta^{(\Phi)}$ only decays as $1/\sqrt{\ell+\ell_0}$, $\eta^{(\Phi)}$ remains dominant over η_f at all scales. Therefore, Eq. (J.1) is valid at all ℓ.

We can now solve Eq. (4.8) using Eq. (J.1). If the Kondo coupling is weak at ℓ_i, $-\eta_f \tilde{J}^V$ dominates over $(\tilde{J}^V)^2$ at short distance scales. This allows us to use $\frac{\partial \tilde{J}^V(\ell)}{\partial \ell} = -\eta_f(\ell)\tilde{J}^V(\ell)$ to find $\tilde{J}^V(\ell)$ before

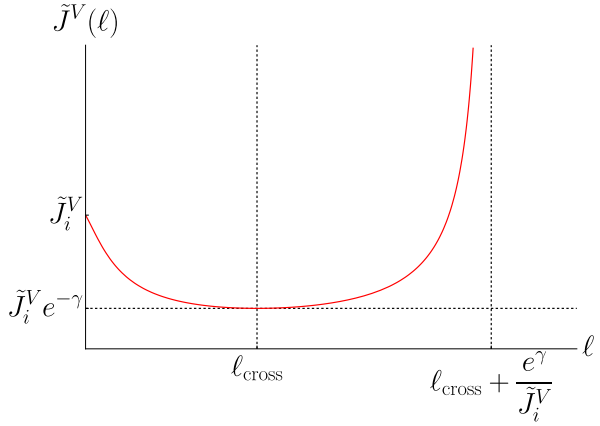

Figure J.1: A schematic RG flow of Kondo coupling $\tilde{J}^V$ in the small $\tilde{J}_i^V$ limit. At short distances below a crossover scale $\ell_{\rm cross}$, $\tilde{J}^V$ is suppressed by the anomalous dimension η_f. Beyond the crossover scale, the anomalous dimension becomes negligible, and $\tilde{J}^V$ is enhanced as in Fermi liquids. Therefore, the scale at which $\tilde{J}^V$ becomes $O(1)$ is given by $\ell_K \sim \ell_{\rm cross} + \frac{1}{\tilde{J}^V(\ell_{\rm cross})}$.

$(\tilde{J}^V)^2$ becomes dominant: $\tilde{J}^V(\ell) = \tilde{J}_i^V e^{-\gamma_1(\ell)}$ with

$$\gamma_1(\ell) = \tilde{g}_{f,i} \frac{\left\{ \begin{array}{c} \Big[4\sqrt{3}(\ell_0-15)(\ell+\ell_0)^{3/2} - 4\sqrt{3}(\ell+\ell_0)^{5/2} - 30(\ell+\ell_0)^2 \\ +18(\ell_0-15)(\ell+\ell_0) + 18\sqrt{3}(\ell_0-15)\sqrt{\ell+\ell_0} + 27(\ell_0-15)\Big] e^{\frac{2\left(\sqrt{\ell_0+\ell_i}-\sqrt{\ell+\ell_0}\right)}{\sqrt{3}}} \\ -4\sqrt{3}(\ell_0-15)(\ell_0+\ell_i)^{3/2} + 4\sqrt{3}(\ell_0+\ell_i)^{5/2} + 30(\ell_0+\ell_i)^2 - 18(\ell_0-15)(\ell_0+\ell_i) \\ -18\sqrt{3}(\ell_0-15)\sqrt{\ell_0+\ell_i} - 27(\ell_0-15) \end{array} \right\}}{4\pi^3(\ell_0+\ell_i)}. \tag{J.2}$$

At short distance scales, Kondo coupling is exponentially suppressed due to $\tilde{g}_f$. For $\ell > \sqrt{\ell_0}$, however, $\tilde{g}_f$ becomes exponentially small, slowing down the decay of $\tilde{J}^V$. Therefore, a crossover from the $\eta_f \tilde{J}^V$-dominated flow to the $(\tilde{J}^V)^2$-dominated flow occurs at the crossover scale $\ell_{\rm cross,1}$ which is determined by $\eta_f(\ell_{\rm cross,1}) = \tilde{J}_I^V(\ell_{\rm cross,1})$. We note that $\ell_{\rm cross,1} > \sqrt{\ell_0}$ in the small $\tilde{J}_i^V$ limit. At scale greater than $\sqrt{\ell_0}$, Eq. (J.2) saturates to

$$\tilde{J}_I^V(\ell \gg \sqrt{\ell_0}) = \tilde{J}_i^V e^{-\frac{3\tilde{g}_{f,i}\ell_0}{\pi^3}}, \tag{J.3}$$

and $\ell_{\rm cross,1}$ satisfies $\sqrt{\ell_{\rm cross,1}+\ell_0} - \sqrt{\ell_0} - \frac{\sqrt{3}}{2}\log\left(\frac{(\ell_{\rm cross,1}+\ell_0)\ell_{\rm cross,1}}{\ell_0}\right) = \frac{\sqrt{3}}{2}\log\left(\frac{\tilde{g}_{f,i}}{\pi^3}\right) + \frac{3^{\frac{3}{2}}\tilde{g}_{f,i}\ell_0}{2\pi^3} + \frac{\sqrt{3}}{2}\log\left(\frac{1}{\tilde{J}_i^V}\right)$. To the leading in $\tilde{J}^V$, the crossover scale is given by

$$\ell_{\rm cross,1} = \frac{3\sqrt{3}\tilde{g}_{f,i}\ell_0^{3/2}}{\pi^3} + \sqrt{3}\sqrt{\ell_0}\log\left(\frac{\tilde{g}_{f,i}}{\pi^3\tilde{J}_i^V}\right) + \frac{3\tilde{g}_{f,i}^2\left(\frac{\pi^3\log\left(\frac{\tilde{g}_{f,i}}{\pi^3\tilde{J}_i^V}\right)}{\tilde{g}_{f,i}} + 3\ell_0\right)^2}{4\pi^6}. \tag{J.4}$$

For $\ell \gg \ell_{\rm cross,1}$, the flow of the Kondo coupling is governed by $\frac{\partial\tilde{J}^V(\ell)}{\partial\ell} = \left(\tilde{J}^V(\ell)\right)^2$, and its solution is

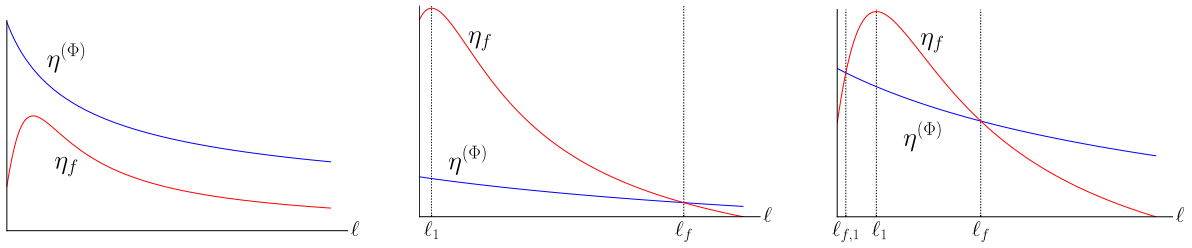

(a) (b) (c)

Figure J.2: The renormalization group flow of the boson-impurity coupling (g_f) is controlled by $\eta^{(\Phi)}(\ell)$, the correction to the anomalous dimension of the boson at non-zero nesting angle, and $\eta_f(\ell) = \tilde{g}_f(\ell)\ell/\pi^3$, the anomalous dimension generated from g_f itself. g_f exhibits different behaviours, depending on the relative magnitudes of $\eta_i^{(\Phi)} \sim 1/\sqrt{\ell_0}$ and $\sqrt{\tilde{g}_{f,i}}$. (a) In this case, $\tilde{g}_{f,i}$ is small enough that η_f remains negligible compared to $\eta^{(\Phi)}$ at all scales (Appendix C J.1). (b) In this case, $\tilde{g}_f$ is dominant over $\eta^{(\Phi)}$ from the UV scale all the way to a crossover scale $\ell_f \sim \sqrt{\ell_0}$ (Appendix C J.2 a). (c) This is similar to case (b) except that there is an additional window of scale $\ell_i < \ell < \ell_{f,1}$ in which $\eta^{(\Phi)}$ is larger than η_f (Appendix C J.2 b).

$\tilde{J}_I^V(\ell \geq \ell_{\text{cross},1}) = \frac{1}{\left(\tilde{J}_I^V(\ell_{\text{cross},1})\right)^{-1} - (\ell - \ell_{\text{cross},1})}$. This results in the Kondo scale,

$$\ell_K = \ell_{\text{cross},1} + \frac{e^{\frac{3\tilde{g}_{f,i}\ell_0}{\pi^3}}}{\tilde{J}_i^V}. \tag{J.5}$$

In the small $\tilde{J}^V$ limit, ℓ_K is given by $\frac{e^{\frac{3\tilde{g}_{f,i}\ell_0}{\pi^3}}}{\tilde{J}_i^V}$ to the leading order. Compared to the Fermi liquid with the same electronic density of states, ℓ_K is larger by factor of $e^{\frac{3\tilde{g}_{f,i}\ell_0}{\pi^3}}$.

J.2 $1/\ell_0 \ll \tilde{g}_{f,i}$

In this case, the boson-impurity coupling plays the dominant role, and the behaviour of Kondo coupling exhibits a strong departure from that of Fermi liquids. Below, we present the solution of the beta function for two sub-cases separately: (a) $1/\sqrt{\ell_0} \ll \tilde{g}_{f,i}$, (b) $1/\ell_0 \ll \tilde{g}_{f,i} \ll 1/\sqrt{\ell_0}$.

J.2.1 $1/\sqrt{\ell_0} \ll \tilde{g}_{f,i}$

In this case, $\tilde{g}_f$ is dominant so that one can ignore $\eta^{(\Phi)}$ in the beta function of g_f at short distance scale. g_f obeys $\frac{\partial g_f(\ell)}{\partial \ell} = -\frac{g_f^3(\ell)\ell}{\pi^3 c^2}$ with its solution $g_f(\ell) = \pm\frac{\pi^{5/2}|g_{f,i}|}{\sqrt{\pi^5 + 16 g_{f,i}^2\left(2\ell^3 + 3\ell^2\ell_0 - \ell_i^2(3\ell_0 + 2\ell_i)\right)}}$. Then, $\tilde{g}_f$ becomes

$$\tilde{g}_f(\ell) = \frac{3\pi^3 \tilde{g}_{f,i}(\ell + \ell_0)}{3\pi^3(\ell_0 + \ell_i) + \tilde{g}_{f,i}(2\ell^3 + 3\ell^2\ell_0 - \ell_i^2(3\ell_0 + 2\ell_i))}. \tag{J.6}$$

While $\tilde{g}_f(\ell) \approx \tilde{g}_{f,i}$ at short distance scales, it takes a universal form, $\tilde{g}_f(\ell) \approx \frac{3(\ell+\ell_0)\pi^3}{2\ell^3 + 3\ell^2\ell_0}$ at long distance scales. This crossover occurs around

$$\ell_1 \approx \sqrt{\frac{\pi^3}{\tilde{g}_{f,i}}} \ll \ell_0^{1/4}. \tag{J.7}$$

According to Eq. (J.6), $\tilde{g}_f\ell$ decays faster than $\eta^{(\Phi)}$ with increasing ℓ. Therefore, there must be a crossover scale ℓ_f above which $\tilde{g}_f\ell$ becomes smaller than $\eta^{(\Phi)}$. Equating $\eta^{(\Phi)}(\ell_f)$ and $\tilde{g}_f\ell_f/\pi^3$ gives

$\ell_f^2 - 2\sqrt{3\ell_0}\ell_f + \ell_1^2 = 0$ whose only positive solution is

$$\ell_f = \sqrt{3\ell_0} + \sqrt{3\ell_0 - \ell_1^2} \approx 2\sqrt{3\ell_0}. \tag{J.8}$$

For $\ell_0 \gg 1$, we have a hierarchy $\ell_1 \ll \ell_f \ll \ell_0$. For $\ell \gg \ell_f$, the beta function for g_f is given by $\frac{\partial g_f(\ell)}{\partial \ell} = -\frac{1}{4\pi} w \log\left(\frac{1}{w}\right) g_f(\ell)$ whose solution is given by $g_f(\ell \geq \ell_f) = e^{-\frac{\sqrt{\ell+\ell_0}-\sqrt{\ell_0+\ell_f}}{\sqrt{3}}} g_f(\ell_f)$. This gives $\tilde{g}_f(\ell)$ that decays exponentially,

$$\tilde{g}_f(\ell \geq \ell_f) = \frac{\pi^3(\ell_0+\ell)}{\ell_f^2(\ell_0+\ell_f)} e^{-\frac{2\left(\sqrt{\ell+\ell_0}-\sqrt{\ell_0+\ell_f}\right)}{\sqrt{3}}}. \tag{J.9}$$

With $\tilde{g}_f$, we can now understand how Kondo scale ℓ_K depends on $\tilde{J}_i^V$. As $\tilde{J}_i^V$ decreases, ℓ_K continuously increases such that it passes three crossover scales ℓ_f. Therefore, we consider the following two limiting cases: *i)* $\ell_K \ll \ell_f$, and *ii)* $\ell_f \ll \ell_K$.

$\ell_K \ll \ell_f$ In this case, the flow of g_f is dominated by η_f at all scales up to ℓ_K. Using the large ℓ_0 expression of Eq. (J.6), $\tilde{g}_f(\ell) \approx \frac{\tilde{g}_{f,i}\pi^3}{\pi^3 + \tilde{g}_{f,i}(\ell^2 - \ell_i^2)}$, we obtain the solution for Eq. (4.8) is

$$\tilde{J}^V(\ell) = \frac{\sqrt{\frac{\pi^3}{\tilde{g}_{f,i}}}\tilde{J}_i^V}{\sqrt{\frac{\pi^3}{\tilde{g}_{f,i}} + \ell^2 - \ell_i^2}\left(\sqrt{\frac{\pi^3}{\tilde{g}_{f,i}}}\tilde{J}_i^V \log\left(\frac{\sqrt{\frac{\pi^3}{\tilde{g}_{f,i}}}+\ell_i}{\ell+\sqrt{\frac{\pi^3}{\tilde{g}_{f,i}}+\ell^2-\ell_i^2}}\right)+1\right)}. \tag{J.10}$$

With $\ell_i \sim O(1)$, the Kondo length scale is given by

$$\ell_K = \sqrt{\frac{\pi^3}{\tilde{g}_{f,i}}} \sinh\left(\sqrt{\frac{\tilde{g}_{f,i}}{\pi^3}}\frac{1}{\tilde{J}_i^V}\right). \tag{J.11}$$

For $\tilde{J}_i^V/\sqrt{\tilde{g}_{f,i}} \gg 1$, the bare Kondo coupling is relatively strong that the boson-impurity coupling plays only a minimal role, and ℓ_K is essentially reduced to that of Fermi liquids with a small correction, $\ell_K \approx \frac{1}{\tilde{J}_i^V}\left(1 + \frac{\tilde{g}_{f,i}}{6\pi^3\left(\tilde{J}_i^V\right)^2}\right)$. For $\tilde{J}_i^V/\sqrt{\tilde{g}_{f,i}} \ll 1$, on the other hand, the boson-impurity coupling significantly suppresses Kondo coupling, and ℓ_K becomes much larger than that of Fermi liquids, $\ell_K \approx \frac{1}{2}\sqrt{\frac{\pi^3}{\tilde{g}_{f,i}}} e^{\sqrt{\frac{\tilde{g}_{f,i}}{\pi^3}}\frac{1}{\tilde{J}_i^V}}$. Remarkably, the logarithmic Kondo scale ℓ_K grows exponentially as $\tilde{J}_i^V$ decreases.

$\ell_f \ll \ell_K$ In the small $\tilde{J}_i^V$ limit, ℓ_K becomes greater than ℓ_f. In this case, one has to solve the beta function for the Kondo coupling in multiple steps. At short distance scales, the beta function can be approximated as $\frac{\partial \tilde{J}^V(\ell)}{\partial \ell} = -\frac{\tilde{g}_f(\ell)\ell}{\pi^3}\tilde{J}^V(\ell)$. Its solution is $\tilde{J}^V(\ell) = \tilde{J}_i^V e^{-\gamma_2(\ell)}$ with

$$\gamma_2(\ell) = \frac{\left\{\begin{array}{c}\Big[4\sqrt{3}(\ell_0-15)(\ell+\ell_0)^{3/2} - 4\sqrt{3}(\ell+\ell_0)^{5/2} - 30(\ell+\ell_0)^2 + 18(\ell_0-15)(\ell+\ell_0) + 18\sqrt{3}(\ell_0-15)\sqrt{\ell+\ell_0} \\ +27(\ell_0-15)\Big] e^{\frac{2\left(\sqrt{\ell_0+\ell_f}-\sqrt{\ell+\ell_0}\right)}{\sqrt{3}}} - 4\sqrt{3}(\ell_0-15)(\ell_0+\ell_f)^{3/2} + 4\sqrt{3}(\ell_0+\ell_f)^{5/2} + 12\ell_0(\ell_0+\ell_f) \\ +30\ell_f(\ell_0+\ell_f) + 270(\ell_0+\ell_f) - 18\sqrt{3}(\ell_0-15)\sqrt{\ell_0+\ell_f} - 27\ell_0 + 405\end{array}\right\}}{4\ell_f^2(\ell_0+\ell_f)}. \tag{J.12}$$

This $\tilde{J}^V$-linear beta function is valid up to a crossover scale $\ell_{\text{cross},2}$ above which $(\tilde{J}^V)^2$ term dominates. At the crossover scale, Eq. (J.12) saturates to

$$\tilde{J}^V(\ell_{\text{cross},2}) = e^{-\frac{3}{4}} \frac{\tilde{J}_i^V}{2} \sqrt{\frac{\pi^3}{3\tilde{g}_{f,i}\ell_0}} \tag{J.13}$$

for sufficiently small $\tilde{J}_i^V$. From $\eta_f(\ell_{\text{cross},2}) = \tilde{J}_{IIb}^V(\ell_{\text{cross},2})$, we obtain the crossover scale,

$$\begin{aligned}\ell_{\text{cross},2} =& -\frac{3}{4}\left(\log\left(\frac{\sqrt{\frac{3\tilde{g}_{f,i}\ell_0}{\pi^3}}}{6\ell_0(\ell_0+2\sqrt{3\ell_0})\tilde{J}_i^V}\right)+\frac{3}{4}\right)^2 + \sqrt{3}\sqrt{\ell_0+2\sqrt{3\ell_0}}\log\left(\frac{\sqrt{\frac{3\tilde{g}_{f,i}\ell_0}{\pi^3}}}{6\ell_0(\ell_0+2\sqrt{3\ell_0})\tilde{J}_i^V}\right) \\ &+\frac{3}{4}\sqrt{3}\sqrt{\ell_0+2\sqrt{3\ell_0}}+2\sqrt{3\ell_0}.\end{aligned} \tag{J.14}$$

For $\ell \gg \ell_{\text{cross},2}$, the Kondo coupling runs as in Fermi liquids, $\tilde{J}_{IIb}^V(\ell \geq \ell_{\text{cross},2}) = \frac{1}{\left(\tilde{J}_{IIa}^V(\ell_{\text{cross},2})\right)^{-1}-(\ell-\ell_{\text{cross},2})}$, and the Kondo scale is given by

$$\ell_K = \ell_{\text{cross},2} + \frac{2e^{\frac{3}{4}}}{\tilde{J}_i^V}\sqrt{\frac{3\tilde{g}_{f,i}\ell_0}{\pi^3}}. \tag{J.15}$$

To the leading order in $1/\tilde{J}_i^V$, the Kondo scale becomes $\ell_K \sim \frac{1}{\tilde{J}_i^V}\frac{g_{f,i}}{v_{0,i}\log 1/v_{0,i}}$, where $v_{0,i} \sim 1/(\ell_0 \log \ell_0)$. For fixed $\tilde{J}_i^V$ and $g_{f,i}$, the Kondo length scale diverges as the bare nesting angle $v_{0,i}$ approaches zero. The $v_{0,i}$ and $g_{f,i}$ dependences of ℓ_K are confirmed through the numerical solution of the beta functions, as is shown in Fig. 4.3. There is a discrepancy in the prefactor A for $\ell_K = \frac{A}{\tilde{J}_i^V}\frac{g_{f,i}}{v_{0,i}\log 1/v_{0,i}}$ between the analytic estimation and the numerical solution: $A_{\text{analytic}} = \frac{8e^{3/4}}{\sqrt{\pi}}$ vs. $A_{\text{numeric}} \approx \frac{8e^{3/4}}{3\sqrt{\pi}}$. This is because Eq. (J.15) does not accurately account for the ℓ-dependent anomalous dimension around the crossovers from the η_f-dominated flow to the the $\eta^{(\Phi)}$-dominated flow. Since we only keep only one dominant term between $\eta^{(\Phi)}$ and η_f for the flow of g_f, our analytic result overestimates g_f. This, in turn, makes η_f larger, causing an underestimaion of $\tilde{J}^V$, and hence $\ell_{K,\text{analytic}} > \ell_{K,\text{numeric}}$. However, this does not affect how ℓ_K depends on $g_{f,i}$ and $v_{0,i}$.

J.2.2 $1/\ell_0 \ll \tilde{g}_{f,i} \ll 1/\sqrt{\ell_0}$

In this case, $\eta_i^{(\Phi)}$ is larger than $\tilde{g}_{f,i}$ at the UV cut off scale ℓ_i, but is not large enough to stay dominant over $\tilde{g}_f$ at all scales. Since $\eta_f(\ell)$ initially grows as a function of ℓ, there is a crossover $\ell_{f,1}$, where the term $\tilde{g}_f\ell/\pi^3$ in the beta function of g_f dominates over $\eta^{(\Phi)}$ at crossover scale set by $\eta^{(\Phi)}(\ell_{f,1}) = \eta_f(\ell_{f,1})$. The crossover scale is given by

$$\ell_{f,1} \approx \frac{\pi^3}{2\sqrt{3\ell_0}\tilde{g}_{f,i}}. \tag{J.16}$$

At this crossover scale, the Kondo coupling becomes $\tilde{J}_i^V e^{-\frac{\pi^3}{24\tilde{g}_{f,i}\ell_0}}$ in the small $\tilde{J}_i^V$ limit. The flow in $\ell > \ell_{f,1}$ is then identical to the previous case discussed in Sec. J.2. If $\ell_K \ll \ell_f$, $\tilde{J}^V(\ell)$ is given by Eq. (J.10) with the replacement of $\ell_i \to \ell_{f,1}$ and $\tilde{J}_i^V \to \tilde{J}_i^V e^{-\frac{\pi^3}{24\tilde{g}_{f,i}\ell_0}}$. This gives the Kondo scale that is analogous to Eq. (J.11),

$$\ell_K = \frac{\pi^3}{2\sqrt{3\ell_0}\tilde{g}_{f,i}}\cosh\left(\sqrt{\frac{\tilde{g}_{f,i}}{\pi^3}}\frac{e^{\frac{\pi^3}{24\tilde{g}_{f,i}\ell_0}}}{\tilde{J}_i^V}\right) + \sqrt{\frac{\pi^3}{\tilde{g}_{f,i}}}\sinh\left(\sqrt{\frac{\tilde{g}_{f,i}}{\pi^3}}\frac{e^{\frac{\pi^3}{24\tilde{g}_{f,i}\ell_0}}}{\tilde{J}_i^V}\right). \tag{J.17}$$

On the other hand, if $\ell_K \gg \ell_f$, the Kondo scale is given by Eq. (J.15) with $\tilde{J}_i^V \to \tilde{J}_i^V e^{-\frac{\pi^3}{24\tilde{g}_{f,i}\ell_0}}$:

$$\begin{aligned}\ell_K =& \frac{2\sqrt{3}e^{\frac{\pi^3}{24\tilde{g}_{f,i}\ell_0}+\frac{3}{4}}\sqrt{\tilde{g}_{f,i}\ell_0}}{\pi^{3/2}\tilde{J}_i^V} - \frac{3}{4}\left(\log\left(\frac{\sqrt{\frac{3\tilde{g}_{f,i}\ell_0}{\pi^3}}e^{\frac{\pi^3}{24\tilde{g}_{f,i}\ell_0}}}{6\tilde{J}_i^V\ell_0(\ell_0+2\sqrt{3\ell_0})}\right)+\frac{3}{4}\right)^2 \\ &+\sqrt{3}\sqrt{\ell_0+2\sqrt{3\ell_0}}\log\left(\frac{\sqrt{\frac{3\tilde{g}_{f,i}\ell_0}{\pi^3}}e^{\frac{\pi^3}{24\tilde{g}_{f,i}\ell_0}}}{6\tilde{J}_i^V\ell_0(\ell_0+2\sqrt{3\ell_0})}\right)+\frac{3}{4}\sqrt{3}\sqrt{\ell_0+2\sqrt{3\ell_0}}+2\sqrt{3\ell_0}\end{aligned} \tag{J.18}$$

to the leading order.

Bibliography

[1] Ar. Abanov and A. Chubukov. "Anomalous Scaling at the Quantum Critical Point in Itinerant Antiferromagnets". In: *Phys. Rev. Lett.* 93 (25 Dec. 2004), p. 255702. DOI: 10.1103/PhysRevLett.93.255702. URL: http://link.aps.org/doi/10.1103/PhysRevLett.93.255702.

[2] Ar. Abanov and Andrey V. Chubukov. "Spin-Fermion Model near the Quantum Critical Point: One-Loop Renormalization Group Results". In: *Phys. Rev. Lett.* 84 (24 June 2000), pp. 5608–5611. DOI: 10.1103/PhysRevLett.84.5608. URL: http://link.aps.org/doi/10.1103/PhysRevLett.84.5608.

[3] Ar. Abanov, Andrey V. Chubukov, and J. Schmalian. "Quantum-critical theory of the spin-fermion model and its application to cuprates: Normal state analysis". In: *Adv. Phys.* 52.3 (2003), pp. 119–218. DOI: 10.1080/0001873021000057123. URL: http://dx.doi.org/10.1080/0001873021000057123.

[4] Elihu Abrahams and Peter Wölfe. "Critical quasiparticle theory applied to heavy fermion metals near an antiferromagnetic quantum phase transition". In: *Proc. Natl. Acad. Sci.* 109 (2012), p. 3238. DOI: 10.1073/pnas.1200346109. URL: http://www.pnas.org/content/109/9/3238.abstract.

[5] A. A. Abrikosov. "Electron scattering on magnetic impurities in metals and anomalous resistivity effects". In: 2.1 (), pp. 5–20. ISSN: 0554-128X. DOI: 10.1103/physicsphysiquefizika.2.5.

[6] Ian Affleck. "A current algebra approach to the Kondo effect". In: *Nuclear Physics B* 336.3 (1990), pp. 517–532. ISSN: 0550-3213. DOI: https://doi.org/10.1016/0550-3213(90)90440-0. URL: https://www.sciencedirect.com/science/article/pii/0550321390904400.

[7] Ian Affleck and Andreas W.W. Ludwig. "The Kondo effect, conformal field theory and fusion rules". In: *Nuclear Physics B* 352.3 (1991), pp. 849–862. ISSN: 0550-3213. DOI: https://doi.org/10.1016/0550-3213(91)90109-B. URL: https://www.sciencedirect.com/science/article/pii/055032139190109B.

[8] Vivek Aji, Chandra M. Varma, and Ilya Vekhter. "Kondo effect in an antiferromagnetic metal: Renormalization group analysis and a variational calculation". In: *Phys. Rev. B* 77 (22 June 2008), p. 224426. DOI: 10.1103/PhysRevB.77.224426. URL: https://link.aps.org/doi/10.1103/PhysRevB.77.224426.

[9] Ahmed Almheiri et al. "Black holes: complementarity or firewalls?" In: *Journal of High Energy Physics* 2013.2 (Feb. 2013). ISSN: 1029-8479. DOI: 10.1007/jhep02(2013)062. URL: http://dx.doi.org/10.1007/JHEP02(2013)062.

[10] B. L. Altshuler, L. B. Ioffe, and A. J. Millis. "Low-energy properties of fermions with singular interactions". In: *Phys. Rev. B* 50 (19 Nov. 1994), pp. 14048–14064. DOI: 10.1103/PhysRevB.50.14048. URL: http://link.aps.org/doi/10.1103/PhysRevB.50.14048.

[11] Daniel J. Amit and Victor Martin-Mayor. *Field Theory, the Renormalization Group, and Critical Phenomena*. 3rd. World Scientific, 2005. DOI: 10.1142/5715. eprint: https://www.worldscientific.com/doi/pdf/10.1142/5715. URL: https://www.worldscientific.com/doi/abs/10.1142/5715.

[12] B. Amorim et al. "Novel effects of strains in graphene and other two dimensional materials". In: *Physics Reports* 617 (Mar. 2016), pp. 1–54. DOI: 10.1016/j.physrep.2015.12.006. URL: https://doi.org/10.1016%2Fj.physrep.2015.12.006.

[13] P. W. Anderson. "A poor man's derivation of scaling laws for the Kondo problem". In: *Journal of Physics C: Solid State Physics* 3.12 (1970), pp. 2436–2441. ISSN: 0022-3719. DOI: 10.1088/0022-3719/3/12/008.

[14] P. W. Anderson. "Localized Magnetic States in Metals". In: *Phys. Rev.* 124 (1 Oct. 1961), pp. 41–53. DOI: 10.1103/PhysRev.124.41. URL: https://link.aps.org/doi/10.1103/PhysRev.124.41.

[15] N. Andrei. "Diagonalization of the Kondo Hamiltonian". In: *Phys. Rev. Lett.* 45 (5 Aug. 1980), pp. 379–382. DOI: 10.1103/PhysRevLett.45.379. URL: https://link.aps.org/doi/10.1103/PhysRevLett.45.379.

[16] N. Andrei and C. Destri. "Solution of the Multichannel Kondo Problem". In: *Phys. Rev. Lett.* 52 (5 Jan. 1984), pp. 364–367. DOI: 10.1103/PhysRevLett.52.364. URL: https://link.aps.org/doi/10.1103/PhysRevLett.52.364.

[17] N. Andrei, K. Furuya, and J. H. Lowenstein. "Solution of the Kondo problem". In: *Rev. Mod. Phys.* 55 (2 Apr. 1983), pp. 331–402. DOI: 10.1103/RevModPhys.55.331. URL: https://link.aps.org/doi/10.1103/RevModPhys.55.331.

[18] N. P. Armitage et al. "Anomalous Electronic Structure and Pseudogap Effects in $Nd_{1.85}Ce_{0.15}CuO_4$". In: *Phys. Rev. Lett.* 87 (14 Sept. 2001), p. 147003. DOI: 10.1103/PhysRevLett.87.147003. URL: https://link.aps.org/doi/10.1103/PhysRevLett.87.147003.

[19] N.W. Ashcroft and N.D. Mermin. *Solid State Physics*. Cengage Learning, 2011. ISBN: 9788131500521. URL: https://books.google.ca/books?id=x_s_YAAACAAJ.

[20] Abhay Ashtekar, Luca Bombelli, and Oscar Reula. "THE COVARIANT PHASE SPACE OF ASYMPTOTICALLY FLAT GRAVITATIONAL FIELDS". In: *Mechanics, Analysis and Geometry: 200 Years After Lagrange*. Ed. by Mauro Francaviglia. North-Holland Delta Series. Amsterdam: Elsevier, 1991, pp. 417–450. DOI: https://doi.org/10.1016/B978-0-444-88958-4.50021-5. URL: https://www.sciencedirect.com/science/article/pii/B9780444889584500215.

[21] Sven Badoux et al. "Change of carrier density at the pseudogap critical point of a cuprate superconductor". In: *Nature* 531.7593 (2016), pp. 210–214.

[22] J. Bardeen, L. N. Cooper, and J. R. Schrieffer. "Microscopic Theory of Superconductivity". In: *Phys. Rev.* 106 (1 Apr. 1957), pp. 162–164. DOI: 10.1103/PhysRev.106.162. URL: https://link.aps.org/doi/10.1103/PhysRev.106.162.

[23] J. Bardeen, L. N. Cooper, and J. R. Schrieffer. "Theory of Superconductivity". In: *Phys. Rev.* 108 (5 Dec. 1957), pp. 1175–1204. DOI: 10.1103/PhysRev.108.1175. URL: https://link.aps.org/doi/10.1103/PhysRev.108.1175.

[24] G. Baym and C. Pethick. *Landau Fermi-Liquid Theory: Concepts and Applications*. A Wiley-Interscience publication. Wiley, 1991. ISBN: 9780471824183. URL: https://books.google.ca/books?id=zDBnNEPAu2MC.

[25] E. Berg, M. Metlitski, and S. Sachdev. "Sign-Problem–Free Quantum Monte Carlo of the Onset of Antiferromagnetism in Metals". In: *Science* 338 (6088 2012), p. 1606. DOI: 10.1126/science.1227769. URL: http://science.sciencemag.org/content/338/6114/1606.

[26] Erez Berg et al. *Monte Carlo Studies of Quantum Critical Metals*. 2018. eprint: arXiv:1804.01988.

[27] N. D. Birrell and P. C. W. Davies. *Quantum Fields in Curved Space*. Cambridge Monographs on Mathematical Physics. Cambridge University Press, 1982. DOI: 10.1017/CBO9780511622632.

[28] Francisco Borges and Sung-Sik Lee. "Emergence of curved momentum-spacetime and its effect on cyclotron motion in the antiferromagnetic quantum critical metal". In: *Physical Review B* 108.24 (2023), p. 245112.

[29] Francisco Borges, Peter Lunts, and Sung-Sik Lee. "Ultraviolet/infrared mixing-driven suppression of Kondo screening in the antiferromagnetic quantum critical metal". In: (May 2025). DOI: 10.48550/ARXIV.2505.01561. arXiv: 2505.01561 [cond-mat.str-el].

[30] Francisco Borges et al. "Field-theoretic functional renormalization group formalism for non-Fermi liquids and its application to the antiferromagnetic quantum critical metal in two dimensions". In: *Annals of Physics* 450 (2023), p. 169221. ISSN: 0003-4916. DOI: https://doi.org/10.1016/j.aop.2023.169221. URL: https://www.sciencedirect.com/science/article/pii/S0003491623000064.

[31] Jens Braun, Holger Gies, and Daniel D. Scherer. "Asymptotic safety: A simple example". In: *Phys. Rev. D* 83 (8 Apr. 2011), p. 085012. DOI: 10.1103/PhysRevD.83.085012. URL: https://link.aps.org/doi/10.1103/PhysRevD.83.085012.

[32] Sergey Bravyi, David P. DiVincenzo, and Daniel Loss. "Schrieffer–Wolff transformation for quantum many-body systems". In: *Annals of Physics* 326.10 (2011), pp. 2793–2826. ISSN: 0003-4916. DOI: 10.1016/j.aop.2011.06.004.

[33] Henrik Bruus and Karsten Flensberg. *Many-body quantum theory in condensed matter physics - an introduction*. English. United States: Oxford University Press, 2004.

[34] Vanuildo S. de Carvalho and Hermann Freire. "Breakdown of Fermi liquid behavior near the hot spots in a two-dimensional model: A two-loop renormalization group analysis". In: *Nuclear Physics B* 875.3 (2013), pp. 738 –756. ISSN: 0550-3213. DOI: 10.1016/j.nuclphysb.2013.07.016. URL: http://www.sciencedirect.com/science/article/pii/S0550321313003829.

[35] Vanuildo S. de Carvalho and Hermann Freire. "Evidence of a short-range incommensurate d-wave charge order from a fermionic two-loop renormalization group calculation of a 2D model with hot spots". In: *Annals of Physics* 348 (2014), pp. 32 –49. ISSN: 0003-4916. DOI: 10.1016/j.aop.2014.05.009. URL: http://www.sciencedirect.com/science/article/pii/S0003491614001171.

[36] R. J. Cava et al. "Bulk superconductivity at 91 K in single-phase oxygen-deficient perovskite $Ba_2YCu_3O_{9-\delta}$". In: *Phys. Rev. Lett.* 58 (16 Apr. 1987), pp. 1676–1679. DOI: 10.1103/PhysRevLett.58.1676. URL: https://link.aps.org/doi/10.1103/PhysRevLett.58.1676.

[37] Joseph G. Checkelsky et al. "Flat bands, strange metals and the Kondo effect". In: *Nature Reviews Materials* 9.7 (2024), pp. 509–526. DOI: 10.1038/s41578-023-00644-z. URL: https://doi.org/10.1038/s41578-023-00644-z.

[38] Gennady Y. Chitov and Andrew J. Millis. "Leading Temperature Corrections to Fermi-Liquid Theory in Two Dimensions". In: *Phys. Rev. Lett.* 86 (23 June 2001), pp. 5337–5340. DOI: 10.1103/PhysRevLett.86.5337. URL: https://link.aps.org/doi/10.1103/PhysRevLett.86.5337.

[39] Gennady Y. Chitov and David Sénéchal. "Fermi liquid as a renormalization-group fixed point: The role of interference in the Landau channel". In: *Phys. Rev. B* 57 (3 Jan. 1998), pp. 1444–1456. DOI: 10.1103/PhysRevB.57.1444. URL: https://link.aps.org/doi/10.1103/PhysRevB.57.1444.

[40] Gennady Y. Chitov and David Sénéchal. "Renormalization-group study of interacting electrons". In: *Phys. Rev. B* 52 (18 Nov. 1995), pp. 13487–13496. DOI: 10.1103/PhysRevB.52.13487. URL: https://link.aps.org/doi/10.1103/PhysRevB.52.13487.

[41] Debanjan Chowdhury et al. "Translationally Invariant Non-Fermi-Liquid Metals with Critical Fermi Surfaces: Solvable Models". In: *Phys. Rev. X* 8 (3 July 2018), p. 031024. DOI: 10.1103/PhysRevX.8.031024. URL: https://link.aps.org/doi/10.1103/PhysRevX.8.031024.

[42] L. Classen, N. J. Robinson, and A. M. Tsvelik. "Ladder-like optical conductivity in the spin-fermion model". In: *ArXiv e-prints* (Nov. 2018). arXiv: 1811.01103 [cond-mat.str-el].

[43] Alberto Cortijo and María A.H. Vozmediano. "Effects of topological defects and local curvature on the electronic properties of planar graphene". In: *Nuclear Physics B* 763.3 (2007), pp. 293–308. ISSN: 0550-3213. DOI: https://doi.org/10.1016/j.nuclphysb.2006.10.031. URL: https://www.sciencedirect.com/science/article/pii/S055032130600856X.

[44] C Crnkovic. "Symplectic geometry of the convariant phase space". In: *Classical and Quantum Gravity* 5.12 (Dec. 1988), p. 1557. DOI: 10.1088/0264-9381/5/12/008. URL: https://dx.doi.org/10.1088/0264-9381/5/12/008.

[45] Thomas L. Curtright, Xiang Jin, and Cosmas K. Zachos. "Renormalization Group Flows, Cycles, and c-Theorem Folklore". In: *Phys. Rev. Lett.* 108 (13 Mar. 2012), p. 131601. DOI: 10.1103/PhysRevLett.108.131601. URL: https://link.aps.org/doi/10.1103/PhysRevLett.108.131601.

[46] J. Custers et al. "The break-up of heavy electrons at a quantum critical point". In: *Nature* 424 (July 2003), 524 EP –. URL: https://doi.org/10.1038/nature01774.

[47] J. Custers et al. "The break-up of heavy electrons at a quantum critical point". In: *Nature* 424.6948 (July 2003), pp. 524–527. DOI: 10.1038/nature01774. URL: https://doi.org/10.1038%2Fnature01774.

[48] Denis Dalidovich and Sung-Sik Lee. "Perturbative non-Fermi liquids from dimensional regularization". In: *Phys. Rev. B* 88 (24 Dec. 2013), p. 245106. DOI: 10.1103/PhysRevB.88.245106. URL: http://link.aps.org/doi/10.1103/PhysRevB.88.245106.

[49] Seth M. Davis and Matthew S. Foster. "Geodesic geometry of 2+1-D Dirac materials subject to artificial, quenched gravitational singularities". In: *SciPost Phys.* 12 (2022), p. 204. DOI: 10.21468/SciPostPhys.12.6.204. URL: https://scipost.org/10.21468/SciPostPhys.12.6.204.

[50] Nicolas Doiron-Leyraud et al. "Quantum oscillations and the Fermi surface in an underdoped high-Tc superconductor". In: *Nature* 447.7144 (May 2007), pp. 565–568. DOI: 10.1038/nature05872. URL: https://doi.org/10.1038%2Fnature05872.

[51] S. Doniach. "The Kondo lattice and weak antiferromagnetism". In: *Physica B+C* 91 (1977), pp. 231–234. ISSN: 0378-4363. DOI: https://doi.org/10.1016/0378-4363(77)90190-5. URL: https://www.sciencedirect.com/science/article/pii/0378436377901905.

[52] Maxim Dzero et al. "Topological Kondo Insulators". In: *Phys. Rev. Lett.* 104 (10 Mar. 2010), p. 106408. DOI: 10.1103/PhysRevLett.104.106408. URL: https://link.aps.org/doi/10.1103/PhysRevLett.104.106408.

[53] Andreas Eberlein. "Fermionic two-loop functional renormalization group for correlated fermions: Method and application to the attractive Hubbard model". In: *Phys. Rev. B* 90 (11 Sept. 2014), p. 115125. DOI: 10.1103/PhysRevB.90.115125. URL: https://link.aps.org/doi/10.1103/PhysRevB.90.115125.

[54] Andreas Eberlein. "Self-energy effects in functional renormalization group flows of the two-dimensional $t-t'$ Hubbard model away from van Hove filling". In: *Phys. Rev. B* 92 (23 Dec. 2015), p. 235146. DOI: 10.1103/PhysRevB.92.235146. URL: https://link.aps.org/doi/10.1103/PhysRevB.92.235146.

[55] Andreas Eberlein and Walter Metzner. "Effective interactions and fluctuation effects in spin-singlet superfluids". In: *Phys. Rev. B* 87 (17 May 2013), p. 174523. DOI: 10.1103/PhysRevB.87.174523. URL: https://link.aps.org/doi/10.1103/PhysRevB.87.174523.

[56] Dominic V. Else, Ryan Thorngren, and T. Senthil. "Non-Fermi Liquids as Ersatz Fermi Liquids: General Constraints on Compressible Metals". In: *Phys. Rev. X* 11 (2 Apr. 2021), p. 021005. DOI: 10.1103/PhysRevX.11.021005. URL: https://link.aps.org/doi/10.1103/PhysRevX.11.021005.

[57] Ilya Esterlis et al. "Large-N theory of critical Fermi surfaces". In: *Phys. Rev. B* 103 (23 June 2021), p. 235129. DOI: 10.1103/PhysRevB.103.235129. URL: https://link.aps.org/doi/10.1103/PhysRevB.103.235129.

[58] W. Felsch and K. Winzer. "Magnetoresistivity of (La, Ce)Al2 alloys". In: *Solid State Communications* 13.5 (1973), pp. 569–573. ISSN: 0038-1098. DOI: 10.1016/s0038-1098(73)80015-8.

[59] A. Liam Fitzpatrick et al. "Non-Fermi-liquid fixed point in a Wilsonian theory of quantum critical metals". In: *Phys. Rev. B* 88 (12 Sept. 2013), p. 125116. DOI: 10.1103/PhysRevB.88.125116. URL: http://link.aps.org/doi/10.1103/PhysRevB.88.125116.

[60] G. Gabrielse et al. "New Determination of the Fine Structure Constant from the Electron g Value and QED". In: *Phys. Rev. Lett.* 97 (3 July 2006), p. 030802. DOI: 10.1103/PhysRevLett.97.030802. URL: https://link.aps.org/doi/10.1103/PhysRevLett.97.030802.

[61] Antoine Georges and Gabriel Kotliar. "The Hund-metal path to strong electronic correlations". In: *Physics Today* 77.4 (Apr. 2024), pp. 46–53. ISSN: 0031-9228. DOI: 10.1063/pt.wqrz.qpjx. eprint: https://pubs.aip.org/physicstoday/article-pdf/77/4/46/20086423/46_1_pt.wqrz.qpjx.pdf. URL: https://doi.org/10.1063/pt.wqrz.qpjx.

[62] Max H. Gerlach et al. "Quantum critical properties of a metallic spin-density-wave transition". In: *Phys. Rev. B* 95 (3 Jan. 2017), p. 035124. DOI: 10.1103/PhysRevB.95.035124. URL: http://link.aps.org/doi/10.1103/PhysRevB.95.035124.

[63] Holger Gies and Lukas Janssen. "UV fixed-point structure of the three-dimensional Thirring model". In: *Phys. Rev. D* 82 (8 Oct. 2010), p. 085018. DOI: 10.1103/PhysRevD.82.085018. URL: https://link.aps.org/doi/10.1103/PhysRevD.82.085018.

[64] Holger Gies et al. "Phase transition and critical behavior of $d = 3$ chiral fermion models with left-right asymmetry". In: *Phys. Rev. D* 81 (2 Jan. 2010), p. 025009. DOI: 10.1103/PhysRevD.81.025009. URL: https://link.aps.org/doi/10.1103/PhysRevD.81.025009.

[65] Vitaly L. Ginzburg. In: *Sov. Phys. Sol. State* 2.1824 (1960).

[66] Stanisław D. Głazek. "Limit cycles of effective theories". In: *Phys. Rev. D* 75 (2 Jan. 2007), p. 025005. DOI: 10.1103/PhysRevD.75.025005. URL: https://link.aps.org/doi/10.1103/PhysRevD.75.025005.

[67] Stanisław D. Głazek and Kenneth G. Wilson. "Limit Cycles in Quantum Theories". In: *Phys. Rev. Lett.* 89 (23 Nov. 2002), p. 230401. DOI: 10.1103/PhysRevLett.89.230401. URL: https://link.aps.org/doi/10.1103/PhysRevLett.89.230401.

[68] Swee K. Goh et al. *Quantum Oscillations in the High Pressure Metallic State of Ca_2RuO_4*. 2012. DOI: 10.48550/ARXIV.1205.3045. arXiv: 1205.3045 [cond-mat.str-el]. URL: https://arxiv.org/abs/1205.3045.

[69] Victor Gorbenko, Slava Rychkov, and Bernardo Zan. "Walking, weak first-order transitions, and complex CFTs". In: *Journal of High Energy Physics* 2018.10 (2018), p. 108. DOI: 10.1007/JHEP10(2018)108. URL: https://doi.org/10.1007/JHEP10(2018)108.

[70] V. Grinenko et al. "Selective mass enhancement close to the quantum critical point in BaFe2(As1-x P x)2". In: *Scientific Reports* 7.1 (July 2017). DOI: 10.1038/s41598-017-04724-3. URL: https://doi.org/10.1038%2Fs41598-017-04724-3.

[71] M. Gurvitch and A. T. Fiory. "Resistivity of $La_{1.825}Sr_{0.175}CuO_4$ and $YBa_2Cu_3O_7$ to 1100 K: Absence of saturation and its implications". In: *Phys. Rev. Lett.* 59 (12 Sept. 1987), pp. 1337–1340. DOI: 10.1103/PhysRevLett.59.1337. URL: https://link.aps.org/doi/10.1103/PhysRevLett.59.1337.

[72] W. J. de Haas, J. de Boer, and G. J. van dën Berg. "The electrical resistance of gold, copper and lead at low temperatures". In: *Physica* 1.7-12 (1934), pp. 1115–1124. ISSN: 0031-8914. DOI: 10.1016/s0031-8914(34)80310-2.

[73] Christoph J. Halboth and Walter Metzner. "Renormalization-group analysis of the two-dimensional Hubbard model". In: *Phys. Rev. B* 61 (11 Mar. 2000), pp. 7364–7377. DOI: 10.1103/PhysRevB.61.7364. URL: https://link.aps.org/doi/10.1103/PhysRevB.61.7364.

[74] F. D. M. Haldane. "Berry Curvature on the Fermi Surface: Anomalous Hall Effect as a Topological Fermi-Liquid Property". In: *Phys. Rev. Lett.* 93 (20 Nov. 2004), p. 206602. DOI: 10.1103/PhysRevLett.93.206602. URL: https://link.aps.org/doi/10.1103/PhysRevLett.93.206602.

[75] F D M Haldane. "Luttinger liquid theory of one-dimensional quantum fluids. I. Properties of the Luttinger model and their extension to the general 1D interacting spinless Fermi gas". In: *Journal of Physics C: Solid State Physics* 14.19 (July 1981), pp. 2585–2609. DOI: 10.1088/0022-3719/14/19/010. URL: https://doi.org/10.1088%2F0022-3719%2F14%2F19%2F010.

[76] Sean A. Hartnoll et al. "Quantum critical response at the onset of spin-density-wave order in two-dimensional metals". In: *Phys. Rev. B* 84 (12 Sept. 2011), p. 125115. DOI: 10.1103/PhysRevB.84.125115. URL: http://link.aps.org/doi/10.1103/PhysRevB.84.125115.

[77] K. Hashimoto et al. "A Sharp Peak of the Zero-Temperature Penetration Depth at Optimal Composition in BaFe2(As1-xPx)2". In: *Science* 336 (6088 2012), p. 1554. DOI: 10.1126/science.1219821. URL: http://science.sciencemag.org/content/336/6088/1554.

[78] T. Helm et al. "Magnetic Breakdown in the Electron-Doped Cuprate Superconductor $Nd_{2-x}Ce_xCuO_4$: The Reconstructed Fermi Surface Survives in the Strongly Overdoped Regime". In: *Phys. Rev. Lett.* 105 (24 Dec. 2010), p. 247002. DOI: 10.1103/PhysRevLett.105.247002. URL: http://link.aps.org/doi/10.1103/PhysRevLett.105.247002.

[79] John A. Hertz. "Quantum critical phenomena". In: *Phys. Rev. B* 14 (3 Aug. 1976), pp. 1165–1184. DOI: 10.1103/PhysRevB.14.1165. URL: http://link.aps.org/doi/10.1103/PhysRevB.14.1165.

[80] Alexander Cyril Hewson. *The Kondo Problem to Heavy Fermions*. Vol. 2. Cambridge Studies in Magnetism. Cambridge: Cambridge University Press, 1993. ISBN: 9780511470752. DOI: doi.org/10.1017/CBO9780511470752. URL: https://www.cambridge.org/core/books/kondo-problem-to-heavy-fermions/EDBEDC3F4492DD3EE27E02259935705A.

[81] F. Höfling, C. Nowak, and C. Wetterich. "Phase transition and critical behavior of the d=3 Gross-Neveu model". In: *Phys. Rev. B* 66 (20 Nov. 2002), p. 205111. DOI: 10.1103/PhysRevB.66.205111. URL: https://link.aps.org/doi/10.1103/PhysRevB.66.205111.

[82] Tobias Holder. "Electrons flow like falling cats: Deformations and emergent gravity in quantum transport". In: *arXiv preprint arXiv:2111.07782* (2021). URL: https://arxiv.org/abs/2111.07782.

[83] Tobias Holder and Walter Metzner. "Anomalous dynamical scaling from nematic and U(1) gauge field fluctuations in two-dimensional metals". In: *Phys. Rev. B* 92 (4 July 2015), p. 041112. DOI: 10.1103/PhysRevB.92.041112. URL: http://link.aps.org/doi/10.1103/PhysRevB.92.041112.

[84] T. Holstein, R. E. Norton, and P. Pincus. "de Haas-van Alphen Effect and the Specific Heat of an Electron Gas". In: *Phys. Rev. B* 8 (6 Sept. 1973), pp. 2649–2656. DOI: 10.1103/PhysRevB.8.2649. URL: http://link.aps.org/doi/10.1103/PhysRevB.8.2649.

[85] Carsten Honerkamp. "Density Waves and Cooper Pairing on the Honeycomb Lattice". In: *Phys. Rev. Lett.* 100 (14 Apr. 2008), p. 146404. DOI: 10.1103/PhysRevLett.100.146404. URL: https://link.aps.org/doi/10.1103/PhysRevLett.100.146404.

[86] J.D. Jackson. *Classical electrodynamics*. Wiley, 1975. ISBN: 9780471431329. URL: https://books.google.ca/books?id=_7rvAAAAMAAJ.

[87] P. Jakubczyk and A. Eberlein. "Thermodynamics of the two-dimensional XY model from functional renormalization". In: *Phys. Rev. E* 93 (6 June 2016), p. 062145. DOI: 10.1103/PhysRevE.93.062145. URL: https://link.aps.org/doi/10.1103/PhysRevE.93.062145.

[88] Lukas Janssen and Holger Gies. "Critical behavior of the $(2+1)$-dimensional Thirring model". In: *Phys. Rev. D* 86 (10 Nov. 2012), p. 105007. DOI: 10.1103/PhysRevD.86.105007. URL: https://link.aps.org/doi/10.1103/PhysRevD.86.105007.

[89] Lukas Janssen and Igor F. Herbut. "Antiferromagnetic critical point on graphene's honeycomb lattice: A functional renormalization group approach". In: *Phys. Rev. B* 89 (20 May 2014), p. 205403. DOI: 10.1103/PhysRevB.89.205403. URL: https://link.aps.org/doi/10.1103/PhysRevB.89.205403.

[90] H.-C. Jiang et al. "Non-Fermi-liquid d-wave metal phase of strongly interacting electrons". In: *Nature* 493 (2013), p. 39. DOI: 10.1038/nature11732. URL: http://www.nature.com/nature/journal/v493/n7430/full/nature11732.html.

[91] Leo P. Kadanoff. "Scaling laws for ising models near T_c". In: *Physics Physique Fizika* 2 (6 June 1966), pp. 263–272. DOI: 10.1103/PhysicsPhysiqueFizika.2.263. URL: https://link.aps.org/doi/10.1103/PhysicsPhysiqueFizika.2.263.

[92] David B. Kaplan et al. "Conformality lost". In: *Phys. Rev. D* 80 (12 Dec. 2009), p. 125005. DOI: 10.1103/PhysRevD.80.125005. URL: https://link.aps.org/doi/10.1103/PhysRevD.80.125005.

[93] Yong Baek Kim et al. "Gauge-invariant response functions of fermions coupled to a gauge field". In: *Phys. Rev. B* 50 (24 Dec. 1994), pp. 17917–17932. DOI: 10.1103/PhysRevB.50.17917. URL: http://link.aps.org/doi/10.1103/PhysRevB.50.17917.

[94] Motoi Kimata et al. "Cyclotron Resonance and Mass Enhancement by Electron Correlation in KFe_2As_2". In: *Phys. Rev. Lett.* 107 (16 Oct. 2011), p. 166402. DOI: 10.1103/PhysRevLett.107.166402. URL: https://link.aps.org/doi/10.1103/PhysRevLett.107.166402.

[95] A. Kitaev. *A simple model of quantum holography*. Apr. 2015. URL: https://online.kitp.ucsb.edu/online/entangled15/kitaev/.

[96] W. Kohn and J. M. Luttinger. "New Mechanism for Superconductivity". In: *Phys. Rev. Lett.* 15 (12 Sept. 1965), pp. 524–526. DOI: 10.1103/PhysRevLett.15.524. URL: https://link.aps.org/doi/10.1103/PhysRevLett.15.524.

[97] Jun Kondo. "Resistance Minimum in Dilute Magnetic Alloys". In: *Progress of Theoretical Physics* 32.1 (July 1964), pp. 37–49. ISSN: 0033-068X. DOI: 10.1143/PTP.32.37. eprint: https://academic.oup.com/ptp/article-pdf/32/1/37/5193092/32-1-37.pdf. URL: https://doi.org/10.1143/PTP.32.37.

[98] Jerzy Kowalski-Glikman. "LIVING IN CURVED MOMENTUM SPACE". In: *International Journal of Modern Physics A* 28.12 (May 2013), p. 1330014. DOI: 10.1142/s0217751x13300147. URL: https://doi.org/10.1142/s0217751x13300147.

[99] Shubham Kukreja, Afshin Besharat, and Sung-Sik Lee. "Projective fixed points for non-Fermi liquids: A case study of the Ising-nematic quantum critical metal". In: *Phys. Rev. B* 110 (15 Oct. 2024), p. 155142. DOI: 10.1103/PhysRevB.110.155142. URL: https://link.aps.org/doi/10.1103/PhysRevB.110.155142.

[100] L. Landau. "Oscillations in a Fermi liquid". In: *Sov. Phys. JETP* 5 (1957), p. 101. URL: http://www.jetp.ac.ru/cgi-bin/dn/e_005_01_0101.pdf.

[101] L. Landau. "The theory of a Fermi liquid". In: *Sov. Phys. JETP* 3 (1957), p. 920. URL: http://www.jetp.ac.ru/cgi-bin/dn/e_003_06_0920.pdf.

[102] Lev Landau. "Zur Theorie der Phasenumwandlungen I". In: *Sov. Phys. JETP* 7.19 (1937).

[103] Lev Landau. "Zur Theorie der Phasenumwandlungen II". In: *Phys. Z. Sowjetunion* 11.26-35 (1937).

[104] A. I. Larkin and V. I. Melnikov. "MAGNETIC IMPURITIES IN AN ALMOST MAGNETIC METAL". In: *Sov. Phys. JETP* 34 (3 1972), p. 656.

[105] André LeClair, José María Román, and Germán Sierra. "Russian doll renormalization group and superconductivity". In: *Phys. Rev. B* 69 (2 Jan. 2004), p. 020505. DOI: 10.1103/PhysRevB.69.020505. URL: https://link.aps.org/doi/10.1103/PhysRevB.69.020505.

[106] Joohan Lee and Robert M. Wald. "Local symmetries and constraints". In: *Journal of Mathematical Physics* 31.3 (1990), pp. 725–743. DOI: 10.1063/1.528801. eprint: https://doi.org/10.1063/1.528801. URL: https://doi.org/10.1063/1.528801.

[107] Junhyun Lee, Philipp Strack, and Subir Sachdev. "Quantum criticality of reconstructing Fermi surfaces in antiferromagnetic metals". In: *Phys. Rev. B* 87 (4 Jan. 2013), p. 045104. DOI: 10.1103/PhysRevB.87.045104. URL: https://link.aps.org/doi/10.1103/PhysRevB.87.045104.

[108] Patrick A. Lee. "Gauge field, Aharonov-Bohm flux, and high-T_c superconductivity". In: *Phys. Rev. Lett.* 63 (6 Aug. 1989), pp. 680–683. DOI: 10.1103/PhysRevLett.63.680. URL: http://link.aps.org/doi/10.1103/PhysRevLett.63.680.

[109] Patrick A. Lee and Naoto Nagaosa. "Gauge theory of the normal state of high-T_c superconductors". In: *Phys. Rev. B* 46 (9 Sept. 1992), pp. 5621–5639. DOI: 10.1103/PhysRevB.46.5621. URL: http://link.aps.org/doi/10.1103/PhysRevB.46.5621.

[110] Sung-Sik Lee. "Low-energy effective theory of Fermi surface coupled with U(1) gauge field in $2+1$ dimensions". In: *Phys. Rev. B* 80 (16 Oct. 2009), p. 165102. DOI: 10.1103/PhysRevB.80.165102. URL: http://link.aps.org/doi/10.1103/PhysRevB.80.165102.

[111] Sung-Sik Lee. "Quantum renormalization group and holography". In: *Journal of High Energy Physics* 2014.1 (2014), p. 76. DOI: 10.1007/JHEP01(2014)076. URL: https://doi.org/10.1007/JHEP01(2014)076.

[112] Sung-Sik Lee. "Recent Developments in Non-Fermi Liquid Theory". In: *Annu. Rev. of Condens. Matter Phys.* 9.1 (2018), pp. 227–244. DOI: 10.1146/annurev-conmatphys-031016-025531. URL: https://doi.org/10.1146/annurev-conmatphys-031016-025531.

[113] A. J. Leggett et al. "Dynamics of the dissipative two-state system". In: *Rev. Mod. Phys.* 59 (1 Jan. 1987), pp. 1–85. DOI: 10.1103/RevModPhys.59.1. URL: https://link.aps.org/doi/10.1103/RevModPhys.59.1.

[114] A. Legros et al. "Evolution of the cyclotron mass with doping in $La_{2-x}Sr_xCuO_4$". In: *Phys. Rev. B* 106 (19 Nov. 2022), p. 195110. DOI: 10.1103/PhysRevB.106.195110. URL: https://link.aps.org/doi/10.1103/PhysRevB.106.195110.

[115] Arkady. P. Levanyuk. In: *Sov. Phys. JETP* 36.571 (1959).

[116] Zi-Xiang Li et al. "Nature of the effective interaction in electron-doped cuprate superconductors: A sign-problem-free quantum Monte Carlo study". In: *Phys. Rev. B* 95 (21 June 2017), p. 214505. DOI: 10.1103/PhysRevB.95.214505. URL: https://link.aps.org/doi/10.1103/PhysRevB.95.214505.

[117] Zi-Xiang Li et al. "What makes the Tc of monolayer FeSe on SrTiO3 so high: a sign-problem-free quantum Monte Carlo study". In: *Science Bulletin* 61.12 (2016), pp. 925 –930. ISSN: 2095-9273. DOI: 10.1007/s11434-016-1087-x. URL: http://www.sciencedirect.com/science/article/pii/S2095927316300962.

[118] Zi Hong Liu et al. *EMUS-QMC: Elective Momentum Ultra-Size Quantum Monte Carlo*. 2017. eprint: arXiv:1801.00127.

[119] Zi Hong Liu et al. *Itinerant Quantum Critical Point with Fermion Pockets and Hot Spots*. 2018. eprint: arXiv:1808.08878.

[120] Zi Hong Liu et al. "Itinerant quantum critical point with frustration and a non-Fermi liquid". In: *Phys. Rev. B* 98 (4 July 2018), p. 045116. DOI: 10.1103/PhysRevB.98.045116. URL: https://link.aps.org/doi/10.1103/PhysRevB.98.045116.

[121] Hilbert v. Löhneysen et al. "Fermi-liquid instabilities at magnetic quantum phase transitions". In: *Rev. Mod. Phys.* 79 (3 Aug. 2007), pp. 1015–1075. DOI: 10.1103/RevModPhys.79.1015. URL: http://link.aps.org/doi/10.1103/RevModPhys.79.1015.

[122] Peter Lunts, Michael S. Albergo, and Michael Lindsey. "Non-Hertz-Millis scaling of the antiferromagnetic quantum critical metal via scalable Hybrid Monte Carlo". In: *arXiv e-prints*, arXiv:2204.14241 (Apr. 2022), arXiv:2204.14241. arXiv: 2204.14241 [cond-mat.str-el].

[123] Peter Lunts, Andres Schlief, and Sung-Sik Lee. "Emergence of a control parameter for the antiferromagnetic quantum critical metal". In: *Phys. Rev. B* 95 (24 June 2017), p. 245109. DOI: 10.1103/PhysRevB.95.245109. URL: https://link.aps.org/doi/10.1103/PhysRevB.95.245109.

[124] J. M. Luttinger. "Fermi Surface and Some Simple Equilibrium Properties of a System of Interacting Fermions". In: *Phys. Rev.* 119 (4 Aug. 1960), pp. 1153–1163. DOI: 10.1103/PhysRev.119.1153. URL: https://link.aps.org/doi/10.1103/PhysRev.119.1153.

[125] J. M. Luttinger and J. C. Ward. "Ground-State Energy of a Many-Fermion System. II". In: *Phys. Rev.* 118 (5 June 1960), pp. 1417–1427. DOI: 10.1103/PhysRev.118.1417. URL: https://link.aps.org/doi/10.1103/PhysRev.118.1417.

[126] H. Maebashi, K. Miyake, and C. M. Varma. "Singular Effects of Impurities near the Ferromagnetic Quantum-Critical Point". In: *Phys. Rev. Lett.* 88 (22 May 2002), p. 226403. DOI: 10.1103/PhysRevLett.88.226403. URL: https://link.aps.org/doi/10.1103/PhysRevLett.88.226403.

[127] H. Maebashi, K. Miyake, and C. M. Varma. "Undressing the Kondo Effect near the Antiferromagnetic Quantum Critical Point". In: *Phys. Rev. Lett.* 95 (20 Nov. 2005), p. 207207. DOI: 10.1103/PhysRevLett.95.207207. URL: https://link.aps.org/doi/10.1103/PhysRevLett.95.207207.

[128] Gerald D. Mahan. *Many-Particle Physics*. 2000. DOI: 10.1007/978-1-4757-5714-9.

[129] Stefan A. Maier, Andreas Eberlein, and Carsten Honerkamp. "Functional renormalization group for commensurate antiferromagnets: Beyond the mean-field picture". In: *Phys. Rev. B* 90 (3 July 2014), p. 035140. DOI: 10.1103/PhysRevB.90.035140. URL: https://link.aps.org/doi/10.1103/PhysRevB.90.035140.

[130] Stefan A. Maier and Philipp Strack. "Universality in antiferromagnetic strange metals". In: *Phys. Rev. B* 93 (16 Apr. 2016), p. 165114. DOI: 10.1103/PhysRevB.93.165114. URL: http://link.aps.org/doi/10.1103/PhysRevB.93.165114.

[131] Juan Maldacena and Douglas Stanford. "Remarks on the Sachdev-Ye-Kitaev model". In: *Phys. Rev. D* 94 (10 Nov. 2016), p. 106002. DOI: 10.1103/PhysRevD.94.106002. URL: https://link.aps.org/doi/10.1103/PhysRevD.94.106002.

[132] Ipsita Mandal. "UV/IR mixing in non-Fermi liquids: higher-loop corrections in different energy ranges". In: *The European Physical Journal B* 89.12 (Dec. 2016), p. 278. DOI: 10.1140/epjb/e2016-70509-4.

[133] Ipsita Mandal and Sung-Sik Lee. "Ultraviolet/infrared mixing in non-Fermi liquids". In: *Phys. Rev. B* 92 (3 July 2015), p. 035141. DOI: 10.1103/PhysRevB.92.035141. URL: http://link.aps.org/doi/10.1103/PhysRevB.92.035141.

[134] Jinhai Mao et al. "Evidence of flat bands and correlated states in buckled graphene superlattices". In: *Nature* 584.7820 (Aug. 2020), pp. 215–220. DOI: 10.1038/s41586-020-2567-3. URL: https://doi.org/10.1038%2Fs41586-020-2567-3.

[135] Nicola Marzari et al. "Maximally localized Wannier functions: Theory and applications". In: *Rev. Mod. Phys.* 84 (4 Oct. 2012), pp. 1419–1475. DOI: 10.1103/RevModPhys.84.1419. URL: https://link.aps.org/doi/10.1103/RevModPhys.84.1419.

[136] Samir D. Mathur. "The Fuzzball proposal for black holes: An Elementary review". In: *Fortsch. Phys.* 53 (2005). Ed. by E. Kiritsis, pp. 793–827. DOI: 10.1002/prop.200410203. arXiv: hep-th/0502050.

[137] Daniel C. Mattis and Elliott H. Lieb. "Exact Solution of a Many-Fermion System and Its Associated Boson Field". In: *Journal of Mathematical Physics* 6.2 (1965), pp. 304–312. DOI: 10.1063/1.1704281. eprint: https://doi.org/10.1063/1.1704281. URL: https://doi.org/10.1063/1.1704281.

[138] A. Menth, E. Buehler, and T. H. Geballe. "Magnetic and Semiconducting Properties of SmB_6". In: *Phys. Rev. Lett.* 22 (7 1969), pp. 295–297. DOI: 10.1103/PhysRevLett.22.295. URL: https://link.aps.org/doi/10.1103/PhysRevLett.22.295.

[139] D. Mesterházy, J. Berges, and L. von Smekal. "Effect of short-range interactions on the quantum critical behavior of spinless fermions on the honeycomb lattice". In: *Phys. Rev. B* 86 (24 Dec. 2012), p. 245431. DOI: 10.1103/PhysRevB.86.245431. URL: https://link.aps.org/doi/10.1103/PhysRevB.86.245431.

[140] Max A. Metlitski and Subir Sachdev. "Quantum phase transitions of metals in two spatial dimensions. I. Ising-nematic order". In: *Phys. Rev. B* 82 (7 Aug. 2010), p. 075127. DOI: 10.1103/PhysRevB.82.075127. URL: https://link.aps.org/doi/10.1103/PhysRevB.82.075127.

[141] Max A. Metlitski and Subir Sachdev. "Quantum phase transitions of metals in two spatial dimensions. II. Spin density wave order". In: *Phys. Rev. B* 82 (7 Aug. 2010), p. 075128. DOI: 10.1103/PhysRevB.82.075128. URL: http://link.aps.org/doi/10.1103/PhysRevB.82.075128.

[142] Max A. Metlitski et al. "Cooper pairing in non-Fermi liquids". In: *Phys. Rev. B* 91 (11 Mar. 2015), p. 115111. DOI: 10.1103/PhysRevB.91.115111. URL: https://link.aps.org/doi/10.1103/PhysRevB.91.115111.

[143] Walter Metzner et al. "Functional renormalization group approach to correlated fermion systems". In: *Rev. Mod. Phys.* 84 (1 Mar. 2012), pp. 299–352. DOI: 10.1103/RevModPhys.84.299. URL: https://link.aps.org/doi/10.1103/RevModPhys.84.299.

[144] A. J. Millis. "Effect of a nonzero temperature on quantum critical points in itinerant fermion systems". In: *Phys. Rev. B* 48 (10 Sept. 1993), pp. 7183–7196. DOI: 10.1103/PhysRevB.48.7183. URL: http://link.aps.org/doi/10.1103/PhysRevB.48.7183.

[145] Johannes Mitscherling and Walter Metzner. "Non-Hermitian band topology from momentum-dependent relaxation in two-dimensional metals with spiral magnetism". In: *Phys. Rev. B* 104 (20 Nov. 2021), p. L201107. DOI: 10.1103/PhysRevB.104.L201107. URL: https://link.aps.org/doi/10.1103/PhysRevB.104.L201107.

[146] Tim R. Morris. "The exact renormalization group and approximate solutions". In: *Int. J. Mod. Phys. A*. 9.14 (1994), pp. 2411 –2449. DOI: 10.1142/S0217751X94000972. URL: https://www.worldscientific.com/doi/abs/10.1142/S0217751X94000972.

[147] E. M. Motoyama et al. "Spin correlations in the electron-doped high-transition-temperature superconductor Nd2-xCexCuO4±δ". In: *Nature* 445 (Jan. 2007), 186 EP –. URL: https://doi.org/10.1038/nature05437.

[148] David F. Mross et al. "Controlled expansion for certain non-Fermi-liquid metals". In: *Phys. Rev. B* 82 (4 July 2010), p. 045121. DOI: 10.1103/PhysRevB.82.045121. URL: http://link.aps.org/doi/10.1103/PhysRevB.82.045121.

[149] Naoto Nagaosa and Patrick A. Lee. "Kondo Effect in High- T_c Cuprates". In: *Phys. Rev. Lett.* 79 (19 Nov. 1997), pp. 3755–3758. DOI: 10.1103/PhysRevLett.79.3755. URL: https://link.aps.org/doi/10.1103/PhysRevLett.79.3755.

[150] Chetan Nayak and Frank Wilczek. "Non-Fermi liquid fixed point in 2 + 1 dimensions". In: *Nuclear Physics B* 417.3 (1994), pp. 359 –373. ISSN: 0550-3213. DOI: 10.1016/0550-3213(94)90477-4. URL: http://www.sciencedirect.com/science/article/pii/0550321394904774.

[151] P. Nozières. "A "fermi-liquid" description of the Kondo problem at low temperatures". In: *Journal of Low Temperature Physics* 17.1 (1974), pp. 31–42. DOI: 10.1007/BF00654541. URL: https://doi.org/10.1007/BF00654541.

[152] Olivier Parcollet et al. "Overscreened multichannel SU(N) Kondo model: Large-N solution and conformal field theory". In: *Phys. Rev. B* 58 (7 Aug. 1998), pp. 3794–3813. DOI: 10.1103/PhysRevB.58.3794. URL: https://link.aps.org/doi/10.1103/PhysRevB.58.3794.

[153] T. Park et al. "Hidden Magnetism and Quantum Criticality in the Heavy Fermion Superconductor CeRhIn5". In: *Nature* 440 (2006), p. 65. DOI: 10.1038/nature04571. URL: http://www.nature.com/nature/journal/v440/n7080/full/nature04571.html.

[154] Aavishkar A. Patel and Subir Sachdev. "dc resistivity at the onset of spin density wave order in two-dimensional metals". In: *Phys. Rev. B* 90 (16 Oct. 2014), p. 165146. DOI: 10.1103/PhysRevB.90.165146. URL: https://link.aps.org/doi/10.1103/PhysRevB.90.165146.

[155] Aavishkar A. Patel, Philipp Strack, and Subir Sachdev. "Hyperscaling at the spin density wave quantum critical point in two-dimensional metals". In: *Phys. Rev. B* 92 (16 Oct. 2015), p. 165105. DOI: 10.1103/PhysRevB.92.165105. URL: http://link.aps.org/doi/10.1103/PhysRevB.92.165105.

[156] Adarsh S. Patri and Yong Baek Kim. "Critical Theory of Non-Fermi Liquid Fixed Point in Multipolar Kondo Problem". In: *Phys. Rev. X* 10 (4 Oct. 2020), p. 041021. DOI: 10.1103/PhysRevX.10.041021. URL: https://link.aps.org/doi/10.1103/PhysRevX.10.041021.

[157] Vitor M. Pereira et al. "Geometry, Mechanics, and Electronics of Singular Structures and Wrinkles in Graphene". In: *Phys. Rev. Lett.* 105 (15 Oct. 2010), p. 156603. DOI: 10.1103/PhysRevLett.105.156603. URL: https://link.aps.org/doi/10.1103/PhysRevLett.105.156603.

[158] J. H. Pixley et al. "Quantum criticality in the pseudogap Bose-Fermi Anderson and Kondo models: Interplay between fermion- and boson-induced Kondo destruction". In: *Phys. Rev. B* 88 (24 Dec. 2013), p. 245111. DOI: 10.1103/PhysRevB.88.245111. URL: https://link.aps.org/doi/10.1103/PhysRevB.88.245111.

[159] C. Platt, W. Hanke, and R. Thomale. "Functional renormalization group for multi-orbital Fermi surface instabilities". In: *Advances in Physics* 62.4-6 (2013), pp. 453–562. DOI: 10.1080/00018732.2013.862020. eprint: https://doi.org/10.1080/00018732.2013.862020. URL: https://doi.org/10.1080/00018732.2013.862020.

[160] J. Polchinski. "Effective Field Theory and the Fermi Surface". In: *ArXiv High Energy Physics - Theory e-prints* (Oct. 1992). eprint: hep-th/9210046.

[161] Joseph Polchinski. "Low-energy dynamics of the spinon-gauge system". In: *Nuclear Physics B* 422.3 (1994), pp. 617–633. DOI: 10.1016/0550-3213(94)90449-9. URL: https://www.sciencedirect.com/science/article/pii/0550321394904499?via%3Dihub.

[162] Joseph Polchinski. "Renormalization and effective lagrangians". In: *Nuclear Physics B* 231.2 (1984), pp. 269 –295. ISSN: 0550-3213. DOI: 10.1016/0550-3213(84)90287-6. URL: http://www.sciencedirect.com/science/article/pii/0550321384902876.

[163] I. Ia. Pomeranchuk. "On the Stability of a Fermi liquid". In: *Sov. Phys. JETP* 8 (2 1959), p. 361. URL: http://www.jetp.ac.ru/cgi-bin/dn/e_008_02_0361.pdf.

[164] Victor Nikolaevich Popov and SA Fedotov. "The functional-integration method and diagram technique for spin systems". In: *Zh. Eksp. Teor. Fiz* 94.3 (1988), pp. 183–194.

[165] S. Raghu, S. A. Kivelson, and D. J. Scalapino. "Superconductivity in the repulsive Hubbard model: An asymptotically exact weak-coupling solution". In: *Phys. Rev. B* 81 (22 June 2010), p. 224505. DOI: 10.1103/PhysRevB.81.224505. URL: https://link.aps.org/doi/10.1103/PhysRevB.81.224505.

[166] B. J. Ramshaw et al. "Quasiparticle mass enhancement approaching optimal doping in a high-T_c superconductor". In: *Science* 348.6232 (2015), pp. 317–320. DOI: 10.1126/science.aaa4990. eprint: https://www.science.org/doi/pdf/10.1126/science.aaa4990. URL: https://www.science.org/doi/abs/10.1126/science.aaa4990.

[167] M. Yu. Reizer. "Relativistic effects in the electron density of states, specific heat, and the electron spectrum of normal metals". In: *Phys. Rev. B* 40 (17 Dec. 1989), pp. 11571–11575. DOI: 10.1103/PhysRevB.40.11571. URL: http://link.aps.org/doi/10.1103/PhysRevB.40.11571.

[168] M. Reuter. "Nonperturbative evolution equation for quantum gravity". In: *Phys. Rev. D* 57 (2 Jan. 1998), pp. 971–985. DOI: 10.1103/PhysRevD.57.971. URL: https://link.aps.org/doi/10.1103/PhysRevD.57.971.

[169] Sam P. Ridgway and Chris A. Hooley. "Non-Fermi-Liquid Behavior and Anomalous Suppression of Landau Damping in Layered Metals Close to Ferromagnetism". In: *Phys. Rev. Lett.* 114 (22 June 2015), p. 226404. DOI: 10.1103/PhysRevLett.114.226404. URL: https://link.aps.org/doi/10.1103/PhysRevLett.114.226404.

[170] L. Rosa, P. Vitale, and C. Wetterich. "Critical Exponents of the Gross-Neveu Model from the Effective Average Action". In: *Phys. Rev. Lett.* 86 (6 Feb. 2001), pp. 958–961. DOI: 10.1103/PhysRevLett.86.958. URL: https://link.aps.org/doi/10.1103/PhysRevLett.86.958.

[171] Dietrich Roscher, Emilio Torres, and Philipp Strack. "Dual QED3 at "N F = 1/2" is an interacting CFT in the infrared". In: *Journal of High Energy Physics* 2016.11 (Nov. 2016), p. 17. ISSN: 1029-8479. DOI: 10.1007/JHEP11(2016)017. URL: https://doi.org/10.1007/JHEP11(2016)017.

[172] Subir Sachdev. *Quantum Phase Transitions*. 2nd ed. Cambridge University Press, 2011. DOI: 10.1017/CBO9780511973765.

[173] Subir Sachdev. *Quantum Phases of Matter*. 2023. DOI: 10.1017/9781009212717.

[174] Subir Sachdev and Jinwu Ye. "Gapless spin-fluid ground state in a random quantum Heisenberg magnet". In: *Phys. Rev. Lett.* 70 (21 May 1993), pp. 3339–3342. DOI: 10.1103/PhysRevLett.70.3339. URL: https://link.aps.org/doi/10.1103/PhysRevLett.70.3339.

[175] P. D. Sacramento and P. Schlottmann. "The Kondo system Fe: Comparison of theory and experiment". In: *Solid State Communications* 73.11 (1990), pp. 747–750. ISSN: 0038-1098. DOI: 10.1016/0038-1098(90)90163-6.

[176] K. Samwer and K. Winzer. "Magnetoresistivity of the Kondo-system (La, Ce)B6". In: *Zeitschrift für Physik B Condensed Matter and Quanta* 25.3 (1976), pp. 269–274. ISSN: 0340-224X. DOI: 10.1007/bf01420889.

[177] D. J. Scalapino, E. Loh, and J. E. Hirsch. "*d*-wave pairing near a spin-density-wave instability". In: *Phys. Rev. B* 34 (11 Dec. 1986), pp. 8190–8192. DOI: 10.1103/PhysRevB.34.8190. URL: https://link.aps.org/doi/10.1103/PhysRevB.34.8190.

[178] Harley D. Scammell and Mathias S. Scheurer. "Tunable Superconductivity and Möbius Fermi Surfaces in an Inversion-Symmetric Twisted van der Waals Heterostructure". In: *Phys. Rev. Lett.* 130 (6 Feb. 2023), p. 066001. DOI: 10.1103/PhysRevLett.130.066001. URL: https://link.aps.org/doi/10.1103/PhysRevLett.130.066001.

[179] Yoni Schattner et al. "Competing Orders in a Nearly Antiferromagnetic Metal". In: *Phys. Rev. Lett.* 117 (9 Aug. 2016), p. 097002. DOI: 10.1103/PhysRevLett.117.097002. URL: http://link.aps.org/doi/10.1103/PhysRevLett.117.097002.

[180] Yoni Schattner et al. "Ising Nematic Quantum Critical Point in a Metal: A Monte Carlo Study". In: *Phys. Rev. X* 6 (3 Aug. 2016), p. 031028. DOI: 10.1103/PhysRevX.6.031028. URL: http://link.aps.org/doi/10.1103/PhysRevX.6.031028.

[181] Michael M. Scherer, Stefan Uebelacker, and Carsten Honerkamp. "Instabilities of interacting electrons on the honeycomb bilayer". In: *Phys. Rev. B* 85 (23 June 2012), p. 235408. DOI: 10.1103/PhysRevB.85.235408. URL: https://link.aps.org/doi/10.1103/PhysRevB.85.235408.

[182] Andres Schlief, Peter Lunts, and Sung-Sik Lee. "Exact Critical Exponents for the Antiferromagnetic Quantum Critical Metal in Two Dimensions". In: *Phys. Rev. X* 7 (2 Apr. 2017), p. 021010. DOI: 10.1103/PhysRevX.7.021010. URL: https://link.aps.org/doi/10.1103/PhysRevX.7.021010.

[183] Andrés Schlief, Peter Lunts, and Sung-Sik Lee. "Noncommutativity between the low-energy limit and integer dimension limits in the ϵ expansion: A case study of the antiferromagnetic quantum critical metal". In: *Phys. Rev. B* 98 (7 Aug. 2018), p. 075140. DOI: 10.1103/PhysRevB.98.075140. URL: https://link.aps.org/doi/10.1103/PhysRevB.98.075140.

[184] F. Schmitt et al. "Analysis of the spectral function of $Nd_{1.85}Ce_{0.15}CuO_4$ obtained by angle-resolved photoemission spectroscopy". In: *Phys. Rev. B* 78 (10 Sept. 2008), p. 100505. DOI: 10.1103/PhysRevB.78.100505. URL: https://link.aps.org/doi/10.1103/PhysRevB.78.100505.

[185] A. J. Schofield. "Non-Fermi liquids". In: *Contemporary Physics* 40.2 (1999), pp. 95–115. DOI: 10.1080/001075199181602. eprint: https://doi.org/10.1080/001075199181602. URL: https://doi.org/10.1080/001075199181602.

[186] J. R. Schrieffer and P. A. Wolff. "Relation between the Anderson and Kondo Hamiltonians". In: *Physical Review* 149.2 (), pp. 491–492. ISSN: 0031-899X. DOI: 10.1103/physrev.149.491.

[187] A. Schröder et al. "Onset of antiferromagnetism in heavy-fermion metals". In: *Nature* 407.6802 (2000), pp. 351–355. DOI: 10.1038/35030039. URL: https://doi.org/10.1038/35030039.

[188] Suchitra E Sebastian, Neil Harrison, and Gilbert G Lonzarich. "Towards resolution of the Fermi surface in underdoped high-Tc superconductors". In: *Reports on Progress in Physics* 75.10 (Sept. 2012), p. 102501. DOI: 10.1088/0034-4885/75/10/102501. URL: https://dx.doi.org/10.1088/0034-4885/75/10/102501.

[189] Suchitra E. Sebastian et al. "A multi-component Fermi surface in the vortex state of an underdoped high-Tc superconductor". In: *Nature* 454.7201 (July 2008), pp. 200–203. DOI: 10.1038/nature07095. URL: https://doi.org/10.1038%2Fnature07095.

[190] T. Senthil. "Critical Fermi surfaces and non-Fermi liquid metals". In: *Phys. Rev. B* 78 (3 July 2008), p. 035103. DOI: 10.1103/PhysRevB.78.035103. URL: http://link.aps.org/doi/10.1103/PhysRevB.78.035103.

[191] T. Senthil. *On the mass enhancement near optimal doping in high magnetic fields in the cuprates*. 2014. arXiv: 1410.2096 [cond-mat.str-el].

[192] T. Senthil, Subir Sachdev, and Matthias Vojta. "Fractionalized Fermi Liquids". In: *Phys. Rev. Lett.* 90 (21 May 2003), p. 216403. DOI: 10.1103/PhysRevLett.90.216403. URL: https://link.aps.org/doi/10.1103/PhysRevLett.90.216403.

[193] T. Senthil, Matthias Vojta, and Subir Sachdev. "Weak magnetism and non-Fermi liquids near heavy-fermion critical points". In: *Phys. Rev. B* 69 (3 Jan. 2004), p. 035111. DOI: 10.1103/PhysRevB.69.035111. URL: https://link.aps.org/doi/10.1103/PhysRevB.69.035111.

[194] R. Shankar. "Renormalization-group approach to interacting fermions". In: *Rev. Mod. Phys.* 66 (1 Jan. 1994), pp. 129–192. DOI: 10.1103/RevModPhys.66.129. URL: http://link.aps.org/doi/10.1103/RevModPhys.66.129.

[195] Qimiao Si and Frank Steglich. "Heavy Fermions and Quantum Phase Transitions". In: *Science* 329.5996 (2010), pp. 1161–1166. DOI: 10.1126/science.1191195. eprint: https://www.science.org/doi/pdf/10.1126/science.1191195. URL: https://www.science.org/doi/abs/10.1126/science.1191195.

[196] Qimiao Si et al. "Kondo Destruction and Quantum Criticality in Kondo Lattice Systems". In: *Journal of the Physical Society of Japan* 83.6 (2014), p. 061005. DOI: 10.7566/JPSJ.83.061005. eprint: https://doi.org/10.7566/JPSJ.83.061005. URL: https://doi.org/10.7566/JPSJ.83.061005.

[197] John Singleton et al. "Magnetic Quantum Oscillations in $YBa_2Cu_3\mathbf{O}_{6.61}$ and $YBa_2Cu_3\mathbf{O}_{6.69}$ in Fields of Up to 85 T: Patching the Hole in the Roof of the Superconducting Dome". In: *Phys. Rev. Lett.* 104 (8 Feb. 2010), p. 086403. DOI: 10.1103/PhysRevLett.104.086403. URL: https://link.aps.org/doi/10.1103/PhysRevLett.104.086403.

[198] Tyler B. Smith, Lakshmi Pullasseri, and Ajit Srivastava. "Momentum-space gravity from the quantum geometry and entropy of Bloch electrons". In: *Phys. Rev. Res.* 4 (1 Mar. 2022), p. 013217. DOI: 10.1103/PhysRevResearch.4.013217. URL: https://link.aps.org/doi/10.1103/PhysRevResearch.4.013217.

[199] Tudor D. Stanescu, Victor Galitski, and H. D. Drew. "Effective Masses in a Strongly Anisotropic Fermi Liquid". In: *Physical Review Letters* 101.6 (Aug. 2008). DOI: 10.1103/physrevlett.101.066405. URL: https://doi.org/10.1103%2Fphysrevlett.101.066405.

[200] W. M. Star and G. J. Nieuwenhuys. "The low temperature limit of the kondo effect in copper-iron". In: *Physics Letters A* 30.1 (1969), pp. 22–23. ISSN: 0375-9601. DOI: 10.1016/0375-9601(69)90017-6.

[201] G. R. Stewart. "Heavy-fermion systems". In: *Rev. Mod. Phys.* 56 (4 Oct. 1984), pp. 755–787. DOI: 10.1103/RevModPhys.56.755. URL: https://link.aps.org/doi/10.1103/RevModPhys.56.755.

[202] G. R. Stewart. "Non-Fermi-liquid behavior in d- and f-electron metals". In: *Rev. Mod. Phys.* 73 (4 Oct. 2001), pp. 797–855. DOI: 10.1103/RevModPhys.73.797. URL: http://link.aps.org/doi/10.1103/RevModPhys.73.797.

[203] Philipp Strack and Pawel Jakubczyk. "Fluctuations of Imbalanced Fermionic Superfluids in Two Dimensions Induce Continuous Quantum Phase Transitions and Non-Fermi-Liquid Behavior". In: *Phys. Rev. X* 4 (2 Apr. 2014), p. 021012. DOI: 10.1103/PhysRevX.4.021012. URL: https://link.aps.org/doi/10.1103/PhysRevX.4.021012.

[204] Shouvik Sur and Sung-Sik Lee. "Anisotropic non-Fermi liquids". In: *Phys. Rev. B* 94 (19 Nov. 2016), p. 195135. DOI: 10.1103/PhysRevB.94.195135. URL: http://link.aps.org/doi/10.1103/PhysRevB.94.195135.

[205] Shouvik Sur and Sung-Sik Lee. "Chiral non-Fermi liquids". In: *Phys. Rev. B* 90 (4 July 2014), p. 045121. DOI: 10.1103/PhysRevB.90.045121. URL: http://link.aps.org/doi/10.1103/PhysRevB.90.045121.

[206] Shouvik Sur and Sung-Sik Lee. "Quasilocal strange metal". In: *Phys. Rev. B* 91 (12 Mar. 2015), p. 125136. DOI: 10.1103/PhysRevB.91.125136. URL: http://link.aps.org/doi/10.1103/PhysRevB.91.125136.

[207] Uwe C. Täuber. *Critical Dynamics: A Field Theory Approach to Equilibrium and Non-Equilibrium Scaling Behavior*. Cambridge University Press, 2014. DOI: 10.1017/CBO9781139046213.

[208] Sin-itiro Tomonaga. "Remarks on Bloch's Method of Sound Waves applied to Many-Fermion Problems". In: *Progress of Theoretical Physics* 5.4 (July 1950), pp. 544–569. ISSN: 0033-068X. DOI: 10.1143/ptp/5.4.544. eprint: http://oup.prod.sis.lan/ptp/article-pdf/5/4/544/5430161/5-4-544.pdf. URL: https://dx.doi.org/10.1143/ptp/5.4.544.

[209] Emilio Torres et al. "Fermion-induced quantum criticality with two length scales in Dirac systems". In: *Phys. Rev. B* 97 (12 Mar. 2018), p. 125137. DOI: 10.1103/PhysRevB.97.125137. URL: https://link.aps.org/doi/10.1103/PhysRevB.97.125137.

[210] C. M. Varma. "Quantum Criticality in Quasi-Two-Dimensional Itinerant Antiferromagnets". In: *Phys. Rev. Lett.* 115 (18 Oct. 2015), p. 186405. DOI: 10.1103/PhysRevLett.115.186405. URL: http://link.aps.org/doi/10.1103/PhysRevLett.115.186405.

[211] Chandra M. Varma et al. "Quantum critical singularities in two-dimensional metallic XY ferromagnets". In: *Phys. Rev. B* 97 (8 Feb. 2018), p. 085134. DOI: 10.1103/PhysRevB.97.085134. URL: https://link.aps.org/doi/10.1103/PhysRevB.97.085134.

[212] Boris A. Veytsman. "Limit cycles in renormalization group flows: thermodynamics controls dances of space patterns". In: *Physics Letters A* 183.4 (1993), pp. 315–318. ISSN: 0375-9601. DOI: https://doi.org/10.1016/0375-9601(93)90463-A. URL: https://www.sciencedirect.com/science/article/pii/037596019390463A.

[213] J Voit. "One-dimensional Fermi liquids". In: *Reports on Progress in Physics* 58.9 (Sept. 1995), pp. 977–1116. DOI: 10.1088/0034-4885/58/9/002. URL: https://doi.org/10.1088%2F0034-4885%2F58%2F9%2F002.

[214] M.A.H. Vozmediano, M.I. Katsnelson, and F. Guinea. "Gauge fields in graphene". In: *Physics Reports* 496.4-5 (Nov. 2010), pp. 109–148. DOI: 10.1016/j.physrep.2010.07.003. URL: https://doi.org/10.1016%2Fj.physrep.2010.07.003.

[215] R.M. Wald. *General Relativity*. University of Chicago Press, 2010. ISBN: 9780226870373. URL: https://books.google.ca/books?id=9S-hzg6-moYC.

[216] Chong Wang et al. "Deconfined Quantum Critical Points: Symmetries and Dualities". In: *Phys. Rev. X* 7 (3 Sept. 2017), p. 031051. DOI: 10.1103/PhysRevX.7.031051. URL: https://link.aps.org/doi/10.1103/PhysRevX.7.031051.

[217] Fa Wang et al. "Functional Renormalization-Group Study of the Pairing Symmetry and Pairing Mechanism of the FeAs-Based High-Temperature Superconductor". In: *Phys. Rev. Lett.* 102 (4 Jan. 2009), p. 047005. DOI: 10.1103/PhysRevLett.102.047005. URL: https://link.aps.org/doi/10.1103/PhysRevLett.102.047005.

[218] Jing Wang, Andreas Eberlein, and Walter Metzner. "Competing order in correlated electron systems made simple: Consistent fusion of functional renormalization and mean-field theory". In: *Phys. Rev. B* 89 (12 Mar. 2014), p. 121116. DOI: 10.1103/PhysRevB.89.121116. URL: https://link.aps.org/doi/10.1103/PhysRevB.89.121116.

[219] Xiaoyu Wang et al. "Fragility of Charge Order Near an Antiferromagnetic Quantum Critical Point". In: *Phys. Rev. Lett.* 120 (24 June 2018), p. 247002. DOI: 10.1103/PhysRevLett.120.247002. URL: https://link.aps.org/doi/10.1103/PhysRevLett.120.247002.

[220] Xiaoyu Wang et al. "Superconductivity mediated by quantum critical antiferromagnetic fluctuations: The rise and fall of hot spots". In: *Phys. Rev. B* 95 (17 May 2017), p. 174520. DOI: 10.1103/PhysRevB.95.174520. URL: https://link.aps.org/doi/10.1103/PhysRevB.95.174520.

[221] Yongjun Wang, Zeyang Chi, and Jinxing Liu. "On buckling behaviors of a typical bending-dominated periodic lattice". In: *Composite Structures* 258 (2021), p. 113204. ISSN: 0263-8223. DOI: https://doi.org/10.1016/j.compstruct.2020.113204. URL: https://www.sciencedirect.com/science/article/pii/S0263822320331305.

[222] Christof Wetterich. "Exact evolution equation for the effective potential". In: *Physics Letters B* 301.1 (1993), pp. 90 –94. ISSN: 0370-2693. DOI: 10.1016/0370-2693(93)90726-X. URL: http://www.sciencedirect.com/science/article/pii/037026939390726X.

[223] Marc A. Wilde et al. "Symmetry-enforced topological nodal planes at the Fermi surface of a chiral magnet". In: *Nature* 594.7863 (June 2021), pp. 374–379. DOI: 10.1038/s41586-021-03543-x. URL: https://doi.org/10.1038%2Fs41586-021-03543-x.

[224] Kenneth G. Wilson. "Renormalization Group and Critical Phenomena. I. Renormalization Group and the Kadanoff Scaling Picture". In: *Phys. Rev. B* 4 (9 Nov. 1971), pp. 3174–3183. DOI: 10.1103/PhysRevB.4.3174. URL: https://link.aps.org/doi/10.1103/PhysRevB.4.3174.

[225] Kenneth G. Wilson. "Renormalization Group and Critical Phenomena. II. Phase-Space Cell Analysis of Critical Behavior". In: *Phys. Rev. B* 4 (9 Nov. 1971), pp. 3184–3205. DOI: 10.1103/PhysRevB.4.3184. URL: https://link.aps.org/doi/10.1103/PhysRevB.4.3184.

[226] Kenneth G. Wilson. "The renormalization group: Critical phenomena and the Kondo problem". In: *Rev. Mod. Phys.* 47 (4 Oct. 1975), pp. 773–840. DOI: 10.1103/RevModPhys.47.773. URL: https://link.aps.org/doi/10.1103/RevModPhys.47.773.

[227] Stephen D. Wilson et al. "Resonance in the electron-doped high-transition-temperature superconductor Pr0.88LaCe0.12CuO4-δ". In: *Nature* 442 (July 2006), 59 EP –. URL: https://doi.org/10.1038/nature04857.

[228] Xiaochuan Wu et al. "Candidate theory for the strange metal phase at a finite-energy window". In: *Phys. Rev. B* 98 (16 Oct. 2018), p. 165117. DOI: 10.1103/PhysRevB.98.165117. URL: https://link.aps.org/doi/10.1103/PhysRevB.98.165117.

[229] Di Xiao, Ming-Che Chang, and Qian Niu. "Berry phase effects on electronic properties". In: *Reviews of Modern Physics* 82.3 (July 2010), pp. 1959–2007. DOI: 10.1103/revmodphys.82.1959. URL: https://doi.org/10.1103%2Frevmodphys.82.1959.

[230] Xiao Yan Xu et al. "Non-Fermi Liquid at $(2+1)$D Ferromagnetic Quantum Critical Point". In: *Phys. Rev. X* 7 (3 Sept. 2017), p. 031058. DOI: 10.1103/PhysRevX.7.031058. URL: https://link.aps.org/doi/10.1103/PhysRevX.7.031058.

[231] Weicheng Ye, Sung-Sik Lee, and Liujun Zou. "Ultraviolet-Infrared Mixing in Marginal Fermi Liquids". In: *Phys. Rev. Lett.* 128 (10 Mar. 2022), p. 106402. DOI: 10.1103/PhysRevLett.128.106402. URL: https://link.aps.org/doi/10.1103/PhysRevLett.128.106402.

[232] D. Zanchi and H. J. Schulz. "Weakly correlated electrons on a square lattice: Renormalization-group theory". In: *Phys. Rev. B* 61 (20 May 2000), pp. 13609–13632. DOI: 10.1103/PhysRevB.61.13609. URL: https://link.aps.org/doi/10.1103/PhysRevB.61.13609.

[233] Jean Zinn-Justin. *Quantum Field Theory and Critical Phenomena*. 4th. Oxford University Press, 2002. DOI: 10.1093/acprof:oso/9780198509233.001.0001. URL: http://www.oxfordscholarship.com/view/10.1093/acprof:oso/9780198509233.001.0001/acprof-9780198509233.

[234] Gil Zumbach. "Almost second order phase transitions". In: *Phys. Rev. Lett.* 71 (15 Oct. 1993), pp. 2421–2424. DOI: 10.1103/PhysRevLett.71.2421. URL: https://link.aps.org/doi/10.1103/PhysRevLett.71.2421.